Petrochemistry, Geochronology and Tectonic Implication of the Chiang Khong-Lampang-Tak Volcanic Belt, Northern Thailand

by

Weerapan Srichan
B.S., M.S. (Chiang Mai University)

Submitted in fulfilment of the requirements for the degree of
Doctor of Philosophy

University of Tasmania
Hobart

October, 2008

STATEMENT

This thesis contains the results of research done at CODES, the School of Earth Sciences, University of Tasmania, Hobart, Tasmania, Australia between 2005 and 2008. Part of the material presented in this thesis has been published as:

Srichan, W, Crawford, A.J. and Berry, R.F., 2008, Geochemistry and geochronology of Late Triassic volcanic rocks in the Chiang Khong region, northern Thailand, The Island Arc, *in press*.

This thesis contains no material which has been accepted for the award of any other higher degree of graduate diploma in any tertiary institution and to the best of the author's knowledge and belief. This thesis contains no material previously published or written by another person, except where due references is made in the text of the thesis.

W. Srichan

Weerapan Srichan
October, 2008

CODES Centre of Excellence in Ore Deposits
Department of Geology
School of Earth Sciences
University of Tasmania
Hobart, Tasmania, Australia

ABSTRACT

The Chiang Khong-Lampang-Tak volcanic belt (CLT) is a key element in the central part of the Sukhothai Fold Belt in northern Thailand, lying between the Chiang Mai (Inthanon) Suture and the Nan-Sra-Kaeo Suture. This study reports detailed petrochemical, geochronological and structural aspects of rocks constituting the CLT, and uses this information to elucidate the tectonic evolution of this geologically important part of mainland SE Asia.

The CLT is constituted by a number of sub-belts, and these have been examined in two major study areas, namely, in northernmost Thailand along the Mekong River border region with Laos, and in further south in the Lampang area. Volcanic and dyke rocks in the CLT formed mainly between 220 and 230 Ma, and they display a striking range of compositions and affinities, from low-K rocks with transitional tholeiitic affinities, through medium-K calc-alkaline, to dominant high-K calc-alkaline compositions. Basaltic rocks dominate some sub-belts, whereas felsic rocks predominate in others. Although previous studies have unanimously suggested that these rocks formed in a continental margin volcanic arc, it is suggested here that these rocks formed in a post-collisional, extensional Basin and Range-type setting. It is proposed that crustal thickening due to the Late Middle Triassic collision between the Shan-Thai and Indochina terranes was followed by relaxation rifting and gravitational collapse of the new crustal collage, leading to the post-collisional magmatism of the CLT.

Laser ablation ICP-MS U-Pb dating of zircons in this study has shown that most CLT igneous rocks crystallized in late Middle to early Late Triassic (~220-230 Ma). In many rocks, age histograms for zircons showed a peak at 220 Ma and another at 230 Ma. The cause of these bimodal zircon ages remains uncertain and there are no internal textural differences between the zircon grains in either group. Permian zircons have been found in some Late Triassic CLT igneous rocks and are inherited possibly from basement Permian granites associated with prior subduction.

Detrital zircons in CLT sedimentary rocks indicate that Late Devonian to Early Carboniferous, Permian and Late Triassic rocks were exposed in the provenance areas of

these sandstones. The Devonian to Early Carboniferous and Permian detrital zircons formed in the earlier, subduction-related magmatic events, whereas the Late Triassic zircons are locally derived from the CLT volcanics.

Several structural transects of the CLT, in both the northern and southern study areas, showed that these rocks are dominated by a thin-skinned east-vergent fold and thrust structural style, characterized by upright close to open folds with locally overturned bedding. The steep regional cleavage is axial planar to regional folds and becomes more intense to the east and near thrusts. In some localities, the steep cleavage is overprinted by a shallow dipping cleavage, the latter is possibly related to shallow west-dipping thrusts associated with Late Triassic deformation. The thin-skinned thrust faulting involved mainly east-directed transport and was overprinted by local back thrusts. A west-dipping mylonite zone along the SW margin of the Chiang Khong Central Sub-belt is correlated with the regional deformation event that produced L/S tectonites of the Ban Huak area, southeast of the Chiang Khong area. Anomalous thrust fault orientations in the Ban Huak area represent lateral ramps. It is concluded that the structure of the CLT is similar to the thrust geometry described by previous workers from further east and south in the Sukhothai Fold Belt. The compressional event in the Latest Triassic, after the CLT extensional magmatism, and which disrupted the CLT into the present sub-belts, remains problematic. It possibly represents a final minor event at least 10 m.y. after the accretion of the Shan-Thai to Indochina terranes. Rocks showing the fold and thrust style regional structure of the CLT and the Sukhothai Fold Belt are overlain by Latest Triassic to Early Jurassic Khorat Group molasse and affected by normal and strike-slip faulting. This late structure is related to the extensional rift basin development in northern Thailand and possibly associated with the Eocene collision between the India and Asia.

A new tectonic model for the geodynamic evolution of the northern Thailand region is proposed, based on the new data from this study and a comprehensive review of the extensive published literature. West-directed subduction during the Permian within the ocean basin (Palaeo-Tethys) between the Indochina and Shan-Thai terranes produced a typical West Pacific-type intra-oceanic arc-backarc basin system. Eventual closure of this segment of ocean led to collision of the arc system with the leading (western) edge of Indochina, perhaps in the Late Permian. Following locking of the plate boundary by this collision event, continued convergence between the Indochina Terrane and the Shan-Thai

Terrane forced a subduction polarity reversal, to east-directed subduction beneath the Indochina Terrane. Ongoing Latest Permian east-directed subduction led to construction of the Loei arc on the western edge of the Indochina Terrane, then to arrival of the leading edge of the Shan-Thai Terrane at the trench, and a Late Middle to Early Late Triassic continent-continent collision, which thoroughly reworked and restructured the fold belt formed in the earlier arc-continent collision. Although such an event is expected to generate east-dipping thrusts over much of the area affected by the collision, backthrusting of the older fold belt collage against the buttress of the Indochina Terrane may have produced the widespread west-dipping structures over much of the Sukhothai Fold Belt and Simao Terrane. Relaxation rifting and gravitational collapse of the new crustal collage in Late Triassic led to the post-collisional mainly calc-alkaline magmatism of the Chiang Khong-Lampang-Tak volcanic belt, and subsequent deposition of the Lampang Group. Cessation of extension and post-collisional magmatism may have been followed by Latest Triassic thrust faulting responsible for the present disposition of the sub-belt that constitute the CLT. This thrusting may have been due to further 'locking up' along the Indochina – Shan-Thai suture, but it remains problematic. Finally, the Khorat Group molasse was deposited over the collision zone.

ACKNOWLEDGEMENTS

I would like to greatly thank my supervisors, Prof. Anthony J. Crawford and Assoc. Prof. Ronald F. Berry for their invaluable supervision, patient guidance, expert advice, support, enthusiasm, encouragement, stimulation, critical reading and comment throughout this study project.

I am also very much indebted to Dr. Sebastien Meffre (UTAS) for his expert help with laser ablation ICP-MS zircon dating and careful checking of the relevant material in this thesis, as well as discussions on the tectonic models of the region. Assoc. Prof. Khin Zaw (UTAS), Dr. Andrew McNeill (UTAS), Dr. Clive Burrett (Great South Land Minerals Limited), Assoc. Prof. Yuenyong Panjasawatwong (CMU), Assoc. Prof. Sampan Singharajwarapan (CMU) and Somboon Khositanont (DMR, Thailand) for their stimulating tectonic discussions, support and guidance.

I am grateful for the support and comment of my former teachers and present colleagues especially the young staff in the Department of Geological Sciences, Faculty of Science, Chiang Mai University.

Financial support for this project was provided by the Royal Thai Government and CODES. Special thanks are extended to the Australian UNESCO Committee for the IGCP, via IGCP project 516 and Oxiana Ltd. for their supplementary funding for this research.

The expert help of Dr. Karsten Goemann (Central Science Laboratory, University of Tasmania) with Electron Probe Microanalysis (EMP) and Scanning Electron Microscopy (SEM) is gratefully acknowledged.

I also would like to acknowledge Phil Robinson, Sarah Gilbert and Katie McGoldrick for their advice and support with the XRF and ICP-MS analyses. Niti Mankhemthong and Noppol Pacharapongsakun, Master students of the Department of Geological Sciences, Chiang Mai University, are thanked for their field assistances in northern Thailand.

Simon Stephen (UTAS) and Chantip Punthusa (CMU) are also thanked for their masterful preparation of thin-sections and polished thin-sections.

Thanks are extended to the support staff at CODES and the School of Earth Sciences (UTAS) for all their help, in particular, Dianne Steffens, Christine Higgins, Nilar Hlaing, Keith Dobson, Peter Cornish, Isabella von Lichtan, June Pongratz and Dianne Madden.

To all post-graduate students at CODES: Ben Jones, Paul Cromie, Blackwell Singoyi, Abhisit Salam, Teera Kamvong, Takayuki Manaka, Dinh Sang, Bronto Sutopo, Victor Galvan, Susan Belford, Andrew Stacey, Liezl Cuison, Nathan Fox, Tim Ireland, Wallace Mackay, Claire McMahon, Joe Moye, Anita Parbhakar, Lee Robson, Lee Evans, Adam Bath, Patrick Sack, Sofia Tetroeva, Adel Vantandoost, Wojceich Zukowski, Jaqueline Blackwell, Natalee Bonnici, Kim Denwer, Sarah Gordee, Martin Jutzeler, Rod Maier, Bryan Bowden, Heidi Pass, Olga Vasyukova, Reia Chmielowski, Andrea Agangi, Paul Ferguson, Yansan Gamyanbaatae and many others: thanks for your friendship and support.

I am deeply grateful for the support from my parent and sister. Finally, I would like to give special thanks to Kamolrawee Sintupat for her continual support and encouragement.

TABLE OF CONTENTS

Page

Page

LIST OF FIGURES

Page

Page

Page

Page

Page

LIST OF TABLES

THAI GEOGRAPHIC TERMS

Amphoe = town, district

Ang Keb Nam = reservoir

Ban = village, small community

Changwat = province, city

Doi = mountain

Huai = rivulet, gully, creek

Khaeng = rapids

Khao = isolated hill, mountain

Khlong = stream, canal

Mae Nam = large river

Nam = river

Pha = cliff

Phra That = pagoda

Phu = hill or mountain

Phu Khao = mountain range

Wat = temple

CHAPTER 1

Introduction

1.1 Purpose and Scope of Study

The main aim of this project is to study the occurrence, petrochemistry, geochronology and the tectonic implications of volcanic rocks along Chiang Khong-Lampang-Tak volcanic belt (the central part of the Sukhothai Fold Belt) in northern Thailand. The Chiang Khong-Lampang-Tak volcanic belt (CLT) has been considered to represent fragments of a Permo-Triassic continental volcanic arc in northern Thailand (Jungyusuk & Khositanont, 1992; Panjasawatwong *et al.,* 2003; Sone & Metcalfe, 2008). This volcanic belt (CLT) is now located between the two other volcanic belts of broadly similar age, the Chiang Rai-Chiang Mai volcanic belt and Nan-Chanthaburi suture, respectively (Figure 1.1). New information deriving from this project is then used, along with published information on the latter belts, to evaluate and improve models for the tectonic evolution of this part of Southeast Asia. To carry out this aim, sampling and detailed mapping (including structural analysis) were focussed along a number of regional transects effectively perpendicular to this broadly meridional volcanic belt.

Transects across the CLT include six geological sections (Figures 1.2 and 1.3). The first section extends along the Mae Khong River (Thai-Laos border) from Chiang Khong through to Wiang Kaen. The second and the third extend across the central part of the Chiang Khong area along the road from Doi Luang sub-district to the Phu Chi Fa area. The last three traverses are along the Highway number 11 from the Muang Lampang district to Ban Mae Khaem in the Lampang area. In addition, a detailed structural study of a distinctive metamorphic zone in the southeastern part of the Chiang Khong area (Figure 1.2) was carried out to elucidate the structural and metamorphic history of this region.

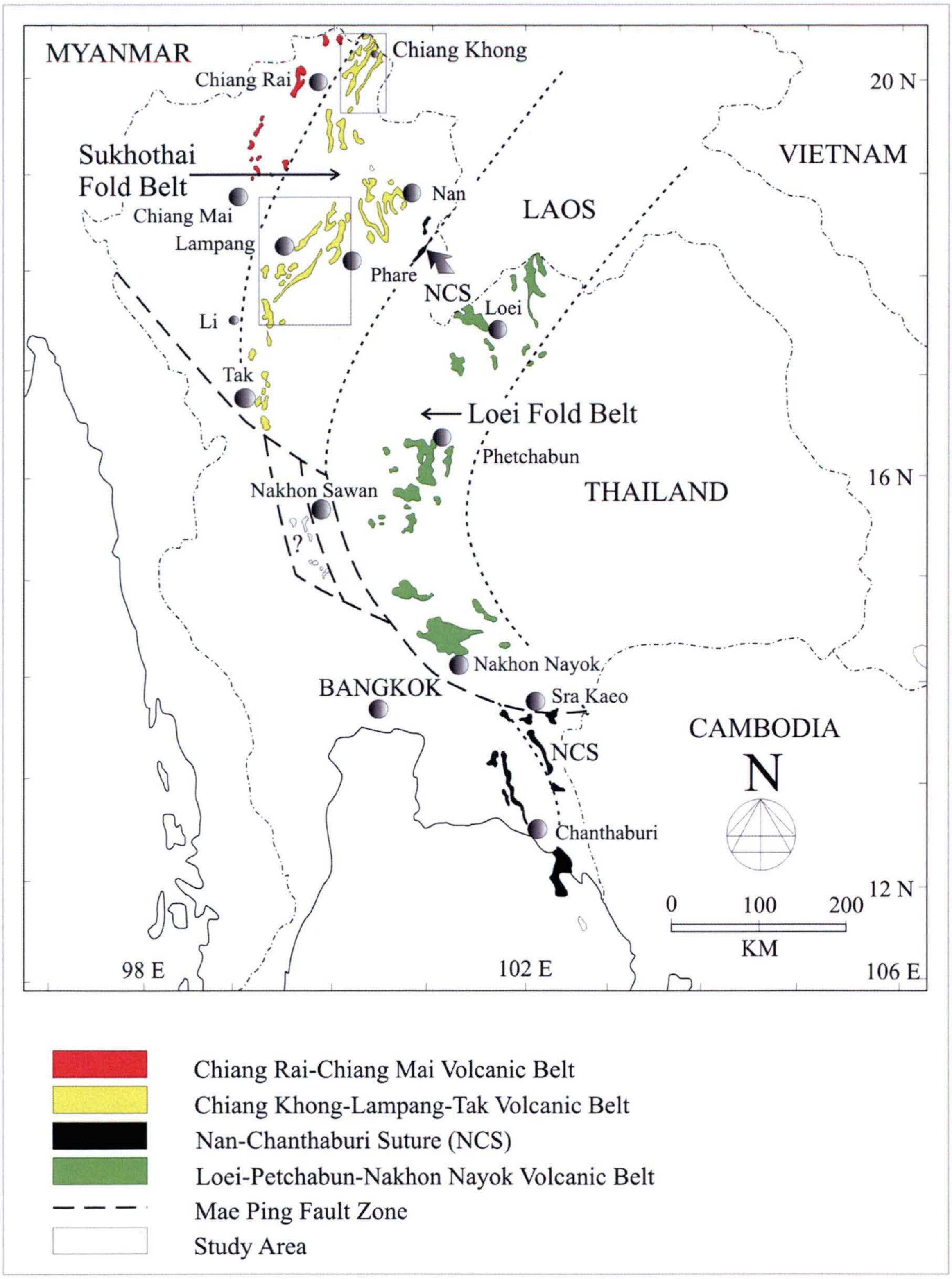

Figure 1.1 Map showing the Sukhothai Fold Belt, Loei Fold Belt, distribution of pre-Jurassic volcanic rocks in Thailand and study areas of the Chiang Khong-Lampang-Tak volcanic belt (after Panjasawatwong *et al.,* 1997 and Kosuwan, 2004).

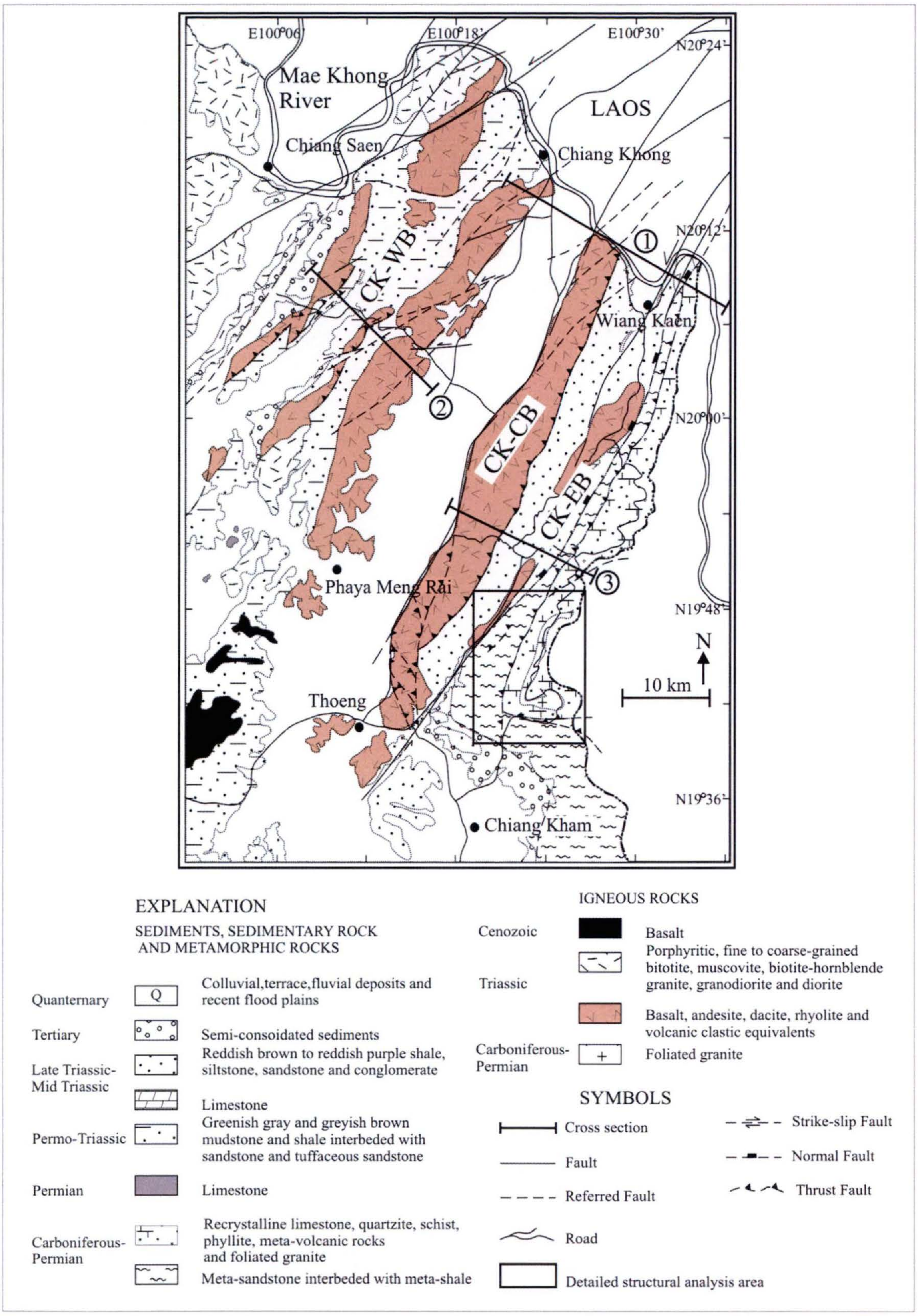

Figure 1.2 Geological map of the Chiang Khong area showing transects and location of the area that was the focus of the detailed structural and metamorphic study (after Bruan & Hahn, 1976; Sukvattananunt *et al.,* 1985a, 1985b; Sukvattananunt & Assawapatchara, 1989a, 1989b, 1989c, 1989d; Tansuwan & Chitmanee, 1990a, 1990b).

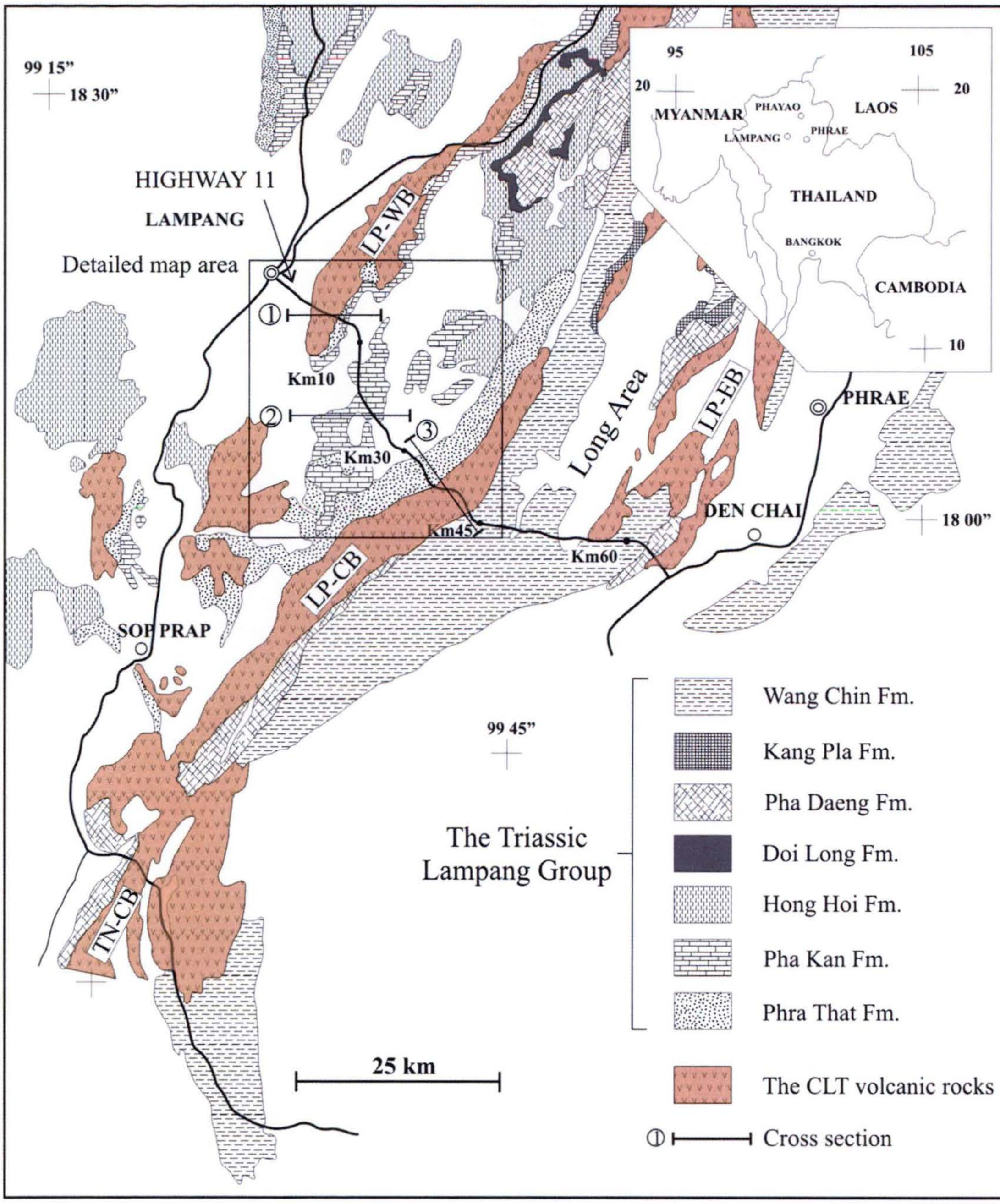

Figure 1.3 Simplified geological map of the Lampang area showing distribution of the CLT volcanics and three cross-sections along the Highway number 11 (after Chaodumrong, 1992).

1.2 Tectonic Setting

Thailand consists of two micro-continents, the Shan-Thai Terrane in the west and the Indochina Terrane in the east, and these two terranes have long been considered to join along the Nan-Chanthaburi suture (Asanachinda, 1978; Bunopas & Vella, 1978;

Chantraramee, 1978; Gatinsky *et al.,* 1978; Thanasuthipitak, 1978; Bunopas, 1981; Barr & Macdonald, 1991; Panjasawatwong, 1991; Singharajwarapan, 1994; Hada *et al.,* 1991, 1999; Metcalfe, 1999; Singharajwarapan & Berry, 2000). The Indochina and Shan-Thai terranes rifted off from Gondwana in Early Devonian and Late Early Permian, respectively and drifted away from the Southern Hemisphere as Palaeo-Tethys opened (Metcalfe, 1999; Sone & Metcalfe, 2008). The Shan-Thai and Indochina terranes converged and collided by Late Triassic (Bunopas & Vella, 1983; Hutchison, 1989; Intasopa, 1993; Charusiri *et al.,* 1994) and produced the Nan-Chantaburi suture (Bunopas, 1981; Panjasawatwong, 1991; Crawford & Panjasawatwong, 1996; Hada *et al.,* 1999; Singharajwarapan & Berry, 2000). This suture is usually considered to lie along the Nan River, and to extend southward to the Sra Kaeo-Chanthaburi area, after which it is believed to extend across the Gulf of Thailand to the Bentong-Raub suture in peninsular Malaysia (Bunopas & Vella, 1983; Hada *et al.,* 1991). Although many plate tectonic models of the collision between the Shan-Thai and Indochina terranes have been proposed to account for the tectonic evolution of Thailand, the geometry and timing of collision have been controversial.

Models of plate convergence between the two terranes have involved both east-directed and west-directed subduction of intervening oceanic crust. Westward subduction of the Indochina Terrane beneath the Shan-Thai Terrane was proposed by Asanachinda (1978), Bunopas & Vella (1978), Chantraramee (1978), Barr & Macdonald (1987), Panjasawatwong (1991), Singharajwarapan (1994), Crawford & Panjasawatwong (1996) and Singharajwarapan & Berry (2000), whereas eastward subduction of Palaeo-Tethys beneath the Indochina Terrane was suggested by Beckinsale *et al.* (1979) and Sone & Metcalfe (2008). However, a pair of subduction zones, one dipping west and the other dipping east, was suggested by Gatinsky *et al.* (1978), Thanasuthipitak (1978), Bunopas (1981) and Cooper *et al.* (1989).

The timing of collision has been interpreted to be Late Triassic (Asanachinda, 1978; Chantraramee, 1978; Bunopas & Vella, 1978; Bunopas, 1981; Panjasawatwong, 1991; Singharajwarapan, 1994; Crawford & Panjasawatwong, 1996; Hada *et al.,* 1999; Barr *et al.,* 2000; Singharajwarapan & Berry, 2000), Late Permian-Early Triassic (Thanasuthipitak, 1978; Cooper *et al.,* 1989), and Middle Permian (Helmcke, 1982, 1986; Helmcke & Kraithong, 1982, Helmcke & Lindenberg, 1983; Barr & Macdonald, 1991).

1.3 The Pre-Jurassic Volcanic Rocks in Thailand

Pre-Jurassic volcanic rocks in Thailand and neighbouring areas provide significant clues to help elucidate the tectonic evolution of this region. These pre-Jurassic volcanic rocks in Thailand are divided into four belts (Figure 1.1), from west to east: the Chiang Rai-Chiang Mai volcanic belt, the Chiang Khong-Lampang-Tak volcanic belt, volcanic rocks along the Nan-Chanthaburi suture, and the Loei-Phetchabun-Nakhon Nayok volcanic belts.

1.3.1 Chiang Rai-Chiang Mai Volcanic Belt

The Chiang Rai-Chiang Mai volcanic belt extends in a NNE-SSW direction from the western part of Chiang Rai province through the northern and eastern parts of Chiang Mai province to the Li district in Lumphun province. The Chiang Rai-Chiang Mai volcanic belt is a structurally complex zone that includes mafic lavas, hyaloclastites, pillow breccias, mafic dikes, and common broken formation and turbiditic sedimentary sequences. The age of the mafic rocks in this belt has been controversial. Previous reports suggested that the basalts were erupted in the Carboniferous (Braun & Hahn, 1976; Macdonald & Barr, 1978; Hess & Koch, 1979; Barr *et al.,* 1990) or Permian to Permo-Triassic (Chuaviroj *et al.,* 1980; Bunopas, 1981; Bunopas & Vella, 1983; Panjasawatwong, 1999). Similarly, the tectonic setting of eruption of these rocks is unclear. It has been claimed that volcanic rocks in the Chiang Rai-Chiang Mai areas were erupted in a subduction environment (Macdonald & Barr, 1978; Barr *et al.,* 1990), a continental within plate environment (Barr *et al.,* 1990), or as seamounts within a major ocean basin or mature backarc basin (Panjasawatwong *et al.*, 1995; Panjasawatwong, 1999; Phajuy *et al.,* 2005). The most recent interpretations (Sone & Metcalfe, 2008; Meffre *et al.,* 2008) of the Chiang Rai – Chiang Mai volcanic belt are that it represents a subduction complex and may define a major suture zone (the Inthanon suture of Sone & Metcalfe, 2008).

1.3.2 Chiang Khong-Lampang-Tak Volcanic Belt

The Chiang Khong-Lampang-Tak volcanic belt (CLT), the focus of this study, is located in the Sukhothai Fold Belt (Figure 1.1) to the east of the Chiang Rai-Chiang Mai volcanic belt, and extends in a NNE-SSW direction from the Chiang Khong district, Chiang Rai province, through Lampang and Phrae provinces to Tak province in the south. Rocks of similar age have also been reported in the eastern part of the Lincang-Jinghong volcanic belt in Yunnan, a possible northern extension of the CLT (Yang *et al.,* 1994; Barr *et al.,* 2000). The CLT is made up of rhyolite, dacite, andesite, basalt and their volcaniclastic equivalents (Panjasawatwong *et al.,* 2003). Two episodes of volcanic activity (Permo-Triassic, and Upper Triassic to Lower Jurassic) have been claimed to exist along this belt, with products of the older volcanism said to be volumetrically dominant over those of the younger episode (Jungyusuk & Khositanont, 1992). The tectonic setting invoked for these Permo-Triassic volcanic suites tends to support formation in an arc environment (Bunopas, 1981; Bunopas & Vella, 1983; Hutchison, 1989; Barr *et al.,* 1990) as products of subduction-related magmatism (Bunopas, 1981; Singharajwarapan, 1994; Crawford & Panjasawatwong, 1996; Barr *et al.,* 2000; Phajuy, 2001; Panjasawatwong *et al.,* 2003; Barr *et al.,* 2006).

1.3.3 Volcanic Rocks along the Nan-Chanthaburi Suture

The Nan-Chanthaburi suture (sometimes referred to as the Nan-Uttaradit suture) is located between the CLT and the Loei-Phetchabun-Nakhon Nayok volcanic belt (Figure 1.1), and some authors have suggested that it extends southwards across the Gulf of Thailand to the Bentong-Raub suture in peninsular Malaysia. It is widely believed to have formed during a Late Triassic collision between the Shan-Thai and Indochina terranes (Crawford & Panjasawatwong, 1996; Singharajwarapan & Berry, 2000), although recent studies have suggested that it may represent an older, possibly Permian suture recording closure of the 'Nan backarc basin' (Sone & Metcalfe, 2008). The pre-Jurassic volcanic rocks along this suture occur as variably sized blocks embedded in foliated serpentinite matrix. Petrochemical studies have revealed that they are constituted by Early to Middle Permian ocean-island basalts, probable Carboniferous lavas erupted in an immature backarc basin, Permo-Triassic arc-type basalts and andesites, and undated MORB-type basalts (Yoshikura, 1990; Panjasawatwong, 1991; Crawford & Panjasawatwong, 1996).

1.3.4 Loei-Petchabun-Nakhon Nayok Volcanic Belt

The Loei-Phetchabun-Nakhon Nayok volcanic belt extends in a NNE - SSW direction from Loei province through Phetchabun province to Nakhon Nayok province. It is composed of lavas and volcaniclastic rocks showing a wide range of compositions, from felsic to mafic, and may well include products erupted in more than one tectonic setting, or over a long time interval. In the Loei area, the volcanic rocks can be separated into eastern, central and western sub-belts. The volcanic rocks of the eastern sub-belt are mainly rhyolitic, whereas those of western sub-belts are largely andesitic (Jungyusuk & Khositanont, 1992). The rocks of eastern and western sub-belts have been interpreted to be Permo-Triassic (Bunopas, 1981). The volcanic rocks in the Nakhon Nayok area in the southern part of the western sub-belt have arc affinities (Kosuwan, 2004). The rhyolitic rocks of the eastern sub-belt, however, have given a Mid-Devonian whole-rock Rb-Sr isochron age of 374 ± 33 Ma (Intasopa & Dunn, 1994). The central sub-belt is made up mainly of pillow lavas, hyaloclastites and pillow breccias assigned a mid-ocean ridge origin. These have yielded a wholerock Rb-Sr isochron age of 341 ± 11 Ma (Intasopa & Dunn, 1994). According to Panjasawatwong *et al.* (1997; 2006) the volcanics of the central Loei volcanic sub-belts in the Pak Chom area include both mid-oceanic ridge basalts and oceanic island-arc lavas, with the arc lavas possibly built on an oceanic basement in a major ocean basin or a mature backarc basin.

Given the variety of tectonic settings interpreted for the pre-Jurassic volcanic belts in Thailand, tectonic models derived from these studies incorporate and reflect significant uncertainty, also evident in the relatively poor knowledge of the complex regional geology of the region. Clearly, an up-to-date review of the petrology, geochemistry and implications of the main volcanic belts is required, and new data is demanded, especially for the relatively poorly known CLT. This is the primary aim of the present study.

1.4 Methods of Study

1.4.1 Field Methods

Rock samples from the CLT for geochemical and geochronology studies were collected from over a large part of the outcrop area of this belt. The first field trip (4 months) was done during January 2005 to April 2005. The second one (2 months) was carried out between December 2005 and January 2006. The last field season (2 months) extended from December 2006 through January 2007.

The more than 200 rocks selected for geochemistry and geochronology were mainly collected from exposures along and adjacent to main and minor roads across this area. The six structural transects (three sections in northern area and three sections in southern area) focused on mesoscopic structures observed in the road-cuttings, stream cuttings, and in the banks of the Mae Khong River and in some quarries.

1.4.2 Analytical Methods

Analytical works in this study include whole-rock major and trace elements analyses, REE and Sm-Nd isotopic analyses, metamorphic mineralogy, and LA-ICP-MS U-Pb zircon and chemical U-Th-Pb monazite age dating. All analytical techniques are detailed in the following sections and Appendix C.

1.5 Thesis Outline

The thesis is divided into the following chapters:

- Chapter 1 is an introduction and review of the pre-Jurassic volcanic rocks and their implications for the tectonic evolution of northern Thailand.

- Chapter 2 is a review of the regional setting of the CLT, as well as an overview of the tectonic evolution of northern Thailand and neighboring areas.

- Chapter 3 presents petrography and whole-rock geochemistry of the CLT rocks including the major element, trace element, REE and Sm-Nd isotopic chemistry of these volcanic rocks.

- Chapter 4 gives the geochronological data for key rock units along the CLT.

- Chapter 5 presents structural information from the regional transects across the CLT, and it offers a structural synthesis of this belt.

- Finally, Chapter 6 discusses tectonic models which have been invoked to explain the tectonic evolution of northern Thailand and neighboring area, and uses the new data to provide a new model.

CHAPTER 2

Overview of the Tectonic Evolution of Northern Thailand and Neighbouring Areas, and Geologic Setting of the Chiang Khong-Lampang-Tak Volcanic Belt

2.1 Overview of the Tectonic Evolution of Northern Thailand and Neighbouring Areas

Northern Thailand and neighbouring areas including NW Laos, NE Myanmar and SW China consist of two continental terranes, the Indochina Terrane in the east and the Shan-Thai Terrane in the west (labelled as Sibumasu in Figure 2.1).

The Indochina Terrane is bounded to the north-east by the Song Ma and the Ailaoshan-Song Da suture zones in northern Vietnam and south China along the Ailaoshan-Red River Fault Zone (Leloup *et al.*, 1995; Lacassin *et al*, 1997) and to the west by the Nan-Chanthaburi suture in Thailand and the Bentong-Raub suture in peninsular Malaysia (Metcalfe, 2000). Metcalfe (1988 & 1994) concluded that the Indochina Terrane probably extended northward to the Simao Terrane in southern China. However, the Simao Terrane has been regarded as a separate, possibly South China-derived, tectonic unit by Wu *et al.* (1995), and recently, Sone & Metcalfe (2008) proposed that the Simao Terrane rifted from the western margin of the Indochina Terrane during Permian opening of the 'Nan backarc basin'. Effectively, the Simao Terrane in northern Thailand corresponds to the northern section of the Sukhothai Fold Belt. Metcalfe (1994 & 1999) proposed that three continental slivers, including the North China, South China and Indochina terranes, rifted from northern Gondwanaland during the opening of the Palaeo-Tethys in the Devonian, and that these blocks drifted into the northern hemisphere. The South China and Indochina terranes were considered to have already amalgamated along the Song Ma suture in the Carboniferous and formed the South China/Indochina Superterrane in the Permian (Metcalfe, 1988, 1996 a, 1996b, 1998 and 1999).

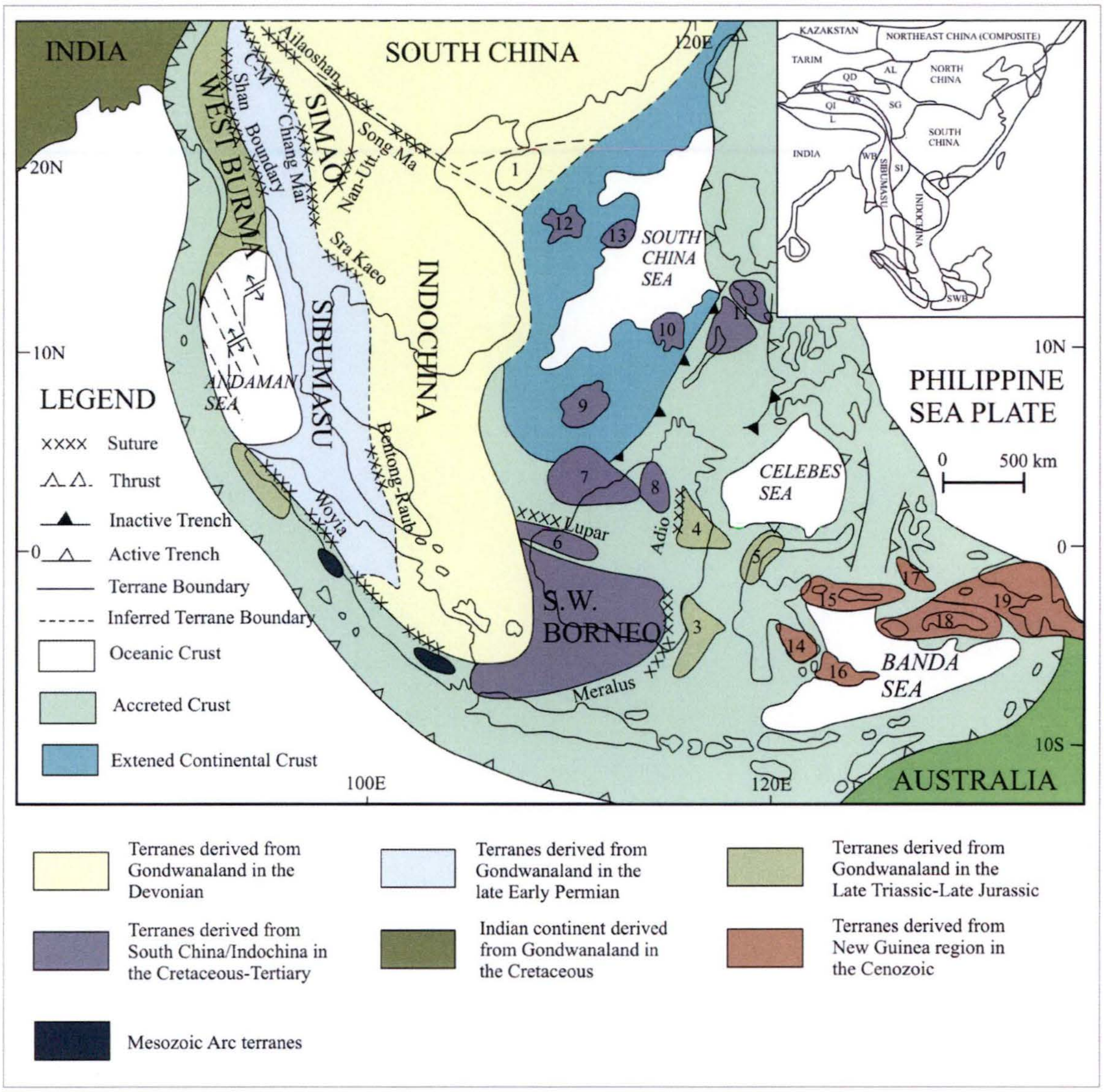

Figure 2.1 Distribution of continental blocks, fragments and terranes of SE and E Asia (after Metcalfe, 2002). Terrane abbreviations in inset map: Wb, West Burma; KL. Kunlun; QD, Qaidam; AL, Ala Shan; QS, Qamdao-Simao; QI, Qiangtang; L, Lhasa; SI, Simao Terrane; SWB, SW Borneo; SG, Songpan Ganzi accretionary complex. Numbered microcontinental blocks: (1) Hainan Island terranes, (2) Sikuleh, (3) Paternoster, (4) Mangkalihat, (5) West Sulawesi, (6) Semitau, (7) Luconia, (8) Kelabit-Longbowan, (9) Spratley Island-Dangerous Ground, (10) Reed Bank, (11) North Palawan, (12) Paracel Island, (13) Macclesfield Bank, (14) East Sulawesi, (15) Bangai-Sula, (16) Buton, (17) Obi-Bacan, (18) Buru-Seram, (19) West Irian Jaya. CM: Changning-Menglian suture.

The Shan-Thai Terrane is bounded to the west by the Shan Boundary Fault (or Sagiang Fault) and the Andaman Sea, and to the southwest by the Woyia suture in Sumatra (Metcalfe, 1996a & b). The eastern boundary is traditionally regarded as being defined by the Changning-Menglian and Lincangjian suture in western Yunnan and Tibet (Metcalfe, 1996 a & b; 1998), the Nan-Chanthaburi suture in Thailand (Hada *et al.*, 1999; Crawford & Panjasawatwong, 1996; Singharajwarapan & Berry, 2000) and the Bentong-Raub suture in peninsular Malaysia (Hutchinson, 1975; Metcalfe, 2000). Metcalfe (2002), Wakita & Metcalfe (2005) and Sone & Metcalfe (2008) have suggested that the eastern boundary of the Shan-Thai Terrane lay further west, and is now marked by the Chiang Rai-Chiang Mai volcanic belt (sometimes referred to as the Chiang Mai suture or Inthanon suture). Based on foraminiferal biogeographic studies in Mae Hong Son, northwestern Thailand, Ueno & Igo (1997) proposed that the eastern limit of the Shan-Thai Terrane could be even further west, along the Mae Yuam Fault zone (Hisada *et al.*, 2004). On palaeogeographic grounds, Burrett & Stait (1985, 1986) and Stait & Burrett (1984) suggested that the Shan-Thai Terrane was closely conjoined to the northern margin of Gondwanaland from the lower Palaeozoic. The rifting of the Shan-Thai Terrane off Gondwanaland occurred in Late Early Permian and it drifted northward to amalgamate with the South China/Indochina Superterrane in the Triassic (Metcalfe, 1999).

The suturing between the South China/Indochina Superterrane and the Shan-Thai Terrane has been widely claimed to have occurred along the Nan-Chanthaburi suture (Asanachinda, 1978; Chantraramee, 1978; Gatinsky *et al.*, 1978; Thanasuthipitak, 1978; Bunopas & Vella, 1978; Bunopas, 1981; Barr & Macdonald, 1991; Panjasawatwong, 1991; Singharajwarapan, 1994; Hada *et al.*, 1999; Metcalfe, 1999; Barr *et al.*, 2000; Singharajwarapan & Berry, 2000). The age and the geometric model of convergence of the Palaeo-Tethys beneath both of these continental terranes are still debated.

Four major pre-Jurassic volcanic belts have been identified in Thailand (see Chapter 1.3). These include the Chiang Rai-Chiang Mai volcanic belt (Inthanon suture in Sone & Metcalfe, 2008) in the west, the Chiang Khong-Lampang-Tak volcanic belt (CLT), the Nan-Chanthaburi suture, and in the east, the Loei-Petchabun-Nakhon Nayok volcanic belt (Jungyusuk & Khositanont, 1992; Panjasawatwong *et al.*, 1997).

The Chiang Rai-Chiang Mai volcanic belt of MacDonald & Barr (1978), Barr *et al.* (1990), Panjasawatwong (1995 & 1999) and Phajuy *et al.* (2005) corresponds with the Chiang Mai suture of Metcalfe (2002) and Wakita & Metcalfe (2005) and the Inthanon suture of Sone & Metcalfe, (2008). It includes packages of basalts interpreted to have formed as intra-oceanic seamounts, ribbon cherts dated by radiolarians as ranging in age from Devonian to Triassic (Caridoit, 1993; Shashida *et al.*, 1993: Shashida & Igo, 1999; Metcalfe, 2002), and interbedded pelagic limestones and bedded chert, pelagic mudstone, rhythmic mudstones, and shallow-marine limestones with fusulinids interpreted as carbonate cap to seamounts (Ueno & Igo, 1997). Meffre *et al.,* (2008) has suggested that these rocks represent a subduction complex at the margin of the Palaeo-Tethys ocean. The most recent study of the least-altered Permian mafic volcanic rocks in this belt, from the Pang Ma Yao area, suggested that these rocks are tholeiitic with compositions similar to T- or rift-type MORB (Phajuy *et al.* (2005) that they may have formed in a major ocean basin rather than in a mature back-arc basin. The rock association of the Chiang Rai-Chiang Mai volcanic belt has been interpreted as a northern continuation of the Bentong-Raub suture of peninsular Malaysia (Metcalfe, 2000). A similar rock suite with the same age range occurs to the north, along the Changning-Menglian suture in Yunnan (SW China) (Wu *et al.*, 1995; Feng, 2002).

The Chiang Khong-Lampang-Tak volcanic belt (CLT), in the central part of the Sukhothai Fold Belt (Singharajwarapan & Berry, 2000), is composed of mafic to felsic volcanic rocks, their volcaniclastic equivalents, and associated intrusive rocks. In the northern part of the CLT, these Triassic volcanic rocks range compositionally from dacite to basalt, and Panjasawatwong *et al.* (2003) and Barr *et al.* (2006) suggested that they formed in a continental margin volcanic arc. Similarly, a petrochemical study of the Triassic dacitic to rhyolitic rocks in the Lampang area (southern part of the CLT) supported an origin at a convergent plate margin, probably in a continental margin arc (Barr *et al.*, 2000). These CLT continental margin arc rocks have been correlated with rocks of similar age and compositional range in the Lincang-Jinhong volcanic belt in southern Yunnan (Barr *et al.*, 2000; Yang *et al.*, 1994). Based on stratigraphic and palaeontological studies, Feng *et al.* (2005) proposed that the mainly Triassic Simao Terrane in Yunnan can be correlated with the Triassic Lampang-Phrae Basin, and northern section of the Sukhothai Fold Belt in northern Thailand. Their results supported the idea that the Sukhothai Fold Belt belongs to the Cathaysian domain and thus was part of the South China/Indochina Superterrane, and not to the Gondwanaland domain. As noted in Chapter 1, the Simao Terrane probably rifted from the South China/Indochina Superterrane in the Early Carboniferous by back-arc extension and subsequent ocean floor spreading (Wang *et al.*, 2000). Metcalfe (2002) reported that the Simao Terrane extended southward into northern Thailand and thus equates with part of the Sukhothai Fold Belt (Figure 2.2). The Simao Terrane and Sukhothai Fold Belt are bounded to the west by the Chiang Rai-Chiang Mai volcanic belt (or Inthanon suture) and to the east and southeast by the Jinshajiang, Ailaoshan and the Nan-Chanthaburi suture, respectively, but its extension to the south is still poorly constrained.

A number of previous workers has concluded that the Nan-Chanthaburi suture delineates the suturing between the Indochina and Shan-Thai terranes and represented the Palaeo-Tethys ocean (Bunopas, 1981; Panjasawatwong, 1991; Crawford & Panjasawatwong, 1996; Stokes *et al.,* 1996; Hada *et al.,* 1999; Singharajwarapan & Berry, 2000). Several previous workers, however, reported that the northern part of the Nan-Chanthaburi suture may represent a back-arc basin which opened in the Carboniferous, rather than a the major ocean basin (Wang *et al.*, 2000; Metcalfe, 2002; Wakita & Metcalfe, 2005; Sone & Metcalfe, 2008). However, based on key relationships of chert/siliciclastic sequences and serpentinite mélange further south, in the Sra Kaeo-Chanthaburi segment of the Nan-Chanthaburi suture, Hada *et al.*, (1999) suggested that this segment does indeed represent the suture between the Shan-Thai and Indochina terranes, with collision occurring in the Late Triassic. Based on studies of deformation and metamorphism in the Sukhothai Fold Belt, Singharajawarapan (1994) and Singharajwarapan & Berry (2000) suggested that the geometry of plate convergence along the Nan-Chanthaburi suture involved a west-dipping subduction zone.

The Loei-Petchabun-Nakhon Nayok volcanic belt is located in the western Khorat Plateau and consists of mafic to felsic volcanic rocks and associated volcaniclastic rocks and dykes. In the Loei area, the volcanic rocks have been divided into Eastern, Central and Western sub-belts. The Eastern and Western sub-belts were interpreted to be a product of Permo-Triassic arc volcanism (Bunopas, 1981). In contrast, the Central sub-belt includes MORB-like tholeiitic basalt and microgabbro dykes, and calc-alkaline oceanic island-arc basalt/andesite lavas (Panjasawatwong *et al.,* 2006) and one sample has yielded a Devonian-Carboniferous whole-rock Rb-Sr isochon age of 374 ± 33 Ma (Inthasopa &

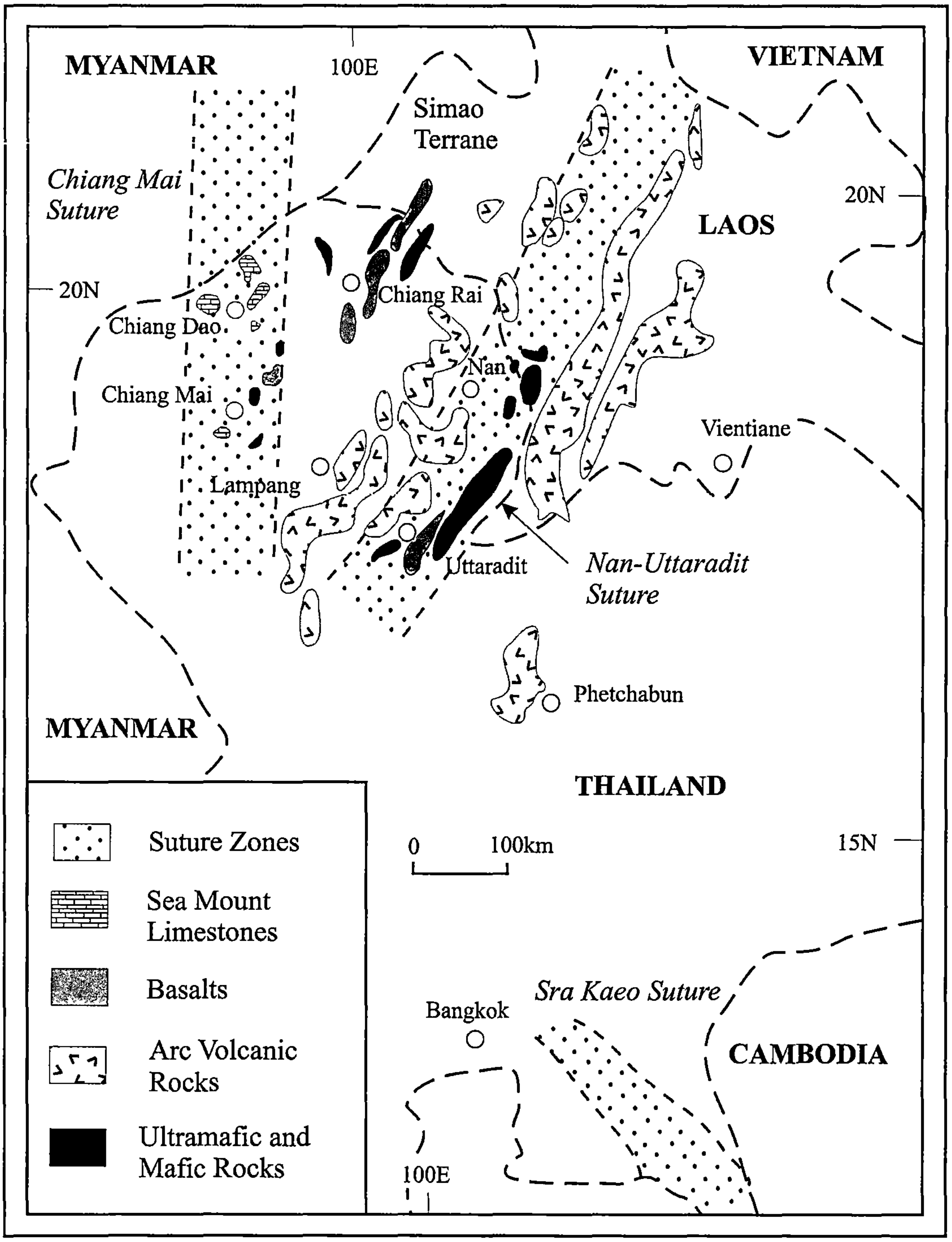

Figure 2.2 Sketch map showing the Chiang Mai (Inthanon), Nan-Uttaradit-Chanthaburi-Sra Kaeo sutures of Thailand in the southern part of the Simao Terrane, and the distribution of volcanic arc rocks, basalts, ultramafic and mafic rocks and seamount carbonates in northern Thailand (after Metcalfe, 2002).

Dunn, 1994). According to Kosuwan (2004), the volcanic rocks in the Nakhon Nayok area, a southern part of Western sub-belt, also have arc affinities.

In summary, there are two interpretations of the present location of the main Palaeo-Tethys suture in SE Asia. Wakita & Metcalfe (2005), Metacalfe (2006) and Sone & Metcalfe (2008) have proposed that it is represented by the Lancangjian, Changning-Menglian and Chiang Mai (Inthanon) sutures, offset to the east further south by the Mae Ping Fault Zone, to continue as the Sra Kaeo - Bentong-Raub sutures (Hada *et al.,* 1999; Metcalfe, 1988, 1996, 2000). In these models, the Jinshajiang, Ailaoshan and Nan-Chanthaburi sutures have been re-interpreted as probably representing the site of closure of a back-arc basin. In contrast, numerous authors have proposed that the latter suture extends south to connect with the Sra Kaeo – Bentong-Raub suture, and that this represents the Palaeo-Tethys suture. Clearly further detailed studies on all sutures are required to resolve these conflicting interpretations.

2.2 Geologic Setting of the Chiang Khong-Lampang-Tak Volcanic Belt

The CLT is located in the central part of the Sukhothai Fold Belt, northern Thailand, between latitudes 16°N and 21°N, and longitude 99°E and 101°E, covering an area of about 4,000 km^2. The CLT forms a NNE-SSW-trending S-shape, starting from the Chiang Khong district in the northern tip, through the central part of Phayao province, along the provincial border between Lampang and Phrae provinces, and finally to the eastern part of Tak province in the south. It may continue further south to the Nakhon Sawan province where it is offset by the Mae Ping Fault Zone (Figure 1.1 in Chapter 1).

Two key sections of the CLT form the nucleus of this study, based largely on availability of good outcrop exposure along roads and rivers. These are the Chiang Khong area in the north, and the Lampang area in the south.

2.2.1 The Chiang Khong Area

The Chiang Khong, or northern, area is located in the eastern part of Chiang Rai province. An important area of higher metamorphic grade that was also examined in detail in this study occurs in the Phu Chi Fa and Ban Huak areas, in the southeastern part of the Chiang Khong area, in the northwestern portion of Chiang Kham district, Phayao province. The

Chiang Khong area is shown on 1:50,000 topographic maps series L 7017 including sheets 5049 I (Amphoe Chiang Khong), 5049 II (Ban Si Don Chai), 5049 III (Ban Pong Noi), and series L7018, including sheets 5048 I (Amphoe Khuntan), 5048 II (Amphoe Chiang Kham), 5048 III (Amphoe Thoeng), 5048 IV (Amphoe Phaya Meng Rai), 5049 IV (Amphoe Chiang Saen) and 5149 III (Amphoe Wiang Kaen).

The Chiang Khong area is accessed via highway 1020 from Muang Chiang Rai to Thoeng and then turn N to the Chiang Khong district at the Thai/Laos border. Alternatively, access is via the Highway number 1 (from Muang Chiang Rai to Mae Chan district) and turn NE via the Chiang Saen district and on to the Chiang Khong by highway 1016 and 1129, respectively. The southeastern part of metamorphic zone (the Phu Chi Fa and Ban Huak areas) covers portion of Khun Tan and Thoeng districts in Chiang Rai province and Chiang Kham district in Phayao province, and can be reached by highway 1155 (from Chiang Khong via Wiang Kaen) and 1093 (from Ban Ratsadon Phakdi to the Phu Chi Fa area). The physiography of the Chiang Khong area is characterized by mountain ranges running parallel to NNE-SSW trending intermountain basins that control major drainages in this area, and are probably controlled by major faults.

The structural cross sections in this study were controlled by good exposures along roads, rivers and in quarries. The northern transect was along the Mae Khong River and roadside outcrops from Chiang Khong to Wiang Kaen. The two other northern transects extend west to east across the central part of these volcanic belts along local road cut number 1098 (from Doi Luang sub-district to Ban Kaen) and local road cut number 3123 and 1093 (from Ban Pa Tan via Ban Phaya Phiphak, Ban Ratsadon Phakdi to the Phu Chi Fa area).

Geological Setting of the Chiang Khong Area

The geologic map of the Chiang Khong area (Figure 2.3) is based on data collected in this project over three field seasons and data compiled from previous works. The first geologic map was made by the German Geological Mission to Thailand at a scale of 1:250,000 (Braun & Hahn, 1976). Detailed geologic maps at 1:50,000, published by the Geological Survey Division, the Department of Mineral Resources, Thailand (Sukvattananunt *et al.,* 1985a, 1985b; Sukvattananunt & Assawapatchara, 1989a, 1989b, 1989c, 1989d; Tansuwan & Chitmanee, 1990a, 1990b), guided much of the sampling for this study.

Metamorphic Rocks

Permo-Carboniferous metamorphic rocks were named the Chiang Kham Group by Tansuwan & Chitmanee (1990a & b). They are mainly distributed in the east and southeastern part of the Chiang Khong area along the Thai/Laos border. The Chiang Kham Group is composed of three formations, the Doi Mun, Nam Bong and Huai Krai formations. The Doi Mun Formation is the structurally lowermost portion of this group and consists of schist, phyllite, meta-volcanic and foliated granitic rocks. The middle unit, Nam Bong Formation consists of slate, quartzite, phyllite and crystalline limestone, and the highest structural unit is the Permo-Carboniferous Huai Krai Formation which is composed of meta-sandstone interbedded with meta-shale. These metamorphic units are cut by faults and unconformably overlain by Tertiary semi-consolidated sediments.

Sedimentary Rocks

Sedimentary rocks in the Chiang Khong area can be separated into five units based on stratigraphic correlation and index fossils. These include Permian limestone, Permo-Triassic sedimentary rocks, Middle to Late Triassic sedimentary rocks, Tertiary semi-consolidated sediments and Quaternary unconsolidated sediments. (Braun & Hahn, 1976; Sukvattananunt *et al.,* 1985a, 1985b; Sukvattananunt & Assawapatchara, 1989a, 1989b, 1989c, 1989d; Tansuwan & Chitmanee, 1990a, 1990b).

Permian limestone, located in southwestern corner of this area as small scattered outcrops, is thick-bedded light to dark gray limestone containing fusulinids, brachiopods and crinoid fossils (Sukvattananunt *et al.,* 1985a, 1985b). Permo-Triassic sedimentary rocks are mainly located in the western part of the CLT belt and comprise dark-greenish-gray sandstone interbedded with siltstone and shale, light gray conglomerate, mudstone and occasional volcaniclastic sandstones (Sukvattananunt & Assavapatchara, 1989c, 1989d).

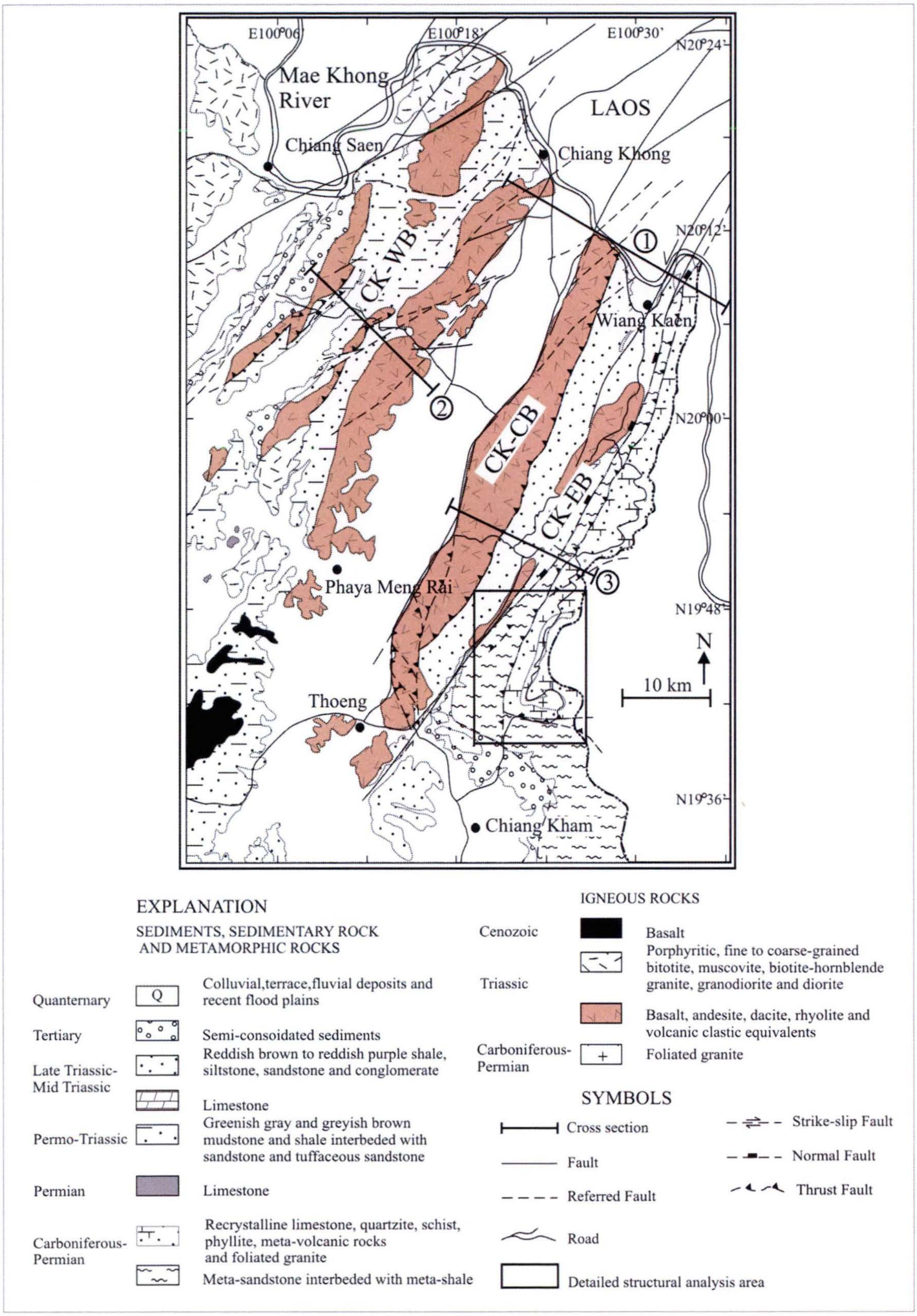

Figure 2.3 Geologic map of the Chiang Khong area compiled from my field work and previous maps (after Bruan & Hahn, 1976; Sukvattananunt *et al.,* 1985a, 1985b; Sukvattananunt & Assawapatchara, 1989a, 1989b, 1989c, 1989d; Tansuwan & Chitmanee, 1990a, 1990b).

Middle to Late Triassic sedimentary rocks occur along the intermontane basin between the central part of the Chiang Khong belt and the metamorphic rocks in the eastern portion of the Chiang Khong area. Three formations have been distinguished, the Huai Fak, Pa Lae and Doi Pong Nok formations (Tansuwan & Chitmanee, 1990a & b). The Huai Fak Formation is composed of greenish-gray and grayish brown mudstone interbedded with sandstone and volcaniclastic sandstone. Fossils of *Posidonia* sp., *Halobia* sp. and *Pteria* sp. have been found in this formation, which is cŏnformably overlain by the Pa Lae Formation, consisting of thick- to thinly bedded gray-black limestone that is slightly recrystallised locally and contains abundant of oncolites, algae, molluscs and crinoid stem fragments. The uppermost portion of this rock association is the Doi Pong Nok Formation, which contains reddish brown to reddish purple shale, sandstone, siltstone and conglomerate. The Huai Fak and Pa Lae Formations are located in small area at Ban Pae Lae and have been grouped as a Triassic limestone unit in this study.

Tertiary semi-consolidated sediments occur in the foothills south of metamorphic rocks and both sides of Huai Nam Bong in northwestern part of the Chiang Khong area. These semi-consolidated sediments comprise grey to greenish grey, conglomerate, sandstone, siltstone and shale with small coal fragments in the sandstone. This unit is unconformably overlain by Quaternary unconsolidated sediments and unconformably underlain by the pre-Tertiary rock units.

Igneous Rocks

Igneous rocks of the Chiang Khong area include both plutonic and volcanic rocks with crystallisation ages ranging from Carboniferous to Late Cenozoic.

Plutonic rocks in this area are divided into three units; Carboniferous-Permian foliated granite, Permo-Triassic mafic-ultramafic rocks, and Triassic granites (Sukvattananunt *et al.,* 1985a, 1985b; Sukvattananunt & Assawapatchara, 1989a, 1989b, 1989c, 1989d). The Carboniferous-Permian foliated granite intrudes metasedimentary rocks in the southeastern corner of the Chiang Khong region and has been grouped into the Doi Mun Formation by Tansuwan & Chimanee (1990a & b). The Permo-Triassic mafic-ultramafic rocks are sparingly exposed in a few localities in the northwestern part of this area and are mainly altered to serpentinite. The outcrops are too small to appear on the geologic map.

The Triassic granites are mainly distributed in the northwestern and western part of this area. The granitic rocks comprise medium- to coarse-grained porphyritic granite-granodiorite and fine-grained diorite that intrude Permo-Triassic sedimentary rocks and are overlain by Tertiary semi-consolidated sediment and Quaternary sediments.

Volcanic rocks in the Chiang Khong area have two discrete ages, Triassic CLT rocks and widespread Late Cenozoic basalts.

In the northern field area, the CLT rocks are geographically separated into three sub-belts from west to east as follows; Chiang Khong Western Belt (CK-WB), Chiang Khong Central Belt (CK-CB) and Chiang Khong Eastern Belt (CK-EB) (Figure 2.3). CK-WB is mainly exposed in the Doi Luang Phrae Muang mountain range, in northwestern part of this area and extends south to the Doi Luang sub-district and Praya Meng Rai district. Exposures of CK-CB trend NNE-SSW along the Doi Yao mountain range in the central part of this area, whereas CK-EB is exposed in the intermontane basin between CK-CB and the metamorphic zone further east around Ban Hauk. The volcanic rocks include basalt, basaltic andesite, andesite, dacite and rhyolite, their volcaniclastic equivalents and associated shallow intrusive rocks. According to Barr *et al.* (2006), these calc-alkalic volcanic suites of the Chiang Khong area formed via subduction-related magmatism. This conclusion was supported by the study of least-altered mafic volcanic rocks in this area by Panjasawatwong *et al.* (2003). The latter authors argued the suite formed in a continental margin volcanic arc.

The CLT rocks in the northern area have been interpreted to result from two episodes of eruption, in the Permo-Triassic and the Late Triassic – Early Jurassic, on the basis of stratrigraphic correlation (Jungyusuk & Khositanont, 1992). Volcanics assigned to the Permo-Triassic suite include intermediate and felsic pyroclastic rocks and rhyolite lavas, whereas the Late Triassic-Early Jurassic rocks are largely andesite, dacite, rhyodacite and rhyolite with associated volcaniclastics (Jungyusuk & Khositanont, 1992; Sukvattananunt, *et al,* 1985a, 1985b; Sukvattananunt & Assawapatchara, 1989a, 1989b, 1989c, 1989d; Tansuwan & Chitmanee, 1990a, 1990b). However, according to Panjasawatwong *et al.* (2003), some of the Late Triassic - Early Jurassic volcanic rocks may actually be Permo-Triassic, based on their geochemistry and a Middle Triassic U-Pb zircon age of 232.9 ± 0.4 Ma for one felsic rock (Barr *et al.,* 2006). The CLT rocks in the northern area rest unconformably on, or are in fault contact with either Permo-Triassic sedimentary rocks or Middle to Late Triassic sedimentary rocks, and are unconformably overlain or in fault contact with Tertiary sediments.

Late Cenozoic basalts are exposed in two areas, and include the Chiang Khong basalt (Barr & Macdonald, 1981; Panjasawatwong & Youngsanong, 1996; Saminpanya, 2000) and the Thoeng basalt (Sriprasert, 1997). The Chiang Khong basalt, a basanite to trachybasalt, occurs in a small area along the Mae Khong River near the Chiang Khong Customs Office. It is regarded as the southerly extent of the Huai Xai basalt in Laos (Barr & Macdonald, 1981; Panjasawatwong & Youngsanong, 1996; Saminpanya, 2000; Phajuy, 2001). The Thoeng basalt, in the southwestern corner of this area, has transitional continental tholeiite affinities (Sriprasert, 1997). Whole-rock K-Ar dating of the Chiang Khong and Thoeng basalts yielded ages of 1.74 ± 0.18 Ma and 1.69 ± 1.25 Ma, respectively (Barr & Macdonald, 1981).

2.2.2 The Lampang Area

The CLT rocks in the Lampang area are distributed across the Muang Lampang, Mae Moh, Mae Thaa, Ko Kha, Sop Prab, Thoen, and Mae Phrik districts in Lampang province, Long, Denchai, and Wang Chin districts in Phrae province, and the Sam Ngao and Ban Tak districts in Tak province. The rocks are exposed across the area shown on the 1:50,000 topographic map series L7018, sheets 4844 I (Amphoe Sop Prab), 4844 II (Ban Saphan Hin), 4844 III (Amphoe Thoen), 4844 IV (Ban Puang), 4845 II (Amphoe Ko Kha), 4944 I (Ban Bo Kaeo), 4944 IV (Amphoe Wang Chin), 4945 II (Amphoe Long), 4945 III (Amphoe Mae Thaa) and 4945 IV (Changwat Lampang). The volcanic rocks in the Lampang area have been separated into four sub-belts including the Lampang Western Belt (LP-WB), Lampang Central Belt (LP-CB), Lampang Eastern Belt (LP-EB) and Thoen Central Belt (TN-CB), as shown in Figure 2.4. Occasional outcrops of CLT rocks also occur in the Long area, in the major valley between the LP-CB and LP-EB. The detailed geologic map and structural transects in this area (Figure 2.5) were based on geological mapping along highway 11 interval km 5 to km 42 (from Muang Lampang via Mae Thaa districts, Lampang province to Long district, Phrae province).

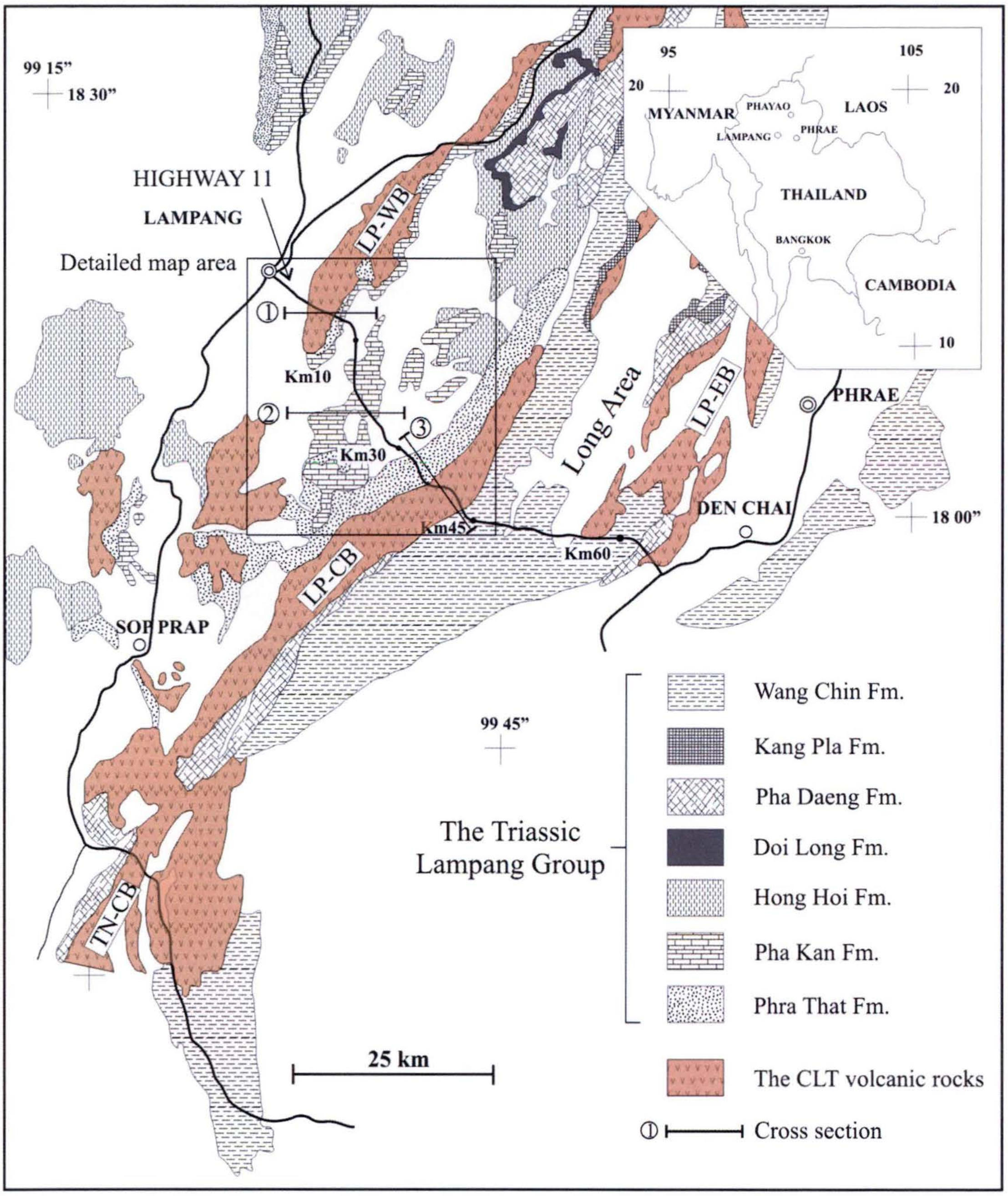

Figure 2.4 Geologic map of the Lampang area showing distribution of sub-belts of the CLT volcanic belt and Triassic sedimentary sequences of the Lampang Group (after Chaodumrong, 1992).

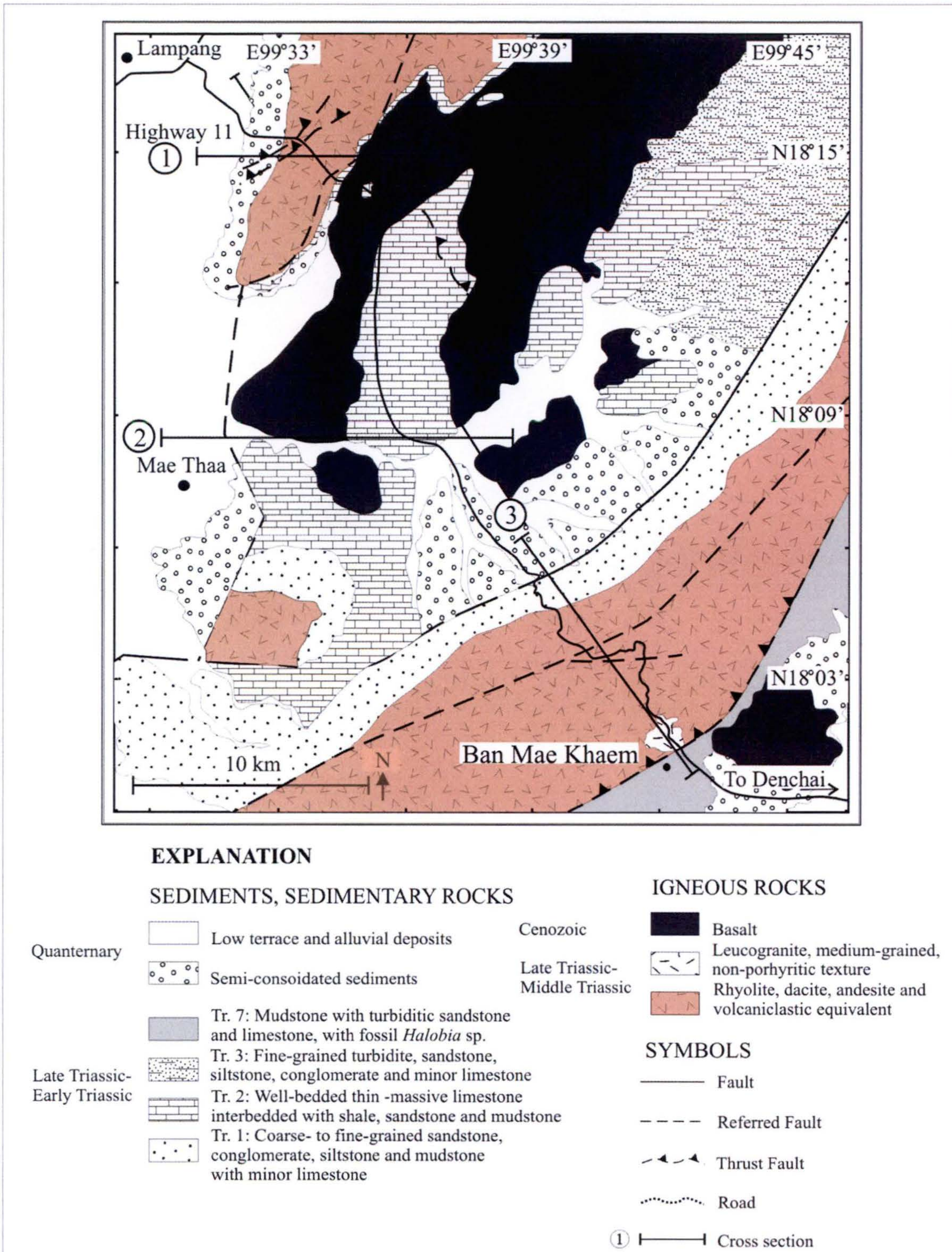

Figure 2.5 Detailed geologic map of the Lampang area compiled from my field work and published maps (Chaodumrong, 1992; Charoenprawat *et al.,* 1994).

Physiographically, the CLT in the Lampang area forms NNE-SSW-trending mountain ranges and is bounded by Tertiary intermontane basins including the Lampang, Mae Moh, Long and Phrae basins. The CLT rocks in the Lampang area are unconformably overlain by the Triassic Lampang Group (Chaodumrong, 1992) and unconformably underlain by the Late Permian Huai Thak Formation (Piyasin, 1972).

Geologic Setting of the Lampang Area

The Lampang area is mainly underlain by Triassic sedimentary sequence of the Lampang Group, and diverse igneous rocks (Charoenprawat *et al.,* 1994) including the Triassic Mae Khaem granite, the CLT rocks, and the Late Cenozoic Mae Thaa and Long basalts.

Sedimentary Rocks

The Triassic Lampang Group is a sequence of red beds, carbonates and turbidites (Chaodumrong, 1992) occurring in two adjacent sub-basins, Lampang sub-basin to the west and Phrae sub-basin to the east. The Lampang Group consists of seven formations, in ascending order, the Phra That (Tr. 1), Pha Kan (Tr. 2), Hong Hoi (Tr. 3), Doi Long (Tr. 4), Pha Daeng (Tr. 5), Kang Pla (Tr. 6) and Wang Chin (Tr. 7) Formations (Chaodumrong, 1992). In my map area, the Phra That, Pha Kan, Hoi Hoi (in the Lampang sub-basin) and the Wang Chin (in the Phrae sub-basin) formations are exposed along the Highway 11 transects (Figure 2.5).

The Phra That Formation (Tr. 1), the lowermost part of Triassic Lampang Group, is characterized by feldspathic sandstone, conglomerate with volcanic clasts, siltstone and mudstone in its lower part. Whereas its upper part consists of grey mudstone and intercalated, thin- to thick-bedded grey sandstone and limestone (Chaodumrong, 1992). This formation unconformably overlies the volcanic rocks of the CLT and Permian sedimentary strata, and it is interpreted that volcanic clasts in the conglomerates are locally derived from CLT volcanic sequences.

The overlying formations of the Lampang Group include carbonates with minor intercalated shale and sandstone in the lower formations and fine-grained turbidites, siltstone, minor limestone and conglomerate in the upper formations of the Lampang Group (Chaodumrong, 1992).

Igneous Rocks

Igneous rocks in the Lampang area include Late Cenozoic basalts, Mae Khaem granitic rock and the CLT rocks.

Late Cenozoic basalts have been found in two areas in the Lampang region, the Mae Thaa and Long districts. The aphyric Mae Thaa basalt consists of several flows and locally volcaniclastic debris associated with volcanic vents (Barr & Macdonald, 1981; Sasada *et al.,* 1987). A K-Ar age of this basalt is 0.6 ± 0.2 Ma (Sasada *et al.,* 1987). The Long basalts are mildly alkalic trachybasalts, basanites and basaltic trachyandesites with continental intraplate affinities (Limptrakun *et al.,* 2005).

The Mae Khaem granitic stock intrudes CLT volcanic rocks and Lampang Group rocks and consists of medium-grained muscovite-bearing leucogranites (Singharajwarapan, 1994). The granite has a U-Pb zircon age of 224 ± 4 Ma (S. Khositanont, *pers. comm.,* 2006).

The CLT rocks in the Lampang area are mainly rhyolitic lavas and volcaniclastic rocks with subordinate andesitic to dacitic volcanic and volcaniclastic rocks that outcrop in three main sub-belts, Lampang Western Belt (LP-WB), Lampang Central Belt (LP-CB), Lampang Eastern Belt (LP-EB); rare outcrops also define a fourth sub-belt, the Thoen Central Belt (TN-CB) (Figure 2.4). LP-WB crops out along the Highway 11 (Lampang-Denchai) at km 5.75 to 9.30 (Doi Ton area) (Barr *et al.,* 2000). The exposures along the road consist of massive dacite, rhyolite, tuff, lapilli tuff and volcanic breccia with intervening thin mudstone and tuffaceous sandstone (Singharajwarapan, 1994). The LP-CB has been named as the Doi Luang volcanic rocks (Singharajwarapan, 1994 and Barr *et al.,* 2000). The Doi Luang volcanic rocks form the mountains between Lampang and Phrae sub-basin. They are exposed along the Highway 11 at interval km 32.10 to km 41.30. The LP-CB is characterized by massive dacitic tuff, cataclastic tuff, carbonaceous shale and tuffaceous sandstone (Singharajwarapan, 1994). LP-EB crops out between 60.45 and km 63.70 (Doi Mak Fire area) and between km 69.00 and km 73.00 (the Ban Kaeng Luang area) along Highway 11. Volcanic rocks at Doi Mak Fire are mainly massive tuff and volcaniclastic breccia whereas at the Ban Kaeng Luang area they consist of massive tuff and minor volcanic breccia. Volcanic clasts are mainly dacite and rhyolite (Singharajwarapan, 1994). Finally, the TN-CB is located in the southern portion of LP-

CB, east of Thoen district and similar rocks have also been reported in Tak volcanic province (Jungyusuk & Khositanont, 1992). It comprises poorly outcropping andesite, rhyolite, ignimbrite, volcaniclastic rocks and associated shallow intrusive rocks. Scattered outcrops of CLT rocks also occur in the Long intermontane basin between the LP-CB and LP-EB. At the time of my study, these rocks were being examined as part of a (now completed) MSc at Chiang Mai University (Osataporn, 2007).

Two representative rhyolites of LP-CB (Doi Luang) and LP-WB (Ban Kaeng Luang) yielded U-Pb zircon ages of 240 ± 1 Ma (early Mid-Triassic) and 229 ± 4 Ma (late Mid-Triassic), respectively (Barr *et al.,* 2000 and S. Khositanont *pers. comm.,* 2006).

In summary, the CLT in the northern (Chiang Khong) and southern (Lampang) study areas occurs as a number of broadly meridional sub-belts that form mountain ranges. Although some studies have suggested on regional correlation grounds that the CLT volcanic rocks range in age from Permian to Triassic, only Triassic ages have been measured to date. Furthermore, there has been no demonstration that the rocks in the Chiang Khong sub-belts are age- and compositional correlates of those occurring further south in the Lampang sub-belts, nor has it been demonstrated whether the rocks forming each sub-belt in both regions are similar in terms of age and compositional affinities. Addressing these problems is a key aim of this study.

CHAPTER 3

Petrochemistry of the Chiang Khong-Lampang-Tak Volcanic Belt

3.1 Introduction

The Chiang Khong-Lampang-Tak volcanic belt (CLT) is composed of several subparallel volcanic sub-belts that include lavas, volcaniclastic rocks and associated intrusive/dyke rocks. Geochronological studies (Chapter 4) have demonstrated that most igneous rocks in the CLT formed around 230-220 Ma in the latest Middle – to early Late Triassic. This chapter describes the geochemical study of best preserved igneous rocks from across the geographic range of the CLT, aimed at determining their compositional affinities and elucidating their tectonic setting of eruption.

Sampling of rocks from the CLT was focussed on several broadly east-west traverses, one set concentrated in the Chiang Khong and Mae Khong River region in the north, close to the border with Laos (herein the Chiang Khong area), the other in the Lampang area some 200 km further south. The more than 300 rocks selected for this study were mainly collected from exposures along and adjacent to main and minor roads and occasional river and creek traverses. Of these, ~220 of the freshest samples were petrographically examined. The 98 freshest rock samples representative of the compositional and geographic range covered were selected for whole-rock analysis by XRF. Twenty four representative samples were also analysed for low-abundance trace elements and REE by solution ICP-MS. Nine of the latter were selected for Sm-Nd isotopic analysis.

3.2 Sampling and Analytical Methods

3.2.1 Chiang Khong Area Rocks

The CLT in the Chiang Khong area comprises three major sub-parallel belts (Figure 3.1), from west to east, the Chiang Khong Western Belt (CK-WB), Chiang Khong Central Belt (CK-CB) and Chiang Khong Eastern Belt (CK-EB). Barr *et al.* (2006) referred to the CK-WB as the Doi Khun Ta Khuan belt, and the CK-CB they referred to as the Doi Yao belt. Volcanic rocks in the CK-WB and CK-CB include mainly intermediate and felsic rocks and their volcaniclastic equivalents, and shallow sub-volcanic dykes, whereas mafic lavas dominate the CK-EB and felsic rocks are absent. The CLT volcanic rocks in this area conformably overlie, or are in fault contact with, Permo-Triassic sedimentary rocks and Middle to Late Triassic sedimentary rocks.

Some 71 new whole-rock major and trace element analyses of lavas and dykes from the Chiang Khong region have been done for this study, 40 from the CK-WB, 20 from the CK-CB and 11 from the CK-EB. Sample locations are given on Figure 3.1. Of these, 16 representative samples were analysed for the low-abundance trace element and REE by LA-ICP-MS, and 5 of these were chosen for Sm-Nd isotopic analysis. Previous petrochemical studies of Chiang Khong region volcanic rocks by Panjasawatwong *et al.* (2003) and Barr *et al.* (2006) reported in total 38 analyses.

3.2.2 Lampang Area Rocks

The CLT in the Lampang area for this geochemical study has been subdivided into three geographical sub-belts (see Chapter 2 and Figure 3.2), the Lampang Western Belt (LP-WB), Lampang Central Belt (LP-CB) and Lampang Eastern Belt (LP-EB). Rocks in the latter sub-belt were poorly exposed; those sampled were strongly silica metasomatised, and thus excluded from this study. However, CLT rocks exposed east of the LP-CB in the Long area, a linear intermontane trough along the Yom River, were being studied as the focus of an MSc project by P. Osataporn at Chiang Mai University during my fieldwork in the region, and were deliberately excluded from my sampling program. Note however, that the data for these rocks are now available (Osataporn, 2007) and are included and discussed in the following presentation of data.

Igneous rocks for petrochemical study were mainly collected along the structural traverse along Highway number 11 (from Lampang to Denchai; locations in Figure 3.2). Comparative geochemical data included LP-WB and LP-CB rocks from Barr *et al.* (2000) and mafic to intermediate rocks from the Long area from Osataporn (2007).

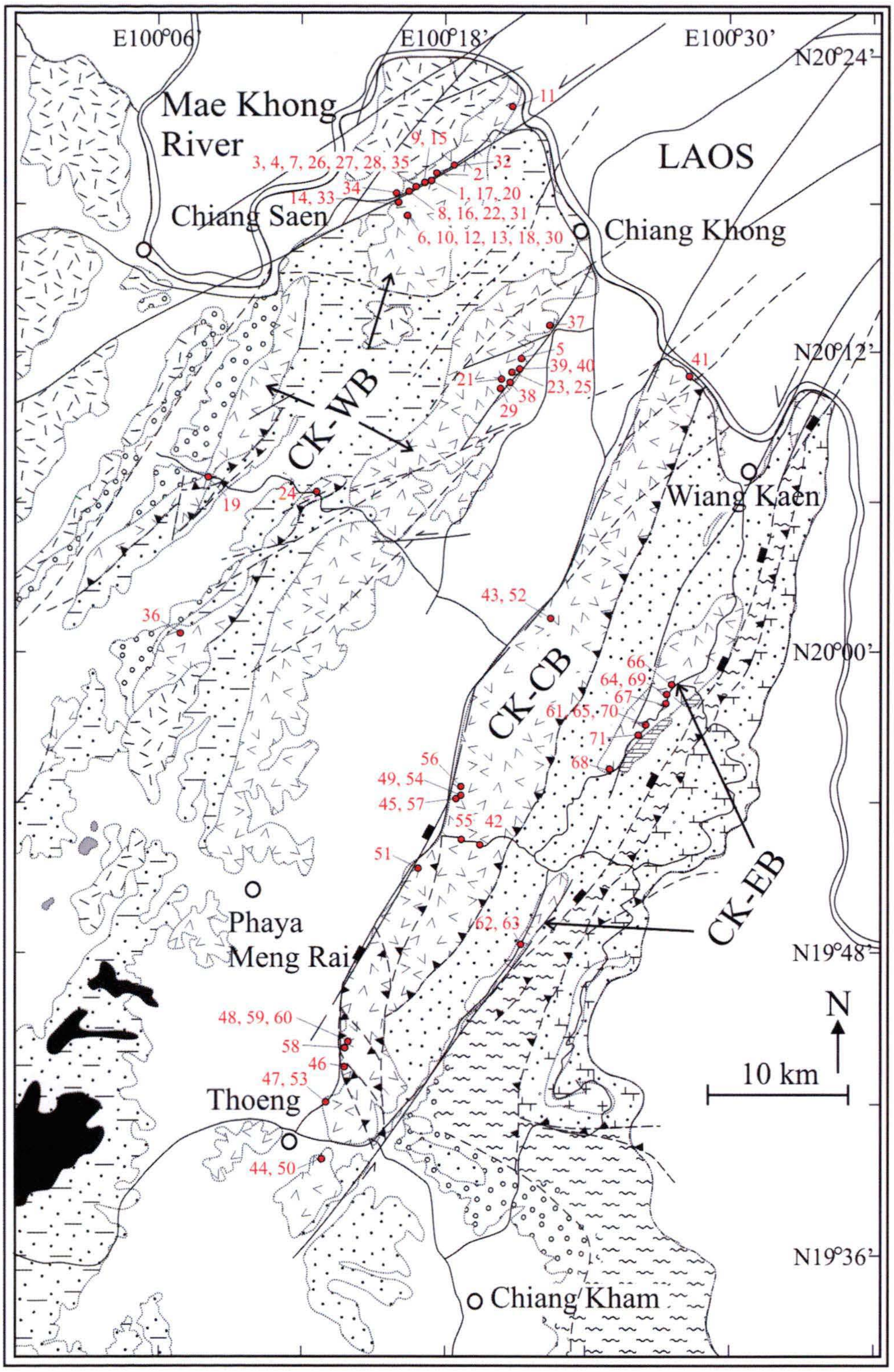

Figure 3.1 Map of the Chiang Khong area showing location of samples for geochemical analysis. Geologic symbols as in Figure 2.3 in Chapter 2. Sample numbers are shown in Table 3.1.

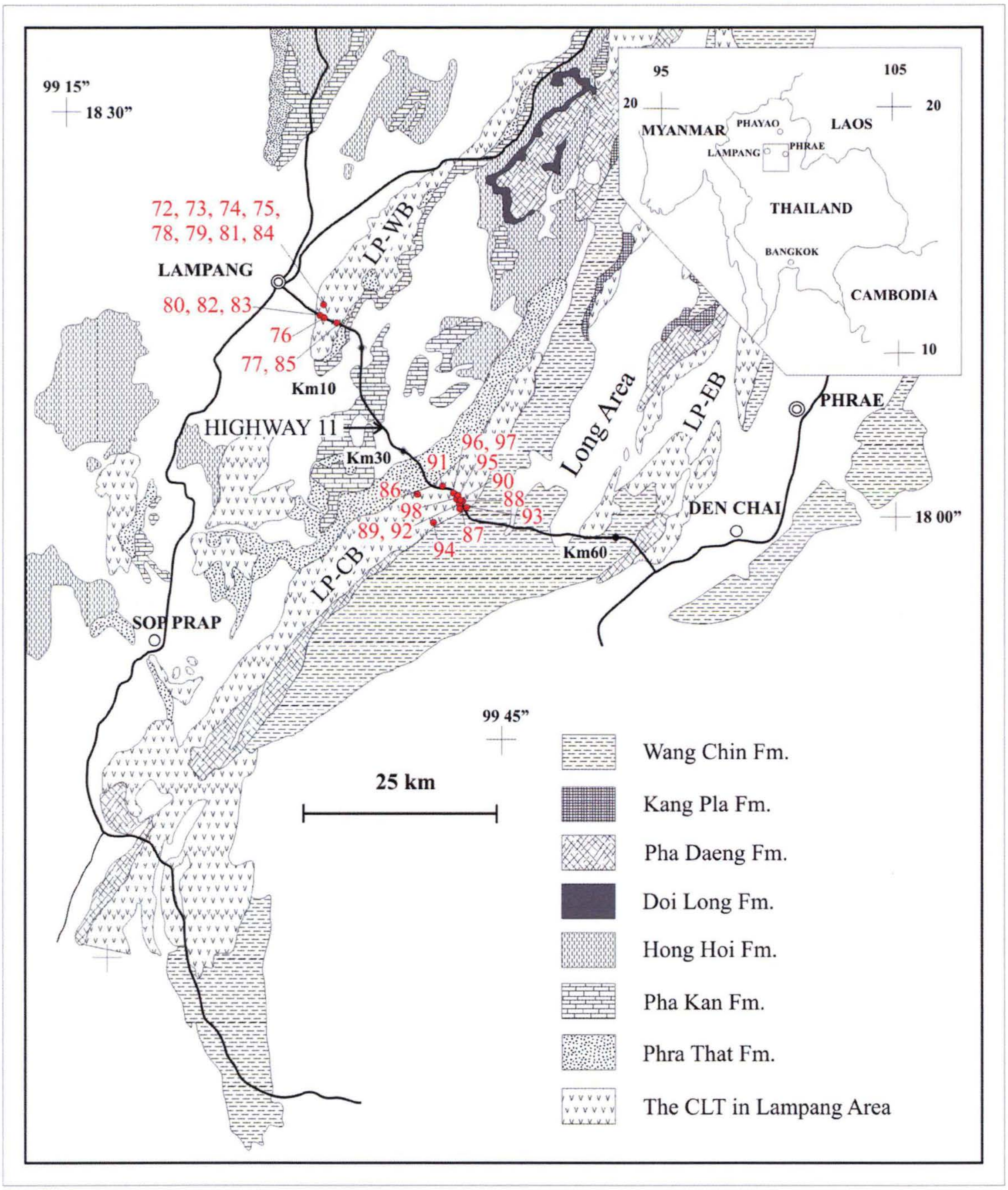

Figure 3.2 Map of the Lampang area showing locations for geochemically analysed samples. Sample numbers are shown in Table 3.1.

Twenty seven representative igneous rocks from the Lampang area were selected for petrochemical study, including 14 samples from LP-WB, and 13 samples from LP-CB. Some 8 samples were selected for low-abundance trace element and REE analysis, and four of these (including two samples from LP-WB and two samples from LP-CB) were selected for the Sm-Nd isotope analysis.

Complementing the new analytical data are 57 analyses from previous petrochemical studies of rocks from the Lampang area, reported by Barr *et al.* (2000) and Osataporn (2007). Barr *et al.* (2000) reported data for 21 samples of mainly felsic composition from the LP-WB, and 9 samples from LP-CB. They also analysed a single rhyolite from LP-WB for its Sm-Nd isotope composition. Twenty-seven whole-rock and five REE analyses for mafic volcanic and shallow intrusive rocks from the Long area were reported by Osataporn (2007).

3.3 Analytical Methods

3.3.1 Introduction

Some 98 representative samples were selected for whole-rock analysis by XRF including 71 samples from the Chiang Khong area and 27 samples from the Lampang area. Of these, 24 representative CLT samples were analysed for low-abundance trace elements and REE by solution ICP-MS. XRF whole-rock analyses and ICP-MS low-abundance trace elements and REE analysis were done at CODES, School of Earth Sciences, University of Tasmania. Analytical results are given in Tables 3.1 and 3.2. Nine selected CLT samples were analysed for Sm-Nd isotopes at School of Earth Science, University of Melbourne.

3.3.2 Major and Trace Element Analysis by XRF

Major and trace elements were analysed using a PANalytical (Philips) PW 1480 X-Ray Fluorescence (XRF) spectrometer. Major elements were measured from fusion discs prepared at 1,100°C in 5%Au/95%Pt crucibles, 0.500g sample, 4.500g 12-22 Flux (lithium tetraborate-metaborate mix) and 0.0606g $LiNO_3$, following the technique described in Robinson (2003). Loss on ignition (LOI) was determined by heating 1-2 g of sample at 1,000°C for 12 hours and reweighing. Pressed powder pellets for trace element analysis were prepared at 3.5 tonnes cm^{-2} with a diameter of 32 mm using 10 g of sample and PVP-MC (Polyvinylpyrrolidone-Methylcellulose) as a binder. Trace elements were measured with a 3kW max. ScMo anode X-Ray tube and 3kW max. Au anode X-Ray tube (Watson, 1996).

3.3.3 Low-abundance Trace Elements and REE Analysis by Solution ICP-MS

The 24 representative CLT samples selected for low-abundance trace element and REE analysis were analysed using a HP4500 Inductively Coupled Plasma Mass Spectrometer (ICP-MS). Sample solutions for ICP-MS analysis were prepared using PicoTrace® high pressure acid (HF/H_2SO_4) digestion. Aliquots (100 mg) of powdered sample were weighed into 30 ml PTFE digestion containers. After wetting the samples with a few drops of ultra-pure water and adding 0.1 ml of μg g $^{-1}$ indium solution to each digestion container, 3 ml HF and 3 ml H_2SO_4 were slowly added. After thorough mixing by shaking a few times, the PTFE containers were left in the digestion block at 180°C for 16 hours. The digestion mixture was then evaporated to dryness at 180°C for four days in the evaporation block. $HClO_4$ (1 ml) was added to the residue and dried before adding the final 2 ml HNO_3 and 1 ml HCl. The residue was dissolved by warming the solution in the digestion block at 60-70°C for ~ 1 hour. After the solution became clear, it was transferred into a polypropylene bottle and diluted to 100 ml (Yu *et al.,* 2001), then analyzed. Comparison between XRF and solution ICP-MS analyses of elements analysed by both techniques showed < 5% variation.

3.3.4 Sm-Nd Isotope Analysis

Sm-Nd isotopic compositions for nine representative CLT igneous rocks were analysed by muti-collector LAM-ICP-MS at the School of Earth Science, University of Melbourne. Sm and Nd concentration were spike-adjusted to yield a mean of 6.59 and 28.8 ppm, respectively, for standard BCR-1. $^{143}Nd/^{144}Nd$ is reported relative to La Jolla Nd = 0.511860 with internal precision (2sd) $\leq \pm$ 0.000012 and external precision (2sd) ±0.000020. CHUR parameters for present-day are $^{147}Sm/^{144}Nd$ = 0.1967 and $^{143}Nd/^{144}Nd$ = 0.512638. ^{147}Sm decay constant is 6.54 E^{-12} yr^{-1}.

Table 3.1 Whole-rock XRF analyses for 98 representative CLT igneous rocks recalculated to 100% volatile-free; loss on ignition and original analytical totals shown.

No	1	2	3	4	5	6	7	8	9	10
Areas	CK WB	CK WB	CK WB	CK WB	CK WB	CK WB	CK WB	CK WB	CK WB	CK WB
Sample name	15'/4(3)	14/6(1)	14/3(5)	14/3(1)	13/2(1)	14/1(1)	14/3(2)	15'/3(2)	14/4(1)	15'/1(5)
Rock types	*I/D	I/D	I/D	I/D	I/D	I/D	I/D	I/D	I/D	I/D
SiO_2	49 27	49 83	50 90	51 20	51 38	53 11	53 22	53 82	54 70	56 82
TiO_2	1 08	1 00	1 53	1 60	0 99	2 15	1 44	1 18	1 04	1 44
Al_2O_3	17 82	17 52	16 42	16 54	20 44	18 18	17 50	18 15	16 85	18 36
FeO*	9 63	9 34	11 27	11 46	9 05	8 70	9 10	7 90	8 18	7 77
MnO	0 18	0 17	0 21	0 23	0 16	0 17	0 16	0 13	0 16	0 21
MgO	8 19	7 87	6 02	6 67	3 74	3 57	4 66	3 50	5 41	2 91
CaO	9 76	9 75	9 51	7 66	10 09	8 56	9 38	8 53	8 77	6 26
Na_2O	3 02	3 30	3 15	3 45	2 83	3 12	2 16	3 75	2 86	4 22
K_2O	0 88	1 07	0 76	0 93	1 07	1 59	1 93	2 57	1 82	1 38
P_2O_5	0 17	0 16	0 23	0 25	0 26	0 85	0 46	0 46	0 21	0 64
Original sum	100 14	100 00	99 50	99 97	100 03	99 86	99 93	100 01	99 95	99 96
Loss inc S-	3 67	3 32	3 30	4 35	1 67	2 33	2 47	1 98	2 72	1 86
Y	22 10	22 80	31 60	33 70	18 30	27 50	24 30	27 50	29 30	33 60
U	<1 5	<1 5	<1 5	<1 5	<1 5	<1 5	1 50	<1 5	<1 5	<1 5
Rb	45 40	63 60	37 30	31 80	24 90	64 70	100 80	135 60	92 90	53 00
Th	1 60	1 50	1 90	2 00	2 90	7 60	8 70	7 40	4 60	7 50
Pb	3 53	1 96	4 03	7 19	5 39	10 59	7 49	9 05	5 22	9 82
Zn	78 70	76 70	107 30	114 70	91 90	100 40	92 80	75 20	87 30	124 90
Cu	55 50	57 30	35 70	32 90	105 30	20 80	32 70	11 60	24 70	12 30
Ni	65 00	68 60	19 00	19 90	10 70	4 90	9 70	15 00	20 70	4 80
Nb	2 70	2 80	5 30	4 80	4 90	9 90	7 60	8 00	6 40	13 00
Zr	82 70	70 70	139 00	128 10	76 70	121 30	128 40	138 80	120 40	134 20
Sr	387 30	467 90	336 20	810 90	512 10	750 60	465 70	621 60	421 70	680 00
Cr	203 00	194 40	48 80	59 20	19 10	6 70	43 00	39 20	148 00	4 40
Ba	131 40	160 70	122 30	261 20	259 50	284 90	292 80	482 10	239 10	342 60
Sc	32 80	32 70	32 40	31 20	28 80	28 00	34 20	25 90	27 90	24 70
V	207 40	206 00	252 80	248 70	284 90	165 70	264 10	195 10	200 30	120 40
La	6 00	5 10	12 00	13 40	12 60	28 70	24 50	21 80	17 10	32 70
Ce	21 10	16 80	26 10	23 00	29 70	59 60	50 70	53 40	38 10	73 50
Nd	10 70	10 10	18 40	16 20	15 00	35 90	27 90	27 90	20 40	42 10

No	11	12	13	14	15	16	17	18	19	20
Areas	CK WB	CK WB	CK WB	CK WB	CK WB	CK WB	CK WB	CK WB	CK WB	CK WB
Sample name	14/8	15'/1(3)	25'/1	15'/2(1)	14/4(2)	15'/3(4)	15'/4(1)	15'/1(1)	26'/10	15'/4(2)
Rock types	I/D	I/D	I/D	I/D	I/D	I/D	I/D	I/D	I/D	lava
SiO_2	57 20	57 62	57 92	62 30	63 62	65 28	66 66	67 65	76 02	49 75
TiO_2	1 06	1 31	0 95	0 92	0 95	0 81	0 73	0 64	0 14	1 02
Al_2O_3	17 34	17 11	16 49	16 48	16 14	15 90	16 35	16 10	13 33	17 66
FeO*	7 26	7 77	7 01	5 67	5 44	4 78	3 97	3 52	1 39	9 28
MnO	0 14	0 19	0 13	0 11	0 14	0 10	0 11	0 10	0 02	0 20
MgO	4 38	3 60	4 43	2 08	2 01	1 72	1 26	1 02	0 13	7 78
CaO	6 10	5 78	7 24	4 99	4 85	3 87	2 39	2 99	0 30	10 45
Na_2O	3 44	2 76	2 74	3 59	3 39	3 59	4 29	4 22	3 50	2 59
K_2O	2 72	3 45	2 83	3 58	3 04	3 62	4 03	3 59	5 13	1 11
P_2O_5	0 36	0 43	0 25	0 29	0 41	0 32	0 21	0 18	0 02	0 17
Original sum	100 01	99 74	99 92	100 19	99 87	99 74	99 56	99 89	99 85	99 99
Loss inc S-	2 36	2 46	1 70	1 46	1 77	1 51	1 76	1 06	0 94	3 23
Y	25 00	27 90	25 80	32 40	35 70	31 40	35 20	38 90	49 10	23 50
U	2 20	2 50	3 10	4 10	4 50	3 70	3 60	4 40	4 30	<1 5
Rb	94 60	182 30	120 90	146 30	101 30	155 40	176 60	131 70	175 20	59 10
Th	8 90	12 90	13 40	17 50	14 80	15 20	15 20	15 40	19 50	1 50
Pb	9 78	13 65	15 82	19 05	42 98	17 68	31 78	20 11	7 64	3 03
Zn	95 30	99 80	78 70	71 90	143 00	61 70	88 80	71 00	25 60	83 10
Cu	36 50	24 50	51 10	17 10	14 00	7 20	8 30	6 60	1 40	57 90
Ni	31 80	6 80	32 00	6 50	6 20	7 30	4 50	4 50	3 90	65 50
Nb	13 40	11 40	12 00	15 70	15 00	16 20	16 90	16 50	17 90	2 80
Zr	183 10	186 20	221 10	240 10	189 90	212 60	257 60	273 00	222 40	81 60
Sr	559 70	379 20	405 30	392 60	445 80	404 80	320 20	376 20	52 50	326 30
Cr	86 90	20 30	90 20	13 00	9 80	9 20	5 10	3 70	1 00	209 60
Ba	599 10	506 60	384 30	506 10	469 20	490 20	593 70	601 40	725 60	142 40
Sc	18 00	20 70	24 00	17 80	18 70	14 00	12 40	12 10	8 70	33 00
V	168 70	183 30	183 80	105 40	88 70	74 50	47 80	37 00	0 30	210 90
La	35 20	29 60	30 60	39 10	38 70	35 00	38 80	40 40	59 50	8 70
Ce	69 60	64 90	64 30	83 30	82 30	74 00	81 40	90 20	120 50	19 40
Nd	35 30	34 40	31 20	39 40	39 50	34 50	39 90	42 70	57 30	11 30

*I/D = Intrusive or dyke

Table 3.1 *(continued)*

No	21	22	23	24	25	26	27	28	29	30
Areas	CK WB	CK WB	CK WB	CK WB	CK WB	CK WB	CK WB	CK WB	CK WB	CK WB
Sample name	13/6(1)	15'/3(5)	13/4(2)	SV-3	13/4(1)	14/3(6)	14/3(7)	14/3(4)	13/7	15'/1(4)
Rock types	lava	lava	lava	lava	lava	lava	lava	lava	lava	lava
SiO_2	50 59	50 96	52 43	52 44	54 65	54 87	54 97	55 00	55 99	57 54
TiO_2	0 85	1 26	1 34	0 90	1 06	1 19	1 17	1 13	1 05	0 94
Al_2O_3	21 73	17 41	16 55	17 27	17 88	18 37	18 04	17 72	18 36	16 43
FeO*	8 51	12 60	11 83	9 22	9 72	7 72	7 52	7 45	8 41	7 02
MnO	0 14	0 26	0 21	0 24	0 18	0 10	0 13	0 14	0 21	0 13
MgO	3 77	5 17	4 53	6 11	3 83	3 90	3 98	3 57	2 97	4 17
CaO	9 50	8 97	8 43	7 87	7 37	8 44	8 22	7 57	5 54	7 77
Na_2O	3 34	3 19	3 07	2 67	4 09	3 21	3 87	4 25	5 82	3 12
K_2O	1 36	0 01	1 21	3 08	0 94	1 76	1 67	2 72	1 31	2 62
P_2O_5	0 21	0 17	0 39	0 21	0 28	0 44	0 43	0 43	0 35	0 27
Original sum	100 46	99 66	99 79	99 97	99 83	99 67	100 02	99 77	99 95	99 92
Loss inc S-	2 36	4 69	0 53	2 08	2 42	1 87	1 71	1 89	2 80	2 24
Y	16 60	28 00	28 30	22 50	20 80	26 40	25 80	26 40	29 10	26 20
U	<1 5	<1 5	<1 5	1 50	2 30	<1 5	<1 5	2 40	2 80	1 70
Rb	41 00	<1	24 30	199 20	19 60	102 30	91 70	120 10	23 30	99 70
Th	3 10	1 50	3 60	5 20	5 00	6 60	6 80	6 20	8 60	10 90
Pb	5 69	7 50	7 79	7 36	8 92	10 09	7 32	7 22	16 06	13 45
Zn	79 40	101 90	123 60	87 10	102 80	56 40	65 70	86 40	117 50	84 20
Cu	91 10	106 60	109 30	38 70	34 30	11 60	33 10	47 80	17 90	43 60
Ni	10 60	10 50	12 00	26 40	2 60	15 20	16 00	16 50	2 10	25 10
Nb	2 20	2 50	6 50	4 50	5 40	9 20	8 70	8 50	9 80	10 40
Zr	59 70	48 30	123 40	76 50	97 50	134 20	132 70	134 30	150 30	161 80
Sr	624 50	1293 80	417 40	478 80	590 20	551 40	569 10	528 80	121 00	421 00
Cr	15 20	25 80	10 80	90 10	1 50	39 80	42 40	42 40	2 90	68 60
Ba	254 00	22 20	281 70	304 70	275 00	343 70	328 70	480 40	192 40	439 10
Sc	26 30	42 80	34 70	28 10	28 10	28 00	26 60	24 90	25 10	25 00
V	268 70	415 00	339 90	227 10	279 40	201 40	200 80	192 30	149 10	178 10
La	6 80	7 30	20 50	12 90	17 10	22 90	22 70	24 60	26 80	29 10
Ce	25 00	14 90	44 50	30 40	35 90	54 20	47 90	46 50	49 90	57 90
Nd	12 80	10 90	23 90	16 50	19 40	29 30	26 00	25 80	25 50	29 90

No	31	32	33	34	35	36	37	38	39	40
Areas	CK WB	CK WB	CK WB	CK WB	CK WB	CK WB	CK WB	CK WB	CK WB	CK WB
Sample name	15'/3(1)	14/7	15'/2(2)	14/2(1)	14/3(3)	18/3(1)	13/1	13/5	13/3(3)	13/3(1)
Rock types	I/D	lava	lava	lava	lava	lava	lava	lava	lava	lava
SiO_2	66 33	63 38	66 76	66 85	67 25	68 54	70 43	75 13	75 22	73 28
TiO_2	0 73	0 91	0 70	0 69	0 66	0 64	0 47	0 32	0 25	0 25
Al_2O_3	16 26	16 51	16 20	16 11	15 95	15 57	14 66	12 91	13 69	14 27
FeO*	4 01	5 73	3 79	3 81	3 62	3 45	3 73	2 48	1 27	1 64
MnO	0 12	0 12	0 12	0 11	0 11	0 16	0 18	0 04	0 03	0 05
MgO	1 27	2 11	1 16	1 25	1 11	0 81	0 79	0 52	0 28	0 35
CaO	3 44	3 93	3 26	3 16	3 18	2 31	0 60	0 43	0 14	0 56
Na_2O	4 19	5 78	4 30	4 27	4 36	4 49	4 63	4 50	3 85	4 40
K_2O	3 44	1 24	3 50	3 56	3 59	3 84	4 38	3 60	5 21	5 15
P_2O_5	0 20	0 30	0 20	0 19	0 18	0 18	0 12	0 07	0 05	0 05
Original sum	100 18	99 85	99 58	100 69	99 72	100 19	99 87	100 03	99 71	99 90
Loss inc S-	1 22	1 16	0 95	1 21	0 88	1 38	1 26	0 74	1 05	0 67
Y	36 60	31 50	37 30	37 00	38 20	47 20	40 90	33 10	158 90	60 20
U	3 10	3 70	2 90	3 80	4 10	4 40	3 10	3 30	5 20	4 70
Rb	124 20	55 30	133 50	144 30	134 50	137 40	139 80	86 50	158 70	160 40
Th	15 90	12 90	14 90	15 30	16 10	15 30	15 30	16 00	18 50	20 80
Pb	21 65	12 66	23 21	21 78	18 61	13 21	2 91	6 61	20 81	50 91
Zn	79 80	79 10	94 70	78 60	67 70	86 10	190 60	131 10	35 00	46 80
Cu	6 40	4 90	8 10	8 90	7 50	3 60	5 20	2 90	7 50	5 30
Ni	4 40	2 90	3 90	5 70	4 60	3 20	3 70	2 90	6 50	3 60
Nb	17 50	16 30	17 10	16 30	16 40	16 90	14 50	16 30	17 70	17 00
Zr	256 40	233 10	265 20	263 70	272 20	261 70	254 10	258 30	235 40	245 50
Sr	398 80	397 90	378 20	372 80	374 90	227 10	125 70	67 20	70 50	111 00
Cr	4 40	3 10	5 30	9 40	4 60	2 10	1 50	0 80	1 00	1 20
Ba	567 10	222 10	565 60	570 00	577 30	573 30	612 60	722 80	743 90	624 10
Sc	14 10	16 10	12 50	13 20	12 70	9 50	12 50	10 10	4 60	4 80
V	46 90	110 90	41 00	46 00	39 60	35 00	7 30	13 60	4 90	6 50
La	37 70	30 60	41 30	38 60	39 70	46 10	34 20	15 70	101 90	66 60
Ce	82 10	70 50	84 10	82 90	85 30	94 80	72 90	43 40	88 60	98 60
Nd	41 70	33 20	40 50	41 40	41 10	45 30	35 50	23 90	113 10	54 10

Table 3.1 *(continued)*

No	41	42	43	44	45	46	47	48	49	50
Areas	CK CB	CK CB	CK CB	CK CB	CK CB	CK CB	CK CB	CK CB	CK CB	CK CB
Sample name	17/10	18/2	16'/2(3)	12/1(2)	16'/6(3)	12/4	12/2(4)	15'/16(2)	16'/5(2)	12/1(1)
Rock types	I/D	I/D	lava	lava	lava	lava	lava	lava	lava	lava
SiO_2	52 48	54 77	51 73	53 46	54 35	54 85	54 97	55 40	55 52	57 52
TiO_2	0 96	1 64	0 87	0 67	0 99	1 11	0 89	1 01	0 95	0 90
Al_2O_3	18 10	15 82	23 38	19 58	16 82	17 77	18 34	17 90	17 70	17 10
FeO*	9 05	10 83	8 04	7 32	9 64	9 14	8 32	8 21	9 09	8 01
MnO	0 16	0 23	0 17	0 13	0 21	0 13	0 17	0 17	0 21	0 16
MgO	5 22	4 15	5 28	4 00	5 33	3 70	4 98	3 81	4 64	4 31
CaO	9 97	7 43	0 93	10 28	7 08	7 67	8 15	6 02	8 30	6 48
Na_2O	2 47	3 64	1 27	4 24	3 85	4 78	3 40	5 35	2 85	4 44
K_2O	1 35	1 08	8 14	0 17	1 51	0 59	0 60	1 89	0 51	0 84
P_2O_5	0 25	0 42	0 17	0 15	0 21	0 25	0 19	0 25	0 23	0 23
Original sum	99 42	99 52	99 86	100 14	99 45	99 80	99 71	100 01	100 21	100 04
Loss inc S-	2 80	2 21	4 59	4 33	2 68	2 36	3 56	2 28	3 24	2 94
Y	19 20	31 90	14 20	12 30	18 60	24 10	16 60	32 00	18 60	18 50
U	<1 5	<1 5	<1 5	<1 5	<1 5	<1 5	<1 5	4 00	<1 5	<1 5
Rb	41 30	28 40	501 90	3 70	60 70	12 70	22 30	109 70	18 40	15 90
Th	2 80	4 70	1 50	1 50	1 60	3 80	4 20	14 60	2 40	4 00
Pb	6 33	12 69	1 40	5 39	3 66	8 93	7 26	13 25	9 33	7 29
Zn	89 30	136 90	154 20	65 30	100 50	98 00	84 10	38 20	166 20	86 10
Cu	118 50	68 10	40 50	43 30	51 40	113 60	20 40	17 30	86 80	32 70
Ni	25 70	17 00	9 80	22 70	16 40	9 60	25 50	4 00	17 60	24 90
Nb	4 40	7 30	3 00	2 50	3 50	5 50	4 20	6 00	4 40	4 60
Zr	80 40	152 80	59 10	47 60	71 00	109 10	85 90	108 70	79 40	98 00
Sr	456 20	475 30	48 60	217 80	428 40	526 20	503 50	323 20	617 60	416 10
Cr	67 70	18 80	6 60	64 50	26 90	17 90	82 10	19 80	41 60	55 70
Ba	242 60	345 40	992 20	52 20	367 80	145 90	113 60	360 70	175 20	424 00
Sc	30 30	32 30	23 20	24 70	33 00	29 10	28 40	24 20	32 10	24 30
V	221 40	323 50	232 70	208 30	258 90	259 10	238 30	241 90	254 60	238 10
La	10 20	18 40	6 10	6 90	7 90	12 20	10 00	14 00	8 70	13 30
Ce	29 00	39 70	15 10	14 80	20 80	29 50	24 90	34 20	22 00	28 00
Nd	14 30	22 50	8 20	8 10	13 50	14 50	12 30	18 00	12 10	14 50

No	51	52	53	54	55	56	57	58	59	60
Areas	CK CB	CK CB	CK CB	CK CB	CK CB	CK CB	CK CB	CK CB	CK CB	CK CB
Sample name	16'/7(1)	16'/2(2)	12/2(3)	16'/5(1)	18/1	16'/4	16'/6(1)	16'/10(1)	15'/16(1)	15'/16(3)
Rock types	lava	lava	lava	lava	lava	lava	lava	lava	lava	lava
SiO_2	57 99	59 02	63 06	65 00	67 58	63 93	73 80	75 14	78 51	75 68
TiO_2	0 95	1 00	0 95	0 92	0 77	0 80	0 48	0 23	0 10	0 21
Al_2O_3	16 48	16 70	15 63	15 96	15 01	15 75	13 62	13 32	11 87	13 11
FeO*	7 58	7 81	7 07	5 17	4 06	5 03	2 62	1 72	0 97	1 62
MnO	0 16	0 14	0 17	0 19	0 05	0 27	0 05	0 05	0 03	0 04
MgO	4 05	3 44	2 45	2 24	0 44	1 53	0 57	0 47	0 18	0 41
CaO	6 78	4 58	3 81	2 60	2 42	3 16	0 20	0 70	0 34	0 75
Na_2O	3 37	4 35	4 75	4 12	6 54	0 51	5 38	4 33	4 08	4 52
K_2O	2 37	2 70	1 82	3 54	2 84	8 76	3 18	4 00	3 90	3 62
P_2O_5	0 27	0 25	0 28	0 28	0 29	0 27	0 09	0 04	0 01	0 04
Original sum	99 73	99 90	100 04	100 41	100 47	99 49	100 09	99 44	99 83	99 84
Loss inc S-	2 28	2 10	1 86	1 98	1 62	1 96	0 82	0 79	0 34	0 69
Y	26 20	26 30	27 00	34 50	31 60	33 30	24 30	34 10	34 80	23 50
U	1 60	<1 5	1 50	2 00	4 20	2 40	3 70	4 40	5 60	<1 5
Rb	85 70	91 70	47 90	114 00	49 30	199 10	73 30	127 00	118 60	54 00
Th	7 20	7 60	7 00	10 10	13 90	33 10	12 30	14 40	17 20	3 90
Pb	14 05	11 95	14 36	13 18	8 55	1985 36	7 52	5 81	4 28	7 92
Zn	102 90	85 30	111 80	242 70	60 40	1499 20	41 80	42 40	13 10	97 00
Cu	67 70	16 80	13 60	14 00	3 60	375 90	3 30	4 30	2 40	147 10
Ni	20 20	10 50	2 60	5 50	5 10	7 90	3 60	3 50	2 70	19 60
Nb	6 80	8 00	8 20	11 80	16 90	9 80	14 30	17 50	15 00	17 90
Zr	147 50	156 20	159 70	217 30	289 30	190 40	234 60	201 80	134 10	201 70
Sr	563 90	426 60	620 00	255 70	79 50	273 80	84 70	118 10	66 40	128 60
Cr	41 70	27 40	1 60	7 40	3 50	11 60	3 80	1 60	1 30	2 50
Ba	505 20	511 70	297 50	554 30	450 20	1169 50	481 70	548 10	479 40	527 00
Sc	25 70	21 70	18 40	13 60	10 00	14 50	7 90	5 40	4 00	5 10
V	198 00	195 60	128 20	89 20	40 70	107 10	34 20	8 80	2 20	9 40
La	21 70	18 20	19 20	27 00	20 00	26 30	22 50	32 00	32 80	30 30
Ce	45 30	39 40	45 10	60 10	54 90	78 70	52 90	71 00	71 00	69 60
Nd	23 90	19 00	22 10	29 90	29 80	32 10	20 60	31 50	34 00	30 10

Table 3.1 *(continued)*

No	61	62	63	64	65	66	67	68	69	70
Areas	CK EB	CK EB	CK EB	CK EB	CK EB	CK EB	CK EB	CK EB	CK EB	CK EB
Sample name	17/7(2)	15'/15(2)	15'/15(1)	17/9(3)	17/7(1)	15'/7(1)	15'/8(2)	15'/13(2)	17/9(2)	17/7(3)
Rock types	I/D	lava	lava	lava	lava	lava	lava	lava	lava	lava
SiO_2	51 94	49 70	50 56	50 65	51 16	51 16	51 45	52 22	52 32	53 62
TiO_2	1 44	1 41	1 35	0 89	1 06	1 39	1 05	1 15	1 11	1 48
Al_2O_3	17 45	17 97	18 83	20 26	17 58	18 83	20 61	18 89	17 05	16 15
FeO*	12 27	10 72	10 48	8 98	10 51	12 63	8 86	10 74	11 07	11 41
MnO	0 23	0 17	0 18	0 15	0 29	0 15	0 17	0 20	0 20	0 21
MgO	5 37	4 45	4 81	4 28	6 20	6 75	4 32	4 07	5 84	4 55
CaO	4 99	12 09	8 27	10 48	9 20	7 75	7 05	7 70	7 41	7 19
Na_2O	5 88	3 09	4 85	3 27	3 21	0 27	4 77	4 06	4 70	3 75
K_2O	0 19	0 11	0 42	0 87	0 60	0 74	1 51	0 75	0 10	1 32
P_2O_5	0 23	0 30	0 26	0 17	0 19	0 32	0 21	0 22	0 19	0 32
Original sum	99 65	99 95	100 27	99 88	99 92	100 10	99 65	99 96	99 66	99 65
Loss inc S-	2 78	4 51	3 29	2 39	3 20	11 23	2 83	2 82	2 81	2 40
Y	21 20	22 80	20 60	13 90	20 30	22 10	16 80	21 20	15 80	25 90
U	<1 5	2 00	<1 5	<1 5	<1 5	<1 5	<1 5	<1 5	<1 5	<1 5
Rb	3 70	3 70	15 70	21 00	14 50	21 80	50 50	15 60	2 80	33 30
Th	1 60	3 10	2 00	1 90	1 50	2 10	1 90	1 60	1 80	3 20
Pb	6 60	12 96	6 53	5 46	5 66	5 43	6 98	6 16	4 73	10 95
Zn	130 60	105 60	113 90	83 60	102 70	141 90	87 30	112 20	100 10	121 90
Cu	30 70	121 50	26 80	283 90	17 20	22 70	78 50	21 40	48 80	51 40
Ni	8 70	50 10	45 90	13 30	34 60	31 50	17 70	9 60	20 00	12 80
Nb	2 50	5 60	3 70	1 70	3 20	3 70	3 00	2 70	1 50	4 60
Zr	62 10	89 00	72 40	44 40	65 70	101 40	73 00	83 60	50 10	108 80
Sr	468 80	352 90	1034 30	539 10	395 90	89 50	901 10	466 80	548 90	577 00
Cr	1 40	121 90	57 60	40 50	64 80	45 60	25 10	9 80	92 20	12 00
Ba	94 50	57 80	158 70	241 40	213 20	145 70	598 00	192 20	77 40	454 00
Sc	31 80	28 70	30 00	35 00	39 80	33 20	24 90	26 70	34 70	32 70
V	348 50	311 80	324 30	290 70	318 50	289 40	243 60	220 00	327 70	327 60
La	8 60	12 70	7 20	5 80	5 40	7 10	8 70	8 90	7 40	12 70
Ce	16 50	22 40	23 90	12 10	21 10	20 30	26 80	18 60	14 50	30 00
Nd	11 30	14 90	14 50	8 00	11 40	13 00	12 80	11 10	9 60	18 80

No	71	72	73	74	75	76	77	78	79	80
Areas	CK EB	LP WB	LP WB	LP WB	LP WB	LP WB	LP WB	LP WB	LP WB	LP WB
Sample name	15'/10(2)	12'/1(5)	12'/1(2-1)	12'/1(1-1)	12'/1(1-3)	5/3	20'/5	12'/1(9)	12'/1(8)	12'/5(3)
Rock types	lava	I/D	I/D	lava	lava	lava	lava	lava	lava	lava
SiO_2	54 14	78 74	78 67	50 67	51 66	75 04	77 31	78 05	77 17	77 25
TiO_2	1 53	0 26	0 41	1 02	1 00	0 47	0 33	0 26	0 24	0 33
Al_2O_3	16 43	11 97	8 70	18 15	18 15	13 34	12 08	11 92	12 60	12 89
FeO*	11 13	2 38	3 80	9 80	9 77	2 72	3 04	2 43	2 37	2 30
MnO	0 24	0 08	0 17	0 39	0 39	0 17	0 05	0 06	0 06	0 04
MgO	5 16	2 11	4 46	7 41	7 42	1 83	1 23	1 61	1 64	0 79
CaO	6 04	0 10	1 68	7 09	6 13	0 38	1 09	0 36	0 12	0 20
Na_2O	4 46	3 10	1 95	5 13	5 24	5 79	4 03	4 65	5 49	5 69
K_2O	0 51	1 23	0 07	0 21	0 13	0 18	0 77	0 62	0 26	0 46
P_2O_5	0 34	0 03	0 08	0 11	0 11	0 08	0 07	0 03	0 03	0 05
Original sum	99 88	100 37	100 82	100 01	99 91	100 24	100 24	100 27	100 18	100 38
Loss inc S-	2 82	2 37	4 74	9 24	9 03	1 67	2 70	1 89	1 76	1 51
Y	27 90	47 10	21 50	19 90	25 40	40 30	38 80	46 10	56 50	30 30
U	<1 5	<1 5	<1 5	<1 5	<1 5	<1 5	<1 5	<1 5	<1 5	<1 5
Rb	13 70	19 30	1 10	3 60	2 10	2 30	16 10	9 50	3 70	7 10
Th	3 30	3 00	3 40	1 50	1 50	2 30	2 70	2 70	2 80	2 90
Pb	7 56	0 30	9 80	6 43	5 90	1 70	14 20	0 83	2 50	0 83
Zn	125 10	74 80	75 20	148 60	146 80	98 00	65 40	76 60	84 80	32 80
Cu	32 50	1 40	17 60	93 80	87 90	2 20	12 30	1 30	0 90	3 30
Ni	11 60	2 00	16 80	38 40	38 90	1 40	2 20	1 90	2 80	2 50
Nb	4 30	4 80	3 00	1 00	1 80	5 00	4 10	4 30	5 00	4 40
Zr	112 50	172 20	71 50	45 90	44 10	185 80	162 30	194 80	179 20	195 60
Sr	473 20	34 80	29 20	86 20	87 20	71 30	55 90	50 80	47 70	55 50
Cr	7 80	0 80	19 90	169 90	170 50	1 40	1 60	1 20	1 70	2 10
Ba	256 20	99 00	10 90	43 50	51 60	52 00	115 50	61 90	38 40	150 20
Sc	32 90	11 20	14 30	45 00	44 30	13 60	11 70	10 00	8 70	7 40
V	350 90	0 70	97 50	298 20	295 00	4 70	6 70	0 60	1 60	17 90
La	12 70	9 00	10 50	2 80	7 20	10 70	8 50	15 20	2 90	7 60
Ce	29 30	22 40	20 50	9 30	14 40	27 30	27 50	32 60	14 30	9 80
Nd	18 30	14 10	13 70	6 70	9 00	18 00	22 90	26 10	9 40	14 10

Table 3.1 *(continued)*

No	81	82	83	84	85	86	87	88	89	90
Areas	LP WB	LP WB	LP WB	LP WB	LP WB	LP CB	LP CB	LP CB	LP CB	LP CB
Sample name	12'/1(1-4)	12'/5(1)	12'/5(2)	5/1	6/5	SV-1	7/2	12'/10	7/4(2)	12'/9
Rock types	lava	lava	lava	lava	lava	I/D	I/D	I/D	lava	lava
SiO_2	76 57	73 77	77 05	76 88	76 27	55 21	75 53	65 94	66 04	79 04
TiO_2	0 38	0 52	0 44	0 26	0 33	1 45	0 16	0 65	0 75	0 14
Al_2O_3	12 89	13 11	12 97	12 52	12 16	16 75	13 37	16 42	15 30	11 49
FeO*	2 60	3 67	1 59	2 84	3 56	8 15	1 67	4 15	5 14	0 94
MnO	0 05	0 28	0 09	0 07	0 08	0 12	0 06	0 09	0 21	0 01
MgO	1 41	2 38	1 06	1 48	1 56	5 63	0 20	1 39	2 39	0 16
CaO	0 28	0 79	0 22	0 10	1 45	6 91	0 16	2 49	1 98	0 02
Na_2O	5 13	5 27	6 46	5 76	3 66	4 13	3 80	3 80	3 52	1 25
K_2O	0 62	0 13	0 04	0 04	0 86	1 34	5 00	4 87	4 44	6 92
P_2O_5	0 07	0 08	0 07	0 04	0 06	0 30	0 04	0 21	0 23	0 04
Original sum	100 04	100 54	100 10	100 31	99 81	100 35	99 68	100 06	100 16	100 24
Loss inc S-	1 73	2 56	1 23	1 39	3 45	2 45	1 02	1 47	2 26	1 08
Y	36 70	41 70	44 20	44 40	41 40	37 40	22 40	31 50	26 60	67 90
U	<1 5	1 50	<1 5	<1 5	0 90	<1 5	12 20	8 40	6 70	3 80
Rb	9 70	2 00	0 40	<1	16 60	18 20	225 60	215 90	165 80	252 00
Th	3 00	3 10	3 10	3 50	2 60	2 40	55 20	37 20	30 10	12 50
Pb	1 63	0 20	1 90	1 80	3 90	1 53	15 49	70 64	58 49	19 07
Zn	51 20	115 40	51 70	78 10	75 60	76 40	11 80	78 40	173 10	42 30
Cu	8 00	1 40	1 00	1 50	7 90	33 70	11 60	12 90	9 00	4 50
Ni	2 70	2 10	3 00	2 40	1 70	24 60	4 10	5 60	17 30	5 60
Nb	3 70	5 40	4 40	4 60	3 90	5 60	15 30	14 50	12 50	9 10
Zr	189 80	194 90	175 10	183 10	160 70	230 30	192 80	371 50	248 30	163 70
Sr	88 20	42 60	49 80	44 80	54 30	303 00	50 30	313 10	348 20	67 40
Cr	2 40	3 00	0 90	3 10	2 30	86 20	1 90	6 10	46 60	1 00
Ba	104 90	38 20	16 70	15 10	66 20	245 50	312 50	1750 20	1404 70	738 70
Sc	10 50	14 80	10 00	11 20	10 30	25 80	2 00	10 20	13 20	5 70
V	14 10	21 50	3 30	3 20	8 20	190 00	5 30	63 70	107 70	4 20
La	10 20	5 90	6 20	9 50	6 80	11 10	39 90	48 30	39 00	72 40
Ce	27 50	27 60	15 50	30 10	21 90	32 10	77 30	92 60	82 80	126 20
Nd	18 80	17 20	12 10	19 80	16 90	22 40	28 30	39 80	35 80	67 90

No	91	92	93	94	95	96	97	98
Areas	LP CB	LP CB	LP CB	LP CB	LP CB	LP CB	LP CB	LP CB
Sample name	12'/6(1)	7/4(1)	7/3(1)	SV-V	7/6	7/7(1)	7/7(2)	12'/8
Rock types	lava	lava	lava	lava	lava	lava	lava	lava
SiO_2	78 93	74 58	75 36	77 26	77 33	77 52	77 61	77 70
TiO_2	0 14	0 16	0 16	0 06	0 07	0 08	0 07	0 08
Al_2O_3	12 33	14 14	13 70	12 59	12 70	13 46	12 81	13 34
FeO*	1 29	1 87	1 09	1 03	1 19	0 67	1 06	0 49
MnO	0 01	0 05	0 01	0 03	0 04	0 01	0 04	0 01
MgO	0 11	0 31	0 24	0 09	0 17	0 14	0 15	0 15
CaO	0 10	1 30	0 44	0 45	0 61	0 07	0 05	0 08
Na_2O	3 84	3 30	4 36	3 74	3 04	2 53	3 32	2 86
K_2O	3 23	4 25	4 60	4 74	4 82	5 49	4 86	5 27
P_2O_5	0 02	0 03	0 04	0 01	0 02	0 02	0 02	0 02
Original sum	99 72	99 73	99 46	100 53	99 47	99 91	100 39	100 14
Loss inc S-	1 67	2 91	0 71	0 65	1 37	1 19	0 99	1 01
Y	23 70	33 40	23 90	35 20	19 10	34 20	29 40	21 10
U	3 20	10 60	13 90	10 70	8 60	11 10	10 40	16 80
Rb	89 50	184 70	157 70	232 80	236 40	271 30	197 50	257 90
Th	13 20	54 50	53 60	50 50	47 80	50 90	49 60	53 70
Pb	8 90	150 11	12 95	23 43	28 09	105 75	125 15	21 06
Zn	11 10	26 60	21 80	16 70	13 90	21 20	24 90	8 70
Cu	4 00	3 60	11 20	6 60	3 20	2 40	2 00	4 90
Ni	2 90	2 90	3 10	3 30	2 40	3 80	3 60	3 30
Nb	9 00	18 60	16 10	18 50	13 10	20 10	18 20	14 30
Zr	193 10	253 90	217 70	114 90	107 80	149 50	149 90	123 90
Sr	94 20	72 90	70 90	40 00	55 50	76 90	48 60	51 50
Cr	1 00	1 90	1 70	0 80	1 00	1 10	1 30	1 00
Ba	901 40	573 70	473 70	71 80	236 60	368 10	380 60	311 00
Sc	4 30	5 00	2 00	2 00	2 00	2 00	2 00	2 00
V	4 80	2 40	5 50	0 00	1 80	1 50	1 10	2 40
La	28 80	68 60	44 70	15 20	21 80	37 20	26 90	27 40
Ce	59 90	142 80	85 40	45 20	50 60	79 80	63 10	53 70
Nd	25 70	55 30	29 80	18 20	16 50	32 00	23 50	18 70

Table 3.2 Low-abundance trace elements and REE compositions (in ppm) for the 24 representative CLT igneous rocks by ICP-MS analysis.

No	1	2	3	4	5	6	7	8	9	10	11	12
Areas	CK WB	CK WB	CK WB	CK WB	CK WB	CK WB	CK WB	CK WB	CK WB	CK WB	CK CB	CK CB
Sample name	15'/4(3)	14/3(5)	14/8	14/4(2)	15'/1(1)	13/4(2)	13/4(1)	15'/1(3)	14/7	13/5	17/10	12/2(3)
Rock types	I/D	I/D	I/D	I/D	I/D	lava	lava	lava	lava	lava	I/D	lava
Li	50 10	50 58	17 37	23 16	12 63	25 06	26 76	49 18	12 84	14 29	38 32	42 37
Be	0 60	0 98	1 71	2 07	2 42	1 06	1 03	0 91	2 20	1 57	0 87	1 45
Sc	37 97	39 00	17 82	16 55	12 50	37 19	29 22	28 38	16 62	12 63	32 66	21 90
V	210 81	252 80	159 86	81 18	36 70	339 90	292 14	265 30	113 64	12 73	219 11	125 20
Cr	179 86	48 80	79 40	7 92	3 01	10 80	102 28	0 77	2 28	0 39	65 20	0 26
Mn	1291 89	1553 51	1073 87	1010 14	776 93	1615 90	1162 05	1323 07	908 48	339 20	1142 14	1340 40
Ni	57 72	18 09	29 24	4 88	2 65	10 52	44 56	2 12	1 37	1 52	22 99	0 92
Cu	54 36	33 94	32 99	11 38	4 51	113 25	121 89	30 98	2 25	2 36	114 24	9 65
Zn	76 09	108 81	95 18	143 48	73 55	128 13	103 89	99 45	79 05	134 87	87 62	108 87
Ga	15 59	18 97	18 99	19 02	18 96	19 29	20 74	19 08	19 04	8 33	18 48	19 30
Rb	42 43	36 22	88 26	93 58	125 32	23 45	3 22	17 93	52 82	85 21	38 75	46 38
Sr	375 36	344 39	542 90	433 95	369 86	426 32	346 27	561 27	392 08	64 44	468 61	621 89
Y	19 42	31 60	21 50	31 44	34 67	28 30	20 38	18 98	28 38	29 49	17 38	24 41
Zr	79 08	139 00	176 16	192 81	261 36	123 40	86 94	94 33	226 32	246 96	83 86	153 53
Nb	2 74	5 51	13 72	14 15	15 85	6 50	4 61	5 51	14 97	12 60	4 53	7 44
Mo	0 29	0 49	0 93	1 41	1 57	0 83	0 39	0 47	1 83	0 60	0 68	0 70
Sn	0 82	1 41	2 01	3 13	3 01	1 21	1 12	1 06	2 43	2 69	0 88	1 41
Sb	3 09	1 47	0 89	1 43	0 44	0 19	0 61	0 12	0 43	0 96	1 17	4 12
Cs	4 06	3 70	5 05	2 94	2 60	2 32	1 08	2 32	2 76	4 92	4 05	2 76
Ba	118 32	122 30	506 01	462 66	544 30	281 70	61 17	257 50	225 09	650 14	234 65	294 13
La	6 70	12 05	35 32	42 73	46 00	18 65	12 00	16 84	41 27	17 29	12 74	23 23
Ce	15 83	27 40	69 29	85 19	90 71	40 68	26 21	34 32	80 71	43 77	27 58	45 78
Pr	2 33	3 84	8 46	10 47	11 07	5 51	3 70	4 39	9 69	5 97	3 71	5 69
Nd	10 98	17 75	33 52	41 87	43 49	24 38	17 01	18 59	37 72	25 30	16 39	23 39
Sm	2 94	4 38	6 44	8 17	8 47	5 44	4 05	3 96	7 26	5 87	3 74	5 05
Eu	1 06	1 54	1 62	1 91	1 99	1 53	1 30	1 26	1 73	1 18	1 15	1 39
Gd	3 38	5 07	5 51	7 18	7 39	5 41	4 24	3 93	6 35	5 43	3 70	4 76
Tb	0 61	0 87	0 79	1 07	1 14	0 86	0 67	0 64	0 96	0 95	0 58	0 76
Dy	3 80	5 41	4 37	6 14	6 56	5 08	4 01	3 73	5 52	5 62	3 44	4 56
Ho	0 78	1 12	0 81	1 19	1 30	1 04	0 78	0 75	1 06	1 17	0 68	0 91
Er	2 35	3 27	2 26	3 45	3 82	2 98	2 27	2 18	3 10	3 56	1 98	2 67
Tm	0 34	0 48	0 31	0 49	0 56	0 44	0 33	0 32	0 45	0 55	0 29	0 40
Yb	2 23	3 13	2 00	3 21	3 69	2 82	2 13	2 11	2 98	3 70	1 88	2 60
Lu	0 35	0 49	0 31	0 50	0 57	0 44	0 33	0 33	0 47	0 60	0 29	0 42
Hf	2 15	3 29	4 60	5 48	7 11	3 13	2 57	2 64	6 04	6 75	2 41	4 13
Ta	0 21	0 46	0 99	1 13	1 46	0 42	0 43	0 47	1 13	1 08	0 41	0 58
Tl	0 29	0 27	0 78	0 98	0 67	0 19	0 02	0 11	0 39	0 77	0 23	0 55
Pb	3 58	4 77	9 15	41 20	19 78	8 32	12 86	8 10	12 65	4 99	7 83	14 18
Bi	0 04	<0 02	0 06	0 13	0 20	<0 02	0 11	0 03	0 14	0 11	0 05	0 15
Th	0 93	1 97	8 35	13 31	14 09	3 05	1 88	4 24	12 51	13 61	2 24	6 74
U	0 27	0 57	2 49	3 47	3 72	0 88	0 66	1 30	3 23	3 19	0 70	1 98

Table 3.2 *(continued)*

No	13	14	15	16	17	18	19	20	21	22	23	24
Areas	CK CB	CK EB	CK EB	CK EB	LP WB	LP WB	LP WB	LP WB	LP WB	LP CB	LP CB	LP CB
Sample name	15'/16 (1)	15'/15 (2)	17/7 (3)	15'/10 (2)	12'/1 (5)	12'/1 (1-1)	12'/1 (1-3)	12'/1 (8)	12'/5 (3)	7/2	12'/10	7/7(1)
Rock types	lava	lava	lava	lava	I/D	lava	lava	lava	lava	I/D	lava	lava
Li	2 89	35 45	18 38	19 93	4 57	7 72	7 79	3 60	1 31	4 24	24 26	8 45
Be	1 84	1 64	1 01	1 13	1 13	0 67	0 70	0 76	0 88	4 01	3 17	2 77
Sc	5 78	23 58	36 17	37 08	12 72	41 81	40 89	10 10	9 28	2 46	12 59	1 16
V	1 81	181 53	327 60	350 90	0 79	298 20	295 00	1 60	18 61	5 42	67 37	1 59
Cr	0 65	20 96	12 00	7 80	1 32	169.90	170 50	1 70	1 24	1 34	5 52	1 15
Mn	226 64	1394 99	1535 94	1812 26	687 46	2724 65	2739 78	413 90	332 05	450 35	754 65	65 29
Ni	1 79	5 72	10 88	10 31	1 65	35 92	36 69	1 36	2 07	2 79	3 89	1 52
Cu	2 48	20 67	52 17	30 99	1 83	97 59	91 01	2 57	4 54	11 60	12 06	2 18
Zn	15 30	101 71	121 39	126 36	79 60	154 63	153 74	92 45	35 38	14 13	84 82	23 45
Ga	12 11	18 69	20 22	19 63	15 70	16 97	16 85	14 46	13 46	15 36	17 32	17 29
Rb	117 18	172 95	32 97	13 37	19 90	3 35	2 00	3 71	7 10	225 93	211 03	270 45
Sr	64 54	373 37	607 33	491 56	34 14	83 92	84 94	45 82	53 80	49 90	283 96	75 01
Y	31 41	25 46	25 90	27 90	44 43	19 90	25 40	56 50	27 55	20 86	29 19	30 62
Zr	129 05	180 92	108 80	112 50	161 78	45 90	44 10	179 20	189 24	191 94	364 23	145 91
Nb	11 35	11 66	4 79	4 96	3 45	0 99	0 88	2 98	3 32	11 04	13 78	13 90
Mo	2 42	1 13	0 54	0 44	0 11	0 10	0 09	0 33	0 07	1 66	1 39	1 27
Sn	2 31	2 18	1 20	1 16	1 73	0 48	0 54	1 14	1 10	3 79	2 53	3 29
Sb	0 42	0 84	0 47	0 61	0 31	0 81	1 09	0 19	0 20	0 29	0 76	1 30
Cs	1 06	5 63	3 11	1 92	0 40	0 33	0 23	0 05	0 04	3 74	7 14	9 86
Ba	503 95	477 63	454 00	256 20	98 98	43 50	51 60	38 40	154 83	327 09	690 14	384 58
La	38 71	33 38	14 16	14 35	9 60	4 70	6 96	6 66	10 18	42 43	48 56	40 06
Ce	77 53	67 95	31 02	31 62	22 31	10 11	12 43	12 76	9 99	77 45	97 04	76 00
Pr	9 32	8 47	4 28	4 35	3 24	1 55	2 09	2 18	3 14	8 25	11 17	8 94
Nd	35 33	34 19	19 66	20 21	14 90	8 09	10 89	10 42	14 03	27 83	41 30	31 75
Sm	6 99	6 88	4 69	4 81	4 39	2 38	3 00	3 36	3 52	5 03	7 54	6 74
Eu	0 55	1 65	1 48	1 45	1 16	1 02	1 33	0 86	0 72	0 49	1 57	0 59
Gd	6 29	5 94	4 86	5 00	5 94	3 04	4 06	5 84	3 71	4 03	6 31	5 87
Tb	1 05	0 89	0 77	0 80	1 19	0 53	0 69	1 29	0 69	0 64	0 98	1 01
Dy	6 29	4 98	4 72	4 88	7 87	3 39	4 21	9 14	4 58	3 66	5 50	5 86
Ho	1 25	0 98	0 92	0 98	1 68	0 70	0 85	1 96	1 02	0 72	1 05	1 11
Er	3 75	2 79	2 72	2 78	5 08	1 95	2 31	5 75	3 34	2 22	3 06	3 28
Tm	0 58	0 40	0 40	0 42	0 75	0 27	0 31	0 85	0 54	0 36	0 45	0 51
Yb	3 85	2 52	2 59	2 63	4 91	1 68	1 89	5 45	3 70	2 45	2 93	3 31
Lu	0 60	0 40	0 41	0 40	0 76	0 26	0 28	0 82	0 60	0 39	0 46	0 50
Hf	4 94	4 99	2 89	2 97	4 76	1 18	1 17	4 46	5 25	6 12	9 19	5 67
Ta	1 14	0 80	0 39	0 35	0 34	0 11	0 17	0 49	0 55	2 01	1 52	1 89
Tl	0 72	0 90	0 19	0 07	0 09	0 02	0 01	0 02	0 03	1 32	1 21	1 89
Pb	3 67	12 69	10 13	7 26	1 04	5 79	5 55	1 88	1 54	15 23	56 26	103 23
Bi	0 04	0 04	<0 02	<0 02	0 00	<0 02	<0 02	0 06	0 02	0 08	0 08	0 07
Th	15 50	10 86	2 40	2 45	2 67	0 39	0 39	2 51	3 01	52 45	31 02	45 79
U	4 46	2 86	0 75	0 79	0 90	0 12	0 13	0 90	0 95	10 55	7 90	10 09

3.4 Petrographic Features of Geochemically Defined Rock Groups

3.4.1 Introduction

A Th-SiO_2 diagram plot for all new data for CLT igneous rocks (Figure 3.3) provides a useful framework for grouping the analysed rocks for presentation of their petrographic details (Appendix A provides petrographic details for all samples). Compositional groups have the suffix –L for rocks considered to be lavas, and –D for dykes and other shallow intrusive rocks. In some instances, particularly in areas of poor outcrop, it proved impossible to determine with confidence whether some rocks were lavas or from narrow dykes, especially for the more mafic composition rocks. Where assigned to a dyke origin, this was either based on outcrop, or on doleritic or medium- to coarse-grained holocrystalline textures. Despite low-grade regional metamorphism (prehnite-pumpellyite to greenschist facies: see below), all analysed samples show excellent textural preservation.

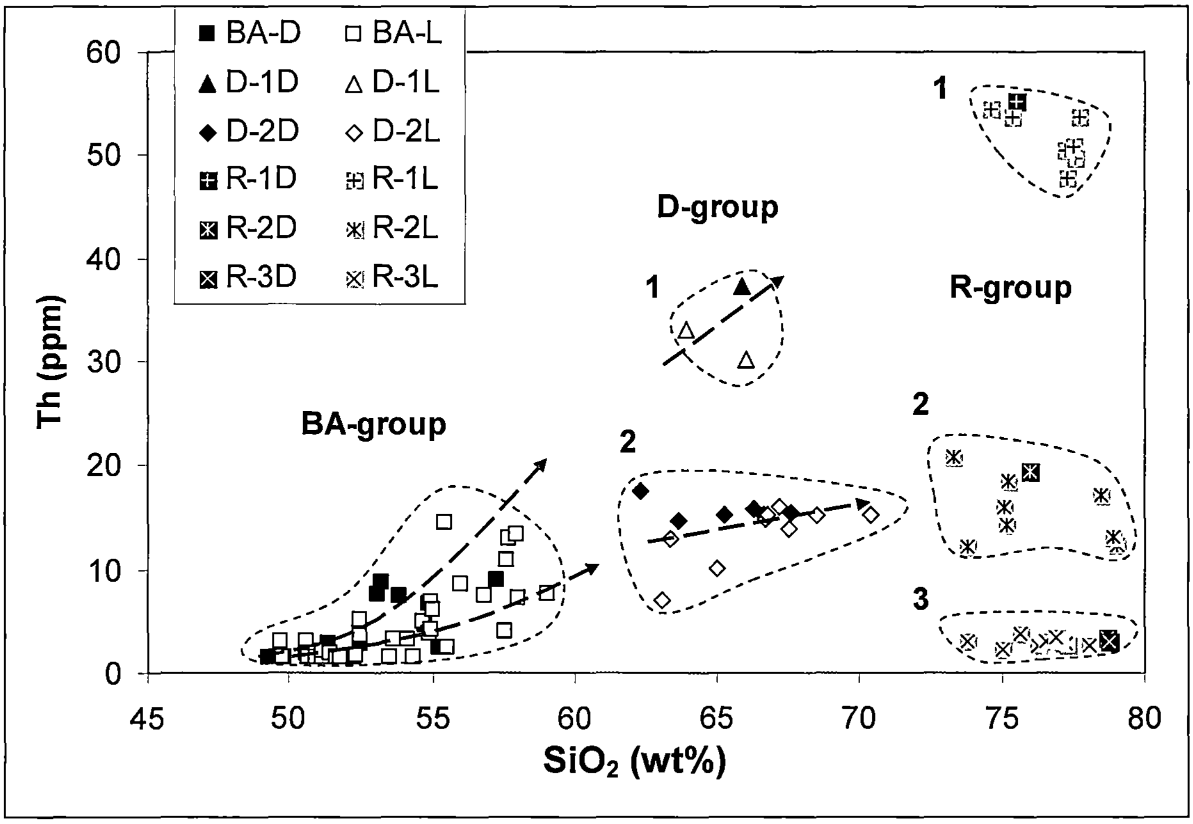

Figure 3.3 CLT rocks can be effectively grouped and classified using a Th- SiO_2 plot (see text for discussion).

3.4.2 Petrography

The BA-Group

The BA-group is composed of mafic to intermediate (basaltic/andesitic composition) dykes/intrusives (BA-D subgroup) and lavas (BA-L subgroup) with 45-60 wt % SiO_2. The intrusive BA-D subgroup rocks include dolerite, microgabbro, microdiorite and basaltic dykes, whereas the extrusive BA-L subgroup comprises basalt, basaltic andesite and andesite lavas. Representative photomicrographs of BA-D and BA-L subgroup rocks are shown in Figures 3.4 (a) to (d), respectively.

Typically, rocks with basaltic to andesitic compositions, whether lavas or dykes, are either aphyric or sparsely plagioclase- or plagioclase+augite-phyric. Doleritic and microgabbroic rocks show subophitic or ophitic textures, and olivine does not appear to have been present. Several of the more dioritic compositions among the BA group rocks carry hornblende and interstitial biotite.

The D-Group

D-group rocks are intermediate, mainly dacitic (60-71 wt % SiO_2) compositions, and these are divided into 4 subgroups, including D-1D, D-1L, D-2D and D-2L based on Th content and petrographic assignment as dykes and lavas.

Subgroups D-1D and *Subgroup D-1L* include intermediate SiO_2/high Th intrusive rocks from LP-CB (one dyke and one lava) and CK-CB (one lava), and are represented by a single analysed dacitic dyke with microphenocrysts of plagioclase, quartz, biotite and clinopyroxene in a microcrystalline quartzo-feldspathic groundmass (Figures 3.4 e & f), and two dacitic lavas with the phenocryst assemblage plagioclase + clinopyroxene (chloritized) + apatite + Fe-Ti oxide in a recrystallized, formerly devitrified glassy groundmass (Figures 3.4 g & h)

Subgroup D-2D comprises diorite, quartz-diorite and monzodiorite dykes and plugs with medium Th contents, all from CK-WB. Representative rocks in this subgroup show holocrystalline textures defined by intergrown clinopyroxene, plagioclase, hornblende, Fe-Ti oxides and minor interstitial altered biotite and quartz (Figures 3.5 a & b).

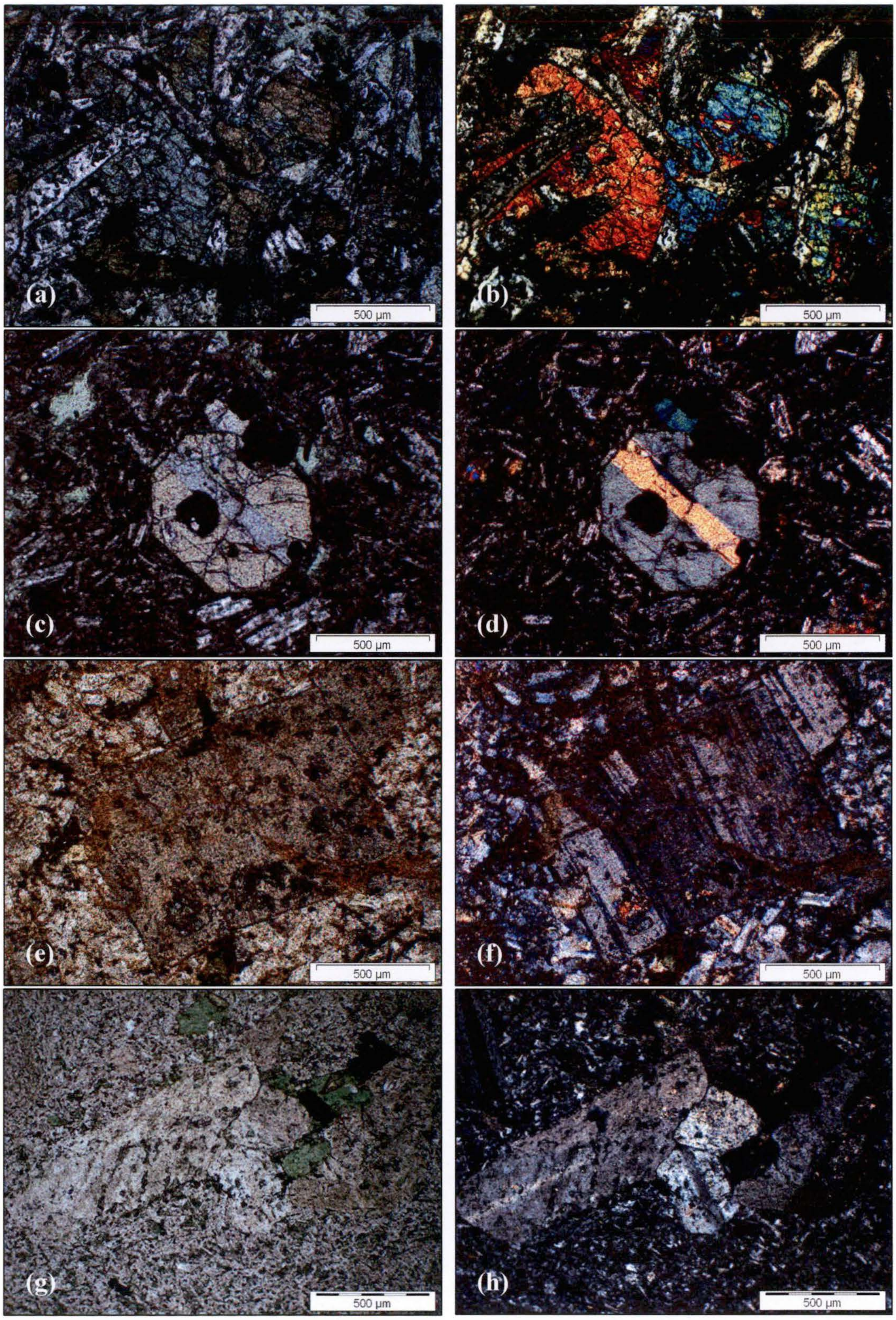

Figure 3.4 Microphotographs showing petrographic features for representative CLT rock sub-groups BA-D (a) & (b), BA-L (c) & (d), D1-D (e) & (f) and D1-L (g) & (h).

Subgroup D-2L includes plagioclase-phyric dacitic lavas from CK-WB and CK-CB. These rocks also contain occasional actinolite-altered clinopyroxene and leucoxene-altered Fe-Ti oxide microphenocrysts in murky, probably originally glassy groundmasses now composed of fine-grained quartzo-feldspathic intergrowths containing common chlorite (Figures 3.5 c & d).

The R-group

R-group felsic compositions are mainly rhyolitic, but include occasional microgranitic-textured dyke rocks. Welded ignimbrites were noted at several locations, as also documented by Barr *et al.,* (2006), but fragmental rocks are considerably less abundant than coherent lavas. On the basis of their Th – SiO_2 relationships (Figure 3.3), rocks in this group are divided into six sub-groups, namely, R-1D, R-1L, R-2D, R-2L, R-3D and R-3L.

Subgroup R-1D includes one high-SiO_2/high-Th intrusive granophyric microgranite, bearing green biotite (Figures 3.5 e & f), from LP-CB.

Subgroup R-1L is composed of plagioclase+quartz-phyric, spherulitic- (Figures 3.5 g & h) and snowflake-textured rhyolitic lavas with high-SiO_2/high-Th content, from the LP-CB.

Subgroup R-2D includes high-SiO_2/medium-Th plagioclase-phyric rhyolitic dykes with granophyric textures (Figures 3.6 a & b) from CK-WB.

Subgroup R-2L comprises high-SiO_2/medium-Th plagioclase+quartz-phyric rhyolitic lavas (Figures 3.6 c & d), and welded rhyolitic ignimbrites from CK-WB, CK-CB and LP-CB. In all samples, formerly glassy groundmasses are now microcrystalline intergrowths of quartz, plagioclase, minor K- feldspar, chlorite and sparse epidote and leucoxene.

Subgroups R-3D and R-3L are high-SiO_2/low-Th plagioclase+quartz-phyric rhyolitic dykes (Figures 3.6 e & f) and lavas (Figures 3.6 g & h).from the LP-WB. Groundmass textures vary from fine-grained holocrystalline quartzo-feldspathic intergrowths in some dykes, to sugary very fine-grained, microcrystalline quartz-feldspar-chlorite intergrowths after glass.

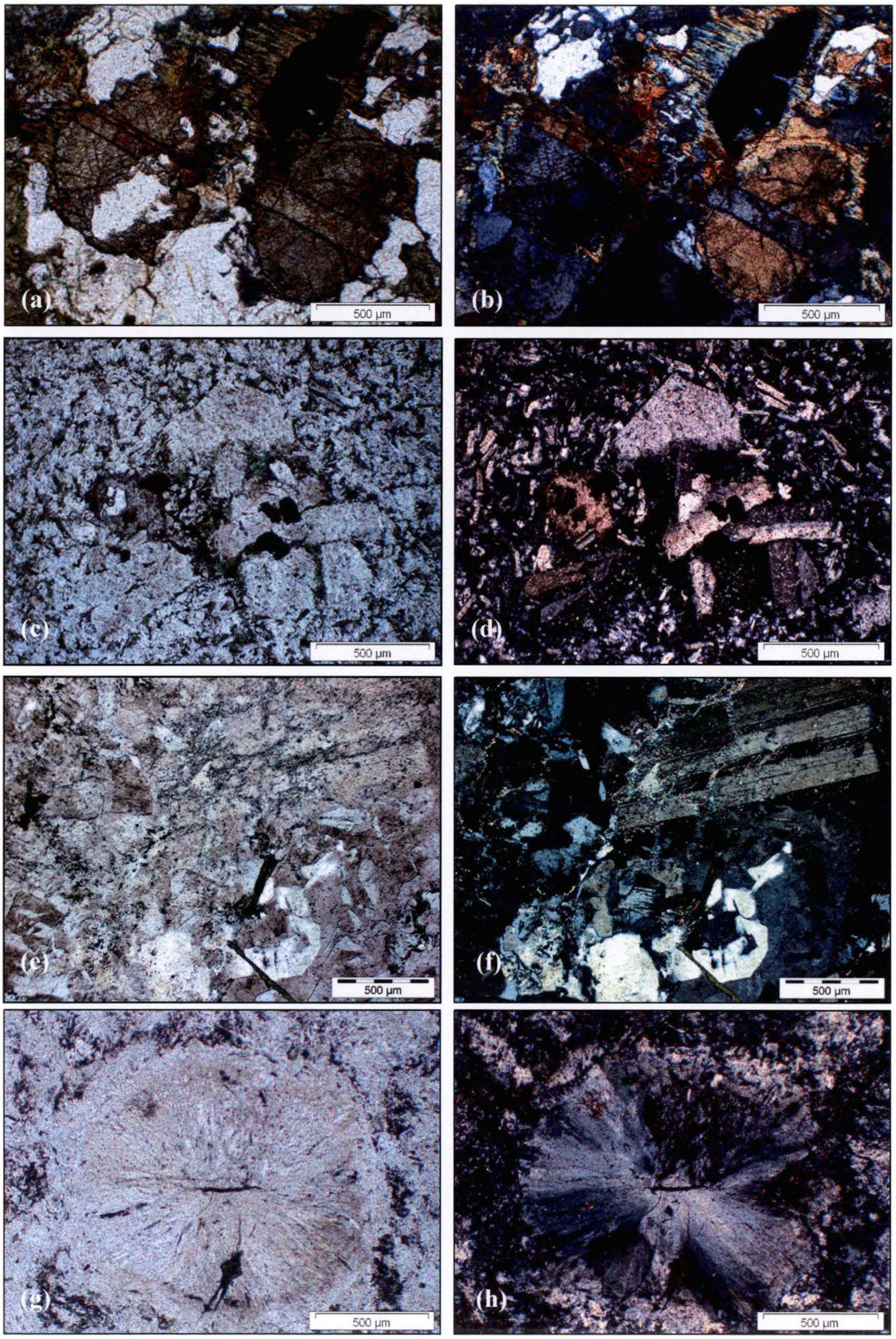

Figure 3.5 Microphotographs showing petrographic features for representative CLT rock sub-groups D2-D (a) & (b), D2-L (c) & (d), R1-D (e) & (f) and R1-L (g) & (h).

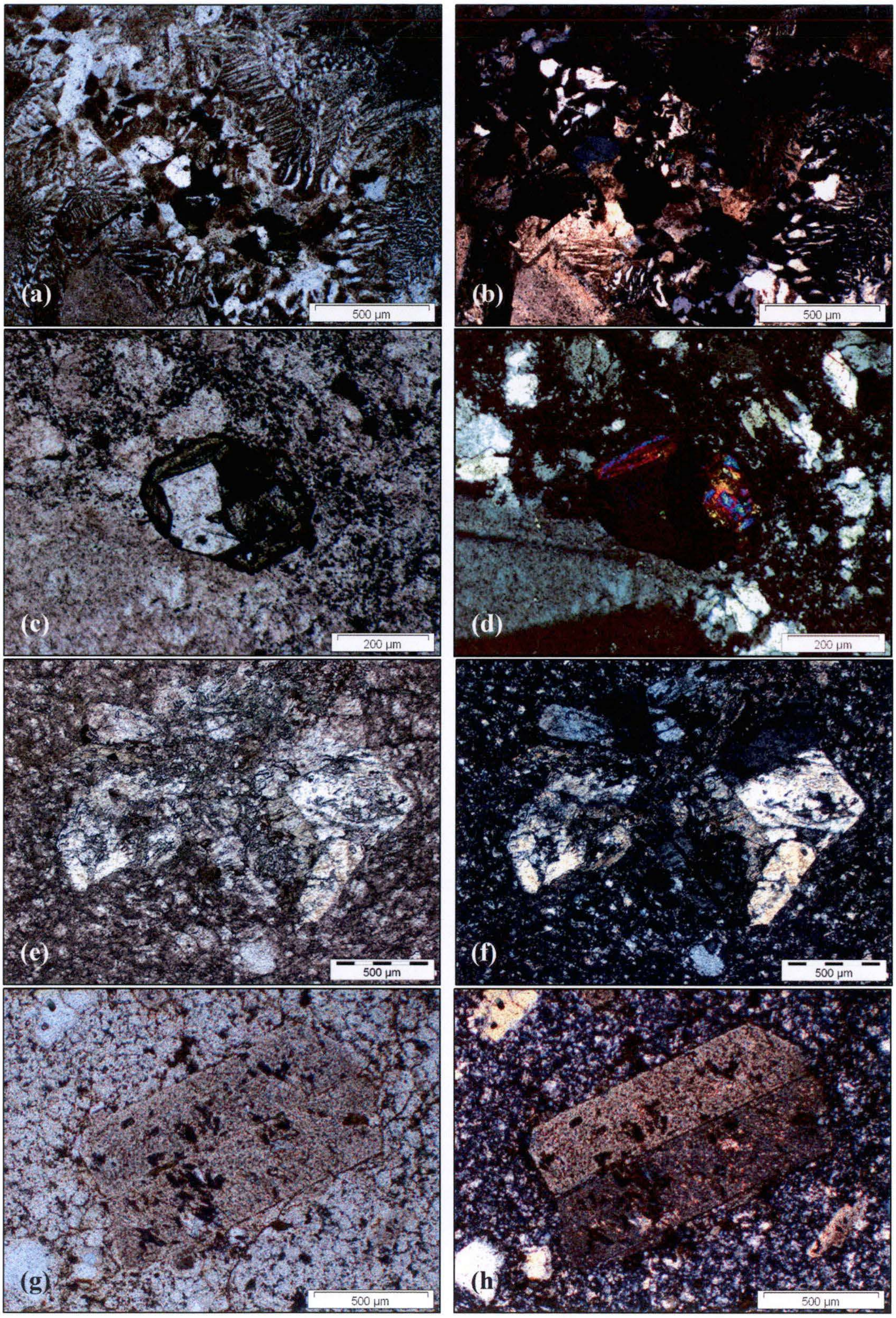

Figure 3.6 Microphotographs showing petrographic features for representative CLT rock sub-groups R2-D (a) & (b), R2-L (c) & (d), R3-D (e) & (f) and R3-L (g) & (h).

3.4.3 Metamorphic Grade and Alteration

All analysed samples show excellent textural preservation. Metamorphic grade varies from prehnite-pumpellyite facies to low greenschist facies, with the latter being defined by the presence of fibrous actinolite usually replacing or fringing clinopyroxene. Plagioclase crystals in both the intrusive and extrusive rocks of all groups may be (i) partly fresh with epidote or sericite alteration, (ii) totally altered to either or both of those minerals, or (iii) totally replaced by clear albite that is sometimes speckled by sericite. Typical assemblages in the BA group rocks include plagioclase-clinopyroxene-epidote-chlorite-albite+/-actinolite+/-prehnite+/-pumpellyite. Carbonate is a rare alteration phase. A detailed study of the CLT metamorphic mineralogy and grade is given in Chapter 5 (Section 5.2.4).

It is well known that regional low-grade alteration of igneous rocks can significantly affect their geochemical compositions. Typically, CaO (and Sr, Ba), the alkaline oxides Na_2O and K_2O, and the K-group trace elements such as Rb, are regarded as being potentially mobile during such alteration, and interpretation of their abundances must be done with care. In contrast, total Fe (measured as Fe_2O_3 via XRF), MgO, Al_2O_3 and the transition (Ni, Cr, V, Sc) and high field strength elements (Ti, P, Zr, Y, Nb, Ta, Hf) are widely regarded as being essentially immobile during low-grade alteration, especially in rocks with excellent textural preservation (summarised in Rollinson, 1993). Therefore, the following evaluation of the geochemical affinities of the Chiang Khong volcanic belt rocks focuses on the immobile elements, but also examines the contents, variation and implications of their K_2O contents.

3.5 Geochemistry of the Chiang Khong Area Igneous Rocks

3.5.1 Major and Trace Element Geochemistry

Of the 71 new whole-rock major and trace element analyses of lavas and dykes from the Chiang Khong area done for this study, 40 are from the CK-WB, 20 from the CK-CB and 11 from the CK-EB (Tables 3.1 and 3.2). Complementing the new data are whole-rock analyses of 8 samples from the CK-WB and 14 from the CK-CB reported by Barr *et al.*, (2006), and 16 analyses of the least altered mafic to intermediate rocks from Panjasawatwong *et al.* (2003), mainly from the CK-WB. Compositional variation diagrams against SiO_2 and MgO are shown for rocks from the CLT volcanic belt in the Chiang Khong region in Figures 3.7 & 3.8. Key points to note from these plots include:

1: Both the CK-WB and CK-CB rock suites show a range of compositions defining broad fractionation trends from mafic to felsic compositions, whereas the CK-EB contains only mafic rocks. Significantly greater major element compositional spread exists at the more mafic end of the compositional spectrum than at the felsic end.

2: Over most of the fractionation range defined by samples from both the CK-WB and CK-CB, the regular decrease in total Fe (reported herein as FeO*) and TiO_2 from mafic to felsic compositions is characteristic of magmas with calc-alkaline affinities.

3: Despite the potential mobility of K_2O, the intermediate and felsic samples from the CK-WB and CK-CB define a high-K calc-alkaline trend, whereas many of the CK-EB mafic rocks fall below that field, suggesting low-K (transitional tholeiitic) or medium-K calc-alkaline affinities for these rocks.

4: Despite the overall similarity in major element variations across the fractionation range for rocks from the CK-WB and CK-CB, HFSE such as Zr, Nb, Y and LREE (Ce shown in Figure 3.8) are consistently slightly higher at any stage of fractionation in CK-WB rocks, suggesting that these suites were derived from different parental magmas, with slightly more HFSE-enriched parental magmas for the Western sub-belt rocks.

5: Most mafic rocks analysed from CK-EB, and a significant suite of mafic rocks (most of them dykes) from the CK-WB show quite high FeO* (11-14%) and more than 1% TiO_2, whereas the CK-CB mafic lavas, and several from the CK-WB, have FeO* and TiO_2 contents <11% and 1.0% respectively (Figure 3.9). A single analysed basaltic dyke from the CK-CB shows the higher FeO* and TiO_2 (12% and 1.6% respectively) characteristic of the higher Fe, higher-Ti group of the CK-WB and CK-EB mafic rocks. The higher-Fe suite is considered to have transitional tholeiitic affinities. Rocks that define this higher-Fe suite in the FeO*-, TiO_2- and V- vs MgO plots (Figures 3.9 a, b & c) also have higher Zr/Nb values (>22) than the other mafic rocks (Figure 3.9d). Since Zr/Nb is unaffected by fractionation, we consider these mafic rocks to be a separate magmatic suite from the high-K calc-alkaline rocks that dominate the CK-WB and CK-CB in the Chiang Khong area. Two REE patterns (Figure 3.9) for the more mafic rocks in the transitional tholeiitic high–Fe, high-Zr/Nb suite show significantly flatter profiles than mafic rocks from the CK-WB and CK-CB, which show typical medium- to high-K calc-alkaline LREE-enriched patterns (Figure 3.10). Notably, the CK-WB high Zr/Nb basaltic dyke with 8.2% MgO has higher chondrite-normalised HREE levels than

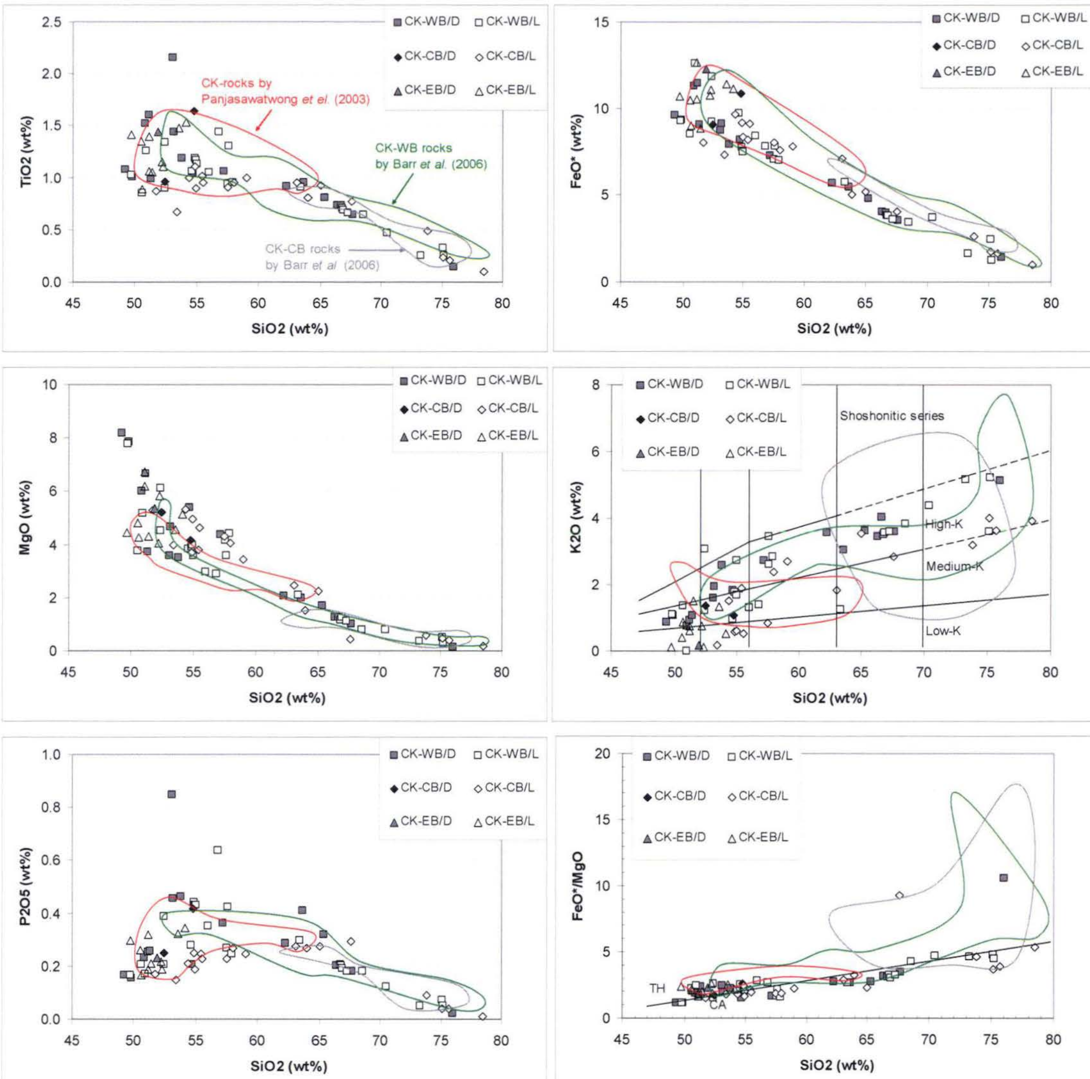

Figure 3.7 Selected major elements vs. SiO_2 (w t% volatile free) variation diagrams of the Chiang Khong area igneous rocks compared to data from Barr *et al.* (2006) and Panjasawatwong *et al.* (2003) from the same belt. CK-WB/D and CK-WB/L = respectively, dykes/intrusive rocks, and lavas, from Chiang Khong Western Belt; CK-CB/D and CK-CB/L = respectively, dykes/intrusive rocks, and lavas, from Chiang Khong Central Belt; CK-EB/D = dykes or intrusive rocks from Chiang Khong Eastern Belt; CK-EB/L = lavas from Chiang Khong Eastern Belt. [K_2O vs. SiO_2 classification scheme after Peccerillo & Taylor (1976) and FeO*/MgO vs. SiO_2 divide after Miyashiro (1974)].

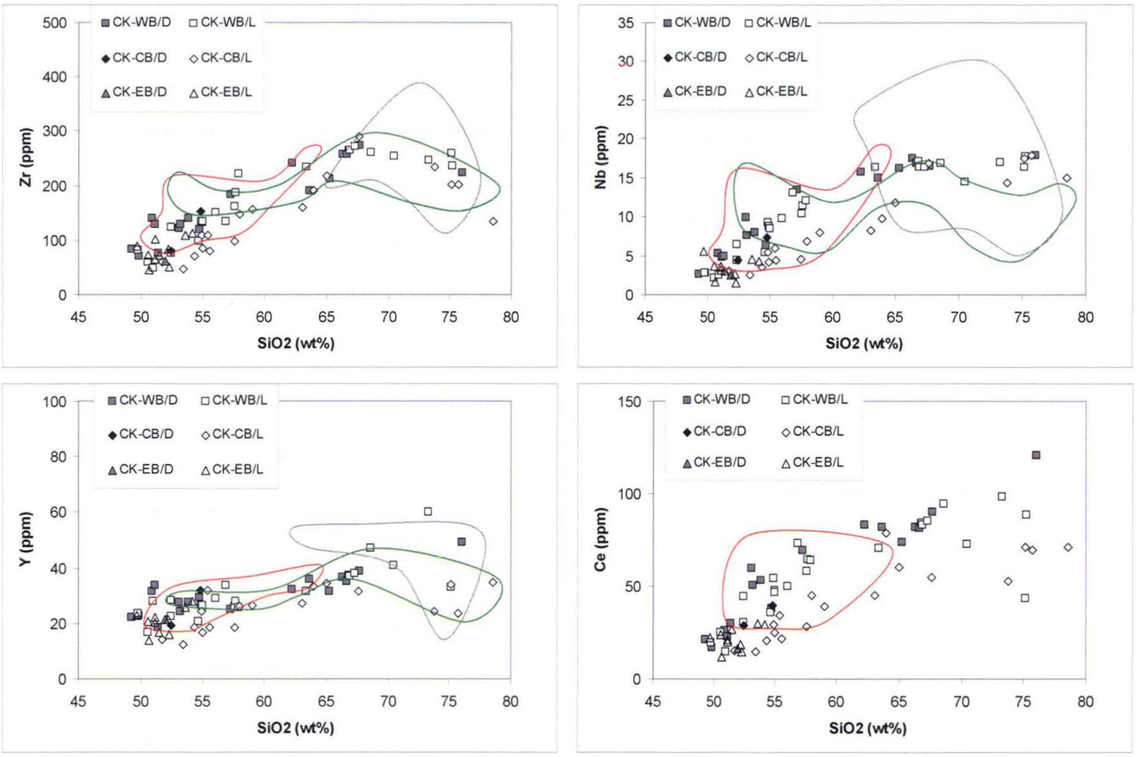

Figure 3.8 Selected immobile high field strength elements, and Ce as representative of LREE, plotted against SiO_2 (wt %) for the Chiang Khong area igneous rocks.

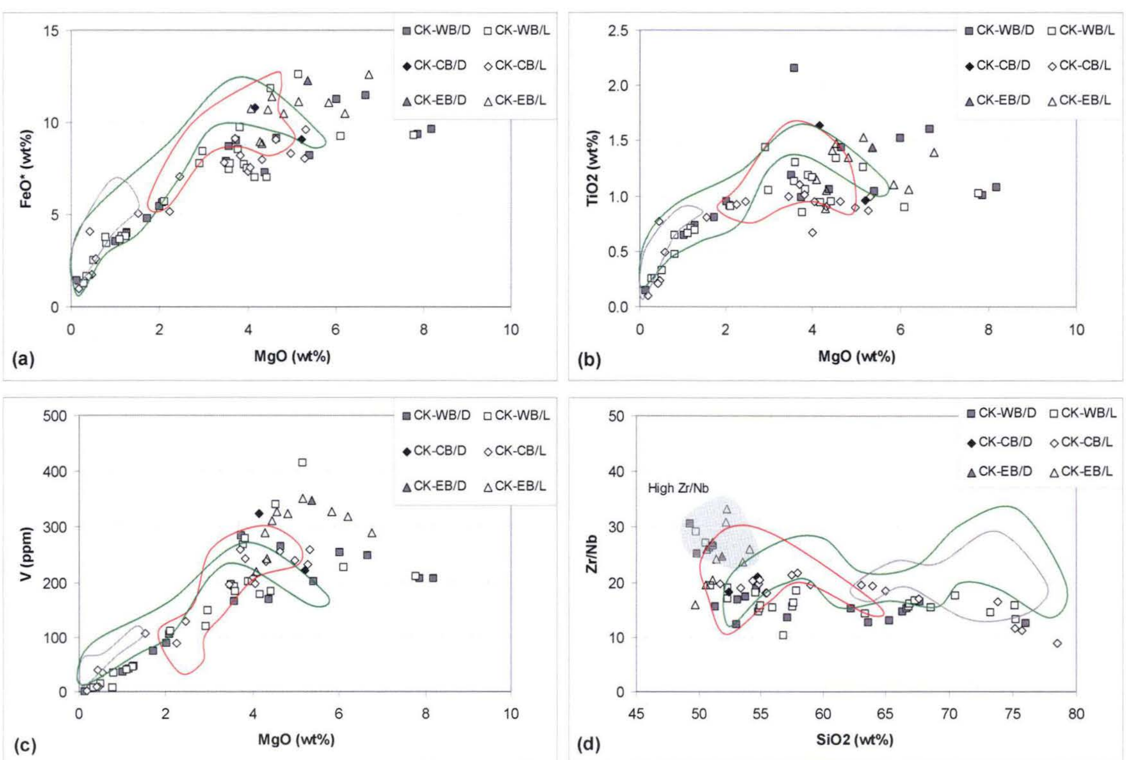

Figure 3.9 Plots of (a) FeO* (wt %), (b) TiO_2 (wt %), and (c) V (ppm) vs. MgO (wt%), and (d) Zr/Nb vs. SiO_2 (wt%) for the Chiang Khong area igneous rocks.

basalts and andesites with 3.8-5.2% MgO from the lower Zr/Nb group (Figure 3.10), and is likely to be comagmatic with the transitional tholeiitic high-Fe rocks in the CK-CB and CK-EB sub-belts.

6: Increasing fractionation from andesitic to dacitic compositions in the calc-alkaline suite rocks leads to higher total REE abundances, but further fractionation to rhyolitic compositions leads to a significant decrease in LREE enrichment, development of a significant negative Eu anomaly, and/or a less pronounced depletion in MREE (Figure 3.11). This late depletion in REE is a common feature of rhyolitic magmas developed via fractionation (or AFC) from dacitic precursors, and can be explained qualitatively by crystallisation and removal of LREE- and MREE-enriched accessory phases such as allanite, monazite and apatite (Miller & Mittlefehldt, 1982).

7: N-MORB-normalised multi-element patterns for all the calc-alkaline lavas (Figure 3.12) show the typical depletion in Nb-Ta relative to adjacent LREE, and the enrichment in LILE relative to HFSE that characterise subduction-related magmas. Patterns for the transitional tholeiitic mafic suite (Figure 3.13) also show significant but relatively subdued Nb-Ta anomalies and LILE enrichment.

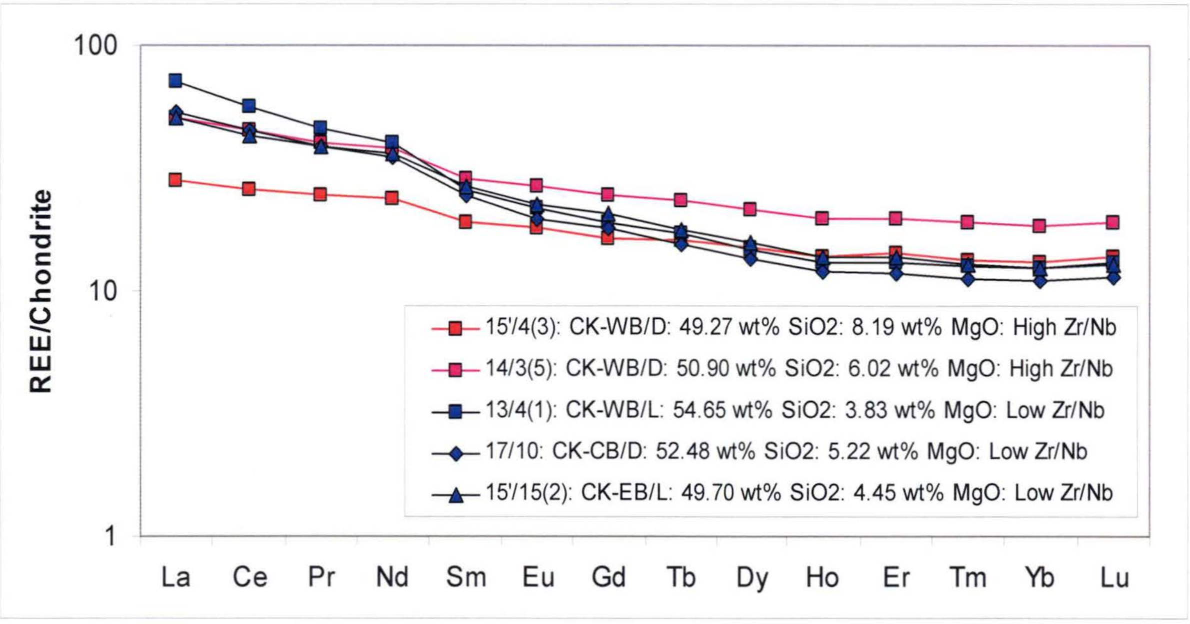

Figure 3.10 Chondrite-normalised REE patterns of representative mafic Chiang Khong area igneous rocks (<55wt% SiO_2). Normalizing values from Sun & McDonough (1989).

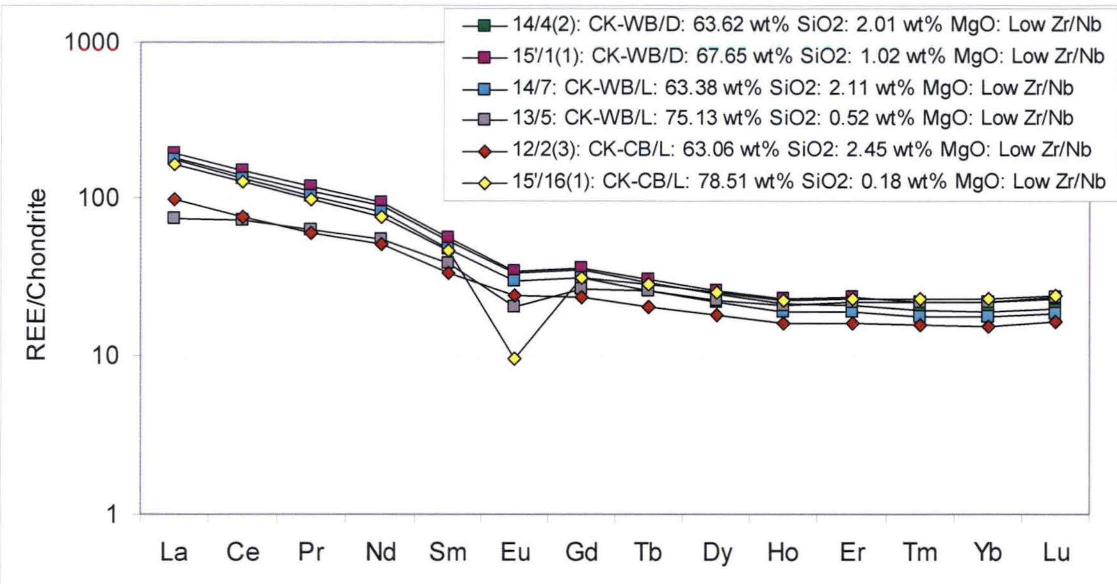

Figure 3.11 Chondrite-normalised REE patterns of representative felsic Chiang Khong area igneous rocks (>60 wt% SiO_2). Normalizing values from Sun & McDonough (1989).

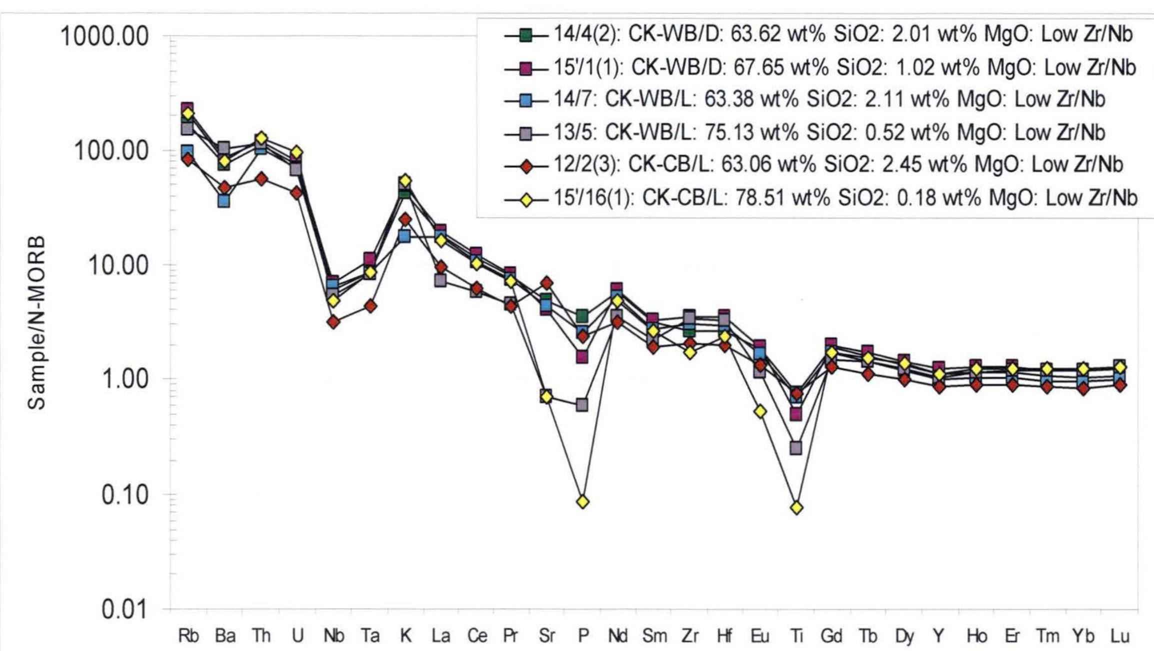

Figure 3.12 N-MORB normalised patterns of representative high-K calc-alkaline intermediate to felsic (>60 wt% SiO_2) rocks from the Chiang Khong area. Normalizing values are from Sun & McDonough (1989).

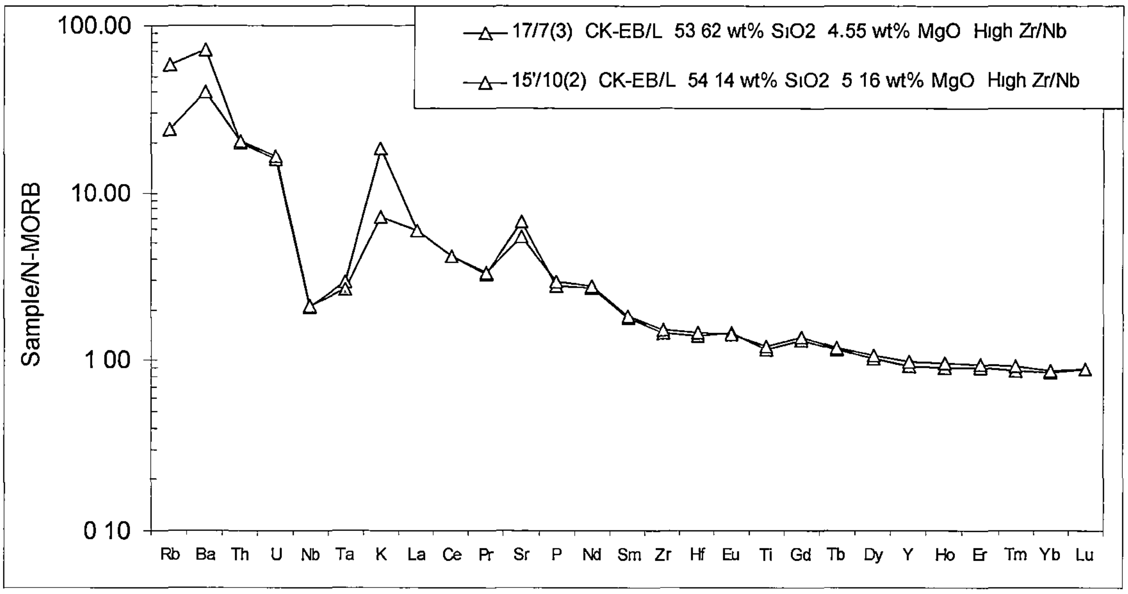

Figure 3.13 N-MORB normalised patterns of representative transitional tholeiitic mafic rocks from the Chiang Khong area. Normalizing values from Sun & McDonough (1989).

3.5.2 Sm-Nd Isotopic Geochemistry of Chiang Khong Area Igneous Rocks

Four samples from mafic to felsic composition from the CK-WB and one basaltic rock from the CK-EB were analysed for Sm and Nd isotopes (Table 3.3). Initial ε_{Nd} values at 220 Ma (ε_{Nd220}) vary from -2.3 to +3.6 with the intermediate to felsic rocks having εNd_{220} = -1.7 to -2.3. This compares with an ε_{Nd240} value of +0.8 reported by Barr *et al.* (2006) for two rhyolites from the CK-CB. Figure 3.14 shows a strong correlation between SiO_2 and initial ε_{Nd} for the analysed samples, strongly implying that significant amounts of crustal contamination accompanied fractionation from basalt to rhyolite in the calc-alkaline suite. The least evolved calc-alkaline mafic rocks from the CK-WB, and the transitional tholeiitic basalt from the CK-EB, have ε_{Nd} values between +1.2 and +3.6, indicating either (1) derivation from a lithospheric mantle source that was significantly enriched in crustal components compared to the convecting asthenosphere at this time, or (2) that even the more mafic magmas in these suites had suffered significant crustal contamination prior to eruption/emplacement. Longer residence times in the upper crustal magma chambers enabling further fractionation through to rhyolitic compositions also allowed more crustal contamination, a common feature in calc-alkaline magmatic systems in which a spectrum of compositions from basalt to rhyolite is present (eg. Ewart *et al.* 1992).

Table 3.3. Neodymium isotopic data for representative Chiang Khong area igneous rocks.

Sample	Sub-belt	Rock type	Sm (ppm)	Nd (ppm)	$^{147}Sm/^{144}Nd$	$^{143}Nd/^{144}Nd$	ε_{Nd} now	Age (Ma)	ε_{Nd} (220 Ma)
15'/4(3)	CK-WB	Dolerite dyke	2.88	10.78	0.1614	0.512770	2.57	220	3.6
13/4(2)	CK-WB	Phyric andesite	5.33	23.13	0.1394	0.512647	0.18	220	1.8
14/7	CK-WB	Dacite	7.02	35.58	0.1193	0.512438	-3.90	220	-1.7
13/5	CK-WB	Rhyolite	5.70	24.16	0.1425	0.512444	-3.78	220	-2.3
15'/15(2)	CK-EB	Basalt	4.02	16.48	0.1473	0.512627	-0.21	220	1.2

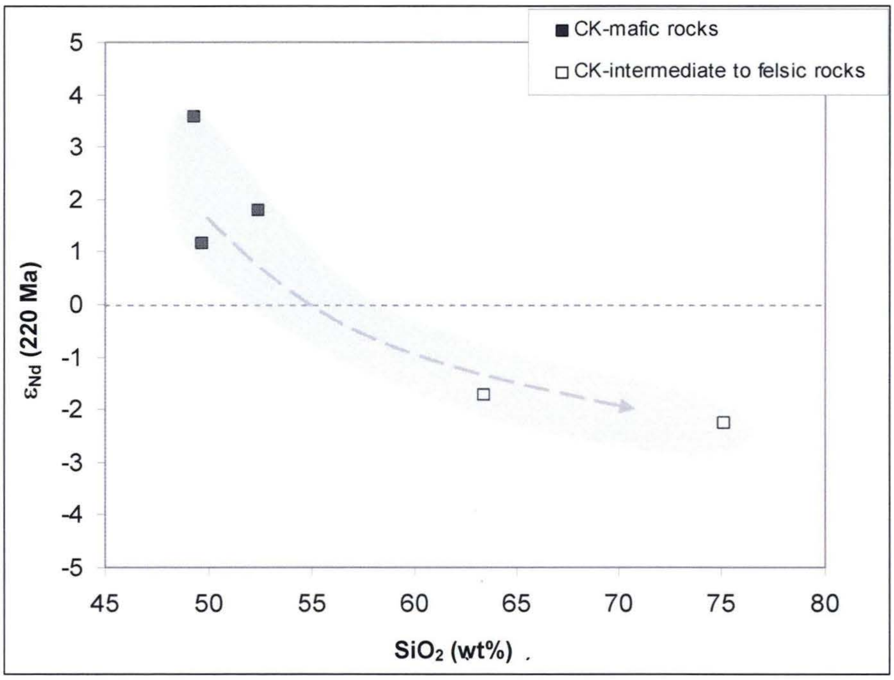

Figure 3.14 Initial ε_{Nd} value at 220 Ma [ε_{Nd} (220 Ma)] plotted against SiO_2 (wt%) for representative igneous rocks from the Chiang Khong area. Although the trend of decreasing ε_{Nd} with increasing SiO_2 is typical of assimilation-fractional crystallisation (AFC) involving relatively older, radiogenic crust, no attempt is made herein to model this process due to the absence of information on the likely crustal contaminants involved.

3.5.3 Summary of Chiang Khong Area Igneous Rocks

Two major rock suites in the Chiang Khong area sub-belts of the CLT volcanic belt have been identified. These include a felsic lava-dominated basalt-andesite-dacite-rhyolite high-K calc-alkaline suite, present in the CK-WB and CK-CB sub-belts, and a mafic-dominated transitional tholeiitic suite represented by lavas in the CK-EB sub-belt, and occasional dykes through the calc-alkaline lavas in the CK-WB and CK-CB. Since our zircon dates for rhyolites in the CK-WB and CK-CB are essentially identical, these sub-belts are presumably sampling formerly more or less adjacent high-K calc-alkaline volcanoes that have been disrupted by thrust faulting (see Chapter 5).

3.6 Geochemistry of the Lampang Area Igneous Rocks

3.6.1 Major and Trace Element Geochemistry

Major and trace element analyses of Lampang area igneous rocks are plotted against SiO_2 in Figures 3.15 & 3.16, in which they are compared with rocks described above from the Chiang Khong area. Note the following key points:

1: Most igneous rocks from the Lampang area have felsic compositions. The LP-CB igneous rocks define a broad, continuous fractionation series from rare mafic/intermediate members to abundant felsic compositions. The fractionation trend of rocks from the LP-CB, with continuously decreasing total Fe and TiO_2 towards felsic compositions, is characteristic of calc-alkaline magmatic affinities. Rocks from the Long area also appear to define a calc-alkaline suite, although for this region felsic rocks are absent.

2: In contrast, LP-WB rocks comprise a bimodal suite, with two mafic lavas and the bulk of the volcanic pile having felsic compositions. The LP-WB felsic rocks show distinctively higher contents of TiO_2, Fe total and MgO compared to the LP-CB suite at any SiO_2 level, and are regarded as a transitional tholeiitic suite.

3: Despite the potential mobility of K_2O, the intermediate and felsic rocks from the LP-CB define a high-K calc-alkaline suite, whereas the bimodal LP-WB mafic and felsic rocks consistently plot as a low-K calc-alkaline or transitional tholeiitic series, an assignment in keeping with their particularly low Th contents.

4: The low-Th felsic suite from the LP-WB shows lower contents of Nb and Ce than the high-Th felsic rocks from the LP-CB (Figures 3.16c, e), and has no compositional correlatives in the Chiang Khong region. These rhyolites have almost flat REE patterns at 15 to 40 times chondritic levels, with negative Eu anomalies (Figure 3.17a).

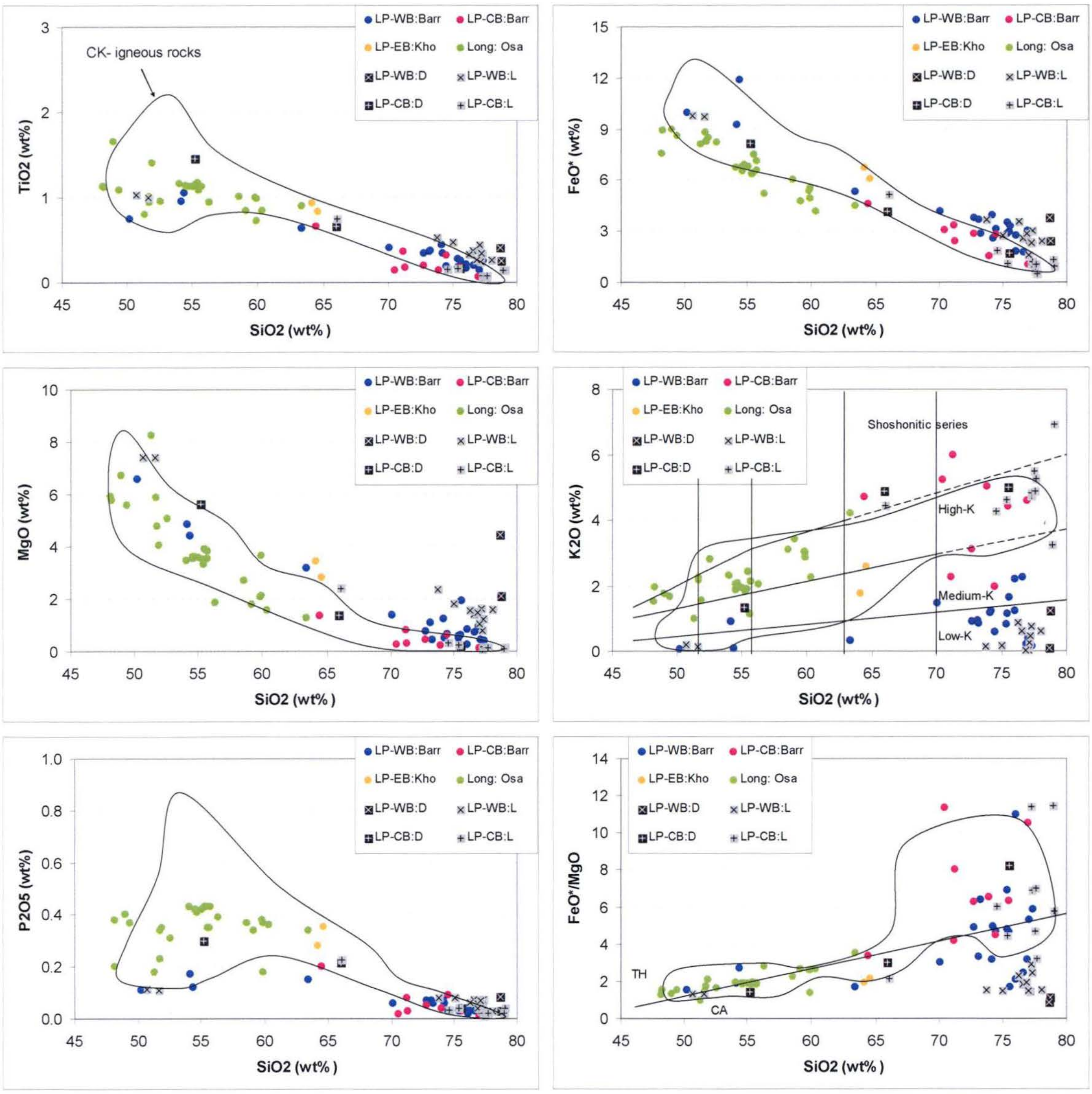

Figure 3.15 Selected major elements vs. SiO_2 (wt% volatile free) variation diagrams for the Lampang region igneous rocks also showing data for LP-WB and LP-CB from Barr *et al.* (2000); and for igneous rocks from the Long area of Osataporn (2007) and fields for igneous rocks from the Chiang Khong area.

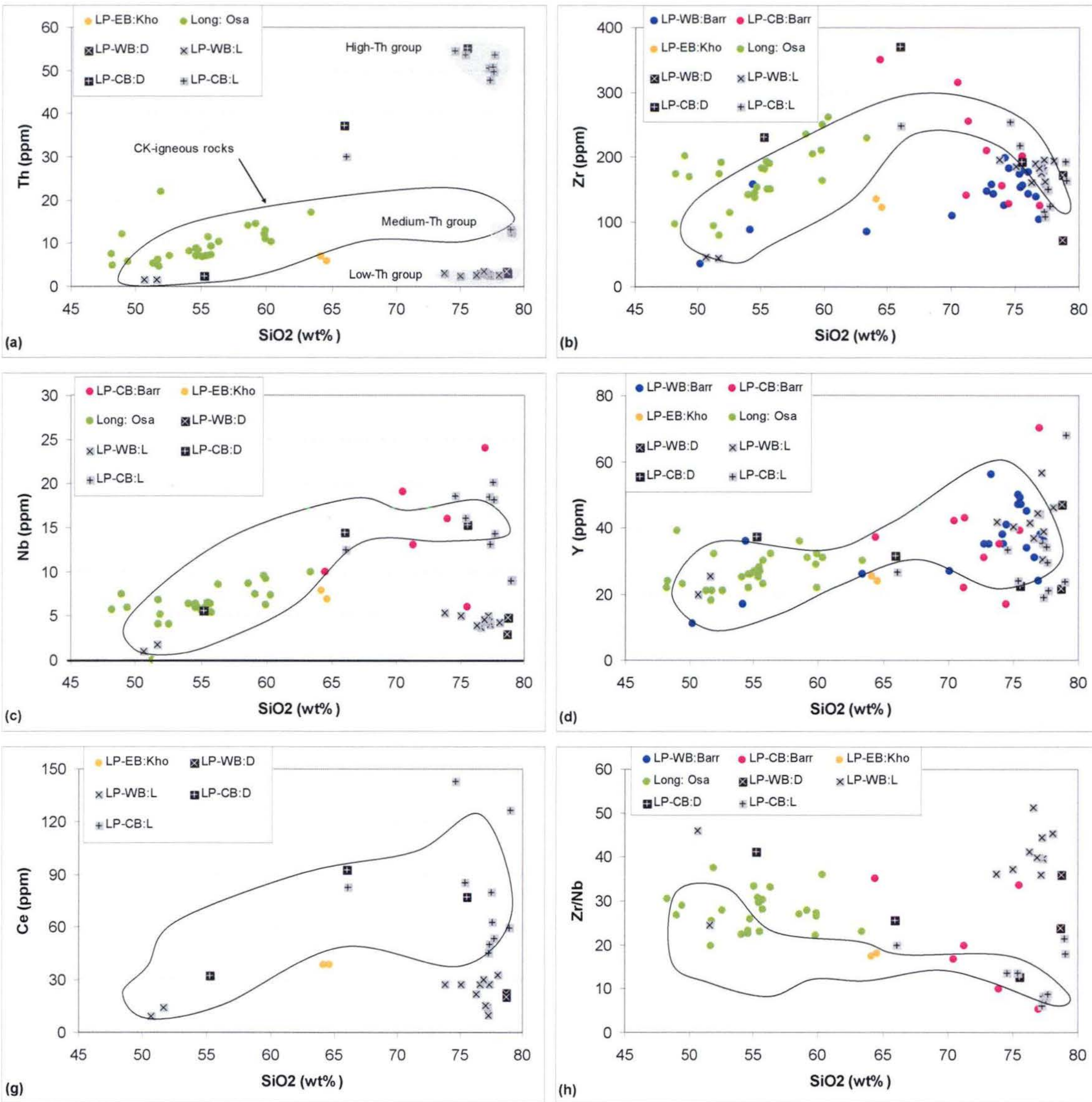

Figure 3.16 Selected immobile high field strength elements in ppm from (a) to (e)] and Zr/Nb (f) plotted against SiO_2 (wt%) for the Lampang belt igneous rocks compared to igneous rocks from the Chiang Khong area.

5: The passage from dacitic to rhyolitic compositions for the LP-CB rocks is marked by a decrease in LREE and MREE contents and the development of significant negative Eu anomalies (Figure 3.17a).

6: REE patterns for the basaltic rocks from the LP-WB are almost flat to very slightly LREE-enriched, with mild HREE depletion (Figure 3.17b) and weak positive Eu anomalies.

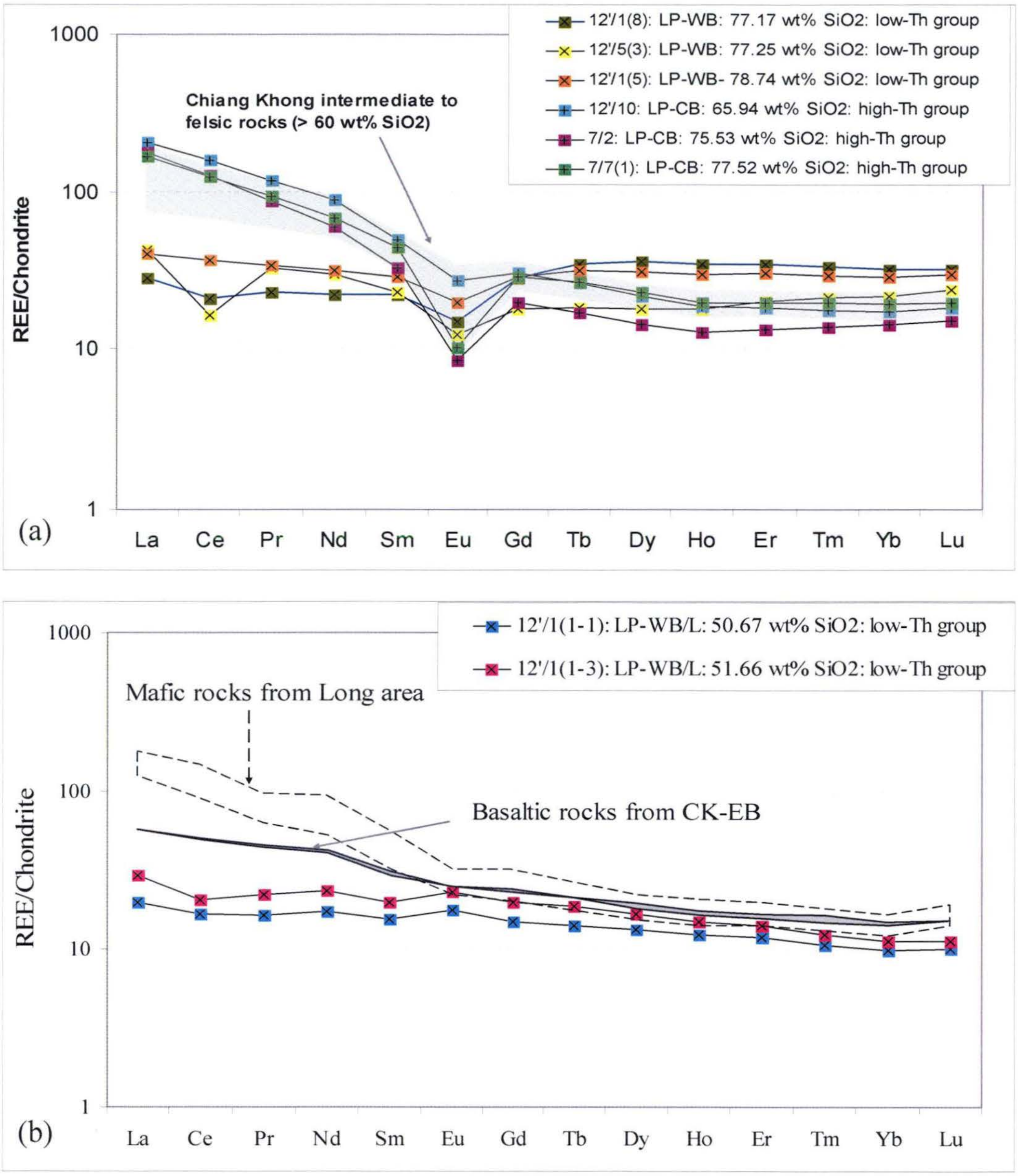

Figure 3.17 Chondrite-normalised REE plots of (a) low-Th LP-WB rhyolites and high-Th felsic rocks from LP-CB, showing shaded field for the Chiang Khong rocks with >60% SiO_2, and (b) for mafic rocks from the LP-WB and comparative field for Long area and CK-EB basalts. Normalising values are from Sun & McDonough (1989).

7: The N-MORB normalised patterns of the LP-WB low-Th group of felsic rocks is distinctly different from the typical high-K calc-alkaline CLT lavas and dykes, with notably lower levels of all LILE (including Nb, Ta, Th, U) (Figure 3.18a). The N-MORB normalized patterns of the LP-WB mafic rocks (Figure 3.18b) show negative Nb, Zr, Hf, Sr and Ti anomalies with small positive peaks at Ba, Nb and Eu.

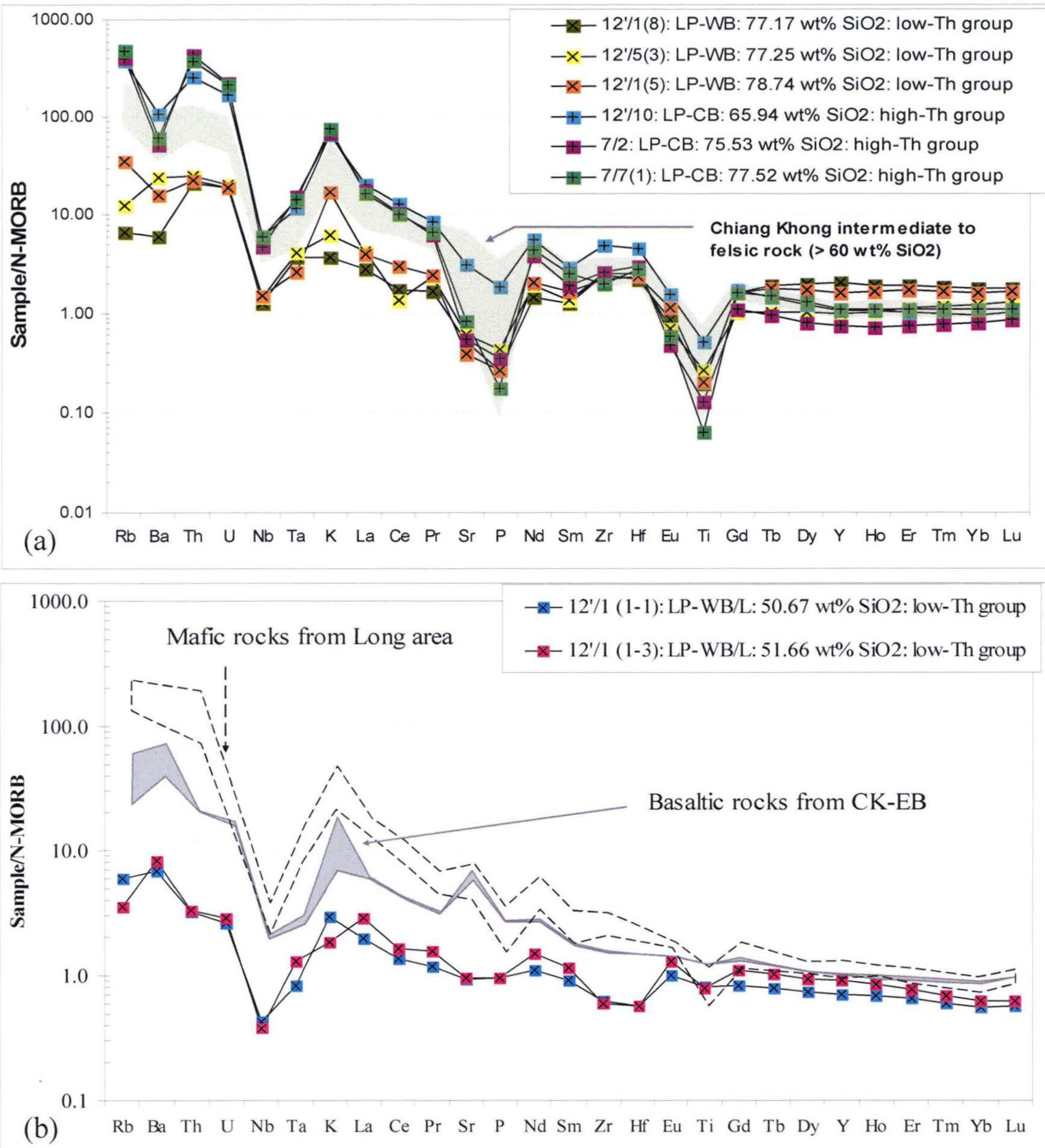

Figure 3.18 N-MORB normalised patterns of (a) felsic rocks from LP-WB and LP-CB compared with field for Chiang Khong rocks with >60% SiO_2, and (b) for representative low-Th mafic rocks of LP-WB compared to mafic rocks from Long area and CK-EB basalt. Normalising values are those of Sun & McDonough (1989).

3.6.2 Sm-Nd Isotopic Geochemistry of Lampang Area Igneous Rocks

Four samples from mafic to felsic composition from the Lampang area were analysed for Sm and Nd isotopes (Table 3.4). Basic to felsic rock for LP-WB have positive ε_{Nd230} values of about + 5. Conversely, intermediate to felsic composition for the LP-CB rocks have highly evolved Nd isotopic characteristics with $\varepsilon_{Nd(230)}$ = -4.6 to -5.6 (Figure 3.19).

Table 3.4 Neodymium isotopic data for representative Lampang igneous rocks.

Sample	Sub-belt	Rock type	Sm (ppm)	Nd (ppm)	$^{147}Sm/^{144}Nd$	$^{143}Nd/^{144}Nd$	ε_{Nd} now	Age (Ma)	$\varepsilon_{Nd}(T)$
12'/1 (1-1)	LP-WB	Basalt	2 26	7 63	0 1796	0 512862	4 37	230	4 9
12'/5 (3)	LP-WB	Rhyolıte	3 37	13.30	0 1534	0 512828	3 71	230	5 0
12'/10	LP-CB	Dacıtıc dyke	7 36	39 60	0 1124	0 512226	-8 04	230	-5 6
7/7 (1)	LP-CB	Granıtıc dyke	6 46	30 28	0 1289	0 512305	-6 50	220	-4 6

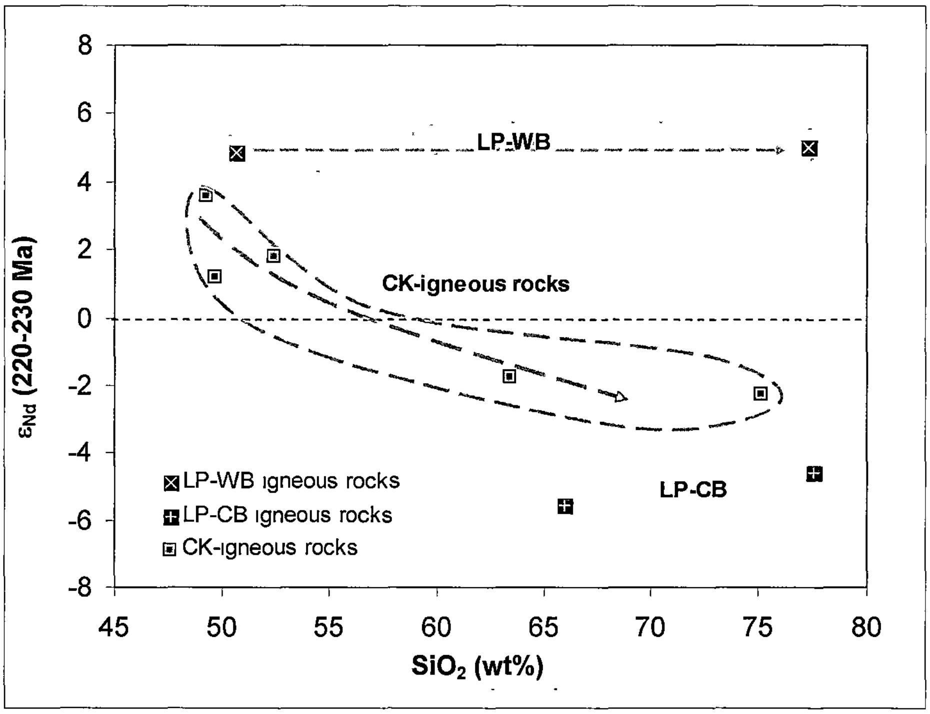

Figure 3.19 Initial ε_{Nd} values at 220 to 230 Ma [ε_{Nd} (220-230 Ma)] vs. SiO_2 (wt%) for representative igneous rocks from the Lampang area compared to igneous rocks from the Chiang Khong area.

Comparative Nd isotope data for two rhyolites from the LP-WB (Doi Ton belt of Barr *et al.,* 2000) have ε_{Nd240} values of about +4.92 (Barr *et al.,* 2000). The positive initial ε_{Nd} values of the LP-WB igneous rocks are slightly higher than those of basalts from the CK-WB dolerite dykes and CK-EB basalts, suggesting derivation from lithospheric mantle or contamination of convecting asthenosphere-derived magmas during ascent. Much lower initial ε_{Nd} values of the LP-CB felsic rocks suggest derivation from mafic precursors via assimilation – fractional crystallisation processes (Figure 3.19).

3.6.3 Summary of Lampang Area Igneous Rocks

Rocks from the LP-WB constitute a distinctive bimodal suite of low-K basalts and rhyolites. The felsic rocks make up a low-Th, low-Nb suite with flat REE patterns and have no compositionally correlative suite from anywhere within the CLT Volcanic Belt. Of two possible petrogenetic scenarios, one involving derivation of these rhyolites via fractional crystallisation from associated basalts, the other via partial melting of low-K metabasic rocks in the fold belt basement, the latter model is favoured (see below).

Mainly felsic lavas constitute the igneous rocks in the LP-CB segment, and intermediate and mafic lavas with high-K calc-alkaline affinities occur in the Long intermontane basin (between the LP-CB and LP-EB). Very limited, poor outcrops of LP-EB were found to be highly altered, silica metasomatised rocks.

3.7 Petrogenesis of Mafic Rocks from the Chiang Khong and Lampang Areas

Table 3.5 presents a summary of the major magmatic groups and affinities represented in each of the sub-belt areas of the Chiang Khong and Lampang regions. As mafic rocks are invariably more useful and diagnostic in determining the tectonic setting of eruption of igneous rock suites, in this section I compare the mafic suites in both regions prior to evaluation of their tectonic affinities.

The general assignment of magmatic affinities shown in Table 3.5 based on K_2O contents is broadly consistent, reflecting the careful petrographic filtering of best preserved samples for analysis. However, in evaluating their magmatic affinities, it is preferable to use those elements widely considered to be immobile during low-grade metamorphism. Typically, these are the high field strength elements (Ti, Zr, Nb, Ta, Hf, Th, P) and the REE. The latter are particularly useful in such an assessment, as enrichment in LREE (ie. chondrite normalised La/Sm) typically correlates closely with enrichment in the more mobile K-group elements (Gill, 1981; Tatsumi & Eggins, 1995), and can be used as a general proxy for K in studies of altered metabasaltic rocks.

Table 3.5 Summary of magmatic affinities of igneous rocks in the CLT, showing occurrence in the various sub-belts.

The Chiang Khong Area	Western sub-belt (CK-WB)	Central sub-belt (CK-CB)	Eastern sub-belt (CK-EB)
	Basalt-andesite-dacite-rhyolite	Basalt-andesite-dacite-rhyolite	Basalt and basaltic andesite
	Mainly medium-K & high-K calc-alkaline, some low-K transitional tholeiitic	Mainly low-K to medium-K calc-alkaline	Low-K transitional tholeiitic
The Lampang Area	Western sub-belt (LP-WB)	Central sub-belt (LP-CB)	Long sub-belt (Long)
	Bimodal	Felsic lava and rare mafic dyke	Basalt and basaltic andesite
	Low-K rhyolite Low- to medium-K transitional tholeiitic	High-K felsic lavas low- to medium-K transitional tholeiitic mafic dyke	High-K calc alkaline

It was noted in Section 3.5.1 that the mafic rocks represented in the Chiang Khong area define a broad spectrum of compositions extending from generally more Fe-rich, lower-K suites that have been assigned transitional tholeiitic affinities, through typically medium-K calc-alkaline suites to rocks that have high-K calc-alkaline affinities. Immobile trace element ratios that reflect source mantle values, exemplified by Zr/Nb, also show a range of values between ~15 and 30. The mafic rocks from the Lampang area (including the Long area), extend this range to include basalts with even less LREE-enrichment (LP-WB) and more strongly LREE-enriched high-K calc-alkaline basalts (Long). Figure 3.17b and 3.18b show the range of REE patterns and N-MORB normalised multi-element patterns, respectively, of mafic rocks from the CLT. Extents of LREE enrichment agree well with K_2O contents, and show that the least LREE-enriched, lowest-K lavas occur in LP-WB, whereas slightly more LREE-enriched basaltic lavas and dykes from the CK-EB have consistently higher incompatible HFSE (e.g., Th, Nb, Ta, P) element abundances and K_2O contents. Basalts from the Long area show the highest K_2O contents (typical of high-K calc-alkaline basalts) and correspondingly, have the strongest LREE- and incompatible element enrichment.

The key point from this comparison is that at the basaltic end of the compositional spectrum, there is a notable diversity of magmatic affinities from low-K transitional tholeiitic-type magmas to high-K calc-alkaline magmas in the CLT belt. Evidence presented in Chapter 4 indicates that these diverse magma types are essentially contemporaneous.

Lower Zr and Nb contents than typical N-MORB at similar levels of fractionation (Figure 3.20) suggest that the source mantle for the CLT mafic rocks was consistently more depleted in HFSE than N-MORB. However, the same rocks show significant, albeit variable, LILE enrichment. Plots of immobile LILE such as Th- and Ce vs Nb (Figures 3.21 a & b; note Long data was not used due to unreliable Th and no Ce reported) show that the source mantle from which the CLT basalts were derived was relatively enriched in LILE and depleted in Nb relative to N-MORB. This coupled HFSE depletion and LILE enrichment is the defining character of magmas derived from subduction-modified (supra-subduction zone) upper mantle.

Available data, therefore, suggest that the CLT parental mafic magmas were generated by partial melting of subduction-modified upper mantle. Furthermore, the range of Zr/Nb values and extents of LREE enrichments indicate that either variable upper mantle compositions with these broad features, or a range of extents of partial melting, were involved in the production of these magmas. However, the Nd isotopic data for CLT rocks showed strong evidence for the operation of assimilation – fractional crystallisation processes (AFC) in generating these suites, with ε_{Nd} values between +4.9 and +1.2, considerably below the values for the Triassic convecting asthenosphere. Plots of Ce vs Nb (Figure 3.21a) and Th vs Nb (Figure 3.21b) show that the more mafic CLT compositions extend between the field of most depleted CLT rocks and that for average upper continental crust, supporting the isotopic data in demonstrating that significant crustal contamination accompanied fractionation of these magmas.

The following section is a discussion of the geochemical information presented above in terms of determining the tectonic setting of eruption of the CLT igneous rocks.

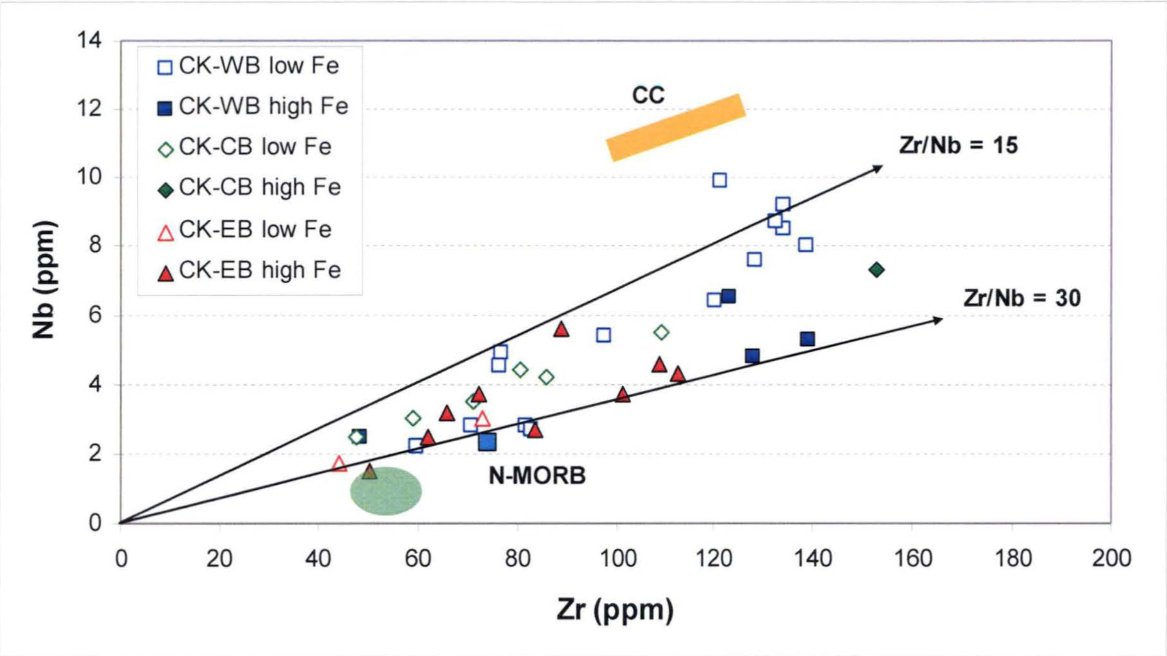

Figure 3.20 Nb vs Zr for mafic rocks (< 55 wt% SiO2) from the Chiang Khong area showing the range of Zr/Nb values within and between the three sub-belts. Samples have been assigned to higher-Fe (>10 wt% FeO*) and lower-Fe (<10 wt% FeO*) groups to emphasize that there appears to be a transition between the more Fe-rich transitional tholeiitic rocks and those with more calc-alkaline affinities. Note; field for continental crust (cc) after Rudnick & Fountain, 1995 and Taylor & McLennan, 1995; N-MORB after Sun & McDonough, 1989; green field represents possible parental magma composition for the least enriched CLT igneous rocks.

3.8 Discussion – Tectonic Setting of Eruption of CLT Igneous Rocks

A defining feature of the CLT igneous rocks is that they represent a series of essentially contemporaneous magmatic suites, varying from basalt to rhyolite, that show a striking compositional range, from low-K transitional tholeiitic rocks, through to high-K calc-alkaline rocks. Parental magmas appear to have been derived from subduction-modified upper mantle, and assimilation-fractional crystallisation processes involving older, radiogenic crust strongly affected the compositions of most samples, especially the felsic rocks. At least one felsic suite, the low-K, low-Th rhyolites in the LP-WB, may represent partial melts of tholeiitic metabasaltic rocks in the fold belt basement.

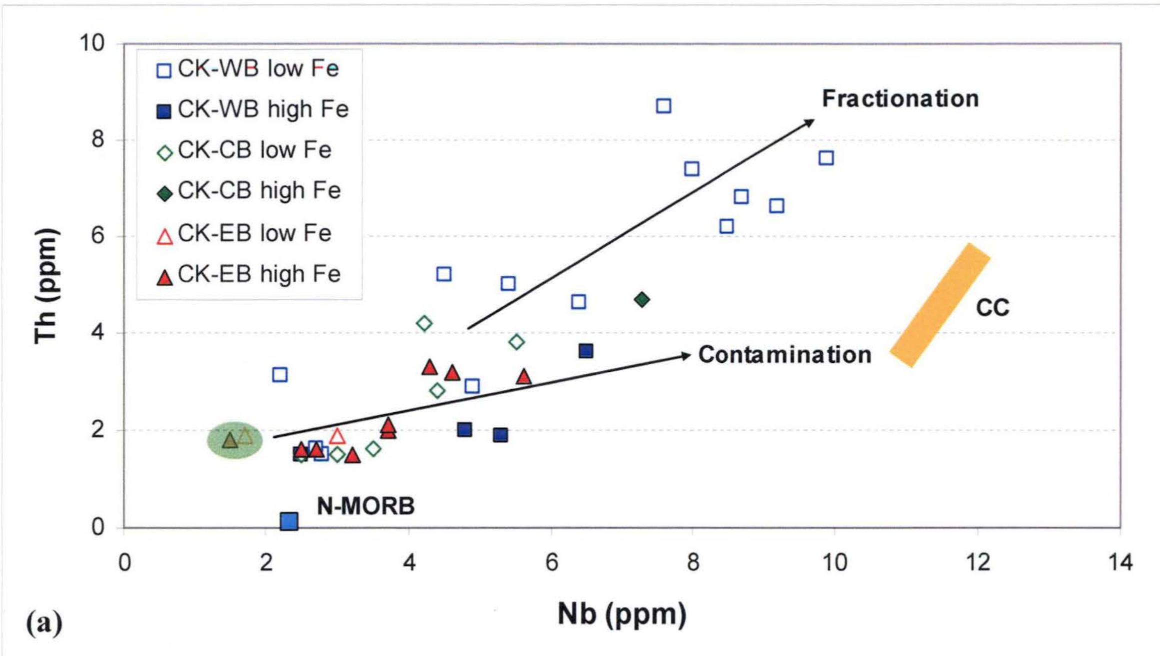

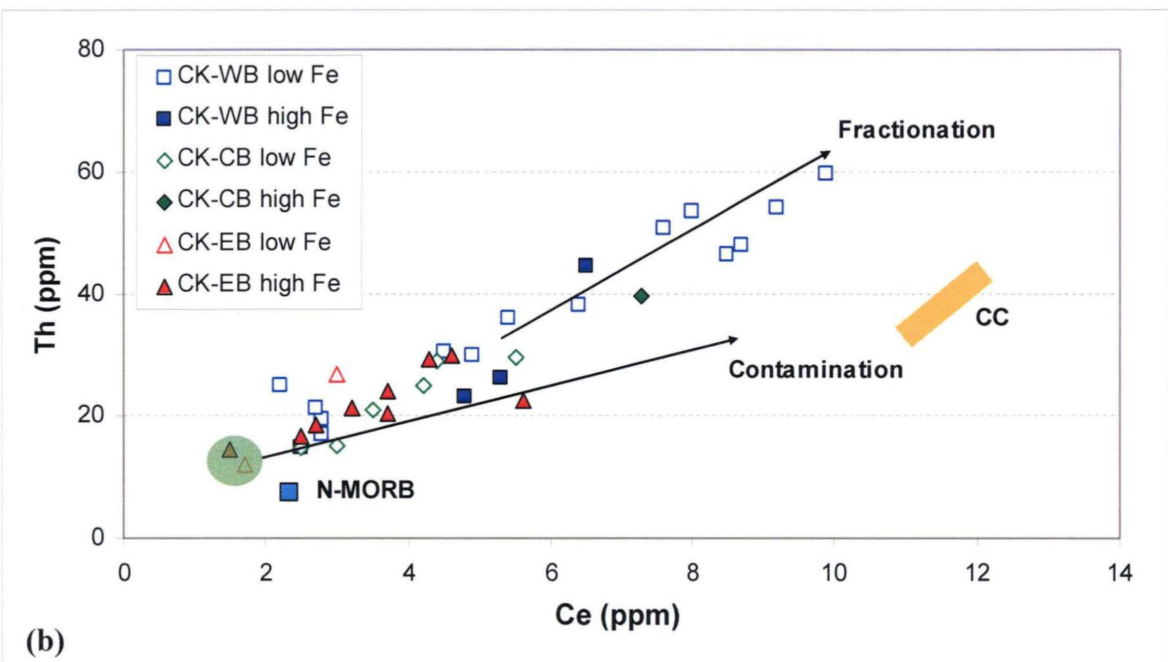

Figure 3.21 Plots of Nb- vs Th (a) and Ce (b) for CLT igneous rocks, showing field of most depleted CLT rocks, field for continental crust and N-MORB. Symbols on diagrams as in Figure 3.20.

Barr *et al.*, (2000 & 2006) suggested that the geochemical data for the CLT lavas, occurrence of welded ignimbrites, and their close association with non-marine red beds, indicated formation in a mature continental margin volcanic arc. In particular, the predominance of felsic lavas and relative paucity of mafic rocks in most of these sequences suggest a substantial thickness of continental crust beneath the region during this Middle to Late Triassic magmatism. Here is noted, however, that the relatively restricted range of radiometric ages recorded from the CLT (230-220 Ma in Chapter 4) and the apparent absence of Early Triassic volcanics is perhaps surprising if the CLT volcanic rocks formed in a continental margin arc, wherein subduction-related magmatism usually shows a long time span.

Although formation of the CLT igneous rock suites in a continental margin arc such as the Andes, Japan or Mexico cannot be absolutely precluded, one other tectonic setting should be considered as a possible scenario for the Late Triassic magmatism in northern Thailand. This is a Basin and Range-type, post-orogenic extensional setting, not necessarily related to contemporaneous subduction, or perhaps related to flat-slab subduction. In either of these latter settings, extension leads to magma generation from the subcontinental lithospheric mantle, which may have been enriched in LILE during some earlier subduction episode, producing calc-alkaline magmas. Calc-alkaline magmas in such settings have been described by Ewart *et al.* (1992), Bryan (2007) and Bryan *et al.* (1997, 2000) for the Whitsunday Volcanic Province of coastal NE Australia, by Hooper *et al.* (1995), Rogers *et al.* (1995) and Hawkesworth *et al.* (1995) for the type Basin and Range area in western USA, by Rottura *et al.* (1998) and Bussy *et al.* (2000) for the Western Alps, by Smedley (1986) for the Late Palaeozoic of Scotland, by Fan *et al.* (2001, 2003) for the Late Cretaceous of NE China, and by Crawford *et al.* (1992) and Crawford & Berry (1992) for the post-collisional Cambrian Mount Read Volcanics of western Tasmania, Australia.

In such post-orogenic settings, extension and magma generation in the sub-continental lithospheric mantle may be related to gravitational collapse of the newly thickened crustal collage, mantle convection-induced lithospheric thinning and/or detachment, or slab breakoff (e.g., England & Houseman, 1989; Davis & von Blanckenburg, 1995). Flat slab scenarios have been proposed for the type Basin and Range province in W USA by Humphreys (1995) and for SE China by Li & Li (2007).

Basin and Range-type magmatism and tectonics in western USA, and in the Cretaceous Whitsunday Province of eastern Australia, is characterised by felsic-dominant magmatism, and transitional tholeiitic to calc-alkaline mafic rocks. Intermediate compositions are considered to be derived largely via magma mixing between the subcontinental mantle-derived mafic rocks and the felsic crustal melts (Ewart *et al.,* 1992; Bryan *et al.*, 1997; Bryan, 2007). Average compositions for the Whitsunday Province define a high-K calc-alkaline suite, and across the compositional range from basalt to rhyolite these lavas and dykes show a striking geochemical similarity to the CLT high-K calc-alkaline suites (Figure 3.22). In particular, Bryan (2007) noted that the Whitsunday mafic lavas show a greater compositional spread than the felsic lavas, and that among the mafic lavas there exist a broad spectrum of compositions from tholeiitic to arc-like (calc-alkaline) compositions. This matches very closely the mafic rocks in the CLT.

Figure 3.23 compares Ti/Y vs. Zr/Y relationships for the CLT igneous rock with three suites of data for a·type continental margin arc, the central and northern Andean arc, and with the calc-alkaline, rift-related Whitsunday volcanic province data. Clearly, the CLT data more closely resemble the Whitsunday rift-related suite than the modern Andean volcanic arcs. Here is noted also that, as pointed out by Miyashiro (1974), a characteristic feature of subduction- related arc volcanics is the predominance of fragmental eruptive products. In contrast, fragmental rocks are less abundant than lavas in the CLT suites, again supporting an extensional rift setting rather than a continental margin arc setting for the CLT volcanic rocks.

There is very little information about the extensional structures active in northern Thailand during the Late Triassic. Stokes *et al.* (1996) suggested that extensional collapse of the Indosinian orogen occurred further east (in Laos) in the Late Triassic and then thermal subsidence continued in the Jurassic and Cretaceous. Their model was based on the widespread deposition of the red-bed Khorat Group molasse, which covered much of north and northeast Thailand and Laos PDR commencing in the latest Triassic. There is no comparable study in northern Thailand to support this interpretation, but it is at least consistent with the suggestion made here, based on igneous geochemistry, that the latest Middle to Late Triassic CLT rocks formed in a post-collisional environment.

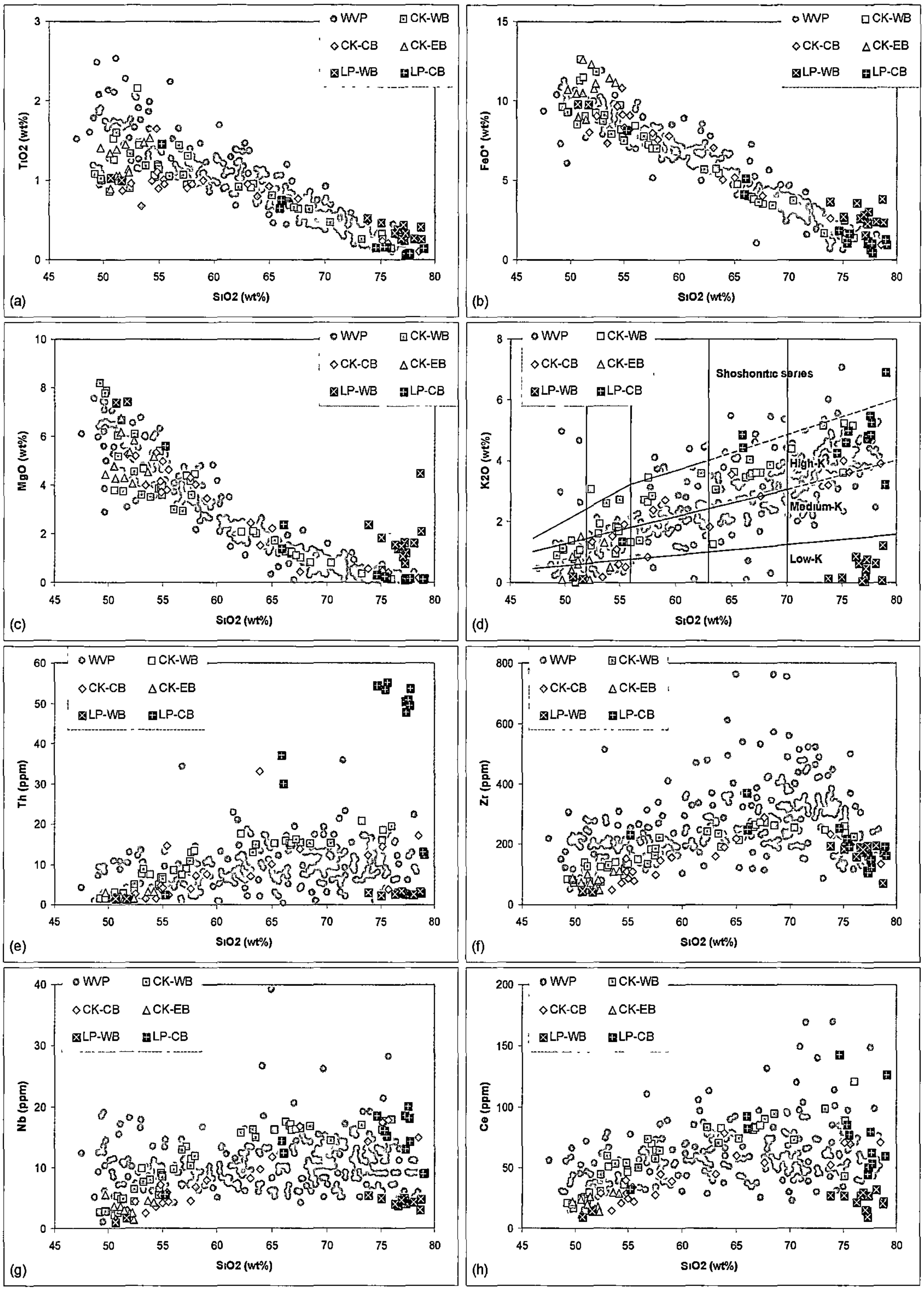

Figure 3.22 Plots of (a to d) selected major elements vs. SiO_2 and (e to h) selected trace elements vs. SiO_2 for the CLT igneous rocks (CK-WB, CK-CB, CK-EB, LP-WB and LP-CB rocks) compared to lavas and dykes from the Cretaceous Whitsunday Volcanic Province (WVP: Ewart *et al.* 1992 and S. Bryan unpublished data).

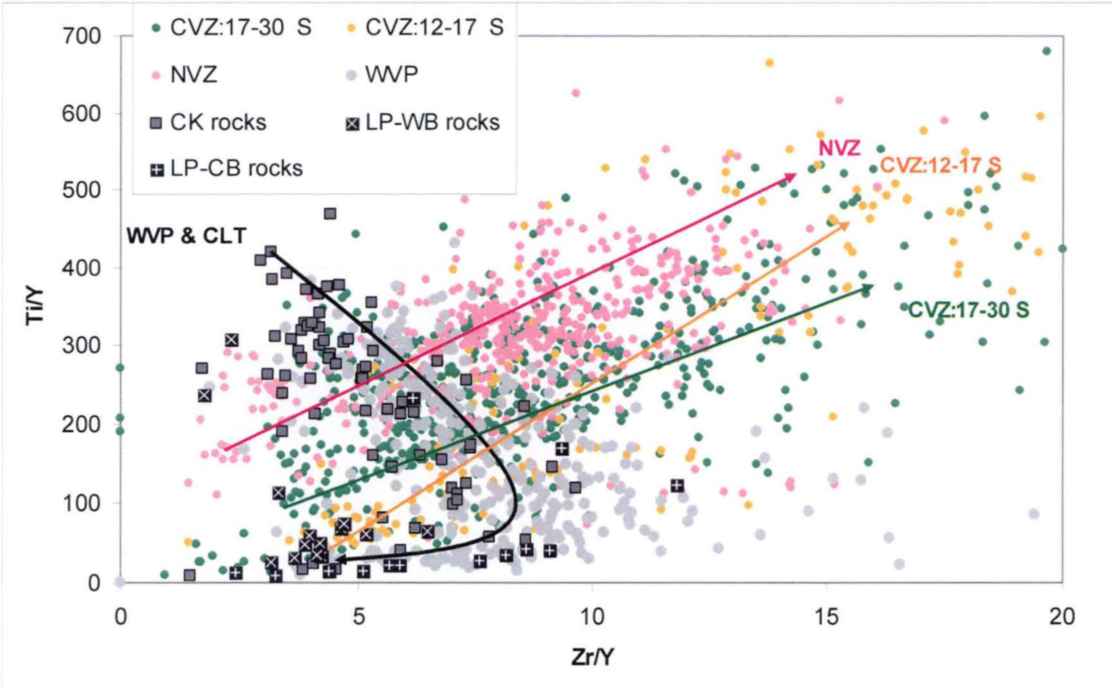

Figure 3.23 Plot of Zr/Y vs. Ti/Y diagram for the CLT igneous rocks (CK , LP-WB and LP-CB rocks) compared to Andean volcanic margin lavas (southern Central Volcanic Zone CVZ: 17-30°S, northern CVZ: 12-17°S, and Northern Volcanic Zone (NVZ) from the web-based GEOROC database: http://georoc.mpch-mainz.gwdg.de/georoc/) and rift-type calc-alkaline rocks of the Whitsunday Volcanic Province (WVP from Ewart *et al.*, 1992 and S. Bryan unpublished data).

Further research is required to evaluate more thoroughly the alternative model for the CLT lavas and volcaniclastics suggested here, in which they are interpreted to have been erupted in a post-orogenic, Basin and Range-type extensional setting. The exact timing of the main deformation event that produced the Sukhothai Fold Belt, involving collision between Indochina and the Shan-Thai (or Sibumasu) terranes is still not well constrained. Earliest unambiguous post-orogenic redbeds of the Khorat Group are generally considered to be latest Triassic age (Metcalfe, 2002; Wakita & Metcalfe, 2005), and stitching plutons are dated around 210-180 Ma (Early Jurassic) (Charusiri *et al.*, 1993).

In summary, crustal thickening resulting from the latest Middle to early Late Triassic collisional event involving the Indochina and Shan-Thai terranes led to gravitational collapse, broad extensional tectonism, and accompanying mainly calc-alkaline magmatism around 230-220 Ma, in a largely non-marine environment. Magmatism may have progressed from high-K felsic-dominant compositions (CK-WB, CK-CB and LP-CB) to later more mafic-dominated, transitional tholeiitic compositions (CK-EB) as extension accelerated, as in the post-collisional history of western Tasmania (Crawford & Berry 1992), since low-K basaltic dykes rocks intrude medium- and high-K calc-alkaline suites in the CK-CB. However, a significant refinement of dating of these rocks is needed to confidently demonstrate this. Strong Tertiary block faulting has overprinted the structural grain of northern Thailand, making it difficult to decipher evidence that unambiguously demonstrates post-orogenic extension in the Late Triassic. In the following chapters, three structural transects across the rocks between Chiang Khong and Lampang, and a geochronological study of the Triassic volcanic rocks in this region help to clarify the tectonic setting of this important part of the southeast Asian Mesozoic orogenic collage, and enable better correlations with regions to the north and south, in Yunnan and southern Thailand-Malaysia respectively.

CHAPTER 4

Geochronology of the Chiang Khong-Lampang-Tak Volcanic Belt

4.1 Introduction and Previous Work

4.1.1 Introduction

The age of igneous and sedimentary rocks in the Chiang Khong-Lampang-Tak volcanic belt was investigated using U-Pb-Th zircon and monazite geochronology. Ten representative igneous rocks, one mylonitic granitoid and seven clastic sedimentary rocks were selected across the area. Sample locations for dated rocks are shown in Figures 4.1 & 4.2.

The morphology of zircon grains was studied using optical microscopy, back-scattered electron imaging (BSE) and cathodoluminescence imaging (CL). The U-Pb zircon age dating was performed using the Laser Ablation Inductively Coupled Plasma Mass Spectrometer (LA-ICP-MS) at CODES, University of Tasmania. The chemical dating of monazite and the CL/BSE images were acquired using a CAMECA SX100 electron probe microanalyser and a FEI Quanta 600 scanning electron microscope equipped with a Gatan PanaCLF detector, housed in the Central Science Laboratory, University of Tasmania. The radiometric ages of rocks in this study are discussed in the context of stratigraphic age relationships shown on the International Stratigraphic Chart of the IUGS (2000).

4.1.2 Previous Work

Previous ages reported from the Chiang Khong-Lampang-Tak volcanic belt rocks have mostly been estimated from stratigraphic correlation. Stratigraphic units range in age from the Late Palaeozoic to Recent (Braun & Hahn, 1976). The oldest age previously inferred for this belt was Carboniferous-Permian for low grade meta-sedimentary rocks in the Ban Huak area (Braun & Hahn, 1976; Tansuwan & Chitmanee, 1990a, b). Most rocks in the CLT belt are Triassic (Chapter 2). Fossil evidence has been presented for the Triassic age of the Lampang Group that overlies the CLT rocks in the southern area (Chapter 2).

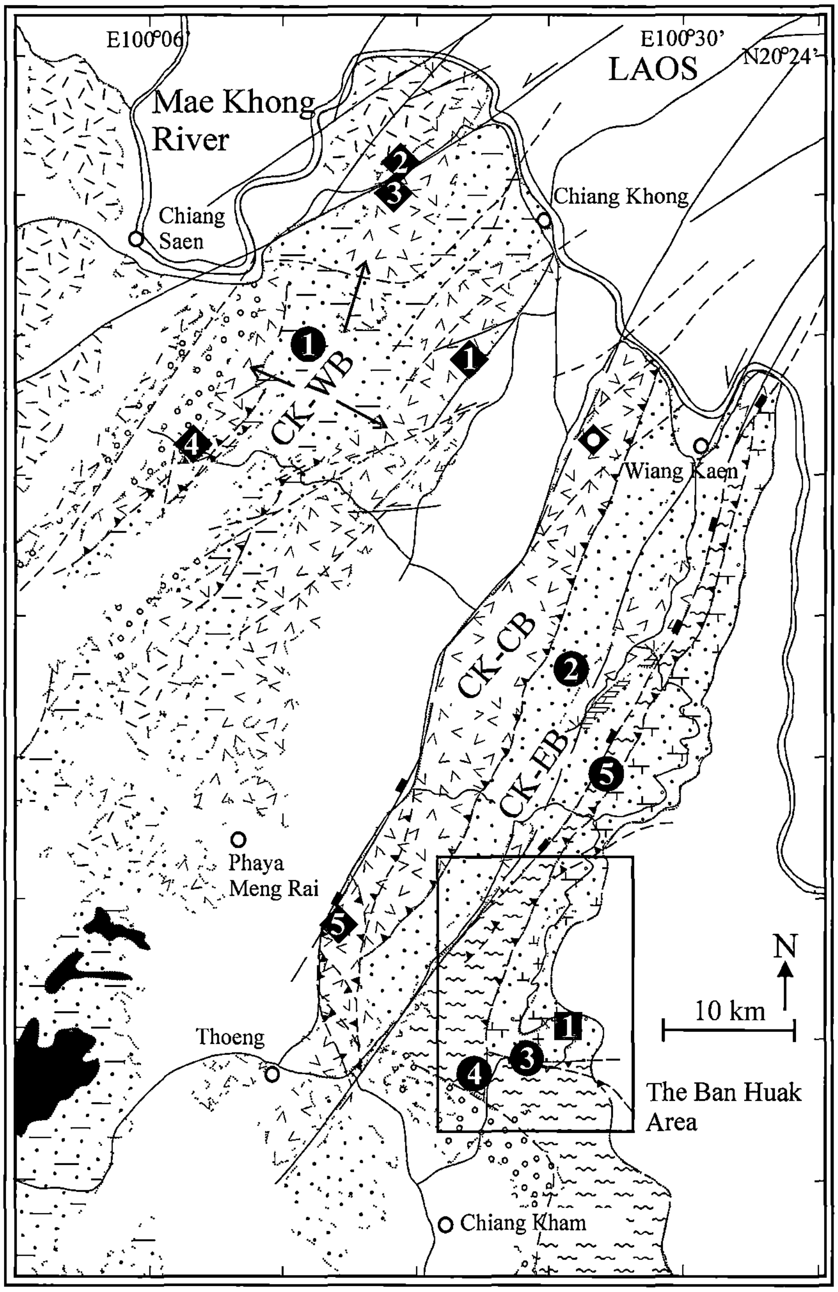

Igneous rocks
- 1 13/3(3) in Figure 4.3
- 2 14/2(1) in Figure 4.4
- 3 15'/1(1) in Figure 4.5
- 4 26'/10 in Figure 4.6
- 5 16'/10 in Figure 4.7

Mylonitic granitoid
- 1 8"-2 in Figure 4.13

Sedimentary rocks
- 1 14-1(2007) in Figure 4.15
- 2 18-3(2007) in Figure 4.16
- 3 St 2-8(2007) in Figure 4.17
- 4 HF-2007 in Figure 4.18
- 5 HH-2007 in Figure 4.19

Sample location from Barr *et al.* (2006)

Figure 4.1 Location of representative igneous, mylonitic granitoid and sedimentary rocks selected for the U-Pb zircon age dating from the Chiang Khong area. See Figure 2.3 for symbols and legend.

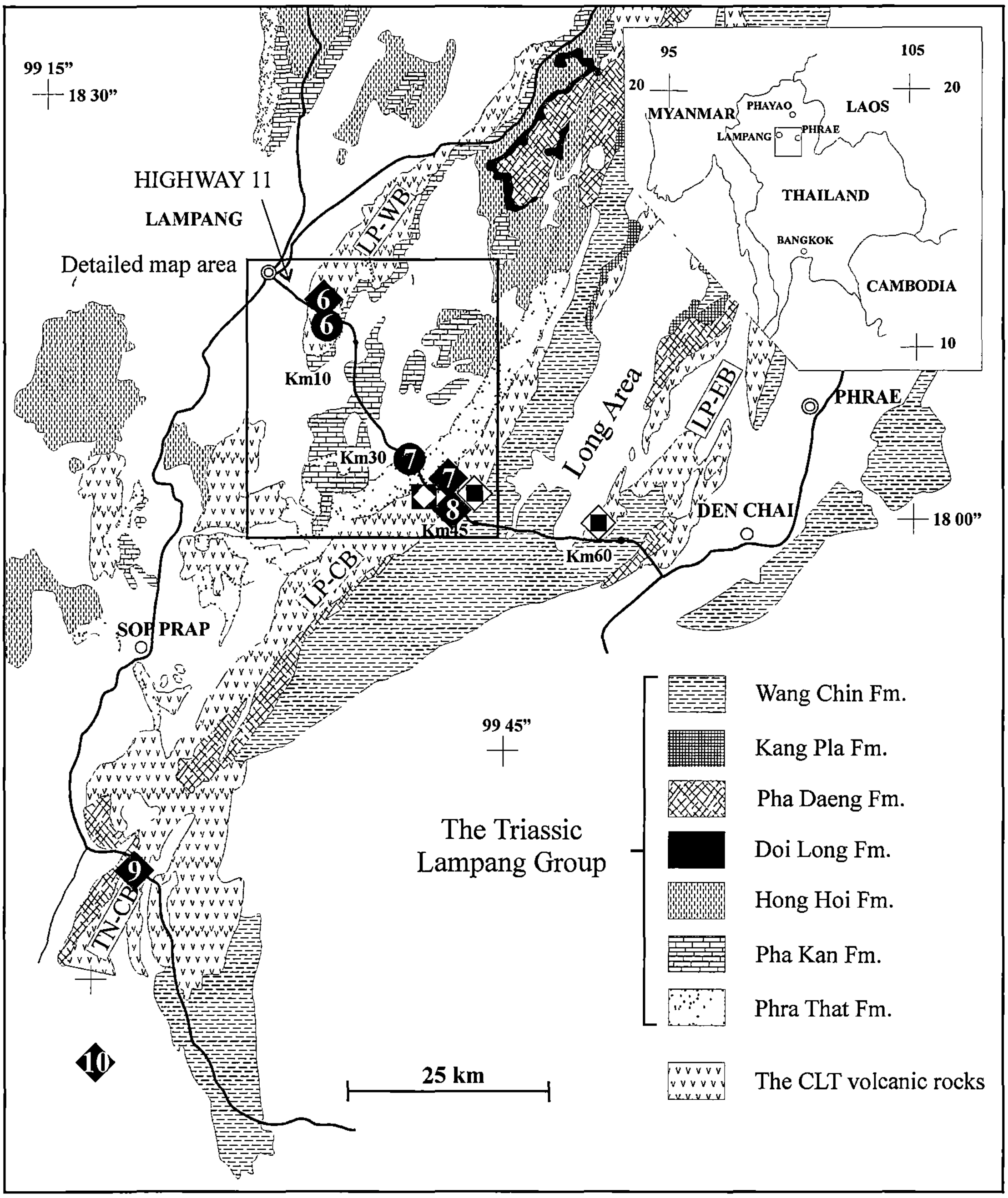

Igneous rock
- 6 12'/5(3) in Figure 4.8
- 7 7/7(2) in Figure 4.9
- 8 12'/10 in Figure 4.10
- 9 13'/3 in Figure 4.11
- 10 13'/11 in Figure 4.12

Sedimentary rock
- 6 DR-2007 in Figure 4.20
- 7 PT-2007 in Figure 4.21

- Sample location from Barr *et al.* (2000)
- Sample locations from Khositanont *pers comm.* (2006)

Figure 4.2 Location of representative igneous and sedimentary rock selected for the U-Pb zircon age dating from the Lampang area.

Plutonic rocks

Plutonic rocks in the CLT have been interpreted as Permo-Triassic based on intrusive relationships and correlations with volcanic and sedimentary rocks from other parts of Thailand (Braun & Hahn, 1976; Tansuwan & Chitmanee, 1990a, b; Jungyusuk & Khositanont, 1992). Direct radiometric ages along this volcanic belt are rare. Most dating of granitic rock has been carried out in the Eastern granitic province in Thailand, to the east of the study area (Beckinsale *et al.,* 1979; Cobbing *et al.,* 1986; Charusiri *et al.,* 1993). An I-type metaluminous granitoid associated with the CLT volcanic rock in the Sukhothai Fold Belt yielded a Triassic (235-220 Ma) age (Charusiri *et al.,* 1993). The U-Pb zircon age of a granite from the Ban Mae Khaem area in the LP-CB was reported as 224 ± 4 Ma (early Late Triassic; S. Khositanont, *pers. comm.,* 2006).

Volcanic Rocks

Volcanic and associated volcaniclastic rocks along the CLT have been previously interpreted to be mostly Permo-Triassic (Bunopas & Vella, 1978; Jungyusuk & Khositanont, 1992; Panjasawatwong *et al.,* 2003) with volumetrically minor Late Triassic to Early Jurassic volcanic rocks recognized in a few places (Jungyusuk & Khositanont, 1992). Recent age dating of a rhyolite from the LP-CB and a rhyolitic tuff from the CK-CB yielded U-Pb zircon ages of 240 ± 1 Ma and 232.9 ± 0.4 Ma, respectively (Barr *et al.,* 2000; Barr *et al.,* 2006). A rhyolite from Ban Kaeng Luang in LP-EB yielded a U-Pb zircon age of 229 ± 4 Ma (S. Khositanont, *pers. comm.,* 2006).

Sedimentary rocks

The Chiang Khong Area

Sedimentary rocks in the Chiang Khong area are shown on current geological maps (Bruan & Hahn, 1976; Sukvattananunt & Assawapatchara, 1989a, b, c, d; Sukvattananunt *et al., 1976;* 1985a, b; Tansuwan & Chitmanee, 1990a, b) as Carboniferous-Permian meta-sedimentary rocks, Carboniferous-Permian foliated limestone, Permo-Triassic sedimentary rocks and Late Triassic to Early Jurassic redbeds with limestone lenses (Figure 4.1). Ages of these rock units were deduced from stratigraphic correlation, with very little direct fossil evidence. Only the limestone lenses interbedded with shale (Late Triassic to Early Jurassic redbeds) had useful fossil evidence based on algae, molluscs, and crinoid stems, *Posidonia sp., Halobia sp.,* and *Pteria sp.* (Tansuwan & Chitmanee, 1990a, b).

The Lampang Area

The Lampang Group rocks along the southern transects (Figures 2.3 in Chapter 2) included the Phra That, Pha Kan and Wang Chin Formations. The Phra That Formation has been interpreted to be the lowermost part of the Lampang Group and is conformably overlain by limestones of the Pha Kan Formation. The Phra That Formation was proposed to be both conformably (Chaodumrong, 1992) and unconformably (Singharajwarapan, 1994) underlain by the CLT volcanics, and sedimentary strata of Permian or older age A faulted contact between the CLT volcanic rocks and the Lampang Group sedimentary sequence has been drawn in one detailed Sukhothai Fold Belt structural cross section (Singharajwarapan, 1994; Singharajwarapan & Berry, 2000). No fossil evidence in the Phra That Formation has been reported from near the Lampang transect but early Scythian to early Anisian (Early-Middle Triassic) fossils have been reported from Ban Tha Si, 30 km north of this area (Chaodumrong, 1992).

The Pha Kan Formation conformably overlies the Phra That Formation. The lower part of the Pha Kan Formation has been interpreted to be early Triassic age (Chaodumrong, 1992). The fossils *Pterria, Pecten, Elegantia, Eumorphotis, Entolium* and *Costatoria* of early Middle Triassic age (Anisian) were found at the Phra That Doi Mueng Kham temple (Chaodumrong, 1992). However, based on a foraminiferal study from limestone outcrops along Highway number 11, the age of this unit near the study transect is Middle to Late Triassic (Kobayashi *et al.,* 2006).

The Wang Chin Formation on the southeastern part of the Lampang area (uppermost unit of the Lampang Group) has been interpreted to be Late Triassic in age. The middle Carnian *Halobia styriaca* has been observed at the km 55.54 point along the Lampang to Denchai section (Chaodumrong, 1992). Sandstone and slate from the km 54.8 point of the Lampang to Denchai section were dated by K-Ar dating of the fine mineral fractions and gave an age of 188-220 Ma (Ahrendt *et al.,* 1993). The Late Triassic biostratigraphic age of the Wang Chin Formation rock is an important control on the age of the deformation and metamorphism of the Sukhothai Fold Belt (Singharajwarapan, 1994).

4.2 Methodology

4.2.1 U-Pb Zircon Age Dating

U-Pb geochronology in zircon is a widely used technique in Earth Sciences to determine the age of igneous rocks. The technique involves measuring the parent to daughter ratio of three distinct radioactive decay series (Harley & Kelly, 2007). The parent isotopes ^{238}U, ^{235}U and ^{232}Th produce, respectively, ^{206}Pb, ^{207}Pb and ^{208}Pb as their final daughter isotopes. Each of these decay series involves several intermediate steps and short-lived intermediate isotopes only need to be considered for age determinations of very young rocks. The whole decay process can be mathematically described by a single decay equation relating the number of ultimate parent atoms remaining (e.g. ^{238}U) and the number of final radiogenic daughter atom (e.g. $^{206}Pb^*$) relative to time:

$$^{206}Pb^*/^{238}U = e^{\lambda 238t} - 1$$

where e is the exponential function, t is time, and λ is the decay constant specific to this decay scheme, i.e. $\lambda^{238} = 1.55125^{e-10}$. $^{206}Pb^*$ refers to the radiogenic ^{206}Pb accumulated in the crystal as a result of the decay of ^{238}U. Similar expressions can be formulated for $^{207}Pb^*$ produced from the decay of ^{235}U and $^{208}Pb^*$ produced from ^{232}Th, with $\lambda^{235} = 9.8485^{e-10}$ and $\lambda^{232} = 4.9475^{e-11}$.

Most of the dates presented in this study are based on the $^{206}Pb/^{238}U$ system with a correction for common-Pb (Pb not derived from *in situ* radioactive decay of U) based on the $^{207}Pb/^{206}Pb$ ratio. In addition to common-Pb, some zircon grains can experience appreciable Pb-loss, recognizable by the skewing of analyses towards younger ages in the U-Pb concordia diagrams (e.g., Figure 4; Harley & Kelly, 2007). Subsequently, the analysis of zircons that have been affected by Pb-loss will return values that represent the minimum age of their growth.

Mezger & Krogstad (1997) argued that, under conditions typical in the continental crust, Pb-loss is only possible in zircons that have experienced significant radiation damage through α-decay and spontaneous fission (metamict zircons). Pb-diffusion in the pristine zircon lattice is insignificant up to temperatures of at least 1000°C. Complete resetting of the U-Pb system in zircon under crustal conditions is only possible through dissolution and reprecipitation of zircon.

Another problem that can be encountered in U-Pb zircon geochronology is inheritance – the presence of older zircon grains in an igneous or metamorphic rock that did not crystallize from that rock's parental magma. Such inherited zircon grains may have been incorporated into a magma through the partial melting of a pre-existing zircon-bearing rock or through assimilation of zircon-bearing country rocks during magma ascent (Harley & Kelly, 2007).

The U-Pb zircon age dating reported here was measured using a HP4500 quadrupole ICP-MS with a 213 nm New Wave quintupled YAG Laser. To improve on precision, some of the zircon were re-analysed using an Agilent 7500 cs ICP-MS with a 193 nm New Wave laser. Zircons were separated from 100 to 200g of rock by crushing to <400 micron in a mortar and pestle or a Cr-steel ring mill, depending on sample hardness. Heavy minerals were then separated using a combination of mechanised panning device (superpan) and a hand pan. The heavy mineral residue was then dried. Magnetic and paramagnetic minerals were removed using a hand magnet and a Franz magnetic separator. For each sample, ~20 to 30 zircons were picked from the non-magnetic heavy mineral separate using a single hair from a fine artist's paint brush, and mounted on double-sided sticky tape. Epoxy glue was then poured into a 2.5 cm diameter mould on top of the zircon grains. Mounts were dried for 12 hours and polished using clean sandpaper and a clean polishing lap, then washed in distilled water in an ultrasonic bath. Zircons were ablated in a He atmosphere in a custom-made chamber with the laser pulsing at 5 Hz, with a 30 micron diameter beam delivering ~ 12 J/cm^2 and drilling at ~1 micron/s. A total of 11 masses were counted (^{96}Zr, ^{146}Nd, ^{178}Hf, ^{202}Hg, ^{204}Pb, ^{206}Pb, ^{207}Pb, ^{208}Pb, ^{232}Th , ^{238}U), with longer counting times on Pb isotopes giving a total quadrupole cycling rate of 0.2s. Each analysis began with a 30 second analysis of background gas followed by 30 seconds with the laser switched on. Four primary (Temora zircons of Black *et al.*, 2003) and two secondary standards (91500 of Wiedenbeck *et al.,* 1995) were analysed before and after every 12 zircon analyses to correct for mass bias, machine drift and down hole fractionation. Repeated monitoring of U/Pb mass fractionation during drilling showed an average fractionation of U/Pb on the Temora standard varying from 0.050 at the start of a

30sec analysis to 0.053 at the deepest level of laser ablation. Monitoring of international standards showed a reproducible standard error of ±0.5-1%. LA- ICP-MS U-Pb isotopic and trace element data for standard zircons from this study are given in Appendix B.

4.2.2 Chemical Monazite Dating

Monazite analyses were acquired using a CAMECA SX100 electron probe microanalyser equipped with five WD spectrometers and operated at 20kV accelerating voltage and a 100nA regulated beam current (faraday cup). A nominal spot size of 3 micron was used. All elements were acquired using a combination of TAP, LiF, and PET analysing crystals. Additional age sensitivity was achieved by using two spectrometers for acquisition for Pb.

X-ray lines were calibrated using a combination of synthetic oxides and minerals, synthetic phosphates (Jarosewich & Boatner, 1991) and well-characterised natural minerals. Peak and background measurement positions were optimised to avoid line overlaps, and where unavoidable, were corrected using on- and off-line procedures. All lines were analysed in PHA differential mode to reduce background and high order overlaps. Data reduction and matrix corrections were performed using the PAP algorithm (Pouchou & Pichoir, 1984). Oxygen was calculated by stoichiometry. Analytical conditions for each element together with peak and background counting times and positions, and standards used, are given in Appendix C-1.

Chemical U-Th-Pb ages (Montel *et al.,* 1996) were calculated using the measured total Pb, Th and U concentrations in monazite. Isotopic U-Th-Pb dating of monazite has shown that monazites are typically concordant. The common Pb is generally insignificant compared with the radiogenic Pb created by decay of Th and U. Age calculations and errors were carried out as in Berry *et al.* (2007) and performed using software developed in-house by Dr. R. Berry and further processed using ISOPLOT (Ludwig, 1998). The accuracy of the method was verified using primary standard RGL04B (Rubatto *et al.*, 2001) and a range of in-house standard monazites of previously determined ages using independent isotopic methods (either SHRIMP or TIMS). The respective ages are given in Appendix C-2.

4.2.3 The CL/BSE Imaging

The cathodoluminescence (CL) and Back Scattered Electron images were obtained on carbon-coated grain mounts with a FEI Quanta 600 scanning electron microscope equipped with a Gatan PanaCLF detector, using an acceleration voltage of 20 kV and an arbitrary spot size of 5.0 μm, corresponding to a probe current of around 0.2 nA.

4.3 Ages of Igneous Rocks

Zircons were separated from ten representative volcanic and shallow intrusive rocks of the CLT, including four rock samples from CK-WB, one from CK-CB, one from LP-WB, two from LP-CB and two from TN-CB. The rock types and zircon morphology are shown in Table 4.1. LA-ICP-MS U-Pb isotopic and trace element data for zircons from these ten igneous rocks are given in Table 4.2.

4.3.1 The Chiang Khong area

Morphology of zircons

Zircons from five representative intermediate to felsic igneous rocks of the Chiang Khong area, including two shallow intrusive rocks (dykes) and three volcanic rocks were separated for U-Pb dating. Zircon morphology was examined using CL/BSE imaging (Figures 4.3b to 4.7b). Zircons are small (30-150 micron) and rare in the volcanic rocks. Zircons from the intrusive rocks are mostly euhedral to subhedral crystals, whereas volcanic zircon crystals are subhedral to anhedral. Zircons from the intrusive rocks generally show oscillatory growth zoning. Older partially resorbed cores were visible in a few zircon grains from sample 15'/1(1) and 26'/10.

Table 4.1 U-Pb zircon age of igneous rocks from the Chiang Khong-Lampang-Tak volcanic belt

Sample number	Location/ geographic belt	Age dating	Rock description	Morphology of zircon
1. 13/3(3) (Figure 4.3)	20.1710°N 100.3543°E/ CK-WB	229 ± 3 Ma	Plagioclase-phyric rhyolite, high-level intrusive rock with granophyric texture. Rare green biotite/hornblende.	Euhedral to subhedral crystals with prismatic shape, 50 to 150 microns. Inclusions and resorbed edges in some grains. Oscillatory growth zoning is observed without inherit cores.
2. 14/2(1) (Figure 4.4)	20.3107°N 100.2817°E/ CK-WB	222 ± 6 Ma	Glassy dacitic lava with flow banding. Groundmass has patchy devitrification.	Small rare zircon grains. Anhedral to subhedral crystals about 30 to 50 micron across. Brightness contrast shown in some grains, most are fairly dark in CL image without growth zoning. Resorbed edges and fracture surface common.
3. 15'/1(1) (Figure 4.5)	20.2981°N 100.2797°E/ CK-WB	223 ± 8 Ma 272 ± 15 Ma	Microdiorite with clinopyroxene, albitised plagioclase, late magmatic green hornblende, and altered biotite. Common interstitial quartz.	Subhedral to euhedral zircon grains, 40 to 120 microns across with stubby to prismatic shape. Growth zoning not obvious but some grains have dark inherited core.
4. 26'/10 (Figure 4.6)	20.1093°N 100.1356°E/ CK-WB	221 ± 2 Ma 231 ± 3 Ma	Plagioclase-phyric rhyolitic intrusive rock with granophyric groundmass and green hornblende, biotite and Fe-Ti oxide.	Euhedral to subhedral prismatic crystal about 50 to 150 microns. Inclusions, fractures and resorbed edges observed. Oscillatory growth zoning is shown on CL image with some inherited dark cores.
5. 16'/10 (Figure 4.7)	19.3183°N 100.2251°E/ CK-CB	220 ± 5 Ma	Quartz and plagioclase phyric rhyolite with flow texture.	Small rare zircon grains 40 to 70 microns. Growth zoning is not obvious, no inherited cores. Crystal shape is short to prismatic subhedral to anhedral.

Table 4.1 *(continued)*

Sample number	Location/ geographic belt	Age dating	Rock description	Zircon morphology
6. 12'/5(3) (Figure 4.8)	18.2560°N 99.5487°E/ LP-WB	233 ± 5 Ma	Quartz and plagioclase phyric rhyolite	Euhedral to anhedral short prismatic crystals, 40 to 100 microns. Resorbed edges and fractures are common. The CL image is very bright without any internal features.
7. 7/7(2) (Figure 4.9)	18.9569°N 99.7029°E/ LP-CB	223 ± 4 Ma	Microsnowflake-textured rhyolitic lava with quartz and plagioclase phenocrysts and occasional zircons.	Euhedral to subhedral crystals, 50 to 120 microns, short and prismatic shapes. Oscillatory growth zoning common but no inherit cores. Internal features not distinctive. Some grains are less dark.
8. 12'/10 (Figure 4.10)	18.9351°N 99.7085°E/ LP-CB	227 ± 4 Ma	Plagioclase-quartz-biotite-clinopyroxene - phyric dacitic intrusive rock	Euhedral to subhedral prismatic crystals, 40 to 120 microns. Oscillatory growth zoning common. Dark cores and inclusions are less common.
9. 13'/3 (Figure 4.11)	17.6239°N 99.3139°E/ TN-CB	233 ± 4 Ma	Granite with green to straw colour biotite	Euhedral to subhedral prismatic crystals 50 to 150 microns. Oscillatory growth zoning is common. Less common inherited dark cores, Rare inclusions.
10. 13'/11 (Figure 4.12)	17.4639°N 99.1780°E/ TN-CB	292 ± 7 Ma	Hornblende-quartz diorite.	Big euhedral to subhedral prismatic crystal: 70 to 200 micron. Oscillatory growth zoning and brightness contrast are distinctive on the CL image. Inclusions, inherit cores and resorbed edges were not found.

Table 4.2 Laser ablation ICPMS U-Pb isotopic and trace element data for zircons from the ten representative CLT igneous rocks.

Sample	206Pb/238U age (Ma)		Isotopic ratios								Trace element data (in ppm)				
analysis no	(207Pb corrected)	+/-1s	206Pb/238U	%rsd	208Pb/232Th	%rsd	207Pb/206Pb	%rsd	207Pb/235U	%rsd	Nd	Hf	Pb	Th	U
13/3 (3) 03*	203	2 1	0 0321	1 0%	0 0110	1 7%	0 051	2 5%	0 219	2 5%	12 5	8621	34	965	922
13/3 (3) 11	216	3 5	0 0347	1 6%	0 0112	3 4%	0 064	4 9%	0 294	4 7%	6 5	9110	11	250	309
13/3 (3) 06	218	3 1	0 0346	1 4%	0 0111	2 0%	0 053	3 1%	0 248	3 1%	10 0	8678	46	1274	1158
13/3 (3) 12	225	2 2	0 0356	1 0%	0 0115	1 7%	0 052	2 3%	0 256	2 2%	2 7	10568	17	287	456
13/3 (3) 07	227	10 3	0 0695	2 7%	0 1305	3 8%	0 438	2 7%	4 011	4 0%	247 9	11579	66	260	460
13/3 (3) 08	228	2 2	0 0361	1 0%	0 0122	1 9%	0 054	2 9%	0 268	2 8%	6 9	10392	14	254	369
13/3 (3) 09	229	2 0	0 0363	0 9%	0 0120	1 5%	0 053	2 2%	0 267	2 2%	10 7	10561	21	394	524
13/3 (3) 02	229	1 9	0 0363	0 8%	0 0117	1 4%	0 051	2 2%	0 256	2 0%	9 8	10256	27	562	670
13/3 (3) 04	230	2 4	0 0364	1 0%	0 0119	1 6%	0 052	2 6%	0 260	2 5%	9 0	8220	17	381	410
13/3 (3) 05	233	2 1	0 0368	0 9%	0 0123	1 6%	0 052	2 2%	0 266	2 0%	5 5	11520	22	381	556
13/3 (3) 10	234	2 5	0 0372	1 1%	0 0127	2 3%	0 054	2 6%	0 277	2 5%	8 3	9419	11	175	264
13/3 (3) 01	235	2 6	0 0372	1 1%	0 0122	2 4%	0 051	3 2%	0 266	3 0%	1 2	10681	7	95	181
14/2(1) 03	218	5 0	0 0344	2 2%	0 0105	5 5%	0 052	9 0%	0 248	8 6%	9 1	9284	19	277	543
14/2(1) 08	218	3 5	0 0350	1 6%	0 0115	3 3%	0 066	4 8%	0 319	5 3%	12 8	9479	18	366	461
14/2(1) 05	219	2 0	0 0346	0 9%	0 0103	1 5%	0 052	2 5%	0 245	2 5%	34 8	9288	130	4656	2796
14/2(1) 04	222	3 3	0 0352	1 5%	0 0105	2 4%	0 054	4 8%	0 260	4 5%	50 5	9447	20	467	503
14/2(1) 07	228	2 4	0 0362	1 0%	0 0103	1 8%	0 055	2 7%	0 272	2 7%	73 1	9912	104	2732	2423
14/2(1) 06	236	4 9	0 0376	2 1%	0 0107	3 4%	0 055	6 2%	0 290	6 2%	17 8	9946	22	446	535
14/2(1) 01*	249	8 0	0 0418	3 0%	0 0188	5 9%	0 098	10 1%	0 528	9 7%	10 5	8877	15	219	277
14/2(1) 02*	897	13 5	0 1518	1 5%	0 0607	4 5%	0 082	3 8%	1 702	3 8%	0 7	13872	249	115	1785
15'/1(1) 06*	213	2 6	0 0350	1 2%	0 0121	1 9%	0 082	3 2%	0 393	3 4%	60 3	8873	69	1858	1467
15'/1(1) 03	213	9 8	0 0339	4 5%	0 0129	7 8%	0 057	15 3%	0 259	13 0%	146 7	8882	12	200	312
15'/1(1) 09	216	5 0	0 0345	2 3%	0 0138	3 8%	0 060	7 0%	0 274	6 9%	87 7	10060	9	133	236
15'/1(1) 05	224	2 2	0 0353	1 0%	0 0103	2 0%	0 049	3 5%	0 234	3 3%	32 3	11467	58	1212	1450
15'/1(1) 07	233	6 5	0 0370	2 8%	0 0148	5 6%	0 055	8 9%	0 280	8 5%	77 9	8867	20	221	509
15'/1(1) 10	261	4 0	0 0413	1 5%	0 0124	2 7%	0 051	5 3%	0 280	5 4%	18 5	8596	25	501	512
15'/1(1) 01	266	3 8	0 0423	1 4%	0 0120	2 4%	0 055	5 5%	0 317	5 6%	20 4	8768	26	510	528
15'/1(1) 04	279	4 7	0 0449	1 6%	0 0163	4 3%	0 064	6 8%	0 397	7 0%	48 3	10892	15	247	295
15'/1(1) 08	280	3 6	0 0443	1 3%	0 0134	3 0%	0 050	4 1%	0 304	4 1%	6 5	10832	34	358	731
15'/1(1) 02*	323	10 9	0 0553	3 1%	0 0281	6 1%	0 110	10 2%	0 783	10 5%	8 0	8969	13	124	172

* Sample analysis number is not used in age calculations. Comment is in text for each sample.

Table 4.2 *(continued)*

Sample	206Pb/238U age (Ma)		Isotopic ratios								Trace element data (in ppm)				
analysis no	(207Pb corrected)	+/-1s	206Pb/238U	%rsd	208Pb/232Th	%rsd	207Pb/206Pb	%rsd	207Pb/235U	%rsd	Nd	Hf	Pb	Th	U
26'/10 04*	186	2 5	0 0294	1 3%	0 0104	1 7%	0 054	2 5%	0 212	2 7%	38 8	8743	29	771	936
26'/10 09	218	3 5	0 0345	1 6%	0 0112	2 1%	0 052	3 0%	0 243	3 0%	368 6	9264	34	982	910
26'/10 12	218	2 5	0 0347	1 2%	0 0114	2 1%	0 056	2 6%	0 264	2 4%	8 7	9445	21	377	507
26'/10 03	222	1 9	0 0356	0 9%	0 0133	2 0%	0 064	2 1%	0 312	2 2%	19 3	9077	9	144	243
26'/10 05	222	2 0	0 0359	0 9%	0 0122	1 6%	0 069	2 2%	0 341	2 3%	9 8	9232	15	282	364
26'/10 10	227	2 6	0 0360	1 2%	0 0119	2 2%	0 053	2 6%	0 264	2 5%	5 6	10274	18	283	438
26'/10 01	228	2 0	0 0361	0 9%	0 0107	1 6%	0 054	1 9%	0 263	1 8%	68 9	8486	14	338	354
26'/10 06	229	1 8	0 0363	0 8%	0 0115	1 3%	0 053	1 8%	0 265	1 7%	5 0	9204	15	253	377
26'/10 11	230	3 5	0 0364	1 5%	0 0117	3 0%	0 052	3 3%	0 263	3 4%	283 1	9278	14	264	356
26'/10 07	234	3 1	0 0370	1 3%	0 0116	2 6%	0 052	3 5%	0 260	3 3%	159 1	9094	8	140	210
26'/10 02	234	2 2	0 0375	0 9%	0 0129	2 0%	0 060	2 5%	0 309	2 3%	2 8	9175	9	118	223
26'/10 08	235	2 9	0 0371	1 2%	0 0116	2 4%	0 051	2 7%	0 255	2 7%	7 8	9136	9	120	221
16'/10(1) 05	210	3 3	0 0335	1 5%	0 0100	3 3%	0 058	6 4%	0 256	6 2%	14 0	9225	14	265	390
16'/10(1) 12	216	3 6	0 0342	1 6%	0 0106	3 4%	0 054	5 8%	0 250	5 7%	42 7	8875	13	258	339
16'/10(1) 06	220	3 7	0 0349	1 7%	0 0109	3 1%	0 055	6 0%	0 262	5 9%	48 2	8669	22	623	499
16'/10(1) 04	221	4 7	0 0354	2 0%	0 0114	4 4%	0 063	7 9%	0 296	7 8%	80 6	7497	11	220	277
16'/10(1) 01	221	3 1	0 0349	1 4%	0 0106	3 0%	0 049	4 9%	0 224	4 9%	5 2	10510	22	320	608
16'/10(1) 09	223	4 2	0 0354	1 8%	0 0113	3 5%	0 054	7 1%	0 264	7 0%	20 1	9328	11	179	271
16'/10(1) 02	224	5 3	0 0366	2 3%	0 0136	4 8%	0 077	8 3%	0 370	8 1%	10 0	8663	7	95	163
16'/10(1) 03	230	5 0	0 0370	2 1%	0 0138	5 1%	0 067	7 9%	0 337	7 8%	73 5	9398	10	134	263
16'/10(1) 10	230	4 7	0 0368	2 0%	0 0116	4 6%	0 062	7 0%	0 303	7 0%	359 8	10990	28	406	684
16'/10(1) 07	236	4 6	0 0376	1 9%	0 0115	4 1%	0 057	6 7%	0 282	7 3%	8 8	10469	18	294	463
16'/10(1) 11	237	4 3	0 0376	1 8%	0 0115	3 4%	0 054	5 7%	0 278	5 8%	7 2	9618	15	308	357
16'/10(1) 08*	254	7 6	0 0402	3 0%	0 0122	5 1%	0 052	11 2%	0 293	11 0%	17 3	8782	16	265	372

* Sample analysis number is not used in age calculations. Comment is in text for each sample.

Table 4.2 *(continued)*

Sample	206Pb/238U age (Ma)		Isotopic ratios								Trace element data (in ppm)				
analysis no	(207Pb corrected)	+/-1s	206Pb/238U	%rsd	208Pb/232Th	%rsd	207Pb/206Pb	%rsd	207Pb/235U	%rsd	Nd	Hf	Pb	Th	U
12'/5(3) 06	224	4 5	0 0359	1 9%	0 0112	4 1%	0 062	7 7%	0 308	7 5%	29 3	9260	10	191	235
12'/5(3) 05	225	3 4	0 0360	1 5%	0 0119	2 6%	0 062	5 2%	0 301	5 0%	391 9	8929	23	570	498
12'/5(3) 08	227	7 0	0 0367	2 9%	0 0135	7 3%	0 071	12 2%	0 393	11 4%	35 5	9682	15	339	337
12'/5(3) 03	230	6 0	0 0369	2 5%	0 0112	5 0%	0 063	12 0%	0 336	11 8%	17 5	9006	13	256	300
12'/5(3) 07	232	3 2	0 0368	1 4%	0 0113	2 6%	0 054	5 9%	0 268	5 7%	37 7	9322	26	663	557
12'/5(3) 11	234	4 4	0 0374	1 8%	0 0131	3 7%	0 062	6 7%	0 315	6 8%	51 0	8855	12	289	267
12'/5(3) 10	236	3 4	0 0374	1 4%	0 0114	2 6%	0 053	5 2%	0 273	5 2%	21 6	9054	26	646	567
12'/5(3) 02	237	3 5	0 0377	1 4%	0 0118	3 5%	0 057	6 5%	0 280	5 7%	41 8	9403	20	422	432
12'/5(3) 12	241	4 2	0 0385	1 7%	0 0126	2 9%	0 060	5 4%	0 342	5 9%	220 1	9418	38	1023	753
12'/5(3) 04	246	4 8	0 0391	1 9%	0 0125	4 2%	0 057	7 9%	0 311	7 4%	47 7	9264	16	340	332
12'/5(3) 09*	256	3 9	0 0407	1 5%	0 0132	3 4%	0 055	6 3%	0 303	6 4%	7 7	9239	14	267	272
12'/5(3) 01*	256	5 6	0 0411	2 1%	0 0132	3 6%	0 063	8 0%	0 367	8 2%	11 9	9157	20	461	398
7/7(2) 06*	168	2 8	0 0279	1 6%	0 0114	3 3%	0 095	4 6%	0 379	5 0%	30 5	10152	75	1993	2115
7/7(2) 02*	205	2 6	0 0331	1 3%	0 0117	2 9%	0 068	4 0%	0 288	3 9%	51 2	13768	170	3003	4367
7/7(2) 04	217	3 2	0 0342	1 4%	0 0107	4 1%	0 051	6 0%	0 253	6 1%	9 2	13883	88	1333	2497
7/7(2) 09	219	4 5	0 0387	1 8%	0 0189	6 0%	0 136	5 4%	0 737	5 7%	9 7	11078	134	2338	2461
7/7(2) 12	221	2 5	0 0359	1 1%	0 0141	2 7%	0 075	3 4%	0 360	3 7%	85 1	12563	124	1909	2894
7/7(2) 03	221	2 7	0 0351	1 2%	0 0113	2 5%	0 057	4 7%	0 263	4 7%	14 1	8861	35	730	863
7/7(2) 08	225	2 8	0 0370	1 2%	0 0139	3 0%	0 081	3 8%	0 421	4 7%	8 3	8159	67	1579	1407
7/7(2) 07	227	2 2	0 0369	0 9%	0 0133	2 1%	0 073	3 3%	0 364	3 4%	13 6	9611	74	1572	1594
7/7(2) 10	227	2 5	0 0358	1 1%	0 0113	2 0%	0 050	3 4%	0 245	3 5%	24 5	9131	78	1672	1883
7/7(2) 05*	228	4 5	0 0463	1 2%	0 0375	3 7%	0 231	3 8%	1 479	4 3%	48 8	10537	211	2128	2626
7/7(2) 11*	238	2 8	0 0376	1 2%	0 0115	2 3%	0 052	3 8%	0 267	3 9%	19 3	9214	55	1128	1240
7/7(2) 01*	431	62 2	0 1148	13 1%	0 1015	17 6%	0 374	8 4%	10 380	18 8%	298 4	8032	1032	6432	3490

* Sample analysis number is not used in age calculations. Comment is in text for each sample.

Table 4.2 *(continued)*

Sample	206Pb/238U age (Ma)		Isotopic ratios								Trace element data (in ppm)				
analysis no	(207Pb corrected)	+/-1s	206Pb/238U	%rsd	208Pb/232Th	%rsd	207Pb/206Pb	%rsd	207Pb/235U	%rsd	Nd	Hf	Pb	Th	U
12'/10 04	219	3 4	0 0346	1 5%	0 0110	2 9%	0 053	6 2%	0 232	5 9%	5 2	9784	15	285	393
12'/10 10	222	2 3	0 0350	1 0%	0 0108	1 9%	0 048	3 7%	0 238	3 6%	53 1	9515	62	1725	1476
12'/10 03	223	3 1	0 0357	1 4%	0 0117	3 0%	0 061	4 7%	0 287	4 6%	198 5	9259	26	433	637
12'/10 07	226	4 2	0 0356	1 9%	0 0105	3 7%	0 049	6 1%	0 234	6 2%	7 0	8876	25	490	624
12'/10 05	227	2 6	0 0360	1 1%	0 0113	2 2%	0 057	3 6%	0 272	3 7%	192 0	9541	98	2458	2144
12'/10 11	228	4 5	0 0364	1 9%	0 0116	4 0%	0 059	7 1%	0 284	7 4%	49 9	9104	16	294	399
12'/10 02	230	3 5	0 0363	1 5%	0 0115	3 0%	0 051	6 1%	0 247	5 5%	27 6	10196	18	381	448
12'/10 01	234	4 0	0 0368	1 6%	0 0120	3 1%	0 049	8 4%	0 242	8 3%	2 3	9991	14	201	341
12'/10 09	235	4 7	0 0376	2 0%	0 0123	3 3%	0 060	6 0%	0 317	6 3%	50 1	8435	53	1485	1203
12'/10 06	237	3 9	0 0382	1 6%	0 0125	2 8%	0 065	6 5%	0 341	6 4%	20 6	7555	21	494	452
12'/10 08*	254	5 2	0 0401	2 0%	0 0132	3 7%	0 051	6 5%	0 269	6 2%	29 2	9556	22	284	486
12'/10 12*	320	8 2	0 0510	2 5%	0 0176	3 9%	0 055	9 6%	0 400	8 9%	6 6	11102	19	205	359
13'/3 05*	110	3 3	0 0310	1 1%	0 0650	1 6%	0 405	2 3%	1 706	2 1%	10 8	9858	82	610	1225
13'/3 09	219	4 8	0 0421	1 8%	0 0257	3 4%	0 195	4 1%	1 094	4 5%	768 9	9673	62	908	935
13'/3 11	225	3 0	0 0357	1 3%	0 0115	2 7%	0 052	4 2%	0 256	3 9%	5 9	12181	42	604	1159
13'/3 06	227	8 4	0 0389	3 5%	0 0218	8 1%	0 116	8 1%	0 645	9 2%	6 1	11471	63	984	1445
13'/3 07	231	2 8	0 0366	1 2%	0 0117	2 5%	0 053	5 0%	0 274	4 7%	44 0	10117	39	844	934
13'/3 10	232	3 5	0 0377	1 4%	0 0150	2 9%	0 073	5 2%	0 379	5 1%	13 9	11678	52	973	1197
13'/3 12	233	3 1	0 0370	1 3%	0 0116	2 5%	0 054	4 9%	0 280	5 1%	11 9	10012	27	526	667
13'/3 04	233	4 1	0 0375	1 7%	0 0134	3 3%	0 064	5 2%	0 325	4 9%	40 8	10694	40	604	971
13'/3 01	234	2 6	0 0371	1 1%	0 0117	2 3%	0 054	4 2%	0 269	4 0%	159 1	10450	29	476	703
13'/3 02	238	4 7	0 0377	1 9%	0 0120	5 3%	0 052	8 0%	0 271	7 7%	2 6	9219	18	229	485
13'/3 03	240	3 6	0 0429	1 2%	0 0217	2 5%	0 145	4 4%	0 841	4 6%	15 0	9765	51	814	837
13'/3 08	244	3 8	0 0386	1 5%	0 0126	2 7%	0 052	5 2%	0 285	5 5%	19 9	10200	24	445	550

* Sample analysis number is not used in age calculations. Comment is in text for each sample.

Table 4.2 *(continued)*

Sample	206Pb/238U age (Ma)		Isotopic ratios								Trace element data (in ppm)				
analysis no	(207Pb corrected)	+/-1s	206Pb/238U	%rsd	208Pb/232Th	%rsd	207Pb/206Pb	%rsd	207Pb/235U	%rsd	Nd	Hf	Pb	Th	U
13'/11 08	274	10	0 0434	3 4%	0 0123	15 5%	0 053	19 8%	0 265	21 8%	1 8	9284	4	39	95
13'/11 01	278	6	0 0444	2 1%	0 0135	5 2%	0 059	7 3%	0 320	7 4%	3 8	7968	16	186	336
13'/11 12	279	5	0 0442	1 8%	0 0119	4 9%	0 052	6 8%	0 281	7 0%	3 8	8443	13	154	280
13'/11 09	283	5	0 0449	1 7%	0 0146	6 3%	0 054	7 0%	0 291	7 0%	0 3	7938	15	120	342
13'/11 02	291	4	0 0462	1 5%	0 0124	3 6%	0 054	4 8%	0 311	4 9%	0 8	7304	36	433	747
13'/11 10	292	6	0 0464	2 1%	0 0145	6 6%	0 054	10 6%	0 287	10 3%	1 6	8347	9	80	177
13'/11 03	297	6	0 0472	2 0%	-0 0441	-1 1%	0 053	7 5%	0 312	7 8%	4 3	8307	6	162	300
13'/11 07	298	9	0 0468	3 0%	0 0133	10 0%	0 043	12 7%	0 235	13 1%	0 8	8489	5	37	103
13'/11 06	298	9	0 0483	3 0%	0 0117	16 0%	0 069	11 7%	0 397	11 6%	0 1	8298	4	23	84
13'/11 05	303	6	0 0481	2 0%	0 0125	5 6%	0 053	6 5%	0 314	6 7%	2 6	7919	14	141	294
13'/11 11	305	5	0 0484	1 5%	0 0141	3 8%	0 051	5 5%	0.306	5 5%	1 7	9293	23	235	449
13'/11 04	306	6	0 0486	1 8%	0 0125	5 6%	0 054	7 7%	0.319	7 9%	3 6	8598	13	145	263

Ages of rocks

CK-WB

13/3(3): Twelve zircon grains were selected for analysis from a porphyritic rhyolite. The 12 analyses are shown in Table 4.2 and Figure 4.3. Most zircon grains are consistent with a mean age of 229 ± 3 Ma. However, three of the analyses yield significantly younger ages of 203-218 Ma (Figures 4.3 a & c). There are no systematic differences between the age of the rims and cores (Figure 4.3b).

There are two possible ways to explain this data – either the sample is Late Triassic (203-218 Ma) and the older zircons were inherited from slightly older underlying rocks, or the older zircons reflect the true age, and the younger grains reflect Pb loss. The older age is preferred because it is based on more dated zircons.

14/2(1): This dacite yielded only eight zircon grains. Analysis number (14/2(1): 01* was rejected due to high common Pb and 14/2(1): 02* is an old Proterozoic inherited core (Table 4.2). The remaining zircons have a mean age of 222 ± 6 Ma with a MSWD of 3.9 (Figures 4.4 a & c). The zircons have few internal features both in CL and BSC images (Figure 4.4 b).

15'/1(1): Ten zircon crystals were separated from this CK-WB. Isotopic and trace element data for these zircon are in Table 4.2. One analysis (15'/1(1): 06*) has been rejected due to high U content and evidence of Pb loss (Table 4.2). Another crystal (15'/1(1): 02*) was broken during analysis. The data forms two distinctive groups, with a weighted average age of 272 ± 15 Ma for the older group and 223 ± 8 Ma for the younger group (Figures 4.5 a & c). There is no evidence of inherited cores in the CL images (Figure 4.5 b). The older ages are interpreted to be inherited grains and the younger ages the crystallisation age.

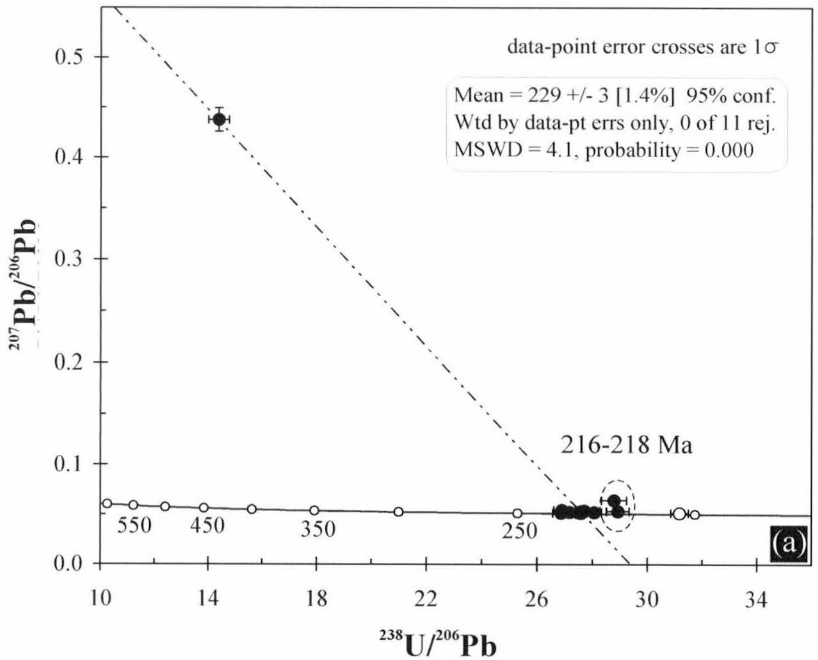

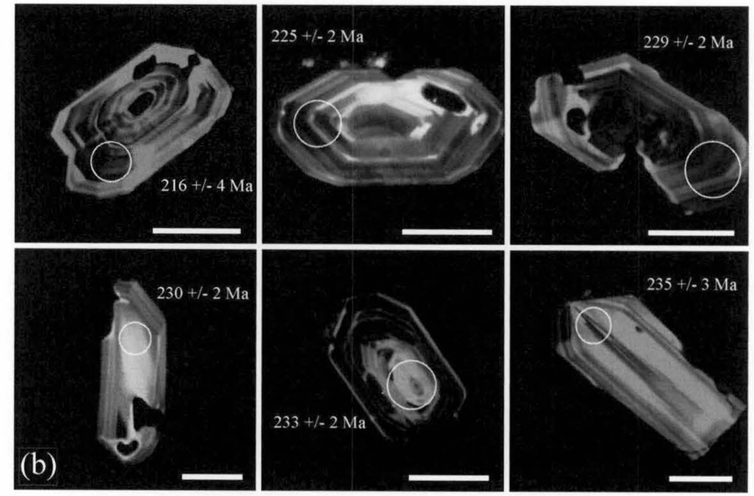

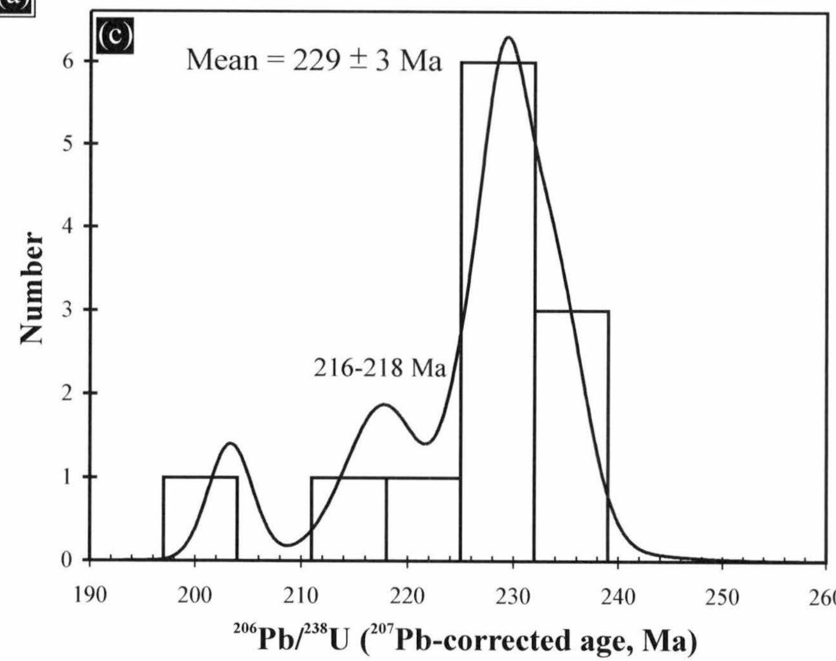

Figure 4.3 Reverse concordia plot of laser ablation ICP-MS zircon U-Pb measurements (a), CL-images (b) and ^{207}Pb-corrected age diagram (c) for rhyolitic rock sample 13/3(3) from the CK-WB. Best fit regression and ^{207}Pb-corrected age calculated using the Isoplot 3.0 software (Ludwig, 2003) assuming common Pb composition based on the 2 stage model of Stacey & Kramer (1975) at 230 Ma. Note; analyses shown in black circle are those used for age calculations whereas white circle are rejected in (a); scale bar is 50 microns long in (b).

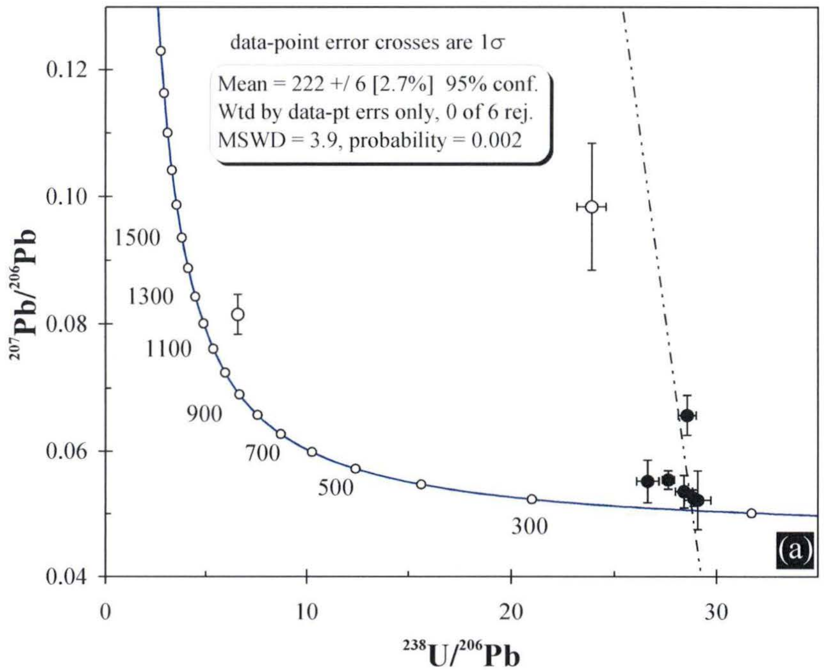

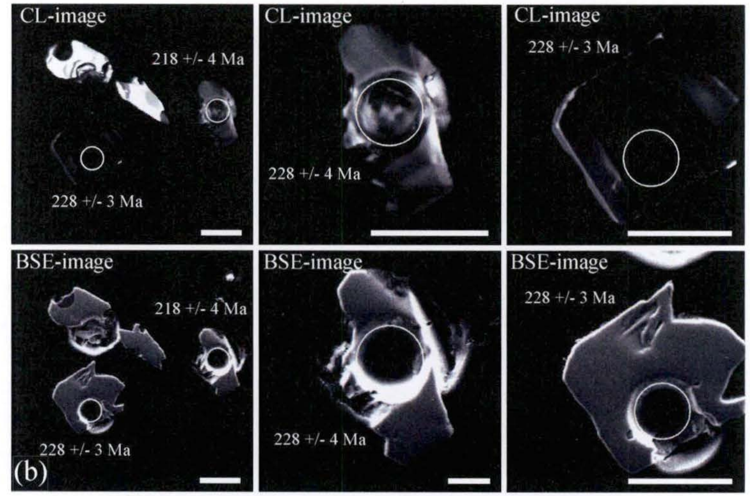

Figure 4.4 Reverse concordia plot of laser ablation ICP-MS zircon U-Pb measurements (a), CL- and BSE-images (b) and ^{207}Pb-corrected age diagram (c) for dacitic rock sample 14/2(1) from the CK-WB. Best fit regression and ^{207}Pb-corrected age calculated using the Isoplot 3.0 software (Ludwig, 2003) assuming common Pb composition based on the 2 stage model of Stacey & Kramer (1975) at 222 Ma. Symbols as in Figure 4.3

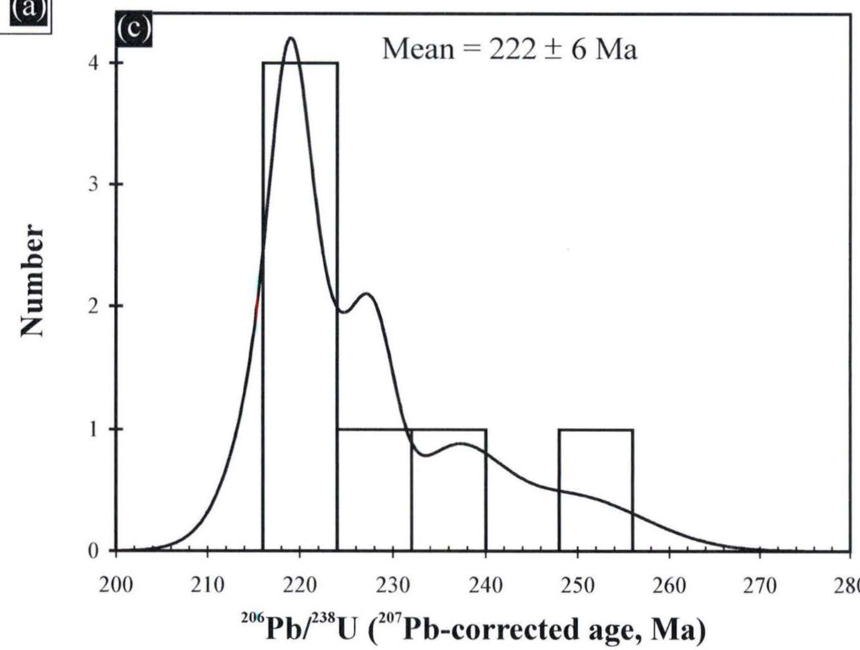

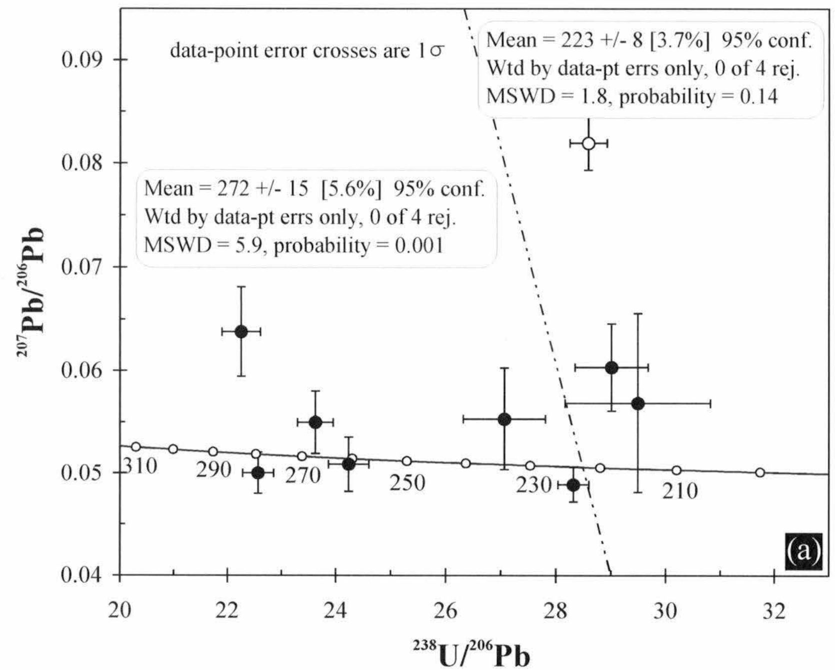

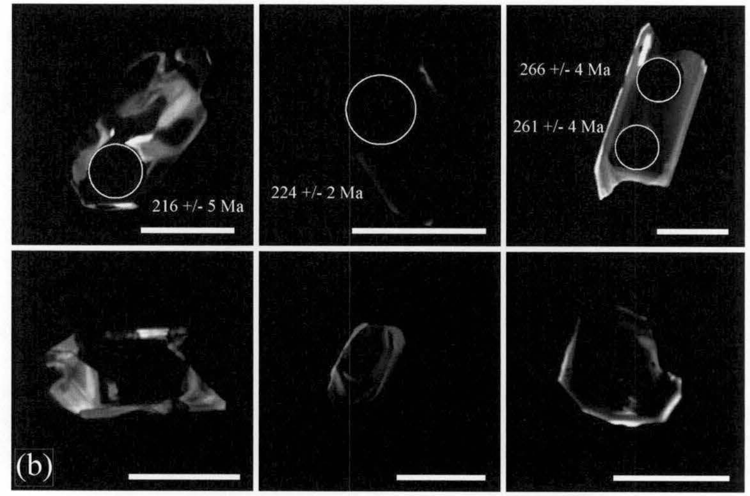

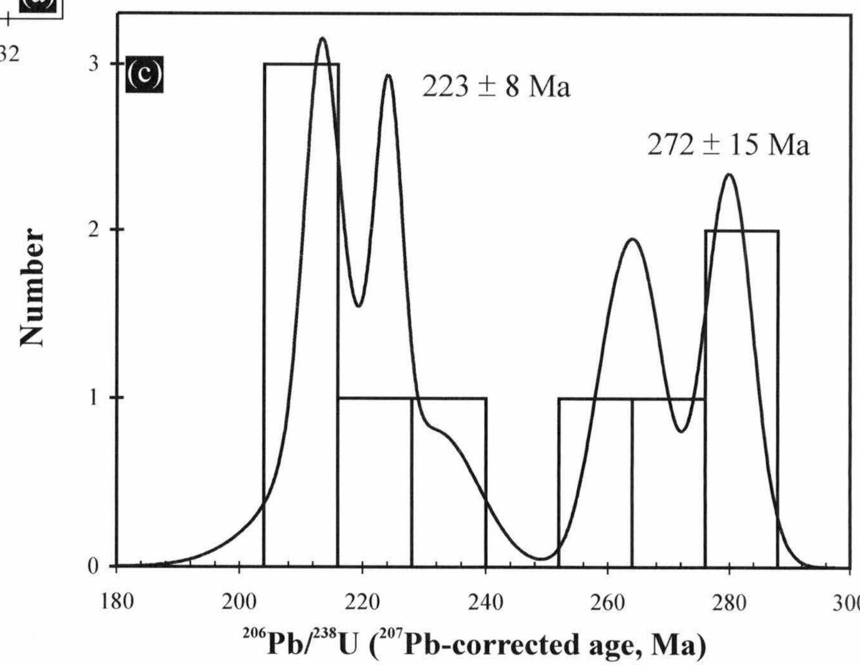

Figure 4.5 Reverse concordia plot of laser ablation ICP-MS zircon U-Pb measurements (a), CL-images (b) and ^{207}Pb-corrected age diagram (c) for microdiorie rock sample 15'/1(1) from the CK-WB. Best fit regression and ^{207}Pb-corrected age calculated using the Isoplot 3.0 software (Ludwig, 2003) assuming common Pb composition based on the 2 stage model of Stacey & Kramer (1975) at 223 Ma. Symbols as in Figure 4.3.

26'/10: Twelve euhedral to subhedral zircon crystals from a CK-WB rhyolitic dyke were analysed. Oscillatory growth zoning is common on CL images and some grains have dark (low U) cores. One analysis (26'/10: 04*) was rejected due to high U content and Pb loss (Table 4.2). The age of the 11 remaining zircons form two distinctive groups (Figures 4.6 a & c), one with lower U contents at 231 ± 3 Ma with a MSWD 1.6 and a higher-U group at 221 ± 2 with a MSWD 0.71. The data suggest that the low U cores of zircons formed at 231 ± 3 Ma and the higher U rims at 221 ± 2 Ma. The high and low U zones could not be analysed individually as they are too small (10 micron).

CK-CB

16'/10(1): Twelve selected zircon grains were analysed from a CK-CB rhyolite (Table 4.2; Figure 4.7a). Three analyses are older than the rest and probably represent early Triassic and Permian inherited cores (Figure 4.7a). The 9 remaining analyses have a mean age of 220 ± 5 Ma with a MSWD of 2.4 (Figures 4.7 a & c).

Summary

The igneous rocks from the Chiang Khong area of the CLT volcanic belt mainly crystallised between 237 Ma and 216 Ma (Middle to Late Triassic age; Figures 4.3-4.7). Most samples contain zircons with two age groups. This feature is especially prominent in sample 26'/10 (Figure 4.6), where the younger zircons average 221 Ma whereas the older age group is around 231 Ma. There are no distinctive internal textural differences between the zircon grains in these two age groups. An older zircon age group, 261 to 280 Ma (mean age = 272 ± 15 of Middle Permian), was recognised in sample number 15'/1(1) (Figure 4.5). This is considered to be inherited by assimilation of zircons from an earlier igneous phase (cf. 8"-2 granite). The preliminary interpretation here is that the younger group in each case is the best indication of the crystallization age of these rocks, except for sample 13/3(3) where only a few poorly clustered younger ages were recovered from mostly high-U zircons.

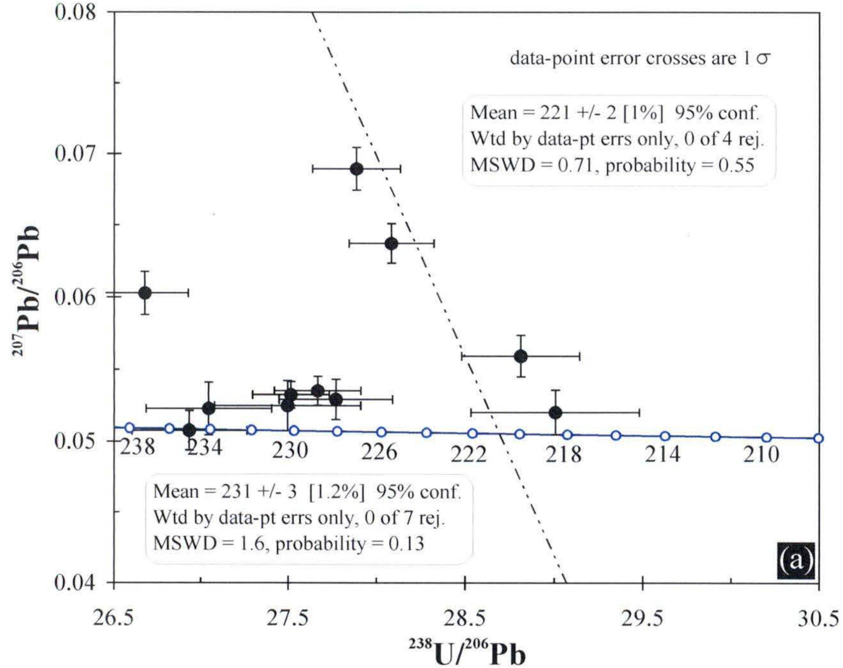

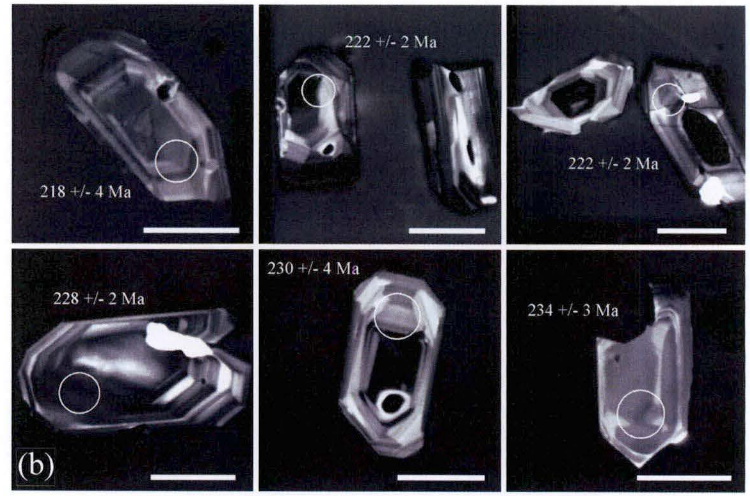

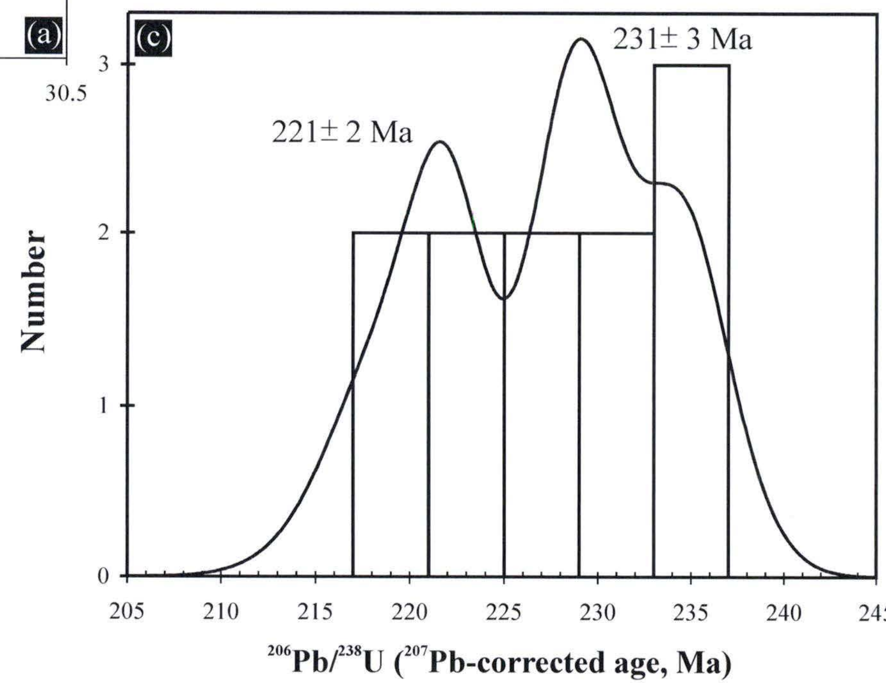

Figure 4.6 Reverse concordia plot of laser ablation ICP-MS zircon U-Pb measurements (a), CL-images (b) and ^{207}Pb-corrected age diagram (c) for rhyolitic intrusive rock sample 26'/10 from the CK-WB. Best fit regression and ^{207}Pb-corrected age calculated using the Isoplot 3.0 software (Ludwig, 2003) assuming common Pb composition based on the 2 stage model of Stacey & Kramer (1975) at 221 Ma. Symbols as in Figure 4.3. Note, one younger high U zircon is out of diagrams (a) & (c).

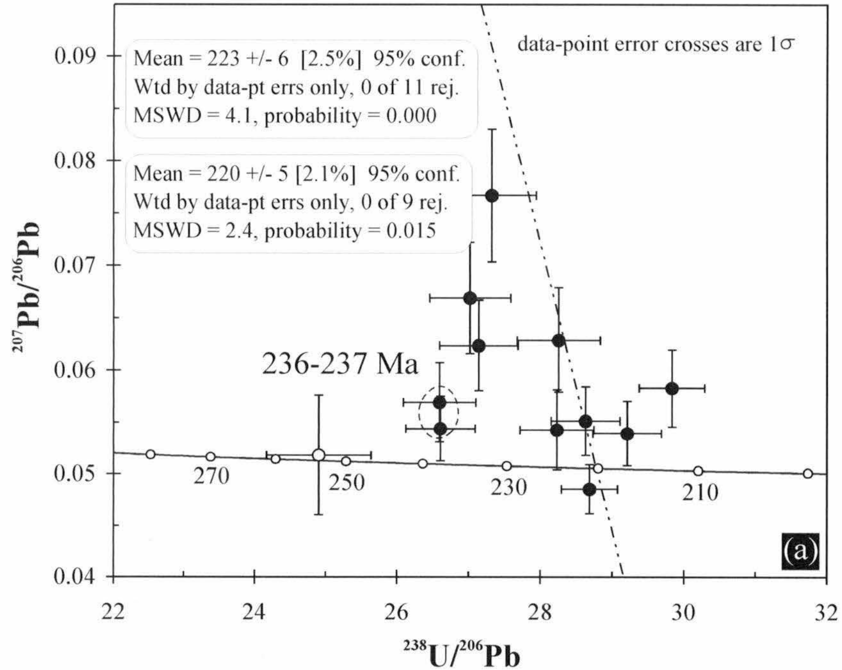

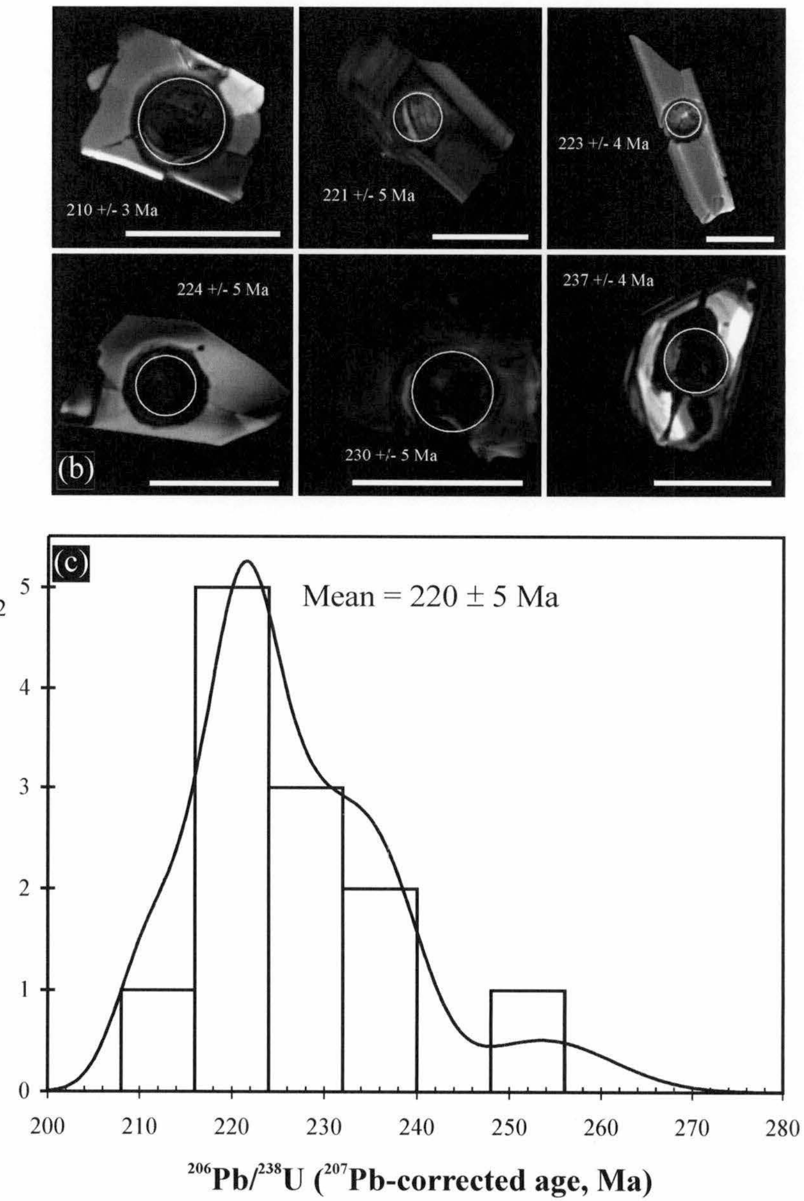

Figure 4.7 Reverse concordia plot of laser ablation ICP-MS zircon U-Pb measurements (a), CL-images (b) and ^{207}Pb-corrected age diagram (c) for rhyolitic rock sample 16'/10 from the CK-CB. Best fit regression and ^{207}Pb-corrected age calculated using the Isoplot 3.0 software (Ludwig, 2003) assuming common Pb composition based on the 2 stage model of Stacey & Kramer (1975) at 220 Ma. Symbols as in Figure 4.3.

4.3.2 The Lampang area

Morphology of zircons

Zircons from CLT rocks in the Lampang area are euhedral to anhedral crystal and 30 to 200 microns in diameter (Figures 4.8b to 4.12b). Zircons from the intrusive rocks are typically bigger than volcanic zircons. The crystal shape is mainly prismatic, dominantly with prism and bipyramidal faces. In the CL images, the zircons commonly show magmatic growth zoning (cf. Corfu *et al.,* 2003), and inherited cores, internal cracks and inclusions are rare. Most zircons are fairly dark in the CL images. There is only one zircon from LP-WB rhyolite shown bright colour in CL emission

Ages of rocks

LP-WB

12'/5(3): Of the twelve grains analysed from LP-WB rhyolite 12'/5(3) (Table 4.2), two analyses (12'/5(3): 09* and 01*) were significantly older than the rest and rejected. The ten remaining analyses have a mean age of 233 ± 5 Ma with a MSWD of 2.6 (Figure 4.8).

LP-CB

7/7(2): Most of the 12 zircons analysed from this sample have oscillatory zoning on the CL images and all have high to very high U content (800-4000 ppm). Consequently, many of the analyses have Pb loss associated with radiation damage (Table 4.2). Analyses 7/7(2): 01*, 02*, 05* and 06* have been rejected, as they show evidence of Pb loss associated with high U contents. On the LA ICP-MS, the isotopes and the age are measured in time-resolved mode, so that the age is measured every 0.1-0.2 micron as the laser is drilling into the crystal. On the very high U zircons such as those in this sample, the analyses show an inverse relationship in the time resolved signal between U content and apparent age because Pb is being lost mostly from the high U parts of crystal. Analysis 7/7(2): 11* is significantly older than the rest probably due to inheritance. Only 7 analyses were used to calculate the age (223 ± 4 Ma of this rock (Figures 4.9 a & c). However, as with many of the analyses from this study, two distinctive age groups are present (225-228 Ma and 217-221 Ma).

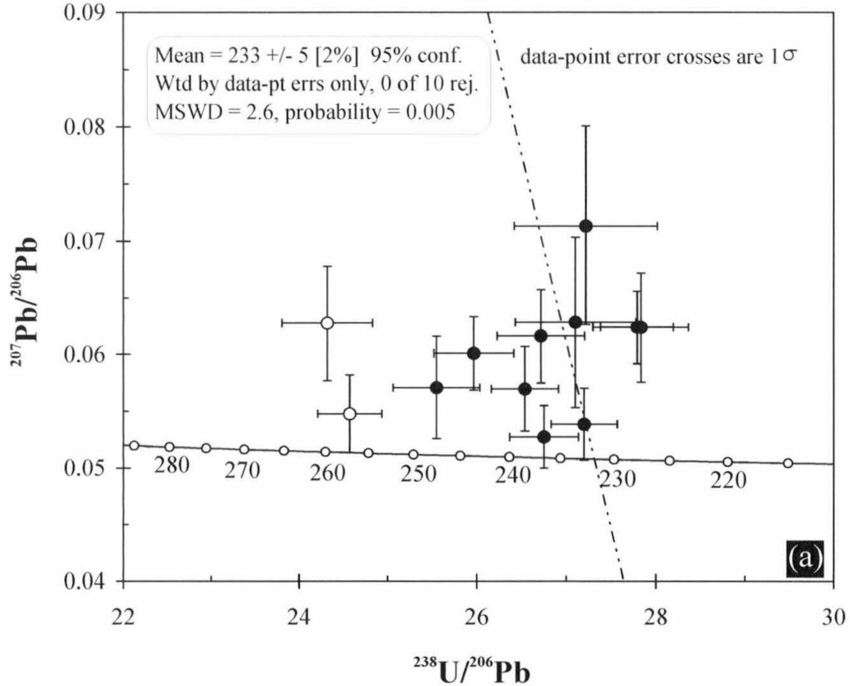

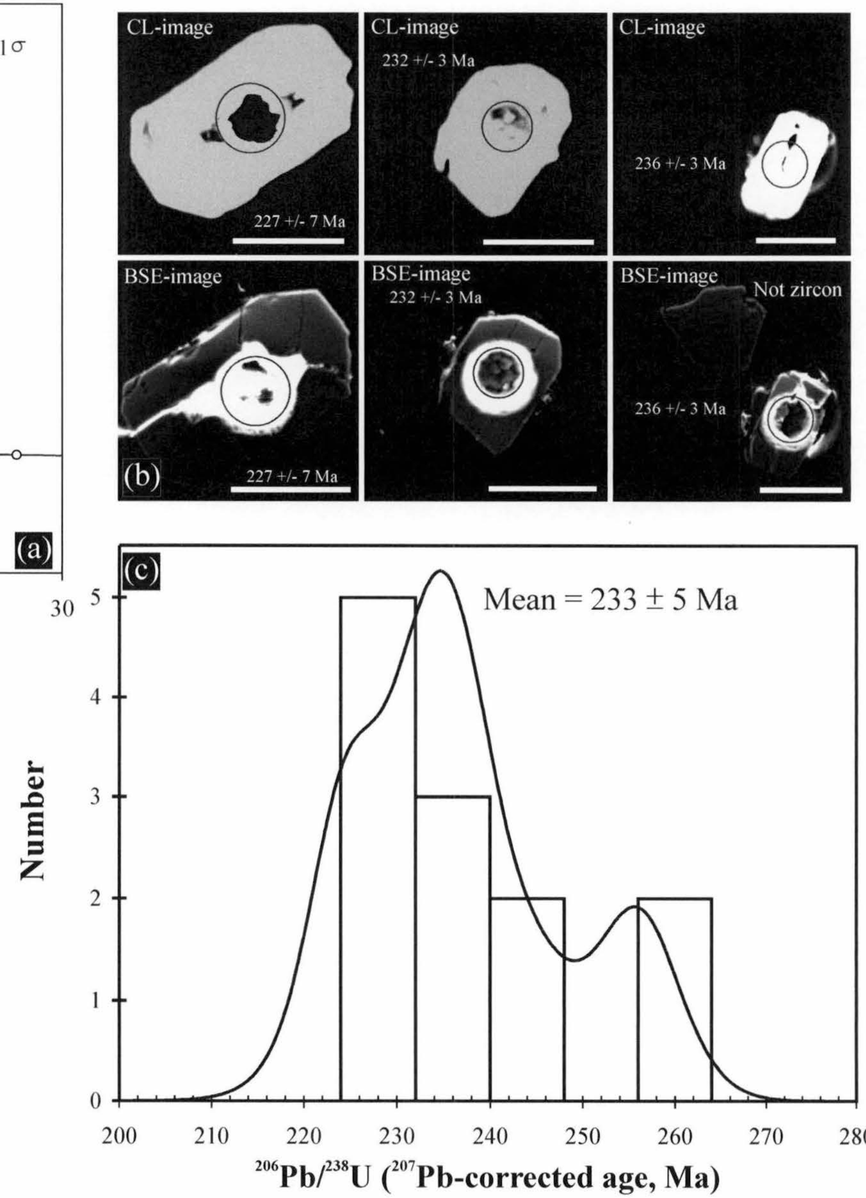

Figure 4.8 Reverse concordia plot of laser ablation ICP-MS zircon U-Pb measurements (a), CL- and BSE-images (b) and ^{207}Pb-corrected age diagram (c) for rhyolitic rock sample 12'/5(3) from the LP-WB. Best fit regression and ^{207}Pb-corrected age calculated using the Isoplot 3.0 software (Ludwig, 2003) assuming common Pb composition based on the 2 stage model of Stacey & Kramer (1975) at 233 Ma. Symbols as in Figure 4.3.

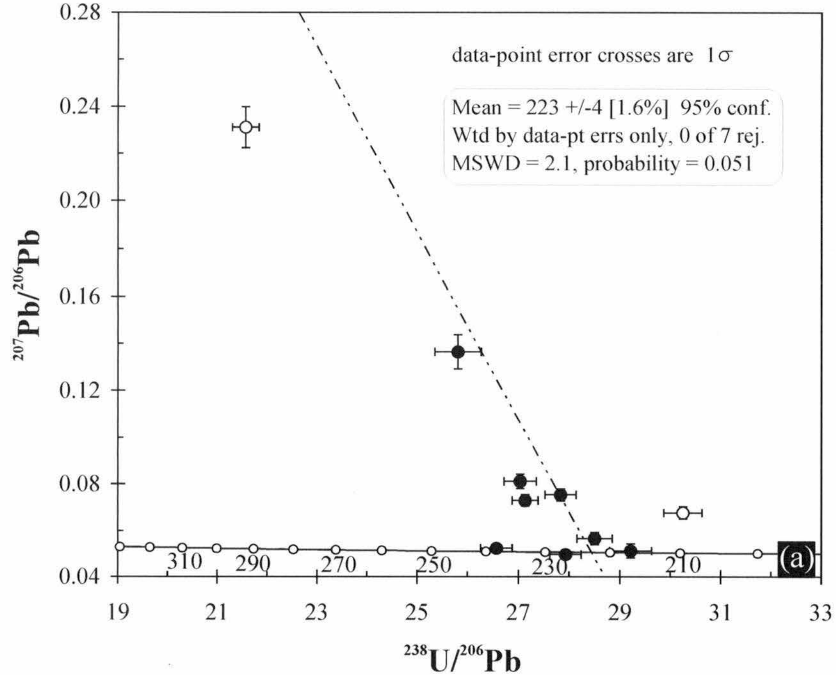

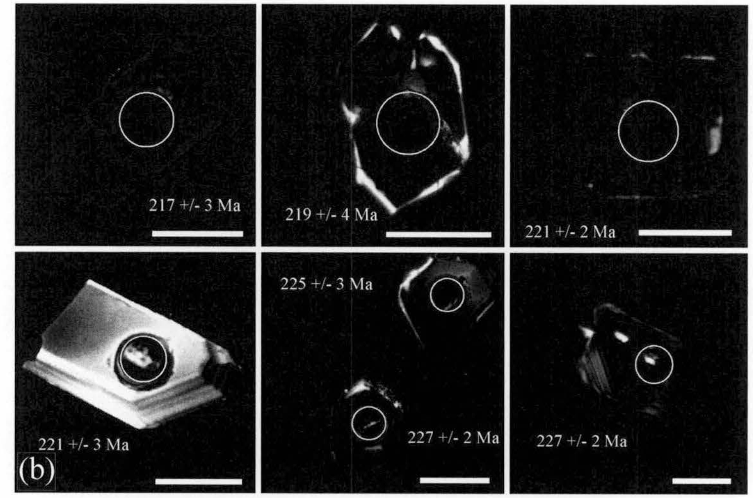

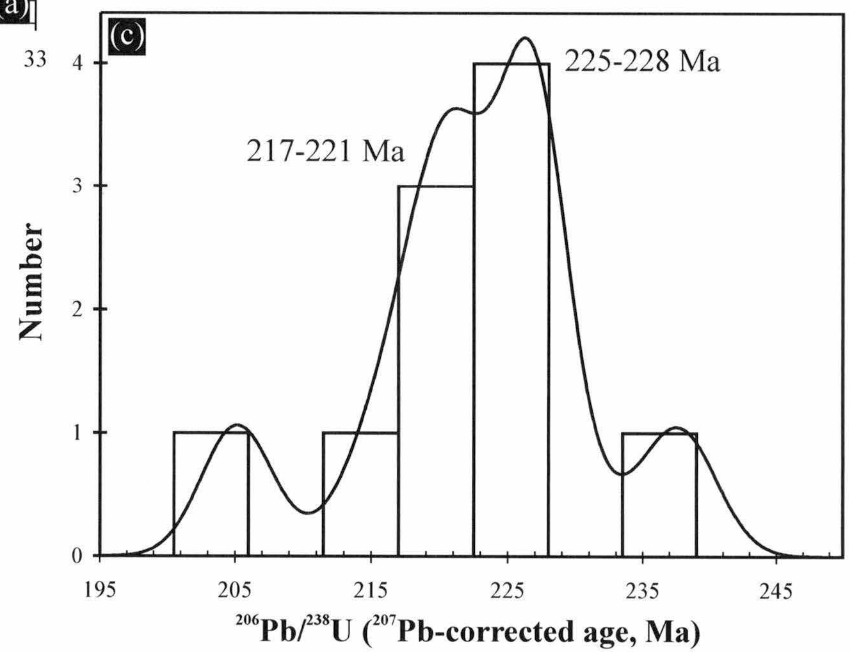

Figure 4.9 Reverse concordia plot of laser ablation ICP-MS zircon U-Pb measurements (a), CL-images (b) and ^{207}Pb-corrected age diagram (c) for rhyolitic rock sample 7/7(2) from the LP-CB. Best fit regression and ^{207}Pb-corrected age calculated using the Isoplot 3.0 software (Ludwig, 2003) assuming common Pb composition based on the 2 stage model of Stacey & Kramer (1975) at 223 Ma. Symbols as in Figure 4.3.

12'/10: Twelve zircon grains were separated from this dacitic dyke in the LP-CB. Two analyses, 12'/10: 8* and 12'/10: 12*, have been rejected as they are significantly older than the rest. There is no distinctive inheritance features in the CL images but the old core ages were detected in some zircon grains (Figure 4.10b). The preferred crystallisation age for this rock is 227 ± 4 Ma (Figures 4.10a & c).

TN-CB

13'/3: 13'/3 is a granite from TN-CB. Oscillatory growth zoning is common in the CL image. No inherited cores were observed in the LA-ICP-MS analyses (Figure 4.11b). One analysis (13'/3: 05* in Table 4.2) has been rejected due to high U content. The eleven remaining crystals have a mean age of 233 ± 4 Ma (Middle Triassic) with a MSWD of 2.9 (Figures 4.11 a & c).

13'/11: A hornblende-quartz diorite from the TN-CN has zircon grains with oscillatory growth zoning and which are very bright in CL images (i.e. low U contents) (Table 4.2). The zircons yield a mean age of 292 ± 7 Ma (Late Carboniferous to Early Permian) with a MSWD of 3.5. Four zircon grains in this sample could form a younger age group at 274-283 Ma. However, there is not sufficient evidence to split the population and a combined group age is preferred here (Figures 4.12 a & c). There is no CL evidence for the existence of inherited cores (Figure 4.12b).

Summary

The ages of the Lampang igneous rocks vary from Middle to Late Triassic age (233 to 217 Ma). Many show evidence for two populations of grains. The younger group is between 221 to 217 Ma, whereas the older group range between 233 and 225 Ma. The origin of these two groups remains uncertain. In this analysis both groups have been accepted as part of one population and a group mean age is the preferred crystallisation age. Zircon from the LP-WB rhyolite (233 ± 5 Ma) and the TN-CB granite (233 ± 4 Ma) are slightly older than the zircon from the LP-CB intrusive rhyolite (mean age = 227 – 223 Ma).

The one sample that is completely different is hornblende diorite 13'/11, which has a crystallisation age of 292 ± 7 Ma (Late Carboniferous-Early Permian age). This is the oldest rock dated in this program and is assumed to be part of an earlier magmatic event.

4.3.3 Summary

Intermediate to felsic volcanic rocks and associated shallow intrusives of the CLT contain magmatic euhedral to subhedral zircon grains 30-200 microns in diameter. Small anhedral grains are rare and limited to the volcanic rocks. CLT zircon varies from short to long prismatic shapes dominated by prism and bipyramidal faces. CL images commonly show oscillatory growth zoning. Inherited cores, inclusions and resorbed edges are uncommon. Most zircons are not very luminescent under the electron beam due to relatively high U contents (mainly >400 ppm). Only those from the LP-WB rhyolite and the older Early Permian granite are bright, with low U and Th concentration (90-600 ppm).

Ages of igneous zircons from the CLT volcanic belt are mainly 230 to 220 Ma (late Middle to early Late Triassic) and they show two distinctive population ages. The younger group is about 220 Ma, whereas the old group is 230 Ma. The origin of these two age groups remains uncertain and there are no distinctive internal textural differences between the zircon grains in the two groups. In this study, late Middle to early Late Triassic is considered to be the preferred crystallisation age of the CLT igneous rocks. Some zircon grains from sample number 15'/1(1), the CK-WB rhyolite, are older, 261-280 Ma (Permian). The grain ages are probably inherited from magmatic rocks in the basement. One such source of these older zircons is the foliated granite from the Ban Huak area (see below). The hornblende diorite from the southern area of TN-CB yielded the oldest age at 292 ± 7 Ma (Carboniferous-Permian).

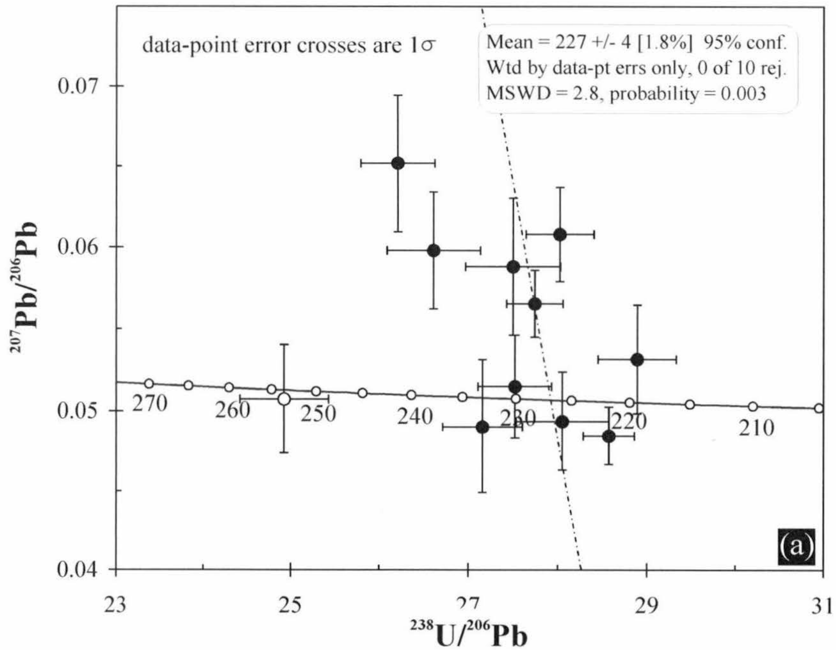

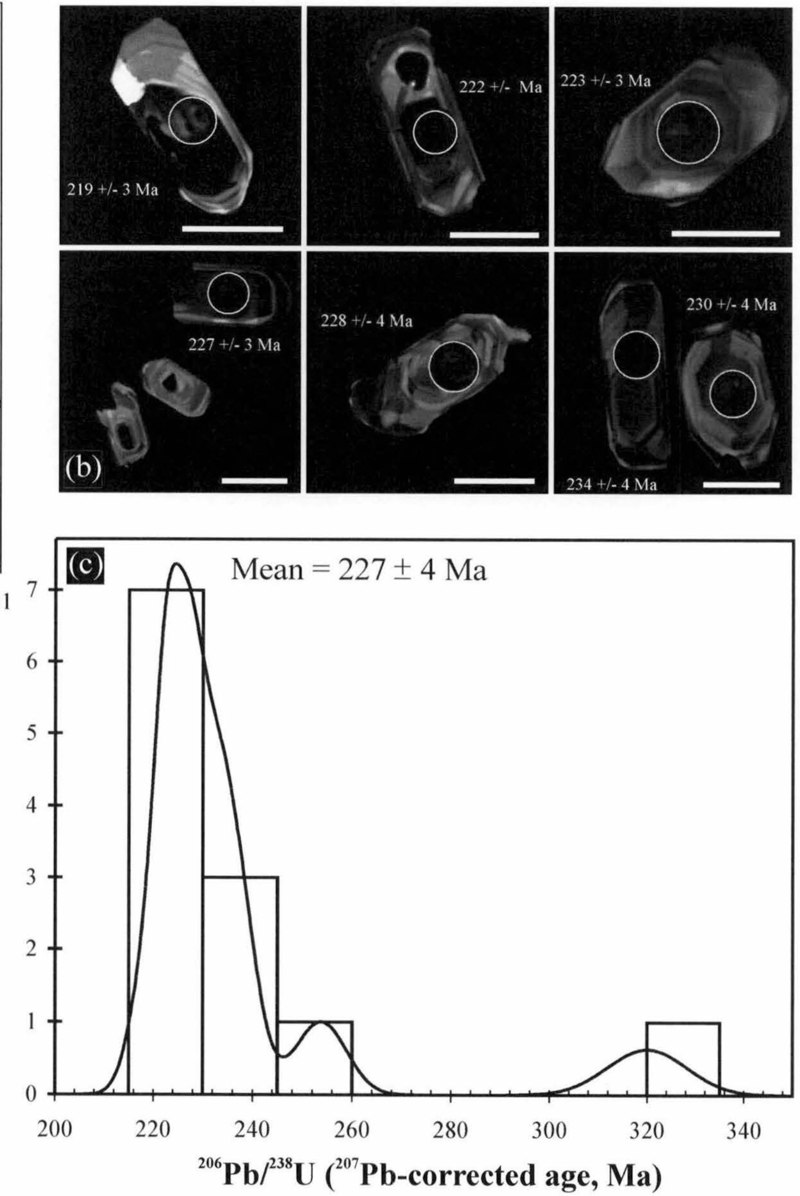

Figure 4.10 Reverse concordia plot of laser ablation ICP-MS zircon U-Pb measurements (a), CL-images (b) and ^{207}Pb-corrected age diagram (c) for dacitic intrusive rock sample 12'/10 from the LP-CB. Best fit regression and ^{207}Pb-corrected age calculated using the Isoplot 3.0 software (Ludwig, 2003) assuming common Pb composition based on the 2 stage model of Stacey & Kramer (1975) at 227 Ma. Symbols as in Figure 4.3.

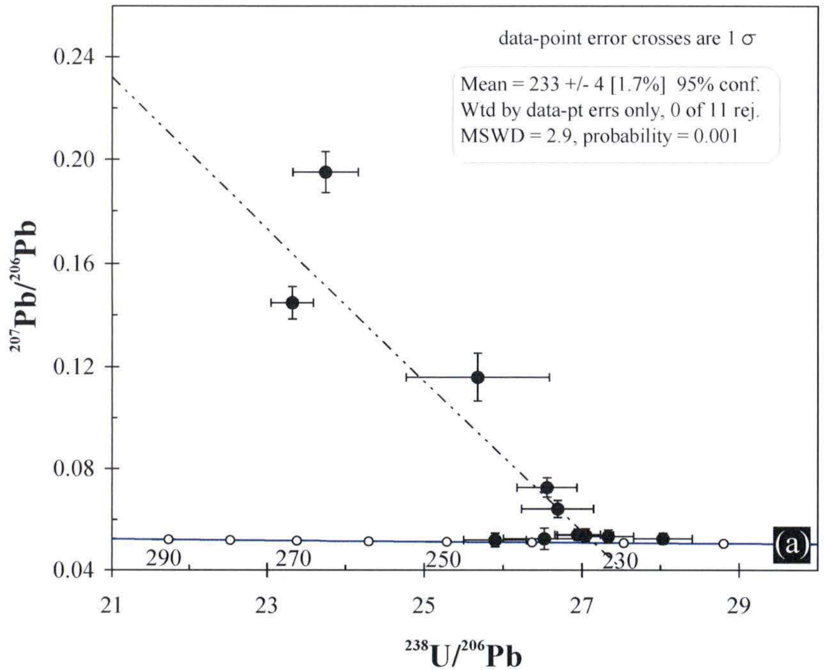

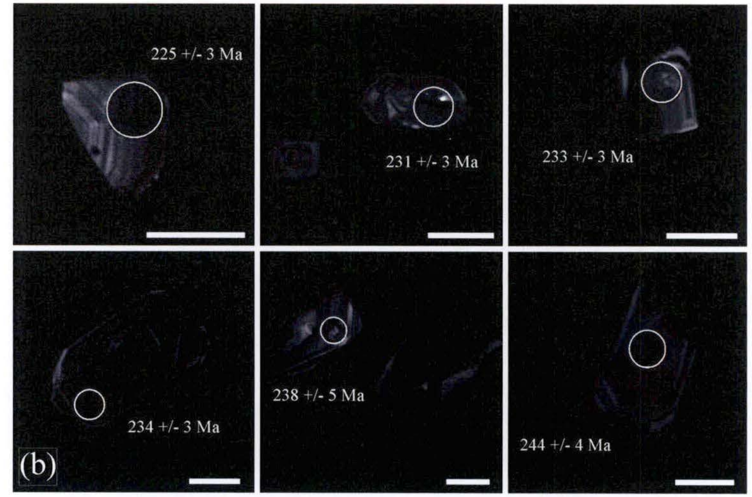

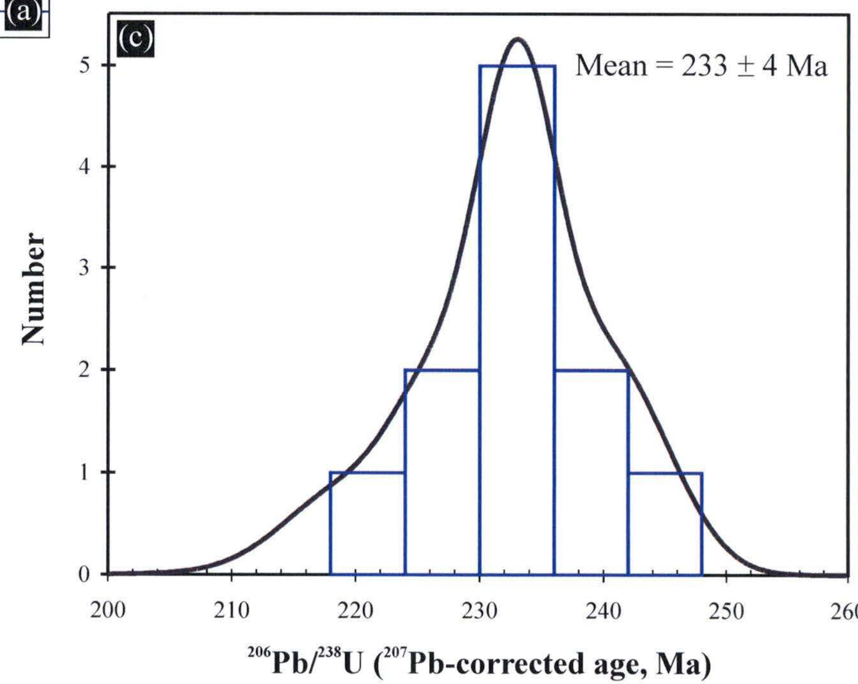

Figure 4.11 Reverse concordia plot of laser ablation ICP-MS zircon U-Pb measurements (a), CL-images (b) and ^{207}Pb-corrected age diagram (c) for granitic rock sample 13'/3 from the TN-CB. Best fit regression and ^{207}Pb-corrected age calculated using the Isoplot 3.0 software (Ludwig, 2003) assuming common Pb composition based on the 2 stage model of Stacey & Kramer (1975) at 233 Ma. Symbols as in Figure 4.3. Note, younger high U zircon is out of diagrams (a) & (c).

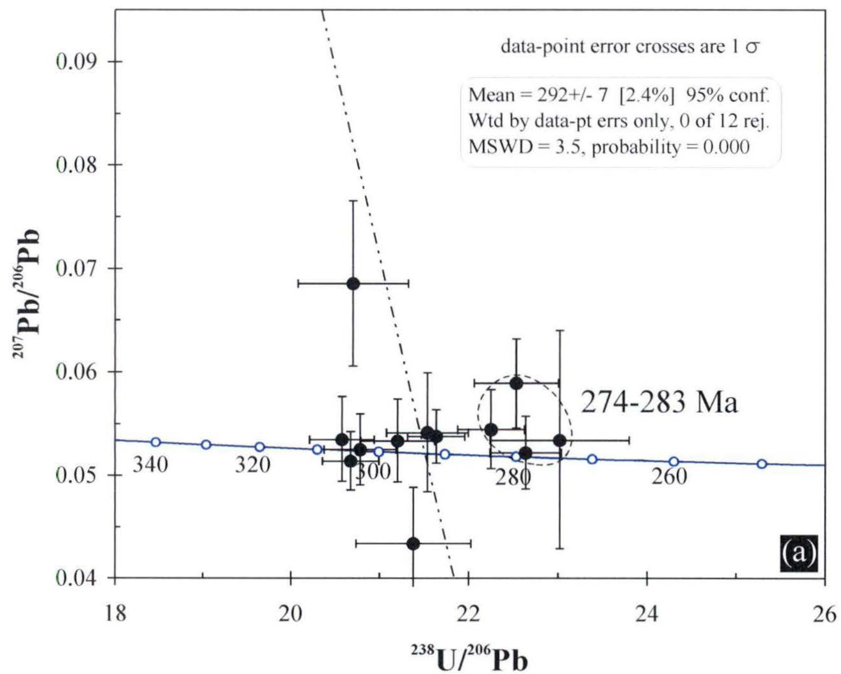

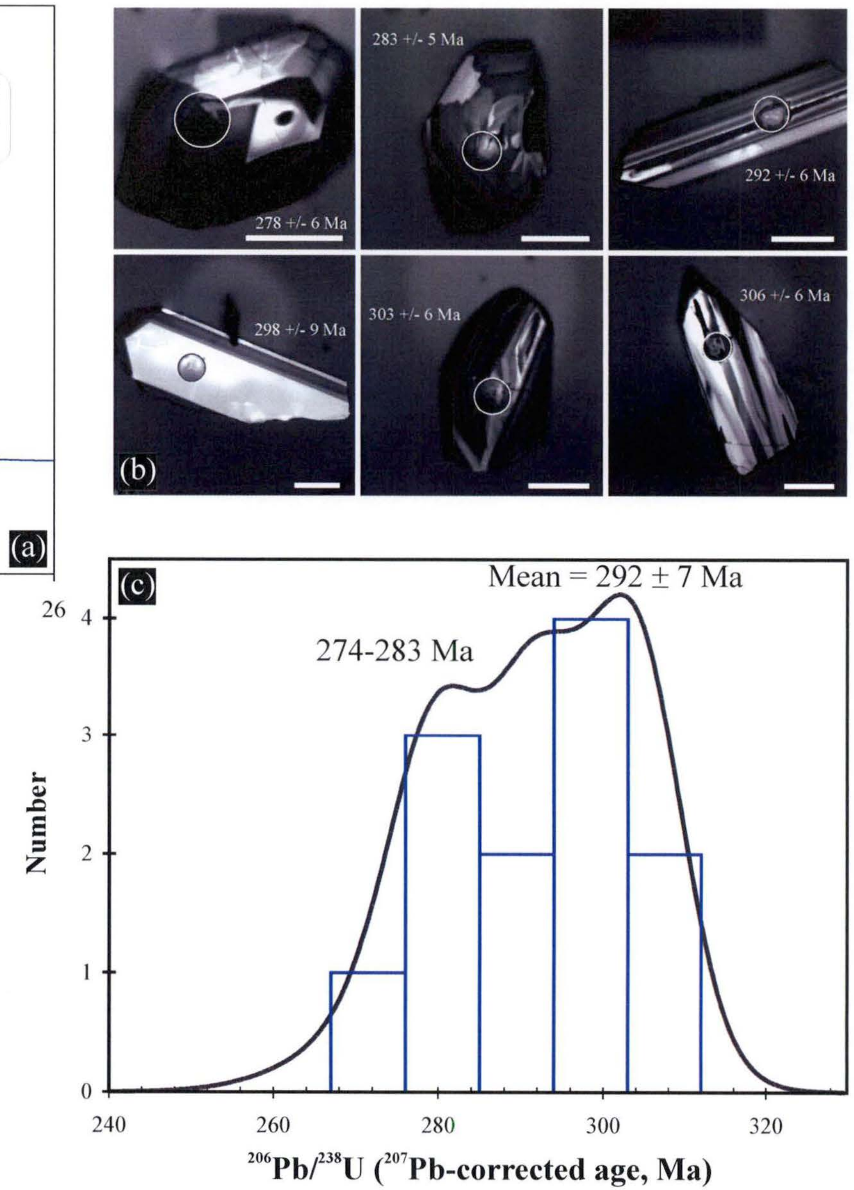

Figure 4.12 Reverse concordia plot of laser ablation ICP-MS zircon U-Pb measurements (a), CL-images (b) and ^{207}Pb-corrected age diagram (c) for hornblende dioritic rock sample 13'/11 from the TN-CB. Best fit regression and ^{207}Pb-corrected age calculated using the Isoplot 3.0 software (Ludwig, 2003) assuming common Pb composition based on the 2 stage model of Stacey & Kramer (1975) at 292 Ma. Symbols as in Figure 4.3.

4.4 Age of Mylonitic Granite

A gneissic granite (8"-2) was collected for U-Pb zircon age dating and chemical monazite age dating. The granite has a metamorphic assemblage quartz-feldspar-chlorite-white mica with a mylonitic texture (8"-2 on Figure 4.1). Zircon separated from this rock has euhedral to subhedral grains with short to long prismatic shapes. The internal features of the zircon grains are not obvious (Figure 4.13b) and they have low Th and U concentrations. Most grains are concordant with three containing some common Pb. The ^{207}Pb-corrected $^{206}Pb/^{238}U$ age forms a single population with a MSWD of 1.2. There is no evidence of inheritance in this data. The zircon $^{206}Pb/^{238}U$ age of this sample is 256 ± 2 Ma (Permian) (Figures 4.13a & c, Table 4.3).

The high strain and recrystallisation in this rock suggested that monazite may be reset to the metamorphic age. To test this, the chemical U-Th-Pb monazite age was measured. Monazite in this mylonitic granite is about 50 microns in diameter (Figures 4.14a & b). Large grains, 100 - 200 microns long, were also detected (Figures 4.14 c & d). The analysis specifications are given with the full chemical analyses and individual spot ages in Appendix E. The analyses were measured over 22 grains. The average Th content is 2.89 wt%. The chemical U-Th-Pb age calculated using this technique is 272 ± 19 Ma. This is within error of the magmatic age and there is no evidence of new grain growth during metamorphism.

The new U-Pb zircon age for the mylonitic granitoid is older than the previously suggested Triassic age (Tansuwan & Chitmanee 1990 a & b).

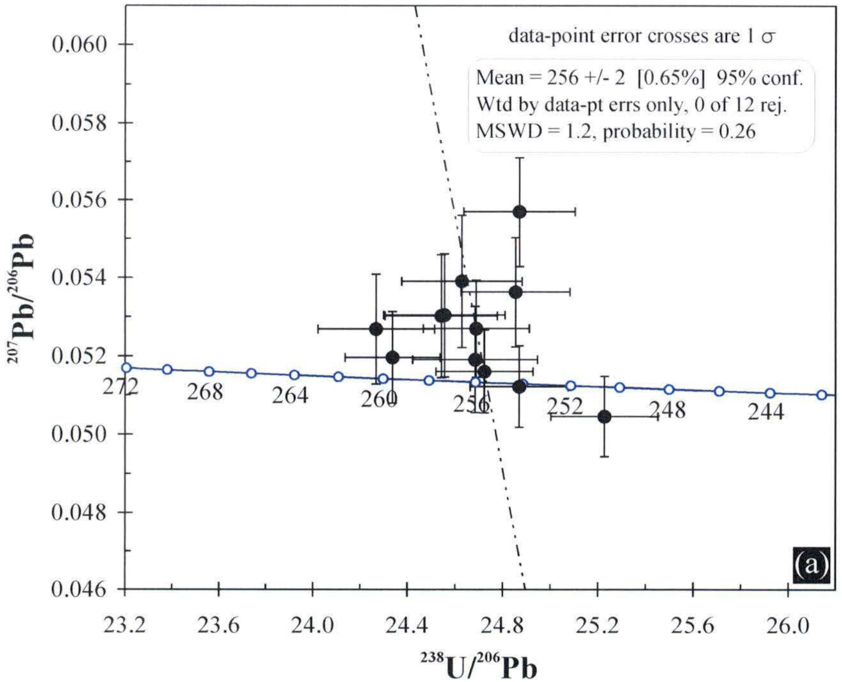

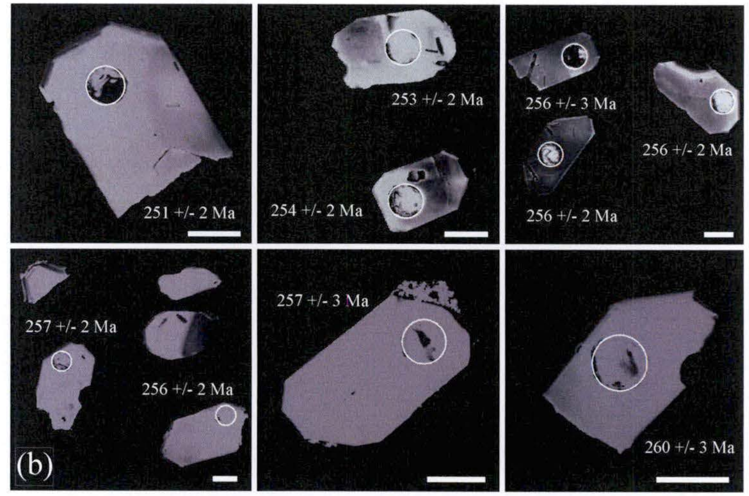

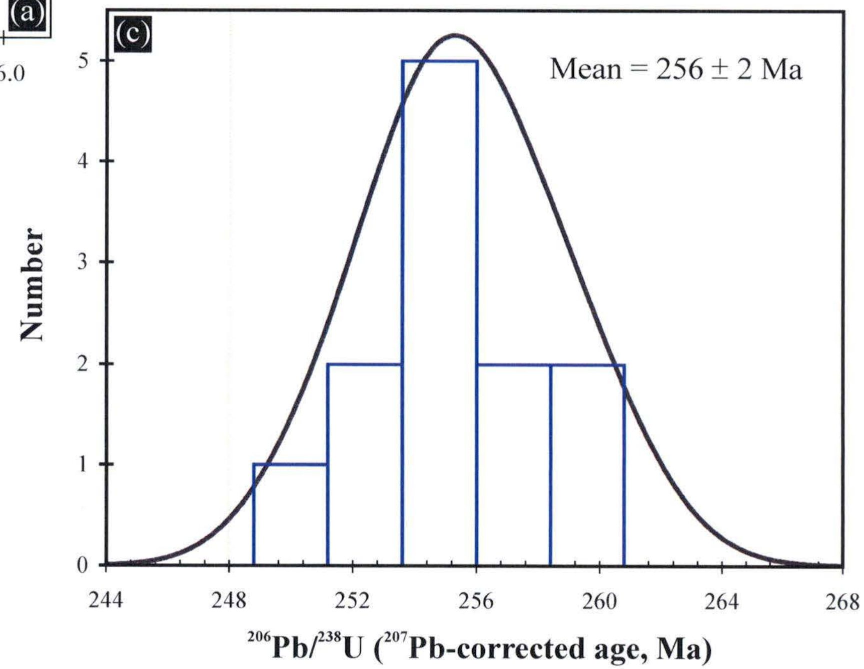

Figure 4.13 Reverse concordia plot of laser ablation ICP-MS zircon U-Pb measurements (a), CL-images (b) and ^{207}Pb-corrected age diagram (c) for mylonitic granitiod sample 8"-2 from the high strain rock area (BH-area). Best fit regression and ^{207}Pb-corrected age calculated using the Isoplot 3.0 software (Ludwig, 2003) assuming common Pb composition based on the 2 stage model of Stacey & Kramer (1975) at 256 Ma. Symbols as in Figure 4.3.

Table 4.3 Laser ablation ICPMS U-Pb isotopic and trace element data for zircons from mylonitic granitoid rock of the high strain rock area (the Ban Huak area).

Sample	206Pb/238U age (Ma)		Isotopic ratios								Trace element data (in ppm)				
analysis no	(207Pb corrected)	+/-1s	206Pb/238U	%rsd	208Pb/232Th	%rsd	207Pb/206Pb	%rsd	207Pb/235U	%rsd	Nd	Hf	Pb	Th	U
8"-2 11	251	2 2	0 0396	0 9%	0 0133	1 5%	0 050	2 0%	0 282	1 9%	7 0	9964	11	264	257
8"-2 03	253	2 4	0 0402	0 9%	0 0136	1 9%	0 056	2 5%	0 311	2 4%	77 1	10235	7	109	159
8"-2 04	254	2 3	0 0402	0 9%	0 0135	1 7%	0 054	2 6%	0 301	2 5%	12 4	10137	7	115	167
8"-2 10	254	2 1	0 0402	0 8%	0 0135	1 5%	0 051	2 0%	0 290	2 0%	3 3	10368	12	188	287
8"-2 07	256	2 1	0 0404	0 8%	0 0132	1 5%	0 052	2 0%	0 296	2 0%	5 1	10766	11	193	270
8"-2 06	256	2 3	0 0405	0 9%	0 0133	1 7%	0 053	2 4%	0 299	2 2%	2 9	10320	8	129	181
8"-2 08	256	2 6	0 0406	1 0%	0 0134	2 5%	0 054	3 1%	0 304	2 9%	2 4	9909	4	58	90
8"-2 12	256	2 7	0 0405	1 1%	0 0134	2 1%	0 052	2 6%	0 295	2 8%	18 2	10939	11	194	274
8"-2 05	257	2 7	0 0407	1 0%	0 0133	2 2%	0 053	3 0%	0 300	2 9%	1 7	9644	5	70	109
8"-2 09	257	2 5	0 0407	1 0%	0 0135	2 2%	0 053	3 0%	0 299	2 8%	1 1	10025	4	59	108
8"-2 02	259	2 1	0 0411	0 8%	0 0134	1 7%	0 052	2 2%	0 298	2 1%	2 6	10511	9	144	210
8"-2 01	260	2 6	0 0412	1 0%	0 0139	2 1%	0 053	2 7%	0 304	2 5%	32 5	9382	5	82	125

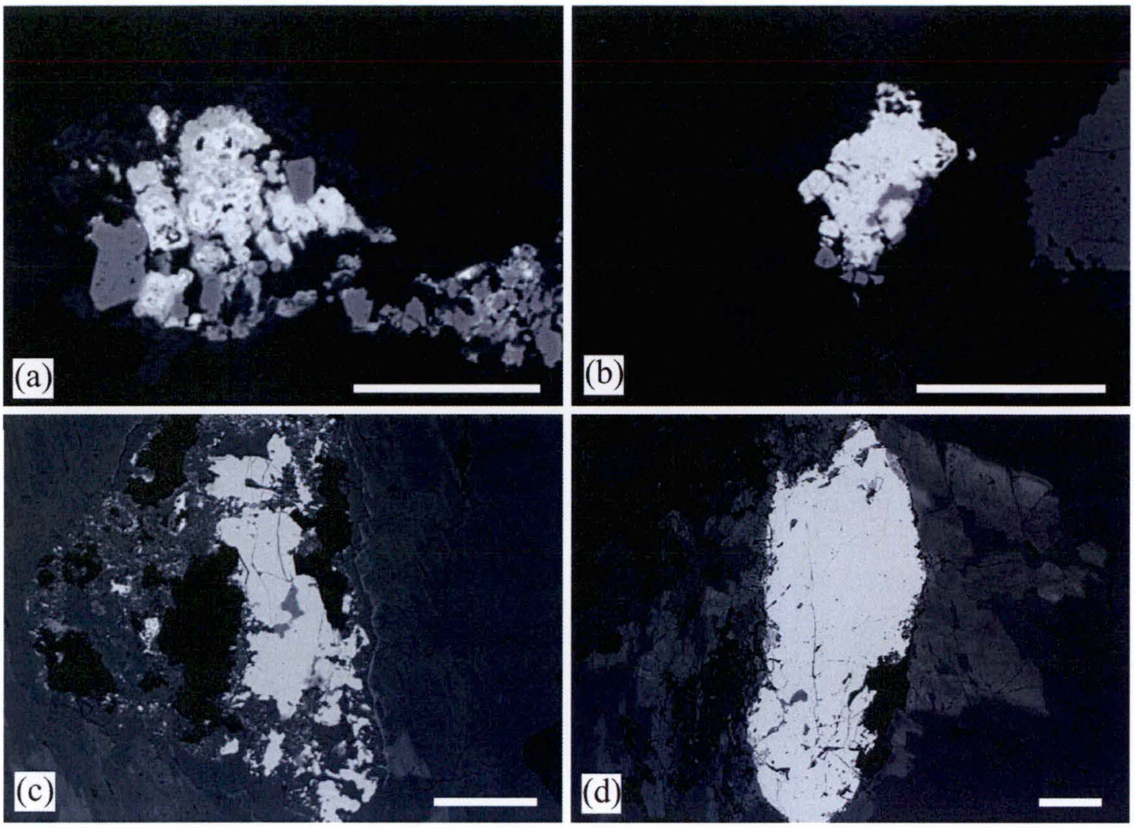

Figure 4.14 Back scattered electron image of monazite in mylonitic granitoid from high strain rocks of the Ban Huak area, southeastern corner of the Chiang Khong area. Note: scale bar is 50 micron long.

4.5 Ages of Sedimentary Rocks

Detrital zircons were separated from seven sedimentary rocks in the CLT, including five samples for the northern area and two samples for the southern area. Descriptions of these sedimentary rocks and morphology of enclosed zircon grains are shown in Table 4.4. Laser ablation ICP-MS U-Pb isotopic and trace element data for these zircons are presented in Table 4.5.

4.5.1 The Chiang Khong area

The five sedimentary rock samples from the Chiang Khong area included one Permo-Triassic sandstone from the CK-WB, three samples of the Carboniferous-Permian meta-sandstone of the Ban Huak area, and one sandstone from the Late Triassic-Early Jurassic

CK-EB redbed sequence. The ages of these rock has been previously deduced by stratigraphic correlation from the geologic mapping (Bruan & Hahn, 1976; Sukvattananunt *et al.* 1985a, b; Sukvattananunt & Assawapatchara, 1989a, b, c, d; Tansuwan & Chitmanee, 1990a, b).

Morphology of zircons

Most detrital zircon grains from the Chiang Khong area are 50 to 170 microns diameter subhedral to euhedral crystals that show typical short to long prismatic shapes with basal, prism and bipyramidal faces dominant (Figures 4.15b to 4.21b). Rare old zircon grains have rounded shapes and are dark on CL images (Figures 4.15b, 16b & 18b). Oscillatory growth zoning and inherited cores are common on CL images. Resorption edges and inclusion traces are less common. Bright zircons (low U) are mostly found in sample St 2-8(2007) from the Ban Huak area (Figure 4.17b) but are uncommon in sample 14-1(2007) (Figure 4.15b).

Ages of rocks

CK-WB

14-1(2007): Twelve zircon grains were analysed from a sandstone in the CK-WB previously identified as Permo-Triassic (Bunopas & Vella, 1978; Jungyusuk & Khositanont, 1992; Panjasawatwong *et al.,* 2003). Maximum age of the sandstone based on the detrital zircon (6 zircon grains) is 255 ± 6 Ma (Late Permian) with a MSWD of 1.9. Older inherited grains are present and have ages of 280-290, 355 and 1675-1740 Ma (Figure 4.15).

CK-EB

18-3(2007): Twelve zircon grains were separated from this reddish brown sandstone from CK-EB for LA-ICP MS analysis (Figure 4.1). Three analyses were rejected due to their Pb loss in high U content (Table 4.5). Five zircons grains are concordant with an age of 219 ± 3 Ma (Late Triassic). Two groups of older age were recognised in this data, 430-470 Ma and 2600 Ma (Figure 4.16).

Table 4.4 Maximum depositional ages based on LA –ICP-MS U-Pb ages of detrital zircons from seven sedimentary rocks from the Chiang Khong-Lampang-Tak volcanic belt.

Sample number	Location/ geographic belt	Maximum Depositional Age	Rock description	Zircon morphology
1. 14-1 (2007) (Figure 4.15)	20.1874°N 100.2185°E/ CK WB	255 ± 6 Ma	Dark greenish grey medium to coarse-grained sandstone with purplish red weather surface	Subhedral to euhedral zircon crystals, 30 to 50 micron. Zircon crystal showing stubby to elongated shape dominated by prism and pyramidal faces. The CL image shows fine-scale oscillatory zoning and some old core. Resorption edges and inclusion traces were observed.
2. 18-3 (2007) (Figure 4.16)	20.0148°N 100.4596°E/ CK-EB	219 ± 3 Ma	Reddish brown medium to coarse-grained sandstone	Subhedral to euhedral zircon grain, 30 to 70 micron. Rounded shapes were observed in some grains. Oscillatory zoning, old cores and brightness contrast are shown in CL images.
3. St 2-8 (2007) (Figure 4.17)	19.6938°N 100.4006°E/ BH area	266 ± 4 Ma	Greenish grey meta-fine-grained sandstone with schistose texture	Zircon crystals show subhedral to euhedral elongate shape and about 30 to 150 micron in ranges. Absorption edges, inclusions and zoning are present in the CL images.
4. HF-2007 (Figure 4.18)	19.6652°N 100.3526°E/ BH area	355 ± 6 Ma	Light grey to white medium to coarse-grained quartz-mica sandstone with some foliated texture	Zircon crystals are subhedral with subrounded to elongate shapes 50 to 150 microns long. CL images show oscillatory zoning, inclusions and old cores. Zircons showing bright and dark CL are present..
5. HH-2007 (Figure 4.19)	19.8931°N 100.4386°E/ PCF area	356 ± 7 Ma	Light grey medium grained sandstone	Subhedral crystal and sub-rounded shape are common. The crystal range from 50 to 120 micron. Old cores, inclusion and oscillatory zoning are observed in the CL images.

Table 4.4 *(continued)*

Sample number	Location/ geographic belt	Age dating	Rock description	Zircon morphology
6. DR-2007 (Figure 4.20)	18.2460°N 99.5676E°/ LP-WB	258 ± 4 Ma	Light grey to light greenish grey fine to coarse grained sandstone with some volcanic clasts	Anhedral to subhedral crystals 20 to 70 microns long. Resorption and irregular edges are observed as well as inclusions, old cores and oscillatory zoning in the CL images.
7. PT-2007 (Figure 4.21)	18.0768°N 99.6568E°/ LP-CB	214 ± 10 Ma	Reddish brown fine to medium-grained sandstone	Zircons are anhedral to subhedral crystals with sub-rounded to elongate shapes. Crystal size is about 40 to 80 microns. Resorption edges, old cores, oscillatory zoning, inclusions and some dark crystal are present in the CL images.

BH-area

St 2-8 (2007): Seven zircon grains were separated from a greenish grey meta-sandstone in the Ban Huak area (Table 4.5), previously identified as Permian-Carboniferous on geological maps (Tansuwan & Chitmanee, 1990a & b). All 7 crystals are within error of each other, with a weighted average age of 266 ± 4 Ma (Permian) with a MSWD of 1.4 (Figures 4.17 a & c). The zircons from this rock have euhedral to subhedral elongate shapes with high brightness contrast, similar to the zircon from the mylonitic granitoid. There is no evidence of inheritance in the CL-images of these grains (Figure 4.17b).

HF-2007: Twelve zircon grains were separated from a light grey sandstone from the BH-area (Table 4.5). The 3 youngest analyses give a maximum age of deposition of 355 ± 6 Ma (Late Devonian to Early Carboniferous). Six other grains range in age up to 440 Ma (Figure 4.18c). Old cores were observed on CL-images have ages of 1425-1576 Ma (HF-2007: 07; HF-2007: 09; HF-2007: 02)(Figures 4.18 b & c).

Table 4.5 Laser ablation ICPMS U-Pb isotopic and trace element data for zircons from the seven representative CLT sedimentary rocks.

Sample	206Pb/238U age (Ma)		Isotopic ratios								Trace element data (in ppm)				
analysis no	(207Pb corrected)	+/-1s	206Pb/238U	%rsd	208Pb/232Th	%rsd	207Pb/206Pb	%rsd	207Pb/235U	%rsd	Nd	Hf	Pb	Th	U
14-1(2007) 12	248	3	0 0393	1 2%	0 0127	3 0%	0 052	4 7%	0 278	4 7%	8 8	9696	21	365	501
14-1(2007) 10	255	4	0 0402	1 4%	0 0123	3 9%	0 049	5 5%	0 264	5 4%	3 6	10603	11	188	244
14-1(2007) 09	257	3	0 0407	1 3%	0 0128	3 4%	0 052	6 0%	0 281	5 7%	3 0	10576	12	228	262
14-1(2007) 07	259	3	0 0411	1 3%	0 0127	3 4%	0 053	4 9%	0 295	4 7%	10 0	8881	15	250	332
14-1(2007) 03	259	5	0 0409	1 7%	0 0132	5 1%	0 050	7 0%	0 274	6 9%	2 8	9598	6	65	132
14-1(2007) 04	267	5	0 0422	1 6%	0 0132	4 4%	0 049	7 5%	0 281	7 4%	8 1	9866	6	98	124
14-1(2007) 05	283	3	0 0447	1 2%	0 0137	3 3%	0 049	5 3%	0 301	5 2%	4 0	11037	14	212	285
14-1(2007) 02	292	4	0 0466	1 3%	0 0144	3 4%	0 056	4 8%	0 365	4 6%	2 6	10532	17	200	341
14-1(2007) 01	294	4	0 0467	1 4%	0 0136	3 1%	0 053	4 0%	0 345	3 9%	6 6	10107	23	232	483
14-1(2007) 08	354	4	0 0566	1 2%	0 0167	4 0%	0 055	4 7%	0 424	4 5%	4 0	11197	14	111	248
14-1(2007) 11	1675	17	0 2987	0 9%	0 0862	2 3%	0 108	2 7%	4 392	2 5%	179 5	10193	76	194	224
14-1(2007) 06	1739	18	0 3087	1 0%	0 0868	2 3%	0 104	2 6%	4 312	3 2%	1 6	12454	66	188	182
18-3(2007) 05*	118	2	0 0202	1 5%	0 0027	2 0%	0 114	2 2%	0 323	2 3%	2123 8	15091	156	39962	3442
18-3(2007) 08*	186	1	0 0297	0 8%	0 0142	2 3%	0 060	1 9%	0 244	2 0%	7 2	15632	98	439	3436
18-3(2007) 09*	300	3	0 0499	1 0%	0 0240	2 5%	0 090	1 9%	0 618	2 1%	2 8	14497	43	116	880
18-3(2007) 07	215	3	0 0340	1 4%	0 0105	3 9%	0 052	4 7%	0 238	4 7%	4 8	12519	12	139	346
18-3(2007) 06	216	3	0 0342	1 4%	0 0107	3 6%	0 053	4 5%	0 237	4 9%	6 6	12640	12	171	333
18-3(2007) 02	218	3	0 0345	1 2%	0 0105	3 4%	0 051	4 2%	0 244	4 2%	3 0	13258	14	175	407
18-3(2007) 12	221	3	0 0349	1 3%	0 0110	3 3%	0 052	4 3%	0 246	4 2%	5 8	12669	12	188	339
18-3(2007) 11	222	3	0 0351	1 3%	0 0107	4 6%	0 051	4 3%	0 245	4 3%	5 5	12984	12	104	346
18-3(2007) 03	434	8	0 0705	1 8%	0 0229	4 0%	0 064	4 4%	0 629	4 6%	10 5	11460	18	127	227
18-3(2007) 04	466	4	0 0765	0 9%	0 0461	2 2%	0 072	2 2%	0 757	2 2%	3 0	13761	61	179	770
18-3(2007) 01	2594	32	0 4966	0 9%	0 1309	2 6%	0 175	1 4%	11 890	1 5%	0 4	12110	308	44	606
18-3(2007) 10	2634	46	0 5209	1 2%	0 1548	2 8%	0 199	2 1%	14 217	2 4%	2 4	9833	29	30	47

* Sample analysis number is not used in age calculations. Comment is in text for each sample.

Table 4.5 *(continued)*

Sample	206Pb/238U age (Ma)		Isotopic ratios								Trace element data (in ppm)				
analysis no	(207Pb corrected)	+/-1s	206Pb/238U	%rsd	208Pb/232Th	%rsd	207Pb/206Pb	%rsd	207Pb/235U	%rsd	Nd	Hf	Pb	Th	U
St2-8(2007) 06	259	4	0 0408	1 4%	0 0125	4 6%	0 049	5 3%	0 267	5 7%	6 0	11907	10	115	227
St2-8(2007) 07	262	4	0 0414	1 6%	0 0124	3 9%	0 050	6 5%	0 271	6 5%	5 3	10597	7	132	150
St2-8(2007) 02	267	6	0 0423	2 1%	0 0128	4 0%	0 052	8 5%	0 289	8 2%	17 5	7923	5	133	90
St2-8(2007) 01	268	3	0 0425	1 2%	0 0129	2 5%	0 052	4 0%	0 303	3 9%	105 7	10186	23	505	453
St2-8(2007) 04	269	4	0 0424	1 4%	0 0129	3 1%	0 049	4 6%	0 288	4 7%	9 3	10686	14	248	293
St2-8(2007) 03	269	7	0 0428	2 6%	0 0117	6 7%	0 055	10 3%	0 300	10 0%	7 1	9739	6	94	120
St2-8(2007) 05	271	3	0 0426	1 1%	0 0135	2 5%	0 046	3 7%	0 273	3 6%	4 5	9664	27	539	534
HH-2007 05	348	4	0 0556	1 2%	0 0172	2 7%	0 054	3 3%	0 416	3 2%	2 6	10672	27	286	461
HH-2007 12	352	5	0 0560	1 4%	0 0173	3 2%	0 052	3 8%	0 398	3 8%	1 9	10837	20	164	345
HH-2007 11	353	5	0 0563	1 5%	0 0179	2 4%	0 053	3 1%	0 409	3 2%	6 9	10586	31	344	517
HH-2007 10	359	4	0 0571	1 2%	0 0172	2 5%	0 052	3 5%	0 399	3 4%	3 3	9901	21	270	339
HH-2007 02	361	5	0 0577	1 5%	0 0165	3 6%	0 056	4 6%	0 445	4 5%	3 7	10111	10	108	166
HH-2007 06	364	5	0 0584	1 4%	0 0182	3 0%	0 058	4 0%	0 451	4 4%	66 3	10668	14	193	218
HH-2007 03	433	6	0 0697	1 3%	0 0220	3 1%	0 057	3 9%	0 536	4 0%	1 9	10071	19	144	256
HH-2007 01	438	5	0 0700	1 2%	0 0226	2 9%	0 053	4 0%	0 502	3 9%	1 1	10377	21	165	280
HH-2007 04	952	15	0 1636	1 6%	0 0408	2 9%	0 093	1 9%	2 097	2 4%	0 3	11954	121	121	773
HH-2007 09	1615	16	0 2872	1 0%	0 0839	2 0%	0 106	1 8%	4 242	1 9%	4 9	9912	125	234	399
HH-2007 07	1830	28	0 3291	1 5%	0 0899	2 4%	0 114	2 1%	5 136	2 3%	3 1	9786	61	86	176
HH-2007 08	2319	43	0 4482	1 6%	0 1356	2 0%	0 172	1 9%	10 616	2 1%	4 1	8152	122	180	229
HF-2007 03	348	5	0 0556	1 5%	0 0166	3 4%	0 056	4 2%	0 436	4 5%	17 5	10835	16	193	259
HF-2007 10	357	4	0 0572	1 1%	0 0175	3 5%	0 058	3 7%	0 468	3 6%	1 1	12555	17	140	280
HF-2007 12	358	6	0 0569	1 7%	0 0174	5 0%	0 051	5 1%	0 419	5 4%	0 7	11371	7	58	115
HF-2007 11	371	5	0 0592	1 3%	0 0183	3 6%	0 053	4 4%	0 438	4 4%	0 6	10705	15	131	240
HF-2007 05	377	4	0 0603	1 1%	0 0185	2 4%	0 054	2 9%	0 464	3 0%	5 3	11078	39	363	593
HF-2007 04	388	6	0 0619	1 5%	0 0188	3 5%	0 052	3 9%	0 448	3 8%	1 9	11594	17	129	259
HF-2007 01	407	6	0 0657	1 4%	0 0222	2 6%	0 062	3 0%	0 562	3 1%	87 9	11618	36	290	502
HF-2007 06	415	5	0 0665	1 2%	0 0213	2 0%	0 054	2 6%	0 494	3 1%	6 3	10163	70	650	956
HF-2007 08	440	4	0 0707	1 0%	0 0223	3 0%	0 056	3 4%	0 561	3 3%	1 0	10812	25	179	336
HF-2007 07	1425	11	0 2472	0 8%	0 0688	2 5%	0 089	1 4%	3 108	2 1%	22 4	13598	291	305	1159
HF-2007 09	1545	14	0 2706	0 9%	0 0778	2 1%	0 095	1 7%	3 650	1 7%	2 6	12702	169	183	606
HF-2007 02	1576	23	0 2766	1 4%	0 0844	2 4%	0 097	2 2%	3 771	2 1%	12 2	10559	72	106	244

Table 4.5 *(continued)*

Sample	206Pb/238U age (Ma)		Isotopic ratios								Trace element data (in ppm)				
analysis no	(207Pb corrected)	+/-1s	206Pb/238U	%rsd	208Pb/232Th	%rsd	207Pb/206Pb	%rsd	207Pb/235U	%rsd	Nd	Hf	Pb	Th	U
PT-2007 04	211	2	0 0336	0 9%	0 0105	2 4%	0 057	2 4%	0 265	2 4%	16 2	13515	66	748	1940
PT-2007 10	214	3	0 0339	1 3%	0 0100	3 8%	0 054	3 9%	0 256	3 9%	2 9	12593	18	154	539
PT-2007 03	218	2	0 0345	1 0%	0 0113	2 3%	0 053	2 3%	0 256	2 3%	2 3	13618	75	708	2198
PT-2007 09	220	2	0 0348	1 0%	0 0108	4 0%	0 051	2 6%	0 244	2 6%	2 0	13514	43	145	1342
PT-2007 02	222	2	0 0351	0 9%	0 0106	2 5%	0 054	2 7%	0 260	2 6%	1 9	13487	43	587	1195
PT-2007 12	224	3	0 0354	1 2%	0 0109	2 4%	0 050	3 4%	0 246	3 4%	4 1	11972	28	535	715
PT-2007 05	228	2	0 0359	1 1%	0 0114	2 5%	0 049	3 3%	0 248	3 3%	3 7	11854	27	457	705
PT-2007 07	241	4	0 0382	1 7%	0 0127	7 7%	0 053	5 9%	0 272	6 1%	0 3	12134	6	27	165
PT-2007 08	250	3	0 0395	1 3%	0 0122	2 8%	0 049	3 4%	0 275	3 5%	4 2	12259	29	270	729
PT-2007 01	962	17	0 1612	1 7%	0 0449	4 5%	0 072	4 8%	1 573	4 7%	1 9	10115	7	32	41
PT-2007 11	1101	13	0 1861	1 2%	0 0553	2 6%	0 076	2 3%	1 976	2 3%	7 0	12443	68	130	355
PT-2007 06	2328	27	0 4340	1 0%	0 1168	1 6%	0 147	1 5%	8 667	2 4%	12 5	9519	236	311	480
DR-2007 12	254	4	0 0403	1 4%	0 0127	4 5%	0 054	5 4%	0 315	5 4%	3 5	9340	7	107	169
DR-2007 05	259	3	0 0411	1 0%	0 0127	2 1%	0 052	2 8%	0 301	2 8%	413 8	11451	46	913	967
DR-2007 08	260	5	0 0413	2 1%	0 0128	5 1%	0 054	6 0%	0 308	5 8%	52 1	9586	6	80	138
DR-2007 06	350	6	0 0559	1 8%	0 0185	5 4%	0 055	6 5%	0 415	6 2%	0 2	10300	6	40	105
DR-2007 10	353	4	0 0562	1 1%	0 0169	2 3%	0 053	3 8%	0 434	3 7%	25 0	9721	21	362	308
DR-2007 03	364	6	0 0579	1 6%	0 0168	4 3%	0 050	5 4%	0 413	5 3%	9 9	9812	8	81	120
DR-2007 07	416	7	0 0666	1 6%	0 0205	2 3%	0 055	2 8%	0 506	2 8%	6 5	10557	56	541	771
DR-2007 04	468	5	0 0755	1 1%	0 0235	2 6%	0 058	3 1%	0 629	3 0%	0 9	10603	26	237	299
DR-2007 09	470	6	0 0754	1 2%	0 0235	2 8%	0 054	3 1%	0 577	3 0%	1 0	11572	26	161	322
DR-2007 11	477	5	0 0768	1 0%	0 0230	2 3%	0 057	2 9%	0 611	2 9%	7 6	10117	36	392	399
DR-2007 02	495	5	0 0798	0 9%	0 0250	2 9%	0 057	2 6%	0 651	2 5%	7 5	12023	58	187	740
DR-2007 01	500	5	0 0807	0 9%	0 0245	1 9%	0 058	2 1%	0 661	2 2%	5 4	9847	95	672	1086

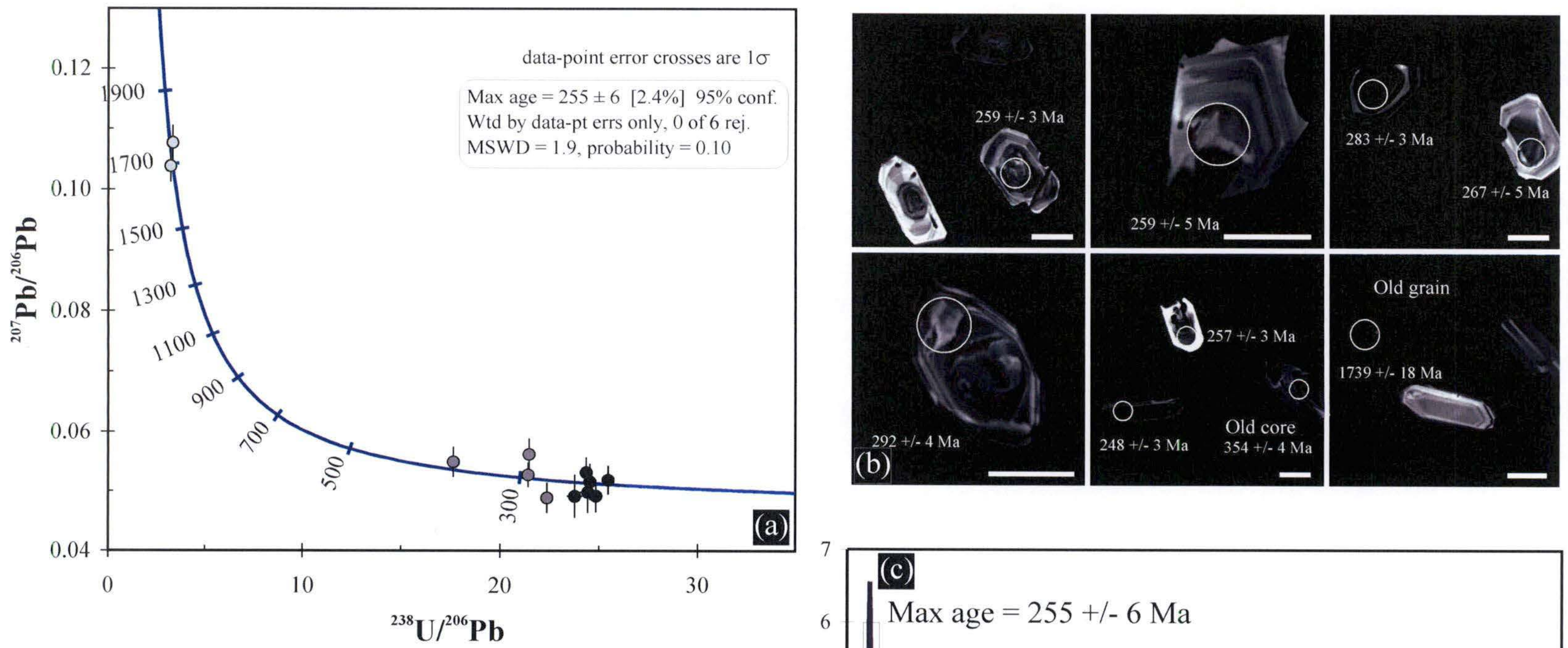

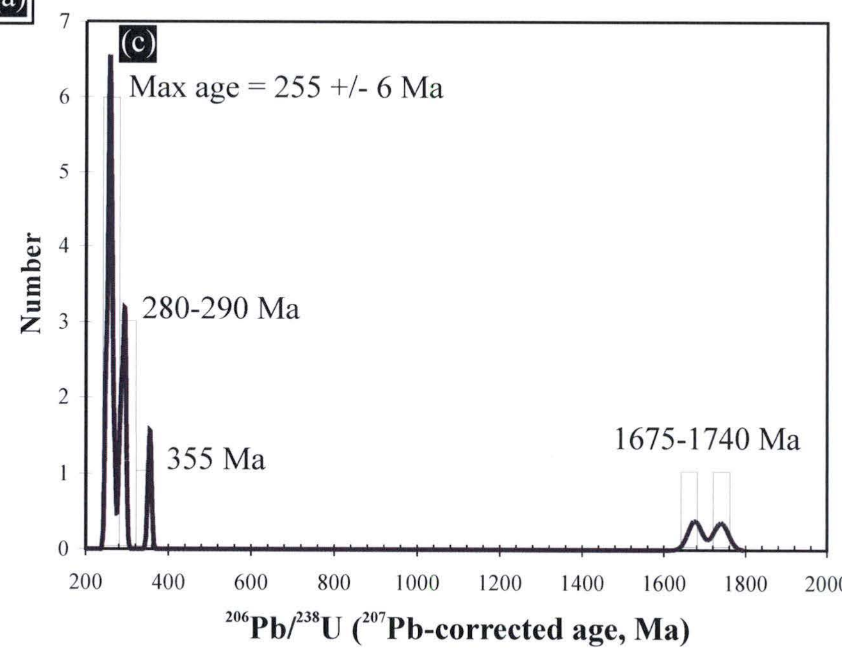

Figure 4.15 Reverse concordia plot of laser ablation ICP-MS zircon U-Pb measurements (a), CL-images (b) and ^{207}Pb-corrected age diagram (c) for sandstone sample 14-1(2007) from the CK-WB. Best fit regression and ^{207}Pb-corrected age calculated using the Isoplot 3.0 software (Ludwig, 2003) assuming common Pb composition based on the 2 stage model of Stacey & Kramer (1975) at 255 Ma. Note; analyses in black are those used for age calculation whereas grey circles are excluded as older; scale bar is 50 microns long in (b).

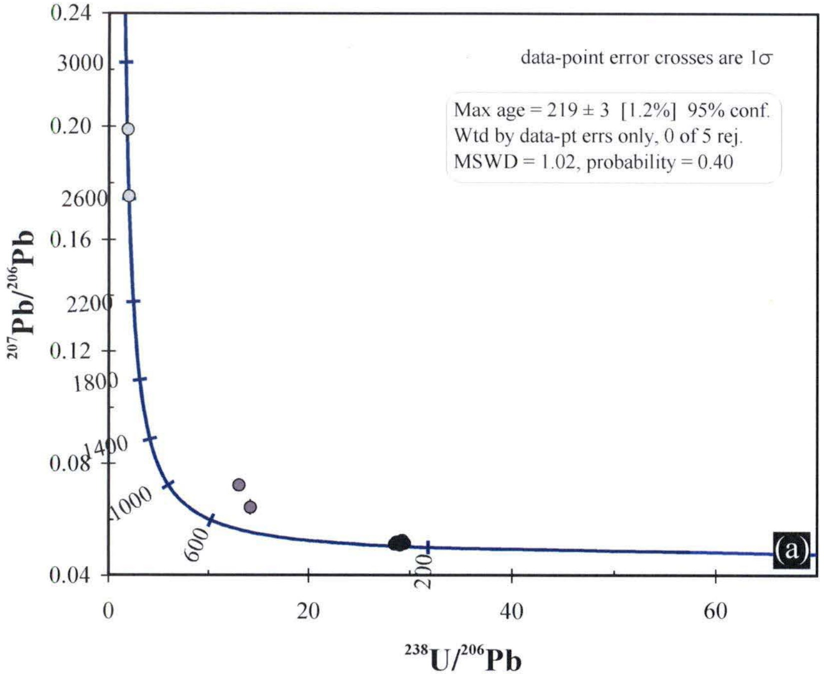

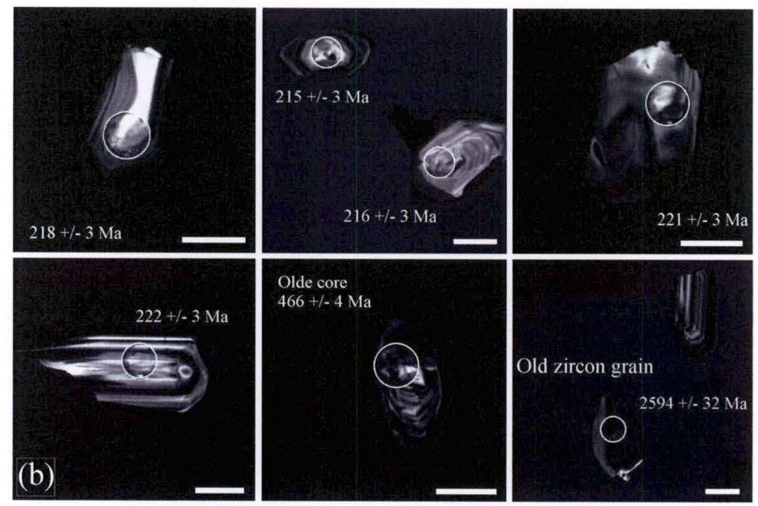

Figure 4.16 Reverse concordia plot of laser ablation ICP-MS zircon U-Pb measurements (a), CL-images (b) and ^{207}Pb-corrected age diagram (c) for sandstone sample 18-3(2007) from the CK-EB. Best fit regression and ^{207}Pb-corrected age calculated using the Isoplot 3.0 software (Ludwig, 2003) assuming common Pb composition based on the 2 stage model of Stacey & Kramer (1975) at 219 Ma. Symbols as in Figure 4.15.

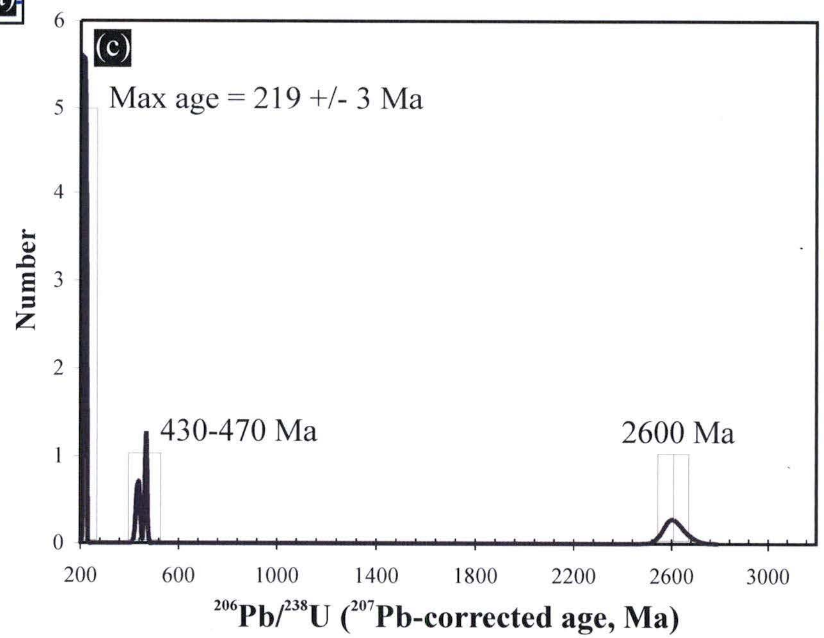

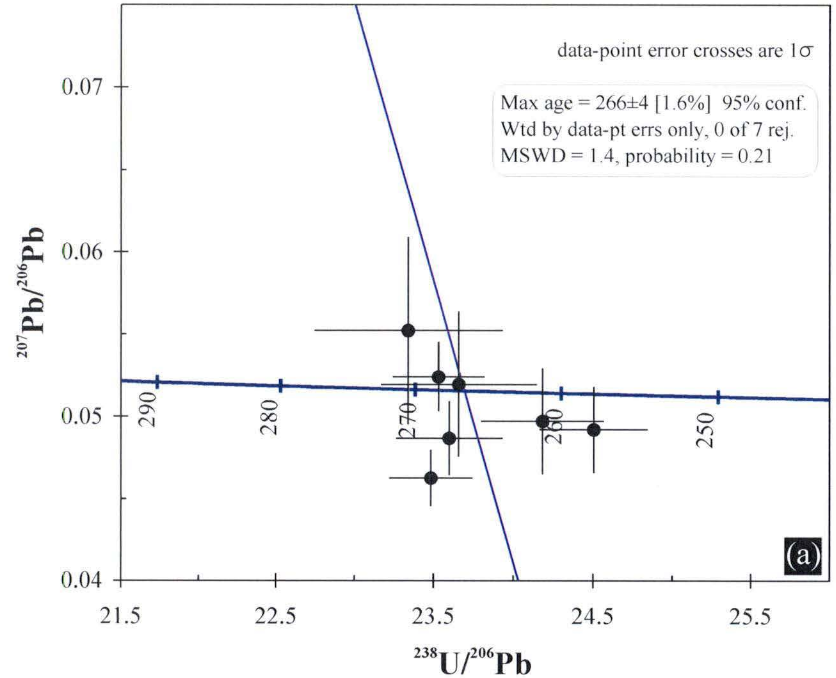

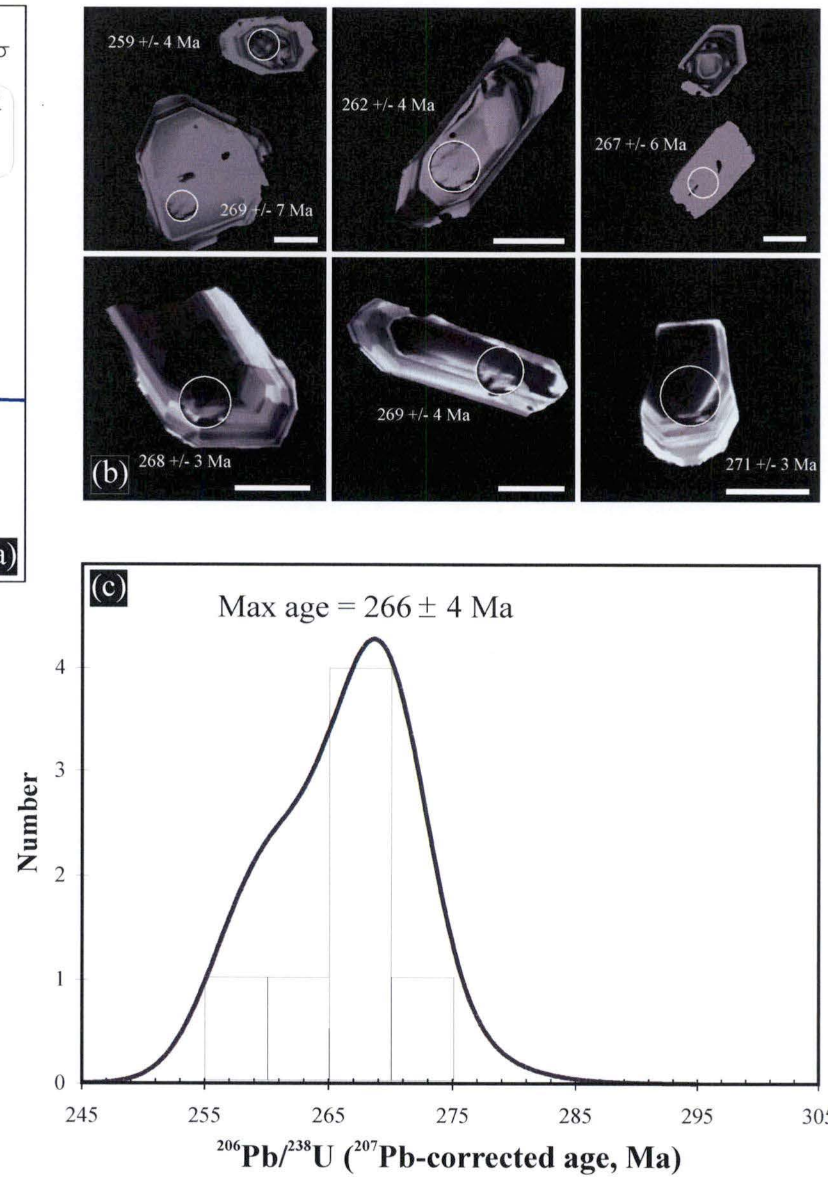

Figure 4.17 Reverse concordia plot of laser ablation ICP-MS zircon U-Pb measurements (a), CL-images (b) and ^{207}Pb-corrected age diagram (c) for meta-sandstone sample St 2-8(2007) from the high strain rock area (BH-area). Best fit regression and ^{207}Pb-corrected age calculated using the Isoplot 3.0 software (Ludwig, 2003) assuming common Pb composition based on the 2 stage model of Stacey & Kramer (1975) at 266 Ma. Symbols as in Figure 4.15.

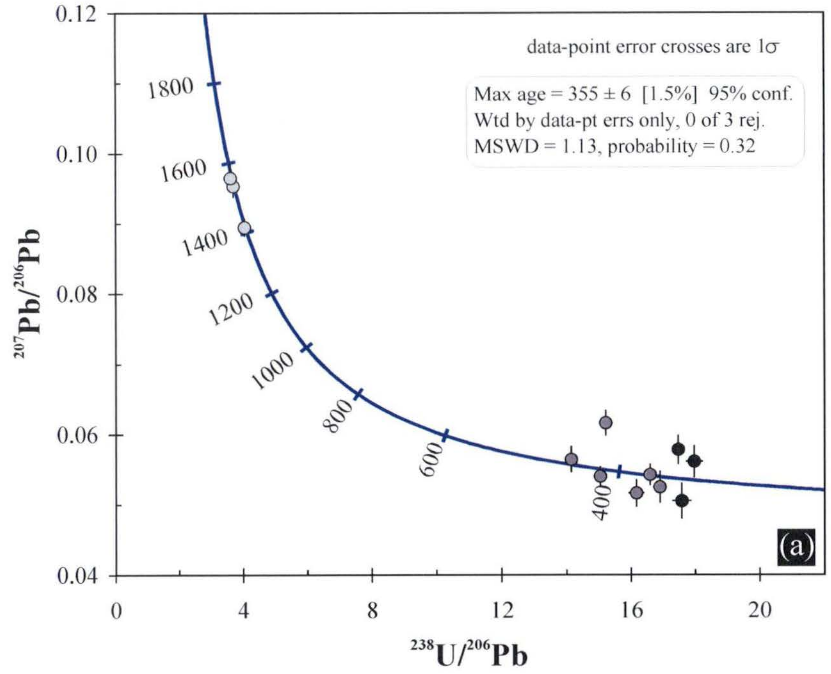

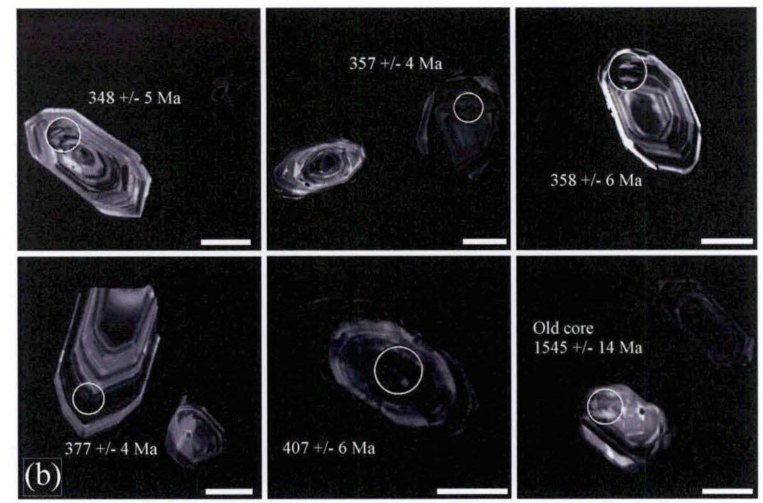

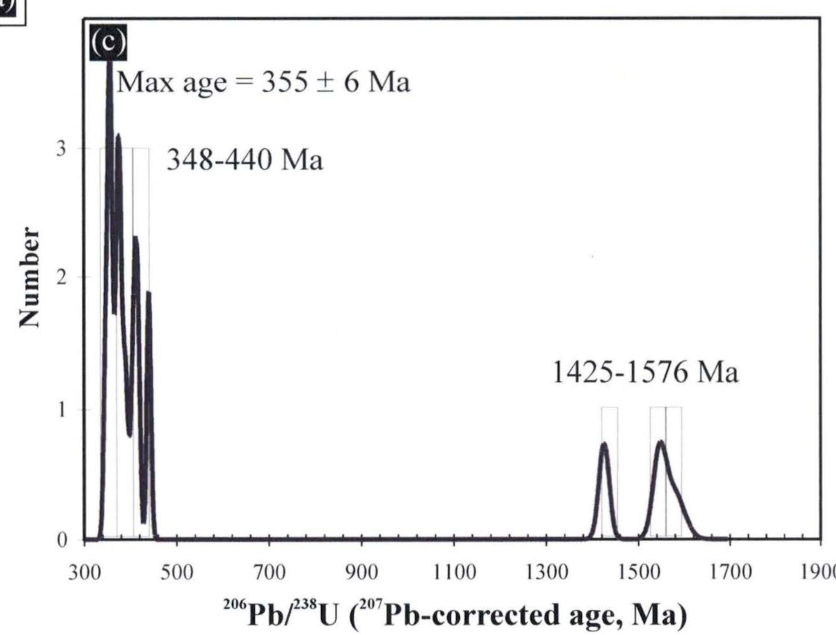

Figure 4.18 Reverse concordia plot of laser ablation ICP-MS zircon U-Pb measurements (a), CL-images (b) and ^{207}Pb-corrected age diagram (c) for meta-sandstone sample HF-2007 from the high strain rock area (BH-area). Best fit regression and ^{207}Pb-corrected age calculated using the Isoplot 3.0 software (Ludwig, 2003) assuming common Pb composition based on the 2 stage model of Stacey & Kramer (1975) at 355 Ma. Symbols as in Figure 4.15.

PCF-area

HH-2007: Twelve zircon grains were separated from a light grey sandstone from the Phu Chi Fa area (Table 4.5). Most of these analyses indicate a maximum depositional age of 356 ± 7 Ma (Late Devonian to Early Carboniferous) (Figures 4.19 a & c). The old cores observed on CL-images (Figure 4.19b) and show three older ages group at 435, 950 and 1615-2320 Ma (Proterozoic ages) (Figures 4.19 a & c).

<u>*Summary*</u>

The sandstones from the Chiang Khong area form three discrete groups based in zircon ages. The youngest zircon grains, from the Late Triassic redbed sandstone from the CK-EB [sample number 18-3(2007)] yield a maximum age of 219 ± 3 Ma (Late Triassic, Figure 4.16]. Older zircon grains from this sample include much older ages, 450 Ma and 2600 Ma.

A second group of samples is dominated by zircons which imply a maximum depositional age of 255 ± 6 Ma in the CK-WB area to 266 ± 4 Ma in the Ban Huak area, with older detrital grains at ~1700 Ma.

The third group of sandstones have maximum depositional age of 355 ± 6 and 356 ± 7 Ma (Devonian to Carboniferous in age). The two rock samples constituting this group are from the "Carboniferous-Permian" meta-sedimentary rock of the Ban Huak and Phu Chi Fa areas (HF-2007 & HH-2007 in Figure 4.18 & 19). The detrital zircon data are compatible with previous inferences about the age of these rocks. The presence of Silurian-Devonian zircons in these samples is compatible with a contribution from the South China/Indochina terranes, as volcanism of that age is common in this compound terrane, but absent from the Shan-Thai Terrane (Metcalfe, 1999; Feng *et al.,* 2005).

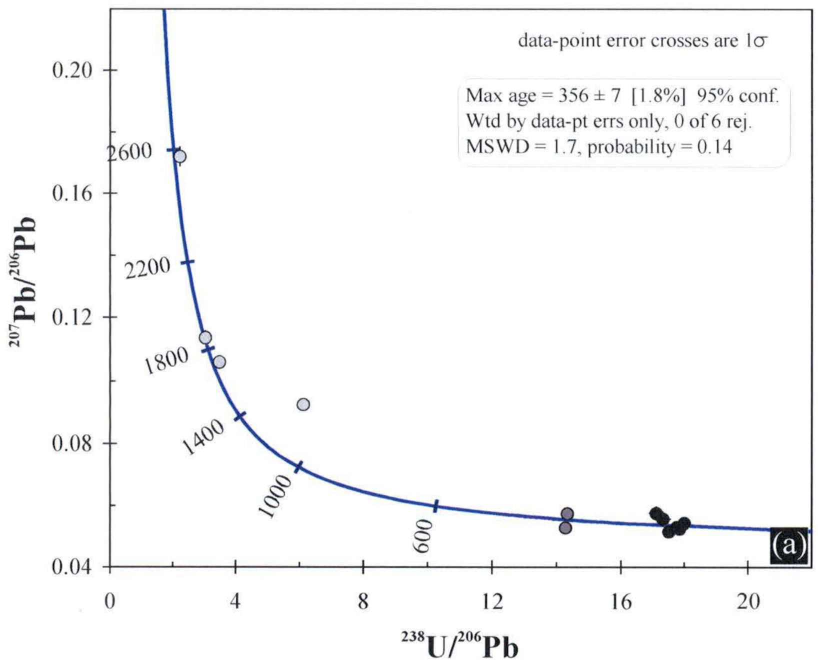

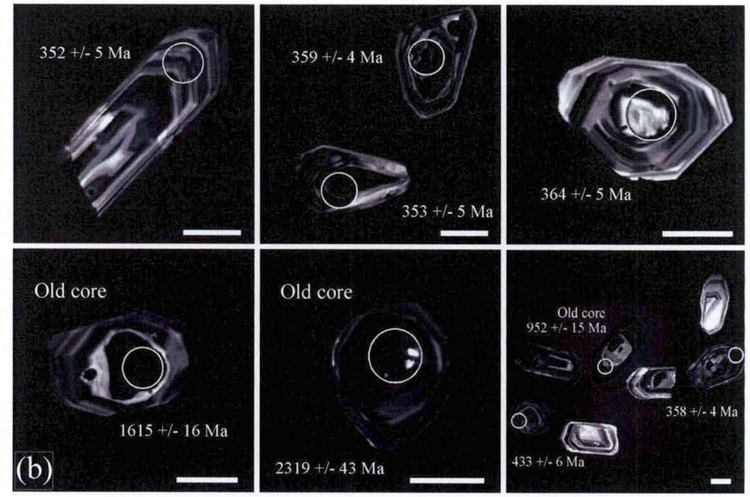

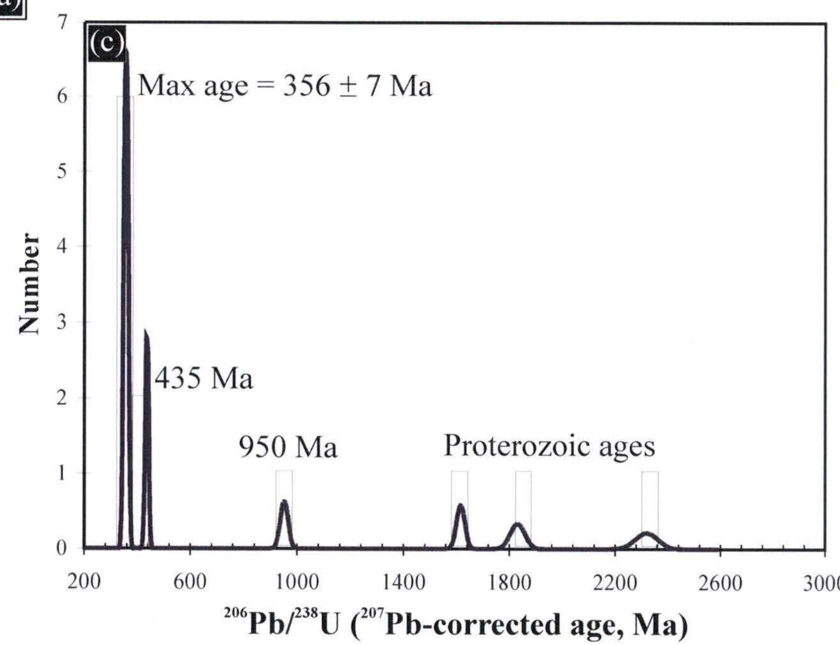

Figure 4.19 Reverse concordia plot of laser ablation ICP-MS zircon U-Pb measurements (a), CL-images (b) and ^{207}Pb-corrected age diagram (c) for meta-sandstone sample HH-2007 from the Phu Chi Fa area. Best fit regression and ^{207}Pb-corrected age calculated using the Isoplot 3.0 software (Ludwig, 2003) assuming common Pb composition based on the 2 stage model of Stacey & Kramer (1975) at 356 Ma. Symbols as in Figure 4.15.

4.5.2 The Lampang area

Two sedimentary rocks from the Lampang area were selected for U-Pb age dating of detrital zircons, including a volcaniclastic sandstone from the LP-WB and a sandstone from the Phra That Formation in the LP-CB.

Morphology of zircons

Detrital zircons from the Lampang area include euhedral to anhedral crystals 30 to 150 micron across (Figures 4.20b & 21b). Prismatic shapes are common whereas broken grains and/or rounded shapes are less common. Resorption edges, fractures, inclusions, oscillatory growth zoning and old cores were observed in the CL images.

Ages of rocks

LP-WB

DR-2007: DR-2007 is a sandstone from the LP-WB (Table 4.5). Zircon ages of these grains range from 254 to 500 Ma (Figures 4.20 a & c). The maximum depositional age is 258 ± 4 Ma (Permian) with older age groups at 360, 410 and 470-500 Ma (Figures 4.20 a & c). Inherited cores visible on CL-images yielded the oldest group of analyses, at 470-500 Ma.

LP-CB

PT-2007: Detrital zircons in a reddish brown LP-CB sandstone (Table 4.5 and Figure 4.21) indicated a maximum age (for the seven youngest zircon grains) at 219 ± 5 Ma, in the Late Triassic. The old cores observed on CL-images (Figure 4.21b) returned ages at 960-1100 Ma and 2300 Ma (Figure 4.21c).

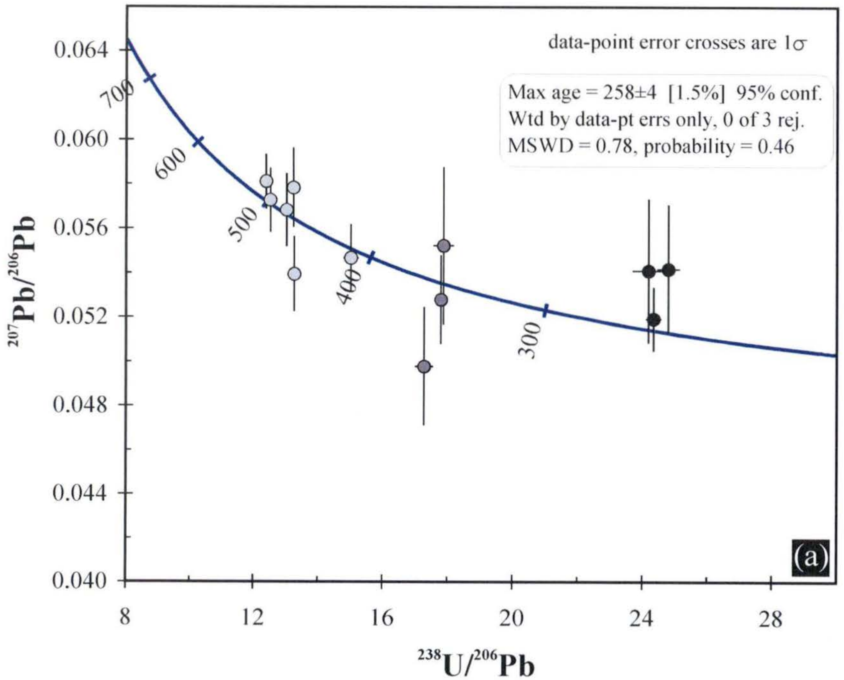

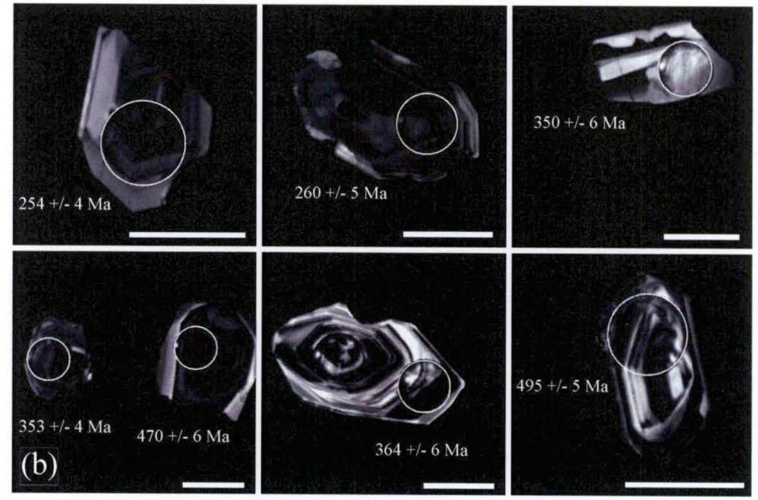

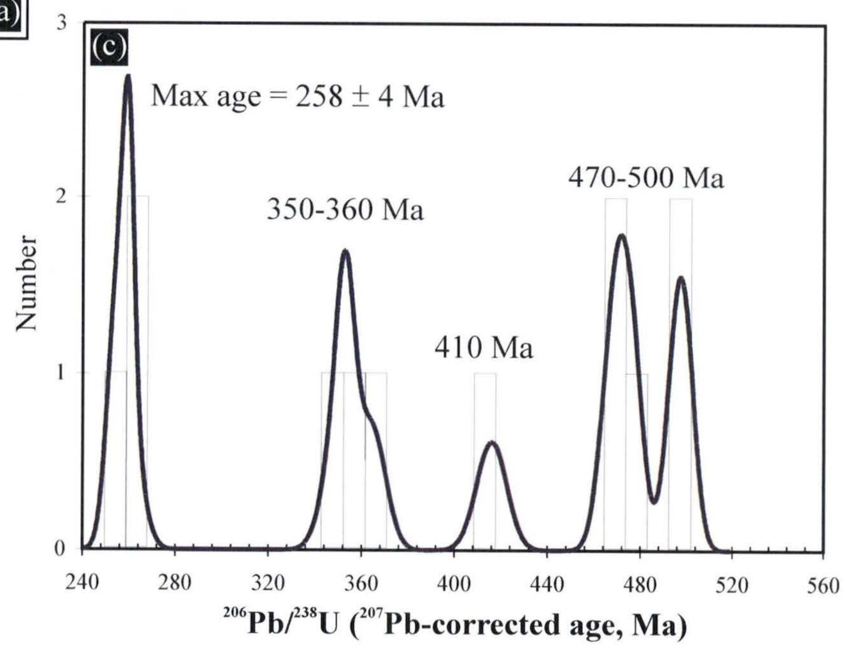

Figure 4.20 Reverse concordia plot of laser ablation ICP-MS zircon U-Pb measurements (a), CL-images (b) and ^{207}Pb-corrected age diagram (c) for volcaniclastic sandstone sample DR-2007 from the LP-WB. Best fit regression and ^{207}Pb corrected age calculated using the Isoplot 3.0 software (Ludwig, 2003) assuming common Pb composition based on the 2 stage model of Stacey & Kramer (1975) at 258 Ma. Symbols as in Figure 4.15.

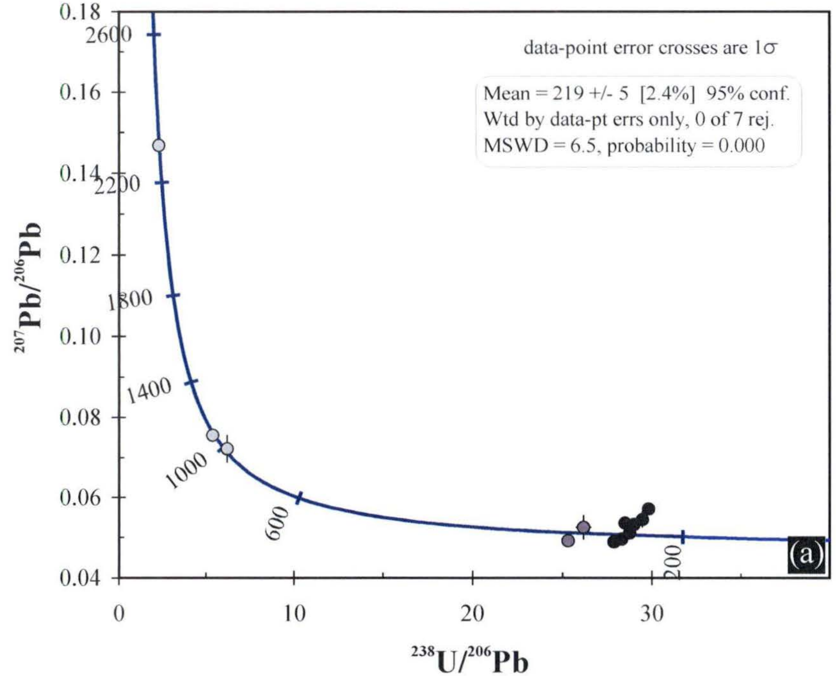

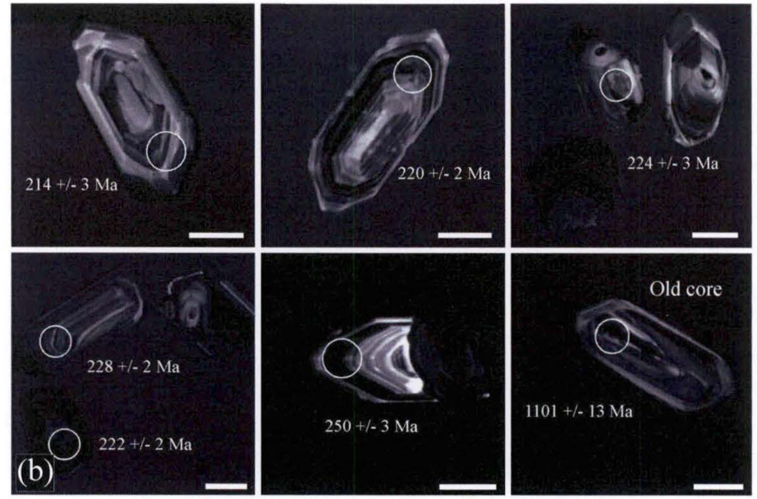

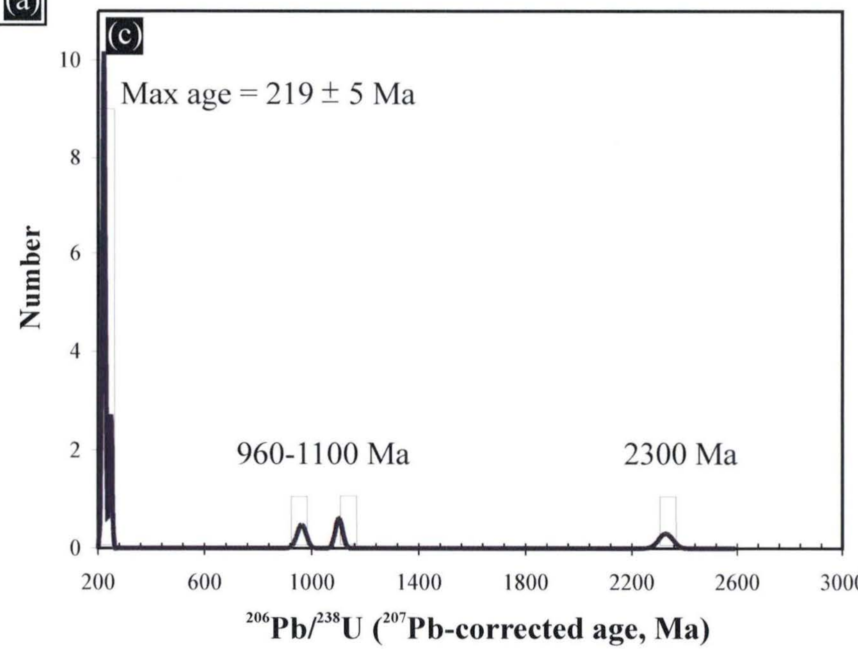

Figure 4.21 Reverse concordia plot of laser ablation ICP-MS zircon U-Pb measurements (a), CL-images (b) and ^{207}Pb-corrected age diagram (c) for sandstone sample PT-2007 from the LP-CB. Best fit regression and ^{207}Pb corrected age calculated using the Isoplot 3.0 software (Ludwig, 2003) assuming common Pb composition based on the 2 stage model of Stacey & Kramer (1975) at 219 Ma. Symbols as in Figure 4.15.

4.5.3 Summary

Most of the detrital zircon grains in sedimentary rocks along the CLT volcanic belt are derived as first cycle magmatic zircons with typical oscillatory growth zoning. The CLT detrital zircons are about 30 -150 microns in size with both euhedral to anhedral crystals. Prismatic shapes with prism and bipyramidal faces are typical. Old and dark zircon grains are present in most samples but less common. Sandstones have three distinct maximum depositional ages based on their U-Pb zircon ages. The youngest rock, a Late Triassic redbed sandstone, has a maximum age of 220 Ma. Most sandstones have maximum depositional ages around 260 Ma, whereas a few samples only contain Carboniferous zircons. Older inherited cores range from 430 Ma to the Archean.

4.6 Discussion and Conclusion

Ages of rocks along the CLT volcanic belt have been determined using LA-ICP-MS U-Pb zircon age dating, and for one sample of mylonitic granite, an EPMA technique for chemical monazite age dating. The major conclusions based on this geochronological study are:

1. Devonian to Carboniferous age: Two meta-sandstones from the Ban Huak area have maximum depositional of 355 ± 6 and 356 ± 7 Ma, and are probably the oldest rock units in the CLT volcanic belt. These ages are consistent with previous data which suggested a Carboniferous-Permian age based on stratigraphic correlation (Tansuwan & Chitmanee, 1990a, b).

2. Carboniferous-Permian age: A hornblende diorite from the TN-CB, south of the Lampang area, has a U-Pb zircon age of 292 ± 7 Ma. This age is the oldest magmatic event recorded in the CLT area. Its relationship to other similar aged rocks, including the Permo-Carboniferous ultramafic rocks of the Chiang Rai-Chiang Mai volcanic belt (Barr *et al.,* 1990), remains unclear.

3. Permian: The mylonitic granite from the Ban Huak area gives a Permian magmatic age (256 ± 2 Ma). The granite may have formed in a Permian magmatic arc. Detrital zircons of Permian age were discovered in three sandstone samples

from the CK-WB, BH area and LP-WB. A Late Triassic rhyolite from the CK-WB also contains inherited Permian zircons.

4. Middle to Late Triassic: A Middle to Late Triassic magmatic event was widely recorded in this study of volcanic and intrusive rocks of the CLT. The rocks analysed from the LP-WB and TN-CB are slightly older than rocks from the Chiang Khong area and the LP-CB. Other studies of volcanic and plutonic rock along the CLT have reported similar ages. These include a rhyolitic tuff from the CK-CB (Barr *et al.,* 2006), a rhyolite from the LP-WB (Barr *et al.,* 2000), a granite from the LP-CB and a rhyolite from the LP-EB (S. Khositanont *pers. comm.* 2006). These rocks all have about the same ages as recorded in this study, whereas the rhyolite from LP-WB is slightly older. The preferred Late Triassic age for a granite intrusion in the Lampang-Denchai section of Singharajwarapan & Berry (2000) has been confirmed age by Khositanont *pers. comm.* (2006). However, the Middle to Late Triassic ages of the CLT are younger than the previous interpretations that this volcanic belt is dominantly of Permo-Triassic age (Bunopas & Vella, 1978; Junkyusuk & Khosittanont, 1992; Panjasawatwong *et al.,* 2003) or Middle Triassic in age (Sone & Metcalfe, 2008).

5. Two redbed sandstones from CK-EB and LP-CB gave maximum depositional ages of 219 ± 3 Ma and 219 ± 5 Ma, respectively. The sandstone from the LP-CB was previously interpreted to be the Lower Triassic Phra That Formation of the Lampang Group (Chaodumrong, 1992). There is no direct fossil evidence for the age of this rock and its age was inferred from stratigraphic correlation (Chaodumrong, 1992). It was collected from the boundary between the Lampang sub-basin and Phrae sub-basin (Chaodumrong, 1992, Chaodumrong & Burrett, 1997). The detrital zircon age supports a correlation of this redbed sandstone with the Pha Daeng Formation (early Late Triassic) rather than the Early Triassic Phra That Formation.

6. Analyses of old detrital zircon grains from CLT sedimentary rocks include 12 of Proterozoic age and two analyses of Archean age. These old zircon ages demonstrate provision from a continental source but no distinct sources can be determined, as too few zircons were analysed for a thorough provenance study.

The Silurian-Devonian zircons in some samples probably reflect a source in the Indochina or South China Terranes, as magmatic rock of that age are common in those areas.

CHAPTER 5

Structure of the Chiang Khong-Lampang-Tak Volcanic Belt

5.1 Introduction

The structure of the Chiang Khong-Lampang-Tak volcanic belt (CLT) has been studied in three transects in the Chiang Khong area and three transects in the Lampang area. These sections are perpendicular to the main structural trend of the volcanic belt. The structural data was mainly collected from road-cuttings, quarries, stream banks, and along the banks of the Mae Khong River. The first section in the northern area extends along the Mae Khong River (Thai-Laos border) from Chiang Khong through Wiang Kaen district. The second and the third transects extend across the central part of northern area along the road from Doi Luang sub-district to the Phu Chi Fa area. The structure data for the Lampang transects was collected along Highway number 11 from the Muang Lampang district to Ban Mae Khaem. The first transect extends across the central part of the LP-WB whereas the second crosses the limestone outcrops in the central part of the area. The last transect in the Lampang area across the LP-CB is slightly modified from, and forms an extension of, a published transect of the western end of the Sukhothai Fold Belt (Singharajwarapan & Berry, 2000). In addition, a more detailed structural study of a distinctive metamorphic zone in the eastern part of the Chiang Khong area (the Ban Huak area) was carried out to elucidate the structural history of this region.

A previous study of the structure and metamorphism of rocks along the CLT was reported by Singharajwarapan (1994) and Singharajwarapan & Berry (2000). Their cross-section across the Lampang-Phrae area was drawn between km 30.00 and km 75.00 on Highway number 11 (Lampang to Denchai). The deformation of rocks on this section is characterized by upright to inclined open to close folds and thrusts. They recognised a single phase of folding with associated northeast-striking regional cleavage (Singharajwarapan & Berry, 2000). On the other hand, the structural style of the Chiang Khong area has only been reported as regional cross sections on 1:50,000 scale geologic maps (Sukvattananunt & Assawapatchara, 1989a, 1989b, 1989c, 1989d; Sukvattananunt, *et al.* 1985a, 1985b; Tansuwan & Chitmanee, 1990a, 1990b).

5.2 Structure of Rocks in the Chiang Khong Area

5.2.1 Introduction

Regional structural data for the Chiang Khong area, collected during three field seasons, includes the orientations of folds, cleavage and faults. The orientation data was first assessed to define the regional distribution of folding and cleavage. The construction of structural transects was a major target for this work. The first transect is approximately 30 km long from Chiang Khong via Waing Kaen district and is located at the northern tip of the CLT. The second and the third transects are across the central part of the Chiang Khong area from Doi Luang to Ban Kaen and Ban Phaya Phiphak to Phu Chi Fa, respectively. The Doi Luang to Ban Kaen transect is 20 km across the CK-WB along the inter-provincial road number 1098. The Ban Phaya Phiphak to Phu Chi Fa transect is 20 km and runs across the central and eastern sub-belts of CLT along a local road. A more detailed regional study of the Ban Huak area was carried out in the high strain zone east of the Thoeng district.

5.2.2 Folds and Cleavages

As noted in Chapters 2 & 3 the Chiang Khong area has been divided into 3 physiographically defined sub-areas including the Chiang Khong Western Belt (CK-WB), Chiang Khong Central Belt (CK-CB) and Chiang Khong Eastern Belt (CK-EB).

Chiang Khong Western Belt

The bedding and cleavage in the CK-WB is dominated by NNE-SSW strike directions (Figures 5.1a & b). Less commonly, NNE-SSW bedding strikes are present in the Permo-Triassic sedimentary rocks and the Middle to Late Triassic volcaniclastic rocks. N-S striking beds at location I in Figure 5.1a are probably the result of drag during late strike-slip fault movement.

The regional NNE-SSW steep cleavage measured at locations B, G and H is shown in Figure 5.1b; it strikes subparallel to bedding in CK-WB rocks and dips sub-vertical to steeply west. Variation in local cleavage strike is observed at several locations and is probably related to local faults (Figure 5.1c). For example, the NE-SW sub-vertical cleavage strike in locations A and C was measured on the Mae Khong River bank outcrops, northeast of the Chiang Saen district. These cleavages are parallel to the major

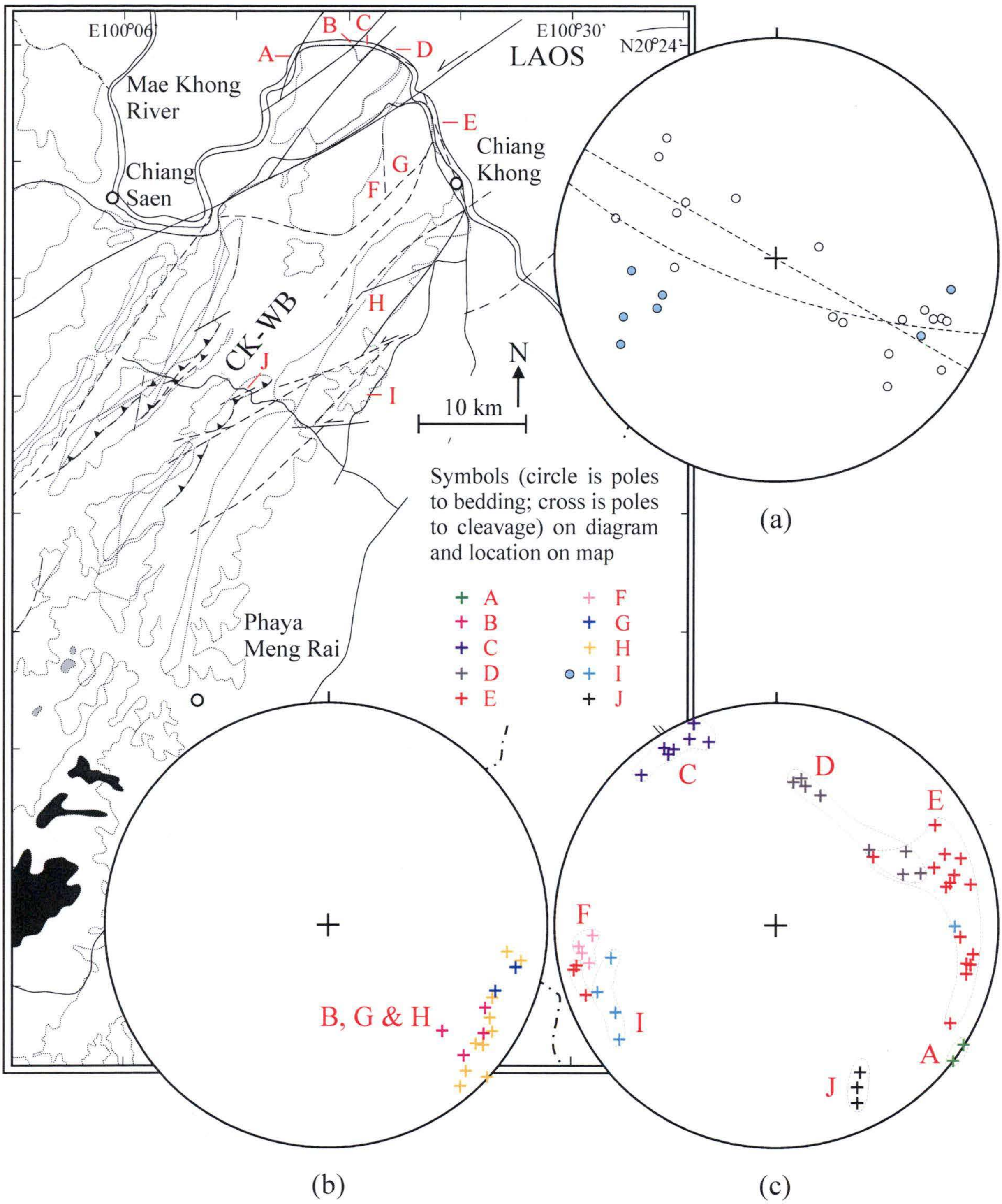

Figure 5.1 Lower-hemisphere equal-area stereographic projection showing poles to regional bedding (a), regional cleavage (b) and cleavage related to local faults (c) of Chiang Khong Western Belt. Note, blue circles in (a) are poles to bedding from location I. Symbols on geologic map as in Figure 2.3.

left lateral strike-slip Mae Chan Fault Zone (Morley, 2007). On the other hand, NW-SE and NNW-SSE cleavage strikes are spatially associated with local faults along the Mae Khong River from location D to A (Figure 5.1c). A N-S striking cleavage measured at Huai Meng Falls, west of Chiang Khong is probably related to a local N-S fault strike (location F in Figure 5.1c). The N-S cleavage that strikes subparallel to bedding at location I is interpreted to have been rotated by late strike-slip fault movement. A NE-SW cleavage at location J along the interprovincial route from Ban Kaen to Doi Luang is spatially associated with a left lateral strike-slip fault movement.

The regional cleavage dips more steeply than bedding. In terms of cleavage/bedding relationships, the major structure of the CK-WB is one limb of a shallowly plunging fold.

Chiang Khong Central Belt and North of the Wiang Kaen District

Cleavage in the north of the Wiang Kaen district was measured along 7 km of the Mae Khong River. The cleavage strikes N-S and dips steeply to the west (Figure 5.2a). At one location, two cleavages were observed both dipping to the west. The second cleavage was probably related to fault movement in that area. There is no evidence that it was regionally significant. A gentle to open upright outcrop-scale fold with S-plunging fold axis was found at 20.1712 ^{o}N 100.5684 ^{o}E.

Cleavages recognised at the northern tip of the CK-CB strike N-S and dip to the west. Two cleavages are present in several outcrops (Figure 5.2b). The steep cleavage (S1) is interpreted to be the regional cleavage whereas the shallow cleavage (S2) is may be associated with later thrust movement.

Bedding at the northern tip of CK-CB strikes N-S and dips steeply to the west (Figure 5.2c). The bedding dips more steeply than the regional cleavage (Figures 5.2b& c) and is interpreted to be an overturned limb (c.f. McClay, 2000).

Further south, cleavage planes in the central part of CK-CB were observed on roadcuts, quarries and reservoir exposures along a 30 km section of road number 1020 (Chiang Khong to Thoeng district) from the Chiang Khong-Wiang Kaen intersection to the Chiang Khong-Ban Phaya Phiphak intersection. The cleavage has been rotated to a NNE-SSW

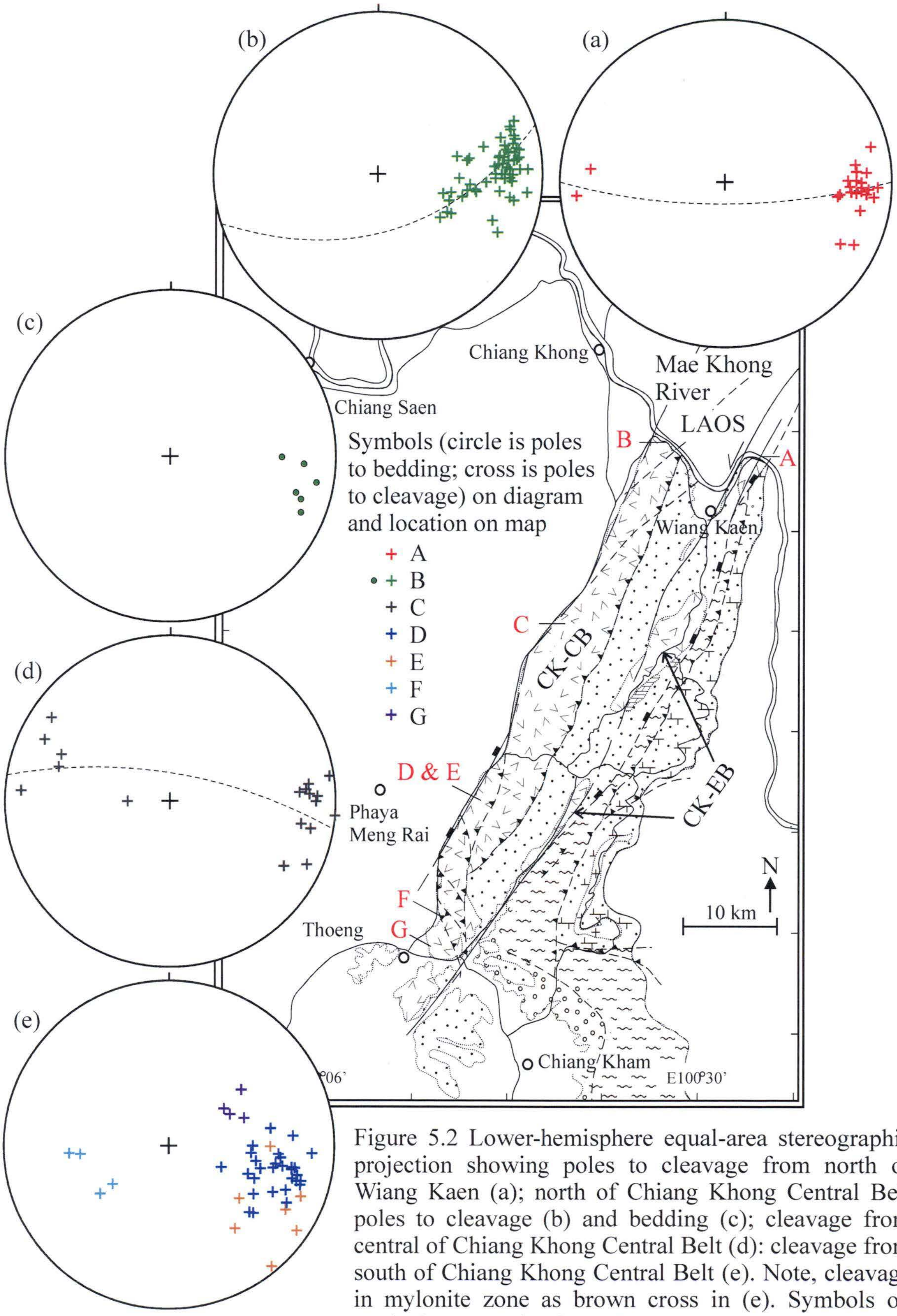

Figure 5.2 Lower-hemisphere equal-area stereographic projection showing poles to cleavage from north of Wiang Kaen (a); north of Chiang Khong Central Belt poles to cleavage (b) and bedding (c); cleavage from central of Chiang Khong Central Belt (d): cleavage from south of Chiang Khong Central Belt (e). Note, cleavage in mylonite zone as brown cross in (e). Symbols on geologic map as in Figure 2.3.

strike (Figure 5.2d), interpreted here as evidence for drag associated with Neogene normal and/or strike slip faults.

Cleavage measurements from the south of CK-CB about 30 km from the Chiang Khong-Ban Phaya Phiphak intersection to the Thoeng district are shown in Figure 5.2e. Cleavage strikes N-S to NNE-SSW and dips W to NW. There is local evidence for two discrete cleavages, including steep and shallow dips to the west. Comparison with the data further north suggests these may represent two distinct generations of cleavage formation. A mylonite zone has been recognised in this area and cleavages in the mylonite zone (brown cross in Figure 5.2e) are subparallel to and also rotated clockwise from the regional cleavage orientation. These are discussed in the mylonite section below. The NW-SE cleavage that dips to the northeast recognised at location F (light blue cross in Figure 5.2e) is interpreted to be associated with a back thrust in that area. At location G, the cleavage strikes NW-SE and shallowly dips to the SW (purple cross in Figure 5.2e). These cleavages are located in the regional hinge zone of a major fold structure in the Chiang Khong area and may have been rotated during folding. They are also close to a NW-striking section of a major fault zone.

Chiang Khong Eastern Belt

The fold and cleavage data in the CK-EB comes from the southeast of the Wiang Kaen district, the Pha Tank area, the Phu Chi Fa area, and the intermontane area between CK-CB and metamorphosed rocks exposed in the mountain range along the Thai-Laos border (Figure 5.3). High strain rocks of the Ban Huak area are described separately below. Fold and cleavage data in this area is more complicated than in the other sub-belts of the Chiang Khong area.

N-S striking cleavages observed in southeast of the Wiang Kaen district (zone A in Figure 5.3a) show a large range in dips. The steep dipping cleavage in this area is similar to orientations measured in the north of the Wiang Kaen district (Figure 5.2a) and is interpreted to be regional cleavage. The shallow cleavage dips may correlate with shallow cleavage recognised in the CK-CB.

Twenty km to the south, in the Pha Tank area, the bedding and cleavage strike NNE-SSW to N-S and dip to the W (Figure 5.3b). The bedding is subparallel to cleavage.

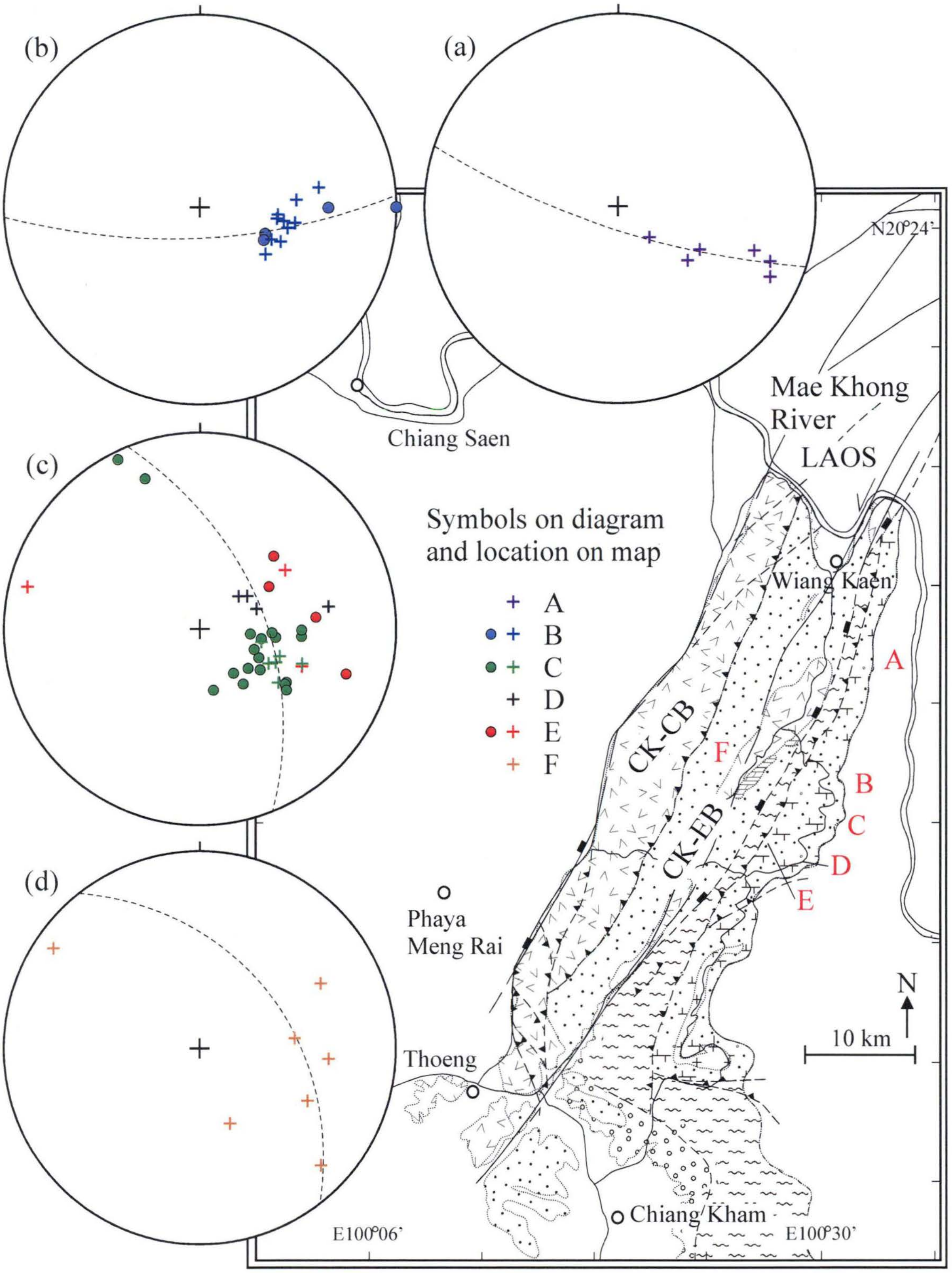

Figure 5.3 Lower-hemisphere equal-area stereographic projection showing poles to cleavage from southeast of Wiang Kaen district in zone A (a); bedding and cleavage from Pha Tank area in zone B (b); bedding and cleavage from Phu Chi Fa area in zone C (c); and cleavage from Late Triassic to Early Jurassic redbeds in zone F (d). Note, coloured circle as pole to bedding and coloured cross as pole to cleavage. Symbols on geologic map as in Figure 2.3.

The Phu Chi Fa area, 40 km south of the Wiang Kaen district, is dominated by Carboniferous-Permian limestone and meta-volcanic rocks and Carboniferous meta-sedimentary rocks. The bedding and regional cleavage in this area strike N-S and dip shallowly to the W (zone C in Figure 5.3c). These bedding and cleavage strikes have been rotated, probably associated with thrust fault movement. The NW-SE cleavage strike and shallow dip to the SW at location D (Figure 5.3c) are interpreted to be related to local thrust movement. Bedding and cleavage at Ban Huai Han (location E in Figure 5.3c) dips more steeply but is otherwise similar. The bedding has a great circle distribution about a SW-plunging fold that must post-date the regional cleavage.

Cleavage orientations in the intermontane lowland between CK-CB and the easternmost high mountain range (Figure 5.3d) are very scattered. These cleavages were measured from the Middle to Late Triassic volcanic rock of CK-EB and the Late Triassic redbeds. The generally NNE-SSW cleavage has been reoriented by drag on a major left lateral strike-slip fault along the Wiang Kaen Basin.

Summary

The dominant structure throughout the area is a NNE-SSW striking regional cleavage that dips steeply west. In the west, the cleavage is steeper and folding is upright and nearly symmetrical. Fold axes are nearly horizontal. In the east, bedding dips consistently west and mostly lies on a right way up limb; bedding orientation is closed to cleavage and in one area a regional overturned limb was recognised. Cleavage intensity increases to the east. The overall structure is most consistent with structural repetition on W-dipping thrust faults. At several locations a moderately W-dipping cleavage was recognised and at least locally this is a separate deformation event. There is no direct evidence for the relative ages of the two cleavage events. The shallow cleavage is interpreted here as the result of additional strain near major thrusts.

Elsewhere around the area there are anomalous cleavage orientations which are spatially correlated to major late faults. In some cases, there is evidence that the orientation is due to fault drag with both bedding and cleavage rotated. In other areas, this is less clear and the cleavage may be a discrete local cleavage unrelated to regional cleavage. Late folds were recognised and these also had a spatial relationship to late faults.

5.2.3 Fault, Fault Rocks and Mylonite

Fractures, fault rock and mylonite in the Chiang Khong area were always associated with fault movement. Fault-related rocks in this study have been discussed using the classification of Sibson (1977) and McClay (2000). Sense of shear was assessed using the criteria outlined by Hanmer & Passchier (1991).

Thrust, normal and strike-slip faults mainly strike subparallel to the dominant NNE-SSW strike of lithological units. For convenience, faults and fault rocks are discussed in three geographic belts (Figure 5.4).

Chiang Khong Western Belt

A major thrust zone is exposed in the CK-WB (location A in Figure 5.4). A foliated fault breccia (Figures 5.5a & b) occurs over 100 m along a roadcut at 20.1105°N 100.1400°E and 20.1095°N 100.1440°E. Minor thrusts within this fault zone strike NE-SW to NNE-SSW and dip NW. Outcrop-scale thrust faults have been observed in the Permo-Triassic sedimentary rocks and locally at the fault contact between Permo-Triassic sedimentary and the CLT rocks. The faults mainly strike NNE-SSW and have north-west dips. A north-dipping fault plane was measured in the westernmost portion of this outcrop section. Outcrop-scale thrusts have been measured along sections A-1 to A-3 and B-1 to B-3 (Figures 5.6 to 5.11). Low angle shear bands and sandstone phacoids were observed in the section A-3 (Figure 5.8).

A strike-slip fault cuts across the NW corner and eastern side of the CK-WB, and a foliation developed within and parallel to this zone is shown in Figure 5.1c (locations A and C). A sub-vertical foliation in quartz-biotite granite strikes NE-SW and parallel to the fault plane at 20.3877°N 100.2584°E (location B in Figures 5.4 & 5.5c).

The NE-SW striking and steeply NW-dipping cleavage in CLT volcaniclastic rocks at location C (in Figures 5.4 & 5.5d) is probably associated with oblique strike-slip movement at 20.3990°N 100.3131°E. The strike-slip faults in this area are interpreted to have a left-lateral movement, especially in the Mae Chan Fault Zone (Leloup *et al.,* 1995 & 2001; Morley, 2002, 2004 & 2007; Uttamo *et al.,* 2003). No exposure of the Mae Chan Fault was observed but the fault trace has been drawn based on the offset of the Mae Khong River and LandSat images. A left-lateral strike-slip fault in the eastern side of

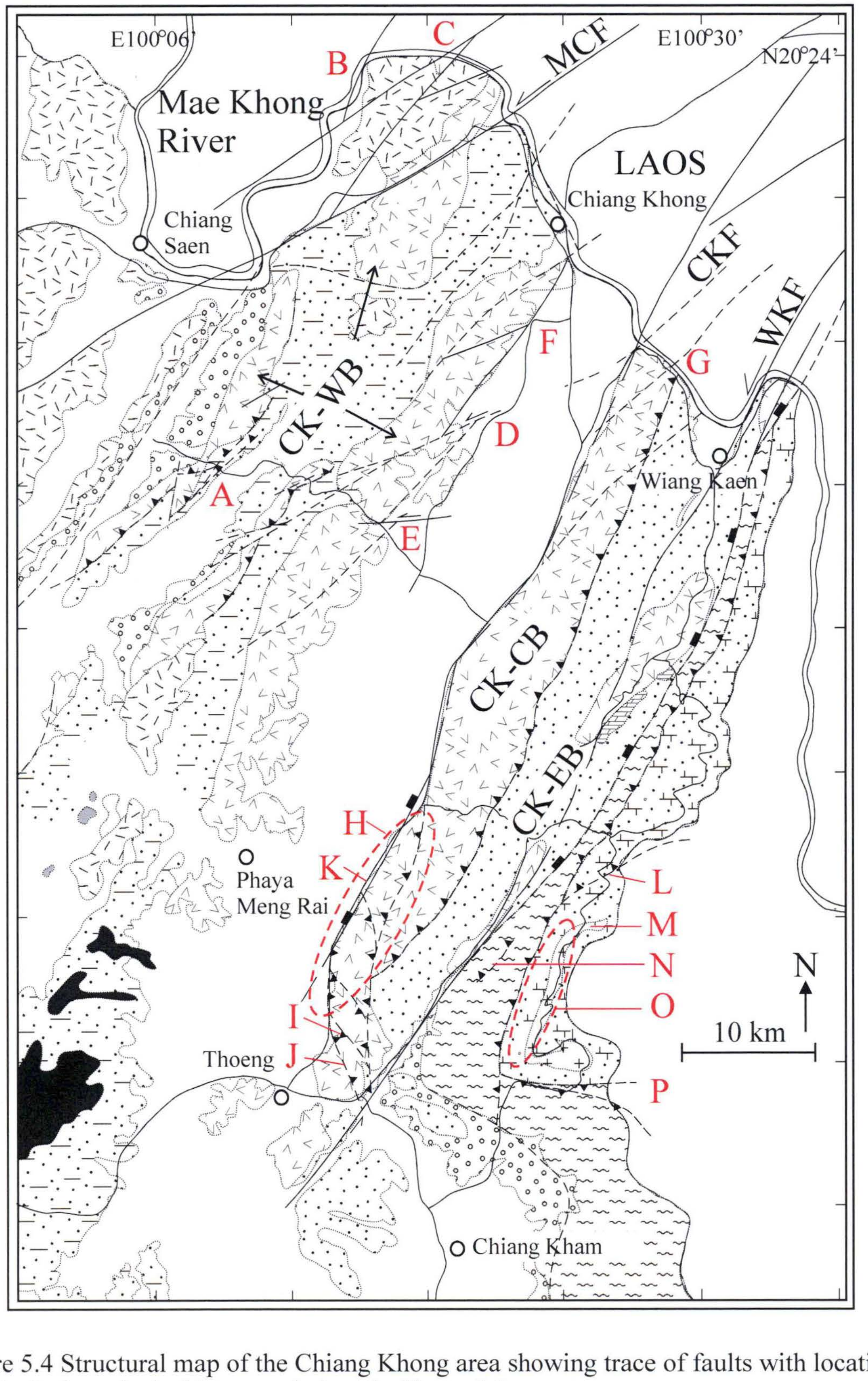

Figure 5.4 Structural map of the Chiang Khong area showing trace of faults with locations used in fault analysis. Note, symbols as in Figure 2.3.

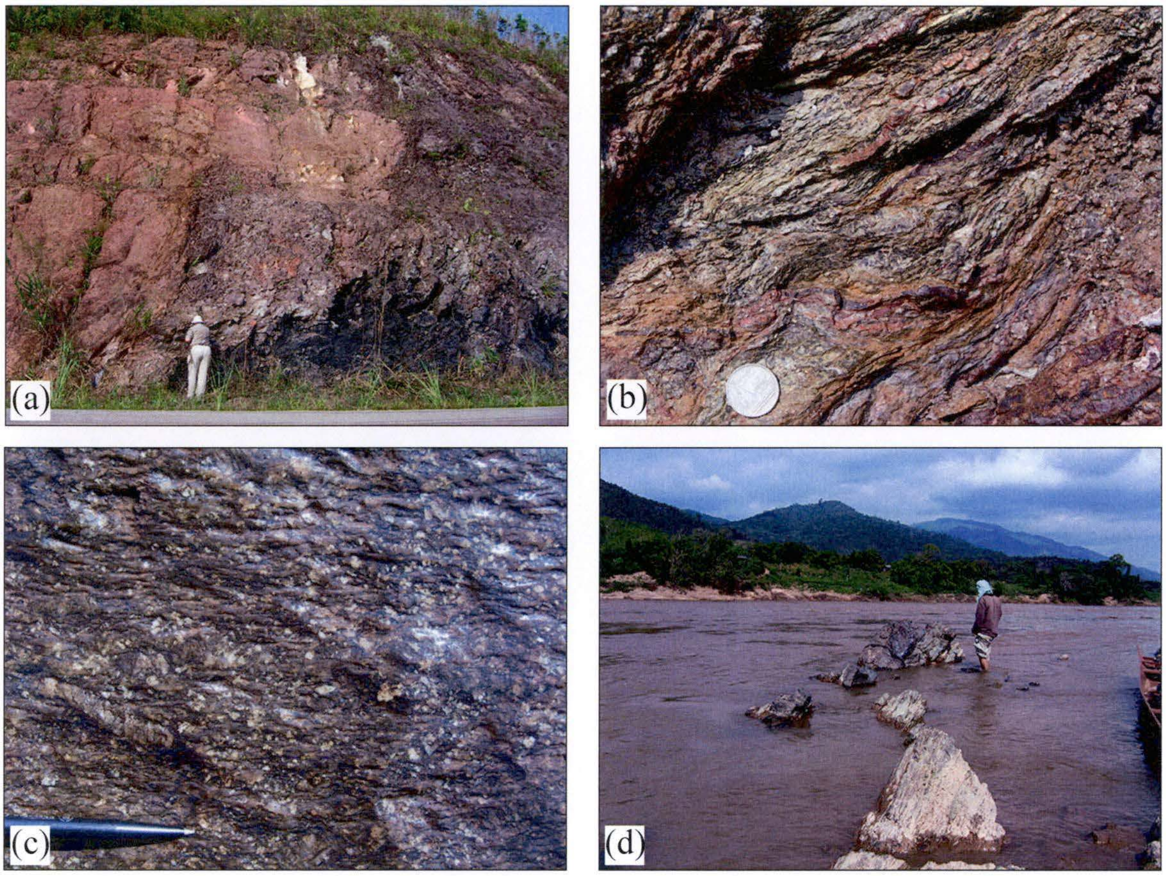

Figure 5.5 Photographs of structural features associated with fault movement in CK-WB. (a) Fracture zone and fault breccia with thrust fault association at location A in Figure 5.4. (b) Close up of foliated fault breccia related to thrust fault movement in (a). (c) Sub-vertical foliation parallel to NNE-SSW strike-slip fault strike at location B in Figure 5.4. (d) The NNE-SSW striking cleavage in volcaniclastic CLT rock at location C in Figure 5.4. Note, man is 180 cm tall in (a); coin is 2 cm in diameter; pen is 4 cm long in field of (c) and man is 178 cm tall in (d).

Section A-1:
Road cut outcrop at 20.1105°N 100.1400°E

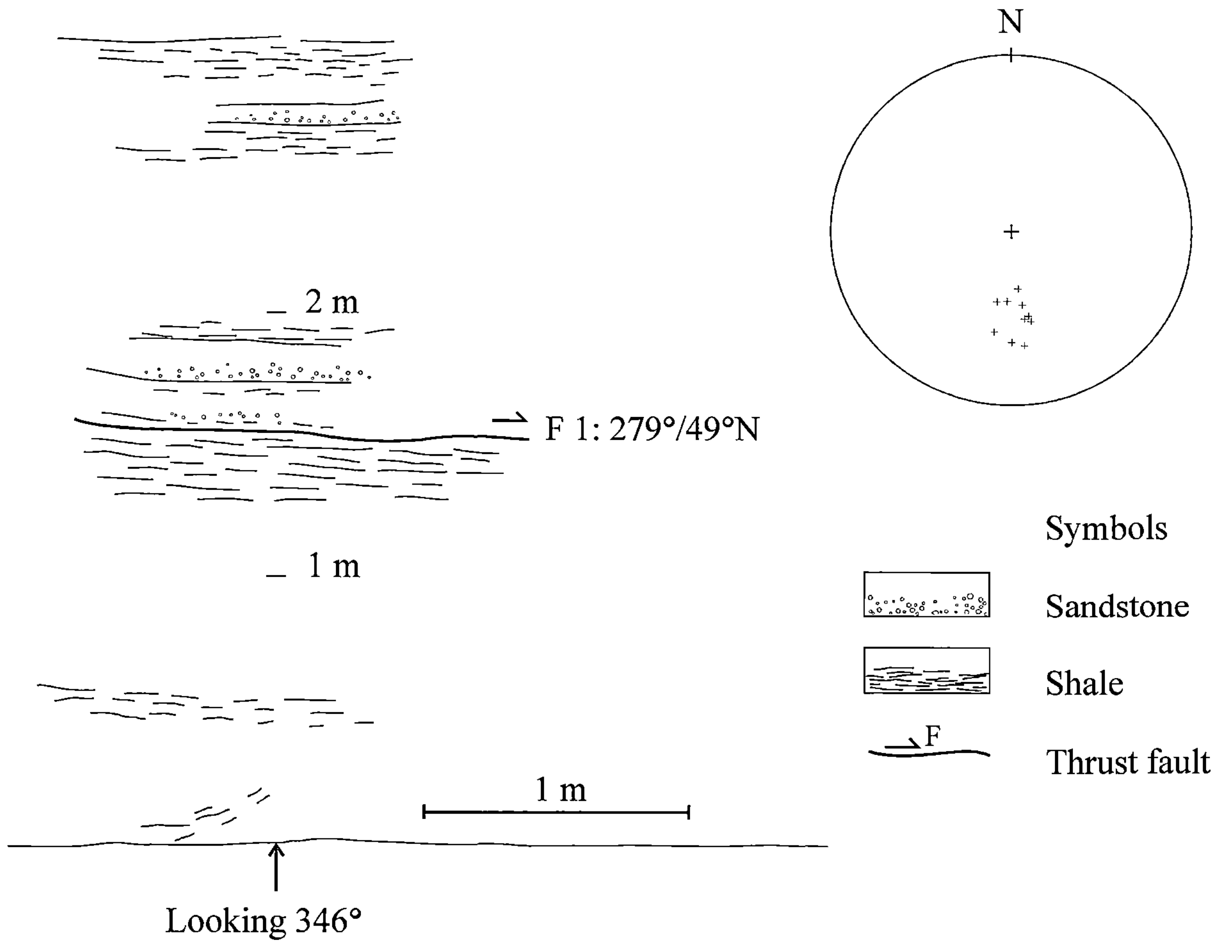

Figure 5.6 Outcrop sketch of A-1 road-cutting section at 20.1105°N 100.1400°E showing geometry of thrust fault (heavy line) in the Permo-Triassic sedimentary rock. Lower-hemisphere equal-area stereographic projection showing poles to bedding (small crosses) of sandstone and shale.

Section A-2:
Road cut outcrop at 20.1105°N 100.1400°E

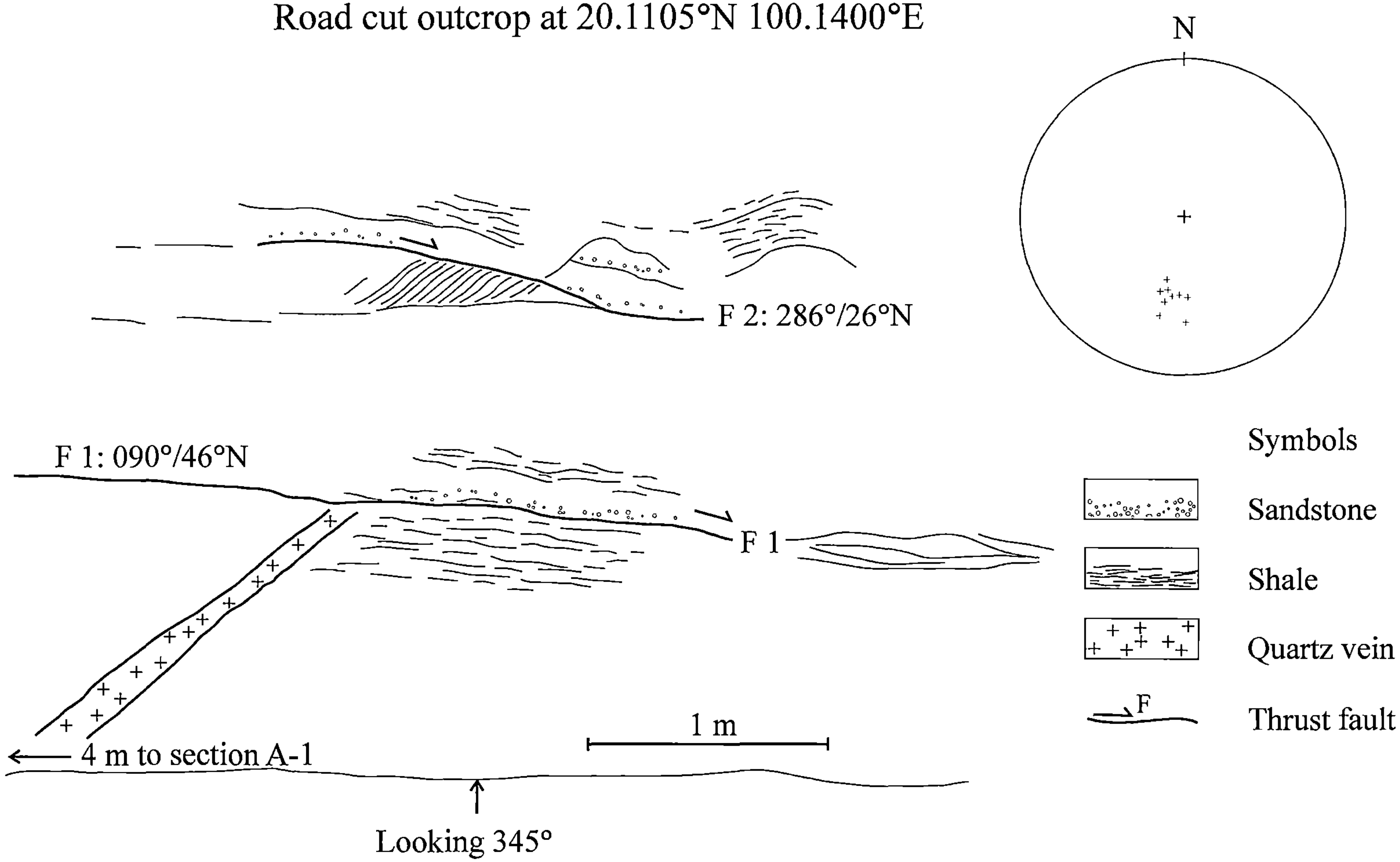

Figure 5.7 Outcrop sketch of A-2 road cutting section at 20.1105°N 100.1400°E showing geometry of thrust faults (F 1 and F 2 in heavy lines) in the Permo-Triassic sedimentary rock. Lower-hemisphere equal-area stereographic projection showing poles to bedding (small crosses) of sandstone and shale.

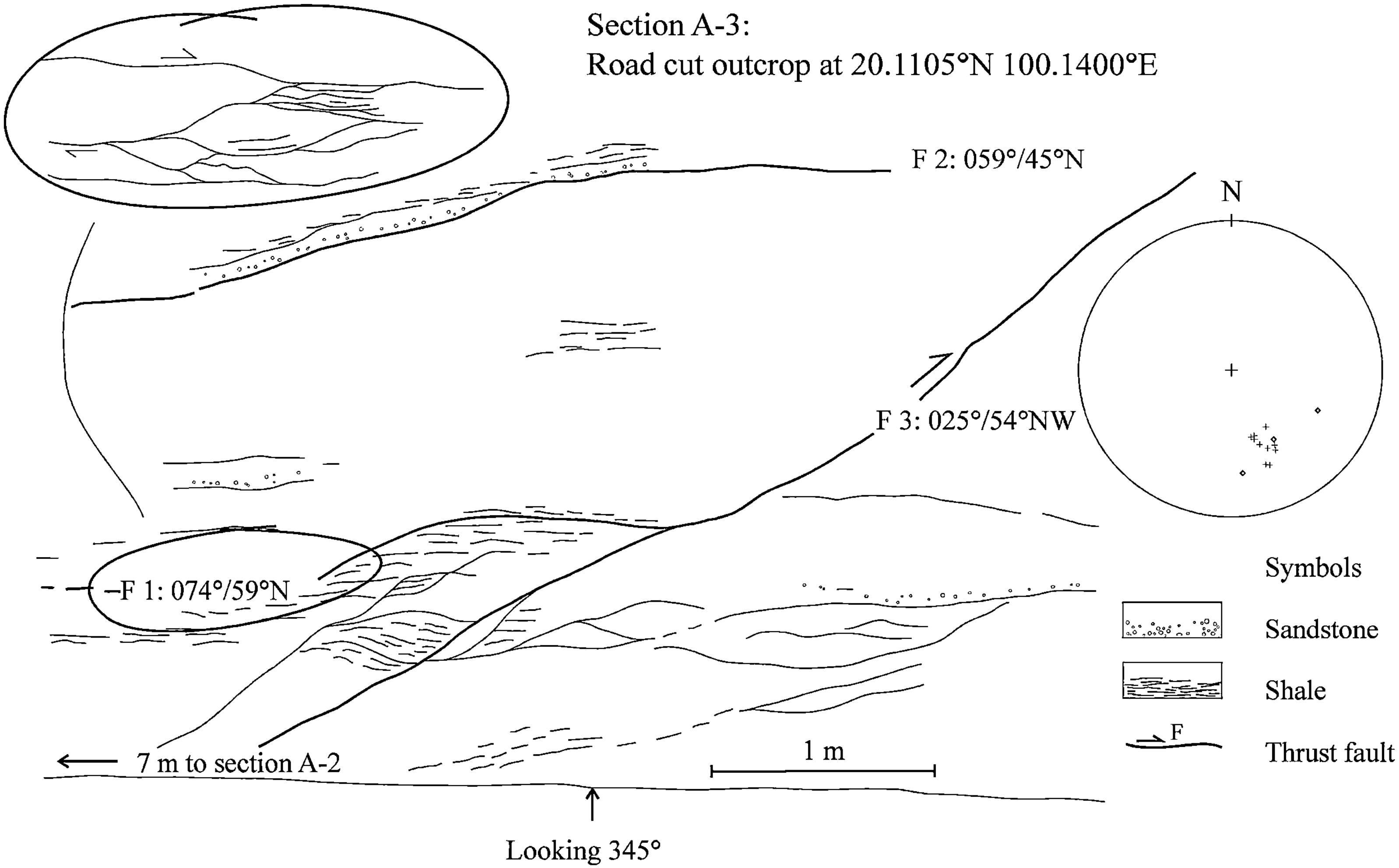

Figure 5.8 Outcrop sketch of A-3 road cutting section at 20.1105°N 100.1400°E showing geometry of thrust faults (F 1, F 2 and F 3 in heavy lines) in the Permo-Triassic sedimentary rock. Lower-hemisphere equal-area stereographic projection showing poles to bedding (small crosses) of sandstone and shale and poles to thrust fault planes (open diamond). Close up line sketch of the low angle shear bands and phacoids shown in the top left.

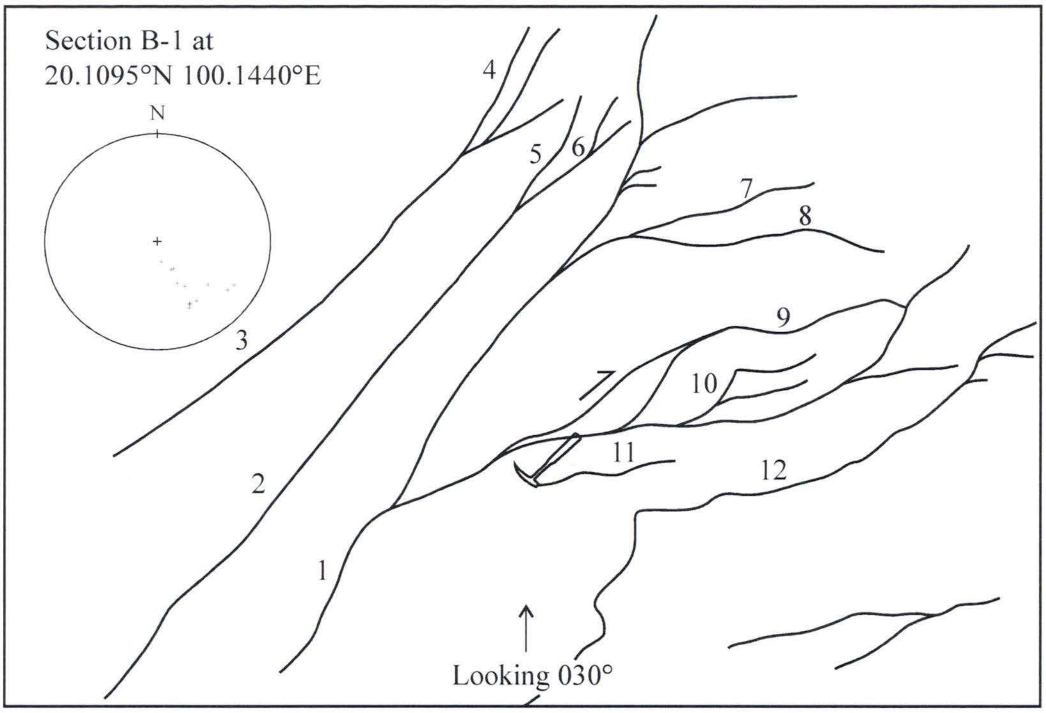

(a)

(b)

Figure 5.9 Line drawing (a) and photograph (b) showing the geometry of thrust faults in outcrop-scale of section B-1 in Permo-Triassic sedimentary rock at 20.1095°N 100.1440°E. Lower-hemisphere equal-area stereographic projection showing poles to fault planes (small crosses). Hammer is 28 cm long.

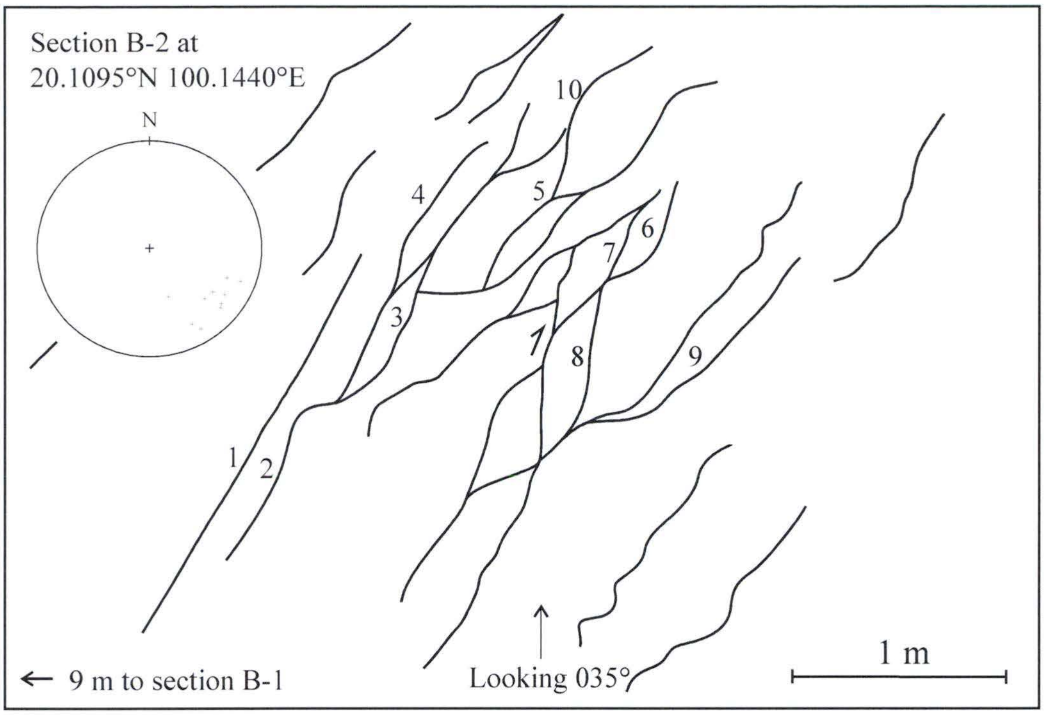

(a)

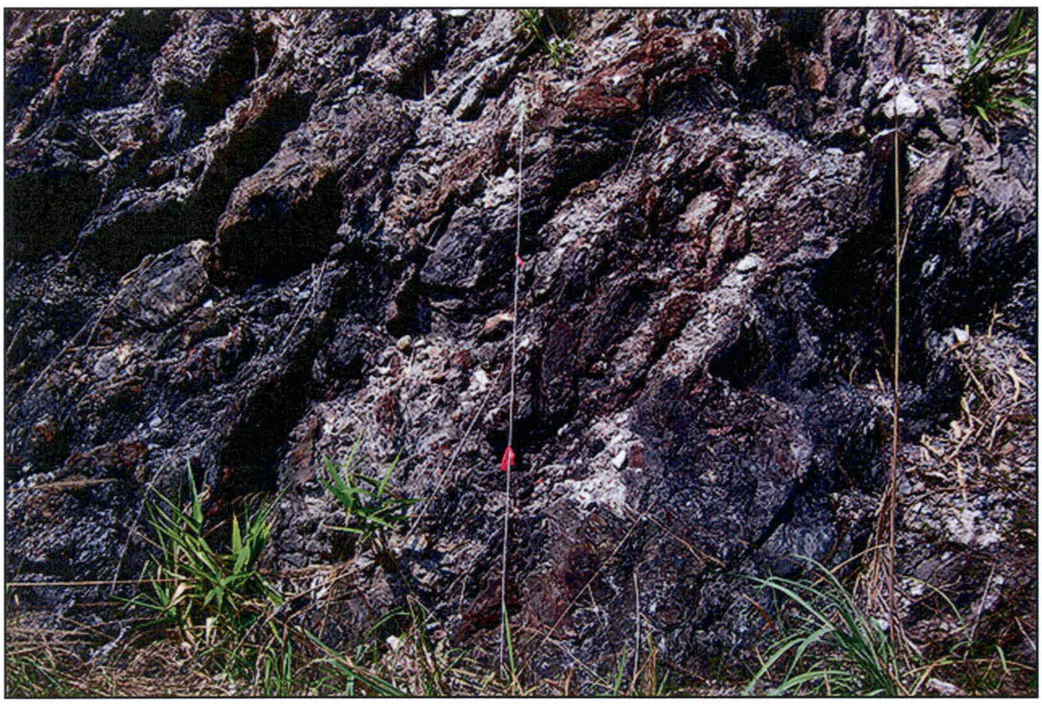

(b)

Figure 5.10 Line drawing (a) and photograph (b) showing the geometry of thrust faults in outcrop-scale of section B-2 in Permo-Triassic sedimentary rock at 20.1095°N 100.1440°E. Lower-hemisphere equal-area stereographic projection showing poles to fault planes (small crosses).

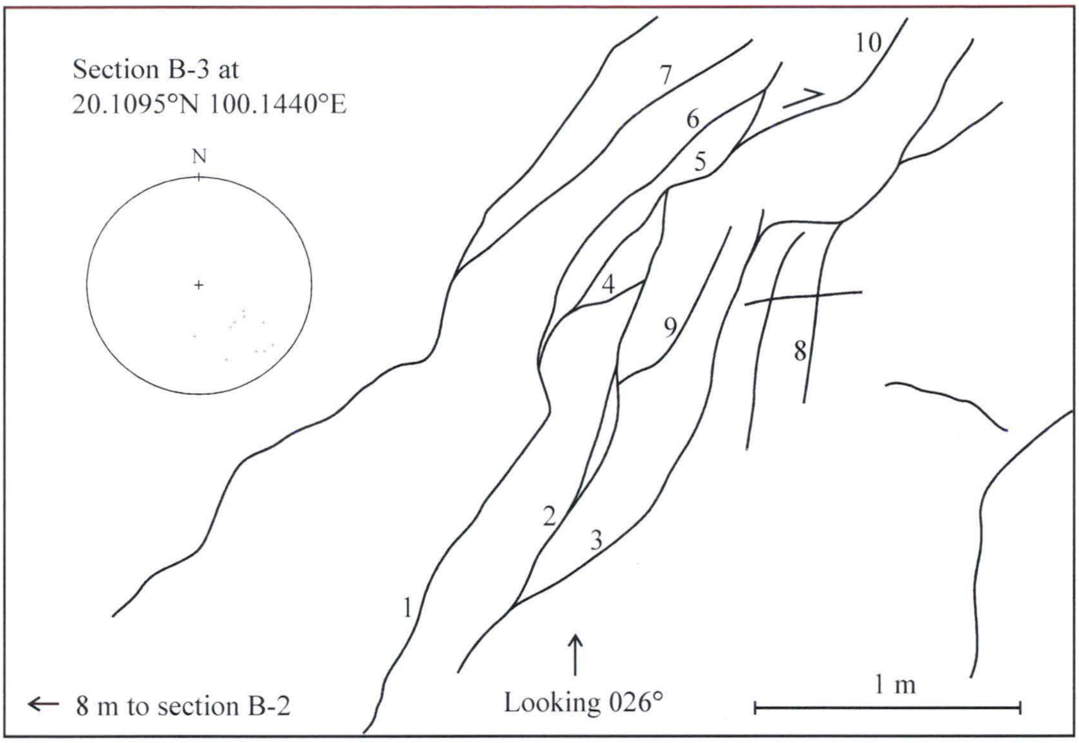

(a)

(b)

Figure 5.11 Line drawing (a) and photograph (b) showing the geometry of thrust faults in outcrop-scale of section B-3 in Permo-Triassic sedimentary rock at 20.1095°N 100.1440°E. Lower-hemisphere equal-area stereographic projection showing poles to fault planes (small crosses). White line on photograph is 3 m long.

CK-WB occurs at 20.1065°N 100.2848°E (location D in Figure 5.4). A vertical fold overprints the NNE-SSW regional trend at 20.0770°N 100.2615°E (location E in Figure 5.4) and this structure is correlated with the late left-lateral strike-slip faults.

Outcrop scale normal faults were found at many locations, and may be linked to late strike-slip fault movement. A NNE-SSW striking and steeply W dipping normal fault was observed at 20.1799°N 100.4874°E (location F in Figure 5.4).

Chiang Khong Central Belt

Both thrust and normal faults were observed along the CK-CB. These faults are dominantly N-S to NNE-SSW striking and subparallel to the mountain range. Strong foliation and mylonite was noted associated with a thrust fault zone in the south of the area.

A NNE-SSW-striking major thrust fault was mapped along a contact between the Middle to Late Triassic CLT and the Late Triassic redbeds. The thrust fault is exposed at 20.1799°N 100.4874°E (location G in Figure 5.4). A strong foliation is present in the volcanic rocks from the south of the CK-CB subparallel to the thrust fault plane (Figure 5.2e).

Mylonite occurs in a thrust fault zone at location H (Figure 5.4). A strong foliation and shear bands in the mylonite mainly strike N-S to NNE-SSW and dip to the W (Figures 5.12a & b), subparallel to the regional cleavage (stereonet in Figure 5.2e). Feldspar and quartz porphyroclasts are very common and show reverse movement on this zone (Figures 5.13 to 5.16). Shear band development (Figure 5.16b) supports this interpretation. The quartz porphyroclasts preserve an original resorbed texture (Figure 5.14) suggesting these rocks were originally a porphyritic volcanic and that the development of the mylonitic texture in this rock has been aided by the primary lithology. The protolith is interpreted to be a Middle to Late Triassic rhyolite or rhyolitic volcaniclastic rock of the CLT.

An outcrop-scale thrust-related fold (Figure 5.17a&b) is present at 19.7284°N 100.2310°E in felsic volcaniclastic rocks (location I in Figure 5.4). Strongly cleaved rocks occur near

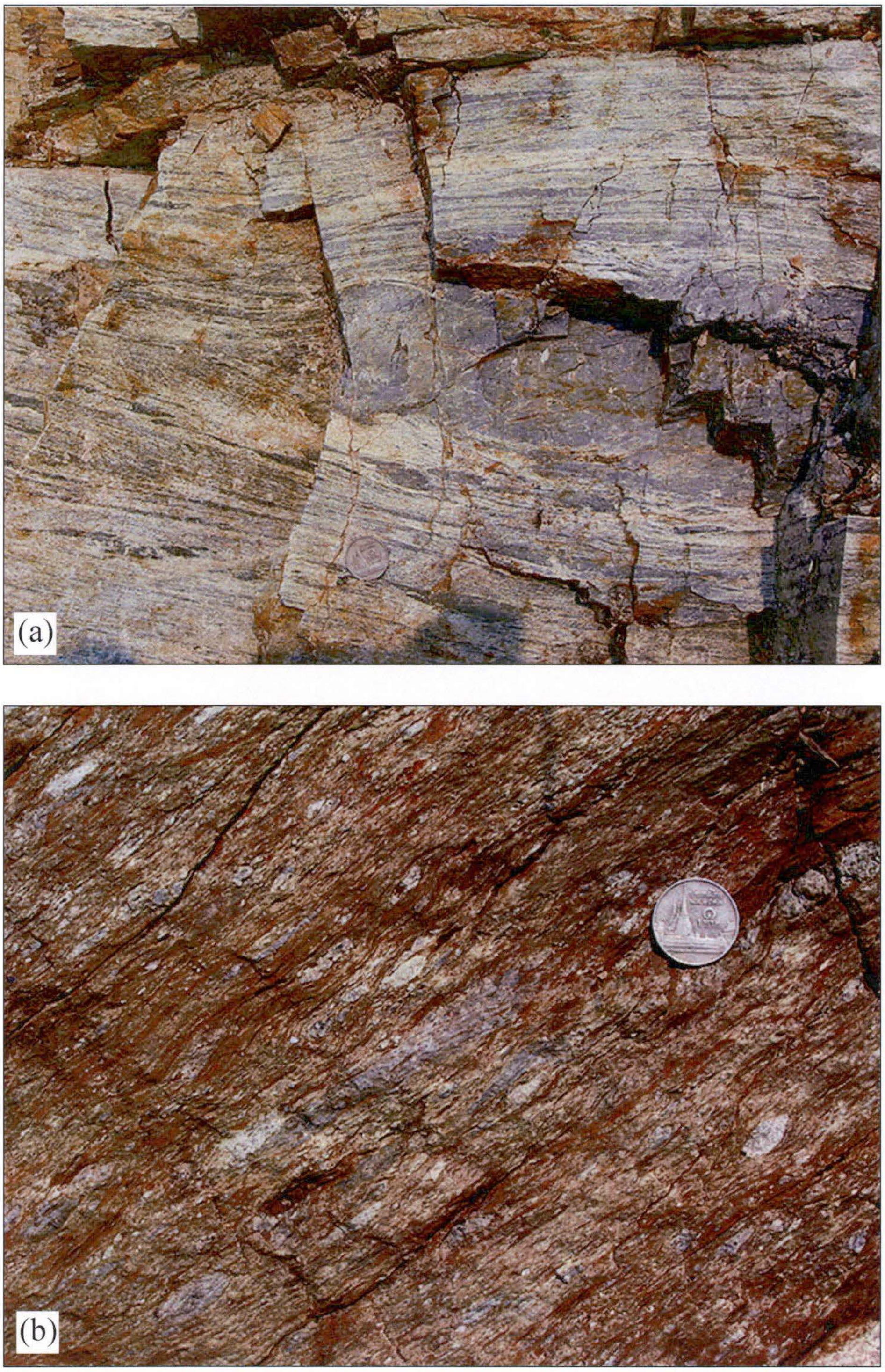

Figure 5.12 Photographs showing foliations, shear bands and porphyroclasts on the mylonite outcrop at (a) 19.8105°N 100.2527°E (looking NW) and (b) 19.3210°N 100.2270°E (looking 030°) from zone H of CK-CB in Figure 5.4. Coin is 2 cm in diameter.

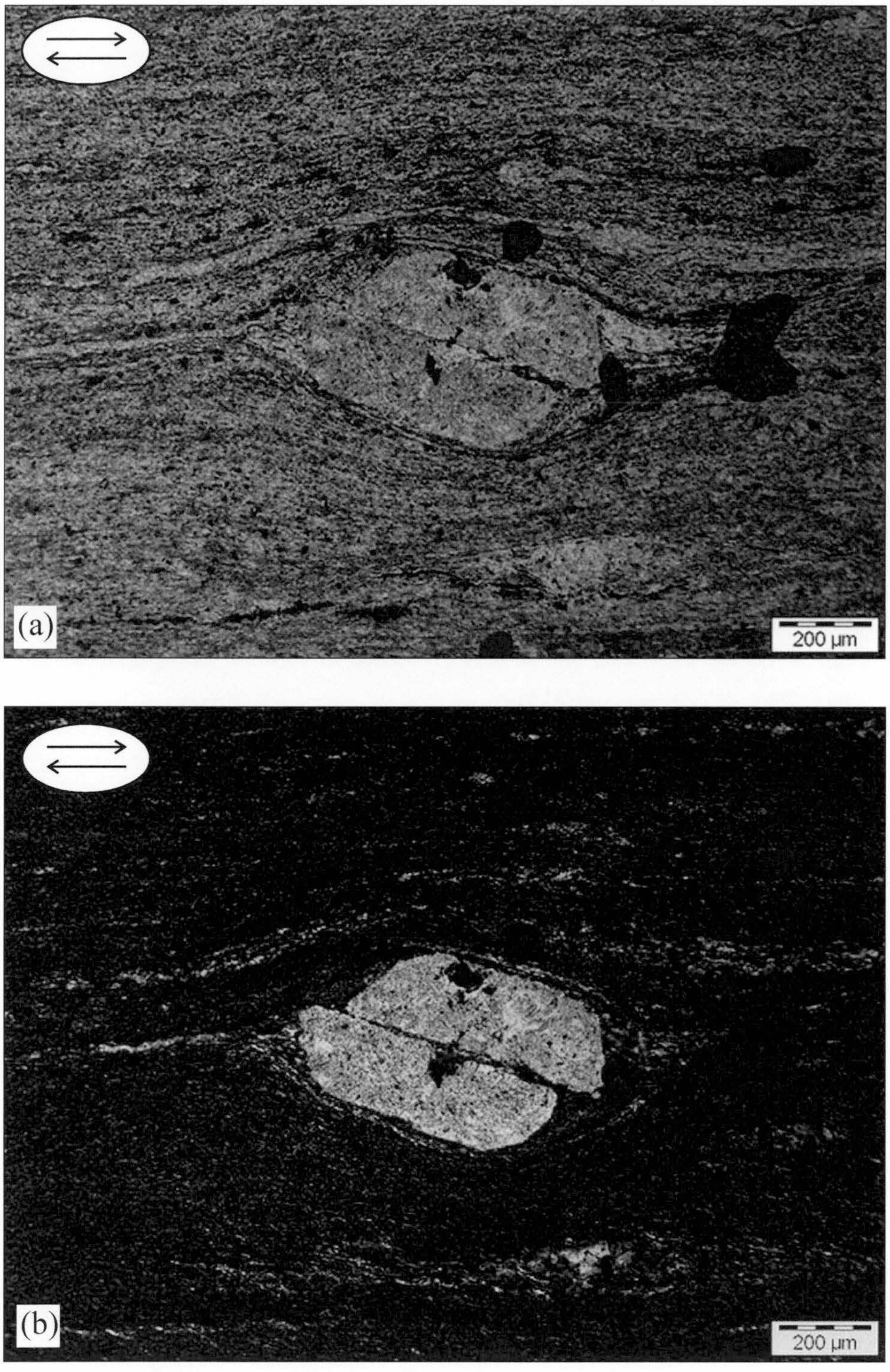

Figure 5.13 Photomicrograph of feldspar porphyroclast enclosed in fine-grained quartz matrix in quartzo-feldpathic mylonite from 19.8105°N 100.2527°E of CK-CB. Feldspar porphyroclast was broken and shows sense of shear top to the right. Note, plane of the photomicrograph is approximately the XZ plane of the finite strain ellipsoid and looking to the north; (a) plane polarized light (b) cross polarized light.

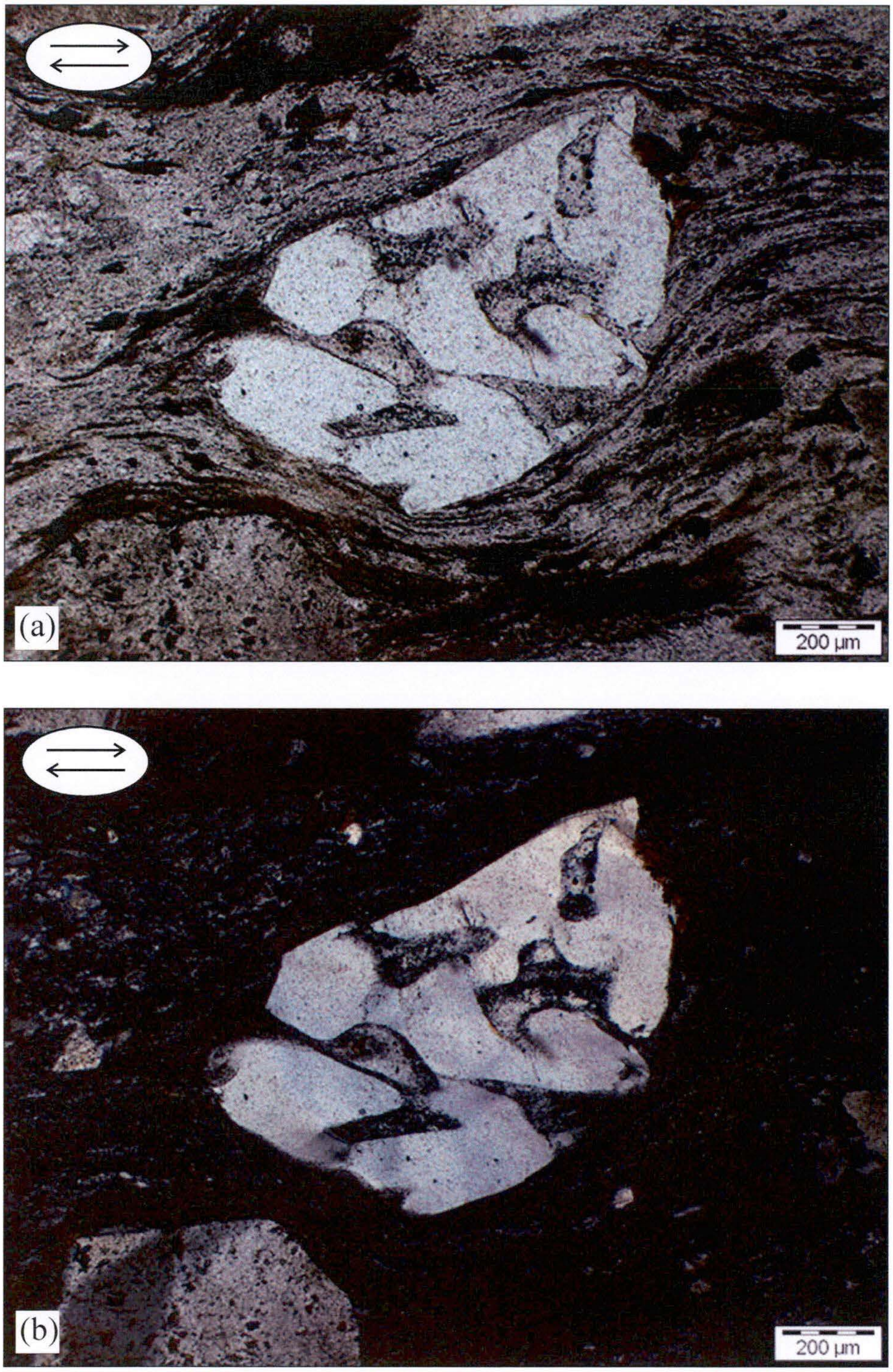

Figure 5.14 Photomicrograph of embayed-quartz porphyroclast with fine-grained recrystallised quartz tail showing top to the right sense of shear in quartzo-feldspathic mylonite from 19.3210°N 100.2270°E (zone H in Figure 5.4). Note, plane of photomicrograph is approximately the XZ plane of the finite strain ellipsoid and looking N, (a) plane polarized light (b) crossed polarized light.

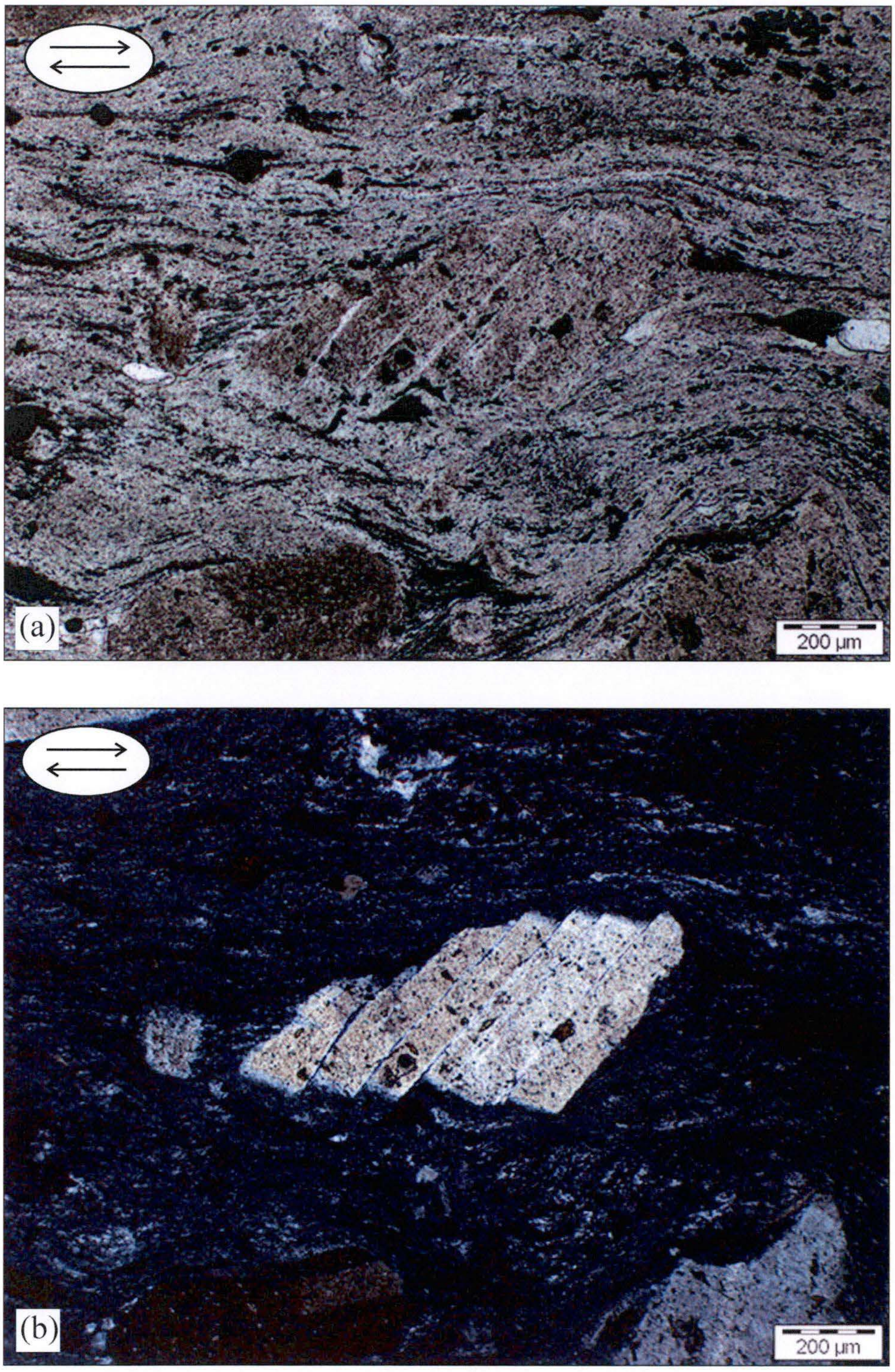

Figure 5.15 Photomicrograph showing dextral shear forming a domino structure of a plagioclase porphyroclast in quartzo-feldspathic mylonite. Note, plane of photomicrograph is approximately the XZ plane of the finite strain ellipsoid and looking N, (a) plane polarized light (b) crossed polarized light.

Figure 5.16 Photomicrograph of quartz-feldspar-epidote porphyroclasts in mylonite from 19.7537°N 100.2398°E showing dextrally rotated 'δ -type' winged epidote-feldspar porphyroclast (a) and C-C' shear band (b). Note, plane is approximately the XZ plane of the finite strain ellipsoid and looking N.

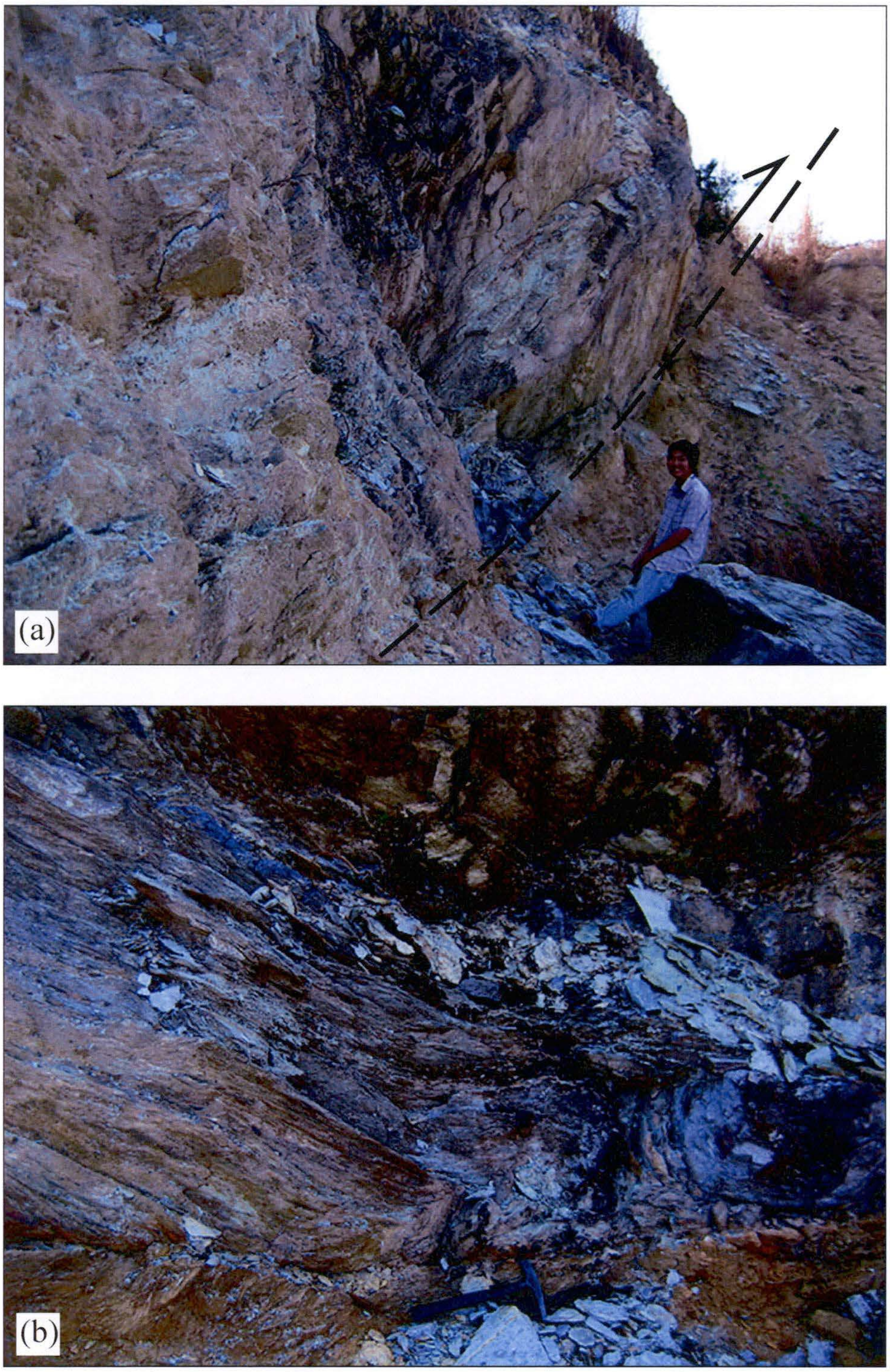

Figure 5.17 Photographs of outcrop-scale thrust fault (a) and intense cleavage near fault (b) in the CK-CB volcaniclastic rocks from 19.7285°N 100.2310°E. Note, looking NW in (a) looking SW in (b), man is 168 cm tall and hammer is 28 cm long.

this fault (Figure 5.17b) and support deformation at conditions within the brittle ductile transition.

A thrust fault zone at the southern tip of CK-CB, 5 to 10 km northeast of Thoeng strikes NNE-SSW to NNW-SSE and dips to the east (locations I and J, Figure 5.4). The structure was observed at 19.7086°N 100.2347°E (location J in Figure 5.4) and is interpreted as a back thrust. There is a strong local cleavage associated with this thrust fault (Figure 5.2e).

The NNE-SSW normal fault on the western side of CK-CB is interpreted as the eastern boundary fault of the Thoeng-Chiang Khong Basin. It was active during Tertiary extension in northern Thailand (Leloup *et al.,* 1995; Morley, 2002 & 2007; Polachan *et al.,* 1991; Uttamo *et al.,* 2003). An outcrop-scale normal fault at 19.8474°N 100.2721°E strikes 024° and dips 77° to the west (location K in Figure 5.4).

Strike-slip faults in the CK-CB were interpreted from the LandSat image. A NNE-SSW strike-slip fault is drawn at the northern tip of CK-CB (Figure 5.4). A NE-SW left-lateral strike-slip fault at the northwest corner of CK-CB has been termed the Chiang Khong Fault (CKF) (Uttamo *et al.,* 2003). The E-W extension of the Thoeng-Chiang Khong Basin may be linked with this sinistral strike-slip tectonics but strike slip faulting continues to the present, although extension was largely active in the Tertiary (Uttamo *et al.,* 2003).

Chiang Khong Eastern Belt and the Ban Huak Area

Thrust, normal and strike-slip faults were also recognised in the CK-EB and in high strain rocks of the Ban Hauk area (Figure 5.4). Fault planes mainly strike NNE-SSW and dip to the west. Thrust faults in the north of high strain area are NE-SW striking and NW-dipping whereas thrust faults in the south are E-W striking and dip south.

A NNE-SSW striking thrust fault was traced through the central part of the area, extending approximately 70 km from east of Wiang Kaen to the north of Chiang Kham (Figure 5.4). It forms a W-dipping fault contact between Carboniferous-Permian meta-sedimentary rocks in the east and Carboniferous-Permian limestone and meta-volcanic rocks in the west. The fault outcrops at 19.886°N 100.4414°E and 19.7868°N 100.3619°E are shown on the Ban Phaya Phiphak to Phu Chi Fa structural transect below.

A NW-dipping thrust fault was inferred in the Phu Chi Fa area (location L in Figure 5.4) from the appearance of strongly foliated limestone at 19.8386°N 100.4435°E. This fault is linked to a NE-SW striking and northwesterly dipping cleavage and NW-plunging lineation in foliated granite at location M in Figure 5.4. The sense of shear is uncertain but the fault repeats stratigraphy and has a strong association with L/S fabrics. Mylonites within the L/S schist zone display reverse sense of displacement (see below). The overturned bedding of the Carboniferous meta-sandstone strikes NE-SW and dips to the NW and is closely related to minor thrust faults at location N in Figure 5.4. The balance of evidence is that this large scale fault also has reverse movement although it may have been reactivated as a normal fault during post-orogenic extensional collapse (Chapter 3) or during Tertiary extension.

Strongly deformed cleavage and lineation were measured in the high strain rocks of the Ban Huak area (see section 5.2.6). The N-S striking and westerly dipping cleavage with W- to SW-plunging lineation is interpreted to be related to the thrust movement (zone O in Figure 5.4). The quartzo-feldspathic mylonite at 19.7192°N 100.3855°E (Figures 5.18a & b) and 19.7940°N 100.4148°E (Figures 5.19a & b) and the epidote porphyroclasts in quartz-chlorite-epidote mylonite from 19.7760°N 100.4003°E (Figures 5.20a & b) all support reverse sense of shear in this area (location zone O, Figure 5.4).

In the far southeast corner of the study area, a thrust fault strikes E-W and dips steeply to the south (location P in Figure 5.4). The thrust fault was interpreted along a fault contact between the Carboniferous-Permian meta-sedimentary rocks and the Carboniferous-Permian limestone and meta-volcanic rocks. A local cleavage is subparallel to the fault and is interpreted to be genetically related to the thrust (see more detailed discussion on the cleavage and folding section).

A regional normal fault in the CK-EB strikes NNE-SSW and steeply dips to the west. This fault was traced from north of Wiang Kaen, through the intermontane basin and ended at southern tip of CK-EB (Figure 5.4). This fault is interpreted at the western contact of the high strain rocks and probably controlled the formation of the Wiang Kaen Basin in the northeastern part of the Chiang Khong area (see detailed schematic on the Ban Phaya Phiphak to Phu Chi Fa transect).

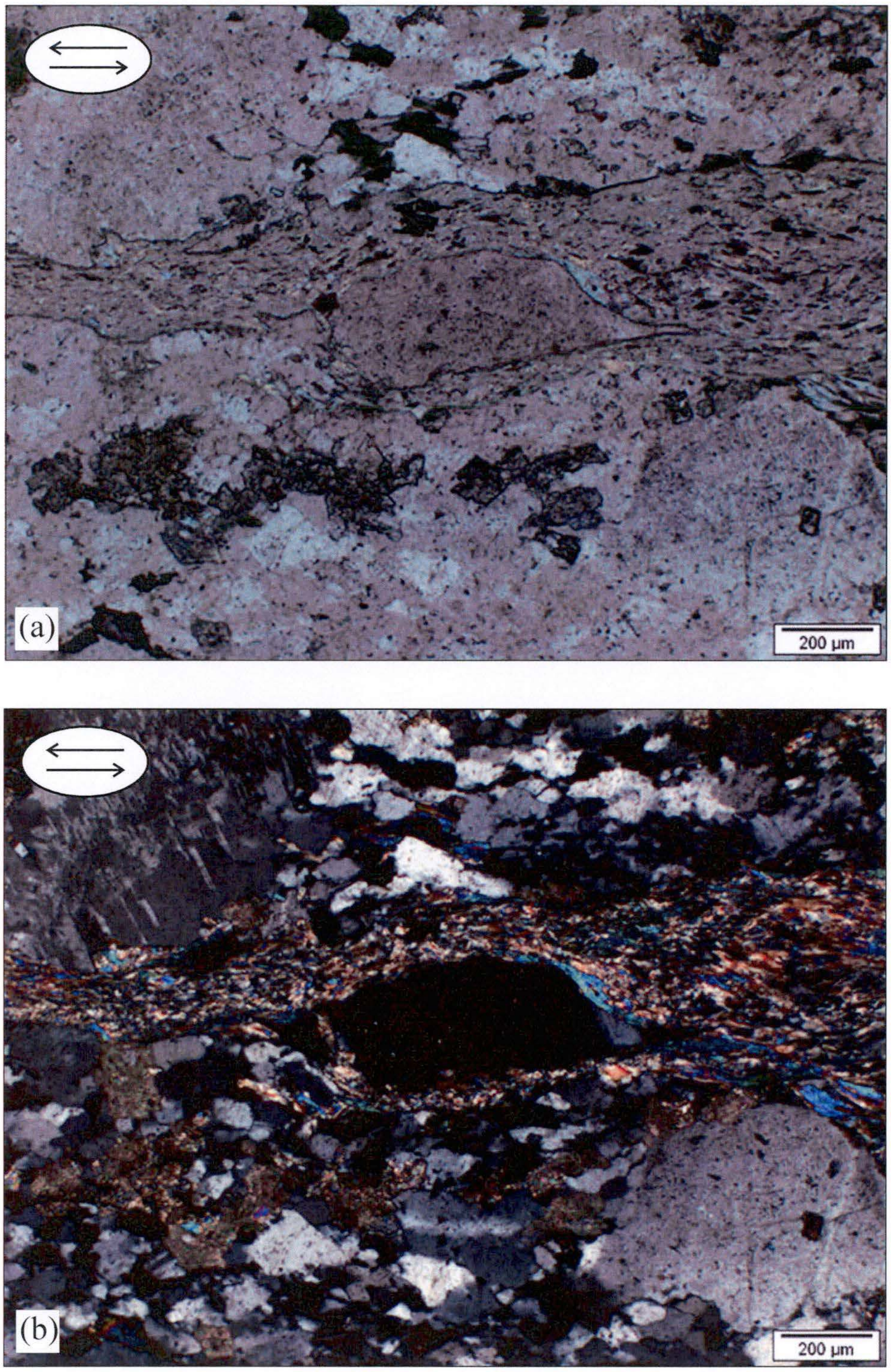

Figure 5.18 Photomicrograph of mylonitic granitoid of the Ban Huak area from 19.7192°N 100.3855°E, shows feldspar porphyroclast with sinistral sense of shear with mica and recrystallised fine-grained quartz tail. Note, the plane of photomicrograph is approximately the XZ plane of the finite strain ellipsoid and looking S; (a) plane polarized light; (b) crossed polarized light.

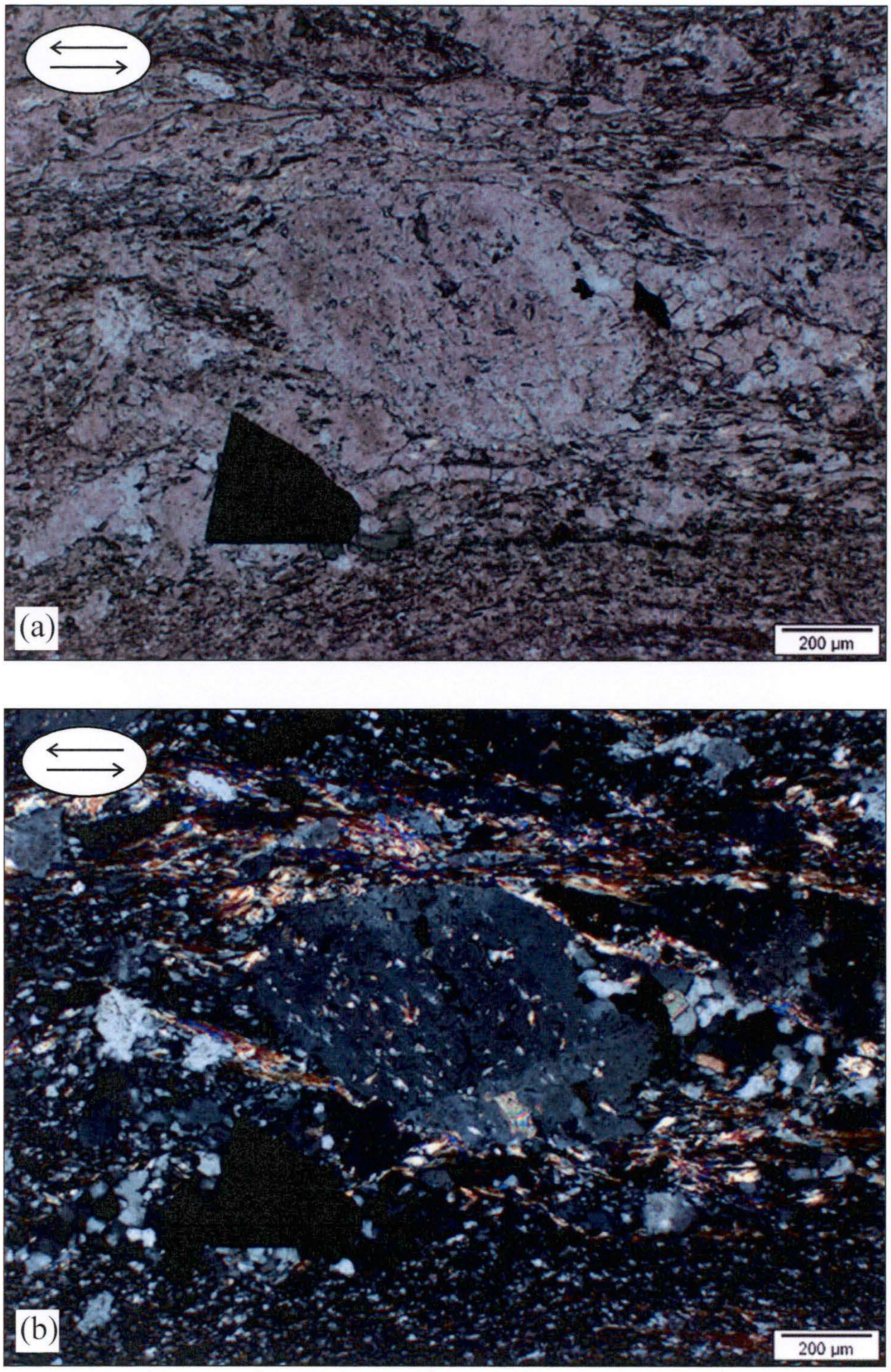

Figure 5.19 Photomicrograph of a σ-type of feldspar porphyroclast with tail of mica and recrystallised fine-grained quartz in mylonite granitoid of Ban Huak area from 19.7940°N 100.4148°E. Note, plane of photomicrograph is approximately the XZ plane of the finite strain ellipsoid and looking S; (a) plane polarized light; (b) crossed polarized light.

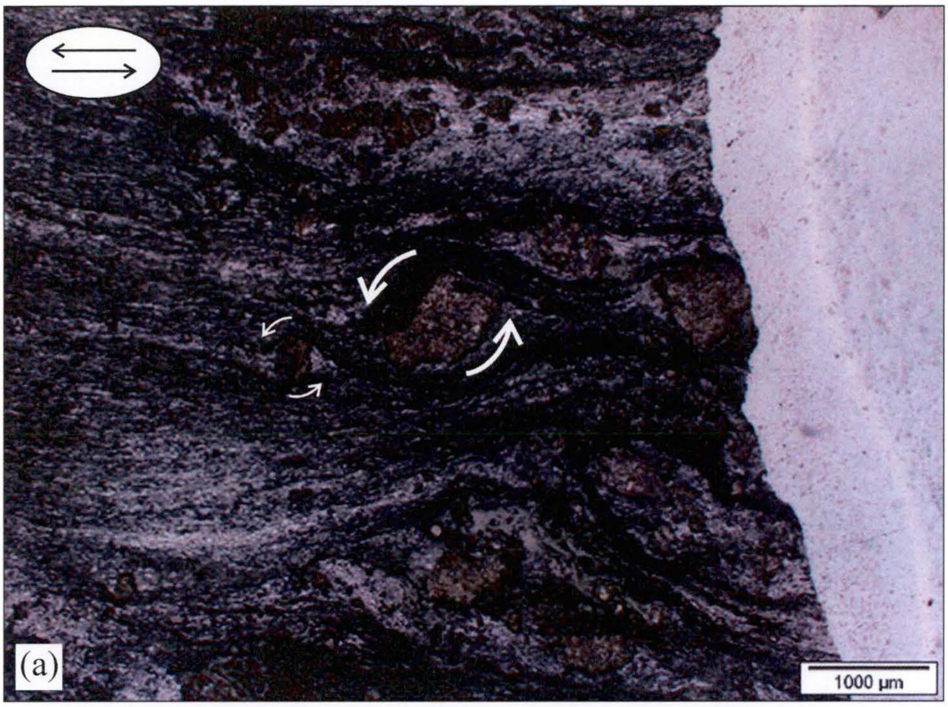

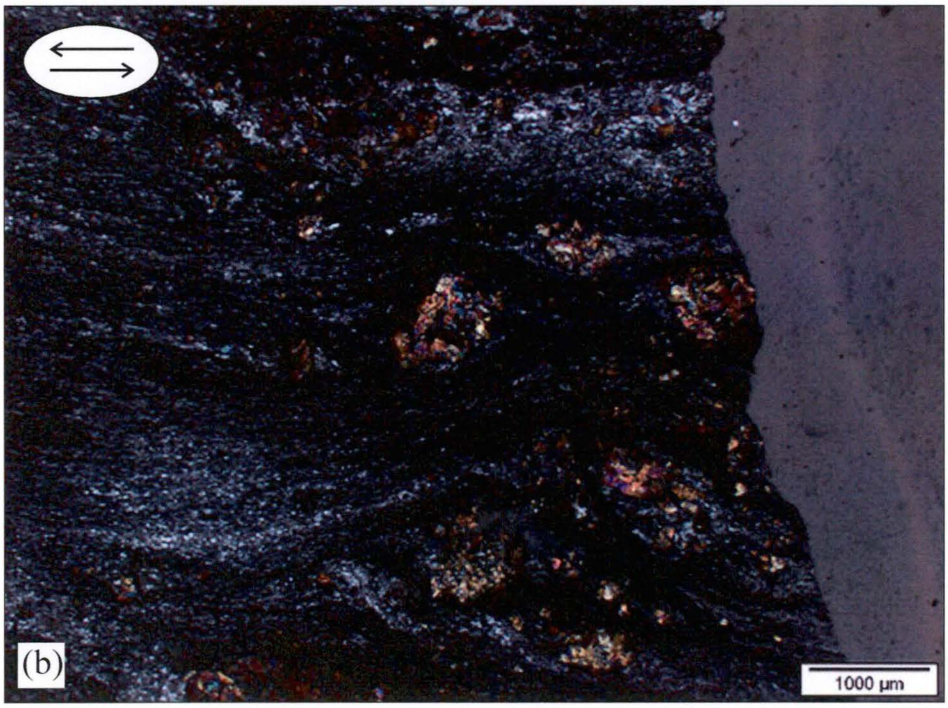

Figure 5.20 Photomicrograph of mafic volcaniclastic mylonite of Ban Huak area from 19.7760°N 100.4003°E, shows 'δ-type' porphyroclast (epidote) with tail of chlorite and recrystallised quartz. Note, plane of photomicrograph is approximately the XZ plane of finite strain ellipsoid and looking S; (a) plane polarized light; (b) crossed polarized light.

A regional NNE-SSW strike-slip fault in the CK-EB has been named the Wiang Kaen Fault (WKF on Figure 5.4). This left lateral strike-slip fault crosses Mae Khong River, north of Wiang Kaen, runs south along the intermontane basin and then east of Thoeng (Figure 5.4). The fault offsets the Mae Khong River by more than 3 km. This movement may be very young (eg. Leloup *et al.* 1995) but was correlated with the Tertiary extension in northern Thailand by Uttamo *et al.* (2003).

Summary

Thrust faults in the Chiang Khong area mainly strike N-S to NNE-SSW, dip W and are associated with regional cleavage development. In the far southeast, thrust faults strike NW. These may be lateral ramps, later thrust faults associated with a separate stress field or partly folded sections of the dominant regional thrusts. In the CK-WB, thrusts are associated with broad zones of foliated fault breccia. In the CK-CB and CK-EB, thrusts are associated with stronger cleavage development and locally mylonite zones. In the far east, there is a broad zone of L/S fabrics including mylonitic fabrics in a granitoid. The whole area is dominated by transport to the ENE. Back thrusts were recognised east of Thoeng. The transition from brittle to ductile textures associated with thrusting is consistent with the metamorphic petrology (section 5.2.4) that demonstrates an increase in metamorphism from prehnite-pumpellyite facies to biotite zone, greenschist facies from east to west across the region.

Late left-lateral strike-slip and normal faults are widespread across the area. They have overprinted the NNE-SSW regional structure and now dominate the topography. Many of these faults may reactivate older structures. For example, parts of the normal faulted margin of the Thoeng-Chiang Khong Basin follow the mylonite zone recognised NE of Thoeng. The NE-SW strike-slip and N-S normal faults were interpreted to be associated with the formation of Tertiary extensional basin in northern Thailand (Lacassin *et al.*, 1997; Leloup *et al.*, 1995; Metcalfe, 1996; Morley, 2002 & 2007; Polachan *et al.*, 1991; Uttamo *et al.*, 2003).

5.2.4 Metamorphism

A reconnaissance study was made of the metamorphic mineral assemblages of rocks in the Chiang Khong area. More than 20 thin sections were studied for index minerals. Nine representative rocks, including 3 samples from CK-WB, two samples from CK-CB, one sample from CK-EB and three samples from the Ban Huak high strain rocks area were selected for metamorphic mineral analysis by electron probe microanalysis. The microanalysis was conducted on a CAMECA SX100 microprobe in the Central Science Laboratory, University of Tasmania. The analytical results for the metamorphic minerals are shown in Appendix D.

The metamorphic grade of rocks in the Chiang Khong area varies from greenschist facies in the southeast corner to prehnite-pumpellyite facies in northwest corner. The metamorphic grade variation and mineral zonation is shown in Figure 5.21. The petrographic features and metamorphic mineralogy for representative rocks are presented in Table 5.1.

Prehnite-pumpellyite facies

Prehnite was observed in the Middle to Late Triassic andesitic CLT rocks in CK-WB and CK-CB from 20.1621°N 100.3427°E (Figure 5.22) and 19.6600°N 100.2019°E, respectively. In addition, pumpellyite has been found in many localities from CK-WB (Figure 5.23) to CK-CB (Figure 5.24) and CK-EB (Figure 5.25). An andesitic lava with veins of actinolite-epidote was found at 20.3348°N 100.3250°E in CK-WB (Figure 5.26). Typical assemblages in the Middle to Late Triassic mafic to intermediate rocks of CLT include plagioclase – clinopyroxene – epidote – chlorite – albite ± actinolite ± prehnite ± pumpellyite. Plagioclase crystals in both the intrusive and extrusive rocks of the CLT varies from partly fresh with epidote or sericite alteration, to totally altered to, or replaced by, clear albite that is sometimes speckled by sericite. These assemblages are typical of prehnite-pumpellyite facies condition and were found over most of the mapped area.

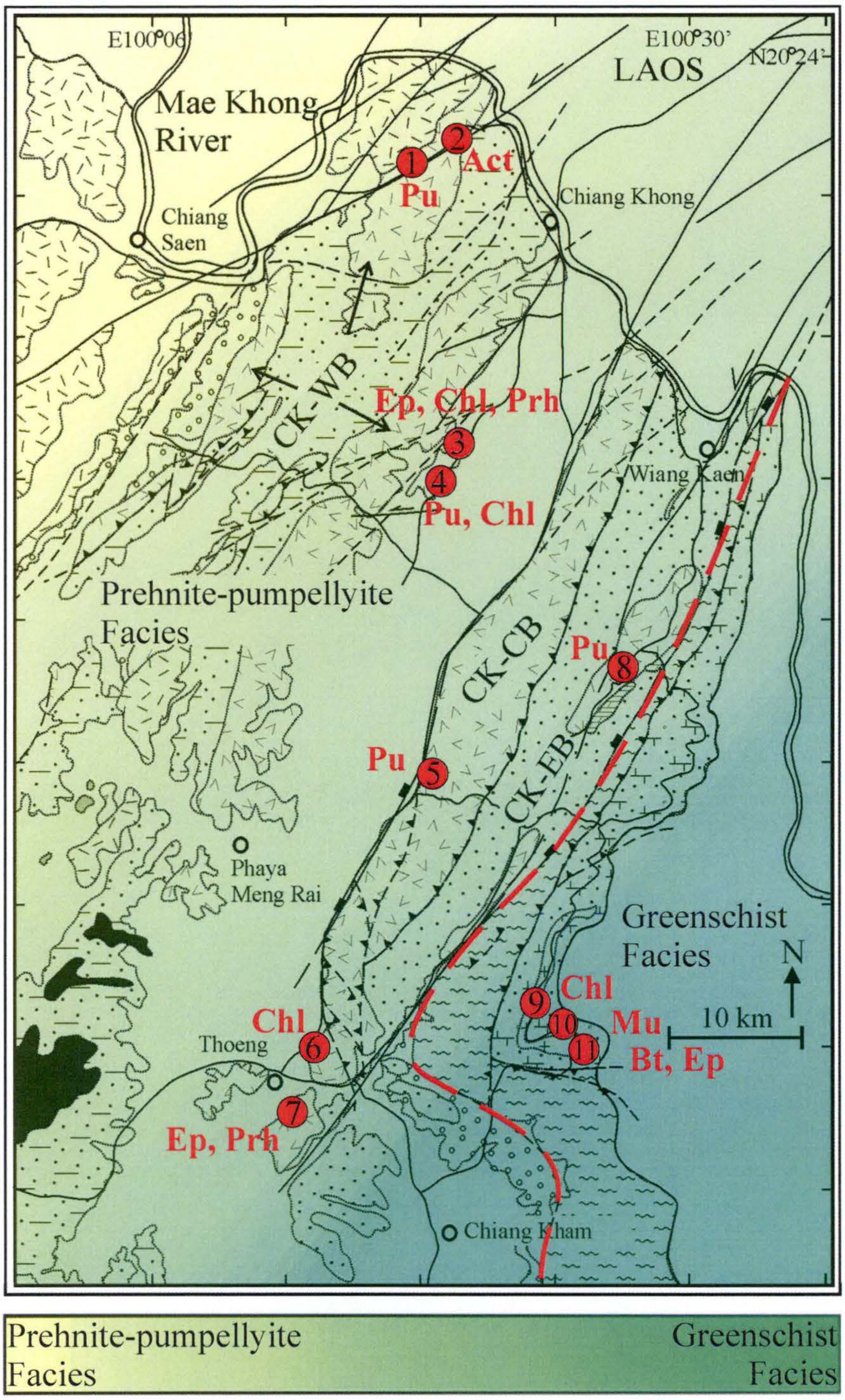

Pu : Pumpellyite Chl : Chlorite Mu : Muscovite
Act : Actinolite Phr : Prehnite Bt : Biotite
Ep : Epidote

Suggested boundary of greenschist facies rocks

Sample number in Table 5.1

Figure 5.21 Map of Chiang Khong area showing metamorphic grade and distribution of index minerals.

Table 5.1 Typical samples containing metamorphic index minerals.

Sample no.	Area	Sample locations	Index minerals	Petrographic features
1. 14/6 (1)	CK-WB	20.3249°N 100.3173°E	Pumpellyite*	Dolerite dyke with fresh clinopyroxene and some pumpellyite in plagioclase crystals.
2. 14/7	CK-WB	20.3348°N 100.3250°E	Actinolite in vein*	Andesitic lava with vein of actinolite-epidote.
3. 13/7	CK-WB	20.1621°N 100.3427°E	Epidote, chlorite and prehnite	Vesicular andesite with albitised plagioclase and rare clinopyroxene mainly replaced by epidote, chlorite and prehnite
4. 13/9 (1)	CK-WB	20.1008°N 100.3231°E	Pumpellyite and chlorite*	Coarse volcaniclastic rock with lithic clasts of felsic formerly glassy plagioclase-phyric dacitic and rhyolitic lavas in a matrix in which vitric ash was the dominant component.
5. 12/5 (1)	CK-CB	19.8843°N 100.2924°E	Pumpellyite*	Strongly plagioclase-phyric andesite lava with intense epidote alteration.
6. 12/2 (3)	CK-CB	19.7033°N 100.2146°E	Chlorite*	Sparsely and finely plagioclase-phyric formerly glassy andesite lava rock with banded fine-grained epidote and chlorite alteration.
7. 12/1(2)	CK-CB	19.6600°N 100.2019°E	Epidote and prehnite	Strongly porphyritic plagioclase+clinopyroxene phyric andesite with epidote+prehnite alteration.
8. 15'/10 (1)	CK-EB	19.9492°N 100.4401°E	Pumpellyite*	Very altered fine-grained mafic lava rock with chlorite-pumpellyite-quartz alteration.
9. 27'/3	BH area	19.7129°N 100.3855°E	Chlorite	Chlorite-sericite altered granite with some allanite grain.
10. 8"/5	BH area	19.7190°N 100.4113°E	Muscovite and chloritized muscovite*	Fine-grained quartz-chlorite-mica schist.
11. 8"/2	BH area	19.7081°N 100.4217°E	Epidote and secondary biotite*	Quartzo-feldspathic mylonitic granitiod with epidote and green biotite alteration.

* Analysis result from EM

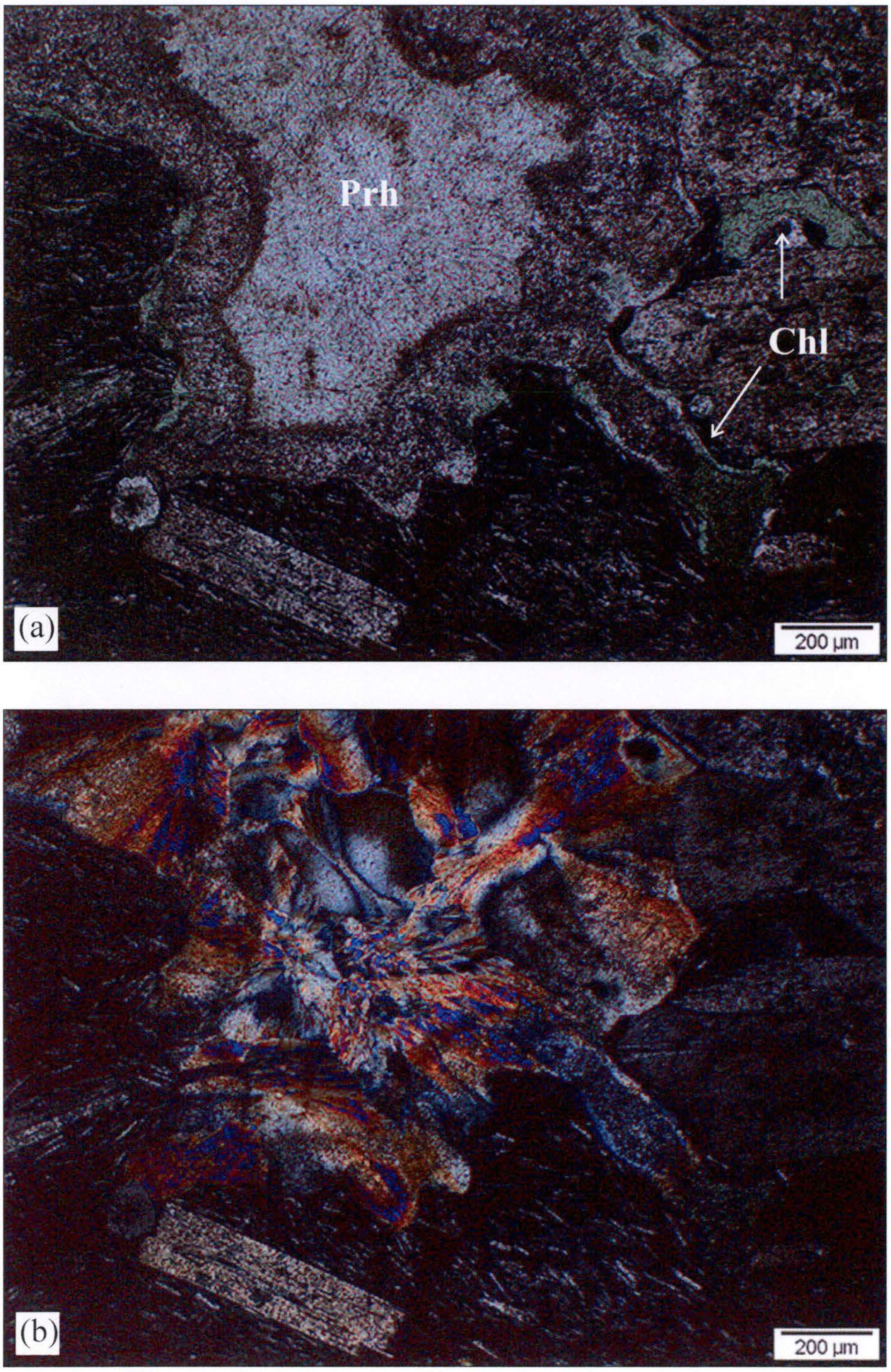

Figure 5.22 Photomicrograph showing prehnite and chlorite in vesicular andesitic lava rock of CK-WB from 20.1621°N 100.3427°E. (a) Plane polarized light (b) crossed polarized light. Note, Prh is prehnite and Chl is chlorite.

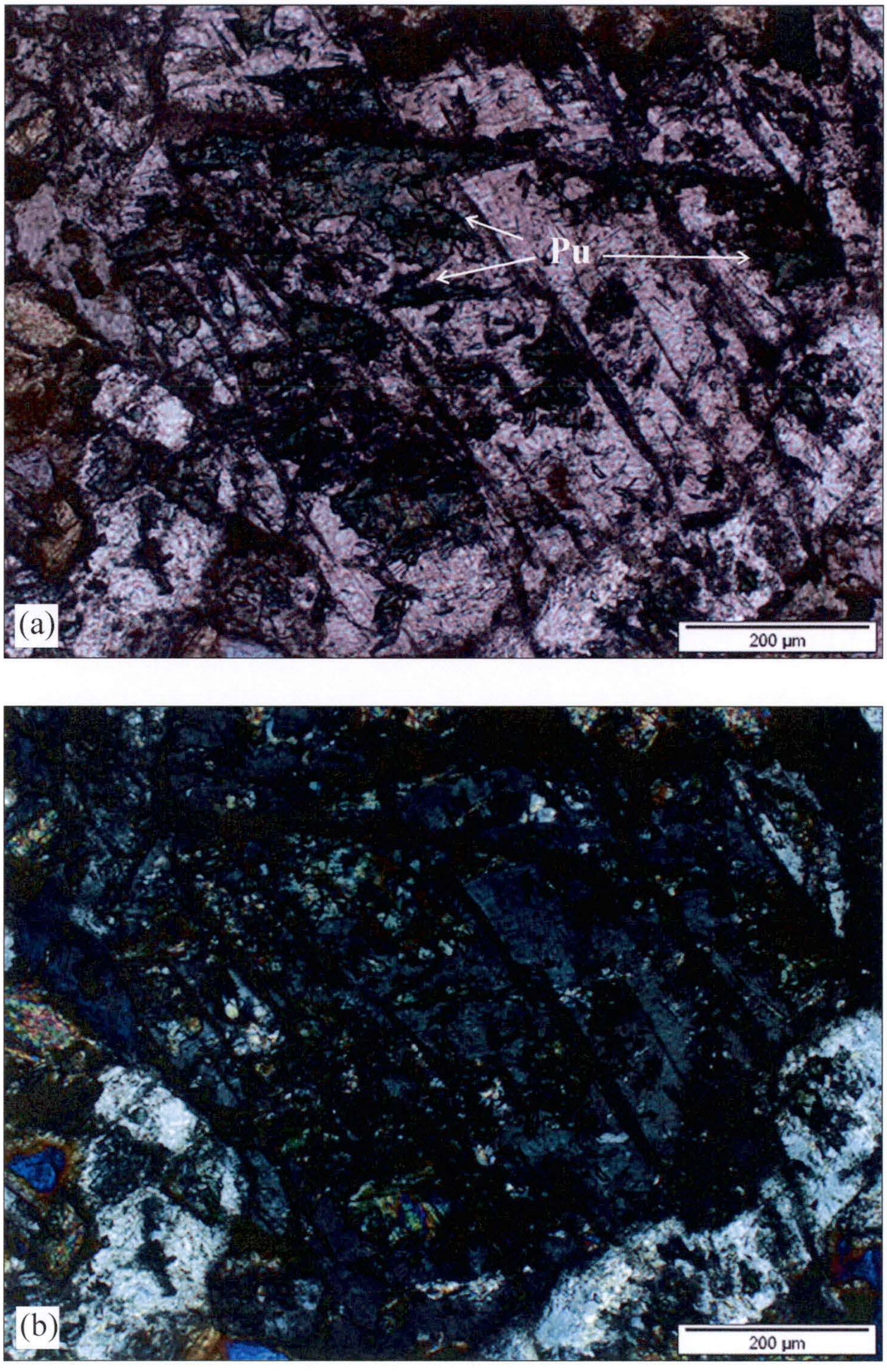

Figure 5.23 Photomicrograph showing pumpellyite (green mineral) in plagioclase crystal in dolerite dyke from CK-WB at 20.3249°N 100.3173°E. (a) Plane polarized light (b) crossed polarized light. Note, Pu is pumpellyite.

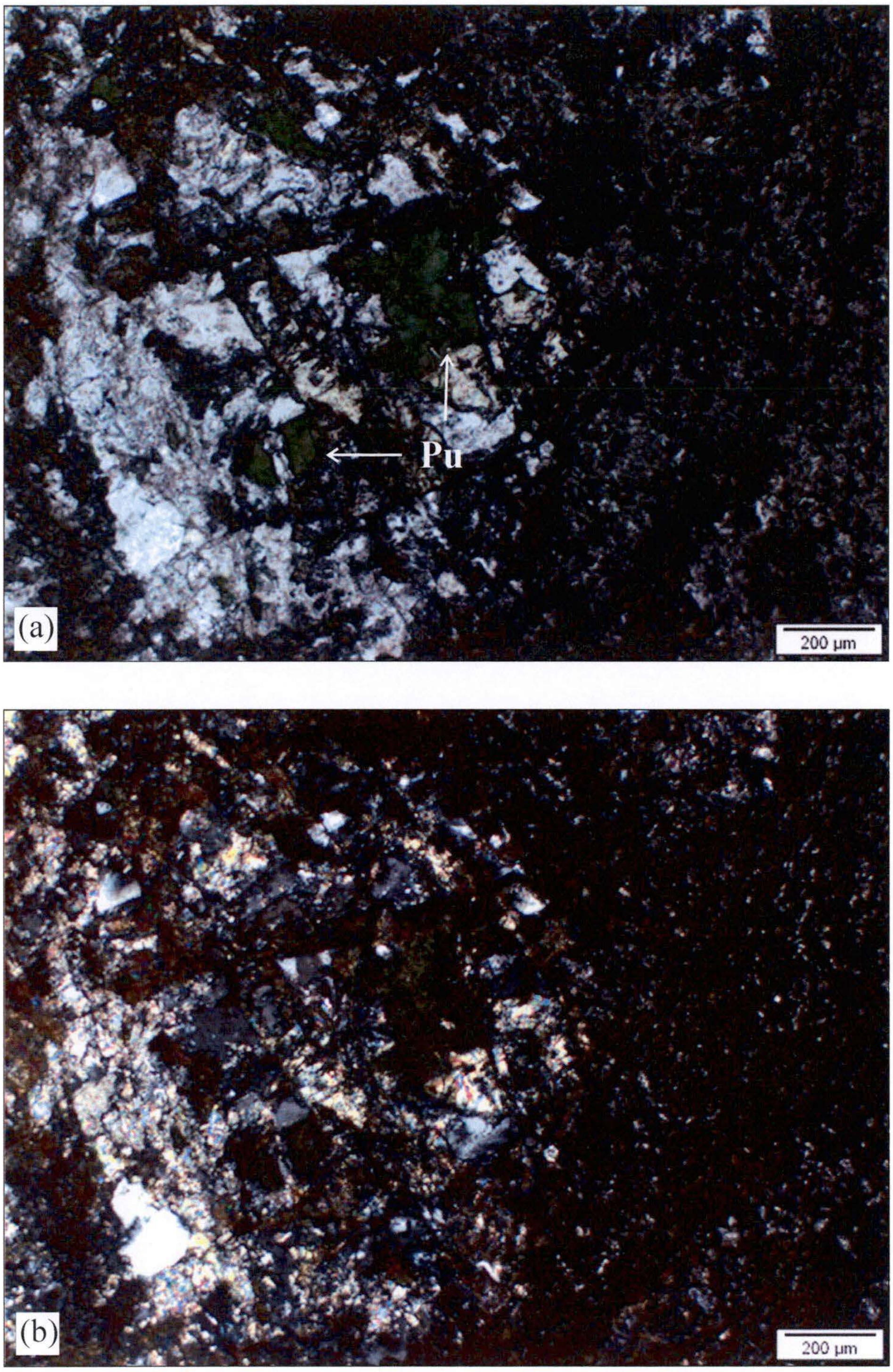

Figure 5.24 Photomicrograph of highly altered plagioclase-phyric andesite with intense epidote alteration and some pumpellyite in plagioclase phynocryst from CK-CB at 19.8843°N 100.2146°E. (a) Plane polarized light (b) crossed polarized light. Note, Pu is pumpellyite.

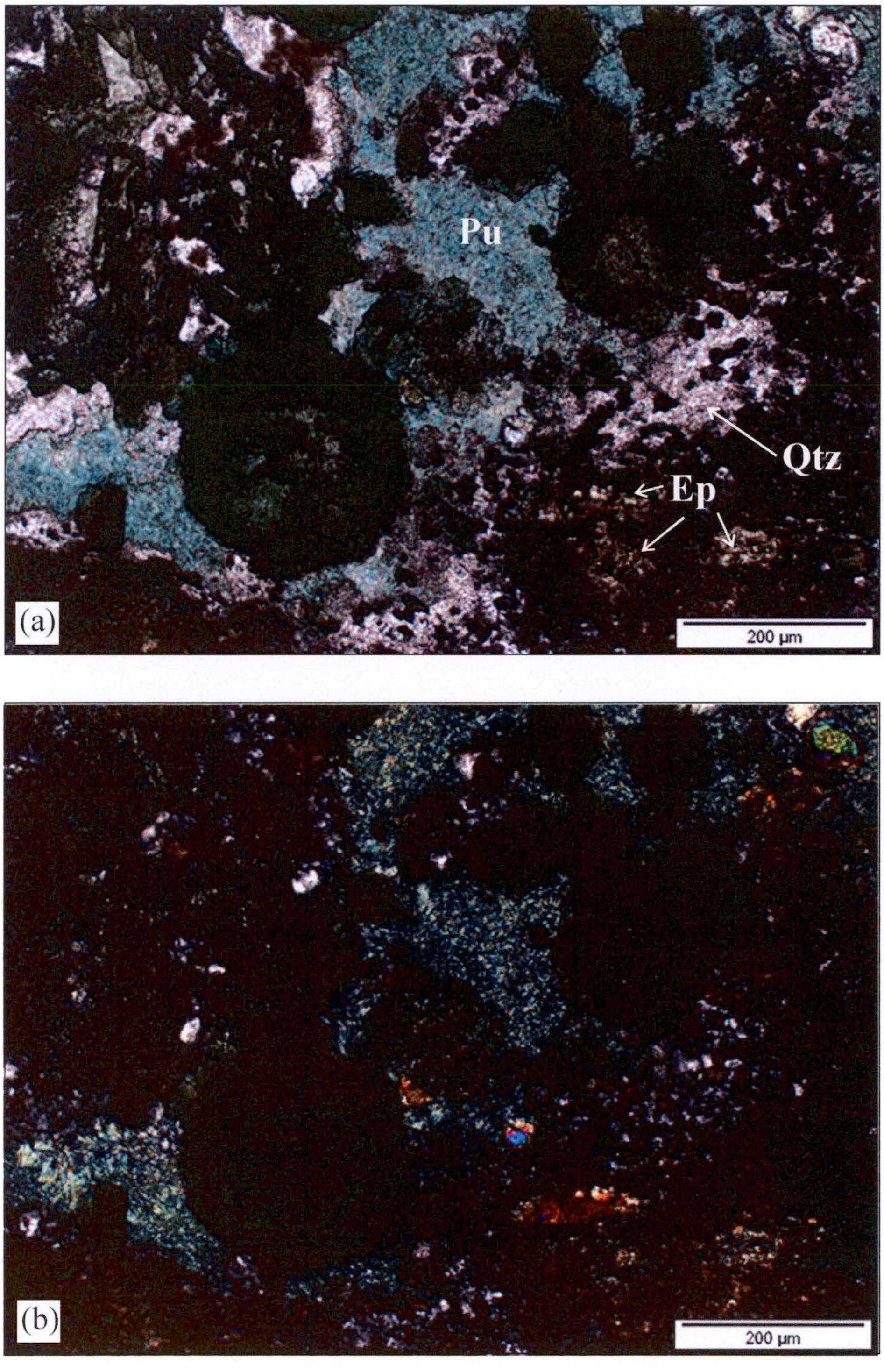

Figure 5.25 Photomicrograph of very altered fine-grained mafic to intermediate volcanic rock with epidote-pumpellyite-quartz alteration from CK-EB at 19.9492°N 100.4401°E. (a) Plane polarized light (b) crossed polarized light. Note, Ep is epidote; Pu is pumpellyite; Qtz is quartz.

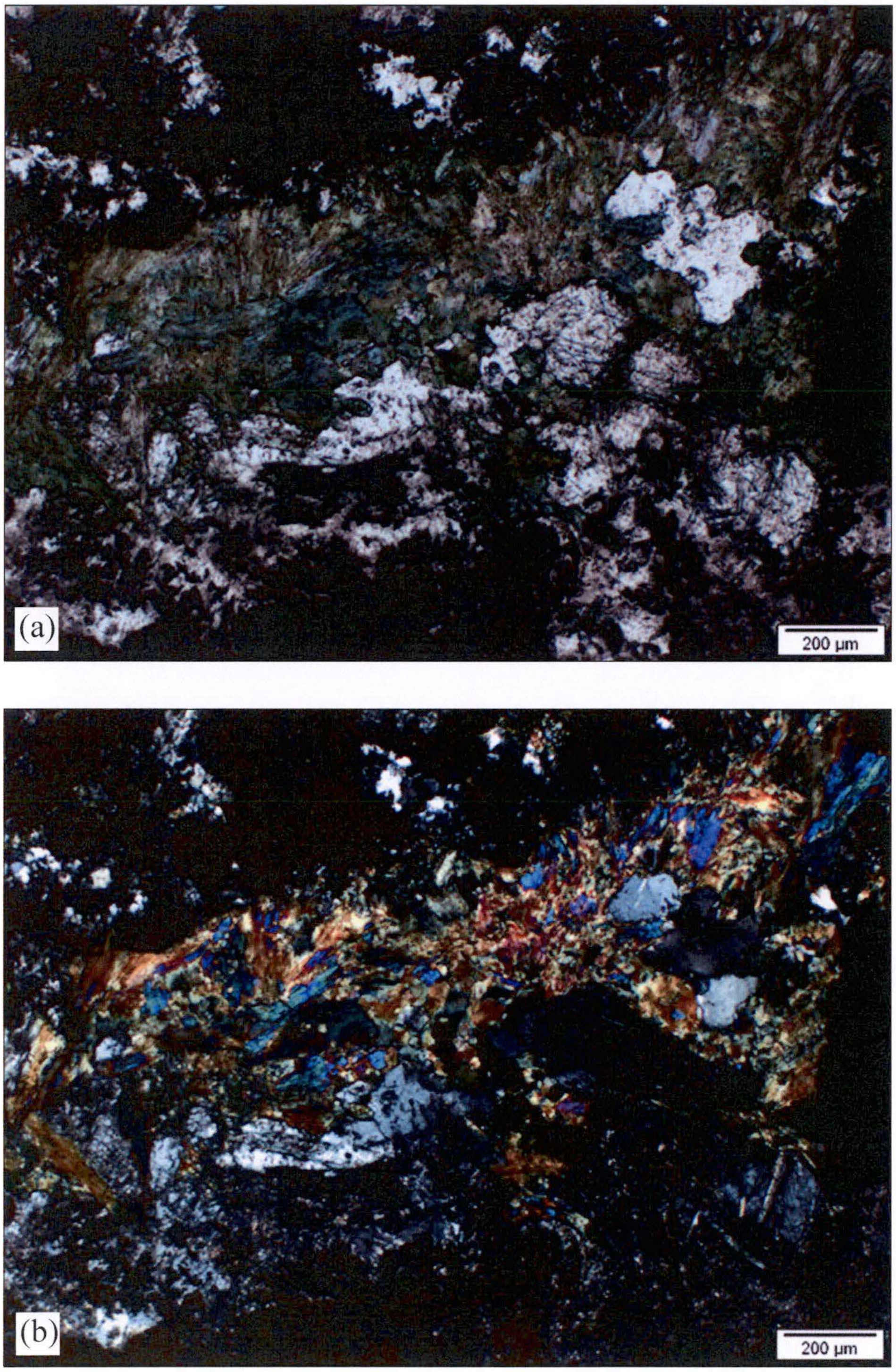

Figure 5.26 Photomicrograph showing actinolite vein in andesitic lava rock of CK-WB from 20.3348°N 100.3250°E. (a) Plane polarized light (b) crossed polarized light.

Greenschist facies

Typical greenschist facies assemblages were found in the southeastern area. The Carboniferous-Permian meta-andesitic rocks from19.7155°N 100.3960°E in the Ban Huak area have been interpreted to be greenschist facies with subordinate actinolite-altered augite phenocrysts (Figure 5.27). Some recrystallized carbonate, quartz, secondary green biotite, chlorite after biotite, and orange needles of stilpnomelane and sphene were observed in the Carboniferous-Permian mylonitic granitoid (Figure 5.28). The biotite + chlorite + muscovite + quartz assemblage in mylonitic granitoid is typical of the biotite zone (c.f. greenschist facies of Miyashiro, 1994).

Summary

The boundary between greenschist and prehnite-pumpellyite metamorphic facies in the Chiang Khong area has been drawn following the boundary of the strong cleavage Carboniferous-Permian meta-sedimentary rocks. The greenschist facies boundary is only located approximately from the observed mineralogy. However, it is shown at the edge of the high strain zone as the increase in cleavage intensity at this boundary suggests it represents a significant increase in metamorphic grade.

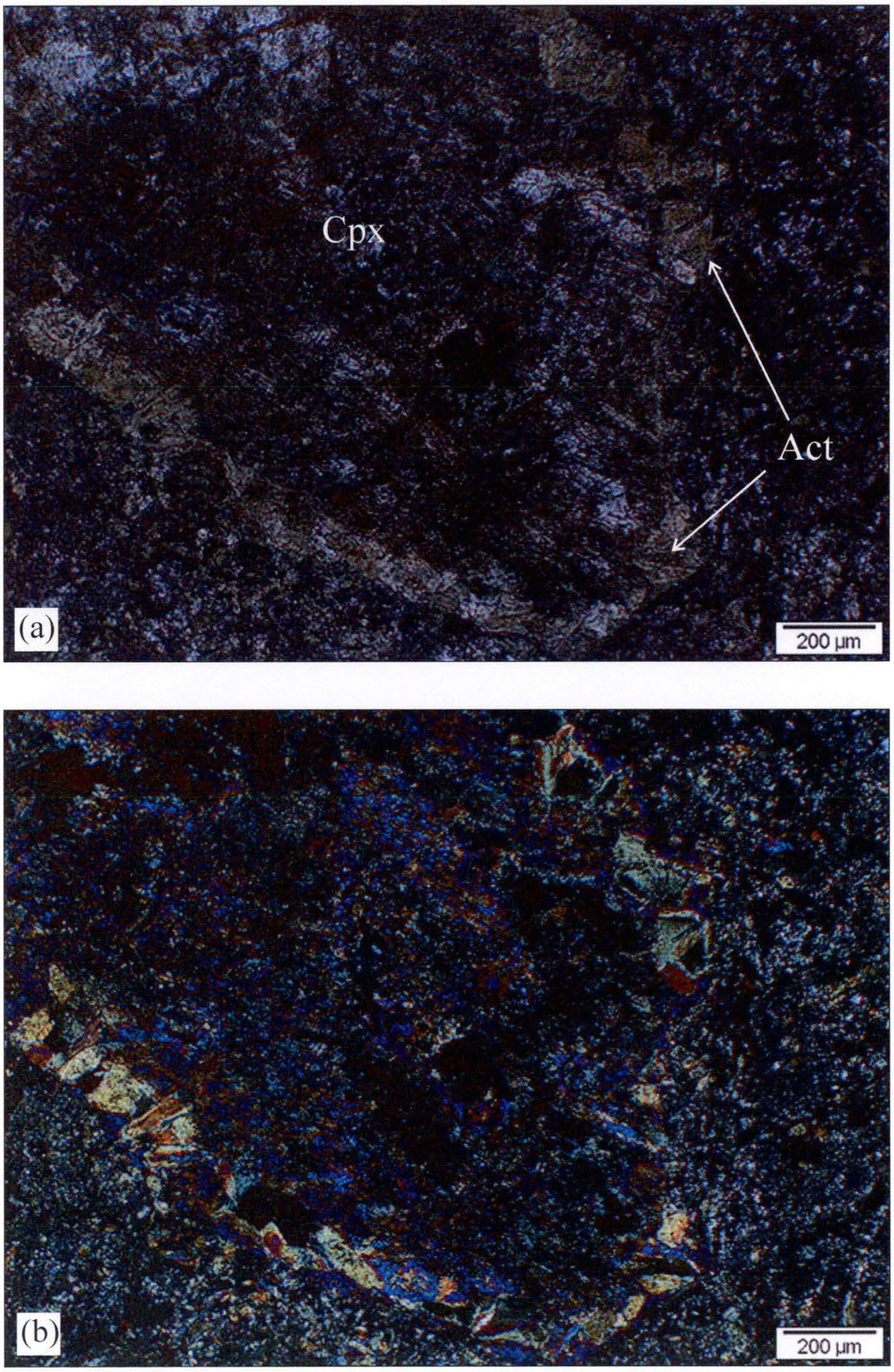

Figure 5.27 Photomicrograph of actinolite-altered blocky clinopyroxene phenocryst in plagioclase-clinopyroxene-olivine phyric andesite from Ban Huak area at 19.7155°N 100.3960°E. (a) Plane polarized light (b) crossed polarized light. Note, Act is actinolite and Cpx is clinopyroxene.

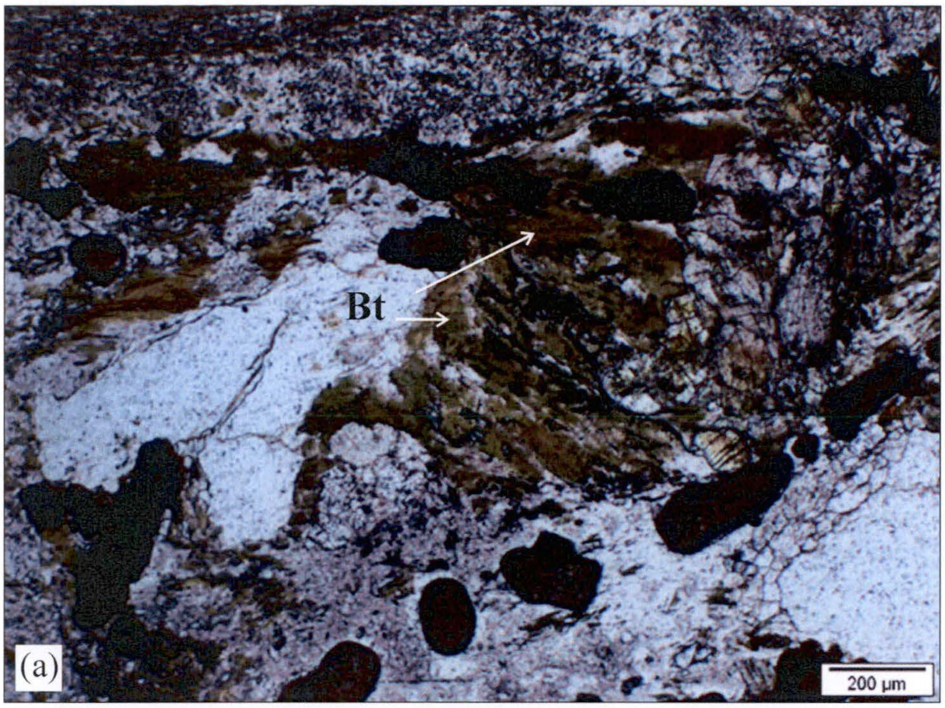

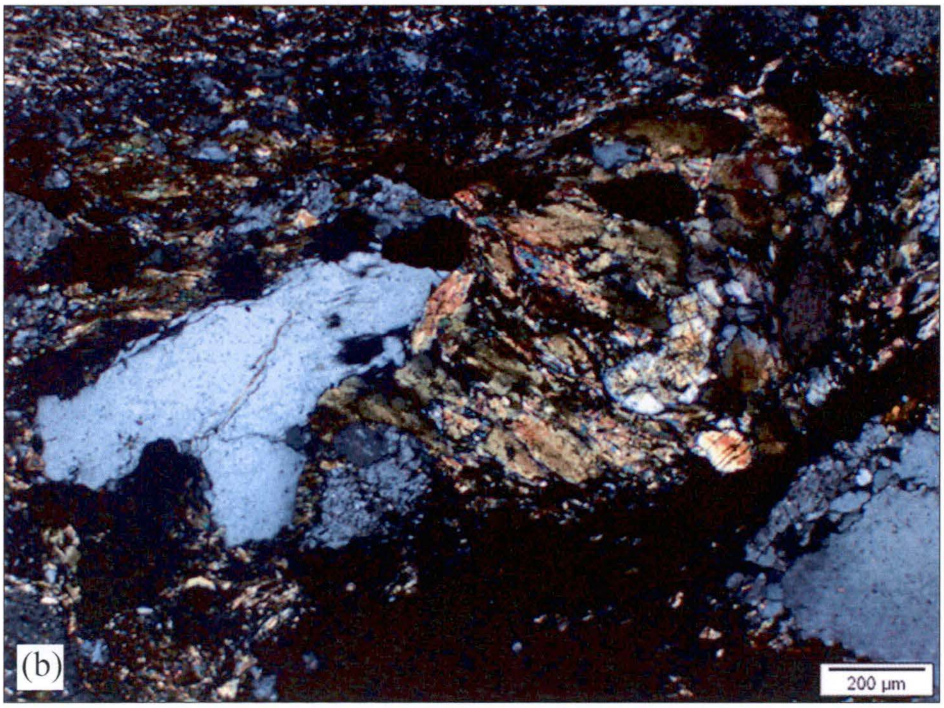

Figure 5.28 Photomicrograph showing green biotite and quartz with some epidote alteration in quartzo-feldspathic mylonitic granitoid from Ban Huak area at 19.7081°N 100.4217°E. (a) Plane polarized light (b) crossed polarized light. Note, Bt is biotite.

5.2.5 Cross-sections

Basic concepts and limitations

The structural study across the Chiang Khong area has been illustrated by three structural transects, including the Chiang Khong-Wiang Kaen, the Doi Luang-Ban Kaen and the Ban Phaya Phiphak-Phu Chi Fa transects, and also a detailed structural map of the Ban Huak area. The cross-section schematic drawing is based on the technique of section balancing of Suppe, 1985 and Woodward, 1988. The limitations of the structural interpretation have been pointed out as follows:

1. The depth of the main detachment surface is inferred to be located within the Carboniferous-Permian meta-sedimentary rocks.

2. The thickness of rock units used for the construction of structural sections is uncertain. An estimated thickness in the range of 800-1500 m is used for the schematic drawing. This thickness is based on the thickness of rock units in the structural section of the Sukhothai Fold Belt (Singharajwarapan, 1994) and the stratigraphic study of the Lampang Group (Chaodumrong, 1992).

3. There is no seismic or drill hole control on the sections. Seismic surveys would help to improve the accuracy in construction of these cross-sections. The structural data is not uniformly distributed and large parts of the sections are inferred based on an assumed style. Sections are more accurate where structural data is available. The distribution of structural data is shown on the maps that accompany each section.

The Chiang Khong to Wiang Kaen Transect

Structure along the Chiang Khong to Wiang Kaen transect was drawn using all the available constraints from observed structure (Figures 5.29 & 5.30). These indicate a thin-skinned style of fold and thrust belt overprinted by steeply dipping normal and strike slip faults. Bedding was rarely observed on this section and the structure is partly projected from other sections.

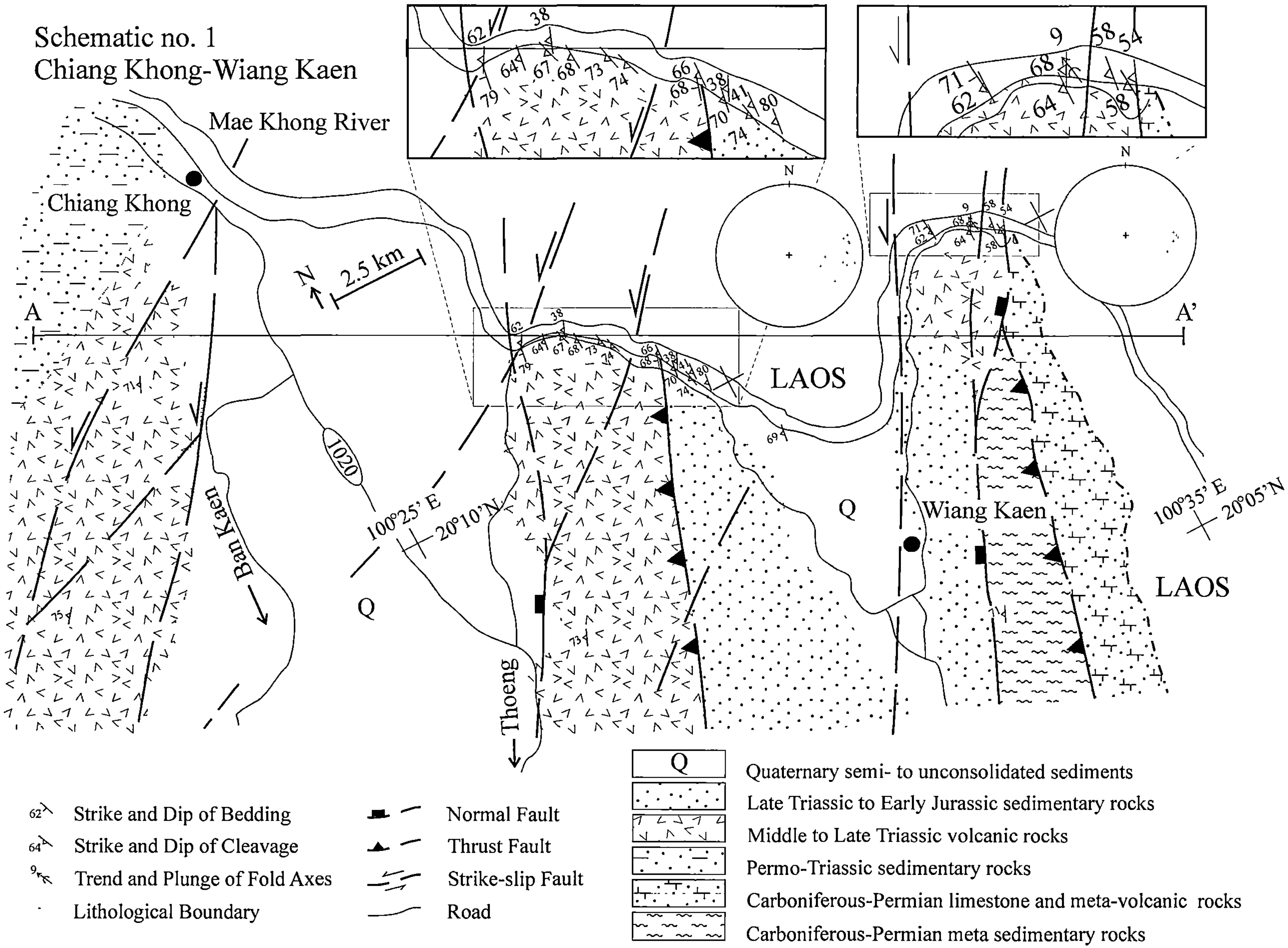

Figure 5.29 Structural map of the Chiang Khong-Wiang Kaen transect.

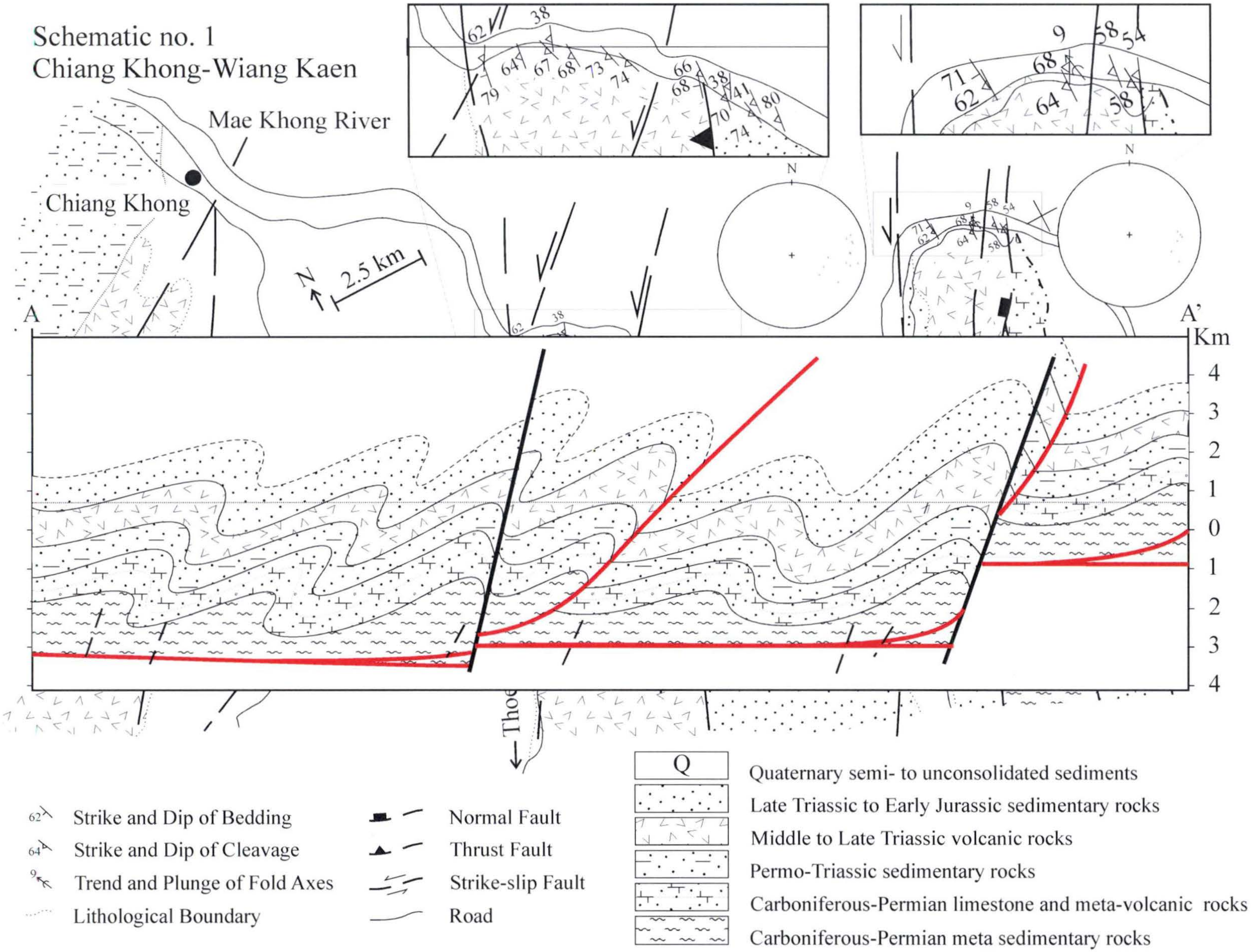

Figure 5.30 Interpretive schematic section of the Chiang Khong-Wiang Kaen transect (along line AA' in Figure 5.29). Note, dashed lines at the bottom of section are represented traces of strike-slip faults.

Folds

An outcrop-scale fold on this transect was observed at 20.1712°N 100.5684E in Middle to Late Triassic volcanic rocks. It is an open upright fold with a S-plunging fold axis.

Cleavage and bedding

The cleavage on this transect strikes N-S and dips to the W (Figures 5.31a to e). Two cleavages were observed at several locations along the northern tip of CK-CB (Figure 5.31e). Only one steep W-dipping cleavage was found north of Wiang Kaen. The steep cleavages on this transect are interpreted to be regional cleavage whereas shallow cleavages were probably associated with additional strain near thrust faults. The bedding dips more steeply than the cleavage along most of this section.

Thrust faults

A small-scale thrust fault was observed in CK-CB at 20.1799°N 100.4874°E (Figure 5.31f), subparallel to a shallow cleavage dipping to the west.

Strike-slip faults

Strike-slip faults on this transect are interpreted to have sinistral displacement based on the offset of the Mae Khong River (Morley, 2007). A 3 km offset of the Mae Khong River reach through the central part of Wiang Kaen Basin represents the largest offset in the Chiang Khong area. The strike-slip faults are presumably sub-vertical.

Normal faults

Several NNE-SSW striking normal faults cross this transect and form the eastern boundary of Chiang Khong-Thoeng Basin (Lacassin *et al,* 1997; Morley, 2007 and Uttamo *et al.,* 2003) and Wiang Kaen Basin. A westward dipping normal fault plane was observed on the Ban Phaya Phiphak to Phu Chi Fa transect.

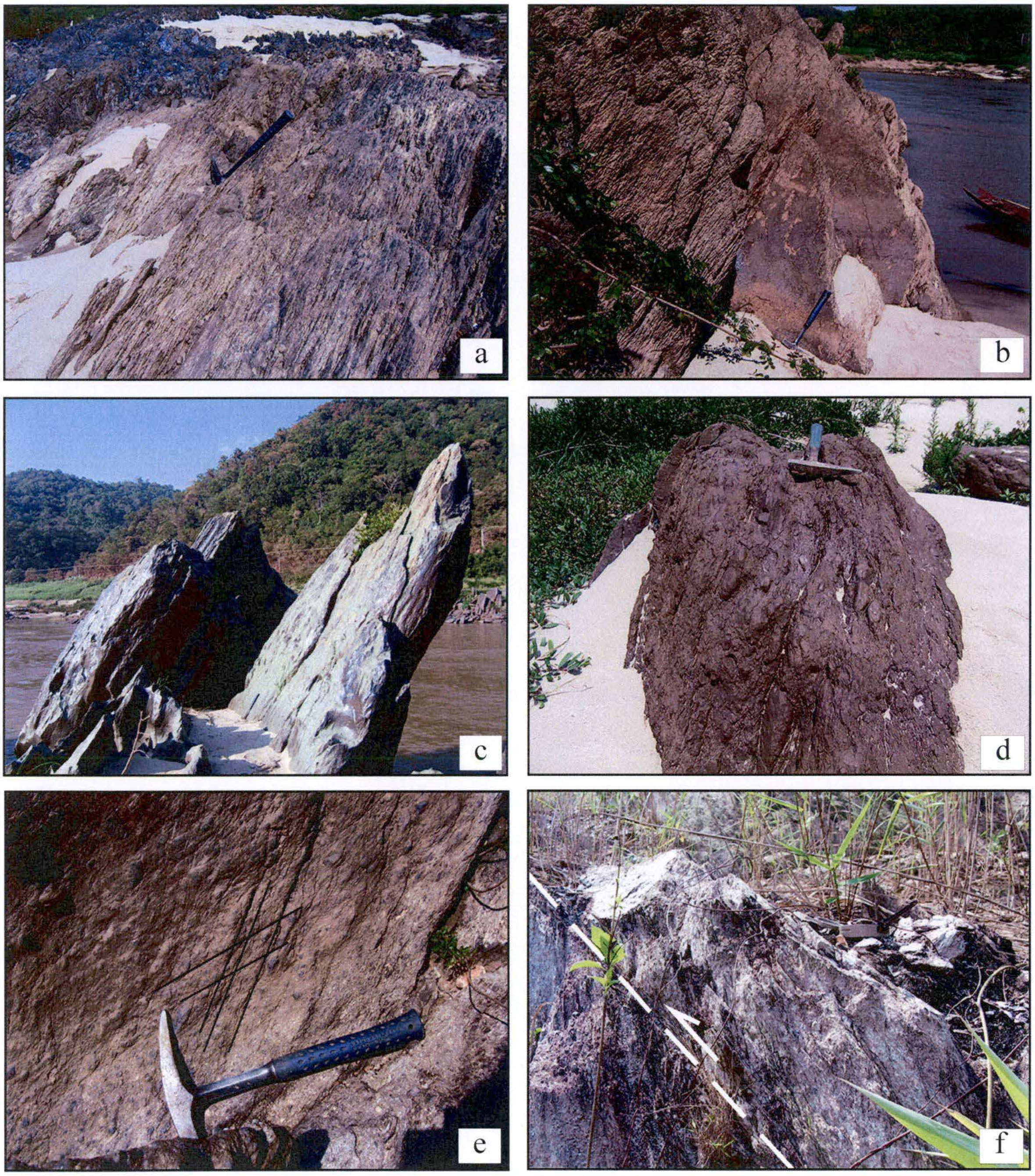

Figure 5.31 Photographs of outcrops with cleavage and thrust fault in the Middle to Late Triassic volcanic rocks. (a)-(e) Strong cleavage in the CLT volcanic and volcaniclastic rocks shown westward dipping cleavage (looking north). Note the two different dip angles in steep and shallow westward dipping cleavage in (e). (f) Outcrop-scale thrust fault in volcaniclastic rocks at 20.1799°N 100.4874°E (looking south). Scale: hammer is 28 cm long; compass is 3 cm thick.

<u>*The Doi Luang to Ban Kaen Transect*</u>

The Doi Luang to Ban Kaen transect is shown in Figures 5.32 and 5.33. The section has been drawn to match the style of observed structures and assumes the same stratigraphy as in the first section.

Folds

The only outcrop-scale fold seen on this transect is an open fold with a vertical fold axis, probably linked to sinistral strike-slip fault movement (Figure 5.34). It was observed in a quarry at 20.0770°N 100.2615°E and overprinted the regional NNE-SSW trending folds.

Cleavages

The cleavage on this transect is moderate to strongly developed with a moderate to steep dip to the northwest. Cleavage was measured in both of Permo-Triassic sedimentary rocks and Middle to Late Triassic volcanic outcrops. Cleavage and folding are closely linked to the thrust geometry.

Thrust faults

Outcrop-scale thrust faults are present in the Permo-Triassic sedimentary rocks and locally at the fault contact between Permo-Triassic sedimentary and CLT rocks. These outcrop-scale thrusts exist in the western end of this section. Thrust faults mainly strike NNE-SSW and dip to northwest. A detail study of these outcrop-scale thrusts (sections A1-3 and B1-3 in Figure 5.6 to 5.11) is shown in section 5.2.3. Low angle shear bands and sandstone phacoids indicate top-to the east sense of shear (Figure 5.35a).

Strike-slip faults

NNE-SSW strike-slip faults outcrop at the Huai Kiang Reservoir (20.1065°N 100.2848°E, Figure 5.35b) north of this transect. A NNE-SSW sinistral strike-slip fault was also found in a CK-WB quarry (20.0770°N 100.2615°E, Figure 5.34).

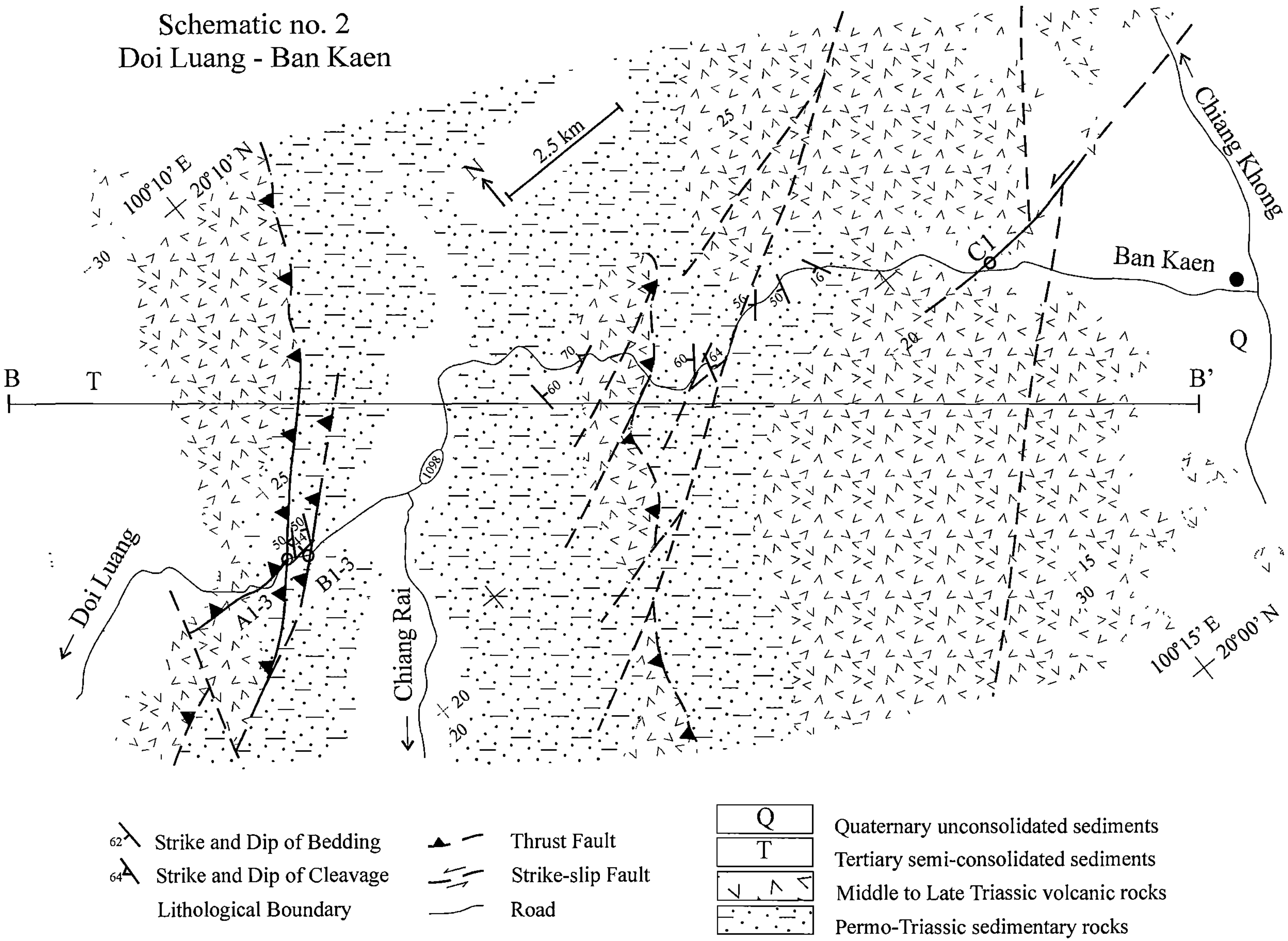

Figure 5.32 Structural map of the Doi Luang-Ban Kaen transect.

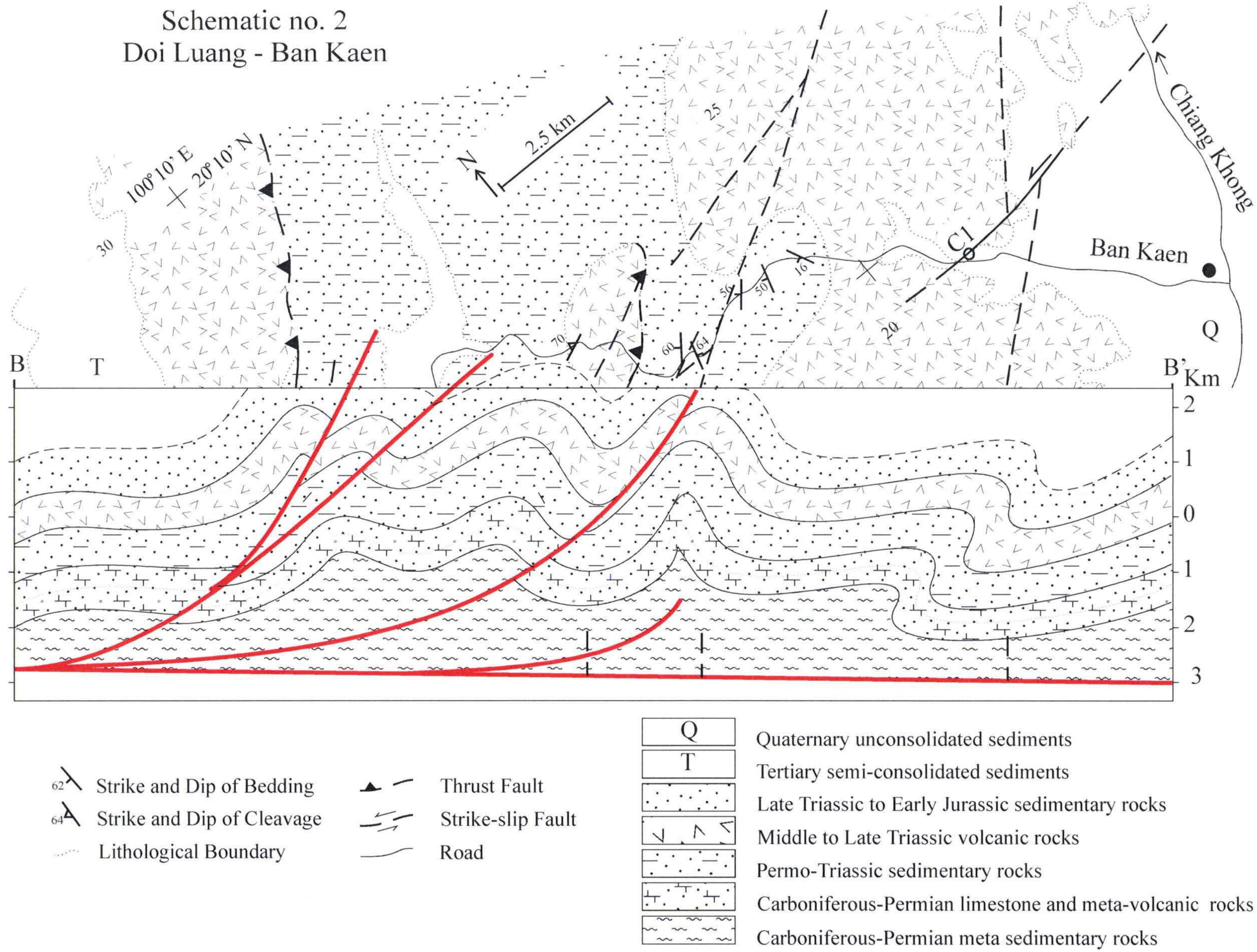

Figure 5.33 Interpretive schematic section of the Doi Luang-Ban Kaen transect (along line BB' in Figure 5.32). Note, vertical dashed lines at the bottom of section are represented traces of strike-slip faults.

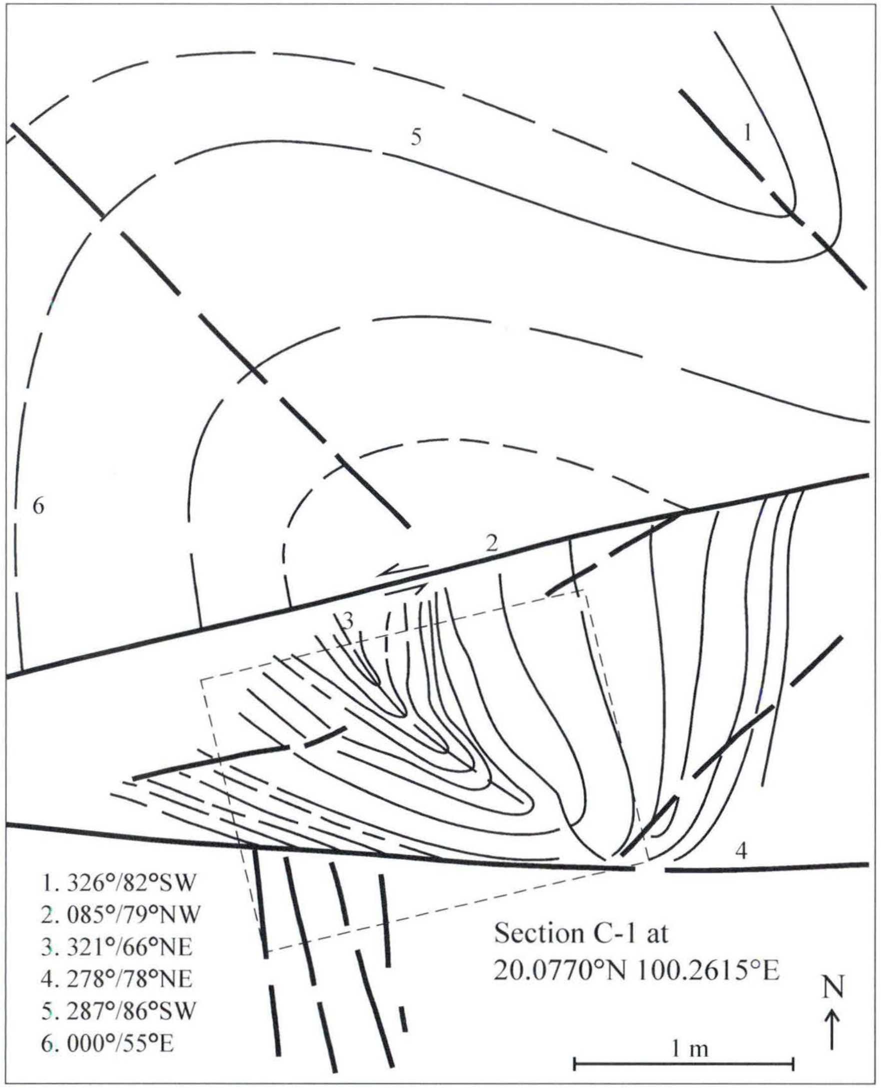

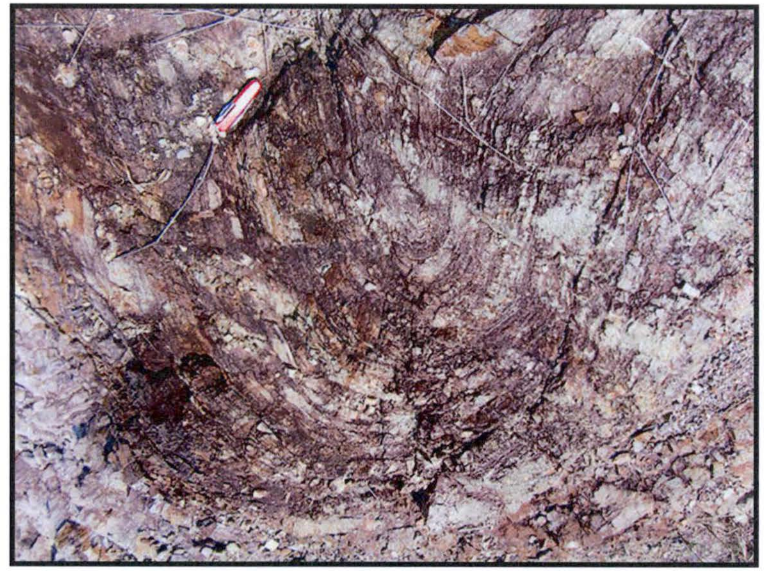

Figure 5.34 Structural sketch and photograph (plan view) showing geometry of close vertical folds and sinistral strike-slip fault (heavy line no. 2) of CLT volcaniclastic rock at 20.0770°N 100.2615°E and C-1 section in Figure 5.32. These folds overprinted the regional NNE-SSW trending folds.

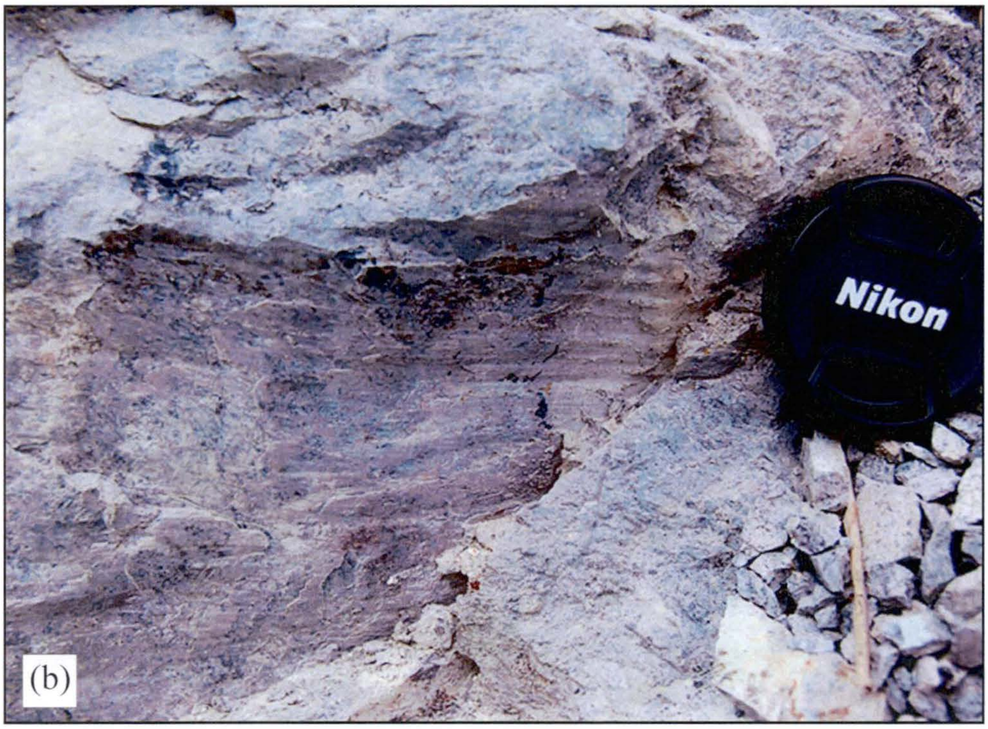

Figure 5.35 Photograph of (a) Sandstone phacoids along thrust fault plane (F 1 in Figure 5.8) in the Permo-Triassic sedimentary rock on section A-3 exposure and (b) slickenside on fault plane (065°/90° trending) showing sinistral strike-slip slicken lines in the CLT volcanic rock at 20.1065°N 100.2848°E. Scale: knife is 8 cm long; lens cap is 5.8 cm in diameter.

The Ban Phaya Phiphak to Phu Chi Fa Transect

The Ban Phaya Phiphak to Phu Chi Fa transect extended across high mountain ranges in the eastern part of Chiang Khong area (Figure 5.36 & 5.37). The repetition of rock units is interpreted to be caused by a NNE-SSW thrust fault striking.

Bedding

Bedding of rocks on this transect strikes NNE-SSW to NE-SW and dips NW to W. Overturned beds occurred in the Carboniferous-Permian meta-sandstone in the southern portion of this transect map at 19.7868°N 100.3619°E and form boudin as shown in Figure 5.38a.

Cleavages

The moderate to strong cleavage along this section is shallowly to steeply dipping to the northwest and west. Steeply dipping cleavages along the western side of CK-CB may be related to normal or thrust faults, whereas shallowly dipping cleavage common on the eastern side is probably related to thrust fault movement. The shallow to moderately dipping cleavage has been measured in the limestone (Figures 5.38b & c). A W- to SW-plunging lineation is also noted in foliated granite further south. A moderate to steep dipping cleavage is present in Late Triassic redbeds (Figure 5.38d), and interpreted to be reoriented by drag on the left-lateral strike-slip movement of the Wiang Kaen Fault.

Folds

An outcrop-scale open fold with northerly fold plunge was observed in the Carboniferous-Permian limestone and meta-volcanic rock at 19.8471°N 100.4411°E. Inclined conjugate kink bands in the Carboniferous-Permian meta-sedimentary rocks at 19.8672°N 100.4059°E are shown in Figure 5.39. Folds and kink bands on this transect are interpreted to be associated with thrusting. A M-shape south-westerly plunging fold was found in the CK-EB at 19.7905°N 100.3514°E.

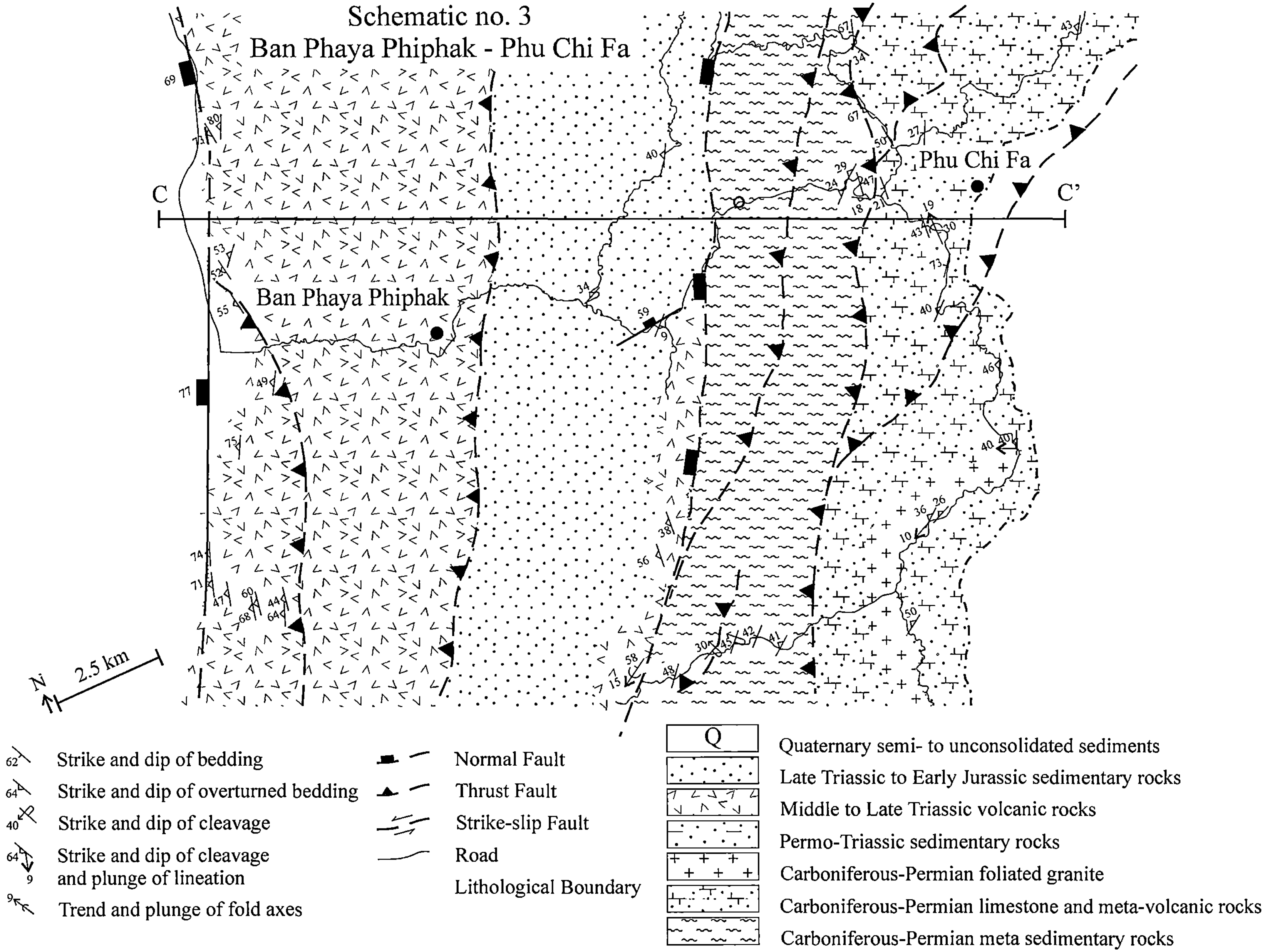

Figure 5.36 Structural map of the Ban Phaya Phiphak-Phu Chi Fa transect.

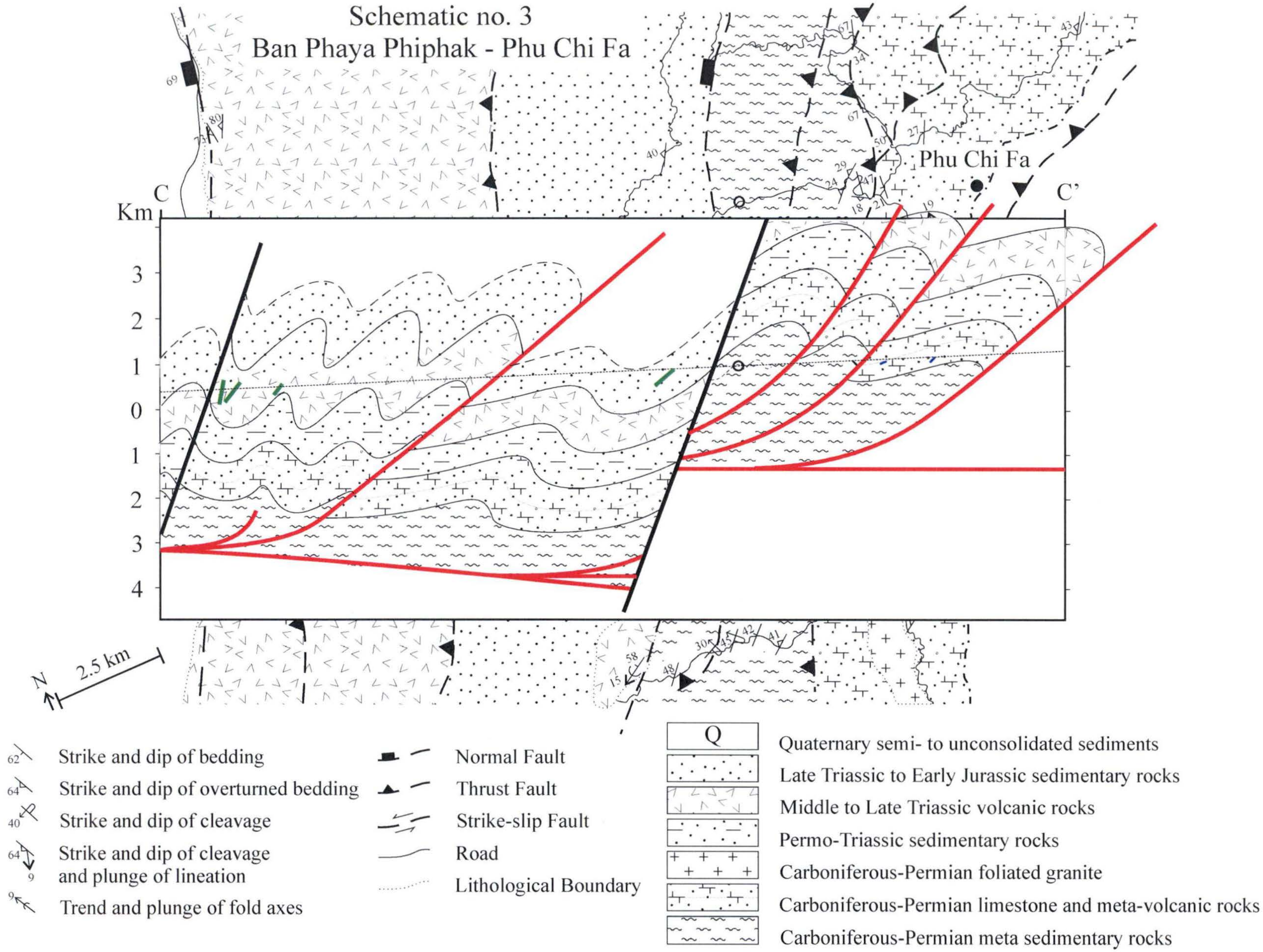

Figure 5.37 Interpretive schematic section of the Ban Phaya Phiphak-Phu Chi Fa transect (along line CC' in Figure 5.36)

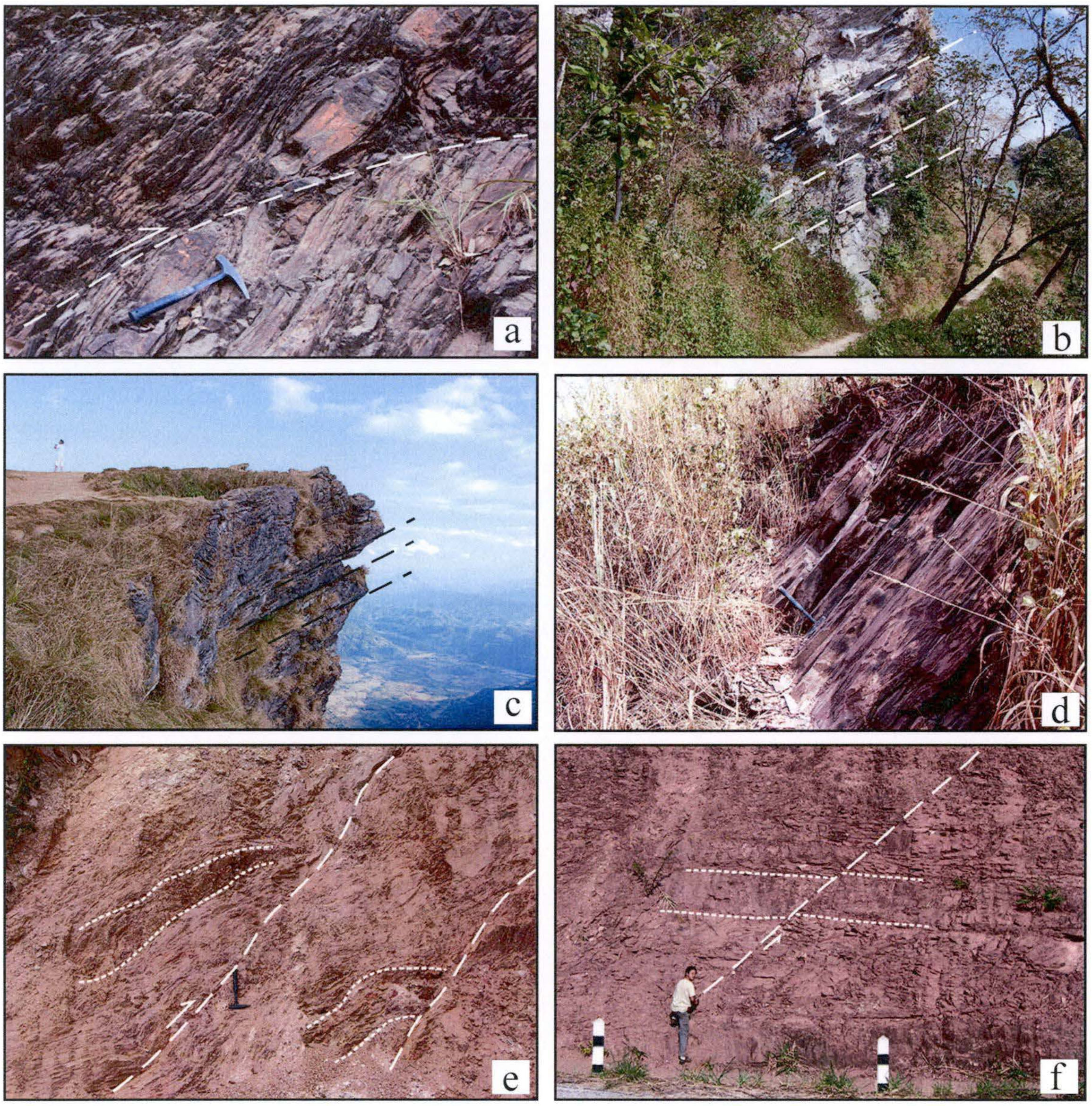

Figure 5.38 Photographs of structural features on the Ban Phaya Phiphak-Phu Chi Fa transect. (a) Outcrop-scale overturned bedding and thrust fault in Carboniferous-Permian meta-sedimentary rocks (looking north). Note the meta-sandstone above the fault formed boudins. (b) and (c) Outcrop-scale cleavage parallel to bedding in Carboniferous-Permian limestone at 19.8327°N 100.4343°E and 19.8506°N 100.4545°E (looking northeast). (d) Outcrop-scale cleavage dipping west in Late Triassic to Early Jurassic sedimentary rocks at 20.0148°N 100.4523°E, north of this transect (looking north). (e) Outcrop-scale thrust fault in Carboniferous-Permian meta-sedimentary rock at 19.8886°N 100.4414°E (looking north). (f) Normal fault in road cutting outcrop in Late Triassic to Early Jurassic sedimentary rock. Scale: hammer is 28 cm long; man is 175 cm tall in (c); man is 170 cm tall in (f).

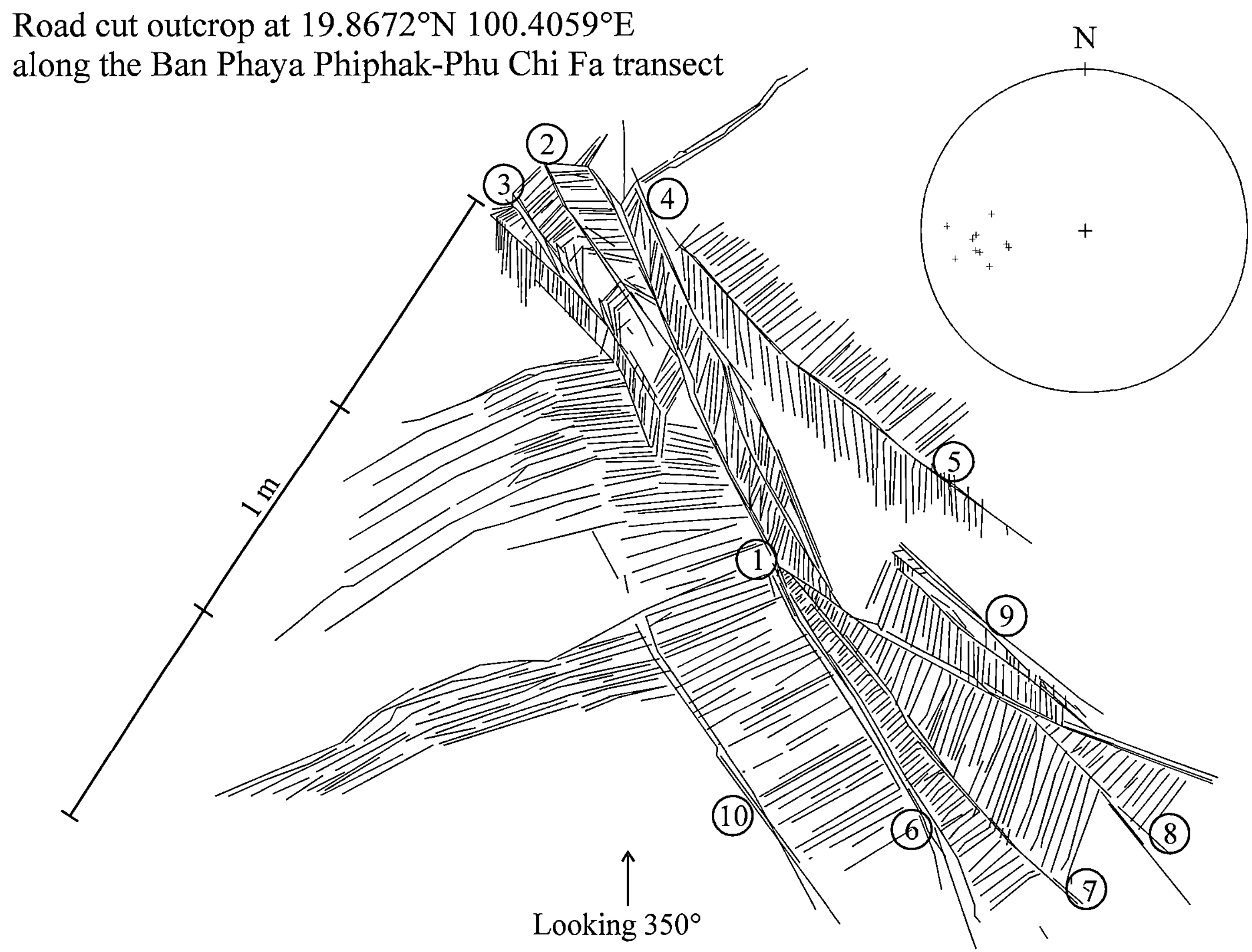

Figure 5.39 Line sketch showing geometry of kink bands in the Carboniferous-Permian meta-sedimentary rocks at 19.8672°N 100.4059°E. Lower-hemisphere equal-area stereographic projection showing poles to kink band boundaries.

Thrust faults

Thrust faults on this transect were measured locally in many rock units. Northwest to west dip of outcrop-scale thrust faults dominates in the Carboniferous-Permian meta-sedimentary rocks at 19.7868°N 100.3619°E (Figure 5.38a) and 19.8886°N 100.4414°E (Figure 5.38e). Thrust faults on this section were recognised from the inverse age stratification of adjacent rocks.

Normal faults

The major NNE-SSW-striking normal fault is subparallel to bedding strike. A steeply west-dipping normal fault occurs at grid reference 19.8474°N 100.2721°E, on the western side of CK-CB. A road cutting outcrop-scale normal fault is exposed locally in the Late Triassic sedimentary rocks at 19.8508°N 100.3825°E (Figure 5.38f).

5.2.6 The Ban Huak Area

The structure of rocks in the Ban Huak area is dominated by a strong cleavage and lineation. A structural map of the Ban Huak area is shown in Figure 5.40.

Bedding

Bedding strikes NE-SW and dips steeply to SE in the southeast corner of the Ban Huak area (Figures 5.40a & 5.41a) whereas bedding in northwestern portion has a NE-SW strike and shallow dip to the NW (Figures 5.40a & 5.41b). A N-S strike and west dip of bedding was observed in some locations in to the south. Overturned bedding in the Carboniferous-Permian meta-sedimentary rocks was measured at 19.7868°N 100.3619°E in the northwest corner (Figure 5.38a). Bedding orientations are very scattered and reflect multiple folding events.

Cleavages and lineations

Cleavage and lineation dominate the outcrops. The regional cleavage varies from E-W to NE-SW striking. The cleavage strikes E-W and dips to the S in the southeast corner (zone A in Figure 5.40b and Figures 5.41c & d). The E-W cleavage strike in zone A has been rotated to N-S strike in zone B and finally NE-SW strike in zone C and D in the north (Figure 5.40b). Poles to the dominant cleavage form a broad great circle distribution everywhere

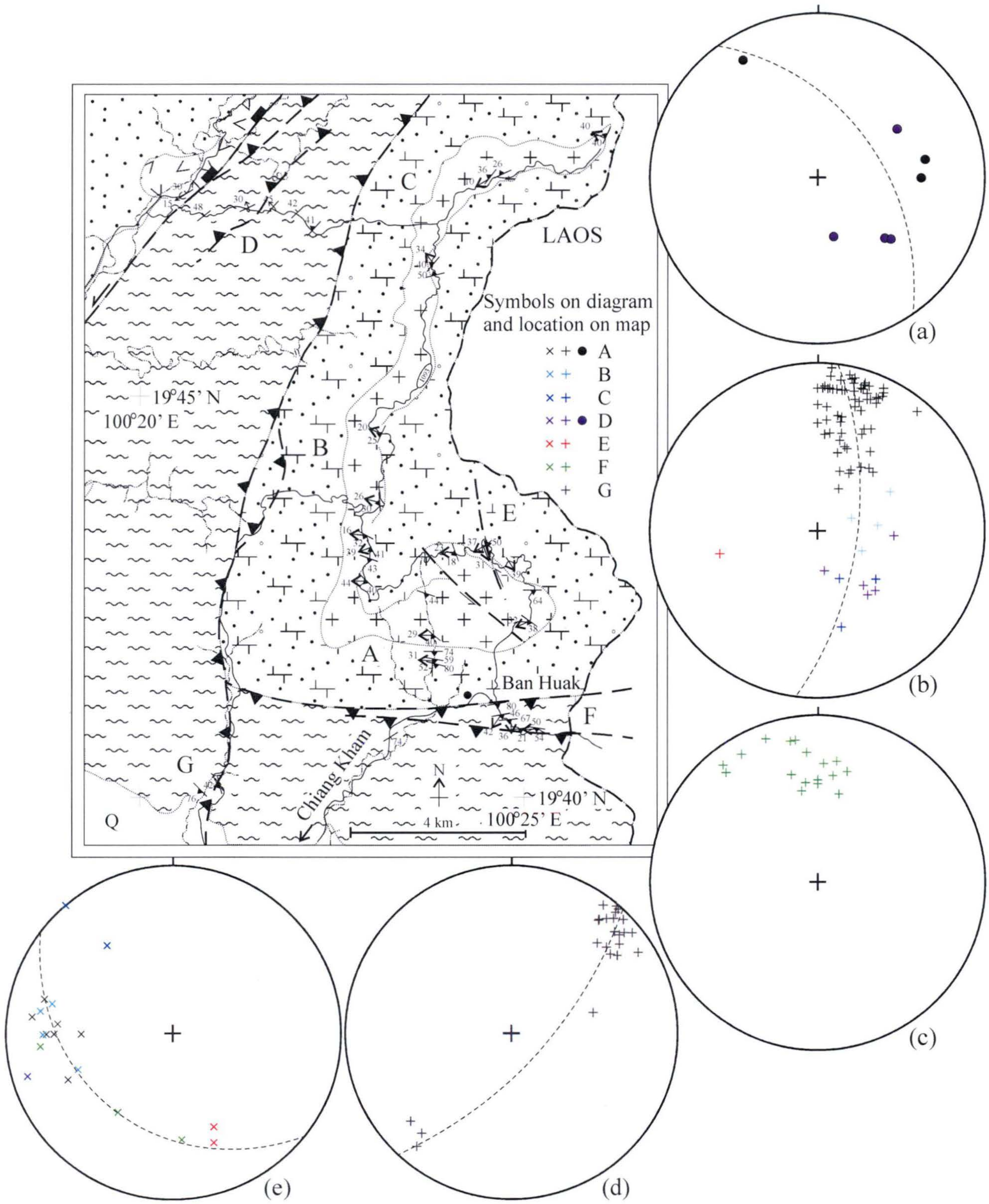

Figure 5.40 Lower-hemisphere equal-area stereographic projection showing poles to bedding (a), poles to cleavage (b) to (d) and lineation (e) of the Ban Huak area. Note, "o" is pole to bedding, "+" is pole to cleavage and "x" is lineation. Symbols on geologic map as in Figure 2.3.

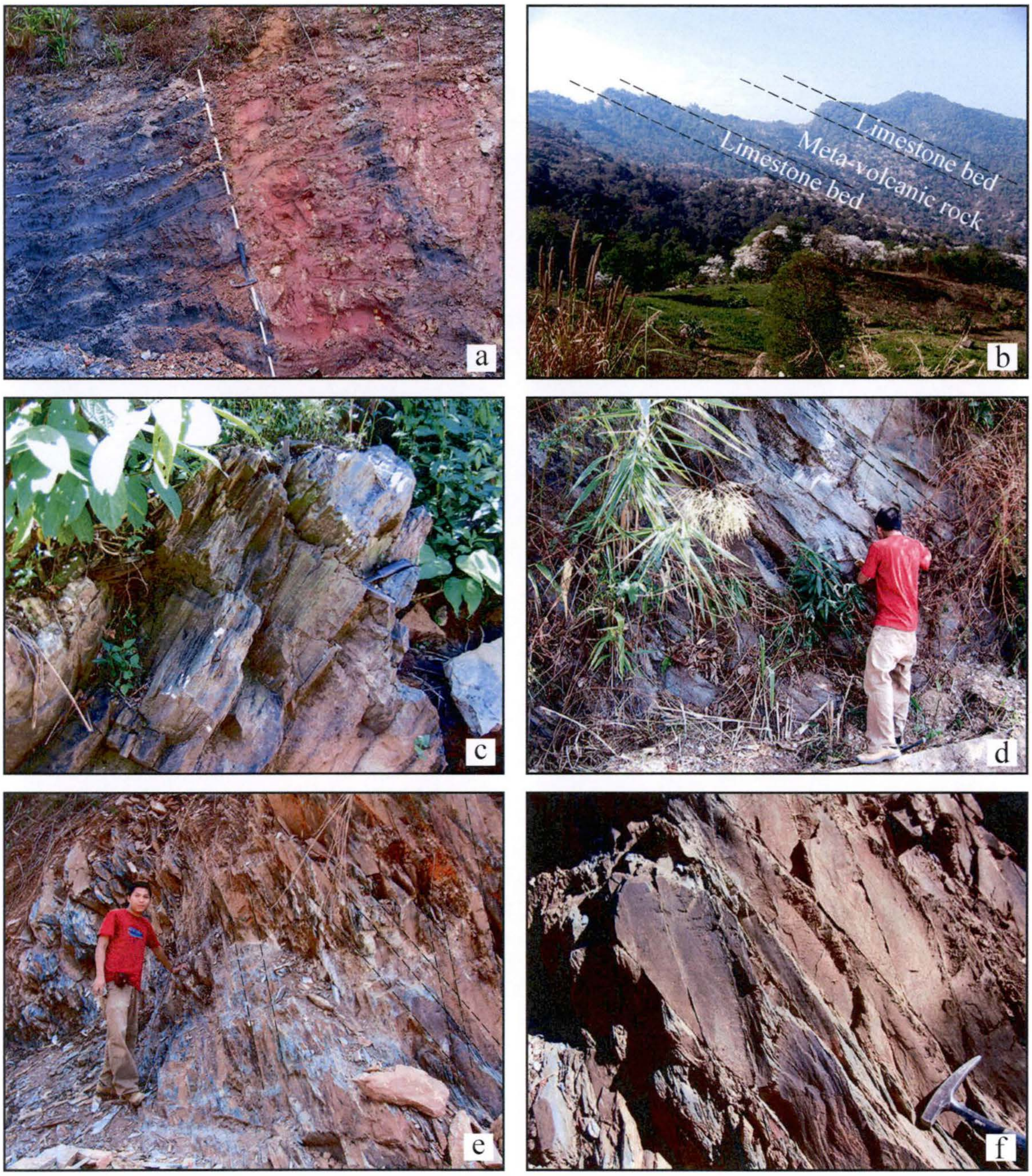

Figure 5.41 Photographs of structural features in the Ban Huak area. (a) Bedding (058°/74°SE) in the Carboniferous-Permian meta-sedimentary rock at 19.6794°N 100.3909°E (looking SE). (b) View showing shallow dip to the west of the Carboniferous-Permian limestone and meta-volcanic rock. View is looking S from 19.8489°N 100.4382°E. (c) Cleavage plane dipping to the south in the Carboniferous-Permian meta-sedimentary rock from 19.6819°N 100.4148°E (looking W). (d) Cleavage in the Carboniferous-Permian foliated granite showing 45° dip to the south at 19.7147°N 100.3865°E (looking SE). (e) and (f) Two cleavages in the Carboniferous-Permian meta-volcanic rock from 19.6982°N 100.4006°E. Note looking SE in (e) and E in (f). Scale: hammer is 28 cm long; man is 168 cm tall; hammer head is 17.5 cm long.

except F and G. The inferred fold axis is shallowly plunging to the W close to the prominent lineation in these rocks. There is some evidence that two distinct cleavages are included in this spread (Figures 5.40b, 5.41e & f).

Location F lies in a fault sliver and includes steep cleavage striking ENE, probably due to drag on the faults Figure 5.40c. The NW-SE striking cleavage in the Huai Fire area, location G in Figure 5.40d, is probably related to the regional hinge fold and/or thrust fault movement in that area and probably not to other cleavages in the Ban Huak area.

The regional lineation on the cleavage plane mainly plunges to the W but plunges to the SE in area E (Figure 5.40e). Area E also has an anomalous cleavage orientation interpreted to be related to drag on a local fault E.

The orientation of cleavage and bedding changes from the south to the north. The EW-striking and southerly dip of area A in Figure 5.40 contrasts with the NS-striking and shallow westerly dip of area B. However, both areas have the same lineation orientation and the cleavage is folded into an antiform with a W-plunging axis.

Faults

The fault traces in this area generally strike sub-parallel to bedding and cleavage. These include thrust, normal and strike-slip faults. The NNE-SSW-striking and NW-dipping thrust faults have been traced through the middle of the Ban Huak area, whereas the EW-striking and southerly dipping thrust faults occur in southern portion. Thrust faults have been interpreted at the contact between the Carboniferous-Permian meta-sedimentary rocks and the Carboniferous-Permian limestone and meta-volcanic rocks. An outcrop-scale thrust fault in the Carboniferous-Permian meta-sedimentary rocks was observed at 19.7868°N 100.3619°E (Figure 5.38a).

Normal and sinistral strike-slip faults are exposed in the northwestern corner of this area. A NNE-SSW-striking and NW-dipping normal fault was interpreted at the fault contact between Carboniferous-Permian meta-sedimentary rocks and Late Triassic sedimentary rocks. A sinistral strike-slip fault has been traced from Mae Khong River offset in the north eastern part of the Chiang Khong area and it extends southwesterly through the Wiang Kaen Basin. Sinistral strike-slip faults have been found locally in the

Carboniferous-Permian meta-volcanic rocks and foliated granite in the southeastern part of the Ban Huak area.

5.2.7 Structure Interpretation of the Chiang Khong Area

The regional bedding and cleavage mainly strike N-S to NNE-SSW and dip to the W, Sections have been selected that are approximately perpendicular to the regional trend of folds and that have accessible exposures. The field work was planned to concentrate on areas that could be projected onto the sections. An asymmetric upright to steeply inclined fold profile has been selected based on the bedding/cleavage relationship (eg. McClay, 2000).

Areas with a shallow dip of cleavage and bedding were interpreted to be related to thrust fault movement, especially in the high strain rocks of the Ban Huak area. The N-S striking and shallowly W-dipping cleavage planes with lineation plunging to the west in the Ban Huak area have been drawn as a the frontal ramp, whereas the E-W striking and steeply S-dipping cleavage with the same direction of lineation is interpreted as evidence for a lateral ramp along that zone (cf. Wilkerson *et al.,* 2002; Marshak & Wilkerson, 2004). For this model, the lateral ramp in the underlying contractional fault-related fold probably produced the W-plunging antiform (Wilkerson *et al.,* 2002). This structure will need to be reinterpreted if the high strain rocks were deformed in an early orogeny (see Chapter 6).

Quartzo-feldspathic mylonite in the southern part of CK-CB and mylonitic granitoid in high strain rocks are correlated with the thrust fault movement. The recrystallised fine-grained quartz and fractured feldspar in the mylonite are typical of strain at 300 to 500 ^{o}C (van der Pluijm & Marshak, 2004) which compares well with the recognition of biotite zone, greenschist facies metamorphism in this area. Elsewhere the metamorphic grade is prehnite-pumpellyite facies.

The structural features of Chiang Khong area are exposed between two major sinistral strike-slip faults, the Mae Chan Fault to the NW and the Wiang Kaen Fault to the east. These late left-lateral strike-slip faults are associated with the collision between India and Asia (Tapponnier *et al,* 1986) and the Tertiary extensional basin in northern Thailand and neighbouring areas (Morley, 2002 & 2007; Uttamo *et al.,* 2003). Normal faults with strike-slip fault association in this area form half graben and are interpreted to form the eastern boundary of the Chiang Khong-Thoeng Basin (Leloup *et al,* 1995; Morley, 2002 & 2007 and Uttamo *et al.*, 2003) and the Wiang Kaen Basin. The NNE-SSW trending normal fault transected the thrust fault zone and separated the CK-WB and CK-CB. Uttamo *et al.* (2003) reported en echelon extensional faults in the southern tip of CK-CB but the field evidence reported here indicates this is a normal fault cutting across a backthrust.

5.3 Structure of the Lampang Area

5.3.1 Introduction

To elucidate the structural history of the Lampang area, outcrop-scale structural data was collected along Highway 11 from the Muang Lampang district to Ban Mae Khaem and used to draw three structural cross sections (Figure 5.42). The last structural section on the southeastern corner of the Lampang area formed an extension of the Sukhothai Fold Belt transect, section Lampang to Denchai of Singharajwarapan & Berry (2000). The eastern end of Figure 5.42 is slightly modified from the previous work.

The structure of this area is dominated by folds and thrusts. Late strike-slip faults are less common than in the Chiang Khong area. There are large basins formed during Tertiary normal faulting. Regional thrust faults have been proposed from bedding orientation in the Pha Kan limestone (Chaodumrong, 1992). Bedding and regional cleavage mainly strikes NNE-SSW (Figures 5.42 a & c). Locally, other orientations are associated with local fault movement (Figure 5.42b). An anomalous E-W strike occurs at locations C, D, E and H (Figures 5.42 b & d). This occurs near normal faults (C) and small left-lateral strike-slip faults (H) with normal fault association. The cause of rotation at C and D is less clear. At D there is a spatial association with a N-dipping thrust.

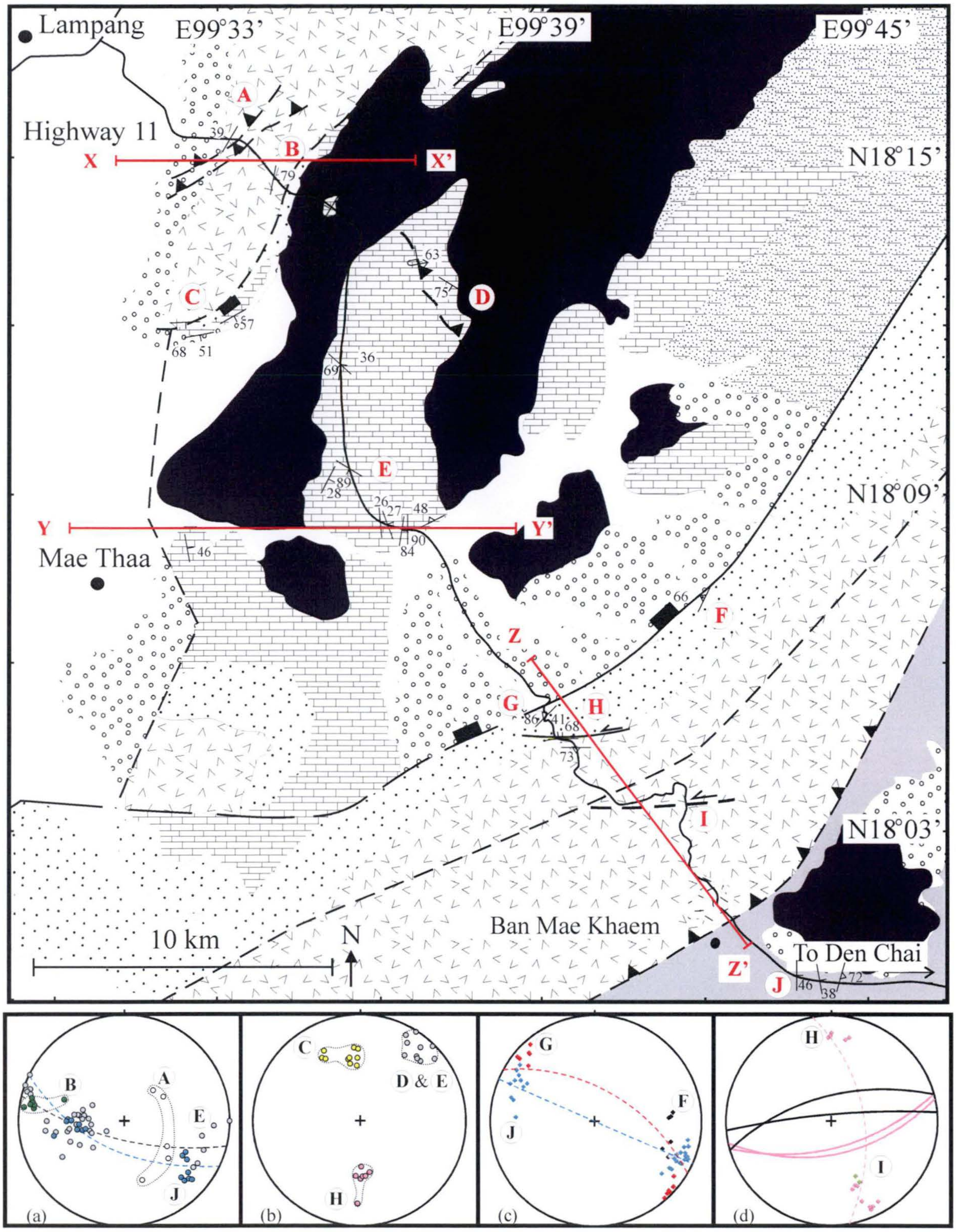

Figure 5.42 Structure map of the Lampang area with lower-hemisphere equal-area stereographic projection showing pole to bedding (circle), pole to cleavage (diamond) and fault planes. (a) pole to bedding from A, B, E and K. (b) anomalous bedding from C, D, E and H. (c) pole to cleavage from F, G and K. (d) pole to cleavage from H and I and fault planes from H and I. Structure from A = white, B = green, C = yellow, D & E = grey, F = black, G = red, H = pink and I = light green. Symbols on geologic map as in Figure 2.5.

5.3.2 Fault, Cleavage and Fold

Fault, fault rock and metamorphism

Thrust and normal faults are common in the Lampang area. Outcrop-scale strike-slip faults are less common in the Triassic Phra That Formation and the CLT rocks in LP-CB.

Thrust faults

Two outcrop-scale thrust faults occur at 18.2560°N 99.553°E and 18.2551°N 99.5572°E in the LP-WB area (location A in Figure 5.42). These thrusts strike NNE-SSW to NE-SW and dip to the NW as shown in (Figures 5.43 & 5.44). A duplex structure with top-to-the-east sense of shear was observed at the latter location. A N-S striking and E-dipping thrust was observed in a limestone quarry at 18.2206°N 99.6119°E (Figure 5.45). Bedding at location D (Figure 5.42b) has a NW-SE strike, different from the regional strike. These beds were probably rotated by local thrust faulting (location D in Figure 5.42). A thrust fault dipping to the west at the Ban Mae Khaem area reported by Singharajwarapan (1994) and Singharajwarapan & Berry (2000) was interpreted from the inverse age stratification of adjacent rocks between the Late Triassic CLT volcanic rock and Late Triassic sedimentary rock of Wang Chin Formation (Tr. 7 in the Lampang Group of Chaodumrong, 1992).

Normal faults

An approximately N-S to NNE-SSW striking normal fault was recognised in volcaniclastic rocks interbedded with sandstone and shale (location B in Figure 5.42). Its geometry is shown in Figure 5.46. A very steep E-W normal fault (Figure 5.47c) was found at Phra That Doi Muang Kham temple at the southern tip of LP-WB. The E-W strike of bedding in this area (Figure 5.43b) is due to fault drag. A normal fault on the western side of LP-CB was interpreted from outcrop-scale measurement at the Sam Kha Reservoir, location F in Figure 5.42 (18.1200°N 99.7061°E). It strikes NE-SW to E-W and dips steeply to the NW (Figure 5.42d). The normal fault has been named the Ban Mai fault segment of the Thoen Fault Zone and is interpreted to be an oblique left-lateral strike-slip fault (Fenton *et al.,* 1997). However, this fault was also interpreted to be the eastern fault boundary of the Mae Moh Basin and named the Mae Moh Fault by Uttamo *et al*, 2003.

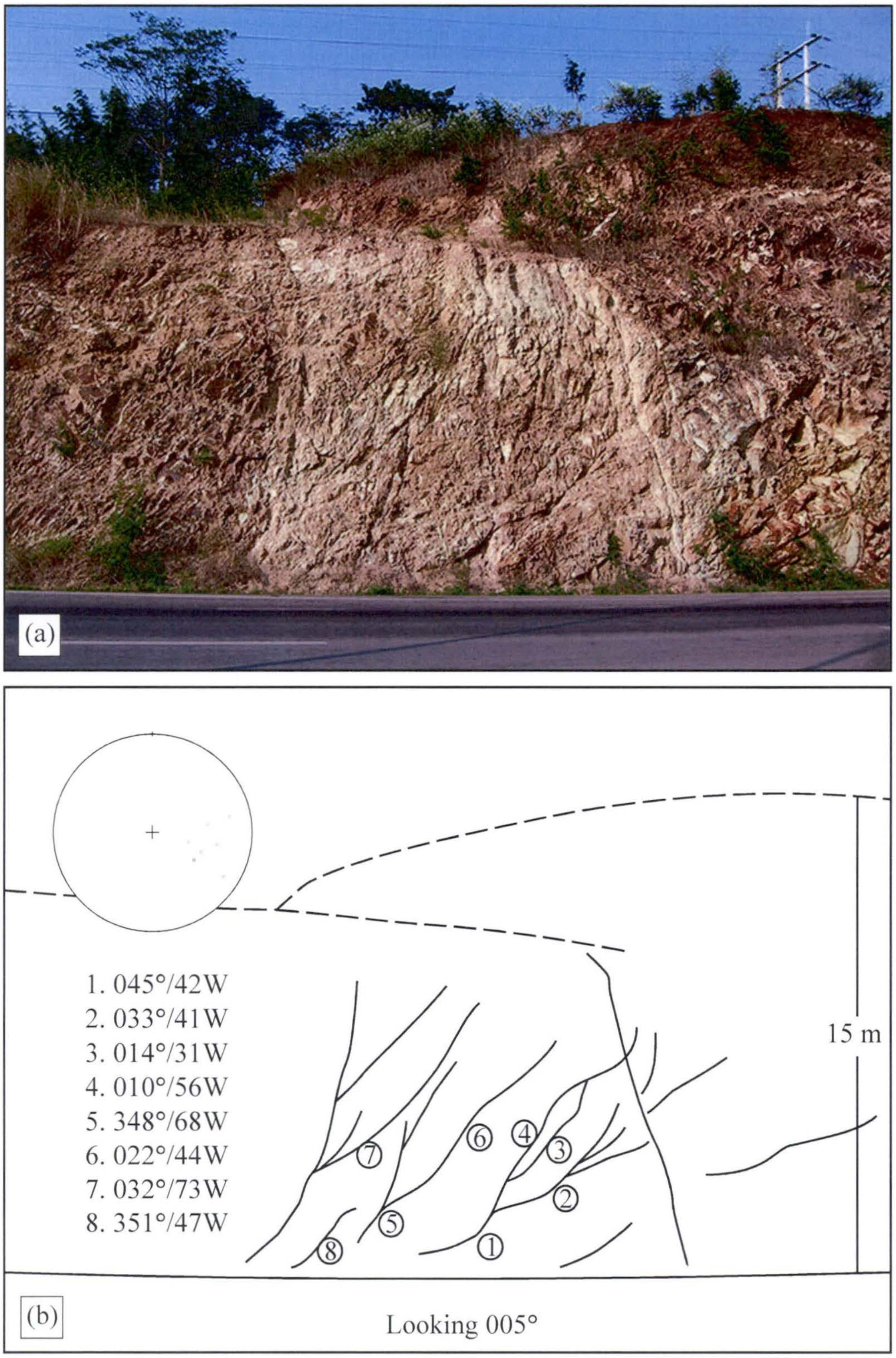

Figure 5.43 Photograph (a) and line drawing (b) showing the geometry of thrust faults at 18.2460°N 99.5676°E in the LP-WB. Lower-hemisphere equal-area stereographic projection showing poles to thrust fault planes.

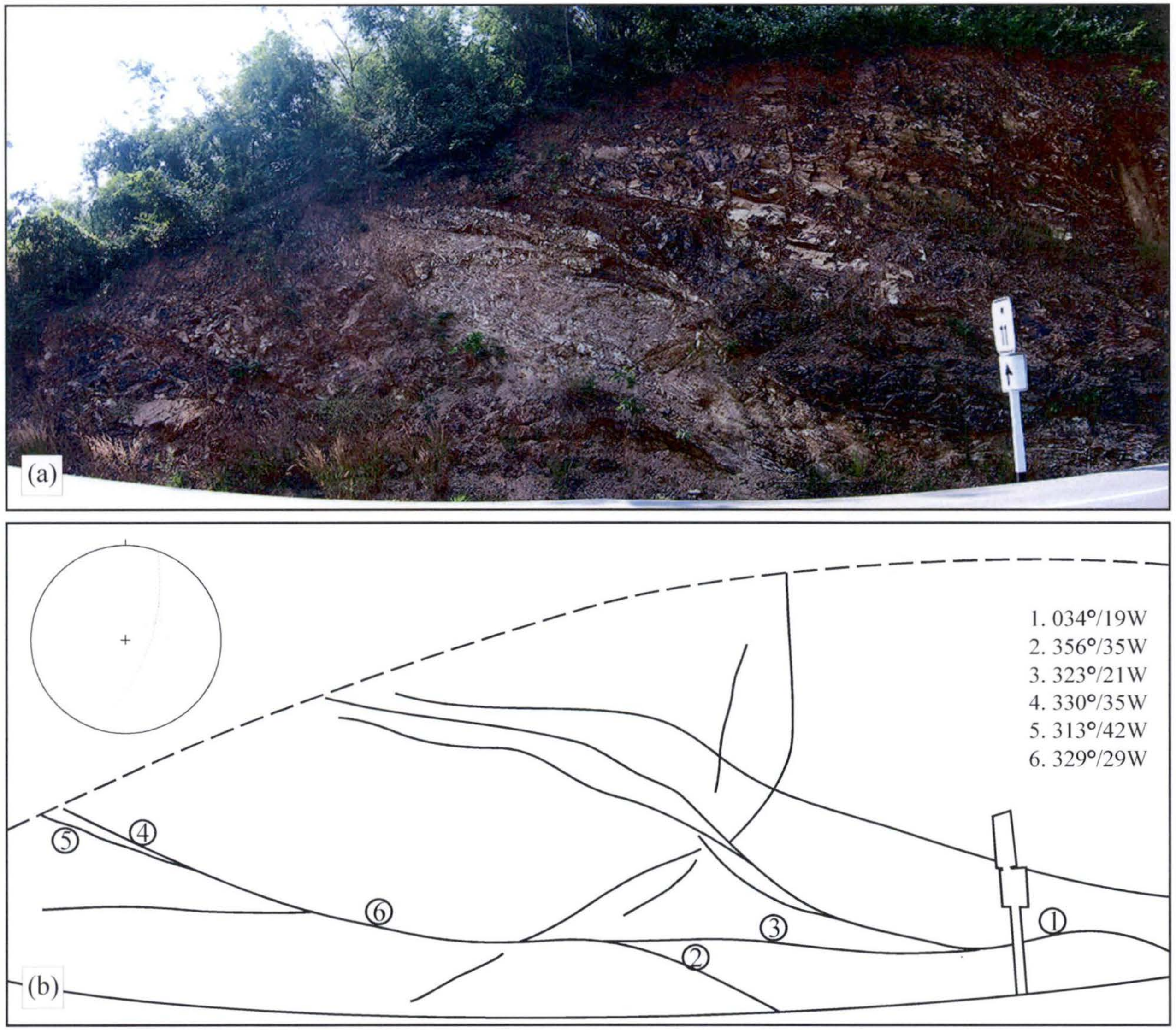

Figure 5.44 Photograph (a) and line drawing (b) of outcrop-scale thrust fault in LP-WB volcanic rocks from 18.2551°N 99.5572°E with lower-hemisphere equal-area stereographic projection showing pole to thrust fault plane. Note, road sign pole is 2.50 m tall; this view is looking 190°.

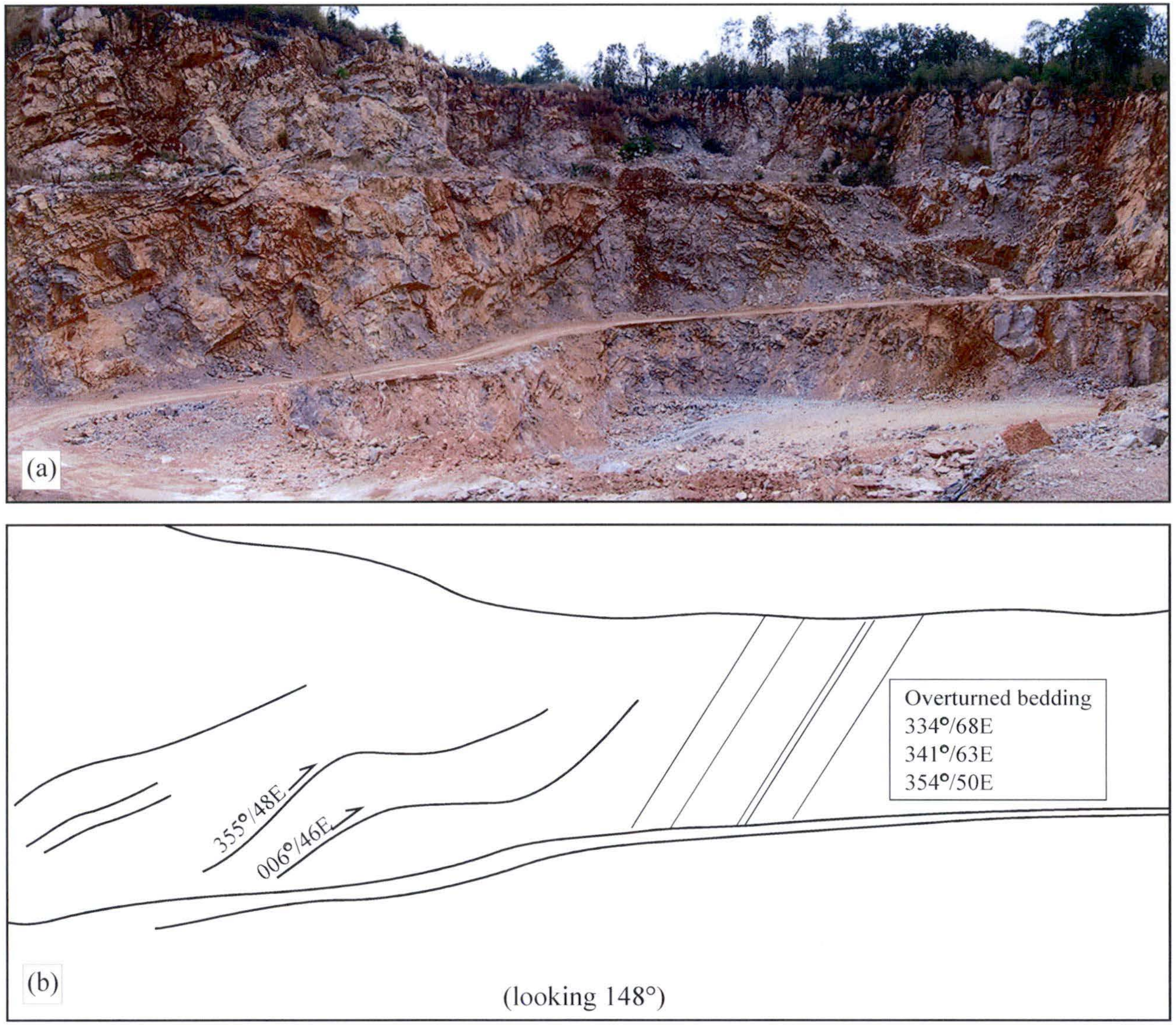

Figure 5.45 Photograph (a) and line drawing (b) showing the geometry of thrust fault and overturned bedding in limestone outcrop of the Pha Kan Formation from 18.2206°N 99.6119°E. Note, outcrop 5 to 7 m height from track.

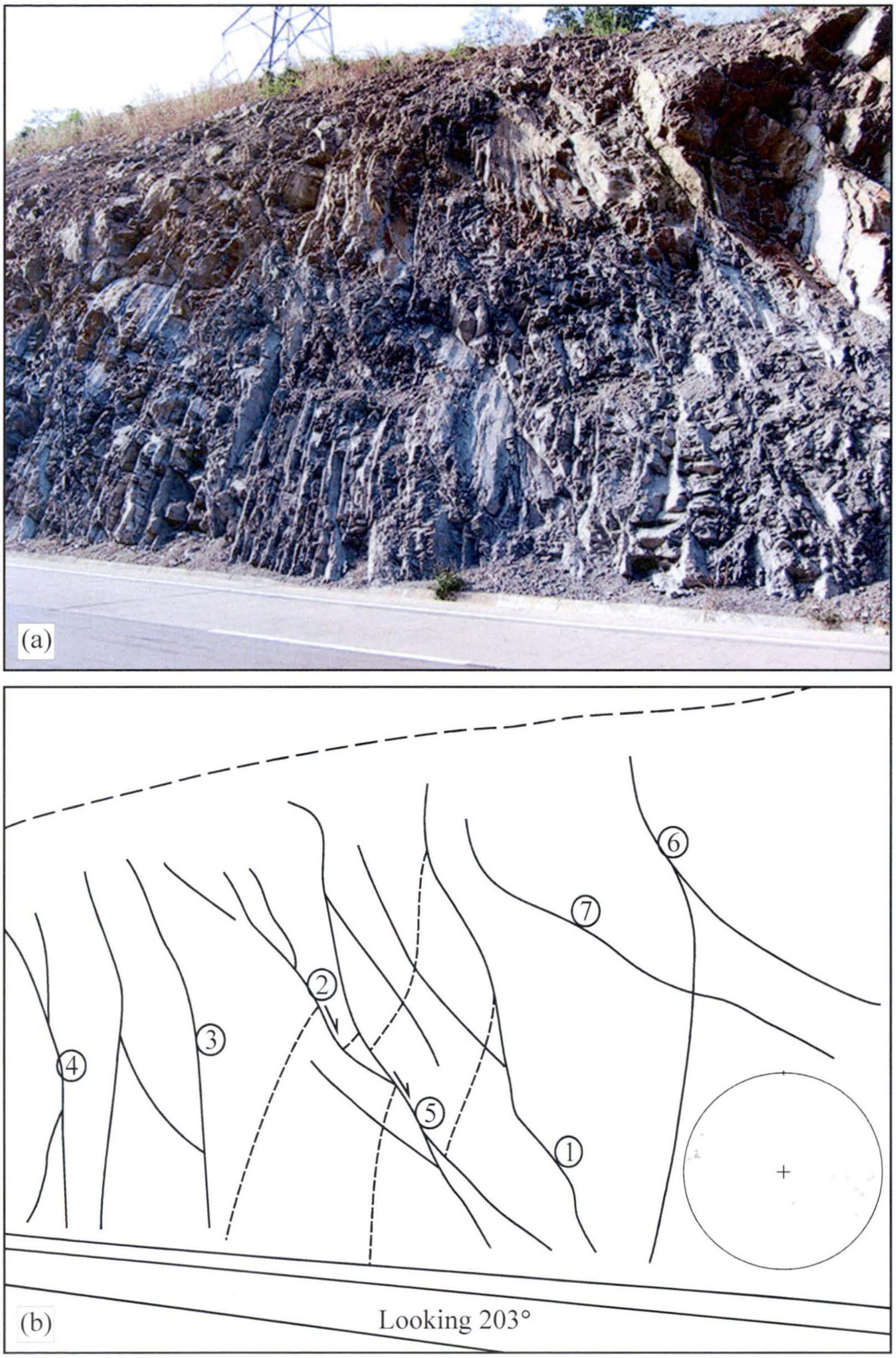

Figure 5.46 Photograph (a) and line drawing (b) showing the geometry of normal fault in outcrop-scale from 18.2460°N 99.5676°E of LP-WB volcaniclastic rock. Lower-hemisphere equal-area stereographic projection showing pole to bedding (cross) and pole to fault plane (open circle). Note, this outcrop is approximately 7 m height.

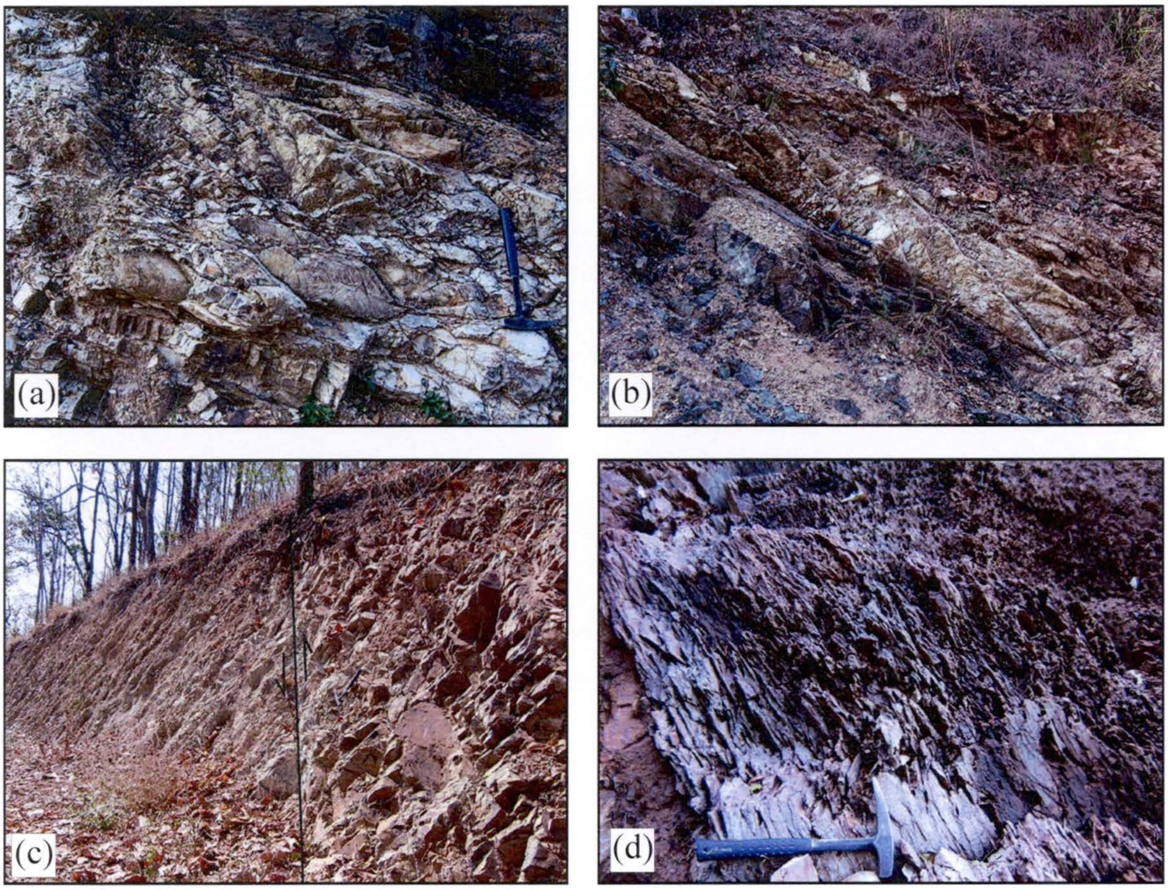

Figure 5.47 Photographs of structural features in the Lampang area. (a) & (b) Duplex structure development on outcrop-scale thrust fault from 18.2551°N 99.5572°E (same location in Figure 5.44) showing top-to-the-east sense of movement (looking SW). (c) The E-W striking and sub-vertical dipping of outcrop-scale normal fault from 18.1991°N 99.5419°E in the LP-WB volcanic rock at the Phra That Doi Muang Kham temple (looking W). (d) Strong cleavage in outcrop-scale of the Phra That Formation at 18.1200°N 99.7061°E (looking S). Note, hammer is 28 cm long.

Strike-slip faults

Two small strike-slip faults were found in the LP-CB at location H and I (Figure 5.42). The left-lateral strike-slip fault (H) strikes E-W, dips steeply south (Figure 5.42d) and has an E-W cleavage associated with this fault. These small scale strike-slips faults were interpreted to be associated with the left-lateral strike-slip movement of the Thoen Fault by Fenton *et al.,* (1997). The strike-slip fault in the middle part of LP-CB was drawn from satellite image interpretation and is probably part of the Thoen Fault Zone.

Fault rock and metamorphism

A duplex and associate fault breccia is associated with thrust fault movement at 18.2551°N 99.5572°E (Figures 5.44, 5.47b & c). A narrow zone of fault gouge was commonly found along most exposed fault planes.

Metamorphism of rocks in the Lampang area was previously described for pelitic rocks of Lampang Group along the Lampang-Denchai transect and illite crystallinity values in range of 0.25-0.36 $\Delta^{o}2\theta$ are indicative of diagenetic to lower anchimetamophic zone (Singharajwarapan 1994; Singharajwarapan & Berry 2000).

Cleavages

Regional cleavage in the Lampang area is common in the Phra That Formation (Tr.1 of Lampang Group), the LP-CB volcanic rocks and the Wang Chin Formation (Tr. 7). The regional cleavage strikes N-S to NNE-SSW (Figures 5.42c & 5.47d). The regional cleavage has been rotated to E-W striking (Figures 5.42 c & d) at locations F, H and I, near the local left-lateral strike-slip fault (Figure 5.42). The E-W cleavage was probably formed during the late normal and strike-slip faults movements associated with formation of Tertiary extensional basins in northern Thailand.

Folds

Outcrop-scale folds were not observed along the highway 11. Thrust fault propagation fold geometry has been drawn in the structure cross section based on the distribution of bedding and lithology (see below). The structure of the central part of the Lampang area is more complicated due to bedding variations in the Pha Kan Limestone. The N-S striking of steep and shallow dipping beds are anomalous and significantly different from the NNE-SSW regional trend (Figure 5.42a). Over 10 km along the road (locations B, E), bedding readings define a N-plunging fold axis despite the fact that the only cleavage data still strikes NNE. The origin of this zone is discussed below. Because of the bedding orientation, sections were drawn EW in this area

5.3.3 The Lampang Transects

Two structural sections were drawn E-W across the LP-WB and the central part of the Lampang area. The last transect on the southeastern area is east of the anomalous zone and was drawn in a NW-SE direction and slightly modified from the western end of the Sukhothai Fold Belt transect of Singharajwarapan & Berry (2000). Stratigraphy and thickness of rock units used in this interpretation are based on previous studies of Lampang Group (Chaodumrong, 1992; Singharajwarapan, 1994). The structure interpretation on the southeastern side of the Lampang area is based on the previously published structural section across the Sukhothai Fold Belt (Singharajwarapan & Berry, 2000).

The first section (X-X' in Figure 5.48) across the LP-WB (XX') is about 10 km long. A W-dipping thrust is dominant on this section. The steep E-facing limb is below the thrust. The duplex structure on the CLT outcrop of the thrust fault indicates top-to-the-east sense of movement (cf. Marshak & Wilkerson, 2004). A steeply dipping normal fault cuts through the eastern side of anticline. Structure of rocks on the eastern side is poorly constrained due to the Tertiary basalt that covers the area. There is no evidence of older rocks in these thrust slices so the thrust detachment on this section is interpreted to be at the bottom of the Middle to Late Triassic CLT volcanic sequence, about 1-2 km below the surface.

The second section (Y-Y' in Figure 5.48) is 15 km long across limestone outcrops in the central part of the Lampang area. The W-dipping thrust has the form of a thrust propagation fold with a very steep E-facing limb above the thrust. However this limb strikes N-S. The anomalous strike is discussed below and it is unlikely the steep limb is entirely due to the thrust geometry here. The eastern part of the section is inferred from the geometry in section ZZ' and is speculative.

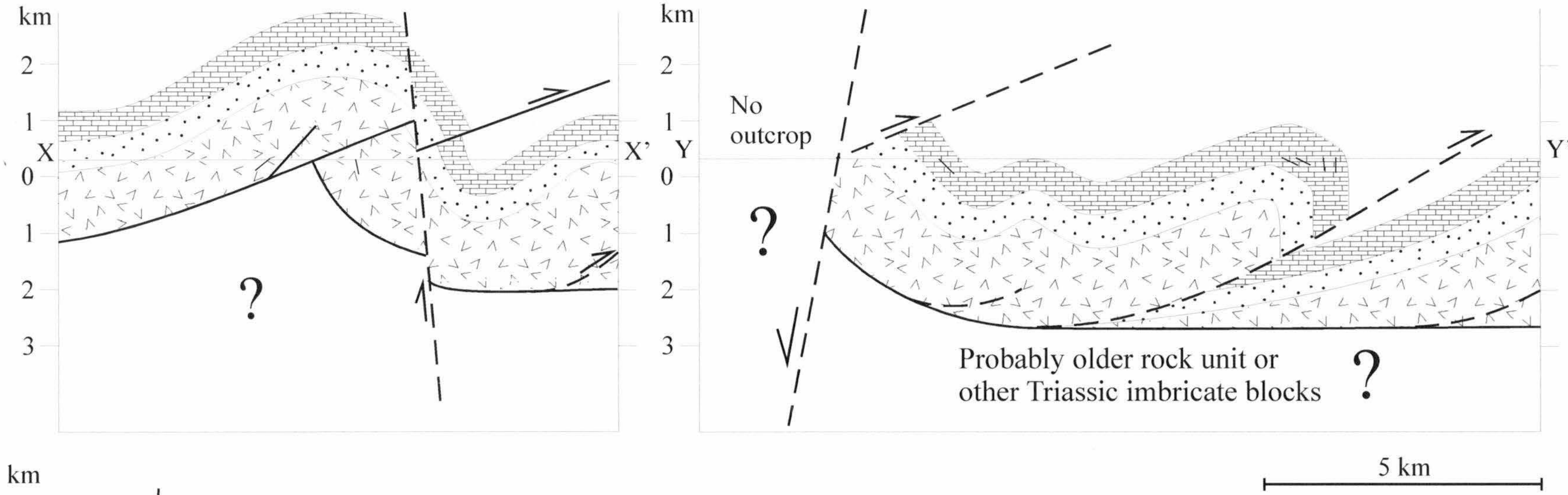

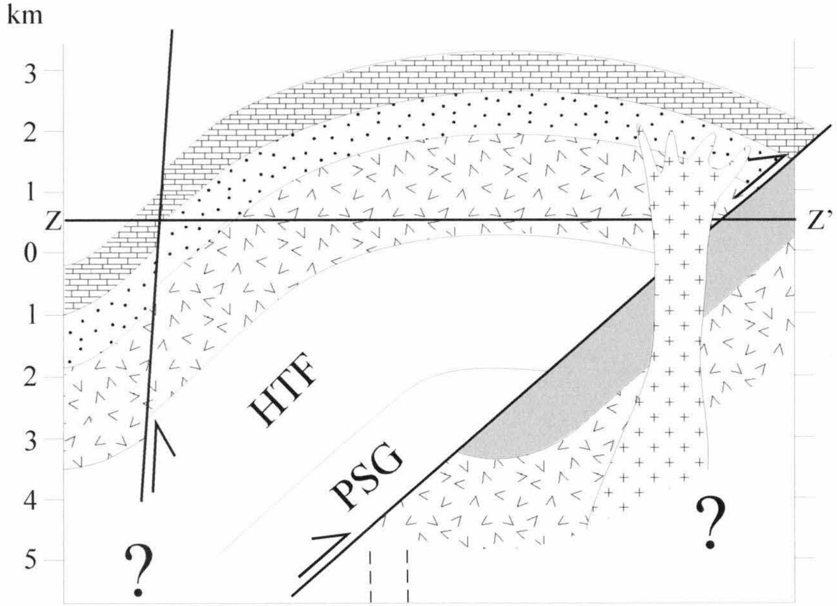

Figure 5.48 Schematic cross sections of the Lampang area (X-X', Y-Y' and Z-Z' transects in Figure 5.42). Symbols as shown in Figure 2.5. Note, the Z-Z' transect is slightly modified from the western part of the Sukhothai Fold Belt transect of Singharajwarapan & Berry (2000); HTF is the Permian Huai Tak Formation and PSG is the Permo-Carboniferous Pha Som Group in Singharajwarapan & Berry (2000).

Z-Z' transect is approximately 12 km long (Figure 5.48), and runs in a NW-SE direction across the LP-CB. This transect is partly modified from the western end of the Lampang – Denchai Transect of Singharajwarapan & Berry (2000). The rock units in this section are shown as a conformable sequence from the Permo-Carboniferous Pha Som Group to the Triassic Lampang Group. The NW-dipping thrust fault with fault propagation fold at the Ban Mae Khaem intersection was modeled to cut through the upper sequence of Lampang Group and brought the CLT volcanics in contact with the Wang Chin Formation (Singharajwarapan & Berry, 2000). The Ban Mae Khaem thrust has been intruded by a Late Triassic granite (Singharajwarapan & Berry, 2000; Khositanont *pers. comm.*, 2006). The normal fault in the western side of LP-CB strikes approximately NE-SW to E-W and steeply dips to the northwest. It has been drawn to cut through the thrust propagation fold and forms the eastern boundary of the Mae Moh Basin (Uttamo *et al.,* 2003). This normal fault was interpreted to be associated with a left-lateral strike-slip fault zone active during the formation of Tertiary extensional basins in northern Thailand (Fenton *et al.,* 1997; Morley, 2007; Polachan *et al.,* 1991; Uttamo *et al.,* 2003).

Two local left-lateral strike-slip faults in the LP-CB strike E-W and dip very steeply to the north. These strike-slip faults have been interpreted as probable fault branchs in the left-lateral strike-slip fault movement of the Thoen Fault Zone (Fenton *et al.,* 1997).

5.3.4 Structure Interpretation

The regional structure of the Lampang area includes areas of NNE-SSW trend but has a large area of anomalous bedding strike. Thrusts were found with NNE strike but there was also a NW-striking thrust. A few normal faults have been observed in the northwestern and southeastern part, and are probably associated with late Tertiary deformation.

The unusual steep N-S limb in the middle part of the Lampang area (on the second structural transect) and the back thrust dipping to the northeast, does not match the typical structure of the Sukhothai Fold Belt. Two possible options are that the limb formed by anticlockwise rotation of the whole block after the Late Triassic folding or that the steep zone nucleated on a structure that predated the late Triassic. Regionally, there is extensive evidence for rotation during in the late Tertiary deformation. A study of magnetostratigraphy of the Mae Moh Basin (about 20 km north of the transect) demonstrated a counterclockwise vertical axis rotation in the Miocene (Benammi *et al.,* 2002). However there is no local evidence for late Tertiary anticlockwise rotation in the Lampang area. The single cleavage plane observed in the area of anomalous bedding has a normal NNE strike. This is more compatible with the steep limb having formed before the Late Triassic thrusting. At this stage there is insufficient evidence to decide which of these options is correct.

The fold thrust belt has been overprinted by late Tertiary structures. This late deformation is dominated by normal and left-lateral strike-slip faults in association with the extensional basin in northern Thailand during Late Oligocene to Early Miocene (Morley, 2007; Uttamo *et al.,* 2003). However, the Mae Moh Basin (further north of these transects) has been interpreted to have developed via the pull-apart basin model (Uttamo *et al.,* 2003). The E-W cleavage and anomalous bedding at locations H and I have been interpreted to have formed during local left lateral strike-slip fault movement that was linked to the left-lateral strike-slip movement of the Thoen Fault Zone (Fenton *et al.,* 1997).

The Triassic Lampang Group has been correlated with the Triassic strata in the Simao Terrane (Feng *et al.,* 2005). Feng *et al.,* (2005) suggested these areas formed on the same continental block. However, no Triassic deformation has been documented from the Simao Terrane. The major NNW-SSE structure of the Simao Terrane has been linked to the late Cenozoic deformation event due to the collision of India with the Asia plate (Leloup *et al.,* 1995, Tapponnier *et al.,* 1990). This remains a weak point in the correlation between the Sukhothai Fold Belt and the Simao Terrane.

5.4 Summary

Structural data has been collected over three field seasons in northern Thailand. The structure of the CLT in northern Thailand has been determined along three structural transects in the Chiang Khong area and three small transects in the Lampang area. These transects are perpendicular to the strike of the volcanic belt. Detailed mapping in the Ban Huak high strain rocks area was also carried out. The structural transects were drawn using concepts of balanced cross-section constructions (e.g. Woodward, 1988). The transect along the Highway number 11 in the southern area is an extension to the structure cross-section across the Sukhothai Fold Belt [Lampang to Denchai transect of Singharajwarapan & Berry (2000)]. Mylonite and fault rocks were identified using the classification of fault rocks by Sibson (1977). Metamorphic mineralogy has been confirmed using electron microprobe analysis to determine the metamorphic grade of rocks in the Chiang Khong area.

The dominant structure in the CLT is a thin-skinned fold and thrust belt style. Mesoscopic structures are characterised by upright close to open folds with locally overturned bedding in the Chiang Khong area. A steep regional cleavage is axial planar to these folds and becomes more intense to the east and near thrusts. In several localities, a second shallower dipping cleavage was recognised. A W-dipping mylonite zone along the SW margin of CK-CB is correlated with the regional folding event as is the L/S tectonites of the southeastern corner of the Chiang Khong study area (the Ban Huak area). Anomalous thrust fault orientations in this area may represent lateral ramps.

Thin-skinned thrust faulting was set as the basic style in construction of sections on both of the Chiang Khong and Lampang structure transects. The sections are consistent with field observation of major E-directed transport overprinted by local backthrusts. This conclusion is the same as the thrust geometry in the Sukhothai Fold Belt proposed by Singharajwarapan & Berry (2000). The fold structure in the Chiang Khong area was drawn with a major detachment in the Carboniferous stratigraphy. In the Lampang area, the fault horses only include Triassic stratigraphy and the main detachment is drawn shallower in these sections.

The eastern margin of the Chiang Khong section includes a deeper stratigraphy, more ductile strain and higher metamorphic grade, suggesting a transition to medium-skinned deformation. This may be partly a response to the post-Triassic uplift history. A similar more cleaved domain was recognised near the Nan-Uttaradit suture by Singharajwarapan & Berry (2000). However no evidence for high pressure metamorphism or oceanic lithologies was recognised in the Ban Huak area. Singharajwarapan & Berry (2000) argued that the high strain rocks in the Nan-Uttaradit suture were formed in an accretionary prism.

Singharajwarapan & Berry,(2000) argued that folding and thrusting in the the Sukhothai Fold Belt was underway by the Late Triassic and was probably related to collision between the Shan-Thai and Indochina terranes in the Late Triassic. The youngest rocks recognised in the fold and thrust belt in this study are the Late Triassic upper sequence of the Lampang Group (the lower Norian Wang Chin Formation) in the southern area. Units younger than 220 Ma (Chaper 4) are deformed and folded. Folding predates the latest Triassic and Early Jurassic sedimentary sequence of Khorat Group in the northern area.

The Triassic stratigraphic sequence of the Lampang Group in northern Thailand has been correlated with the same Triassic units to the Simao Terrane in SW Yunnan (Feng *et al.,* 2005). However, there is a paucity of structural data from the Simao Terrane to support any correlation of the Mesozoic deformation history between the areas. Most of the folding of the Sukhothai Fold Belt predates the folding of the Simao Basin (Lacassin *et al.,* 1997). The S-shape linear trend from the Simao Basin to the Sukhothai Fold Belt has been attributed to the late ENE-WSW strike-slip faulting. Major structure of the Simao Terrane is mainly N-S and NNW-SSW trending parallel to the Red River Fault and Ailaoshan Shear Zone (Heppe *et al.,* 2007; Leloup *et al.,* 1995) and formed during ENE-WSW compression in the late Cenozoic (Tapponier *et al.,* 1990). The available paleomagnetic date from the central part of the Simao Terrane supports a clockwise rotation during the internal deformation (Sato *et al.,* 2007). In contrast, the early fold thrust structure of the CLT is dominantly NNE-SSW with W-dipping thrusts. It has been linked to a range of tectonic models (Chapter 6) but is pre Tertiary in age.

The metamorphism of rocks in the northern area increases from prehnite-pumpellyite in the west to greenschist facies in the east. The lowest grade rocks studied are in the Lampang area (diagenetic to lower anchimetamorphic zone). The textural evidence for cleavage development is consistent with peak metamorphic conditions in these rocks. In the higher grade rocks the metamorphic index minerals are aligned in the cleavage. Metamorphism in these areas probably reached a maximum during the folding and thrusting which produced the cleavage, fault rock and mylonite.

The fold and thrust belt regional structure of the CLT volcanic belt has been overprinted by late normal and left-lateral strike-slip faulting. The Chiang Khong-Thoeng, Wiang Kaen, Lampang , Mae Moh and Long basins formed during these events and disrupted the volcanic belt into many sub-belts. The Tertiary rift basins are linked to the E-W extension associated with the Late Cenozoic collision between India and Asia (Fenton *et al.,* 1997; Lacassin *et al.,* 1997; Leloup *et al.,* 1995 & 2001; Morley, 2002 & 2007; Polachan *et al.,* 1991; Uttamo *et al.,* 2003).

CHAPTER 6

Summary of Results and Regional Implications

6.1 Introduction

The complex tectonic evolution of northern Thailand and neighbouring areas, including NE Myanmar, N Laos, NW Vietnam and SW China, has been keenly debated for more than a decade. Many previous studies have focused on the palaeotectonic reconstructions and timing of terrane accretion in this part of SE Asia. Palaeoenvironmental and palaeomagnetic studies aimed at determining the tectonic evolution of SE Asian fragments have produced sometimes contradictory results [see Metcalfe (2002, 2006) and Li *et al.* (2004), respectively]. Here, new knowledge gained from this study of the Chiang Khong – Lampang – Tak volcanic belt in the central section of the Sukhothai Fold Belt in northern Thailand, is used to evaluate and improve plate tectonic models for the geodynamic development and evolution of this part of SE Asia.

6.2 Summary of the Major Results

This study centred on detailed petrochemical, geochronological and structural aspects of rocks constituting the Chiang Khong – Lampang – Tak volcanic belt. Some 98 representative freshest rocks were analysed, providing a more geographically comprehensive sampling than the published data base. Ten representative igneous rocks, one granitic mylonite and seven sandstone samples were dated via LA ICP-MS U-Pb zircon dating. The granitic mylonite was also dated via the U-Th-Pb monazite (CHIME) method. Six across strike structural transects, including three in the Chiang Khong area and three in the Lampang area, were completed and interpreted to elucidate the structure style of the CLT volcanic belt. Metamorphic mineral assemblages in nine representative (meta)volcanic rocks from the Chiang Khong area were analysed, and a more detailed structural - metamorphic study of a distinctive metamorphic zone in the Ban Huak area (southeastern part of the Chiang Khong region) was carried out to clarify its relationship with the CLT and tectonic significance.

6.2.1 Petrochemistry of the CLT

Previous studies suggested that the CLT volcanic rocks formed in a mature continental margin volcanic arc associated with the subduction (Barr *et al.,* 2000, Barr *et al.,* 2006; Panjasawatwong *et al.,* 2003; Osataporn 2007). However, the relatively restricted range of radiometric ages recorded from the CLT (230-220 Ma in late Middle to early Late Triassic) is not typical a continental margin arc, wherein subduction-related magmatism usually shows a long time span.

The data reviewed in section 3.5 of this study has shown that the volcanic and dyke rocks in the CLT display a striking range of compositions, from low-K rocks with transitional tholeiitic affinities (mainly basaltic compositions but including a low-K, low-Th rhyolite suite from the LP-WB), through medium-K calc-alkaline to dominant high-K calc-alkaline compositions. The latter include areas where the dominant lithologies are mafic to andesitic (Long area in the eastern Lampang sub-belt), to felsic-dominant (CK-WB, CK-CB and LP-CB).

Despite the common occurrence of volcanics with calc-alkaline affinities typically ascribed to subduction-related magmatism, CLT magmatic rocks are suggested to have formed in an extensional Basin and Range-type setting, similar to the Cretaceous Whitsunday Province rift-related magmatism in NE Australia (Bryan, 2007; Ewart *et al.,* 1992). It is proposed that crustal thickening due to the Permian collision between the Shan-Thai and Indochina terranes was followed by gravitational collapse of the new crustal collage, extensional tectonism, and extension-linked CLT magmatism. This model suggests that subduction had ceased well before the 220-230 Ma CLT volcanic rocks were erupted.

6.2.2 Geochronology of rocks along the CLT

As discussed in sections 4.3 and 4.6 of this study, most CLT volcanic belt igneous rocks are considered to be crystallized in late Middle to early Late Triassic (220-230 Ma) and show distinctive age populations of zircons. The younger group is about 220 Ma whereas the old group is 230 Ma. The cause of these two age groups remains uncertain and there are no internal textural differences between the zircon grains in these two groups. Permian zircons (261-280 Ma) have been found in some CLT igneous rocks and are possibly inherited from Permian granites, such as that exposed in the Ban Hauk area in the far east of the CLT belt in the Chiang Khong region.

The detrital zircons in sedimentary rocks within the CLT indicate that Devonian to Carboniferous, Permian and Late Triassic rocks were exposed in the provenance areas of these sandstones. The oldest units in the CLT have a maximum depositional age of 355 ± 6 and 356 ± 7 Ma (Devonian to Carboniferous) and occur in the high strain rocks of Ban Huak area. Permian detrital zircons are present in sandstones from many localities, including in the CK-WB, the Ban Hauk area and LP-EB. Two Late Triassic redbed sandstones from the CK-EB and LP-CB contain Late Triassic zircons sandstones considered to be locally derived from the CLT Late Triassic magmatic rocks.

6.2.3 Structure of the CLT

The Chiang Khong-Lampang-Tak segment of the Sukhothai Fold Belt has been shown to be dominated by a thin-skinned east-vergent fold and thrust structural style characterized by upright close to open folds with locally overturned bedding. The steep regional cleavage is axial planar to regional folds and becomes more intense to the east and near thrusts. In some localities, the steep cleavage is overprinted by a shallow dipping cleavage, the latter possibly related to shallow west-dipping thrusts associated with Late Triassic deformation. The thin-skinned thrust faulting involved mainly east-directed transport and was overprinted by local back thrusts. A west-dipping mylonite zone along the SW margin of the CK-CB is correlated with the regional deformation event that produced the L/S tectonites of the Ban Huak area. Anomalous thrust fault orientations in the Ban Huak area are thought to represent lateral ramps. It is concluded that the structure of the CLT is similar to the thrust geometry described from further east and south in the Sukhothai Fold Belt (Singharajwarapan & Berry, 2000). The fold/thrust structure of the CLT was interpreted by these authors to result from collision between the Shan-Thai Terrane and the fused Simao-Indochina Terrane in Late Triassic but the post-collisional origin of CLT volcanic rocks does not fit this interpretation.

Deformation of the Late Triassic redbeds from the CK-EB and LP-CB is indicated by cleavages associated with the fold/thrust structural style of the CLT. The Latest Triassic age of deformation is also constrained by the deformation elsewhere in the Sukhothai Fold Belt (Singharajwarapan & Berry, 2000) and the cleavage dated at 188-220 Ma in the

Late Triassic Wang Chin Formation (Ahrendt *et al.*, 1993). The post-orogenic history of this area includes the Late Triassic to Early Jurassic less deformed redbeds of the Khorat Group that unconformably overlies CLT rocks and other basement in northern Thailand (Singharajwarapan, 1994; Singharajwarapan & Berry, 2000).

The high strain rocks mapped in the Ban Huak area represent a deeper stratigraphic level, and higher ductile strain and metamorphic grade (transitional between thin- to medium-skinned deformation) than elsewhere in the CLT volcanic belt. Metamorphic grade increases across the CLT volcanic belt from the west to east as the structuring intensifies. The metamorphism reached a maximum upper greenschist facies during the folding and thrusting which produced the cleavage, fault rocks and mylonite.

The fold and thrust regional structure of the CLT has been overprinted by normal and strike-slip faulting. These late structures are related to the extensional rift basin development in northern Thailand, possibly associated with the Late Cenozoic collision between the India and Asia plates (Lacassin *et al.,* 1997; Leloup *et al.,* 1995 & 2000; Morley, 2001 & 2007; Polachan *et al.,* 1991; Uttamo *et al.,* 2003).

6.3 Tectonic Significance of the Chiang Khong-Lampang-Tak Volcanic Belt

6.3.1 Current Tectonic Models of Northern Thailand and Neighbouring Areas

Pre-Permian and Permian Events

There is broad agreement that the Indochina and Shan-Thai terranes rifted from the northern Gondwana margin in the Early or Middle Devonian and Late Early Permian, respectively, and drifted northward as Palaeo-Tethys opened (Metcalfe, 1996a, 1996b, 1998, 1999; Sone & Metcalfe, 2008). Palaeomagnetic data record that the Shan-Thai Terrane was 6000 km from the Simao Terrane - Indochina Terrane in the Early Permian (270 Ma) (Li *et al.,* 2004). At average rates of subduction (100 kmy-1; Schellart *et al,* 2007), it would take at about 60 m.y. for this terrane to reach and collide with the Indochina Terrane (i.e. collision would occur at ~210 Ma in Late Triassic). As noted in Chapter 2, what happened in the East Asia – SE Asia region over the 100 m.y. between earliest Permian and end-Triassic in terms of regional tectonic events remains controversial. In particular, there is little consensus on the initiation and polarity of subduction (one or more subduction zones?), nor on the timing of collisional events as Palaeo-Tethys closed.

A major difference between the numerous tectonic models for this region, with profound implications for the tectonic development of mainland SE Asia, is the subduction polarity during the Permian and Triassic. Existing models fall broadly into three groups: those proposing long-lived east-directed subduction, those arguing for west-directed subduction, and models proposing a pair of opposite-dipping subduction zones. These are reviewed below and then assessed in the light of new information deriving from the present study.

Early models supporting east-directed subduction derived largely from the study of major granitic belts in Thailand (Beckinsale *et al.,* 1979; Mitchell, 1986), and easterly subduction was also tentatively supported by Barr *et al.* (2006). As noted above, the Sone & Metcalfe (2008) model, supported by the work of Meffre *et al.* (2008), also involves long-lived (Middle Devonian to Late Triassic) east-directed subduction of Palaeo-Tethys oceanic crust beneath the western margin of the Indochina Terrane, and assigns the Sukhothai Fold Belt an arc terrane origin, resulting from this subduction. An easterly dip of subducting Palaeo-Tethys beneath the Simao Terrane has also been proposed in SW Yunnan, to form the Jinghong magmatic arc in Middle to Late Triassic on the western side of the Simao Terrane (Okamura *et al.,* 1997; Sone & Metcalfe, 2008), but as noted by the latter authors, special pleading is required for east-directed subduction in southern Yunnan because thrusts sheets are west-dipping and indicate east-directed transport (Zhong & Dalai, 2000), just as they do in the southern part of the Simao Terrane and the Sukhothai Fold Belt in northern Thailand.

Models supporting west-dipping subduction have been proposed by numerous authors (Thanasuthipitak, 1978; Bunopas & Vella, 1978; Bunopas, 1981; Barr & Macdonald, 1991; Panjasawatwong, 1991; Chaodumrong, 1992; Singharajwarapan, 1994; Hada *et al.*, 1997; Metcalfe, 1999; Singharajwarapan & Berry, 2000), all of whom have regarded the Sukhothai Fold Belt as the eastern margin of the Shan-Thai Terrane, formed in a forearc – arc environment during westward subduction beneath the Shan-Thai Terrane of an ocean basin attached to the Indochina Terrane. Collisional suturing between the Shan-Thai and

Indochina terranes is argued, in these models, to have occurred along the Nan Suture in the Late Triassic.

A number of authors have proposed that the Shan-Thai and Indochina oceans were separated by an oceanic realm (Palaeo-Tethys) in which opposite-dipping subduction zones existed, one dipping west beneath Shan-Thai, the other eastward beneath Indochina (Gatinsky *et al.,* 1978; Thanasuthipitak, 1978; Bunopas, 1981; Bunopas & Vella, 1978; Cooper *et al.*, 1989; Hutchison, 1989).

6.3.2 Problems with Existing Tectonic Models

1: Polarity of Subduction during Closure of Palaeo-Tethys

Each of the models above, that is, east-dipping, west-dipping, or two opposite-dipping subduction zones, has problems or uncertainty attached to it. The key problem with those models involving east-dipping subduction is that structural transects along the central section of the Sukhothai Fold Belt along the Nan Suture area by Singharajwarapan & Berry (2000) and further north in Thailand (present study), and also in southern Yunnan (Zhong & Dalai, 2000) showed west-dipping structures that are difficult to relate to east-dipping subduction, and westerly dips to structures in this area are also supported by gravity and magnetic data across the Nan Suture Zone (Pacharapongsakun, 2006).

2: Location of the Magmatic Arc Related to Subduction of Palaeo-Tethys and Timing of Formation and Closure of the Nan Backarc Basin

Rapid northward movement of the Shan-Thai Terrane from cold sub-polar latitudes against Gondwana to warmer, sub-tropical latitudes probably took place in Mid- and Late Permian times (Mantajit, 1999; Metcalfe, 2002; Li *et al.,* 2004), although it may have commenced earlier. This rapid drift should correspond with subduction accommodating this convergence, although it is possible that this subduction was taking place north of the crustal blocks we are dealing with in Thailand and southern China, in the oceanic basin between the North- and South China Terranes (e.g., Metcalfe, 1999).

A major cause of the existing variability in the tectonic models for the mainland SE Asian region centres on the identification and dating of rocks that represent subduction-related arc-type magmatism. In particular, the presence of a well-defined belt of basalt-andesite-dacite-rhyolite rocks of mainly Late Permian age in the Loei Fold Belt (S. Meffre *pers comm.,* 2008), and a subparallel Middle to Late Triassic age belt of similar rocks further west forming the Chiang Khong-Lampang-Tak volcanic belt, has given rise to complex models of subduction polarity (notably the models involving two opposite-dipping subduction zones). What is the evidence for a Permian-Early Triassic arc in the region?

From published studies and work summarised in Meffre *et al.* (2008), there is enough evidence to suggest that a subduction-related magmatic arc is represented by the volcanics that form a broad crescent-shaped belt along the Loei Fold Belt. Although still not well constrained, with the arc constructed on folded Carboniferous volcanics and Carboniferous to Early Permian limestones (S. Meffre *pers. comm.*, 2008). Further west, in the Sukhothai Fold Belt, Singharajwarapan (1994) and Singharajwarapan & Berry (2000) described the Pak Pat Volcanics and the Doi Luang Volcanics in the Lampang – Phrae – Nan area. Both units have arc-type compositional ranges (mainly andesitic to rhyolitic), and include abundant volcaniclastic rocks. The Doi Luang Volcanics underlie the basal Lampang Group formations, making these volcanic rocks Latest Permian to Earliest Triassic, whereas the Pak Pat Volcanics are unconformably overlain by the Huai Lat Formation conglomerates, which are Early to Middle Triassic in age.

In addition to the volcanic rocks of Permian age as noted above, there are numerous reliable dates, including that of the granite studied from the Ban Huak area in this study, and also abundant detrital and inherited zircons documented herein, that give mainly Permian ages for intrusive and extrusive arc-like rocks across central and northern Thailand, including in the Loei Fold Belt, east of the Nan Suture, and across the Sukhothai Fold Belt. There are insufficient data at present to determine whether the volcanic front associated with this convergent plate boundary migrated over time, and there is certainly no reliable information that could constrain the orientation of the Permian subduction zone.

An on-going problem with identifying convergence and subduction-related magmatism in this region has been the tendency to relate any basalt-andesite-dacite-rhyolite suite to formation in a continental margin arc. Thus the Chiang Khong-Lampang-Tak volcanic belt in the central part of the Sukhothai Fold Belt, the focus of my study, has been regarded as being constituted by volcanic arc rocks associated with eastward subduction of Palaeo-Tethys beneath either the Indochina Terrane or a fragment of the latter rifted off during Permian opening of the Nan backarc basin (Barr *et al.,* 2000; Barr *et al.,* 2006; Singharajwarapan & Berry 2000; Panjasawatwong *et al.,* 2003). These Triassic volcanics have been correlated with similar-aged volcanic arc rocks in the Lincang – Jinhong volcanic belt in southern Yunnan in the Simao Terrane (Yang *et al.,* 1994; Barr *et al.,* 2000; Zhong & Dalai, 2000; Barr *et al.,* 2006). In contrast to such models, my study suggests that the Late Triassic volcanics are post-collisional, and unlikely to be associated with any contemporaneous subduction.

3: The Nan Backarc Basin – Timing of Opening and Closing

The recent tectonic model of Sone & Metcalfe (2008) suggested that east-directed subduction of Palaeo-Tethys oceanic crust commenced sometime before Early Permian and constructed the early phase of the 'Sukhothai island arc' on the (current) western side of the Indochina Terrane (Figure 6.1a). In their model, in the Earliest Permian, a fragment of this arc was rifted from the Indochina Terrane via opening of the 'Nan backarc basin' that existed throughout much of the Permian, but closed before Early Triassic. Fragments of this Permian backarc basin are found in the Nan Suture in Thailand, and in correlated extensions of this zone to the north, in the Jinghong Suture Zone in southern Yunnan, and to the south in the Sra Kaeo Suture in southern Thailand (Figure 6.2).

A number of authors (Ueno & Hisada, 2001; Wang *et al.,* 2000; Wakita & Metcalfe, 2005) have claimed or assumed that this backarc basin may have opened in the Carboniferous, but there is no evidence for the existence of Carboniferous oceanic basement or pelagic sediments along this suture zone. Panjasawatwong (1991) and Crawford & Panjasawatwong (1996) have shown that blocks in the serpentinite melange along the Nan Suture include both intra-oceanic arc and backarc basin rocks, both presently undated, but attesting to the existence of a West Pacific-type arc-backarc basin system at some time between the Shan-Thai and Indochina terranes, and its eventual incorporation into the collision zone.

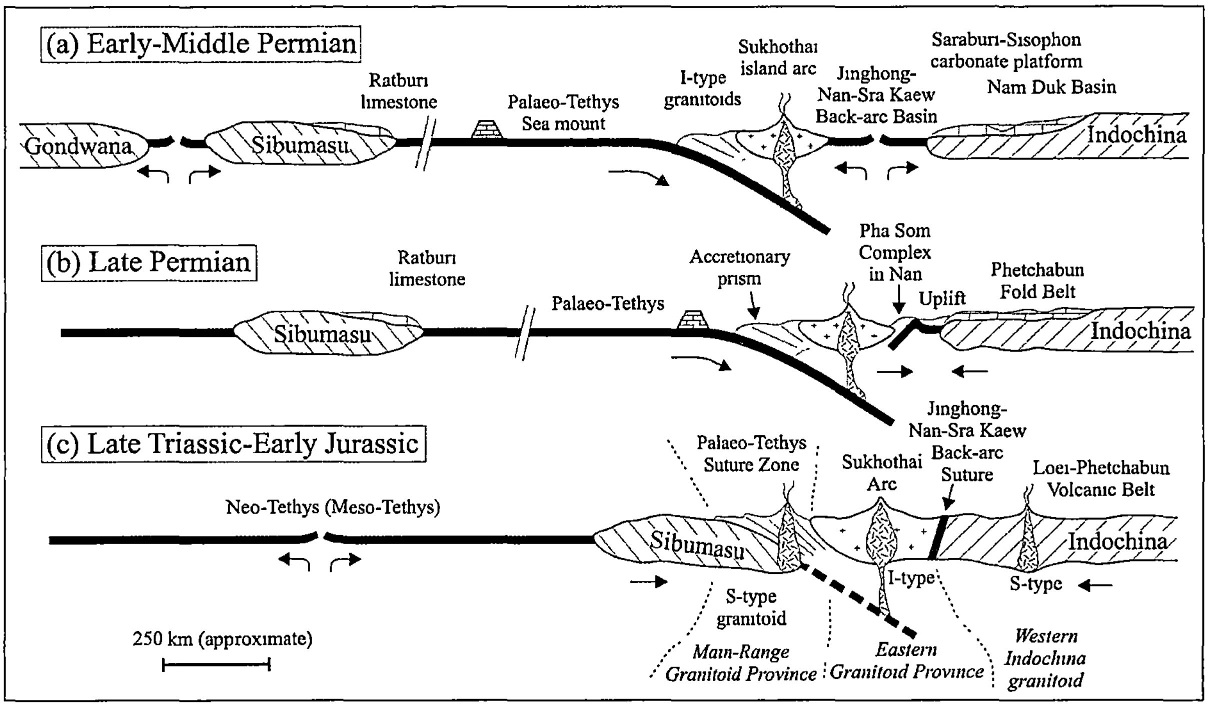

Figure 6.1 Tectonic evolution of mainland SE Asia during the Permian to Early Jurassic, with respect to the formations of the Palaeo-Tethys Suture Zone and the Jinghong-Nan-Sra Kaeo back-arc basin suture (after Sone & Metcalfe, 2008).

Closure of this backarc basin occurred in latest Permian (Figure 6.1b) according to Sone & Metcalfe (2008), whereas a recent U-Pb age of 296 Ma on metamorphic sphenes in a Nan Suture amphibolite suggest a possible Early Permian closure (Meffre *et al.,* 2008; S. Meffre *pers. comm.,* 2008). However, neither model provides any obvious tectonic mechanism or trigger (e.g., a collision event) for this closure, and furthermore, cherts with Late Permian radiolaria have been described from blocks in the Nan Suture melange (Ueno & Hisada, 2001), suggesting that this basin had not closed by this time. It is possible that the amphibolite that yielded these Early Permian ages is recording the scraping off of an intraplate seamount and its incorporation into the subduction complex at the margin of the Palaeo-Tethys, rather than dating the closure of the Nan backarc basin.

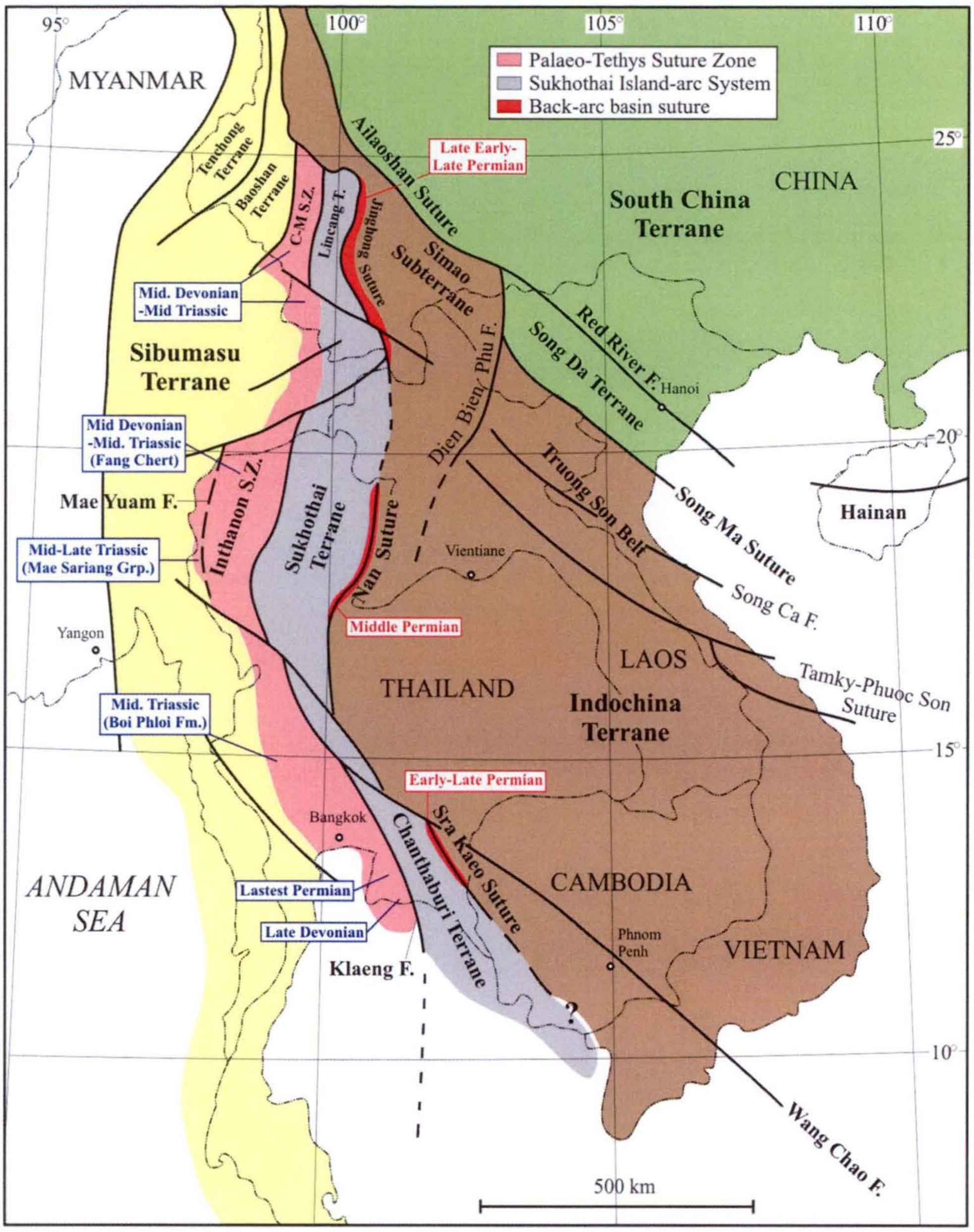

Figure 6.2 Proposed tectonic subdivision of mainland Southeast Asia (after Sone & Metcalfe, 2008), showing the Palaeo-Tethys Suture Zone (in blue) and back-arc sutures (in red). C-M S.Z. = Changning-Menglian Suture Zone.

In the Sone & Metcalfe (2008) model, following formation of the Nan Suture by closure of the Nan backarc basin, continued east-directed subduction led to a more continental flavour for the later (Triassic) Sukhothai arc rocks (including the CLT volcanic belt), and subduction of the remaining Palaeo-Tethys oceanic crust during much of the Triassic saw the Shan-Thai Terrane collide with the complex western margin of the Indochina Terrane around early Late Triassic. The Sone & Metcalfe (2008) model specifically refers to ‘the

Middle Triassic volcanics of the Lampang and Chiang Khong suites' as being a part of the continental margin arc developed along the western margin of the Indochina Terrane. The suture resulting from this collision, and closure of Palaeo-Tethys, is known as the Changning – Menglian – Inthanon Suture Zone, and crustal thickening led to generation of S-type granites through Late Triassic and Early Jurassic (230-180 Ma) and their emplacement in the Sukhothai Fold Belt and the accretionary complex associated with closure of this major ocean basin (Figure 6.1c). Post-collisional sedimentation of the Khorat Group covered a large part of the collision zone during Latest Triassic and Early Jurassic.

4: Shan-Thai - Indochina Collision? Where and When?

It is widely accepted that the Sukhothai Fold Belt and its extension as the Simao Terrane in southern Yunnan formed as a result of collision between the Indochina Terrane and the Shan-Thai Terrane. However, the timing of this collision remains poorly constrained, and, as noted in Chapter 2, has been claimed to be:

(1) Middle Permian (Helmcke, 1986; Burton, 1984; Sengor, 1984; Hahn, 1985; Barr & Macdonald, 1991),
(2) Late Permian to Early Triassic (Thanasuthipitak, 1978; Ridd, 1980; Metcalfe, 1986; Hayashi, 1988, Cooper *et al.*, 1989), and
(3) Late Triassic (Hutchison 1989; Mitchell 1986, 1992; Gatinsky et al. 1978; Macdonald & Barr, 1978; Bunopas & Vella, 1978, 1983; Panjasawatwong, 1991; Hada *et al.,* 1999; Singharajwarapan & Berry, 2000; Li *et al.,* 2004; Meffre *et al.,* 2008; Sone & Metcalfe, 2008)

Data from my study of the CLT volcanic belt suggest that these volcanic rocks are Late Triassic in age (not Middle Triassic as claimed by Sone & Metcalfe, 2008), and did not form in a continental margin arc as a result of subduction. Rather, they are interpreted to be a post-collisional magmatic suite erupted across a broad region (probably including similar aged and composition rocks in the Loei Fold Belt, and also in the Simao Terrane in southern Yunnan (Yang *et al.,* 1994; Barr *et al.,* 2000; Zhong & Dalai., 2000; Barr *et al.,* 2006). The volcanics erupted during extension consequent upon the Late Middle Triassic collision of the Indochina and Shan-Thai terranes.

6.4 Conclusions - A New Tectonic Model for the Northern Thailand Region

A major problem in the unravelling of the tectonic history of this region, as noted above, centres on the orientation and duration of subduction events. There appears to be increasing support for long-lived east-directed subduction (Sone & Metcalfe, 2008; Meffre *et al.,* 2008). However, the widespread west-dipping thrusts and east-directed transport in the Sukhothai Fold Belt and Simao Terrane further north are difficult to accommodate in such a scenario, which would predict east-dipping structures and west-vergent transport as the leading edge of the Shan-Thai Terrane was subducted beneath the Indochina Terrane. Perhaps a simple answer to this apparent problem is that the west-dipping structures in the Sukhothai Fold Belt – Simao Terrane are actually backthrusts, formed where the collision belt abuts the strong buttress of the Indochina Terrane (Figure 6.3).

Figure 6.3 shows a possible sequence of events that led to construction of the continental crust in the Thailand region of mainland SE Asia.

1: West-directed subduction during the Permian within the ocean basin between the Indochina and Shan-Thai terranes produced a typical West Pacific-type intra-oceanic arc-backarc basin system (Figure 6.3a).

2: Eventual closure of this segment of ocean led to collision of the arc system with the leading (western) edge of Indochina, perhaps in the Late Permian. By analogy with arc-continent collisions such as are well preserved in New Caledonia (Eissen *et al.*, 1998; Crawford *et al.*, 2003), this collision would have emplaced one or more large nappes of forearc rocks on to the underthrust thinned continental crust of the Indochina Terrane (Figure 6.3b).

3: Following locking of the plate boundary by this collision event, continued convergence between the Indochina Terrane and the Shan-Thai Terrane led to a subduction reversal, to east-directed subduction beneath the Indochina Terrane (Figure 6.3c). A similar flip in subduction polarity is well demonstrated in the SW Pacific following arc-(micro) continent collision (Crawford *et al.*, 2003).

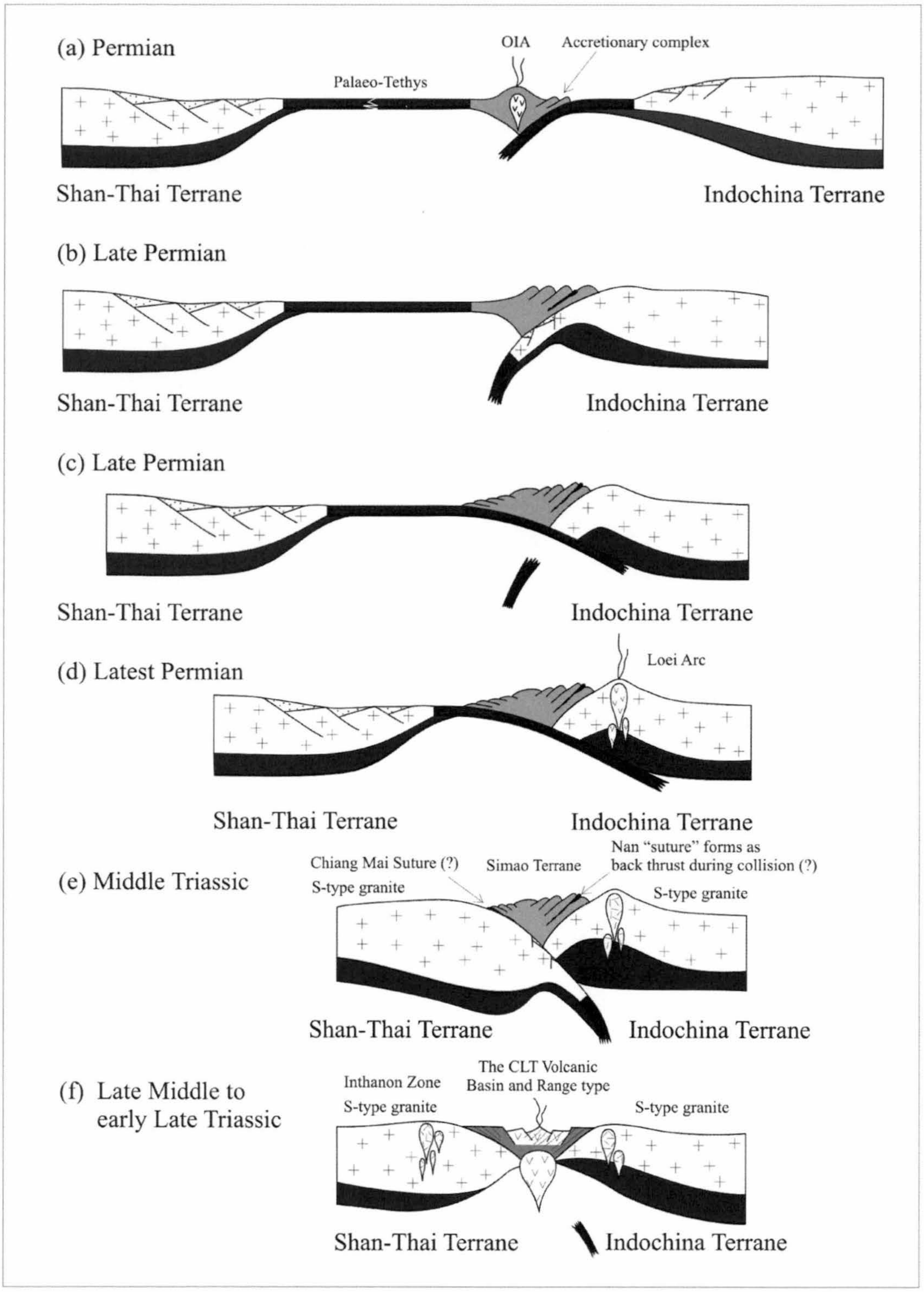

Figure 6.3 Schematic model for tectonic evolution of northern Thailand and neighbouring areas during Permian to Late Triassic (see text for discussion). Note, OIA is ocean island Arc.

4: Ongoing Latest Permian east-directed subduction led to construction of the Loei arc on the western edge of the Indochina Terrane (Figure 6.3d), then to arrival of the leading edge of the Shan-Thai Terrane at the trench, and a Middle Triassic continent-continent collision (Figure 6.3e), which thoroughly reworked and restructured the fold belt formed in the earlier arc-continent collision. Although such an event is expected to generate east-dipping thrusts over much of the area affected by the collision, backthrusting of the older fold belt collage against the buttress of the Indochina Terrane may have produced the widespread west-dipping structures over much of the Sukhothai Fold Belt and Simao Terrane.

5: Relaxation rifting and gravitational collapse of the new crustal collage in Late Triassic led to post-collisional calc-alkaline magmatism of the Chiang Khong – Lampang – Tak Volcanic Belt, and subsequent deposition of the Lampang Group (Figure 6.3f).

6. A final compressional event in the Latest Triassic formed the thin skinned structural style with west-dipping thrusts that dominate the Sukhothai Fold Belt, and disrupted the original extent of the CLT to form the existing CLT sub-belts. Although poorly constrained, this deformation may have been due to further tightening or 'locking up' of the Shan-Thai – Indochina suture zone.

7. Deposition of Khorat Group molasses over the collision zone.

6.5 Suggestions for Further Study

There are numerous opportunities for future studies to test and improve the current tectonic models for the northern Thailand region. Among these, the following are important:

1: Carry out structural transects of the Inthanon Suture west of Chiang Mai – Chiang Rai, and its possible southern continuation as the Sra Kaeo Suture on the Gulf of Thailand to check for the predicted east-dipping structures required by those models that invoke east-dipping subduction before Mid Triassic closure of Palaeo-Tethys.

2: Carry out a careful geochronological and geochemical study of the blocks in the Nan, Inthanon and Sra Kaeo sutures in Thailand, and the Bentong-Raub Suture in Malaysia, to better constrain timing of collision and the nature of the component crustal blocks that were involved.

3: Compare data evolving from 1 and 2 above with new data emerging from the southern Yunnan section of the same crustal provinces that are exposed in northern Thailand, to provide a more comprehensive and regionally extensive understanding of the complex geology of this region.

REFERENCES

Ahrendt, H., Chonglakmani, C., Hansen, B.T. and Helmcke, D., 1993, Geochronological cross section through northern Thailand, Journal of Southeast Asian Earth Sciences, v. 8, p. 207-217.

Asanachinda, P., 1978, The mineralization in the Burmese-Malayan Peninsula-a plate tectonic model, *in*: Nutalaya, P., ed., Proceedings of the Third Regional Conference on Geology and Mineral Resources of Southeast Asia, Bangkok, p. 293-299.

Barr, S.M. and Macdonald, A.S., 1981, Geochemistry and geochronology of Late Cenozoic basalts of Southeast Asia, Geological Society of America Bulletin, v. 92, p. 1069-1142.

Barr, S.M. and Macdonald, A.S., 1987, Nan River suture zone, northern Thailand, Geology, v. 15, p. 907-910.

Barr, S.M. and Macdonald, A.S., 1991, Toward a late Paleozoic-early Mesozoic tectonic model for Thailand, Journal of Thai Geosciences, v. 1, p. 11-22.

Barr, S.M., Macdonald, A.S., Dunning, G.R., Ounchanum, P. and Yaowanoiyothin, W., 2000, Petrochemistry, U-Pb (zircon) age, and palaeotectonic setting of the Lampang volcanic belt, northern Thailand, Journal of the Geological Society, London, v. 157, p. 553-563.

Barr, S.M., Macdonald, A.S., Ounchanum, P. and Hamilton, M.A., 2006, Age, tectonic setting and regional implications of the Chiang Khong volcanic suite, northern Thailand, Journal of the Geological Society, London, v. 163, p. 1037-1046.

Barr, S.M., Tantisukrit, C., Yaowanoiyothin, W. and Macdonald, A.S., 1990, Petrology and tectonic implications of Upper Paleozoic volcanic rocks of the Chiang Mai belt, northern Thailand, Journal of Southeast Asian Earth Sciences, v. 4, p. 37-47.

Beckinsale, R.D., Suensilpong, S. and Nakapadungrat, S., 1979, Geochronology and geochemistry of granite magmatism in Thailand in relation to plate tectonic model, Journal of Geological Society, London, v. 136, p. 529-540.

Benammi, M., Urrutia-Fucugauchi, J., Alva-Valdivia, L.M., Chaimanee, Y., Tiamwichanon, S. and Jaeger, J-J., 2002, Magnetostratigraphy of the Middle Miocene continental sedimentary sequences of the Mae Moh Basin in northern

Thailand: evidence for counterclockwise block rotation, Earth and Planetary Sciences Letters, v. 204, p. 373-383.

Berry, R.F., Chmielowski, R.M., Steele, D.A. and Meffre, S., 2007, Chemical U-Th-Pb monazite dating of the Cambrian Tyannan Orogeny, Tasmania, Australian Journal of Earth Sciences, v. 54, p. 757-771.

Black, L. P., Kamo, S.L., Allen, C.M., Aleinikoff, J.N., Davis, D.W., Korsch, R.J. and Foudoulis, C., 2003, TEMORA 1: a new zircon standard for Phanerozoic U–Pb geochronology, Chemical Geology, v. 200, p. 155– 170.

Braun, E.V. and Hahn, L., 1976, Geological map of northern Thailand, scale 1: 250,000, sheet 2 (Chiang Rai), Federal Institute for Geosciences and Natural Resources, Hanover.

Bryan, S.E., 2007, Silicic Large Igneous Provinces, Episodes, v. 30, p. 20-31.

Bryan S.E., Constantine, A.E., Stephens, C.J., Ewart, A., Schon, R.W. and Parianos, J., 1997, Early Cretaceous volcano-sedimentary successions along the eastern Australian continental margin: Implications for break-up of eastern Gondwana, Earth and Planetary Science Letters, v. 153, p. 85-102.

Bryan, S.E., Ewart, A., Stephens, C.J., Parianos, J. and Downers, P.J., 2000, The Whitsunday Volcanic Province, central Queensland, Australia: Lithological and stratigraphic investigations of a silicic-dominated large igneous province, Journal of Volcanology and Geothermal Research, v. 99, p. 55-78.

Bunopas, S., 1981, Paleogeographic History of Western Thailand and Adjacent Parts of South-East Asia – A Plate Tectonic Interpretation, unpublished PhD thesis, Victoria University of Wellington, 810 p.

Bunopas, S. and Vella, P., 1978, Late Paleozoic and Mesozoic structural evolution of northern Thailand: a plate tectonic model, *in*: Nutalaya, P., ed., Proceedings of the Third Regional Conference on Geology and Mineral Resources of Southeast Asia, Bangkok, p. 133-140.

Bunopas, S. and Vella, P., 1983, Tectonic and geologic evolution of Thailand, *in*: Nutalaya, P., ed., Proceeding of the Workshop on Stratigraphic Correlation of Thailand and Malaysia, Haad Yai, p. 307-322.

Burrett, C.F. and Stait, B., 1985, South East Asia as a part of an Ordovician Gondwanaland-a palaeobiogeographic test of a tectonic hypothesis, Earth and Planetary Science Letters, v. 75, p. 184-190.

Burrett, C.F. and Stait, B., 1986, Southeast Asia as a part of an early Palaeozoic Gondwanaland, Geological Society of Malaysia Bulletin, v. 19, p. 103-107.

Burton, C.K., 1984, The tectonic framework of mainland Southeast Asia, *in:* Proceedings of the Conference on Applications of Geology and National Development, Chulalonkorn University, Bangkok, p. 255-266.

Bussy, F., Hernandez, J. and von Raumer, J., 2000, Bimodal magmatism as a consequence of post-collisional readjustment of the thickened Variscan continental lithosphere (Aiguilles-Rouge and Mont-Blanc massifs, Western Alps), Transactions of the Royal Society of Edinburgh, Earth Sciences, v. 91, p. 221-233.

Caridoit, M., 1993, Permian radiolaria from NW Thailand, *in*: Thanasuthipitak, T., ed., Proceedings of the International Symposium on Biostratigraphy of Mainland Southeast Asia: Facies and Paleontology, Chiang Mai, p. 83–91.

Chantraramee, S., 1978, Tectonic synthesis of Lansang area and discussion of regional tectonic evolution, *in*: Nutalaya, P., ed., Proceedings of the Third Regional Conference on Geology and Mineral Resources of Southeast Asia, Bangkok, p. 177-186.

Chaodumrong, P., 1992, Sedimentology of Triassic Lampang Group, Northern Thailand, unpublished PhD thesis, University of Tasmania, 230 p.

Chaodumrong, P. and Burrett, C.F., 1997, Early Late Triassic continental colliding between Shan-Thai and Indochina terranes as indicated by occurrence of fan delta red beds of Pha Daeng Formation, central north Thailand, *in*: Dheeradilok, P., Hinthong, C., Chadumrong, P., Putthapiban, P., Tansathien, W., Utha-aroon, C., Sattayarak, N., Nuchanong, T. and Techawan, S., eds., Proceeding of the International Conference on Stratigraphy and Tectonic Evolution of Southeast Asia and the South Pacific, Bangkok, p. 143-157.

Charoenprawat, A., Chuavirot, S., Hinthong, C. and Chonglakmani, C., 1994, Geologic Map of Changwat Lampang 1: 250,000, Geological Survey Division, Department of Mineral Resources, Bangkok, Thailand.

Charusiri, P., Chonglakmani, C., Doarerk, V., Supananthi, S. and Imsamut, S., 1994, Detailed stratigraphy of the Ban Thasi area, Lampang, northern Thailand: implication for paleoenvironments and tectonic history, *in*: Angsuwathana, P., Wongwanich, T., Tansthien, W., Wongsomsak, S. and Tulyatid, J., eds., Proceeding of the International Symposium on Stratigraphic Correlation of Southeast Asia, Department of Mineral Resources, Bangkok, p. 226-244.

Charusiri, P., Clark, A.H., Farrar, E., Archibald, D. and Charusiri, B., 1993, Granite belts in Thailand: evidence from the $^{40}Ar/^{39}Ar$ geochronological and geological syntheses, Journal of Southeast Asian Earth Sciences, v. 8, p. 127-136.

Chuaviroj, S., Chaturongkawanich, S. and Sukawattananan, P., 1980, Geology of geothermal resources of northern Thailand (Part I, San Kamphaeng), unpublished report of Geological Survey Division, Department of Mineral Resources, Bangkok, Thailand, p. 45.

Cobbing, E.J., Mallick, D.I.J., Pitfield, P.E.J. and Teoh, L.H., 1986, The granites of SE Asian Tin Belt, Journal of Geological Society of London, v. 143, p. 537-550.

Cooper, M.A., Herbert, R. and Hill, G.S., 1989, The structural evolution of Triassic intermontane basin in northeastern Thailand, *in*: Thanasuthipitak, T. and Ounchanum, P., eds., Proceeding of the International Symposium on Intermontane Basins: Geology and Resources, Chiang Mai, p. 231-242.

Corfu, F., Hanchar, J.M., Hoskin, P.W.O. and Kinny, P., 2003, Atlas of zircon textures, *in*: Hanchar J.M. and Hoskin, P.W.O., eds., Zircon, Reviews in Mineralogy and Geochemistry, v. 53, p. 469–500.

Crawford, A.J. and Berry, R.F., 1992, Tectonic implications of Late Proterozoic-Early Palaeozoic igneous rock associations in western Tasmania, Tectonophysics, v. 214, p. 37-56.

Crawford, A.J. and Panjasawatwong, Y., 1996, Ophiolite, ocean crust, and the Nan suture in NE Thailand, *in*: Lee, T.-Y., ed., Program and Extended Abstract of the International Symposium on Lithosphere Dynamics of East Asia, Taipei, p. 38.

Crawford, A.J., Corbett, K.D. and Everard, J., 1992, Geochemistry of the Cambrian volcanic-hosted massive sulfide-rich Mount Read Volcanics, Tasmania, and some tectonic implications, Economic Geology, v. 87, p. 597-619.

Crawford, A.J., Meffre, S. and Symonds, P., 2003, 120 to 0 Ma tectonic evolution of the southwest Pacific and analogous geological evolution of the 600 to 200 Ma Tasman Fold Belt System, *in:* Hillis, R.R. & Muller, R.D., eds., Evolution and Dynamics of the Australian Plate, Geological Society of Australian Special Publication, v. 22, p. 377-397.

Davis, J.H. and von Blanckenburg, F., 1995, Slab breakoff: A model of lithosphere detachment and its test in the magmatism and deformation of collisional orogens, Earth and Planetary Science Letters, v. 129, p. 85-102.

Eissen, J.-P., Crawford, A.J., Cotton, J., Meffre, S., Bellon, H. and Delaune, M., 1998, Geochemistry and tectonic significance of basalts in the Poya Terrane, New Caledonia, Tectonophysics, v. 284, p. 203-219.

England, P.C. and Houseman, G.A., 1989, Extension during continental convergence, with application to the Tibetan Plateau, Journal of Geophysical Research, v. 94, p. 17561-17579.

Ewart, A., Schon, R.W. and Chappell, B.W., 1992, The Cretaceous volcanic-plutonic province of the central Queensland (Australia) coast – a rift related 'calc-alkaline' province, Transactions of the Royal Society of Edinburgh, Earth Sciences, v. 83, p. 327-345.

Fan, W.M., Guo, F., Wang, Y.J. and Lin, G., 2003, Late Mesozoic calc-alkaline volcanism of post-orogenic extension in the northern Da Hinggan Mountains, northeastern China, Journal of Volcanology and Geothermal Research, v. 121, p. 115-135.

Fan, W.M., Guo, F., Wang, Y.J., Lin, G. and Zhang, M., 2001, Post-orogenic bimodal volcanism along the Sulu orogenic belt in eastern China, Physics and Chemistry of the Earth, v. 26, p. 733-746.

Feng, Q., 2002, Stratigraphy of volcanic rocks in the Changning-Menglian Belt in southwestern Yunnan, China, Journal of Asian Earth Sciences, v. 20, p. 657-664.

Feng, Q., Chonglakmani, C., Helmcke, D., Ingavat-Helmcke, R. and Liu, B., 2005, Correlation of Triassic stratigraphy between the Simao and Lampang-Phrae Basins: implications for the tectonopaleogeography of Southeast Asia, Journal of Asian Earth Sciences, v. 24, p. 777-785.

Fenton, C.H., Charusiri, P., Hintong, C., Lumjuan, A. and Mongkonkarn, B., 1997, Late Quaternary faulting in northern Thailand, *in*: Dheeradilok, P., Hinthong, C., Chaodumrong, P., Putthapiban, P., Tansathien, W., Utha-aroon, C., Sattayalak, N., Nuchanong, T. and Techawan, eds., Proceedings of International Conference on Stratigraphy and Tectonic Evolution of Southeast Asia and the South Pacific, Bangkok, p. 436-452.

Gatinsky, Y.G., Mischina, A.V., Vinogradov, I.V. and Kovalev, A.A., 1978, The main metallogenic belts of Southeast Asia as the result of different geodynamic conditions interference, *in*: Nutalaya, P., ed., Proceedings of the Third Regional Conference on Geology and Mineral Resources of Southeast Asia, Bangkok, p. 313-318.

GEOROC database, http://georoc.mpch-mainz.gwdg.de/georoc/

Gill, J.B. 1981, Orogenic Andesites and Plate Tectonics, Springer-Verlag, New York, 390 p.

Hada, S., Bunopas, S., Ishii, K. and Yoshikura, S., 1999, Rift-drift history and the amalgamation of Shan-Thai and Indochina/East Malaya blocks, *in*: Metcalfe, I., Jishun, I., Charvet, J. and Hada, S., eds., Gondwana Dispersion and Asian Accretion, Final Results Volume for IGCP 321, A.A. Balkerma, Rotterdam, p. 67-87.

Hada, S., Bunopas, S., Salyapong, S., Thitisawan, V., Panjasawatwong, Y., Yaowanoiyothin, W., Ishii, K. and Yoshikura, S., 1991, Terrane analysis and tectonics of the Nan-Chanthaburi suture zone, Abstracts of the Seven Regional Conference on Geology, Mineral and Energy Resources of Southeast Asia, Geological Society of Thailand, Bangkok, p. 40-41.

Hahn, L., 1985, The Indosinian orogeny in Thailand and adjacent areas, Memories de la Societe Geologique de France 147, p. 71-82.

Hanmer, S. and Passchier, C., 1991, Shear-sense Indicators: a Review, Geological Survey of Canada, paper no. 90-17, 72 p.

Harley, S.L. and Kelly, N.M., 2007, Zircon: Tiny but Timely, Elements, v. 3, p. 13-18.

Hawkesworth, C., Turner, S., Gallagher, K., Hunter, A., Bradshaw, T. and Rogers, N., 1995, Calc-alkaline magmatism, lithospheric thinning and extension in the Basin and Range, Journal of Geophysical Research, v. 100, p. 10271-10286.

Hayashi, M., 1989, The hydrocarbon potential and tectonics of Indochina, Geological Society of Malaysia Bulletin, v. 225, p. 65-78.

Helmcke, D., 1982, On the Variscan evolution of central mainland Southeast Asia, Earth Evolution Science, v. 4, p. 309-319.

Helmcke, D., 1985, The Permo-Triassic Paleotethys in mainland Southeast Asia and adjacent parts of China, Geologiche Rundschau, v. 74, p. 215-228.

Helmcke, D., 1986, On the geology of Petchabun Fold-Belt (Central Thailand)-implications for the geodynamic evolution of Mainland SE Asia, Geological Society of Malaysia Bulletin, v. 19, p. 79-85.

Helmcke, D. and Kraithong, C., 1982, On the geosynclineal and geological evolution of central and northeastern Thailand, Journal of the Geological Society of Thailand, v. 5, p. 52-74.

Helmcke, D. and Lindenberg, H.G., 1983, New data on the Indosinian orogeny from central Thailand, Geologiche Rundschau, v. 72, p. 317-328.

Heppe, K., Helmcke, D. and Wemmer, K, 2007, The Lancang River Zone of southwestern Yunnan, China: A questionable location for the active continental margin of Paleotethys, Journal of Asian Earth Sciences, v. 30, p. 706-720.

Hess, A. and Koch, K.E., 1979, Geologic Map of Northern Thailand, scale 1: 250,000, sheet 4 (Chiang Dao), Federal Institute for Geosciences and Natural Resources, Hanover.

Hisada, K., Sugiyama, M., Ueno, K., Charusiri, P. and Arai, S., 2004, Missing ophiolitic rocks along the Mae Yuam Fault as the Gondwana-Tethys divide in north-west Thailand, Island Arc, v. 13, p. 119-127.

Hooper, P.R., Bailey, D.G. and McCarley Holder G.A., 1995, Tertiary calc-alkaline magmatism associated with lithospheric extension in the Pacific Northwest, Journal of Geophysical Research, vol. 100, p. 10303-10319.

Humphreys, E.D., 1995, Post-Laramide removal of the Farallon slab, western USA, Geology, v. 23, p. 987-990.

Hutchison, C.S, 1975, Ophiolite in Southeast Asia, Geological Society of America Bulletin, v. 86, p. 797-806.

Hutchison, C.S., 1989, Geological Evolution of Southeast Asia, Claredon Press, Oxford, 368 p.

Intasopa, S., 1993, Petrology and Geochronology of the Volcanic Rocks of the Central Thailand Volcanic Belt, unpublished PhD thesis, University of New Brunswick, 242 p.

Intasopa, S. and Dunn, T., 1994, Petrology and Sr-Nd isotopic system of the basalts and rhyolites, Loei, Thailand, Journal of Southeast Asian Earth Sciences, v. 9, p. 167-180.

Jarosewich, E. and Boatner, L.A., 1991, Rare-earth element reference samples for electron microprobe analysis, Geostandards Newsletter, v. 15, p. 397-399.

Jungyusuk, N and Khositanont, S., 1992, Volcanic rocks and associated mineralization in Thailand, *in*: Piencharoen, C., ed., Proceedings of the National Conference on Geologic Resources of Thailand – Potential for Future Development, Bangkok, p. 528-532.

Kobayashi, F., Martini, R., Rettori, R., Zanienetti, L., Ratanasthien, B., Saegusa, H. and Nakaya, H., 2006, Triassic foraminifers of the Lampang Group (northern Thailand), Journal of Asian Earth Sciences, v. 27, 312-325.

Kosuwan, P., 2004, Petrochemistry and Tectonic Setting of Mafic Volcanic Rocks in the Klong Tha Dan Dam Area, Nakhon Nayok Province, Thailand, unpublished MS thesis, Chiang Mai University, 95 p.

Lacassin, R., Maluski, H., Leloup, P.H., Tapponnier, P., Hinthong, C., Siribhakdi, K., Chuaviroj, S. and Charoenpravat, A., 1997, Tertiary diachronic extrusion and deformation of western Indochina: Structural and $^{40}Ar/^{39}Ar$ evidence from NW Thailand, Journal of Geophysical Research, v. 102, p. 10013-10037.

Leloup, P.H., Arnaud, N., Lacassin, R., Kienast, J.R., Harrison, T.M., Phan Trong, T.T., Replumaz, A. and Tapponnier, P., 2001, New constraints on the structure, thermochronology, and timing of the Ailao Shan-Red River shear zone, SE Asia, Journal of Geophysical Research, v. 106, p. 6683-6732.

Leloup, P.H., Lacassin, R., Tapponnier, P., Scharer, U., Dalai, Z., Xiaohan, L., Liangshang, Z., Shaocheng, J. and Trinh, P.T., 1995, The Ailao Shan-Red River shear zone (Yunnan, China), Tertiary transform boundary of Indochina, Tectonophysics, v. 251, p. 3-84.

Li, P., Rui, G., Junwen, C. and Ye, G., 2004, Paleomagnetic analysis of eastern Tibet: implications for the collisional and amalgamation history of the Three Rivers Region, SW China, Journal of Asian Earth Sciences, v. 24, p. 291-310.

Li, Z.-X. and Li, X.-H., 2007, Formation of the 1300-km-wide intracontinental orogen and postorogenic magmatic province in Mesozoic South China: a flat-slab subduction model, Geology, vol. 35, p.179-182.

Limptrakun, P., Panjasawatwong, Y., Buasamlee, N., Boonsoong, A., Srithai, B. and Srichan, W., 2005, Petrology and geochemistry of Late Cenozoic basalts from Long District, Phrae Province, northern Thailand, *in*: Wannakao, L., Youngme, W., Srisuk, K. and Lertsirivorakul, K., eds., Proceeding of the International Conference on Geology, Geotechnology and Mineral Resources of Indochina (GEO-INDO'2005), Khon Kaen, Thailand, p. 352-357.

Ludwig, K.R., 1998, ISOPLOT/Ex, A Geochronological Toolkit for Microsoft Excel, Email: kludwig@bgc.org

Ludwig, K.R., 2003, Isoplot 3.0: A Geochronological Toolkit for Microsoft Excel, Berkeley Geochronology Center Special Publication, no. 4, 70 p.

Macdonald, A.S and Barr, S.M., 1978, Tectonic significance of a Late Carboniferous volcanic arc in northern Thailand, *in*: Nutalaya, P., ed., Proceedings of the Third Regional Conference on Geology and Mineral Resources of Southeast Asia, Bangkok, p. 151-156.

Mantajit, N, 1999, Thailand and Tethys sea, *in:* Ratanasthien, B. and Rieb, S.L., eds., Proceedings of the International Symposium on Shallow Tethys (ST) 5, Chiang Mai, p. IX.

Marshak, S. and Wilkerson, M.S., 2004, Fold-thrust Belts – an essay, *in*: Van der Pluijm, B. A. and Marshak, S., eds., Earth Structure, Norton & Company, Inc., New York, p. 444-474.

McClay, K.R., 2000, The Mapping of Geological Structure, John Wiley & Sons, London, 161 p.

Meffre, S., Khin Zaw and Khositanont, S., 2008, Tectonic implications of Early Permian metamorphism along the Nan-Uttaradit Fault Zone, Thailand, *in*: Abstract of the International Conference of the Tectonic of Northwest Indochina Region, Chiang Mai, p. 21.

Metcalfe, I., 1988, Origin and assembly of Southeast Asia continental terranes, *in*: Audley-Charles, M.G. and Hallam, A., eds., Gondwana and Tethys, Geological Society Special Publication, no. 37, p. 101-118.

Metcalfe, I., 1994, Gondwanaland origin, dispersion, and accretion of East and Southeast Asian continental terranes, Journal of South American Earth Sciences, v. 7, p. 333-347.

Metcalfe, I., 1996a, Pre-Cretaceous evolution of SE Asian terranes, *in*: Hall, R. and Blundell, D., eds., Tectonic Evolution of Southeast Asia, Geological Society Special Publication, no. 106, p. 97-122.

Metcalfe, I., 1996b, Gondwanaland dispersion, Asian accretion and evolution of Eastern Tethys, Australian Journal of Earth Sciences, v. 43, p. 605-623.

Metcalfe, I., 1998, Paleozoic and Mesozoic geological evolution of SE Asian region: multidisciplinary constraints and implications for biogeography, *in*: Hall, R. and Holloway, J.D., eds., Biogeography and Geological Evolution of SE Asia, Backhuys Publishers, Amsterdam, p. 25-41.

Metcalfe, I., 1999, Gondwana dispersion and Asian accretion: an overview, *in*: Metcalfe, I., Jishun, I., Charvat, J. and Hada, S., eds., Gondwana Dispersion and Asia

Accretion, Final Results Volume for IGCP 321, A.A. Balkerma, Rotterdam, p. 9-28.

Metcalfe, I., 2000, The Bentong-Raub suture zone, Journal of Asian Earth Sciences, v. 18, p. 691-712.

Metcalfe, I., 2002, Permian tectonic framework and paleography of SE Asia, Journal of Asian Earth Sciences, vol. 20, p. 551-566.

Metcalfe, I., 2006, Palaeozoic and Mesozoic tectonic evolution and palaeogeography of East Asian crustal fragments: The Korean Peninsula in context, Gondwana Research, v. 9, p. 24-46.

Mezger, K. and Krogstad, E.J., 1997, Interpretation of discordant U-Pb zircon ages: An evaluation, Journal of Metamorphic Geology, v. 15, p. 127-140.

Miller, C.F. and Mittlefehldt, D.W., 1982, Depletion of light rare earth elements in felsic magma, Geology, v. 10, p. 129-133.

Mitchell, A.H.G., 1986, Mesozoic and Cenozoic regional tectonics and metallogenesis in Mainland SE Asia, Geological Society of Malaysia Bulletin, v. 20, p. 221-239.

Mitchell, A.H.G., 1992, Late Permian-Mesozoic events and the Mergui Group nappe in Myanmar and Thailand, Journal of Southeast Asian Earth Sciences, v. 7, p. 165-178.

Miyashiro, A., 1994, Metamorphic Petrology, UCL Press, London, 404 p.

Miyashiro, A., 1974, Volcanic rocks series in island arcs and active continental margins, American Journal of Science, vol. 274, p. 321-355.

Montel, J.-M., Foret, S., Veschambre, M., Nicollet, C. and Provost, A., 1996, Electron microprobe dating of monazite, Chemical Geology, v. 131, p. 37-53.

Morley, C.K., 2002, A tectonic model for the Tertiary evolution of strike-slip faults and rift basins in SE Asia, Tectonophysics, v. 347, p. 189-215.

Morley, C.K., 2004, Nested strike-slip duplexes, and other evidence for Late Cretaceous-Palaeogene transpressional tectonics before and during India-Eurasia collision, in Thailand, Myanmar and Malaysia, Journal of the Geological Society, London, v. 161, p. 799-812.

Morley, C.K., 2007, Variations in Late Cenozoic-Recent strike-slip and oblique-extensional geometries, within Indochina: The influence of pre-existing fabrics, Journal of Structural Geology, v. 29, p. 36-58.

Okamura, S., Wu, G.Y., Zhao, C.H., Kagami, H., Yoshida, Y. and Kawano, Y., 1997, Geochemistry of Mesozoic intracontinental basalts from Yunnan, southern China:

implications for geochemical evolution of the subcontinental lithosphere, Mineralogy and Petrology, v. 60, p. 81-98.

Osataporn, P., 2007, Petrochemistry and Tectonic Setting of Late Triassic-Early Jurassic Mafic Volcanic Rocks, Long District, Phrae Province, Thailand, unpublished MS thesis, Chiang Mai University, 107 p.

Pacharapongsakun, N., 2006, Structure of Crust and Upper Mantle Beneath Northern Thailand: a Model from Gravity and Magnetic Data, unpublished MS thesis, Chiang Mai University, 107 p.

Panjasawatwong, Y., 1991, Petrology, Geochemistry and Tectonic Implications of Igneous Rocks in the Nan Suture, Thailand, and an Empirical Study of the Effects of Ca/Na, Al/Si and H_2O on Plagioclase-Melt Equilibria at 5-10 kb Pressure, unpublished PhD thesis, University of Tasmania, 239 p.

Panjasawatwong, Y., 1999, Petrology and tectonic setting of eruption of basaltic rocks penetrated in well GTE-1, San Kam Phaeng geothermal field, Chiang Mai, northern Thailand, *in*: Ratanasthien, B. and Rieb, S.L., eds., Proceedings of the International Symposium on Shallow Tethys (ST) 5, Chiang Mai, p. 242-264.

Panjasawatwong, Y. and Youngsanaong, M., 1996, Chiang Khong corundum-bearing basalts, Amphoe Chiang Khong, Changwat Chiang Rai, Journal of Science Faculty, Chiang Mai University, v. 23, p. 39-52.

Panjasawatwong, Y., Chantaramee, S., Limtrakun, P. and Pirarai, K., 1997, Geochemistry and tectonic setting of eruption of central Loei volcanics in the Pak Chom area, Loei, northeast Thailand, *in*: Dheeradilok, P., Hinthong, C., Chaodumrong, P., Putthapiban, P., Tansathien, W., Utha-aroon, C., Sattayalak, N., Nuchanong, T. and Techawan, eds., Proceedings of International Conference on Stratigraphy and Tectonic Evolution of Southeast Asia and the South Pacific, Bangkok, p. 287-302.

Panjasawatwong, Y., Kanpeng, K. and Ruangvatanasirikun, K., 1995, Basalts in Li basin, northern Thailand: Southern extension of Chiang Mai volcanic belt, *in*: Thanvarachorn, S., Hokjaroen, S. and Youngme, W., eds., Proceedings of the International Conference on Geology, Geotechnology and Mineral Resources of Indochina (GEO-INDO'95), Khon Kaen, p. 225-234.

Panjasawatwong, Y., Khin Zaw, Chantaramee, S., Limptrakun, P. and Pirarai, K., 2006, Geochemistry and tectonic setting of the central Loei volcanic rocks, Pak Chom area, Loei, northeast Thailand, Journal of Asian Earth Sciences, v. 26, p. 77-90.

Panjasawatwong, Y., Phajuy, B. and Hada, S., 2003, Tectonic setting of the Permo-Triassic Chiang Khong volcanic rocks, northern Thailand based on petrochemical characteristics, Gondwana Research, v. 6, p. 743-755.

Peccerillo, A. and Taylor, S.R., 1976, Geochemistry of Eocene calc-alkaline volcanic rocks from the Kastamonu Area, northern Turkey, Contributions to Mineralogy and Petrology, v. 58, p. 63-81.

Phajuy, B., 2001, Geochemistry, Petrology and Tectonic Setting of Permo-Triassic Mafic Volcanic Rocks in the Northern Part of Chiang Khong-Tak Volcanic Belt, unpublished MS thesis, Chiang Mai University, 112 p.

Phajuy, B., Panjasawatwong, Y., Osataporn, P., 2005, Preliminary geochemical study of volcanic rocks in the Pang Mayao area, Phrao, Chiang Mai, northern Thailand: tectonic setting of formation, Journal of Asian Earth Sciences, v. 24, p. 765-776.

Piyasin, S., 1972, Geology of Lampang, Report of Investigation no. 14, Department of Mineral Resources, Bangkok, 66 p.

Polachan, S., Pradidtan, S., Tongtaow, C., Janmaha, S., Intarawijitra, K. and Sangsuwan, C., 1991, Development of Cenozoic basin in Thailand, Marine and Petroleum Geology, v. 8, p. 84-97.

Pouchou, J.L. and Pichoir, F., 1984. Un nouveau modele de calcul pour la microanalyse quantitative par spectrometrie de rayons X. L'application a l'analyses d'echantillons homogenes, Recherche Aerospatiale, v. 3, p. 167-192.

Ridd, M.F., 1980, Possible Palaeozoic drift of SE Asia and Triassic collision with China, Journal of Geological Society, London, v. 137, p. 635-640.

Robinson, P., 2003, XRF analysis of flux-fused disc, *in*: Abstract of the 5th International Conference on the Analysis of Geological and Environmental Materials (Geoanalysis 2003), Rovaniemi, Finland, p. 90.

Rollingson, H., 1993, Using Geochemical Data: Evaluation, Presentation, Interpretation, Longman Group UK Limited, 352 p.

Rogers, N.W., Hawkesworth, C.J. and Ormerod, D.S., 1995, Late Cenozoic basaltic magmatism in the Western Great Basin, California and Nevada, Journal of Geophysical Research, v. 100, p. 10287-10301.

Rottura, A., Bargossi, G.M., Caggianelli, A., Del Moro, A., Visona, D. and Tranne, C.A., 1998, Origin and significance of the Permian high-K calc-alkaline magmatism in the central-eastern Southern Alps, Italy, Lithos, v. 45, p. 329-348.

Rubatto, D., Williams, I.S. and Buick I.S., 2001, Zircon and monazite response to prograde metamorphism in the Reynolds Range, central Australia, Contributions to Mineralogy and Petrology, v. 140, p. 458-468.

Rudnick, R.L. and Fountain, D.M., 1995, Nature and composition of the continental crust: a lower crustal perspective, Review in Geophysics, v. 33, p. 267-309.

Saminpanya, S., 2000, Mineralogy and Origin of Gem Corundum Associated with Basalt in Thailand, unpublished PhD thesis, University of Manchester, 395 p.

Sasada, M., Ratanasthien, B. and Soponpongpipat, P, 1987, New K-Ar ages from the Lampang basalt, northern Thailand, Bulletin of the Geological Survey of Japan, v. 38, p. 13-20.

Sato, K., Liu, Y., Wang, Y., Yokoyama, M., Yoshioka, S, Yang, Z. and Otofuji, Y, 2007, Paleomagnetic study of Cretaceous rocks from Pu'er, western Yunnan, China; evidence of internal deformation of the Indochina block, Earth and Planetary Science Letters, v. 258, p. 1-15.

Schellart, W.P., Freeman, J., Stegman, D.R., Moresi, L. and May, D., 2007, Evolution and diversity of subduction zones controlled by slab width, Nature, v. 446, p. 308-311.

Sengor, A.M.C., 1984, The Cimmeride Orogenic System and the Tectonics of Eurasia, Geological Society of America Special Paper, no. 195, 82 p.

Shashida, K. and Igo, H., 1999, Occurrence and tectonic significance of Paleozoic and Mesozoic Radiolaria in Thailand and Malaysia, *in*: Metcalfe, I., Jishun, I., Charvet, J. and Hada, S., eds., Gondwana Dispersion and Asian Accretion, Final Results Volume for IGCP 321, AA Balkerman, Rotterdam, p. 175-196.

Shashida, K., Igo, H., Hisada, K., Nakornsri, N. and Ampornmaha, A., 1993, Preliminary report of the occurrence of Paleozoic and Early Mesozoic radiolaria in Thailand, Journal of Southeast Asian Earth Sciences, v. 8, p. 97-108.

Sibson, R.H., 1977. Fault rocks and fault mechanisms. Journal of the Geological Society, London, v. 133, p. 191-213.

Singharajwarapan, S., 1994, Deformation and Metamorphism of the Sukhothai Fold Belt, Northern Thailand, unpublished PhD thesis, University of Tasmania, 385 p.

Singharajwarapan, S. and Berry, R.F, 2000, Tectonic implications of the Nan Suture Zone and its relationship to the Sukhothai Fold Belt, northern Thailand, Journal of Asian Earth Sciences, v. 18, p. 663-673.

Smedley, P.L., 1986, The relationship between calc-alkaline volcanism and within-plate continental rift volcanism: evidence from Scottish Palaeozoic lavas, Earth and Planetary Science Letters, v. 77, p. 113-128.

Sone, M and Metcalfe, 2008, Parallel Tethys sutures in mainland Southeast Asia: New insights for Palaeo-Tethys closure and implications for the Indosinian orogeny, Comptes Rendus Geoscinece, v. 340, p. 166-179.

Sriprasert, B., 1997, Geochemistry and Petrology of Thoeng Basalt, Changwat Chiang Rai, unpublished MS thesis, Chiang Mai University, 124 p.

Stacey, J.S. and Kramer, J.D., 1975, Approximation of terrestrial lead isotope evolution by a two stage model, Earth and Planetary Science Letters, v. 26, p. 16-25.

Stait, B. and Burrett C.F., 1984, Ordovician nautiloid faunas of central and southern Thailand, Geological Magazine, v. 121, p. 115-124.

Stokes, R.B., Lovatt Smith, P.F. and Soumphophakdy, K., 1996, Timing of the Shan-Thai-Indochina collision: new evidence from the Pak Lay Foldbelt of the Lao PDR, *in*: Hall, R. and Blundell, D., eds., Tectonic Evolution of Southeast Asian, Geological Society Special Publication, no, 106, p. 225-232.

Sukvattananunt, P. and Assawapatchara, S., 1989a, Geological map of Amphoe Chiang Khong (Sheet 5049 I), scale 1:50,000 (in Thai), Geological Survey Division, Department of Mineral Resources, Bangkok.

Sukvattananunt, P. and Assawapatchara, S., 1989b, Geological map of Amphoe Chiang Saen (Sheet 5049 IV), scale 1:50,000 (in Thai), Geological Survey Division, Department of Mineral Resources, Bangkok.

Sukvattananunt, P. and Assawapatchara, S., 1989c, Geological map of Ban Pong Noi (Sheet 5049 III), scale 1:50,000 (in Thai), Geological Survey Division, Department of Mineral Resources, Bangkok.

Sukvattananunt, P. and Assawapatchara, S., 1989d, Geological map of Ban Si Don Chai (Sheet 5049 II), scale 1:50,000 (in Thai), Geological Survey Division, Department of Mineral Resources, Bangkok.

Sukvattananunt, P., Tansathien, W., Prasittikarnkul, K., Mookdee, P. and Prikyai, P., 1985a, Geological map of Amphoe Thoeng (Sheet 5048 III), scale 1:50,000 (in Thai), Geological Survey Division, Department of Mineral Resources, Bangkok.

Sukvattananunt, P., Tansathien, W., Prasittikarnkul, K., Mookdee, P. and Prikyai, P., 1985b, Geological map of Amphoe Phaya Meng Rai (Sheet 5048 IV), scale

1:50,000 (in Thai), Geological Survey Division, Department of Mineral Resources, Bangkok.

Sun, S.S. and McDonough, W.F., 1989, Chemical and isotopic systematics of oceanic basalts: implications for mantle composition and processes, *in*: Saunders, A.D. and Norry, M.J., eds., Magmatism in the Oceanic Basins, Geological Society Special Publications, no. 42, p. 313-345.

Suppe, J., 1985, Principles of Structural Geology, Prentice-Hall, Inc., New Jersey, 537 p.

Tapponnier, P., Lacassin, R., Leloup, P.H., Scharer, U., Zhong, D., Haiwei, W., Liu, X., Ji, S., Zhang, L. and Zhong, J., 1990, The Ailao Shan-Red River metamorphic belt: Tertiary left-lateral shear between Indochina and South China, Nature, v. 343, p. 431-437.

Tansuwan, V. and Chitmanee, S. (1990a) Geological map of Amphoe Chiang Kham (Sheet 5048 II), scale 1:50,000 (in Thai), Geological Survey Division, Department of Mineral Resources, Bangkok.

Tansuwan, V. and Chitmanee, S. (1990b) Geological map of Ban Pa Tan (Sheet 5048 I), scale 1:50,000 (in Thai), Geological Survey Division, Department of Mineral Resources, Bangkok.

Tapponnier, P., Peltzer, G. and Armijo, R., 1986, On the mechanics of collision between India and Asia, *in*: Coward, M.P. and Ries, A.C., eds., Collision Tectonics, Geological Society Special Publication, no. 19, 115-157.

Tatsumi Y. and Eggins, S., 1995, Subduction Zone Magmatism, Blackwell Science, Boston, 211 p.

Taylor, S.R. and McLennan, S.M., 1995, The geochemical evolution of the continental crust (Review), Reviews of Geophysics, v. 33, p. 241-265.

Thanasuthipitak, T., 1978, Geology of Uttaradit area and its implications on tectonic history of Thailand, *in*: Nutalaya, P., ed., Proceedings of the Third Regional Conference on Geology and Mineral Resources of Southeast Asia, Bangkok, p. 187-197.

Ueno, K., Igo, H., 1997, Late Paleozoic foraminifers from the Chiang Dao area, northern Thailand: geologic age, faunal affinity, and palaeobiogeographic implications, *in:* Proceedings of the 13th International Congress on the Carboniferous and Permian, Krakow, Poland, pp. 339–358.

Ueno, K. and Hisada, K.I., 2001, The Nan-Uttaradit-Sa Kaeo Suture as a main Paleo-Tethyan Suture in Thailand: Is it real?, Gondwana Research, v. 4, p. 804-806.

IUGS, 2000, International Stratigraphic Chart, Strasbourg.

Uttamo, W., Elders, C.F. and Nicole, G. J., 2003, Relationships between Cenozoic strike-slip faulting and basin opening in northern Thailand, *in*: Storti, F., Holdsworth, R.E. and Salvini, F., eds., Intraplate Strike-slip Deformation Belts, Geological Society Special Publication, no. 210, p. 89-108.

Van der Pluijm, B.A. and Marshak, S., 2004, Earth Structure (second edition), Norton & Comapany, Inc., New York, 656 p.

Wakita, K. and Metcalfe, I., 2005, Ocean plate stratigraphy in East and Southeast Asia, Journal of Asian Earth Sciences, v. 24, p. 679-702.

Wang, X., Metcalfe, I., Jian, P, He, L. and Wang, C., 2000, The Jinshajiang-Ailaoshan Suture Zone, China: tectonostratigraphy, age and evolution, Journal of Asian Earth Sciences, v. 18, p. 675-690.

Watson, J.S., 1996, Fast, simple method of powder pellet preparation for X-ray fluorescence analysis, X-Ray Spectrometry, vol. 25, p. 173-174.

Wiedenbeck, M., Alle, P., Corfu, F., Griffin W.L., Meier, M., Oberli, F., von Quadt A., Roddick, J.C. and Spiegel, W., 1995, Three natural zircon standards for U-Th-Pb, Lu-Hf, trace-element and REE analyses, Geostandards Newsletter, v. 19, p. 1-23.

Wilkerson, M.S., Apotria. T. and Farid, T., 2002, Interpreting the geologic map expression of contractional fault-related fold terminations: lateral/oblique ramps versus displacement gradients, Journal of Structural Geology, v. 24, p. 593-607.

Woodward, N.B., 1988, Thrust Tectonics Workshop Notes, The International Geological Congress, Washington, 211 p.

Wu, H., Boulter, C.A., Ke, B., Stow, D.A.W. and Wang, Z., 1995, The Changning-Menglian suture zone: a segment of the major Cathaysian-Gondwana divide in Southeast Asia, Tectonophysics, v. 242, p. 267-280.

Yang, K., Mo., X. and Zhu, Q., 1994, Tectono-volcanic belts and late Paleozoic – early Mesozoic evolution of southwestern Yunnan, China, Journal of Southeast Asian Earth Sciences, v. 10, p. 245-262.

Yoshikura, S., 1990, Geology of the Nan-Chanthaburi suture zone (II)-Petrology of basaltic rocks, *in*: Abstracts of Technical Conference on Development Geology for Thailand into the Year 2000, Department of Geology, Chulalongkorn University, Bangkok, p. 11-13.

Yu, Z., Robinson, P. and McGoldrick, P., 2001, An evaluation of methods for the chemical decomposition of geological materials for trace element determination using ICP-MS, Geostandards Newsletter, vol. 25, p. 199-217.

Zhong, D. and Dalai, Z., 2000, Paleotethysides in West Yunnan and Sichuan, Science Press, Utrecht, 248 p.

Appendix A

Petrographic feature of the 98 representative Chiang Khong-Lampang-Tak volcanic belt igneous rocks for the geochemical analyses

No.	Areas	Sample Name	Rock Types	Latitude (°N)**	Longitude (°E)**	Petrographic Features
1	CK-WB[1]	15'/4(3)	I/D*	20 3146	100 2831	Aphyric tholeiitic basalt/dolerite dyke with fresh clinopyroxene
2	CK-WB	14/6(1)	I/D	20 3261	100 3138	Dolerite dyke with fresh clinopyroxene
3	CK-WB	14/3(5)	I/D	20 3173	100 2850	Sparsely plagioclase-phyric coarse-grained basalt or dolerite dyke with abundant fresh clinopyroxene
4	CK-WB	14/3(1)	I/D	20 3173	100 2850	Aphyric tholeiitic basaltic dyke with medium-grained fresh clinopyroxene
5	CK-WB	13/2(1)	I/D	20 1884	100 3615	Strongly plagioclase-phyric basaltic dyke with strong micro-crystalline epidote alteration of plagioclase but small fresh clinopyroxene in places
6	CK-WB	14/1(1)	I/D	20 2992	100 2763	Green-schist facies microgabbro, plagioclase altered to micro-crystalline epidote, clinopyroxene to actinolite, common interstitial quartz and abundant Fe-Ti oxide
7	CK-WB	14/3(2)	I/D	20 3173	100 2850	Microgabbro with occasional late magmatic olive-hornblende and common big apatites
8	CK-WB	15'/3(2)	I/D	20 3146	100 2831	Dolerite with fresh often euhedral clinopyroxene, mainly altered plagioclase and occasional brown hornblende
9	CK-WB	14/4(1)	I/D	20 2801	100 2943	Weakly vesicular basaltic dyke with fresh groundmass clinopyroxene
10	CK-WB	15'/1(5)	I/D	20 2992	100 2763	Strongly plagioclase+clinopyroxene-phyric dyke, probably basaltic andesite composition, with fresh clinopyroxene, altered plagioclase, and common interstitial quartz Abundant big apatites
11	CK-WB	14/8	I/D	20 3628	100 3544	Sparsely clinopyroxene-phyric diorite dyke
12	CK-WB	15'/1(3)	I/D	20 2992	100 2763	Leucogabbro with more interstitial quartz and big apatites
13	CK-WB	25'/1	I/D	20 2992	100 2763	Fairly evolved diorite dyke with fresh Fe-rich clinopyroxene, plagioclase, Fe-Ti oxide with biotite overgrowths (late magmatic) and granophyre in the interstices
14	CK-WB	15'/2(1)	I/D	20 3056	100 2706	Quartz diorite with abundant brown-green hornblende with common apatites
15	CK-WB	14/4(2)	I/D	20 2801	100 2943	Quartz diorite or monzodiorite, lots of apatite, some fresh brown biotite, interstitial quartz
16	CK-WB	15'/3(4)	I/D	20 3146	100 2831	Holocrystalline quartz diorite with altered biotite, big apatites, abundant granophyric textured

No.	Areas	Sample Name	Rock Types	Latitude (°N)**	Longitude (°E)**	Petrographic Features
17	CK-WB	15'/4(1)	I/D	20 3252	100 3071	Diorite with fresh clinopyroxene, mainly altered plagioclase and occasional brown hornblende
18	CK-WB	15'/1(1)	I/D	20 2992	100 2763	Microdiorite with fresh clinopyroxene, albitised plagioclase, some late magmatic green hornblende, and altered biotite, with common interstitial quartz
19	CK-WB	26'/10	I/D	20 1105	100 1322	Magnificent sparsely plagioclase-phyric rhyolitic high-level intrusive rock with wonderful granophyric texture Rare green biotite/hornblende
20	CK-WB	15'/4(2)	Lava	20 3252	100 3071	Porphyritic basalt with lacking lithic clasts, and all plagioclase is thoroughly albite-sericite altered
21	CK-WB	13/6(1)	Lava	20 1660	100 3393	Very strongly plagioclase-phyric basaltic lava or dyke with strong microcrystalline epidote alteration of much of the plagioclase
22	CK-WB	15'/3(5)	Lava	20 3146	100 2831	Plagioclase+clinopyroxene-phyric andesitic lava with altered devitrified groundmass
23	CK-WB	13/3(2)	Lava	20 1713	100 3479	Trachytic textured sparsely plagioclase-phyric andesite with lacking the abundant plagioclase phenocrysts
24	CK-WB	SV-3	Lava	20 1060	100 2117	Basalt with occasional altered olivine phenocrysts, fresh clinopyroxene phenocrysts, vesicular with chlorite-epidote in vesicles
25	CK-WB	13/4(1)	Lava	20 1713	100 3479	Well preserved plagioclase-phyric basalt but lacking the same epidote alteration Occasional small fresh clinopyroxene phenocrysts
26	CK-WB	14/3(6)	Lava	20 3173	100 2850	Green-schist facies andesitic lava with altered plagioclase, clinopyroxene and Fe-Ti oxide phenocrysts in altered formerly glassy groundmass
27	CK-WB	14/3(7)	Lava	20 3173	100 2850	Andesitic lave with slightly altered plagioclase, clinopyroxene and Fe-Ti oxide
28	CK-WB	14/3(4)	Lava	20 3173	100 2850	Green-schist facies andesitic lava with altered phenocrysts of clinopyroxene, plagioclase and Fe-Ti oxide
29	CK-WB	13/7	Lava	20 1633	100 3393	Flow-textured vesicular andesite lava with albitised plagioclase, rare clinopyroxene mainly replaced by epidote/chlorite/prehnite Vesicles filled by quartz, chlorite, prehnite and calcite
30	CK-WB	15'/1(4)	Lava	20 2992	100 2763	Flow-banded andesitic lava with common fresh zoned plagioclase and small chloritised mafics
31	CK-WB	15'/3(1)	Lava	20 3146	100 2831	Vesicular quenched dacitic lava, chlorite+epidot-filled vesicles common
32	CK-WB	14/7	Lava	20 3360	100 3216	Dacitic lava, vein of actinolite-epidote indicating lowest greenschist facies assemblage
33	CK-WB	15'/2(2)	Lava	20 3056	100 2706	Plagioclase+altered hornblende+Fe-Ti oxide+apatite-phyric dacitic lava with occasional lithic clasts and devitrified glassy groundmass

No.	Areas	Sample Name	Rock Types	Latitude (°N)**	Longitude (°E)**	Petrographic Features
34	CK-WB	14/2(1)	Lava	20 3119	100 2783	Intermediate/felsic lava or ashflow with common largely fresh plagioclase phenocrysts and occasional actinolite-altered former clinopyroxene phenocrysts and small Fe-Ti oxide Occasional lithic clasts
35	CK-WB	14/3(3)	Lava	20 3173	100 2850	Glassy dacitic lava with flow banding in groundmass which is patchily devitrified
36	CK-WB	18/3(1)	Lava	20 0059	100 0990	Plagioclase-phyric dacitic lava or lava breccia, formerly glassy groundmass
37	CK-WB	13/1	Lava	20 2172	100 3790	Plagioclase-phyric dacitic lava, sparse altered clinopyroxene, some Fe-Ti oxide microphenocrysts
38	CK-WB	13/5	Lava	20 1642	100 3412	Plagioclase-phyric rhylite
39	CK-WB	13/3(3)	Lava	20 1722	100 3508	Moderately plagioclase-phyric rhyolite with patchy groundmass texture and occasional chloritised hornblende phenocrysts as well as common plagioclase
40	CK-WB	13/3(1)	Lava	20 1722	100 3508	Moderately plagioclase-phyric glassy rhyolite with strong crystallization of the groundmass and excellent big secondary sphene
41	CK-CB[2]	17/10	I/D	20 1856	100 4772	Dolerite dyke with occasional fresh clinopyroxene
42	CK-CB	18/2	I/D	19 8705	100 3257	Fairly strongly epidote-altered basaltic dyke
43	CK-CB	16'/2(3)	Lava	19 9690	100 3256	Phyric andesitic lava with large altered plagioclase and totally altered clinopyroxene
44	CK-CB	12/1(2)	Lava	19 6600	100 2019	Strongly porphyritic plagioclased+clinopyroxene-phyric andesite and some epidote+prehnite alteration
45	CK-CB	16'/6(3)	Lava	19 8987	100 2992	Sparsely clinopyroxene-phyric basaltic lava with moderate microcrystalline epidote alteration
46	CK-CB	12/4	Lava	19 7537	100 2398	Strongly plagioclase+clinopyroxene-phyric andesitic lava
47	CK-CB	12/2(4)	Lava	19 7033	100 2146	Altered plagioclase+clinopyroxene+sparse altered olivine-phyric basalt or basaltic andesite
48	CK-CB	15'/16(2)	Lava	19 3210	100 2270	Abundantly plagioclase-phyric andesitic to basaltic lava
49	CK-CB	16'/5(2)	Lava	19 8987	100 3011	Plagioclase-phyric andesitic lava with intense microcrystalline epidote alteration
50	CK-CB	12/1(1)	Lava	19 6600	100 2019	Fresh clinopyroxene+altered plagioclase-phyric andesite to basalt lava
51	CK-CB	16'/7(1)	Lava	19 8654	100 2875	Plagioclase+clinopyroxene-phyric andesite lava with formerly glassy groundmass
52	CK-CB	16'/2(2)	Lava	19 9690	100 3256	Plagioclase+clinopyroxene+Fe-Ti oxide-phyric andesitic lava with fresh clinopyroxene, albitised plagioclase
53	CK-CB	12/2(3)	Lava	19 7033	100 2146	Sparsely and finely plagioclase-phyric formerly glassy dacitic lava Banded fine-grained epidote alteration
54	CK-CB	16'/5(1)	Lava	19 8987	100 3011	Strongly foliated plagioclase+clinopyroxne-phyric dacite with sparse quartz fragments
55	CK-CB	18/1	Lava	19 8779	100 3124	Plagioclase-phyric formerly glassy welded dacitic tuff
56	CK-CB	16'/4	Lava	19 9005	100 3021	Plagioclase+clinopyroxene-phyric dacitic lava

No.	Areas	Sample Name	Rock Types	Latitude (°N)**	Longitude (°E)**	Petrographic Features
57	CK-CB	16'/6(1)	Lava	19 8987	100 2992	Foliated plagioclase-phyric rhyolitic lava with sparse quartz fragments
58	CK-CB	16'/10(1)	Lava	19 3183	100 2251	Quartz+plagioclase-phyric welded rhyolite
59	CK-CB	15'/16(1)	Lava	19 3210	100 2270	Excellent quartz+plagioclase-phyric welded rhyolitic tuff or lava
60	CK-CB	15'/16(3)	Lava	19 3210	100 2270	Excellent more crystalline rhyolitic lava with quartz and plagioclase phenocrysts
61	CK-EB[3]	17/7(2)	I/D	19 9536	100 4449	Sparsely plagioclase-phyric basaltic dyke
62	CK-EB	15'/15(2)	Lava	19 8062	100 3538	Distinctive big-plagioclase basalt with rare altered former olivine phenocrysts and large abundant albitised plagioclase phenocrysts
63	CK-EB	15'/15(1)	Lava	19 8062	100 3538	Fairly altered sparserly porphyritic andesitic lava
64	CK-EB	17/9(3)	Lava	19 9734	100 4613	Strongly plagioclase-phyric basaltic lava with moderate epidote alteration, with occasional altered olivine phenocrysts (now microcrystalline quartz-chlorite)
65	CK-EB	17/7(1)	Lava	19 9536	100 4449	Olivine(altered)+clinopyroxene+plagioclase-phyric basaltic lava
66	CK-EB	15'/7(1)	Lava	19 9851	100 4605	Sparsely vesicular olivine+plagioclase-phyric basalt Very altered, no primary phases preserved
67	CK-EB	15'/8(2)	Lava	19 9770	100 4604	Plagioclase+ sparsely clinopyroxene-phyric andesite
68	CK-EB	15'/13(2)	Lava	19 9033	100 4062	Sparsely porphyritic andesitic lava with moderate alteration
69	CK-EB	17/9(2)	Lava	19 9734	100 4613	Sparsely plagioclase-phyric andesitic lava
70	CK-EB	17/7(3)	Lava	19 9536	100 4449	Trachytic textured andesitic lava, no fresh plagioclase Occasional vesicles with chlorite and epidote
71	CK-EB	15'/10(2)	Lava	19 9492	100 4401	Trachytic textured sparsely plagioclase+clinopyroxene-phyric andesite lava
72	LP-WB[4]	12'/1(5)	I/D	18 2136	99 5429	Slightly coarse-grained fairly altered rhyolitic dyke
73	LP-WB	12'/1(2-1)	I/D	18 2136	99 5429	Fairly altered rhyolitic dyke
74	LP-WB	12'/1(1-1)	Lava	18 2136	99 5429	Slightly CO3-altered weakly vesicular aphyric basalt or basaltic andesite
75	LP-WB	12'/1(1-3)	Lava	18 2136	99 5429	Vesicular aphyric basalt or basaltic andesite with some altered olivine phenocrysts and altered plagioclase phenocrysts
76	LP-WB	5/3	Lava	18 2551	99 5562	Sparsely and finely plag-phyric rhyoltic lava
77	LP-WB	20'/5	Lava	18 2460	99 5676	Quartz+plagioclase-phyric microspherulitic rhyolitic lava Plagioclase altered to clays
78	LP-WB	12'/1(9)	Lava	18 2136	99 5429	Sparsely quartz and plagioclase-phyric rhyolitic glassy lava in which all glass has gone to spherulitic textured quartzo-feldspathic intergrowths and slightly small phenocrysts
79	LP-WB	12'/1(8)	Lava	18 2136	99 5429	Quartz+plagioclase-phyric rhyolite with spherlutitic textured quatrzo-felspathic intergrowths
80	LP-WB	12'/5(3)	Lava	18 2560	99 5487	Excellent quartz+plagioclase-phyric rhyolite

No.	Areas	Sample Name	Rock Types	Latitude (°N)**	Longitude (°E)**	Petrographic Features
81	LP-WB	12'/1(1-4)	Lava	18 2136	99 5429	Strongly porphyritic rhyolitic lava with big quartz and plagioclase phenocrysts, occasional altered former mafic and Fe-Ti oxide
82	LP-WB	12'/5(1)	Lava	18 2560	99 5487	Very nice microspherulitic textured formerly glassy sparsely plagioclase-phyric rhyolitic lava
83	LP-WB	12'/5(2)	Lava	18 2560	99 5487	Finely plagioclase-phyric rhyolite
84	LP-WB	5/1	Lava	18 2624	99 5440	Sparsely and finely plagioclase-phyric rhyolitic lava
85	LP-WB	6/5	Lava	18 2460	99 5676	Spherulitic quartz+plagioclase-phyric,rhyolite glassy lava with clay alteration of plagioclase
86	LP-CB[5]	SV-1	I/D	18 4246	99 3357	Fine-grained dolerite with fresh clinopyroxene
87	LP-CB	7/2	I/D	18 9270	99 7132	Plagioclase-phyric granite with strong development of granophyre
88	LP-CB	12'/10	I/D	18 9351	99 7085	More dacitic dyke texture, plagioclase-quartz-biotite-clinopyroxene-phyric
89	LP-CB	7/4(2)	Lava	18 9333	99 7094	Plagioclase+clinopyroxene (chloritised)+apatite + Fe-Ti oxide–phyric dacitic lava
90	LP-CB	12'/9	Lava	18 9388	99 7057	Excellent plagioclase+quartz-phyric felsic ignimbrite (?) with abundant pumice fragments
91	LP-CB	12'/6(1)	Lava	18 9623	99 6963	Plag-phyric formerly glassy rhyolitic lava
92	LP-CB	7/4(1)	Lava	18 9333	99 7094	Formerly glassy plag-phyric rhyolitic lava
93	LP-CB	7/3(1)	Lava	18 9243	99 7180	Almost aphyric formerly glassy rhyolitic lava
94	LP-CB	SV-5	Lava	17 9750	99 6367	Beautiful spherulitic textured quartz+sanidine+albite-phyric rhyolitic lava
95	LP-CB	7/6	Lava	18 9460	99 7048	Spherulitic texturedd quartz+plagioclase-phyric rhyolitic lava
96	LP-CB	7/7(1)	Lava	18 9569	99 7029	Quartz+feldspar-phyric glassy rhyolitic lava
97	LP-CB	7/7(2)	Lava	18 9569	99 7029	Excellent microsnowflake-textured felsic lava with quartz and plagioclase phenocrysts and occasional big zircons
98	LP-CB	12'/8	Lava	18 9433	99 7028	Plagioclase+quartz-phyric snowflake textured spherulitic rhyolitic lava

[1]CK WB = Chiang Khong Western Belt

[2]CK CB = Chiang Khong Central Belt

[3]CK EB = Chiang Khong Eastern Belt

[4]LP WB = Lampang Western Belt

[5]LP-CB = Lampang Central Belt

*I/D = Intrusive or Dyke

** WGS-84 grid system

Appendix B

Appendix B-1: Laser ablation ICPMS U-Pb isotopic and trace element data for standard zircon of the CLT igneous rock analysis.

Sample	206Pb/238U age (Ma)		Isotopic ratios								Trace element data (in ppm)				
analysis no	(207Pb corrected)	+/-1s	206Pb/238U	%rsd	208Pb/232Th	%rsd	207Pb/206Pb	%rsd	207Pb/235U	%rsd	Nd	Hf	Pb	Th	U
Temora	401	8	0 0653	1 9%	0 0202	5 8%	0 068	8 1%	0 552	7 5%	1 8	8070	7	31	100
Temora	406	8	0 0656	2 0%	0 0214	5 1%	0 061	7 9%	0 527	7 4%	3 0	8367	6	35	96
Temora	408	6	0 0653	1 3%	0 0199	3 3%	0 055	4 9%	0 468	5 1%	7 5	9314	19	142	275
Temora	414	7	0 0666	1 6%	0 0203	3 8%	0 058	6 3%	0 511	6 0%	9 4	7637	14	114	189
Temora	415	8	0 0669	2 0%	0 0214	5 8%	0 061	7 8%	0 514	7 1%	1 1	8291	9	37	135
Temora	416	5	0 0668	1 3%	0 0200	3 1%	0 056	4 3%	0 515	4 5%	4 2	9641	27	193	379
Temora	416	8	0 0668	1 8%	0 0201	4 6%	0 056	8 1%	0 482	7 5%	6 1	8883	9	61	130
Temora	417	9	0 0669	2 0%	0 0227	6 0%	0 057	7 9%	0 502	7 7%	2 1	8913	8	37	113
Temora	418	5	0 0671	1 3%	0 0201	3 1%	0 057	4 3%	0 517	4 5%	4 2	9641	27	193	379
Temora	418	9	0 0672	2 0%	0 0228	6 0%	0 057	7 9%	0 504	7 6%	2 1	8913	8	37	113
Temora	420	7	0 0673	1 6%	0 0219	4 1%	0 055	6 5%	0 494	6 6%	4 0	9314	13	84	194
Temora	421	10	0 0677	2 3%	0 0207	6 2%	0 058	8 0%	0 519	8 0%	2 5	8084	7	30	114
Temora	422	6	0 0676	1 4%	0 0210	3 3%	0 054	5 1%	0 475	4 7%	6 2	9314	19	132	266
Temora	422	7	0 0677	1 6%	0 0200	4 0%	0 055	7 0%	0 490	6 7%	6 6	8627	11	79	156
Temora	422	4	0 0679	1 0%	0 0199	2 1%	0 059	2 6%	0 533	2 8%	1 6	8389	84	554	1235
Temora	423	8	0 0677	1 9%	0 0212	3 7%	0 055	6 9%	0 504	6 6%	7 4	8518	11	82	167
Temora	424	7	0 0678	1 7%	0 0225	4 9%	0 052	6 9%	0 482	7 3%	2 8	8548	11	51	172
Temora	425	11	0 0703	2 4%	0 0376	7 7%	0 080	8 8%	0 756	8 8%	0 9	8946	6	27	82
Temora	426	8	0 0684	1 9%	0 0212	6 1%	0 057	7 6%	0 522	7 8%	1 9	8548	7	32	99
Temora	426	7	0 0683	1 6%	0 0202	3 7%	0 055	5 4%	0 502	5 5%	7 9	8899	14	96	197
Temora	426	8	0 0685	1 9%	0 0213	6 1%	0 057	7 6%	0 523	7 8%	1 9	8548	7	32	99
Temora	429	7	0 0681	1 8%	0 0198	4 8%	0 048	7 9%	0 433	8 0%	7 1	8481	9	62	127
Temora	429	12	0 0702	2 7%	0 0336	9 0%	0 071	6 9%	0 704	8 3%	3 1	8443	26	80	367
Temora	433	9	0 0690	2 0%	0 0220	4 7%	0 050	7 8%	0 458	7 9%	3 7	8618	9	53	131
Temora	434	10	0 0695	2 3%	0 0198	6 8%	0 054	10 3%	0 510	10 3%	0 9	8761	5	24	65
Temora	437	7	0 0699	1 6%	0 0226	3 7%	0 053	5 9%	0 498	5 8%	3 2	8733	16	83	233
Temora	437	10	0 0705	2 2%	0 0248	7 9%	0 060	11 0%	0 529	10 5%	1 2	8675	5	23	66
Temora	439	10	0 0708	2 2%	0 0249	7 9%	0 060	10 9%	0 531	10 4%	1 2	8675	5	23	66

Appendix B-1 *(continued)*

Sample	206Pb/238U age (Ma)		Isotopic ratios								Trace element data (in ppm)				
analysis no	(207Pb corrected)	+/-1s	206Pb/238U	%rsd	208Pb/232Th	%rsd	207Pb/206Pb	%rsd	207Pb/235U	%rsd	Nd	Hf	Pb	Th	U
Temora	440	9	0 0713	2 0%	0 0231	5 3%	0 064	6 5%	0 588	6 6%	3 1	8953	10	56	146
Temora	443	13	0 0718	2 9%	0 0254	9 0%	0 063	11 3%	0 606	11 4%	1 7	8889	5	24	67
Temora	445	13	0 0721	2 9%	0 0255	9 0%	0 064	11 3%	0 609	11 4%	1 7	8889	5	24	67
Temora	455	11	0 0732	2 4%	0 0259	10 2%	0 056	9 7%	0 528	10 1%	1 0	8691	4	22	60
91500	1088	22	0 1829	2 0%	0 0533	6 3%	0 071	8 0%	1 627	8 0%	0 2	5463	15	27	77
91500	1059	22	0 1795	2 1%	0 0514	4 3%	0 079	5 8%	1 907	5 8%	0 2	6094	16	34	93
91500	1061	19	0 1799	1 7%	0 0556	4 6%	0 079	5 2%	1 931	5 0%	0 0	6215	15	30	86
91500	1020	16	0 1729	1 6%	0 0583	5 6%	0 080	5 2%	1 863	5 0%	0 2	6282	14	26	79
91500	1067	15	0 1800	1 4%	0 0574	3 8%	0 075	4 8%	1 773	4 6%	0 3	6147	16	30	85
91500	1047	16	0 1774	1 6%	0 0530	3 8%	0 079	4 6%	1 829	4 6%	0 2	5714	14	27	76
91500	1058	18	0 1795	1 8%	0 0536	4 4%	0 080	4 4%	1 883	4 5%	0 2	5809	15	30	85
91500	1040	16	0 1767	1 5%	0 0515	4 5%	0 082	5 0%	1 969	5 2%	0 2	5958	14	28	81
91500	1046	16	0 1769	1 6%	0 0538	4 1%	0 078	4 4%	1 839	4 4%	0 1	5924	15	28	82
91500	1076	18	0 1829	1 6%	0 0532	3 9%	0 081	5 4%	1 934	4 7%	0 1	5867	15	29	81
91500	1027	14	0 1737	1 4%	0 0510	3 8%	0 078	4 7%	1 847	5 0%	0 3	5782	15	30	84
91500	1058	17	0 1782	1 6%	0 0518	4 5%	0 074	5 5%	1 713	5 1%	0 2	5998	15	28	79
91500	1032	16	0 1743	1 5%	0 0516	4 0%	0 077	5 3%	1 801	5 2%	0 7	5855	15	30	85
91500	1025	17	0 1727	1 6%	0 0501	5 2%	0 075	5 4%	1 787	5 3%	0 7	5950	14	27	78
91500	1058	16	0 1774	1 5%	0 0519	4 2%	0 070	5 0%	1 662	5 1%	0 3	5743	15	29	84
91500	1020	17	0 1719	1 7%	0 0510	4 3%	0 076	5 2%	1 750	5 1%	0 3	5791	14	27	77
91500	1049	18	0 1777	1 7%	0 0514	4 8%	0 079	5 5%	1 852	5 5%	0 1	5798	15	29	83
91500	1045	17	0 1753	1 7%	0 0537	4 7%	0 071	5 3%	1 691	5 2%	0 4	6285	15	29	84

Appendix B-2: Laser ablation ICPMS U-Pb isotopic and trace element data for standard zircon of the CLT sandstone analysis.

Sample	206Pb/238U age (Ma)		Isotopic ratios								Trace element data (in ppm)				
analysis no	(207Pb corrected)	+/-1s	206Pb/238U	%rsd	208Pb/232Th	%rsd	207Pb/206Pb	%rsd	207Pb/235U	%rsd	Nd	Hf	Pb	Th	U
Temora	388	10	0 0625	2 7%	0 0202	6 8%	0 060	7 1%	0 493	7 6%	1 3	8905	4	23	58
Temora	405	7	0 0649	1 8%	0 0200	6 5%	0 055	6 5%	0 520	6 2%	1 0	9229	4	25	67
Temora	405	6	0 0652	1 4%	0 0200	4 3%	0 060	4 7%	0 554	4 6%	6 6	8651	10	75	145
Temora	407	7	0 0653	1 7%	0 0192	6 0%	0 057	6 3%	0 514	6 2%	6 2	8793	7	50	103
Temora	409	7	0 0656	1 6%	0 0217	5 0%	0 055	5 8%	0 492	5 6%	5 6	8286	7	51	101
Temora	409	6	0 0656	1 4%	0 0199	4 4%	0 056	4 8%	0 513	4 6%	6 2	8559	8	59	123
Temora	412	7	0 0656	1 7%	0 0223	5 3%	0 051	6 5%	0 453	6 4%	4 2	8125	6	45	82
Temora	407	6	0 0656	1 4%	0 0201	4 4%	0 060	5 6%	0 509	5 4%	5 9	8932	7	51	100
Temora	413	5	0 0661	1 3%	0 0211	3 2%	0 054	3 4%	0 496	3 5%	1 5	9553	24	116	371
Temora	415	5	0 0662	1 3%	0 0206	4 1%	0 050	4 0%	0 474	3 9%	1 9	9530	14	61	225
Temora	411	7	0 0662	1 7%	0 0212	6 2%	0 059	6 2%	0 554	6 1%	1 6	8450	5	24	79
Temora	415	7	0 0662	1 7%	0 0188	4 7%	0 051	6 5%	0 457	6 2%	5 0	8140	6	46	83
Temora	414	10	0 0662	2 4%	0 0204	3 3%	0 054	3 5%	0 499	3 7%	6 5	9441	30	227	416
Temora	412	5	0 0663	1 3%	0 0181	4 3%	0 058	3 9%	0 547	3 9%	6 1	9217	11	80	162
Temora	414	7	0 0663	1 6%	0 0223	4 2%	0 054	5 3%	0 504	5 0%	6 2	8109	7	58	106
Temora	414	10	0 0663	2 4%	0 0204	3 3%	0 054	3 5%	0 500	3 7%	6 5	9441	30	227	416
Temora	414	9	0 0664	2 2%	0 0200	6 0%	0 056	5 5%	0 511	5 3%	1 6	8250	7	31	110
Temora	415	6	0 0664	1 4%	0 0215	4 3%	0 054	5 2%	0 496	5 2%	5 9	9008	9	62	129
Temora	415	7	0 0665	1 7%	0 0212	4 0%	0 054	4 7%	0 507	4 6%	7 3	8434	10	74	147
Temora	418	6	0 0667	1 6%	0 0211	5 3%	0 051	5 7%	0 488	5 5%	3 5	8308	8	48	120
Temora	418	7	0 0669	1 7%	0 0209	3 6%	0 055	3 6%	0 498	3 6%	3 9	9496	17	106	247
Temora	419	9	0 0669	2 2%	0 0212	5 1%	0 052	6 1%	0 480	6 0%	3 7	8864	6	37	83
Temora	420	7	0 0672	1 8%	0 0229	4 0%	0 054	5 1%	0 488	5 1%	6 2	8443	8	55	116
Temora	421	8	0 0673	1 9%	0 0238	6 4%	0 053	6 6%	0 492	6 7%	1 5	7828	5	22	80
Temora	419	6	0 0673	1 4%	0 0159	4 2%	0 056	4 6%	0 531	4 7%	10 2	8126	10	106	140
Temora	422	7	0 0675	1 7%	0 0213	4 3%	0 053	6 0%	0 505	5 8%	5 5	9030	8	56	110
Temora	421	8	0 0675	2 0%	0 0234	4 3%	0 055	5 8%	0 495	5 5%	5 5	8525	9	53	130
Temora	419	8	0 0675	1 9%	0 0219	5 8%	0 060	6 0%	0 544	5 9%	0 7	8700	5	34	72
Temora	422	5	0 0676	1 1%	0 0206	3 3%	0 054	3 0%	0 504	3 1%	2 1	9349	31	158	455
Temora	420	8	0 0676	1 9%	0 0219	5 8%	0 060	6 0%	0 544	5 9%	0 7	8700	5	34	72
Temora	421	7	0 0677	1 6%	0 0214	5 7%	0 058	5 7%	0 531	5 5%	1 3	9629	5	31	79
Temora	421	9	0 0678	2 2%	0 0209	5 2%	0 058	6 0%	0 540	5 8%	1 6	9053	7	34	99

Appendix B-2 *(continued)*

Sample	206Pb/238U age (Ma)		Isotopic ratios								Trace element data (ın ppm)				
analysıs no	(207Pb corrected)	+/-1s	206Pb/238U	%rsd	208Pb/232Th	%rsd	207Pb/206Pb	%rsd	207Pb/235U	%rsd	Nd	Hf	Pb	Th	U
Temora	420	7	0 0679	1 7%	0 0176	5 2%	0 061	5 3%	0 555	5 3%	6 1	8369	6	45	83
Temora	432	8	0 0691	2 0%	0 0220	4 5%	0 052	5 5%	0 480	5 3%	6 1	8254	9	63	131
Temora	434	7	0 0691	1 5%	0 0218	4 1%	0 050	5 2%	0 474	5 1%	3 2	8911	8	51	110
Temora	435	9	0 0699	2 0%	0 0231	3 5%	0 056	4 1%	0 554	4 2%	4 2	8905	12	77	170
91500	1026	14	0 1742	1 3%	0 0539	3 9%	0 081	3 2%	1 987	3 4%	0 3	5929	15	30	83
91500	1034	14	0 1743	1 4%	0 0541	3 9%	0 075	3 6%	1 824	3 4%	0 3	5927	14	28	80
91500	1029	14	0 1746	1 3%	0 0546	3 9%	0 081	3 3%	1 973	3 4%	0 3	5929	15	30	83
91500	1040	15	0 1751	1 5%	0 0528	4 3%	0 074	3 5%	1 788	3 4%	0 1	6015	15	31	85
91500	1040	15	0 1752	1 5%	0 0528	4 3%	0 074	3 5%	1 789	3 4%	0 1	6015	15	31	85
91500	1041	15	0 1758	1 4%	0 0506	4 1%	0 076	3 3%	1 855	3 3%	0 3	6041	14	27	77
91500	1046	15	0 1764	1 4%	0 0550	3 9%	0 075	3 6%	1 828	3 5%	0 3	5896	14	28	81
91500	1050	14	0 1773	1 3%	0 0552	4 3%	0 076	3 4%	1 859	3 3%	0 2	5783	15	28	81
91500	1058	15	0 1782	1 4%	0 0547	4 0%	0 074	3 6%	1 845	3 5%	0 2	5892	13	26	74
91500	1057	15	0 1787	1 5%	0 0521	4 1%	0 077	3 6%	1 919	3 6%	0 4	5939	15	27	80
91500	1068	15	0 1799	1 4%	0 0537	4 0%	0 073	3 6%	1 785	3 5%	0 6	5861	15	28	84
91500	1062	19	0 1802	1 8%	0 0508	4 0%	0 080	3 3%	2 042	3 6%	0 4	5768	15	30	85
91500	1070	15	0 1804	1 4%	0 0556	4 1%	0 074	3 6%	1 849	3 6%	0 2	5861	14	26	75
91500	1068	20	0 1806	1 9%	0 0551	4 1%	0 077	3 4%	1 904	3 5%	0 3	5765	14	27	80
91500	1081	14	0 1826	1 3%	0 0577	4 2%	0 075	3 6%	1 887	3 6%	0 1	5788	14	25	76
91500	1084	19	0 1828	1 8%	0 0553	3 9%	0 074	3 7%	1 809	3 7%	0 1	5964	16	32	88
91500	1094	14	0 1838	1 3%	0 0570	4 4%	0 070	3 2%	1 833	3 4%	0 3	5759	15	27	79
91500	1171	34	0 1981	3 0%	0 0558	3 7%	0 074	4 1%	1 946	4 0%	0 5	6010	16	30	85

Appendix C

Appendix C-1: Analytical conditions for monazite CHIME age analysis. Cameca SX100 electron probe microanalyser, Central Science Laboratory, University of Tasmania. 'LPET' and 'LLiF' indicate large area crystals. (1) An additional off-line overlap correction was applied for the Ce interference on Pb.

Element	Line	Spec. No.	Crystal	Peak/Bg. (s)	Rel. Bg. Pos. ($\sin\theta \cdot 10^5$) / slope	Standard	Corrected overlaps for
Al	Kα	4	TAP	20/20	+900 / 1.048	Gahnite	-
As	Lα	4	TAP	30/30	+700 / 1.118	GaAs	Dy, Sm
Ca	Kα	3	LPET	10/2x5	-800, +850	Ap Snarum	-
Fe	Kα	2	LLiF	10/10	-3850 / 0.72	Hematite	-
K	^{2}Kα	4	TAP	60/60	+300 / 1.02	Microcline	U
P	Kα	5	LPET	10/10	+1750 / 1.095	ScPO4	-
S	Kα	3	LPET	10/10	+632 / 1.10	Celestite	-
Si	Kα	4	TAP	30/30	+400 / 1.176	Huttonite	Nd, La
Sr	Lα	4	TAP	20/20	-565 / 0.944	Celestite	-
Y	Lα	5	LPET	10/10	-1600 / 0.815	Y oxide	-
Pb	Mβ	3+5	2xLPET	2x(180/2x90)	-2695, +4016	K227 glass	U, Ce(1)
Th	Mβ	1	PET	40/2x20	-1300, +800	Huttonite	-
U	Mβ	1	PET	150/150	-1250 / 0.89	U oxide	Th, Sm
La	Lα	1	PET	10/10	+540 / 1.05	$LaPO_4$	Nd
Ce	Lα	1	PET	10/10	+1740 / 1.18	$CePO_4$	-
Pr	Lβ	2	LLiF	15/15	-500 / 1.0	$PrPO_4$	-
Nd	Lβ	2	LLiF	10/10	-1930 / 0.83	$NdPO_4$	-
Sm	Lβ	2	LLiF	15/15	-525 / 0.939	$SmPO_4$	-
Eu	Lβ	2	LLiF	30/30	-3450 / 0.75	$EuPO_4$	Th, Dy
Gd	Lβ	2	LLiF	20/2x10	-500, +470	$GdPO_4$	-
Dy	Lβ	2	LLiF	20/20	-305 / 0.98	$DyPO_4$	Gd, Sm
Er	Lβ	2	LLiF	20/20	-850 / 0.95	$ErPO_4$	Gd, Eu
Yb	Lα	2	LLiF	10/10	+600 / 1.03	$YbPO_4$	Sm, Dy

Appendix C-2: Electron microprobe analysis for chemical U-Pb-Th monazite age dating of a foliated granite (sample 8"-2) from the Ban Huak area

Sample no	Pb (ppm)	Th (ppm)	U (ppm)	Age (Ma)	1sig age	Si (%)	Al (%)	K (%)	Fe (%)	Ca (%)	Pb (%)	Y (%)	Th (%)	U (%)	La (%)	Ce (%)	Pr (%)	Nd (%)	Sm (%)	Gd (%)	Dy (%)	Yb (%)	Er (%)	P (%)	As (%)	O (%)	Total
8"-2 28	339	12475	809	440	54	0 23	0 00	0 01	0 02	0 07	0 03	1 35	1 25	0 08	14 32	27 32	2 78	8 90	1 15	0 77	0 34	0 07	0 17	11 91	0 03	25 72	96 51
8"-2 29	231	5566	803	513	95	0 11	0 00	0 00	0 02	0 04	0 02	1 22	0 56	0 08	14 78	28 15	2 73	8 92	1 10	0 78	0 30	0 06	0 10	12 19	0 03	25 99	97 18
8"-2 30	106	6153	659	176	86	0 11	0 00	0 01	0 01	0 04	0 01	1 30	0 62	0 07	14 57	27 63	2 83	9 05	1 17	0 85	0 38	0 02	0 09	12 18	0 02	25 94	96 88
8"-2 31	430	22691	1079	333	32	0 38	0 00	0 02	0 03	0 07	0 04	1 19	2 27	0 11	14 33	27 06	2 74	8 75	1 17	0 83	0 32	0 06	0 09	11 93	0 01	25 94	97 34
8"-2 32	139	5850	782	260	90	0 14	0 01	0 01	0 02	0 04	0 01	1 21	0 59	0 08	14 80	27 97	2 79	9 00	1 15	0 81	0 28	0 06	0 08	12 14	0 03	25 98	97 19
8"-2 33	277	12383	787	353	54	0 24	0 03	0 01	0 02	0 06	0 03	1 14	1 24	0 08	14 86	27 57	2 76	8 90	1 04	0 79	0 34	0 05	0 08	11 94	0 03	25 83	97 03
8"-2 34	529	40730	1093	248	19	0 50	0 00	0 01	0 05	0 08	0 05	1 27	4 07	0 11	13 59	26 30	2 62	8 74	1 17	0 81	0 28	0 05	0 06	11 76	0 03	25 86	97 41
8"-2 35	451	26943	1075	302	28	0 38	0 00	0 01	0 02	0 11	0 05	1 44	2 69	0 11	14 24	26 71	2 70	8 63	1 17	0 87	0 39	0 07	0 16	11 98	0 01	26 07	97 80
8"-2 36	382	22824	1031	292	31	0 29	0 01	0 02	0 04	0 22	0 04	1 30	2 28	0 10	14 01	26 96	2 71	8 83	1 22	0 86	0 38	0 06	0 11	12 15	0 03	26 18	97 78
8"-2 37	431	29169	465	285	27	0 38	0 00	0 01	0 07	0 23	0 04	0 27	2 92	0 05	14 37	27 39	2 84	9 37	1 19	0 60	0 11	0 00	0 03	12 03	0 04	26 12	98 09
8"-2 38	21	19334	287	-25	23	0 26	0 01	0 01	0 05	0 09	0 00	0 13	1 93	0 03	15 22	28 75	2 84	9 03	0 89	0 44	0 10	0 00	0 00	12 13	0 02	26 11	98 03
8"-2 39	523	32879	1717	282	22	0 54	0 00	0 01	0 03	0 15	0 05	1 37	3 29	0 17	14 08	26 35	2 61	8 50	1 18	0 82	0 34	0 07	0 09	11 95	0 03	26 15	97 76
8"-2 40	471	28574	1235	296	25	0 49	0 00	0 01	0 04	0 17	0 05	1 18	2 86	0 12	14 30	26 82	2 72	8 65	1 07	0 73	0 28	0 11	0 09	11 87	0 02	26 03	97 61
8"-2 41	401	29579	933	248	25	0 37	0 00	0 02	0 08	0 13	0 04	1 12	2 96	0 09	14 32	26 98	2 74	8 69	1 10	0 73	0 30	0 02	0 08	12 06	0 01	26 16	98 02
8"-2 42	359	22961	1101	269	31	0 35	0 00	0 02	0 02	0 10	0 04	1 16	2 30	0 11	14 21	27 11	2 71	8 99	1 17	0 77	0 30	0 07	0 08	12 21	0 02	26 29	98 02
8"-2 43	307	17549	988	287	39	0 31	0 00	0 01	0 03	0 14	0 03	1 13	1 75	0 10	14 66	27 46	2 75	8 95	1 19	0 72	0 32	0 03	0 11	12 33	0 02	26 46	98 49
8"-2 44	341	23545	957	253	31	0 35	0 01	0 01	0 06	0 54	0 03	0 97	2 35	0 10	14 66	26 96	2 68	8 54	1 08	0 69	0 28	0 03	0 10	12 10	0 02	26 23	97 78
8"-2 45	301	34718	1045	154	22	0 51	0 05	0 01	0 09	0 24	0 03	0 71	3 47	0 10	14 43	27 24	2 73	8 66	1 03	0 54	0 22	0 03	0 06	11 70	0 02	25 90	97 75

Appendix D

Electron microprobe analysis for metamorphic minerals of the representative CLT rocks

Sample no	14/6 (1)			14/7			13/9(1)			12/5 (1)			12/2 (3)		
Analysis no	1	2	3	1	2	3	1	2	3	1	2	3	1	2	3
SiO_2	36 18	36 63	36 97	52 46	52 88	48 67	36 48	27 78	36 10	36 66	36 67	35 83	26 94	27 27	27 43
TiO_2	0 04	0 03	0 02	0 19	0 11	0 43	trace	0 03	0 02	trace	0 05	0 05	0 00	0 00	0 05
Al_2O_3	21 00	21 77	20 32	2 17	2 02	4 78	21 01	17 30	19 35	21 58	21 68	21 67	18 08	17 53	17 88
MgO	2 46	2 24	2 43	14 50	14 68	12 07	2 85	18 00	2 69	1 75	1 79	1 98	16 42	16 90	16 67
FeO	9 34	8 91	10 37	14 98	14 23	17 80	8 65	20 91	10 32	8 71	8 70	8 37	24 68	25 25	24 42
CaO	22 50	22 86	22 09	12 39	12 21	11 90	22 65	0 09	22 49	22 42	22 34	22 06	0 08	0 06	0 06
Na_2O	0 01	0 02	0 01	0 28	0 26	0 75	0 03	trace	0 08	0 08	trace	0 02	0 04	0 04	0 09
K2O	0 01	0 02	0 01	0 08	0 17	0 34	0 02	0 06	0 00	trace	0 01	0 02	0 03	0 06	trace
MnO	0 10	0 08	0 12	0 68	0 81	0 73	0 30	1 72	0 32	0 14	0 18	0 10	1 11	0 91	1 04
ZnO	0 05	0 00	0 02	0 12	0 02	0 02	0 11	0 13	trace	0 07	trace	0 06	0 08	0 06	0 10
NiO	trace	0 02	trace	trace	0 05	0 04	0 02	trace	0 01	0 03	0 03	trace	0 04	0 04	0 02
Cl	0 01	0 00	0 00	0 04	0 04	0 24	0 01	0 01	0 00	0 01	trace	0 01	0 01	0 02	0 01
SO_3	0 04	trace	0 01	0 01	0 00	trace	0 02	0 03	0 01	0 07	0 10	0 09	trace	0 00	0 00
P_2O_5	0 02	0 00	0 01	0 00	0 00	trace	0 02	trace	0 02	0 03	trace	0 00	0 00	trace	trace
SrO	0 01	0 01	0 02	trace	0 01	trace	trace	0 00	trace	0 07	trace	trace	0 00	trace	0 00
Cr_2O_3	0 00	0 03	0 00	trace	0 02	0 00	trace	trace	0 03	0 06	trace	0 01	0 00	trace	0 01
BaO	0 10	trace	trace	trace	trace	0 13	trace	trace	trace	0 00	trace	0 12	0 00	0 13	0 00
V_2O_5	0 14	0 05	0 12	0 06	0 07	trace	0 22	0 00	0 44	1 36	1 23	1 27	0 02	trace	0 03
F	0 12	0 08	0 11	0 09	0 11	0 18	0 28	0 07	0 29	0 10	0 04	0 11	0 03	0 00	0 01
Total	92 14	92 75	92 62	98 04	97 69	98 07	92 66	86 12	92 17	93 14	92 82	91 76	87 56	88 26	87 84
Comment	[1]Pu	Pu	Pu	[2]Act	Act	Act	Pu	[3]Chl	Pu	Pu	Pu	Pu	Chl	Chl	Chl

Sample no	15'/10 (1)			27'/3			8"-5			8"-2		
Analysis no	1	2	3	1	2	3	1	2	3	1	2	3
SiO_2	48 62	35 66	36 35	23 47	23 50	23 98	46 99	38 73	42 26	37 54	36 34	36 52
TiO_2	0 05	0 00	0 02	0 03	0 06	0 08	0 16	0 28	0 22	0 03	2 49	2 10
Al_2O_3	10 74	18 49	19 17	17 95	18 12	18 26	29 17	24 39	28 19	23 05	14 32	14 86
MgO	8 59	2 56	2 60	8 70	6 91	7 07	1 54	1 22	1 58	0 02	7 30	7 42
FeO	16 54	12 12	11 04	35 95	38 35	38 16	5 21	15 99	10 05	12 38	23 05	22 73
CaO	0 08	22 35	22 06	0 01	0 08	0 06	0 08	0 31	0 20	23 02	0 92	0 47
Na_2O	0 00	0 02	0 06	0 02	0 04	0 02	0 26	0 24	0 18	0 00	0 03	0 08
K2O	8 07	trace	trace	0 02	0 04	0 08	9 94	6 64	8 22	0 04	8 35	8 29
MnO	0 08	0 09	0 13	0 25	0 14	0 01	0 03	0 00	0 03	0 42	0 36	0 39
ZnO	trace	trace	0 07	0 06	0 11	0 14	trace	0 09	trace	0 15	trace	0 10
NiO	0 03	0 05	0 06	0 01	trace	trace	trace	trace	trace	trace	0 01	trace
Cl	0 01	0 02	0 01	0 00	0 01	0 02	0 03	0 05	0 00	0 01	0 15	0 17
SO_3	0 01	trace	0 02	0 03	0 01	0 02	0 02	0 03	trace	trace	0 00	0 01
P_2O_5	trace	0 08	trace	0 02	0 03	0 01	0 19	0 53	0 22	0 06	0 05	0 01
SrO	trace	trace	0 00	trace	trace	trace	0 00	0 02	0 00	0 08	0 06	trace
Cr_2O_3	trace	0 04	0 02	0 00	0 03	trace	trace	0 00	0 01	trace	0 03	trace
BaO	0 07	0 14	0 02	0 03	trace	trace	0 10	0 18	0 10	0 06	0 02	trace
V_2O_5	0 13	trace	0 04	trace	0 08	0 03	0 06	0 04	0 06	0 09	0 03	trace
F	trace	trace	0 02	0 01	0 00	0 02	0 11	0 14	0 08	0 02	0 46	0 48
Total	93 02	91 61	91 68	86 57	87 51	87 96	93 87	88 86	91 39	96 97	93 97	93 63
Comment	[4]Bt	Pu	Pu	Chl	Chl	Chl	[5]Mu	Chl-Mu	Mu-Chl	[6]Ep	Bt	Bt

[1]Pu = Pumpellyite [2]Act = Actinolite [3]Chl = Chlorite

[4]Bt = Biotite [5]Mu = Muscovite [6]Ep = Epidote

Appendix E

Sample catalogue (LP= Lampang area, CK=Chiang Khong area, CM=Chiang Mai area, R = rock specimen, PD = rock powder, TS = Thin/polished section)

No	Utas#	Field Number	Latitude (decimal)	Longitude (decimal)	Geographical Area	Position Details	Hand specimen	Powder	Thin Section
1	160463	SV I	18 4246	99 3357	N Thailand	LP	R	PD	1TS
2	160464	SV II	20 3990	100 3090	N Thailand	CK	R		1TS
3	160465	SV III	20 2013	100 2015	N Thailand	CK	R	PD	1TS
4	160466	SV IV	20 1722	100 3508	N Thailand	CK	R		1TS
5	160467	SV V	17 9750	99 6367	N Thailand	LP	R	PD	1TS
6	160468	SV IV	17 6493	99 2730	N Thailand	LP	R		1TS
7	160469	12/1 (1)	19 6600	100 2019	N Thailand	CK	R	PD	1TS
8	160470	12/1 (2)	19 6600	100 2019	N Thailand	CK	R	PD	1TS
9	160471	12/2 (1)	19 7033	100 2146	N Thailand	CK	R		1TS
10	160472	12/2 (2)	19 7033	100 2146	N Thailand	CK	R		1TS
11	160473	12/2 (3)	19 7033	100 2146	N Thailand	CK	R	PD	1TS
12	160474	12/2 (4)	19 7033	100 2146	N Thailand	CK	R	PD	2TS
13	160475	12/3	19 7429	100 2283	N Thailand	CK	R		1TS
14	160476	12/4	19 7537	100 2398	N Thailand	CK	R	PD	1TS
15	160477	12/5 (1)	19 8843	100 2924	N Thailand	CK	R		1TS
16	160478	12/5 (2)	19 8843	100 2924	N Thailand	CK	R		2TS
17	160479	13/1	20 2172	100 3790	N Thailand	CK	R	PD	1TS
18	160480	13/2 (1)	20 1884	100 3615	N Thailand	CK	R	PD	2TS
19	160481	13/3 (1)	20 1722	100 3508	N Thailand	CK	R	PD	2TS
20	160482	13/3 (3)	20 1722	100 3508	N Thailand	CK	R	PD	1TS
21	160483	13/3 (4)	20 1722	100 3508	N Thailand	CK	R		1TS
22	160484	13/3 (5)	20 1722	100 3508	N Thailand	CK	R		1TS
23	160485	13/4 (1)	20 1713	100 3479	N Thailand	CK	R	PD	1TS
24	160486	13/4 (2)	20 1713	100 3479	N Thailand	CK	R	PD	1TS
25	160487	13/5	20 1642	100 3412	N Thailand	CK	R	PD	1TS
26	160488	13/6 (1)	20 1660	100 3393	N Thailand	CK	R	PD	1TS
27	160489	13/6 (2)	20 1660	100 3393	N Thailand	CK	R		1TS
28	160490	13/7 (1)	20 1633	100 3393	N Thailand	CK	R	PD	2TS
29	160491	13/8 (1)	20 1091	100 3340	N Thailand	CK	R		1TS
30	160492	13/8 (2)	20 1091	100 3340	N Thailand	CK	R		1TS
31	160493	13/8 (3)	20 1091	100 3340	N Thailand	CK	R		1TS
32	160494	13/9 (1)	20 1020	100 3196	N Thailand	CK	R		2TS
33	160495	13/9 (3)	20 1020	100 3196	N Thailand	CK	R		2TS
34	160496	13/10	20 0993	100 3186	N Thailand	CK	R		1TS
35	160497	13/11	20 0912	100 3109	N Thailand	CK	R		1TS
36	160498	14/1 (1)	20 2992	100 2763	N Thailand	CK	R	PD	1TS
37	160499	14/1 (2)	20 2992	100 2763	N Thailand	CK	R		2TS
38	160500	14/2 (1)	20 3119	100 2783	N Thailand	CK	R	PD	2TS
39	160501	14/3 (1)	20 3173	100 2850	N Thailand	CK	R	PD	1TS
40	160502	14/3 (2)	20 3173	100 2850	N Thailand	CK	R	PD	1TS
41	160503	14/3 (3)	20 3173	100 2850	N Thailand	CK	R	PD	1TS
42	160504	14/3 (4)	20 3173	100 2850	N Thailand	CK	R	PD	1TS
43	160505	14/3 (5)	20 3173	100 2850	N Thailand	CK	R	PD	1TS
44	160506	14/3 (6)	20 3173	100 2850	N Thailand	CK	R	PD	1TS

No	Utas#	Field Number	Latitude (decimal)	Longitude (decimal)	Geographical Area	Position Details	Hand specimen	Powder	Thin Section
45	160507	14/3 (7)	20 3173	100 2850	N Thailand	CK	R	PD	1TS
46	160508	14/4 (1)	20 2801	100 2943	N Thailand	CK	R	PD	1TS
47	160509	14/4 (2)	20 2801	100 2943	N Thailand	CK	R	PD	1TS
48	160510	14/4 (3)	20 2801	100 2943	N Thailand	CK	R		1TS
49	160511	14/5 (1)	20 3261	100 3081	N Thailand	CK	R		2TS
50	160512	14/6 (1)	20 3261	100 3138	N Thailand	CK	R	PD	2TS
51	160513	14/7	20 3360	100 3216	N Thailand	CK	R	PD	1TS
52	160514	14/8 (1)	20 3628	100 3544	N Thailand	CK	R	PD	2TS
53	160515	16/1 (1)	19 7001	100 4006	N Thailand	CK	R		2TS
54	160516	16/2	19 6938	100 4006	N Thailand	CK	R		1TS
55	160517	16/3 (1)	19 7155	100 3960	N Thailand	CK	R		1TS
56	160518	16/3 (2)	19 7155	100 3960	N Thailand	CK	R		1TS
57	160519	16/3 (3)	19 7155	100 3960	N Thailand	CK	R		1TS
58	160520	16/4	19 7120	100 3855	N Thailand	CK	R		1TS
59	160521	16/5	19 7147	100 3865	N Thailand	CK	R		1TS
60	160522	16/6	19 7201	100 3855	N Thailand	CK	R		1TS
61	160523	16/7	19 7336	100 3895	N Thailand	CK	R		1TS
62	160524	17/2	19 8720	100 4862	N Thailand	CK	R		1TS
63	160525	17/7 (1)	19 9536	100 4449	N Thailand	CK	R	PD	1TS
64	160526	17/7 (2)	19 9536	100 4449	N Thailand	CK	R	PD	1TS
65	160527	17/7 (3)	19 9536	100 4449	N Thailand	CK	R	PD	1TS
66	160528	17/8	19 9563	100 4478	N Thailand	CK	R		1TS
67	160529	17/9 (2)	19 9734	100 4613	N Thailand	CK	R	PD	1TS
68	160530	17/9 (3)	19 9734	100 4613	N Thailand	CK	R	PD	2TS
69	160531	17/10 (1)	20 1856	100 4772	N Thailand	CK	R	PD	2TS
70	160532	17/11	20 1884	100 4734	N Thailand	CK	R		1TS
71	160533	18/1	19 8779	100 3124	N Thailand	CK	R	PD	1TS
72	160534	18/2	19 8705	100 3257	N Thailand	CK	R	PD	1TS
73	160535	18/3 (1)	20 0059	100 0990	N Thailand	CK	R	PD	1TS
74	160536	18/3 (2)	20 0059	100 0990	N Thailand	CK	R		1TS
75	160537	18/5	20 1055	100 2001	N Thailand	CK	R		1TS
76	160538	5/1	18 2624	99 5440	N Thailand	LP	R	PD	1TS
77	160539	5/2	18 2551	99 5562	N Thailand	LP	R		1TS
78	160540	5/3	18 2551	99 5562	N Thailand	LP	R	PD	1TS
79	160541	5/4	18 2551	99 5562	N Thailand	LP	R		1TS
80	160542	6/1	17 9544	99 9500	N Thailand	LP	R		1TS
81	160543	6/2	17 9636	99 9274	N Thailand	LP	R		1TS
82	160544	6/3	17 9918	99 8737	N Thailand	LP	R		1TS
83	160545	6/4	18 9522	99 7409	N Thailand	LP	R	PD	1TS
84	160546	6/5	18 2460	99 5676	N Thailand	LP	R	PD	1TS
85	160547	7/2	18 9270	99 7132	N Thailand	LP	R	PD	1TS
86	160548	7/3 (1)	18 9243	99 7180	N Thailand	LP	R	PD	1TS
87	160549	7/3 (2)	18 9243	99 7180	N Thailand	LP	R		1TS
88	160550	7/3 (3)	18 9243	99 7180	N Thailand	LP	R		1TS
89	160551	7/3 (4)	18 9243	99 7180	N Thailand	LP	R		1TS
90	160552	7/4 (1)	18 9333	99 7094	N Thailand	LP	R-chip	PD	1TS
91	160553	7/4 (2)	18 9333	99 7094	N Thailand	LP	Missing	PD	1TS
92	160554	7/4 (3)	18 9333	99 7094	N Thailand	LP	R		1TS
93	160555	7/5	18 9351	99 7066	N Thailand	LP	R	PD	1TS
94	160556	7/6	18 9460	99 7048	N Thailand	LP	R	PD	1TS
95	160557	7/7 (1)	18 9569	99 7029	N Thailand	LP	R	PD	1TS
96	160558	7/7 (2)	18 9569	99 7029	N Thailand	LP	R	PD	1TS

No	Utas#	Field Number	Latitude (decimal)	Longitude (decimal)	Geographical Area	Position Details	Hand specimen	Powder	Thin Section
97	160559	9/1	17 5298	99 3458	N Thailand	LP	R		1TS
98	160560	9/2	17 5434	99 3232	N Thailand	LP	R		1TS
99	160561	12'/1 (1-1)	18 2136	99 5429	N Thailand	LP	R	PD	1TS
100	160562	12'/1 (1-2)	18 2136	99 5429	N Thailand	LP	R		1TS
101	160563	12'/1 (1-3)	18 2136	99 5429	N Thailand	LP	R	PD	1TS
102	160564	12'/1 (1-4)	18 2136	99 5429	N Thailand	LP	Missing	PD	1TS
103	160565	12'/1 (2-1)	18 2136	99 5429	N Thailand	LP	R	PD	1TS
104	160566	12'/1 (2-2)	18 2136	99 5429	N Thailand	LP	R		1TS
105	160567	12'/1 (3-1)	18 2136	99 5429	N Thailand	LP	R	PD	1TS
106	160568	12'/1 (3-2)	18 2136	99 5429	N Thailand	LP	R		1TS
107	160569	12'/1 (4)	18 2136	99 5429	N Thailand	LP	R		1TS
108	160570	12'/1 (5)	18 2136	99 5429	N Thailand	LP	R	PD	1TS
109	160571	12'/1 (6)	18 2136	99 5429	N Thailand	LP	R		1TS
110	160572	12'/1 (7)	18 2136	99 5429	N Thailand	LP	R		1TS
111	160573	12'/1 (8)	18 2136	99 5429	N Thailand	LP	R	PD	1TS
112	160574	12'/1 (9)	18 2136	99 5429	N Thailand	LP	R	PD	1TS
113	160575	12'/2 (1)	18 2904	99 5535	N Thailand	LP	R		1TS
114	160576	12'/2 (2)	18 2904	99 5535	N Thailand	LP	R	PD	1TS
115	160577	12'/3 (1)	18 2886	99 5563	N Thailand	LP	R		1TS
116	160578	12'/3 (2)	18 2886	99 5563	N Thailand	LP	R		1TS
117	160579	12'/4	18 2849	99 5592	N Thailand	LP	R		1TS
118	160580	12'/5 (1)	18 2560	99 5487	N Thailand	LP	R	PD	1TS
119	160581	12'/5 (2)	18 2560	99 5487	N Thailand	LP	R	PD	1TS
120	160582	12'/5 (3)	18 2560	99 5487	N Thailand	LP	R	PD	1TS
121	160583	12'/5 (4)	18 2560	99 5487	N Thailand	LP	R		1TS
122	160584	12'/6 (1)	18 9623	99 6963	N Thailand	LP	R	PD	1TS
123	160585	12'/6 (2)	18 9623	99 6963	N Thailand	LP	R		1TS
124	160586	12'/6 (3)	18 9623	99 6963	N Thailand	LP	R		1TS
125	160587	12'/7 (1)	18 9605	99 7010	N Thailand	LP	R		2TS
126	160588	12'/8	18 9433	99 7028	N Thailand	LP	R	PD	1TS
127	160589	12'/9	18 9388	99 7057	N Thailand	LP	R	PD	1TS
128	160590	12'/10	18 9351	99 7085	N Thailand	LP	Missing	PD	1TS
129	160591	12'/11	17 9690	99 9265	N Thailand	LP	R		1TS
130	160592	13'/3	17 6239	99 3139	N Thailand	LP	R	PD	1TS
131	160593	13'/5	17 6148	99 3214	N Thailand	LP	Missing		1TS
132	160594	13'/7	17 4469	99 1761	N Thailand	LP	R		1TS
133	160595	13'/8	17 4505	99 1771	N Thailand	LP	R		1TS
134	160596	13'/9	17 4749	99 1884	N Thailand	LP	R	PD	1TS
135	160597	13'/10	17 4704	99 1818	N Thailand	LP	R		1TS
136	160598	13'/11 (1)	17 4677	99 1780	N Thailand	LP	R	PD	1TS
137	160599	13'/11 (2)	17 4677	99 1780	N Thailand	LP	R		1TS
138	160600	15'/1 (1)	20 2992	100 2763	N Thailand	CK	R	PD	1TS
139	160601	15'/1 (2)	20 2992	100 2763	N Thailand	CK	R		1TS
140	160602	15'/1 (3)	20 2992	100 2763	N Thailand	CK	R	PD	1TS
141	160603	15'/1 (4)	20 2992	100 2763	N Thailand	CK	Missing	PD	1TS
142	160604	15'/1 (5)	20 2992	100 2763	N Thailand	CK	R	PD	1TS
143	160605	15'/2 (1)	20 3056	100 2706	N Thailand	CK	R	PD	1TS
144	160606	15'/2 (2)	20 3056	100 2706	N Thailand	CK	R	PD	1TS
145	160607	15'/3 (1)	20 3146	100 2831	N Thailand	CK	R	PD	1TS
146	160608	15'/3 (2)	20 3146	100 2831	N Thailand	CK	R	PD	1TS
147	160609	15'/3 (3)	20 3146	100 2831	N Thailand	CK	R		1TS
148	160610	15'/3 (4)	20 3146	100 2831	N Thailand	CK	R	PD	1TS

No	Utas#	Field Number	Latitude (decimal)	Longitude (decimal)	Geographical Area	Position Details	Hand specimen	Powder	Thin Section
149	160611	15'/3 (5)	20 3146	100 2831	N Thailand	CK	R	PD	1TS
150	160612	15'/4 (1)	20 3252	100 3071	N Thailand	CK	R	PD	1TS
151	160613	15'/4 (2)	20 3252	100 3071	N Thailand	CK	R	PD	1TS
152	160614	15'/4 (3)	20 3252	100 3071	N Thailand	CK	R	PD	1TS
153	160615	15'/5	20 3519	100 3687	N Thailand	CK	R		1TS
154	160616	15'/6	20 1957	100 4601	N Thailand	CK	R		1TS
155	160617	15'/7	19 9851	100 4605	N Thailand	CK	R	PD	1TS
156	160618	15'/8	19 9770	100 4604	N Thailand	CK	R	PD	1TS
157	160619	15'/9 (1)	19 9662	100 4574	N Thailand	CK	R		1TS
158	160620	15'/9 (2)	19 9662	100 4574	N Thailand	CK	R		1TS
159	160621	15'/10 (1)	19 9492	100 4401	N Thailand	CK	R		1TS
160	160622	15'/10 (2)	19 9492	100 4401	N Thailand	CK	R	PD	1TS
161	160623	15'/11	19 9429	100 4333	N Thailand	CK	R		1TS
162	160624	15'/12 (1)	19 9060	100 4101	N Thailand	CK	R		1TS
163	160625	15'/12 (2)	19 9060	100 4101	N Thailand	CK	R		1TS
164	160626	15'/13 (1)	19 9033	100 4062	N Thailand	CK	R		1TS
165	160627	15'/13 (2)	19 9033	100 4062	N Thailand	CK	R	PD	1TS
166	160628	15'/13 (3)	19 9033	100 4062	N Thailand	CK	R		1TS
167	160629	15'/14	19 8088	100 3605	N Thailand	CK	R		1TS
168	160630	15'/15 (1)	19 8062	100 3538	N Thailand	CK	R	PD	1TS
169	160631	15'/15 (2)	19 8062	100 3538	N Thailand	CK	R	PD	1TS
170	160632	15'/15 (3)	19 8062	100 3538	N Thailand	CK	R		1TS
171	160633	15'/16 (1)	19 3210	100 2270	N Thailand	CK	R	PD	1TS
172	160634	15'/16 (2)	19 3210	100 2270	N Thailand	CK	R	PD	1TS
173	160635	15'/16 (3)	19 3210	100 2270	N Thailand	CK	R	PD	1TS
174	160636	16'/1	19 9852	100 3305	N Thailand	CK	R		1TS
175	160637	16'/2 (1)	19 9690	100 3256	N Thailand	CK	R		1TS
176	160638	16'/2 (2)	19 9690	100 3256	N Thailand	CK	R	PD	1TS
177	160639	16'/2 (3)	19 9690	100 3256	N Thailand	CK	R	PD	1TS
178	160640	16'/4	19 9005	100 3021	N Thailand	CK	R	PD	1TS
179	160641	16'/5 (1)	19 8987	100 3011	N Thailand	CK	R	PD	1TS
180	160642	16'/5 (2)	19 8987	100 3011	N Thailand	CK	R	PD	1TS
181	160643	16'/6 (1)	19 8987	100 2992	N Thailand	CK	R	PD	1TS
182	160644	16'/6 (2)	19 8987	100 2992	N Thailand	CK	R		1TS
183	160645	16'/6 (3)	19 8987	100 2992	N Thailand	CK	R	PD	1TS
184	160646	16'/7 (1)	19 8654	100 2875	N Thailand	CK	R	PD	1TS
185	160647	16'/7 (2)	19 8654	100 2875	N Thailand	CK	R		1TS
186	160648	16'/8	19 8492	100 2730	N Thailand	CK	R		1TS
187	160649	16'/9	19 8105	100 2527	N Thailand	CK	R		1TS
188	160650	16'/10 (1)	19 3183	100 2251	N Thailand	CK	R	PD	1TS
189	160651	16'/10 (2)	19 3183	100 2251	N Thailand	CK	R		1TS
190	160652	16'/11 (1)	18 1832	100 3710	N Thailand	CM	R		1TS
191	160653	16'/11(2)	18 1832	100 3710	N Thailand	CM	R		1TS
192	160654	20'/1	18 2460	99 5676	N Thailand	LP	R		1TS
193	160655	20'/2 (1)	18 2460	99 5676	N Thailand	LP	R		1TS
194	160656	20'/3 (1)	18 2460	99 5676	N Thailand	LP	R		3TS
195	160657	20'/4	18 2460	99 5676	N Thailand	LP	R		1TS
196	160658	20'/5	18 2460	99 5676	N Thailand	LP	R	PD	1TS
197	160659	20'/6	18 2460	99 5676	N Thailand	LP	R	PD	1TS
198	160660	24'/2	17 6411	99 3036	N Thailand	LP	R		1TS
199	160661	24'/5	17 6094	99 3261	N Thailand	LP	R		1TS
200	160662	24'/9	17 7277	99 3971	N Thailand	LP	R		1TS

No	Utas#	Field Number	Latitude (decimal)	Longitude (decimal)	Geographical Area	Position Details	Hand specimen	Powder	Thin Section
201	160663	25'/1	20 2992	100 2763	N Thailand	CK	R	PD	1TS
202	160664	26'/2	20 1091	100 3283	N Thailand	CK	R		1TS
203	160665	26'/10	20 1105	100 1322	N Thailand	CK	R	PD	1TS
204	160666	27'/3	19 7129	100 3855	N Thailand	CK	R		1TS
205	160667	27'/4	19 7201	100 3855	N Thailand	CK	R		1TS
206	160668	12"/3	17 8263	99 3397	N Thailand	LP	R		1TS
207	160669	8"-2	19 7081	100 4217	N Thailand	CK	R		1TS
208	160670	8"-3	19 7144	100 4179	N Thailand	CK	R		1TS
209	160671	8"-4	19 7181	100 4132	N Thailand	CK	R		1TS
210	160672	8"-5	19 7190	100 4113	N Thailand	CK	R		1TS
211	160673	8"-6	19 7163	100 4046	N Thailand	CK	R		1TS
212	160674	8"-8	19 7183	100 3865	N Thailand	CK	R		1TS
213	160675	8"-9	19 7192	100 3855	N Thailand	CK	R		1TS
214	160676	8"-11	19 7309	100 3885	N Thailand	CK	R		1TS
215	160677	8"-12	19 7418	100 3895	N Thailand	CK	R		1TS
216	160678	8"-14	19 7760	100 4003	N Thailand	CK	R		1TS
217	160679	8"-15	19 7940	100 4148	N Thailand	CK	R		1TS
218	160680	27'/8	19 8571	100 4335	N Thailand	CK	R		1TS
219	160681	28'/2	20 1954	100 4684	N Thailand	CK	R		1TS
220	160682	28'/6	20 1666	100 5779	N Thailand	CK	R		1TS
221	160683	29'-2	19 8105	100 2527	N Thailand	CK	R		1TS
222	160684	29'/3	19 3210	100 2270	N Thailand	CK	R		1TS
223	160685	29'/4	19 7537	100 2398	N Thailand	CK	R		1TS
224	160686	2/4	19 6942	100 3472	N Thailand	CK	R		1TS
225	160687	2/8*	19 6938	100 4006	N Thailand	CK	R		1TS
226	160688	3/1*	19 6846	100 4139	N Thailand	CK	R		1TS
227	160689	3/5*	19 6819	100 4148	N Thailand	CK	R		1TS
228	160690	9/1*	20 2237	100 1872	N Thailand	CK	R		1TS
229	160691	10/1*	20 3877	100 2584	N Thailand	CK	R		1TS
230	160692	12/3*	19 9248	100 5121	N Thailand	CK	R		1TS
231	160693	12/4*	19 9194	100 5073	N Thailand	CK	R		1TS

Appendix F

Submitted paper for *The Island Arc (in press)*

Geochemistry and Geochronology of Late Triassic Volcanic Rocks in the Chiang Khong Region, Northern Thailand

Weerapan Srichan*, Anthony J. Crawford and Ronald F. Berry

CODES ARC Centre of Excellence in Ore Deposits, University of Tasmania, Private Bag 79, Hobart, Tasmania, 7001, Australia (srichanw@utas.edu.au)

Abstract

The Chiang Khong segment of the Chiang Khong-Lampang-Tak Volcanic Belt is composed of three broadly meridional sub-belts of mafic to felsic volcanic, volcaniclastic and associated intrusive rocks. Associated sedimentary rocks are largely non-marine redbeds and conglomerates. Three representative Chiang Khong lavas have Late Triassic (223 - 220 Ma) laser ablation ICPMS U-Pb zircon ages. Felsic-dominated sequences in the Chiang Khong Western and Central Sub-belts are high-K calc-alkaline rocks that range from basaltic to dominant felsic lavas with rare mafic dykes. The Western Sub-belt lavas have slightly lower HFSE contents at all fractionation levels than equivalent rocks from the Central Sub-belt. In contrast, the Eastern Sub-belt is dominated by mafic lavas and dykes with compositions transitional between E-MORB and back-arc basin basalts. The Eastern Sub-belt rocks have higher FeO* and TiO_2 and less LREE-enrichment than basalts in the high-K sequences. Basaltic and doleritic dykes in the Western and Central Sub-belts match the composition of the Eastern Sub-belt lavas and dykes.

A recent geochemical study of the Chiang Khong rocks concluded that they were erupted in a continental margin volcanic arc setting. However, based on the dominance of felsic lavas and the mainly non-marine associated sediments, we propose an alternative origin, in a post-collisional extensional setting. A major late Middle to early Late Triassic collisional orogenic event is well documented in northern Thailand and Yunnan. We believe that the paucity of radiometric dates for arc-like lavas in the Chiang Khong-Lampang-Tak Volcanic Belt that precede this orogenic event, coupled with the geochemistry of the Chiang Khong rocks, and strong compositional analogies with other post-collisional

magmatic suites, are features that are more typical of volcanic belts formed in a rapidly evolving post-collisional, Basin and Range-type extensional setting.

Keywords: Thailand tectonics, Chiang Khong-Lampang-Tak Volcanic Belt, post-collisional magmatism, Late Triassic volcanic rocks.

Introduction

Four major pre-Jurassic volcanic belts have been identified in Thailand (Fig. 1): the Chiang Rai-Chiang Mai Volcanic Belt in the west, the Chiang Khong - Lampang - Tak Volcanic Belt, the Nan - Chanthaburi Suture Zone, and in the east, the Loei – Petchabun - Nakhon Nayok Volcanic Belt (Jungyusuk & Khositanont 1992; Panjasawatwong *et al.* 1997; Kosuwan 2004). The age and tectonic setting of eruption of magmatic rocks in these belts are important ingredients in any model for the tectonic evolution in northern Thailand and neighboring areas.

The Chiang Rai-Chiang Mai Volcanic Belt has been suggested to be one or more slices of Palaeo-Tethyan oceanic crust (Macdonald & Barr 1987; Barr *et al.* 1990; Panjasawatwong *et al.* 1995; Panjasawatwong 1999; Metcalfe 2002; Wakita & Metcalfe 2005; Phajuy *et al.* 2005), and the rock association of this belt has been interpreted to correlate with, and form a northern continuation of the Bentong - Raub Suture of peninsular Malaysia to the south (Metcalfe 2000), and a southern extension of the Changning - Menglian Suture in Yunnan (SW China) to the north (Wu *et al.* 1995). Further east, volcanics in the Chiang Khong – Lampang - Tak Belt in the central part of Sukhothai Fold Belt (Singharajwarapan & Berry 2000) have been interpreted to represent a continental margin arc assemblage (Barr *et al.* 2000, 2006; Panjasawatwong *et al.* 2003; Phajuy 2001) and correlated with volcanic rocks of similar age in the Lincang - Jinghong Volcanic Belt in southern Yunnan (Yang *et al.* 1994; Barr *et al.* 2000).

The Nan - Chanthaburi Suture Zone was interpreted to represent the collisional suture formed when westward subduction beneath the Shan-Thai Terrane resulted in collision between this block and the Indochina Terrane to the east (Panjasawatwong 1991; Singharajwarapan 1994; Crawford & Panjasawatwong 1996; Hada *et al.* 1999; Singharajwarapan & Berry 2000). Volcanic rocks in the Loei - Petchabun - Nakhon Nayok Volcanic Belt have been interpreted to represent arc-related volcanism (Bunopas 1981; Intasopa & Dunn 1994; Kosuwan 2004), although MORB-like tholeiitic basalts and microgabbro dykes have been recorded in some areas (Panjasawatwong *et al.* 2006).

Wakita & Metcalfe (2005) proposed that the Palaeo-Tethys Ocean is represented in East and Southeast Asia by both oceanic and marginal basins. They also suggested that the main Palaeo-Tethys oceanic basin is represented by a progression of sutures that extend southward from the Lancangjiang and Changning - Menglian zones in Yunnan, through the Chiang Rai - Chiang Mai Volcanic Belt in northern Thailand, the Sra Kaeo belt in eastern Thailand and the Bentong - Raub Suture in Malaya. The Jinshajiang and Ailaoshan (Yunnan) and Nan-Chanthaburi suture zones have been re-interpreted as representing the site of a back-arc basin (Wang *et al.* 2000; Metcalfe 2002; Wakita & Metcalfe 2005) rather than the collisional suture between the Shan-Thai and Indochina terranes.

The variety of tectonic settings interpreted for the pre-Jurassic volcanic belts in Thailand reflects significant uncertainty, also evident in the relatively poor knowledge of the complex regional geology of the region. Clearly, further data on the petrochemistry, geochronology and tectonic significance of the main volcanic belts is required, especially for the relatively poorly known Chiang Khong-Lampang-Tak Volcanic Belt.

Geological Setting of Chiang Khong-Lampang-Tak Volcanic Belt

The Chiang Khong-Lampang-Tak Volcanic Belt (CLT) is located in the central part of Sukhothai Fold Belt, northern Thailand, between latitudes 16°N and 20°N, and longitude 99°E and 101°E, covering an area of about 4,000 km^2. The CLT forms a NNE-SSW S-shaped trend, distributed from the Chiang Khong district in the north, through the central part of Phayao province, along the border region between Lampang and Phrae provinces, and terminates in the south in the eastern part of Tak province (Fig. 1).

Our on-going studies of the CLT volcanic belt focus on two regions, the northern, or Chiang Khong area extending some 80 km south from the Mae Khong River border with Laos, and the southern, or Lampang area. Here, we report new geochemical and geochronological data for the Chiang Khong area, where sampling concentrated on relatively continuous, better exposed sections along the Mae Khong River, and along road and creek exposures. Our comprehensive data is compared to existing information on the volcanic rocks in this belt provided in Panjasawatwong *et al.* (2003) and Barr *et al.* (2006).

The Chiang Khong Area

Geological Setting

The Chiang Khong area is located in the eastern part of Chiang Rai province, and is characterized by relatively high mountain ranges trending NNE-SSW and parallel intermontane basins, with these strong linear trends probably controlled by major faults.

The first geological map of the region was made by the German Geological Mission to Thailand at 1:250,000 (Braun & Hahn 1976). The geological map of the Chiang Khong area in Fig. 2 was assembled from existing 1:50,000 mapping by the Geological Survey Division, Department of Mineral Resources, Thailand (Sukvattananunt *et al.* 1985a, 1985b; Sukvattananunt & Assawapatchara 1989a, 1989b, 1989c, 1989d; Tansuwan & Chitmanee 1990a, 1990b), and new mapping carried out by the first author during three field seasons in 2005 and 2006.

The Chiang Khong-Lampang-Tak Volcanic Belt in the Chiang Khong region comprises three sub-parallel belts, from west to east, the Chiang Khong Western Belt (CK-WB), Chiang Khong Central Belt (CK-CB) and Chiang Khong Eastern Belt (CK-EB) (Fig. 2). Barr *et al.* (2006) referred to the CK-WB as the Doi Khun Ta Khuan belt, and our CK-CB they referred to as the Doi Yao belt. Volcanic rocks in the Western and Central belts include mainly intermediate and felsic rocks and their volcaniclastic equivalents, and shallow sub-volcanic dykes. Mafic volcanics occur only in the Eastern Belt, whereas mafic rocks in Western and Central Belts are dykes. On the basis of previous stratigraphic correlations (Jungyusuk & Khositanont 1992), these rocks have been interpreted to have been emplaced in two magmatic events, one Permo-Triassic and the other in Late Triassic – Early Jurassic. The Chiang Khong-Lampang-Tak Volcanic Belt rocks in this area conformably overlie, or are in fault contact with, Permo-Triassic sedimentary rocks and Middle to Late Triassic sedimentary rocks.

CK-WB rocks are exposed along the Doi Luang - Phrae Muang and Doi Khun Ta Khuan mountain ranges, west of the Chiang Khong district, and they extend south to the Doi Luang and Praya Mengrai districts. Outcrops show strong structural control by regional strike slip faults of Tertiary age. The CK-WB rocks comprise volcaniclastics, lavas and dykes, and range from mafic to felsic compositions. Mafic rocks occur mainly as shallow intrusives or dykes. The CK-WB rocks lie unconformably above, or are in fault contact with, Permo-Triassic sedimentary rocks, and are unconformably overlain by, or are in fault contact with, Tertiary and Quaternary semi –consolidated and unconsolidated sediments.

CK-CB rocks form the NNE-SSW-trending Doi Yao mountain range. Volcanic rocks in this sub-belt are mainly intermediate to felsic volcaniclastics and lavas. Mafic rocks are rare in CK-CB and crop out along Mae Khong River as dykes cutting andesitic lavas. Rhyolitic lava is locally exposed in the southern part of CK-CB, where flows around 4 m thick overlie andesitic volcaniclastics that dip to the southwest. A west- to southwest-dipping well developed cleavage is common in outcrops of CK-CB rocks. These rocks are unconformably overlain by and in fault contact with the Late Triassic red beds and Quaternary unconsolidated sediments.

The CK-EB rocks differ from the CK-WB and CK-CB sequences in being dominated by mafic lavas and dykes. They crop out occasionally in the low relief intermontane basin between the CK-CB and the metamorphic zone. Volcanic rocks in the CK-EB are conformably overlain by, or are in fault contact with, Late Triassic sedimentary rocks in some places, and are in fault contact with Carboniferous meta-sandstone and shale further east (Tansuwan & Chitmanee 1990a, 1990b).

Samples and Analytical Methods

Our mapping and sampling of rocks from the Chiang Khong section of the Chiang Khong-Lampang-Tak Volcanic Belt covered effectively the entire belt, from the Mae Khong River in the north at the border with Laos, south to the Thoeng district. The more than 150 rocks selected for this study were mainly collected from exposures along and adjacent to main and minor roads across this area. Approximately 100 representative fresh rock samples were petrographically examined, and the 71 freshest rock samples were selected for whole-rock analysis by XRF. Sixteen representative samples were also analysed for low-abundance trace elements and REE by solution ICP-MS. Three representative dacitic/rhyolitic rocks were dated for this study via U-Pb in zircon using ICP-MS. All petrographic, geochemical and U-Pb zircon age dating were done in the School of Earth Sciences, University of Tasmania.

Major and trace elements were analysed using a PANalytical (Philips) PW 1480 X-Ray Fluorescence (XRF) spectrometer. Major elements were measured from fusion discs prepared at 1,100°C in 5%Au/95%Pt crucibles, 0.500g sample, 4.500g 12-22 Flux (lithium tetraborate-metaborate mix) and 0.0606g $LiNO_3$, following the technique described in

Robinson (2003). Loss on ignition (LOI) was determined by heating 1-2 g of sample at 1,000°C for 12 hours and reweighing. Pressed powder pellets for trace element analysis were prepared at 3.5 tonnes cm^{-2} with a diameter of 32 mm using 10 g of sample and PVP-MC (Polyvinylpyrrolidone-Methylcellulose) as binder. Trace elements were measured with a 3kW max. ScMo anode X-Ray tube and 3kW max. Au anode X-Ray tube (Watson 1996).

The 16 representative Chiang Khong samples selected for low-abundance trace element and REE analysis were analysed using a HP4500 Inductively Coupled Plasma Mass Spectrometer (ICP-MS). Sample solutions for ICP-MS analysis were prepared using PicoTrace® high pressure acid (HF/H_2SO_4) digestion. Aliquots (100 mg) of powdered sample were weighed into 30 ml PTFE digestion containers. After wetting the samples with a few drops of ultra-pure water and adding 0.1 ml of $\mu g\ g^{-1}$ indium solution to each digestion container, 3 ml HF and 3 ml H_2SO_4 were slowly added. After thorough mixing by shaking a few times, the PTFE containers were left in the digestion block at 180°C for 16 hours. The digestion mixture was then evaporated to dryness at 180°C for four days in the evaporation block. $HClO_4$ (1 ml) was added to the residue and dried before adding the final 2 ml HNO_3 and 1 ml HCl. The residue was dissolved by warming the solution in the digestion block at 60-70°C for ~ 1 hour. After the solution became clear, it was transferred into a polypropylene bottle and diluted to 100 ml (Yu *et al.* 2001), then analyzed. Comparison between XRF and solution ICP-MS analyses of elements analysed by both techniques showed < 5% variation.

The U-Pb zircon age dating used an HP4500 quadrupole ICP-MS with a 213 nm New Wave Laser. Zircons were separated from 100 to 200g of rock by crushing to < 400 micron in a mortar and pestle or a Cr-steel ring mill, depending on sample hardness. Heavy minerals were then separated using a combination of mechanised panning device (superpan) and a hand pan. The heavy mineral residue was then dried. Magnetic and paramagnetic minerals were removed using a hand magnet and a Franz magnetic separator. Approximately 20 to 30 zircons were picked from the non-magnetic heavy mineral separate using a single hair from a paint brush, and mounted on double sided sticky tape. Epoxy glue was then poured into a 2.5 cm diameter mould on top of zircon grains. The mount was dried for 12 hours and polished using clean sandpaper and a clean polishing lap. The samples were then washed in distilled water in an ultrasonic bath. Zircons were ablated in a He atmosphere in a custom-made chamber with the laser pulsing at 5 Hz and a

30 micron diameter beam delivering ~ 12 J/cm^2 and drilling at approximately 1 micron/s. A total of 11 masses were counted (^{96}Zr, ^{146}Nd, ^{178}Hf, ^{202}Hg, ^{204}Pb, ^{206}Pb, ^{207}Pb, ^{208}Pb, ^{232}Th , ^{238}U), with longer counting times on Pb isotopes giving a total quadrupole cycling rate of 0.2s. Each analysis began with a 30 seconds analysis of background gas followed by 30 seconds with the laser switched on. Four primary (Temora zircons of Black *et al.* 2004) and 2 secondary standards (91500 of Wiedenbeck *et al.* 1995) were analysed both before and after every 12 zircon analyses to correct for mass bias, machine drift and down hole fractionation. Repeated monitoring of U/Pb mass fractionation during drilling showed an average fractionation of U/Pb varying from 0.050 at the start of a 30sec analysis to 0.053 at the deepest level of laser ablation. Monitoring of international standards showed a reproducible error of +/-2 m.y.

Age of Volcanic Rocks

Previous studies (Sukvattananunt *et al.* 1985a, 1985b; Sukvattananunt & Assawapatchara 1989a, 1989b, 1989c, 1989d; Tansuwan & Chitmanee 1990a, 1990b; Jungyusuk & Khositanont 1992) have suggested that the Chiang Khong rocks interpreted as Permo-Triassic volcanics, comprise rhyolitic lavas and volcaniclastics, and andesitic volcaniclastics, whereas the sequence interpreted to be Late Triassic-Early Jurassic in age by Jungyusuk and Khositanont (1992) is composed of andesitic, dacitic, and rhyolitic lavas and their volcaniclastic equivalents. However, on the basis of whole-rock geochemical data, Panjasawatwong *et al.* (2003) argued that at least some of the rocks previously considered to be Late Triassic to Early Jurassic in age are probably better correlated with the Permo-Triassic sequences.

Radiometric ages for these sequences are sparse. A representative rhyolitic volcaniclastic rock from the northern end of the Central Belt (CK-CB) yielded a Middle Triassic U-Pb zircon age of 232.9 ± 0.4 Ma (Barr *et al.* 2006). We have determined LA-ICP-MS U-Pb zircon ages for three samples from the Chiang Khong area, including two rhyolitic lavas from the Western Belt (Fig. 3) that gave ages of 222 ± 6 Ma and 223 ± 8 Ma, and a rhyolitic lava from the central section of the Central Belt that gave an age of 220 ± 4 Ma (Table 1). We note a minor Mid-Paleozoic inheritance in our analysed zircons (Fig. 3), and suggest that the ~10 m.y. difference between our ages and the older 233 Ma age reported by Barr et al. (2006) may be due to the presence of this inherited component among the zircons dated via TIMS technique by Barr et al. (2006). The consistency of these ages for the Central Belt and Western Belt felsic lavas, plus the lithological and geochemical similarity of these belts, strongly supports the suggestion of Barr *et al.* (2006) that they represent slices of the same original Middle to Late Triassic volcanic pile, now repeated by faulting (Fig. 2).

In contrast, the CK-EB is dominated by mafic lavas and dykes for which we have no radiometric ages. However, the CK-EB volcanic rocks show stratigraphic contacts with sedimentary rocks of Late Triassic age, and several dykes compositionally akin to the CK-EB lavas and dykes intrude felsic rocks in the CK-WB and CK-CB, suggesting that the CK-EB sequence may be younger than the western and central volcanic sub-belts.

Petrology and Geochemistry of Chiang Khong Volcanic Belt Rocks

Previous petrochemical study of Chiang Khong volcanic rocks by Panjasawatwong *et al.* (2003) and Barr *et al.* (2006) reported in total 38 analyses and concluded that these rocks had subduction-related calc-alkaline affinities, with both the compositional range and the relatively abundant felsic lavas (often ignimbritic) best matching those formed in modern continental margin volcanic arcs. Our 71 new whole-rock analyses span the geographic range of the Chiang Khong volcanic belt, and representative analyses recalculated to 100 wt% volatile-free are given in Table 3.

Virtually all analysed samples show excellent textural preservation. The metamorphic grade varies from prehnite-pumpellyite facies to low greenschist facies, with the latter being defined by the presence of fibrous actinolite usually replacing clinopyroxene. Plagioclase crystals in both the intrusive and extrusive rocks of all groups vary from partly fresh with epidote or sericite alteration, to totally altered to either or both of those minerals, or totally replaced by clear albite that is sometimes speckled by sericite. Carbonate minerals are rare. Petrographic details of the representative Chiang Khong volcanic rocks are presented in Table 2 and summarised below. In the geochemical tables and discussion, lavas have the suffix –L, and –D for dykes and other shallow intrusive rocks, although in areas of poor outcrop, we experienced considerable difficulty in determining whether some more mafic units were flows or narrow dykes.

It is well known that regional low-grade alteration of igneous rocks can significantly affect their geochemical compositions. Typically, CaO (and Sr), the alkaline oxides Na_2O and K_2O, and Ba and Rb are regarded as being potentially mobile during such alteration, and interpretation of their abundances must be done with care. In contrast, total Fe (measured as Fe_2O_3 via XRF), MgO, Al_2O_3 and the transition (Ni, Cr, V, Sc) and high field strength elements (Ti, P, Zr, Y, Nb, Ta, Hf) have been regarded as being essentially immobile during low-grade alteration, especially in rocks with excellent textural preservation. Therefore, the following evaluation of the geochemical affinities of the Chiang Khong Volcanic Belt rocks focuses on the immobile elements, but also examines the contents, variation and implications of their K_2O contents.

Petrography

Typically, rocks with basaltic to andesitic compositions, whether lavas or dykes, are either aphyric or sparsely plagioclase- or plagioclase+augite-phyric. Evolved andesitic to dacitic (60-71 wt % SiO_2) rocks include plagioclase+clinopyroxene (chloritized)+apatite +Fe-Ti oxide-phyric lavas with devitrified glassy groundmasses. Included in this group are diorite, quartz diorite and monzodiorite with holocrystalline textures defined by intergrown clinopyroxene, plagioclase, hornblende, Fe-Ti oxides and minor altered biotite. Felsic rocks with rhyolitic compositions comprise plagioclase+quartz-phyric lavas, and welded ignimbrites were noted at several locations, as also documented by Barr *et al.* (2006).

Major and Trace Element Geochemistry

Some 71 new whole-rock major and trace element analyses of lavas and dykes from the Chiang Khong area have been done for this study, 40 from the CK-WB, 20 from the CK-CB and 11 from the CK-EB. Representative analyses are given in Tables 3 and 4. Complementing our data are whole-rock analyses of 8 samples from the CK-WB and 14 from the CK-CB reported by Barr *et al.* (2006), and 16 analyses of the least altered mafic to intermediate rocks from Panjasawatwong *et al.* (2003), mainly from the CK-WB. A series of compositional variation diagrams against SiO_2 and MgO are shown for rocks from the CLT Volcanic Belt in the Chiang Khong region in Figs. 4 and 5. Key points to note from these plots include:

1: Both the CK-WB and CK-CB show a range of compositions defining broad fractionation trends from mafic to felsic compositions, whereas the CK-EB contains only mafic rocks. Significantly greater compositional spread exists at the more mafic end of the compositional spectrum than at the felsic end.

2: Over most of the fractionation range defined by samples from both the CK-WB and CK-CB, the regular decrease in total Fe (reported herein as Fe_2O_3) and TiO_2 from mafic to felsic compositions is characteristic of magmas with calc-alkaline affinities.

3: Despite the potential mobility of K_2O, our intermediate and felsic samples from the CK-WB and CK-CB define a high-K calc-alkaline trend, whereas many of the CK-EB mafic rocks fall below that field, suggesting low-K or medium-K calc-alkaline affinities for these rocks.

4: Despite the overall similarity in major element variations across the basalt to rhyolite range for rocks from the CK-WB and CK-CB, high field strength elements such as Zr, Nb, Y and LREE (Ce shown in Fig. 6) are consistently slightly higher at any stage of fractionation in CK-WB rocks, suggesting slightly more HFSE-enriched parental magmas for the Western sub-belt rocks.

5: Most mafic rocks analysed from CK-EB, and a significant suite of mafic rocks (most of them dykes) from the CK-WB show quite high Fe_2O_3 (11-14%) and more than 1% TiO_2, whereas the CK-CB mafic lavas, and several from the CK-WB, have Fe_2O_3 and TiO_2 contents <11% and 1.0% respectively. A single analysed basaltic dyke from the CK-CB shows the higher Fe_2O_3 and TiO_2 (12% and 1.6% respectively) characteristic of the higher Fe, higher-Ti group of the CK-WB and CK-EB mafic rocks. In the Fe_2O_3-, TiO_2- and V- vs MgO plots (Fig. 5a, b and c), the majority of high-Fe, high-Ti group rocks have higher Zr/Nb values (>22) than the other mafic rocks (Fig. 5d). Since Zr/Nb is unaffected by fractionation, we consider these mafic rocks to be a separate magmatic suite from the high-K calc-alkaline rocks that dominate the CK-WB and CK-CB in the Chiang Khong area. Two REE patterns (Fig. 7) for the more mafic rocks in the high Zr/Nb suite show significantly flatter profiles than the other mafic rocks from the CK-WB and CK-CB, which show typical medium- to high-K calc-alkaline LREE-enriched patterns (Fig. 7). Notably, the CK-WB high Zr/Nb basaltic dyke with 8.2% MgO has higher chondrite-normalised HREE levels than lower Zr/Nb basalts and andesites with 3.8-5.2% MgO (Fig. 7).

6: Increasing fractionation from andesitic to dacitic compositions leads to higher total REE abundances, but further fractionation to rhyolitic compositions leads to a significant decrease in LREE enrichment, development of a significant negative Eu anomaly, and/or a less pronounced depletion in MREE (Fig. 8). This late depletion in REE is a common feature of rhyolitic magmas developed via fractionation (or AFC) from dacitic precursors, and can be explained qualitatively by crystallisation and removal of LREE- and MREE-enriched accessory phases such as allanite, monazite and apatite (Miller & Mittlefehldt 1982).

7: N-MORB-normalised multi-element patterns for the calc-alkaline lavas (Fig. 9) show the typical depletion in Nb-Ta relative to adjacent LREE, and the enrichment in LILE relative to HFSE that characterise subduction-related magmas. Patterns for the transitional tholeiitic mafic suite (Fig. 10) also show significant but relatively subdued Nb-Ta anomalies and LILE enrichment.

In summary, we identify two major rock suites in the Chiang Khong region sub-belts of the Chiang Khong-Lampang-Tak Volcanic Belt. These include a basalt-andesite-dacite-rhyolite high-K calc-alkaline suite, represented in the CK-WB and CK-CB sub-belts, in which felsic lavas dominate, and a mafic-dominated transitional tholeiitic suite represented by lavas in the CK-EB sub-belt, and dykes through the calc-alkaline felsic lavas in the CK-WB and CK-CB.

Discussion

Felsic-dominated sequences in the CK-WB and CK-CB constitute high-K calc-alkaline rocks, with the suite that dominates the CK-WB having slightly lower HFSE contents at any fractionation level than those rocks forming the CK-CB. Since our zircon dates for rhyolites in the CK-WB and CK-CB are essentially identical, these sub-belts are presumably sampling formerly more or less adjacent high-K calc-alkaline volcanoes.

Barr *et al.* (2006) suggested that the geochemical data for the Chiang Khong Volcanic Belt lavas, occurrence of welded ignimbrites, and their close association with non-marine red beds, indicated formation in a mature continental margin volcanic arc. In particular, the predominance of felsic lavas and relative paucity of mafic rocks in these sequences suggest a substantial thickness of continental crust beneath the region during this Late Triassic magmatism. We note, however, that the relatively restricted range of radiometric ages recorded from the Chiang Khong Volcanic Belt (232-220 Ma) and the apparent absence of Early- and Middle Triassic volcanics is perhaps surprising if the Chiang Khong rocks formed in a continental margin arc, wherein subduction-related magmatism usually shows a long time span.

Although we cannot preclude formation in a continental margin arc such as Japan or Mexico, one other tectonic setting should be considered as a possible scenario for the Late Triassic magmatism in northern Thailand. This is a Basin and Range-type post-orogenic extensional setting, not necessarily related to contemporaneous subduction, or perhaps related to flat-slab subduction. In either of these latter settings, extension leads to magma generation from the subcontinental lithospheric mantle, which may have been enriched in LILE during some preceding subduction episode, producing calc-alkaline magmas. Calc-alkaline magmas in such settings have been described by Ewart *et al.* (1992), Bryan (2007) and Bryan *et al.* (1997; 2000) for the Whitsunday Volcanic Province of coastal NE Australia, by Hooper *et al.* (1995), Rogers *et al.* (1995) and Hawkesworth *et al.* (1995) for the type Basin and Range area in western USA, by Rottura *et al.* (1998) and Bussy *et al.* (2000) for the Western Alps, by Smedley (1986) for the Late Palaeozoic of Scotland, by Fan *et al.* (2001, 2003) for the Late Cretaceous of NE China, and by Crawford *et al.* (1992) and Crawford and Berry (1992) for the post-collisional Cambrian Mount Read Volcanics of western Tasmania, Australia.

In such post-orogenic settings, extension and magma generation in the sub-continental lithospheric mantle may be related to gravitational collapse of the newly thickened crustal collage, mantle convection-induced lithospheric thinning and/or detachment, or slab breakoff (eg. England & Houseman 1989; Davis & von Blanckenburg 1995). Flat slab scenarios have been proposed for the type Basin and Range province in W USA by Humphreys (1995) and for SE China by Li and Li (2007).

Basin and Range-type magmatism and tectonics in western USA, and in the Cretaceous Whitsunday Province of eastern Australia, is characterised by felsic-dominant magmatism, and transitional tholeiitic to calc-alkaline mafic rocks. Intermediate compositions are considered to be derived largely via magma mixing between the subcontinental mantle-derived mafic rocks and the felsic crustal melts (Ewart *et al.* 1992; Bryan *et al.* 1997; Bryan, 2007). Average compositions for the Whitsunday Province define a high-K calc-alkaline suite, and across the compositional range from basalt to rhyolite these lavas and dykes show a striking geochemical similarity to the Chiang Khong high-K calc-alkaline suites (Figs. 11a, b). In particular, Bryan (2007) noted that the Whitsunday mafic lavas show a greater compositional spread than the felsic lavas, and that among the mafic lavas there exists a broad spectrum of compositions from tholeiitic to transitional arc-like (calc-alkaline) compositions. This matches very closely the mafic rocks in the Chiang Khong Volcanic Belt calc-alkaline and transitional tholeiitic series described above.

Figure 12 compares Ti/Y vs Zr/Y relationships for the Chiang Khong igneous rock with three suites of data for the central and northern Andean arc and with calc-alkaline rift-related Whitsunday volcanic province data. Clearly, the Chiang Khong data more closely resemble the Whitsunday rift-related suite than the modern Andean volcanic arcs. We note also, as pointed out by Miyashiro (1974) that a characteristic feature of subduction-related arc volcanics is the predominance of fragmental eruptive products. In contrast, fragmental rocks are scarce in the Chiang Khong suites we have studied, again supporting an extensional rift setting rather than a continental margin arc setting for the Chiang Khong rocks.

Further research is required to evaluate more thoroughly the alternative model for the Chiang Khong volcanic belt lavas and volcaniclastics suggested here in which they are interpreted to have been erupted in a post-orogenic, Basin and Range-type setting. The exact timing of the main deformation event that produced the Sukhothai Fold Belt, involving collision between Indochina and the Shan-Thai (or Sibumasu) terranes is still not well constrained. Earliest unambiguous post-orogenic redbeds of the Khorat Group are generally considered to be latest Triassic age (Metcalfe 2002; Wakita & Metcalfe 2005), and stitching plutons are dated around 210-180 Ma (Early Jurassic) (Charusiri *et al.* 1993). The youngest chert or limestone blocks in the melanges along the Chiang Mai Suture west of the Chiang Khong volcanic belt, and its northern analogue, the Changning-Menglian Suture in Yunnan, and southern extension as the Bentong-Raub Suture in Malaysia, are Middle Triassic in age (Metcalfe, 2002; Wakita & Metcalfe 2005).

In summary, we suggest that following the latest Middle to early Late Triassic collisional event involving the Indochina and Shan-Thai terranes, crustal thickening resulting from the collision led to gravitational collapse, broad extensional tectonism, and accompanying mainly calc-alkaline magmatism around 230-220 Ma, in a largely non-marine environment. Magmatism may have progressed from high-K felsic-dominant compositions (CK Western- and Central sub-belts) to later more mafic-dominated, transitional tholeiitic compositions (Eastern sub-belt) as extension accelerated. Strong Tertiary block faulting has overprinted the structural grain of northern Thailand, making it difficult to decipher evidence that unambiguously demonstrates post-orogenic extension in the Late Triassic. Our on-going studies include three structural transects across the Chiang Khong belt rocks between Chiang Khong and Lampang, and a detailed geochemical and geochronological study of the Triassic volcanic rocks in the Lampang region; these may help to clarify the tectonic setting of this important part of the southeast Asian Mesozoic orogenic collage, and enable better correlations with regions to the north and south, in Yunnan and southern Thailand-Malaysia respectively.

Acknowledgements

This project was funded by the Royal Thai Government Scholarship and the ARC Centre of Excellence in Ore Deposits (CODES –UTasmania). Presentation of this work at the Quezon City IGCP 516 conference was financially supported by the Australian UNESCO Committee for IGCP and the IGCP 516 Organizing Committee. We thank Drs Sebastien Meffre and Khin Zaw for useful discussions on Thailand geology. Niti Mankhengthong and Noppol Pacharapongsakun, Master students of the Department of Geological Sciences, Chiang Mai University, are thanked for their field assistances in northern Thailand. Drs Y Panjasawatwong and S Barr provided helpful journal reviews of the paper.

References

BARR S. M., MACDONALD A. S., DUNNING G. R., OUNCHANUM P. & YAOWANOIYOTHIN W. 2000. Petrochemistry, U-Pb (zircon) age, and palaeotectonic setting of the Lampang volcanic belt, northern Thailand. *Journal of the Geological Society of London* **157**, 553-63.

BARR S. M., MACDONALD A. S., OUNCHANUM P. & HAMILTON M. A. 2006. Age, tectonic setting and regional implications of the Chiang Khong volcanic suite, northern Thailand. *Journal of the Geological Society of London* **163**, 1037-46.

BARR S. M., TANTISUKRIT C., YAOWANOIYOTHIN W. & MACDONALD A. S. 1990. Petrology and tectonic implications of upper Paleozoic volcanic rocks of the Chiang Mai belt, northern Thailand. *Journal of Southeast Asian Earth Sciences* **4**, 37-47.

BLACK L. P, KAMO S. L, ALLEN C. M *et al.* 2004. Improved $^{206}Pb/^{238}U$ microprobe geochronology by the monitoring of a trace-element related matrix effect; SHRIMP, ID-TIMS, ELA-ICP-MS, and oxygen isotope documentation for a series of zircon standards. *Chemical Geology* **205**, 115-40.

BRAUN E. V. & HAHN L. 1976. *Geologic map of northern Thailand, sheet 2 (Chiang Rai).* Federal Institute for Geosciences and Natural Resources, Germany. (scale 1:250,000).

BRYAN S. E. 2007. Silicic large igneous provinces. *Episodes* **30**, 20-31.

BRYAN S. E., CONSTANTINE A. E., STEPHENS C. J., EWART A. E., SCHON R. W. & PARIANOS J. 1997. Early Cretaceous volcano-sedimentary successions along the eastern Australian continental margin: implications for break-up of eastern Gondwana. *Earth and Planetary Science Letters* **153**, 85–102.

BRYAN S. E., EWART A., STEPHENS C. J., PARIANOS J. & DOWNERS P. J. 2000. The Whitsunday Volcanic Province, central Queensland, Australia: Lithological and Stratigraphic investigations of a silicic-dominated large igneous province. *Journal of Volcanology and Geothermal Research* **99**, 55-78.

BUNOPAS S. 1981. Paleogeographic history of western Thailand and adjacent parts of Southeast Asia-a plate tectonic interpretation. PhD Thesis, Victoria University of Wellington, Wellington, New Zealand.

BUSSY F., HERNANDEZ J. & VON RAUMER J. 2000. Bimodal magmatism as a consequence of the post-collisional readjustment of the thickened Variscan continental lithosphere (Aiguilles-Rouges and Mont-Blanc massifs, Western Alps). *Transactions of the Royal Society of Edinburgh: Earth Sciences* **91 (1-2)**, 221-33.

CHARUSIRI P., CLARK A. H., FARRAR E., ARCHIBALD D. & CHARUSIRI B. 1993. Granite belts in Thailand: evidence from the $^{40}Ar/^{39}Ar$ geochronological and geological syntheses. *Journal of Southeast Asian Earth Sciences* **8**, 127-36.

CRAWFORD A. J. & BERRY R. F. 1992. Tectonic implications of Late Proterozoic - early Palaeozoic igneous rock associations in W Tasmania. *Tectonophysics* **214**, 37-56.

CRAWFORD A. J., CORBETT K. D. & EVERARD J. 1992. Geochemistry and tectonic setting of a Cambrian VMS-rich volcanic belt: the Mount Read Volcanics, W Tasmania. *Economic Geology* **87**, 597-19.

CRAWFORD A. J. & PANJASAWATWONG Y. 1996. Ophiolite, ocean crust, and the Nan suture in NE Thailand. *In* Lee, T.-Y. (ed). *Proceedings of the International Symposium on Lithosphere Dynamics of East Asia*, pp. 84-89. Taipei, Taiwan, R.O.C.

DAVIS J. H. & VON BLANCKENBURG F. 1995. Slab breakoff: a model of lithosphere detachment and its test in the magmatism and deformation of collisional orogens. *Earth and Planetary Science Letters* **129**, 85-102.

ENGLAND P. C. & HOUSEMAN G. A. 1989. Extension during continental convergence, with application to the Tibet Plateau. *Journal of Geophysical Research* **94**, 17561-79

EWART A., SCHON R. W. & CHAPPELL B. W. 1992. The Cretaceous volcanic-plutonic province of the central Queensland (Australia) coast - a rift related 'calc-alkaline' province. *Transactions of the Royal Society of Edinburgh: Earth Sciences* **83**, 327-45.

FAN W. M, GUO F., WANG Y. J. & LIN G. 2003. Late Mesozoic calc-alkaline volcanism of post-orogenic extension in the northern Da Hinggan Mountains, northeastern China. *Journal of Volcanology and Geothermal Research* **121**, 115-35.

FAN W. M., GUO F., WANG Y. J., LIN G. & ZHANG M. 2001. Post-orogenic bimodal volcanism along the Sulu Orogenic Belt in eastern China. *Physics and Chemistry of the Earth* **A 26**, 733-46.

HADA S., BUNOPAS S., ISHII K. & YOSHIKURA S. 1999. Rift-drift history and the amalgamation of Shan-Thai and Indochina/East Malaya Blocks: *In* Metcalfe I. *et al.* (eds). *Gondwana Dispersion and Asian Accretion – IGCP 321 final results volume*, pp. 67-87, A. A. Balkema Publishers, Rotterdam.

HAWKESWORTH C. J., TURNER S., GALLAGHER K., HUNTER A., BRADSHAW T. & ROGERS N. 1995. Calc-alkaline magmatism, lithospheric thinning and extension in the Basin and Range. *Journal of Geophysical Research* **100**, 10271-86.

HOOPER P. R., BAILEY, D. G. & MCCARLEY HOLDER G. A. 1995. Tertiary calc-alkaline magmatism associated with lithospheric extension in the Pacific Northwest. *Journal of Geophysical Research* **100**, 10303-19.

HUMPHREYS E. D. 1995. Post-Laramide removal of the Farallon slab, western USA. *Geology* **23**, 987-90.

INTASOPA S. & DUNN T. 1994. Petrology and Sr-Nd isotropic systems of basalts and rhyolites, Loei, Thailand, *Journal of Southeast Asian Earth Sciences* **9**, 167-80.

JUNGYUSUK N. & KHOSITANONT S. 1992. Volcanic rocks and associated mineralization in Thailand, *In* Piencharoen, C. (ed). *Proceedings of the National Conference on Geologic Resources of Thailand: Potential for Future Development*, pp. 528-32. Bangkok.

KOSUWAN P. 2004. Petrochemistry and tectonic setting of mafic volcanic rocks in the Khlong Tha Dan Dam area, Nakhon Nayok province, Thailand. MS Thesis, Chiang Mai University, Chiang Mai, Thailand.

LI Z. X. & LI X. H. 2007. Formation of the 1300-km-wide intracontinental orogen and post-orogenic magmatic province in Mesozoic South China: a flat-slab subduction model. *Geology* **35**, 179-82.

LUDWIG K. R. 2003. Isplot 3.0: A Geochronological Toolkit for Microsoft Excel. *Berkeley Geochronology Center Special Publication* **4**, p. 70, Berkeley, California.

MACDONALD A. S. & BARR S. M. 1987. Tectonic significance of a Late Carboniferous volcanic arc in northern Thailand. *In* Nutalaya P. (ed). *Proceedings of the Third Regional Conference on Geology and Mineral Resources of SE Asia,* pp. 151-56, Bangkok and Pattaya.

METCALFE I. 2000. The Bentong-Raub suture zone. *Journal of Asian Earth Sciences* **18**, 691-12.

METCALFE I. 2002. Permian tectonic framework and paleography of SE Asia. *Journal of Asian Earth Sciences* **20**, 551-66.

MILLER C. F. & MITTLEFEHLDT D. W. 1982. Depletion of light rare earth elements in felsic magmas, *Geology* **10**, 129-33.

MIYASHIRO A. 1974. Volcanic rocks series in island arcs and active continental margins, *American Journal of Science* **274**, 321-55.

PANJASAWATWONG Y. 1991. Petrology, geochemistry and tectonic implications of igneous rocks in the Nan suture, Thailand, and an empirical study of the effects of Ca/Na, Al/Si and H_2O in plagioclase-melt equilibria at 5-10 kb pressure. PhD Thesis, University of Tasmania, Tasmania, Australia.

PANJASAWATWONG Y. 1999. Petrology and tectonic setting of eruption of basaltic rocks penetrated in well GTE-1, San Kamphaeng geothermal field, Chiang Mai, northern Thailand. *In* Rattanasathien B & Rieb S. L. (eds). *Proceedings of the International Symposium on Shallow Tethys (ST) 5*, pp. 242-64, Chiang Mai.

PANJASAWATWONG Y., CHANTARAMEE S., LIMTRAKUN P. & PIRARAI K. 1997. Geochemistry and tectonic setting of eruption of central Loei volcanic in the Pak Chom area, Loei, northeast Thailand. *In* Dheeradilok P. *et al.* (eds). *Proceedings of the International Conference on Stratigraphy and Tectonic Evolution of Southeast Asia and South Pacific*, pp. 287-02, Bangkok.

PANJASAWATWONG Y., KANPENG K. & RUENGVATANASIRIKUN K. 1995. Basalts in Li basin, northern Thailand: Southern extension of Chiang Mai volcanic belt. *In* Thanvarachron S. *et al.* (eds). *Proceedings of the International Conference on Geology, Geotechnology and Mineral Resources of Indochina (GEO-INDO' 95)*, pp. 225-34, Khon Kaen.

PANJASAWATWONG Y., KHIN ZAW, CHANTARAMEE S., LIMTRAKUN P. & PIRARAI K. 2006. Geochemistry and tectonic setting of eruption of central Loei volcanic rocks, Pak Chom area, Loei, northeastern Thailand. *Journal of Asian Earth Sciences* **26**, 77-90.

PANJASAWATWONG Y., PHAJUY B. & HADA S. 2003. Tectonic setting of the Permo-Triassic Chiang Khong volcanic rocks, northern Thailand, based on petrochemical characteristics. *Gondwana Research* **6**, 743-55.

PECCERILLO A. & TAYLOR S. R. 1976. Geochemistry of Eocene calc-alkaline volcanic rocks from the Kastamonu Area, northern Turkey. *Contributions to Mineralogy and Petrology* **58**, 63-81.

PHAJUY B. 2001. Geochemistry, petrology and tectonic setting of Permo-Triassic mafic volcanic rocks in the northern part of Chiang Khong-Tak volcanic belt. MS Thesis, Chiang Mai University, Chiang Mai, Thailand.

PHAJUY B., PANJASAWATWONG Y. & OSATAPORN P. 2005. Preliminary geochemical study of volcanic rocks in the Pang Mayao area, Phrao, Chiang Mai, northern Thailand: Tectonic setting of formation. *Journal of Asian Earth Sciences* **24**, 765-76.

ROBINSON P. 2003. XRF analysis of flux-fused discs. Geoanalysis 2003. *The 5th International Conference on the Analysis of Geological and Environmental Materials*, p. 90 (abstracts), Rovaniemi, Finland.

ROGERS N. W., HAWKESWORTH C. J. & ORMEROD D. S. 1995. Late Cenozoic basaltic magmatism in the Western Great Basin, California and Nevada. *Journal of Geophysical Research* **100**, 10287-301.

ROTTURA A., BARGOSSI G. M., CAGGIANELLI A., DEL MORO A., VISONA D. & TRANNE C. A. 1998. Origin and significance of the Permian high-K calc-alkaline magmatism in the central-eastern Southern Alps, Italy. *Lithos* **45**, 329-48.

SINGHARAJWARAPAN S. & BERRY R. F. 2000. Tectonic implications of the Nan suture zone and its relationship to the Sukhothai Fold Belt, northern Thailand. *Journal of Asian Earth Sciences* **18**, 663-73.

SINGHARAJWARAPAN S. 1994. Deformation and metamorphism of the Sukhothai Fold Belt, northern Thailand. PhD Thesis, University of Tasmania, Tasmania, Australia.

SMEDLEY P. L. 1986. The relationship between calc-alkaline volcanism and within-plate continental rift volcanism: evidence from Scottish Palaeozoic lavas. *Earth and Planetary Science Letters* **77**, 113-28.

STACEY J. S. & KRAMER J. D. 1975. Approximation of terrestrial lead isotope evolution by a two stage model. *Earth and Planetary Science Letters* **26**, 16-25.

SUKVATTANANUNT P. & ASSAWAPATCHARA S. 1989a. *Geological map of Amphoe Chiang Khong (Sheet 5049 I).* Geological Survey Division, Department of Mineral Resources, Bangkok, Thailand (scale 1:50,000).

SUKVATTANANUNT P. & ASSAWAPATCHARA S. 1989b. *Geological map of Amphoe Chiang Saen (Sheet 5049 IV).* Geological Survey Division, Department of Mineral Resources, Bangkok, Thailand (scale 1:50,000).

SUKVATTANANUNT P. & ASSAWAPATCHARA S. 1989c. *Geological map of Ban Pong Noi (Sheet 5049 III).* Geological Survey Division, Department of Mineral Resources, Bangkok, Thailand (scale 1:50,000).

SUKVATTANANUNT P. & ASSAWAPATCHARA S. 1989d. *Geological map of Ban Si Don Chai (Sheet 5049 II).* Geological Survey Division, Department of Mineral Resources, Bangkok, Thailand (scale 1:50,000).

SUKVATTANANUNT P., TANSATHIEN W., PRASITTIKARNKUL K., MOOKDEE P. & PRIKYAI P. 1985a. *Geological map of Amphoe Phaya Mengrai (Sheet 5048 III).* Geological Survey Division, Department of Mineral Resources, Bangkok, Thailand (scale 1:50,000).

SUKVATTANANUNT P., TANSATHIEN W., PRASITTIKARNKUL K., MOOKDEE P. & PRIKYAI P. 1985b. *Geological map of Amphoe Thoeng (Sheet 5048 IV).* Geological Survey Division, Department of Mineral Resources, Bangkok, Thailand (scale 1:50,000).

SUN S. S. & MCDONOUGH W. F. 1989. Chemical and isotopic systematics of oceanic basalts: Implications for mantle composition and processes. *In* Saunders A. D & Norry M. J (eds). *Magmatism in the Ocean Basins*, Geological Society of Special Publications **42**, pp. 313-45. Geological Society of London and Blackwell Scientific Publications, London.

TANSUWAN V. & CHITMANEE S. 1990a. *Geological map of Amphoe Chiang Kham (Sheet 5048 II).* Geological Survey Division, Department of Mineral Resources, Bangkok, Thailand (scale 1:50,000).

TANSUWAN V. & CHITMANEE S. 1990b. *Geological map of Ban Pa Tan (Sheet 5048 I).* Geological Survey Division, Department of Mineral Resources, Bangkok, Thailand (scale 1:50,000).

WAKITA K. & METCALFE I. 2005. Ocean plate stratigraphy in E and SE Asia. *Journal of Asian Earth Sciences* **24**, 679-702.

WANG X., METCALFE I., JIAN P., HE L. & WANG C. 2000. The Jinshajiang-Ailaoshan suture zone, tectonic-stratigraphy, age and evolution. *Journal of Asian Earth Sciences*. **18**, 675-90.

WATSON J. S. 1996. Fast, simple method of powder pellet preparation for X-ray fluorescence analysis. *X-Ray Spectrometry* **25**, 173-74.

WIEDENBECK M., ALLE P., CORFU F. *et al.* 1995. 3 Natural zircon standards for U-Th-Pb, Lu-Hf, trace-element and REE analyses. *Geostandards Newsletter: Journal of Geostandards and Geoanalysis* **19**, 1-23.

WU H., BOULTER C. A., KE B., STOW, D. A. V. & WANG Z. 1995. The Changning-Menglian suture zone; a segment of the major Cathaysian-Gondwana divide in Southeast Asia. *Tectonophysics* **242**, 267-80.

YANG K., MO. X. & ZHU Q. 1994. Tectono-volcanic belts and late Paleozoic-early Mesozoic evolution of southwestern Yunnan, China. *Journal of Southeast Asian Earth Sciences* **10**, 245-62.

YU Z., ROBINSON P. & MCGOLDRICK P. 2001. An evaluation of methods for the chemical decomposition of geological materials for trace element determination using ICP-MS. *Geostandards Newsletter: Journal of Geostandards and Geoanalysis* **25**, 199-217.

List of Figures

Fig. 7 Chondrite-normalised REE patterns of representative mafic Chiang Khong belt igneous rocks (< 55 wt% SiO_2). The normalizing values used are those of Sun & McDonough (1989).

Fig. 8 Chondrite-normalised REE patterns of representative dacitic to felsic Chiang Khong belt igneous rocks (60-80 wt% SiO_2). The normalizing values used are those of Sun & McDonough (1989).

Fig. 9 N-MORB normalised patterns of representative high-K calc-alkaline intermediate to felsic rocks of Chiang Khong Volcanic Belt (60 – 80 wt% SiO_2). The normalizing values used are those of Sun & McDonough (1989).

Fig. 10 N-MORB normalised patterns of representative transitional tholeiitic mafic rocks of Chiang Khong Volcanic Belt. The normalizing values used are those of Sun & McDonough (1989).

Fig. 11 Plots of (a) selected major elements vs. SiO_2 (b) selected trace elements vs. SiO_2 for Chiang Khong belt igneous rocks compared to lavas and dykes from the Cretaceous Whitsunday Volcanic Province (WVP: Ewart *et al.* 1992 and S. Bryan unpublished data). Symbols as in Fig. 4.

Fig. 12 Plot of Zr/Y vs. Ti/Y diagram for the Chiang Khong igneous rocks (CK) compared to Andean volcanic margin lavas (southern Central Volcanic Zone CVZ: 17-30°S, northern CVZ: 12-17°S, and Northern Volcanic Zone (NVZ) from the web-based GEOROC database: http://georoc.mpch-mainz.gwdg.de/georoc/) and rift-type calc-alkaline rocks of the Whitsunday Volcanic Province (WVP from Ewart *et al.* 1992 and S. Bryan unpublished data).

List of Tables

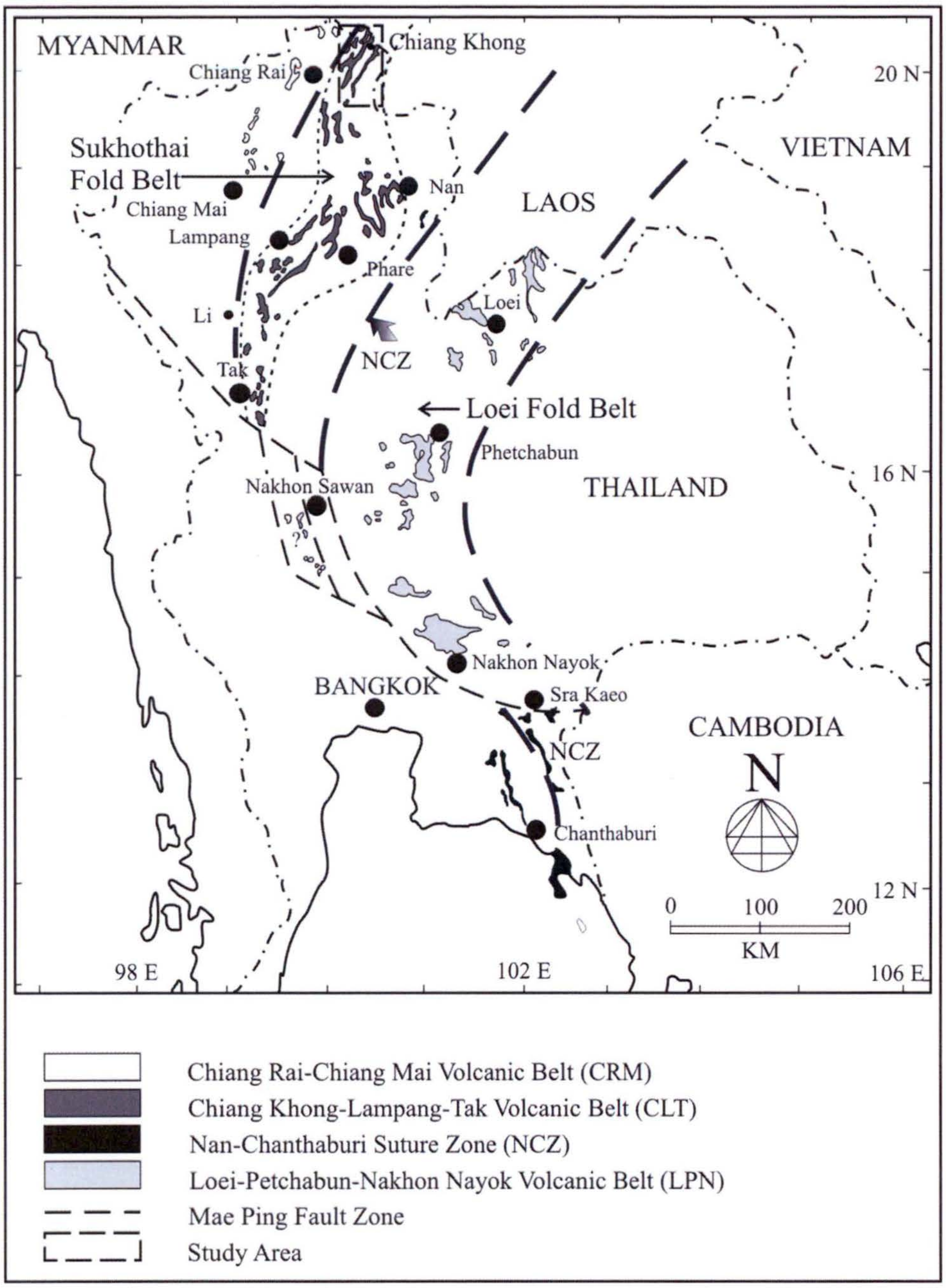

Fig. 1 Map showing the Sukhothai Fold Belt, Loei Fold Belt, distribution of pre-Jurassic volcanic rocks in Thailand and study area of the Chiang Khong Volcanic Belt (after Panjasawatwong *et al.* 1997 and Kosuwan 2004).

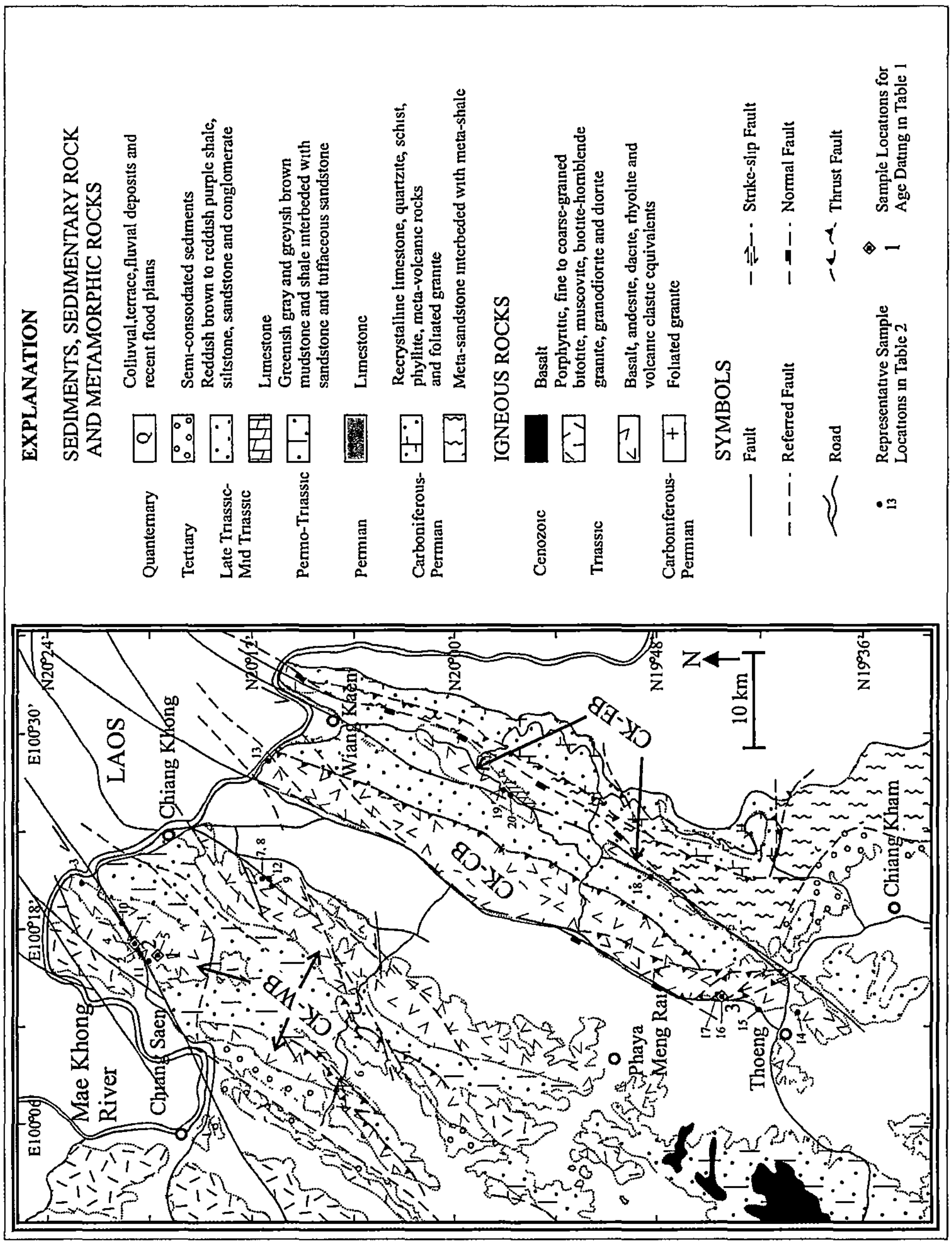

Fig. 2 Geologic map of Chiang Khong area compiled from field work by the first author, and previous maps (Braun & Hahn 1976; Sukvattananunt *et al.* 1985a, 1985b; Sukvattananunt & Assawapatchara 1989a, 1989b, 1989c, 1989d; Tansuwan & Chitmanee 1990a, 1990b; Panjasawatwong *et al.* 2003). Location of map is shown in Fig. 1.

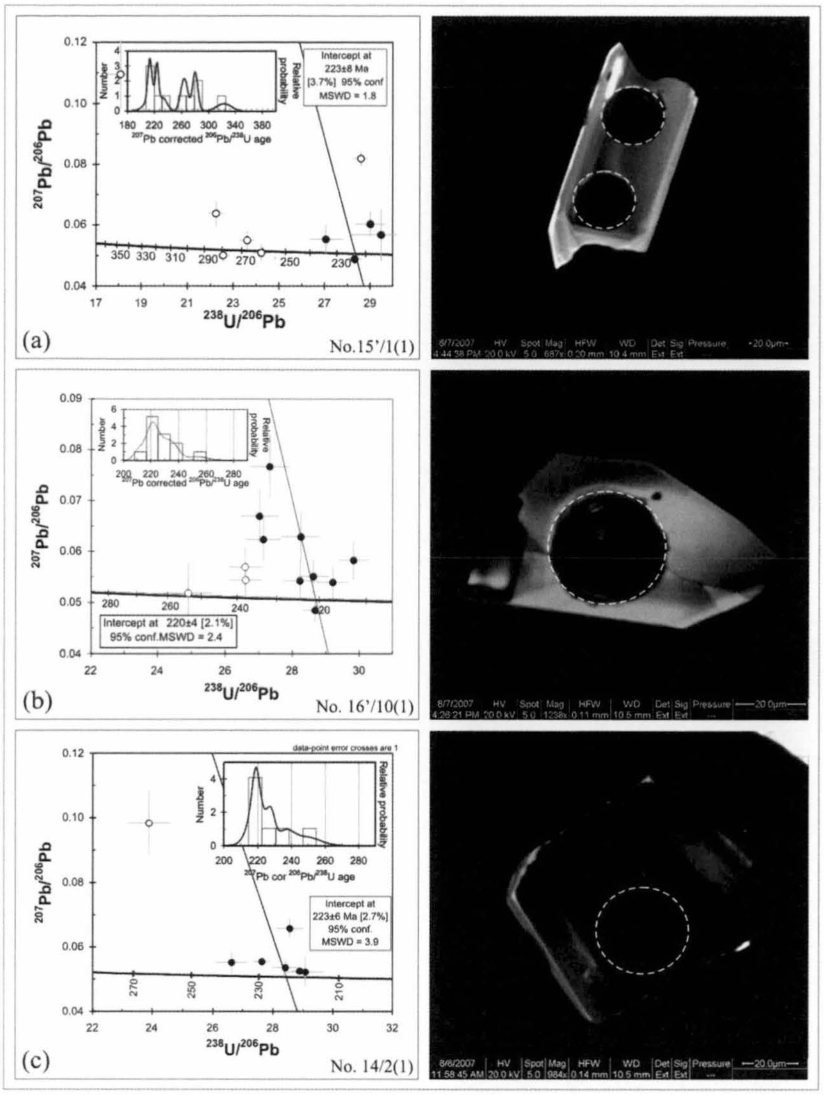

Fig. 3 Reverse concordia plot of laser ablation ICP-MS zircon U-Pb measurements and CL-images for the three representative CLT samples [(a) sample no 15'/1(1) from location 1 in Fig. 2, (b) sample no 16'/10(1) from location 2 in Fig. 2 and (c) sample no 14/2(1) from location 3 in Fig. 2] from Chiang Khong area. Best fit regression and ^{207}Pb corrected age calculated using the Isoplot 3.0 software (Ludwig 2003) assuming common Pb composition based on the 2 stage model of Stacey & Kramer (1975).

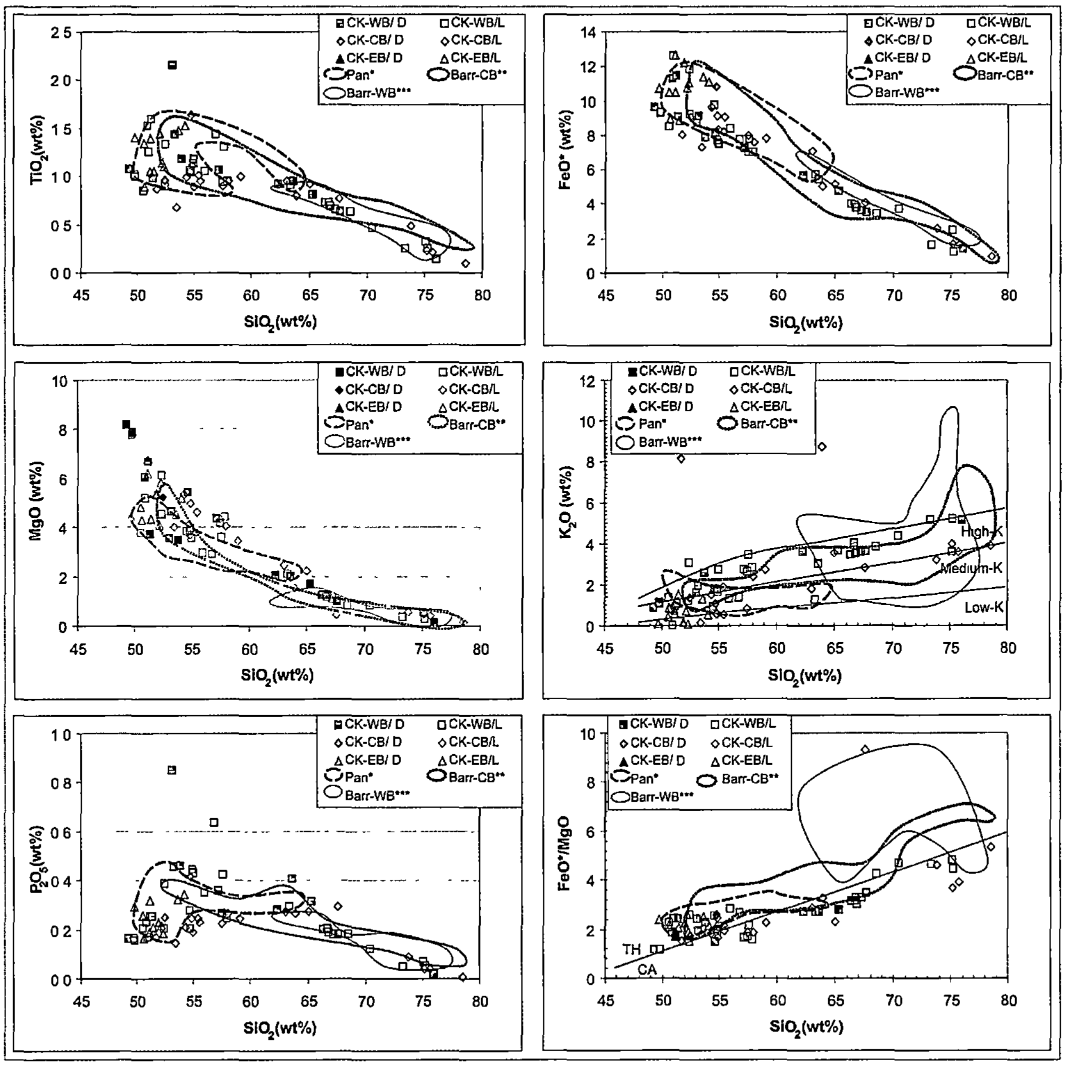

Fig. 4 Selected major elements vs. SiO_2 (all in w t% volatile free) variation diagrams of the Chiang Khong belt igneous rocks compared to data from Barr *et al.* (2006) and Panjasawatwong *et al.* (2003) from the same belt. CK-WB/D = dykes or intrusive rocks from Chiang Khong Western Belt; CK-WB/L = lavas from Chiang Khong Western Belt; CK-CB/D = dykes or intrusive rocks from Chiang Khong Central Belt; CK-CB/L = lavas from Chiang Khong Central Belt; CK-EB/D = dykes or intrusive rocks from Chiang Khong Eastern Belt; CK-EB/L = lavas from Chiang Khong Eastern Belt; Pan* = Igneous rocks in Chiang Khong area by Panjasawatwong *et al.* (2003); Barr-CB** = Igneous rocks from Chiang Khong Central Belt by Barr *et al.* (2006); Barr-WB*** = Igneous rocks from Chiang Khong Western Belt by Barr *et al.* (2006). [K_2O vs. SiO_2 after Peccerillo & Taylor (1976) and FeO^*/MgO vs. SiO_2 after Miyashiro (1974)].

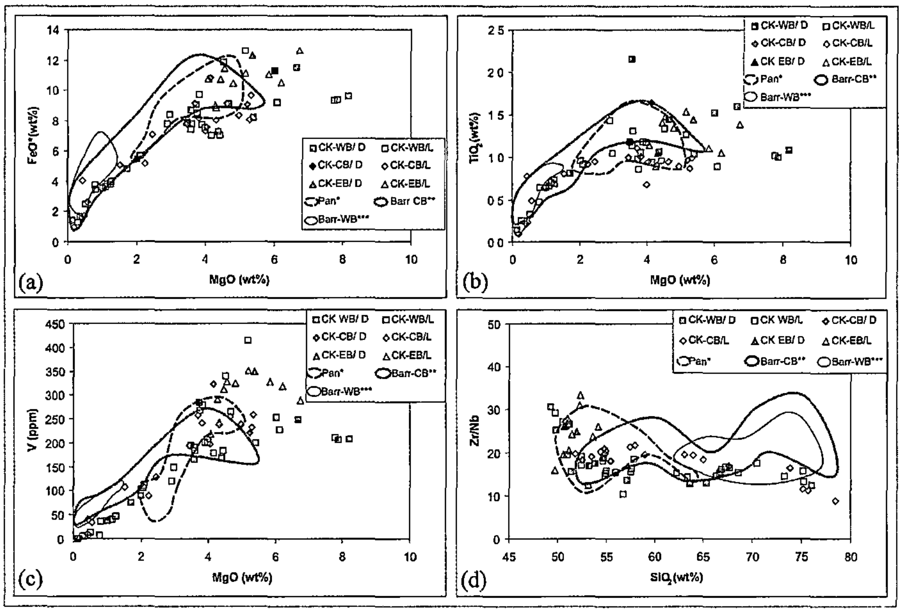

Fig. 5 Plots of (a) FeO* (wt %) vs. MgO (wt %), (b) TiO_2 (wt %) vs. MgO (wt %), (c) V (ppm) vs. MgO (wt %) and (d) Zr/Nb vs. SiO_2 (wt%) diagrams of Chiang Khong belt igneous rocks. Symbols as in Fig. 4.

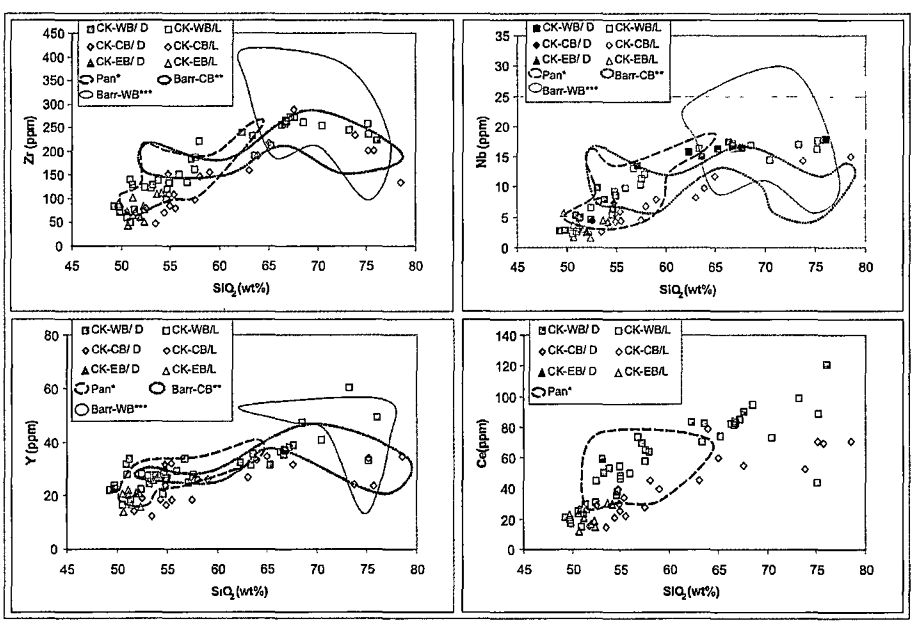

Fig. 6 Selected high field strength elements (HFSE), trace elements and LREE (in ppm) plotted against SiO_2 (wt %) for the Chiang Khong belt igneous rocks. Symbols as in Fig. 4.

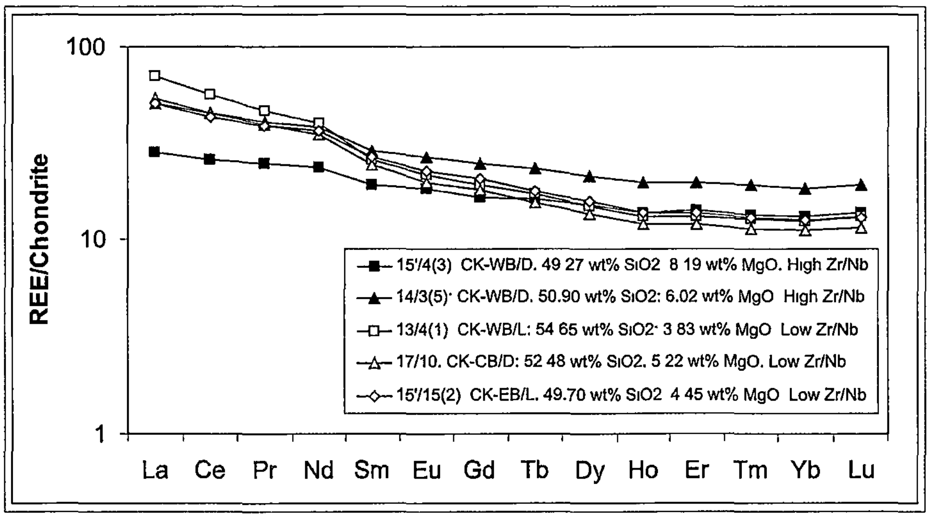

Fig. 7 Chondrite-normalised REE patterns of representative mafic Chiang Khong belt igneous rocks (< 55 wt% SiO_2). The normalizing values used are those of Sun & McDonough (1989).

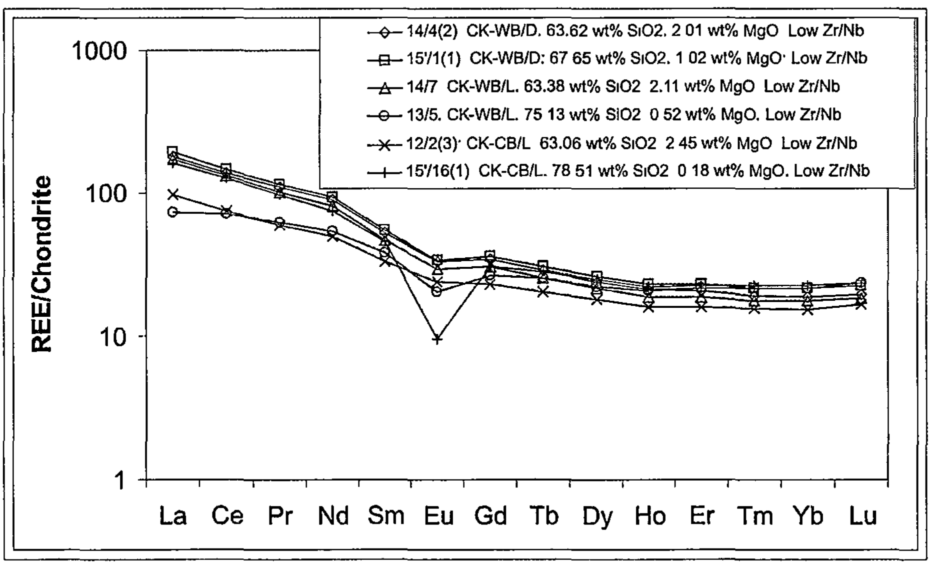

Fig. 8 Chondrite-normalised REE patterns of representative dacitic to felsic Chiang Khong belt igneous rocks (60-80 wt% SiO_2). The normalizing values used are those of Sun & McDonough (1989).

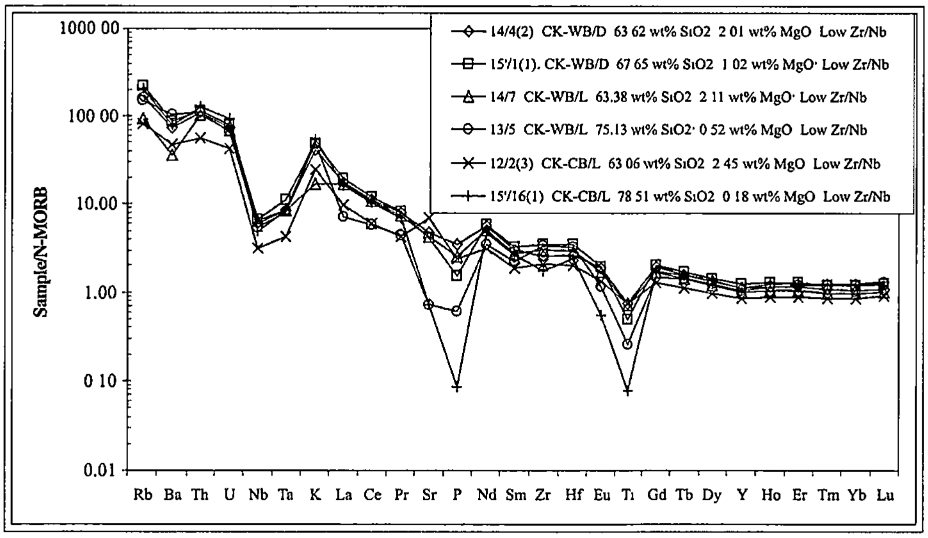

Fig. 9 N-MORB normalised patterns of representative high-K calc-alkaline intermediate to felsic rocks of Chiang Khong Volcanic Belt (60 – 80 wt% SiO_2). The normalizing values used are those of Sun & McDonough (1989).

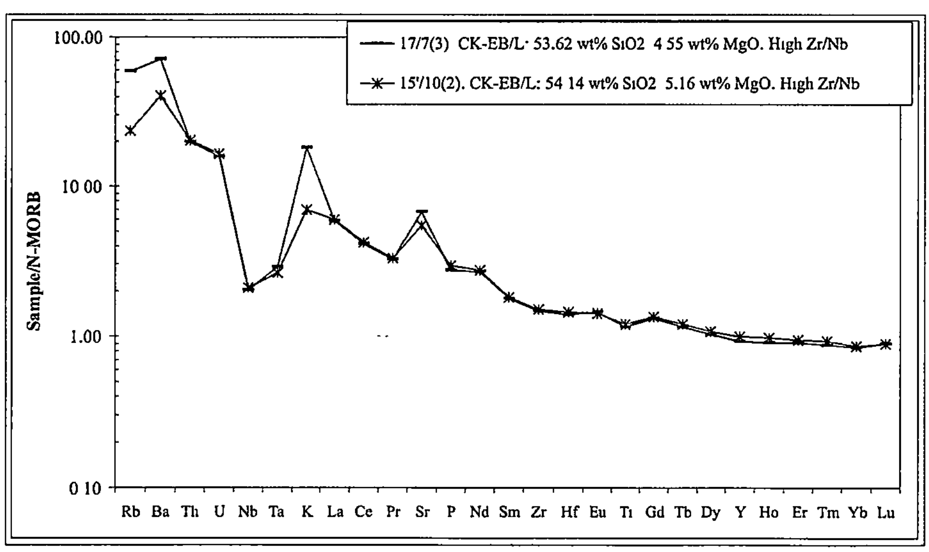

Fig. 10 N-MORB normalised patterns of representative transitional tholeiitic mafic rocks of Chiang Khong Volcanic Belt. The normalizing values used are those of Sun & McDonough (1989).

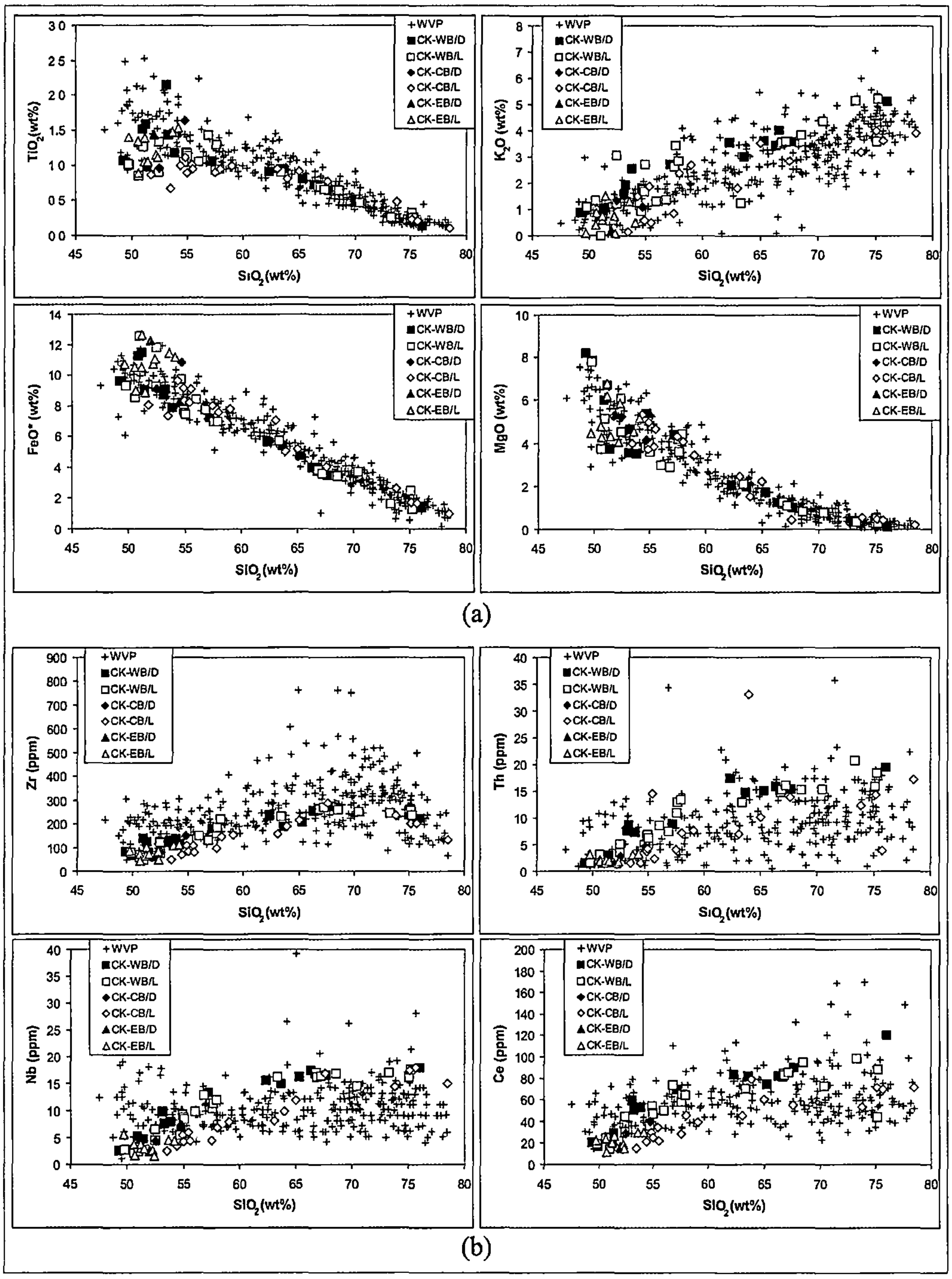

Fig. 11 Plots of (a) selected major elements vs. SiO_2 (b) selected trace elements vs. SiO_2 for Chiang Khong belt igneous rocks compared to lavas and dykes from the Cretaceous Whitsunday Volcanic Province (WVP: Ewart *et al.* 1992 and S. Bryan unpublished data). Symbols as in Fig. 4.

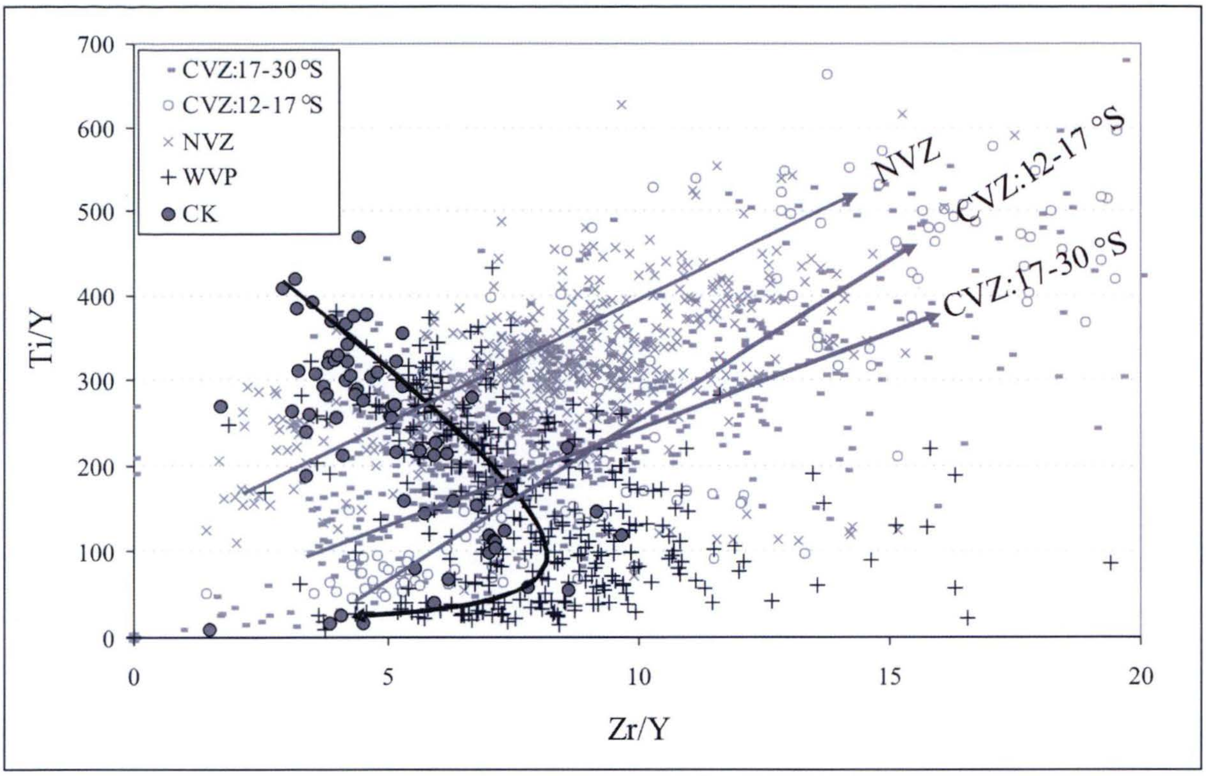

Fig. 12 Plot of Zr/Y vs. Ti/Y diagram for the Chiang Khong igneous rocks (CK) compared to Andean volcanic margin lavas (southern Central Volcanic Zone CVZ: 17-30°S, northern CVZ: 12-17°S, and Northern Volcanic Zone (NVZ) from the web-based GEOROC database: http://georoc.mpch-mainz.gwdg.de/georoc/) and rift-type calc-alkaline rocks of the Whitsunday Volcanic Province (WVP from Ewart *et al.* 1992 and S. Bryan unpublished data).

Table 1 Laser ablation ICPMS U-Pb isotopic and trace element data for zircons from representative Chiang Khong igneous rocks.

Analysis no	206Pb/238U age (207corr)		206Pb/238U		208Pb/232Th		207Pb/206Pb		207Pb/235U		Nd	Hf	Pb	Th	U
Sample-spot	(Ma)	+/-1s		%rse		%rse		%rse		%rse	(in ppm)				
15'/1(1)-1[A]	213	2 6	0 0350	1 2%	0 0121	1 9%	0 0819	3 2%	0 3925	3 4%	60	8873	69	1858	1467
15'/1(1)-2[A]	213	9 8	0 0339	4 5%	0 0129	7 8%	0 0568	15 3%	0 2590	13 0%	147	8882	12	200	312
15'/1(1)-3	216	5 0	0 0345	2 3%	0 0138	3 8%	0 0603	7 0%	0 2736	6 9%	88	10060	9	133	236
15'/1(1)-4	224	2 2	0 0353	1 0%	0 0103	2 0%	0 0489	3 5%	0 2342	3 3%	32	11467	58	1212	1450
15'/1(1)-5	233	6 5	0 0370	2 8%	0 0148	5 6%	0 0553	8 9%	0 2803	8 5%	78	8867	20	221	509
15'/1(1)-6[B]	261	4 0	0 0413	1 5%	0 0124	2 7%	0 0509	5 3%	0 2799	5 4%	18	8596	25	501	512
15'/1(1)-7[B]	266	3 8	0 0423	1 4%	0 0120	2 4%	0 0550	5 5%	0 3166	5 6%	20	8768	26	510	528
15'/1(1)-8[B]	279	4 7	0 0449	1 6%	0 0163	4 3%	0 0638	6 8%	0 3970	7 0%	48	10892	15	247	295
15'/1(1)-9[B]	280	3 6	0 0443	1 3%	0 0134	3 0%	0 0500	4 1%	0 3036	4 1%	6	10832	34	358	731
15'/1(1)-10[C]	323	10 9	0 0553	3 1%	0 0281	6 1%	0 1095	10 2%	0 7826	10 5%	8	8969	13	124	172
16'/10(1)-1	210	3 3	0 0335	1 5%	0 0100	3 3%	0 0583	6 4%	0 2558	6 2%	14	9225	14	265	390
16'/10(1)-2	216	3 6	0 0342	1 6%	0 0106	3 4%	0 0539	5 8%	0 2497	5 7%	43	8875	13	258	339
16'/10(1)-3	220	3 7	0 0349	1 7%	0 0109	3 1%	0 0551	6 0%	0 2621	5 9%	48	8669	22	623	499
16'/10(1)-4	221	4 7	0 0354	2 0%	0 0114	4 4%	0 0629	7 9%	0 2963	7 8%	81	7497	11	220	277
16'/10(1)-5	221	3 1	0 0349	1 4%	0 0106	3 0%	0 0485	4 9%	0 2238	4 9%	5	10510	22	320	608
16'/10(1)-6	223	4 2	0 0354	1 8%	0 0113	3 5%	0 0543	7 1%	0 2644	7 0%	20	9328	11	179	271
16'/10(1)-7	224	5 3	0 0366	2 3%	0 0136	4 8%	0 0767	8 3%	0 3698	8 1%	10	8663	7	95	163
16'/10(1)-8	230	5 0	0 0370	2 1%	0 0138	5 1%	0 0669	7 9%	0 3367	7 8%	74	9398	10	134	263
16'/10(1)-9	230	4 7	0 0368	2 0%	0 0116	4 6%	0 0624	7 0%	0 3032	7 0%	360	10990	28	406	684
16'/10(1)-11	236	4 6	0 0376	1 9%	0 0115	4 1%	0 0569	6 7%	0 2820	7 3%	9	10469	18	294	463
16'/10(1)-12	237	4 3	0 0376	1 8%	0 0115	3 4%	0 0544	5 7%	0 2775	5 8%	7	9618	15	308	357
16'/10(1)-13[B]	254	7 6	0 0402	3 0%	0 0122	5 1%	0 0518	11 2%	0 2932	11 0%	17	8782	16	265	372
14/2(1)-1	218	5 0	0 0344	2 2%	0 0105	5 5%	0 0522	9 0%	0 2484	8 6%	9	9284	19	277	543
14/2(1)-2	218	3 5	0 0350	1 6%	0 0115	3 3%	0 0657	4 8%	0 3193	5 3%	13	9479	18	366	461
14/2(1)-3	219	2 0	0 0346	0 9%	0 0103	1 5%	0 0525	2 5%	0 2452	2 5%	35	9288	130	4656	2796
14/2(1)-4	222	3 3	0 0352	1 5%	0 0105	2 4%	0 0535	4 8%	0 2601	4 5%	51	9447	20	467	503
14/2(1)-5	228	2 4	0 0362	1 0%	0 0103	1 8%	0 0554	2 7%	0 2720	2 7%	73	9912	104	2732	2423
14/2(1)-6	236	4 9	0 0376	2 1%	0 0107	3 4%	0 0552	6 2%	0 2897	6 2%	18	9946	22	446	535
14/2(1)-7[D]	249	8 0	0 0418	3 0%	0 0188	5 9%	0 0984	10 1%	0 5285	9 7%	11	8877	15	219	277
14/2(1)-8[B]	897	13 5	0 1518	1 5%	0 0607	4 5%	0 0815	3 8%	1 7016	3 8%	1	13872	249	115	1785

A = High U; B = Old core; C = Sample exploded; D = Common lead

Table 2 Petrographic features of representative Chiang Khong igneous rocks.

No.	Areas	Sample name	Latitude (°N)	Longitude (°E)	Petrographic features
1	CK WB	15'/4(3)	20.3134	100.2865	Aphyric tholeiitic basalt/dolerite dyke with fresh clinopyroxene.
2	CK WB	14/3(5)	20.3161	100.2885	Plagioclase-phyric coarse-grained basalt or dolerite dyke with abundant fresh clinopyroxene.
3	CK WB	14/8	20.3616	100.3578	Sparsely clinopyroxene-phyric diorite dyke.
4	CK WB	14/4(2)	20.2790	100.2977	Quartz diorite with apatite, some fresh brown biotite and interstitial quartz.
5	CK WB	15'/1(1)	20.2981	100.2797	Microdiorite with fresh clinopyroxene, albitised plagioclase, some late magmatic green hornblende, and altered biotite, with common interstitial quartz.
6	CK WB	26'/10	20.1093	100.1356	Plagioclase-phyric rhyolitic high-level intrusive rock with granophyric texture and rare green biotite/hornblende.
7	CK WB	13/4(2)	20.1701	100.3514	Trachytic textured sparsely plagioclase-phyric andesite.
8	CK WB	13/4(1)	20.1701	100.3514	Plagioclase-phyric andesite with occasional small fresh clinopyroxene phenocryst and some epidote alteration.
9	CK WB	13/7	20.1621	100.3427	Flow-textured vesicular andesite lava with albitised plagioclase, rare clinopyroxene mainly replaced by epidote/chlorite/prehnite. Vesicles filled by quartz, chlorite, prehnite and calcite.
10	CK WB	14/7	20.3348	100.3250	Dacitic lava, vein of actinolite-epidote indicating lowest greenschist facies assemblage.
11	CK WB	14/2(1)	20.3107	100.2817	Intermediate/felsic lava with common largely fresh plagioclase phenocrysts and occasional actinolite-altered former clinopyroxene phenocrysts and small Fe-Ti oxide.
12	CK WB	13/5	20.1630	100.3446	Plagioclase-phyric rhyolite.
13	CK CB	17/10	20.1844	100.4807	Dolerite dyke with occasional fresh clinopyroxene.
14	CK CB	12/1(2)	19.6600	100.2019	Plagioclase+clinopyroxene-phyric andesite and some epidote+prehnite alteration.
15	CK CB	12/2(3)	19.7033	100.2146	Sparsely and finely plagioclase-phyric formerly glassy dacitic lava. Banded fine-grained epidote alteration.
16	CK CB	16'/10(1)	19.3183	100.2251	Quartz+plagioclase-phyric rhylite.
17	CK CB	15'/16(1)	19.3210	100.2270	Fresh quartz+plagioclase-phyric welded rhyolitic tuff or lava.
18	CK EB	15'/15(2)	19.8062	100.3538	Distinctive big-plagioclase basalt with rare altered former olivine phenocrysts and large abundant albitised plagioclase phenocrysts.
19	CK EB	17/7(3)	19.9536	100.4449	Trachytic textured andesitic lava, no fresh plagioclase. Occasional vesicles with chlorite and epidote.
20	CK EB	15'/10(2)	19.9492	100.4401	Trachytic textured sparsely plagioclase+clinopyroxene-phyric andesite.

Table 3 Major and trace elements composition of the Chiang Khong igneous rocks

No in Table 2	1	2	3	4	5	6	7	8	9	10
Areas	CK WB	CK WB	CK WB	CK WB	CK WB	CK WB	CK WB	CK WB	CK WB	CK WB
Sample name	15'/4(3)	14/3(5)	14/8	14/4(2)	15'/1(1)	26'/10	13/4(2)	13/4(1)	13/7	14/7
Rock types	I/D	I/D	I/D	I/D	I/D	I/D	lava	lava	lava	lava
SiO2	49 27	50 90	57 20	63 62	67 65	76 02	52 43	54 65	55 99	63 38
TiO2	1 08	1 53	1 06	0 95	0 64	0 14	1 34	1 06	1 05	0 91
Al2O3	17 82	16 42	17 34	16 14	16 10	13 33	16 55	17 88	18 36	16 51
FeO*	9 63	11 27	7 26	5 44	3 52	1 39	11 83	9 72	8 41	5 73
MnO	0 18	0 21	0 14	0 14	0 10	0 02	0 21	0 18	0 21	0 12
MgO	8 19	6 02	4 38	2 01	1 02	0 13	4 53	3 83	2 97	2 11
CaO	9 76	9 51	6 10	4 85	2 99	0 30	8 43	7 37	5 54	3 93
Na2O	3 02	3 15	3 44	3 39	4 22	3 50	3 07	4 09	5 82	5 78
K2O	0 88	0 76	2 72	3 04	3 59	5 13	1 21	0 94	1 31	1 24
P2O5	0 17	0 23	0 36	0 41	0 18	0 02	0 39	0 28	0 35	0 30
Original sum	100 14	99 50	100 01	99 87	99 89	99 85	99 79	99 83	99 95	99 85
Loss inc S-	3 67	3 30	2 36	1 77	1 06	0 94	0 53	2 42	2 80	1 16
Y	22 10	31 60	25 00	35 70	38 90	49 10	28 30	20 80	29 10	31 50
U	<1 5	<1 5	2 20	4 50	4 40	4 30	<1 5	2 30	2 80	3 70
Rb	45 40	37 30	94 60	101 30	131 70	175 20	24 30	19 60	23 30	55 30
Th	1 60	1 90	8 90	14 80	15 40	19 50	3 60	5 00	8 60	12 90
Pb	3 53	4 03	9 78	42 98	20 11	7 64	7 79	8 92	16 06	12 66
Zn	78 70	107 30	95 30	143 00	71 00	25 60	123 60	102 80	117 50	79 10
Cu	55 50	35 70	36 50	14 00	6 60	1 40	109 30	34 30	17 90	4 90
Ni	65 00	19 00	31 80	6 20	4 50	3 90	12 00	2 60	2 10	2 90
Nb	2 70	5 30	13 40	15 00	16 50	17 90	6 50	5 40	9 80	16 30
Zr	82 70	139 00	183 10	189 90	273 00	222 40	123 40	97 50	150 30	233 10
Sr	387 30	336 20	559 70	445 80	376 20	52 50	417 40	590 20	121 00	397 90
Cr	203 00	48 80	86 90	9 80	3 70	1 00	10 80	1 50	2 90	3 10
Ba	131 40	122 30	599 10	469 20	601 40	725 60	281 70	275 00	192 40	222 10
Sc	32 80	32 40	18 00	18 70	12 10	8 70	34 70	28 10	25 10	16 10
V	207 40	252 80	168 70	88 70	37 00	0 30	339 90	279 40	149 10	110 90
La	6 00	12 00	35 20	38 70	40 40	59 50	20 50	17 10	26 80	30 60
Ce	21 10	26 10	69 60	82 30	90 20	120 50	44 50	35 90	49 90	70 50
Nd	10 70	18 40	35 30	39 50	42 70	57 30	23 90	19 40	25 50	33 20

No in Table 2	11	12	13	14	15	16	17	18	19	20
Areas	CK WB	CK WB	CK CB	CK CB	CK CB	CK CB	CK CB	CK EB	CK EB	CK EB
Sample name	14/2(1)	13/5	17/10	12/1(2)	12/2(3)	16'/10(1)	15'/16(1)	15'/15(2)	17/7(3)	15'/10(2)
Rock types	lava	lava	I/D	lava	lava	lava	lava	lava	lava	lava
SiO2	66 85	75 13	52 48	53 46	63 06	75 14	78 51	49 70	53 62	54 14
TiO2	0 69	0 32	0 96	0 67	0 95	0 23	0 10	1 41	1 48	1 53
Al2O3	16 11	12 91	18 10	19 58	15 63	13 32	11 87	17 97	16 15	16 43
FeO*	3 81	2 48	9 05	7 32	7 07	1 72	0 97	10 72	11 41	11 13
MnO	0 11	0 04	0 16	0 13	0 17	0 05	0 03	0 17	0 21	0 24
MgO	1 25	0 52	5 22	4 00	2 45	0 47	0 18	4 45	4 55	5 16
CaO	3 16	0 43	9 97	10 28	3 81	0 70	0 34	12 09	7 19	6 04
Na2O	4 27	4 50	2 47	4 24	4 75	4 33	4 08	3 09	3 75	4 46
K2O	3 56	3 60	1 35	0 17	1 82	4 00	3 90	0 11	1 32	0 51
P2O5	0 19	0 07	0 25	0 15	0 28	0 04	0 01	0 30	0 32	0 34
Original sum	100 69	100 03	99 42	100 14	100 04	99 44	99 83	99 95	99 65	99 88
Loss inc S-	1 21	0 74	2 80	4 33	1 86	0 79	0 34	4 51	2 40	2 82
Y	37 00	33 10	19 20	12 30	27 00	34 10	34 80	22 80	25 90	27 90
U	3 80	3 30	<1 5	<1 5	1 50	4 40	5 60	2 00	<1 5	<1 5
Rb	144 30	86 50	41 30	3 70	47 90	127 00	118 60	3 70	33 30	13 70
Th	15 30	16 00	2 80	1 50	7 00	14 40	17 20	3 10	3 20	3 30
Pb	21 78	6 61	6 33	5 39	14 36	5 81	4 28	12 96	10 95	7 56
Zn	78 60	131 10	89 30	65 30	111 80	42 40	13 10	105 60	121 90	125 10
Cu	8 90	2 90	118 50	43 30	13 60	4 30	2 40	121 50	51 40	32 50
Ni	5 70	2 90	25 70	22 70	2 60	3 50	2 70	50 10	12 80	11 60
Nb	16 30	16 30	4 40	2 50	8 20	17 50	15 00	5 60	4 60	4 30
Zr	263 70	258 30	80 40	47 60	159 70	201 80	134 10	89 00	108 80	112 50
Sr	372 80	67 20	456 20	217 80	620 00	118 10	66 40	352 90	577 00	473 20
Cr	9 40	0 80	67 70	64 50	1 60	1 60	1 30	121 90	12 00	7 80
Ba	570 00	722 80	242 60	52 20	297 50	548 10	479 40	57 80	454 00	256 20
Sc	13 20	10 10	30 30	24 70	18 40	5 40	4 00	28 70	32 70	32 90
V	46 00	13 60	221 40	208 30	128 20	8 80	2 20	311 80	327 60	350 90
La	38 60	15 70	10 20	6 90	19 20	32 00	32 80	12 70	12 70	12 70
Ce	82 90	43 40	29 00	14 80	45 10	71 00	71 00	22 40	30 00	29 30
Nd	41 40	23 90	14 30	8 10	22 10	31 50	34 00	14 90	18 80	18 30

* I/D = Intrusive or dyke

Table 4 Low-abundance trace elements and REE compositions (in ppm) determined via ICP-MS analysis for the 16 representative Chiang Khong igneous rocks.

Areas	CK WB	CK WB	CK WB	CK WB	CK WB	CK WB	CK WB	CK WB	CK WB	CK WB	CK CB	CK CB	CK CB	CK EB	CK EB	CK EB
Sample name	15'/4(3)	14/3(5)	14/8	14/4(2)	15'/1(1)	13/4(2)	13/4(1)	15'/1(3)	14/7	13/5	17/10	12/2(3)	15'/16(1)	15'/15(2)	17/7(3)	15'/10(2)
Rock types	I/D	I/D	I/D	I/D	I/D	lava	lava	lava	lava	lava	I/D	lava	lava	lava	lava	lava
Li	50 10	50 58	17 37	23 16	12 63	25 06	26 76	49 18	12 84	14 29	38 32	42 37	2 89	35 45	18 38	19 93
Be	0 60	0 98	1 71	2 07	2 42	1 06	1 03	0 91	2 20	1 57	0 87	1 45	1 84	1 64	1 01	1 13
Sc	37 97	39 00	17 82	16 55	12 50	37 19	29 22	28 38	16 62	12 63	32 66	21 90	5 78	23 58	36 17	37 08
V	210 81	252 80	159 86	81 18	36 70	339 90	292 14	265 30	113 64	12 73	219 11	125 20	1 81	181 53	327 60	350 90
Cr	179 86	48 80	79 40	7 92	3 01	10 80	102 28	0 77	2 28	0 39	65 20	0 26	0 65	20 96	12 00	7 80
Mn	1291 89	1553 51	1073 87	1010 14	776 93	1615 90	1162 05	1323 07	908 48	339 20	1142 14	1340 40	226 64	1394 99	1535 94	1812 26
Ni	57 72	18 09	29 24	4 88	2 65	10 52	44 56	2 12	1 37	1 52	22 99	0 92	1 79	5 72	10 88	10 31
Cu	54 36	33 94	32 99	11 38	4 51	113 25	121 89	30 98	2 25	2 36	114 24	9 65	2 48	20 67	52 17	30 99
Zn	76 09	108 81	95 18	143 48	73 55	128 13	103 89	99 45	79 05	134 87	87 62	108 87	15 30	101 71	121 39	126 36
Ga	15 59	18 97	18 99	19 02	18 96	19 29	20 74	19 08	19 04	8 33	18 48	19 30	12 11	18 69	20 22	19 63
Rb	42 43	36 22	88 26	93 58	125 32	23 45	3 22	17 93	52 82	85 21	38 75	46 38	117 18	172 95	32 97	13 37
Sr	375 36	344 39	542 90	433 95	369 86	426 32	346 27	561 27	392 08	64 44	468 61	621 89	64 54	373 37	607 33	491 56
Y	19 42	31 60	21 50	31 44	34 67	28 30	20 38	18 98	28 38	29 49	17 38	24 41	31 41	25 46	25 90	27 90
Zr	79 08	139 00	176 16	192 81	261 36	123 40	86 94	94 33	226 32	246 96	83 86	153 53	129 05	180 92	108 80	112 50
Nb	2 74	5 51	13 72	14 15	15 85	6 50	4 61	5 51	14 97	12 60	4 53	7 44	11 35	11 66	4 79	4 96
Mo	0 29	0 49	0 93	1 41	1 57	0 83	0 39	0 47	1 83	0 60	0 68	0 70	2 42	1 13	0 54	0 44
Sn	0 82	1 41	2 01	3 13	3 01	1 21	1 12	1 06	2 43	2 69	0 88	1 41	2 31	2 18	1 20	1 16
Sb	3 09	1 47	0 89	1 43	0 44	0 19	0 61	0 12	0 43	0 96	1 17	4 12	0 42	0 84	0 47	0 61
Cs	4 06	3 70	5 05	2 94	2 60	2 32	1 08	2 32	2 76	4 92	4 05	2 76	1 06	5 63	3 11	1 92
Ba	118 32	122 30	506 01	462 66	544 30	281 70	61 17	257 50	225 09	650 14	234 65	294 13	503 95	477 63	454 00	256 20
La	6 70	12 05	35 32	42 73	46 00	18 65	12 00	16 84	41 27	17 29	12 74	23 23	38 71	33 38	14 16	14 35
Ce	15 83	27 40	69 29	85 19	90 71	40 68	26 21	34 32	80 71	43 77	27 58	45 78	77 53	67 95	31 02	31 62
Pr	2 33	3 84	8 46	10 47	11 07	5 51	3 70	4 39	9 69	5 97	3 71	5 69	9 32	8 47	4 28	4 35
Nd	10 98	17 75	33 52	41 87	43 49	24 38	17 01	18 59	37 72	25 30	16 39	23 39	35 33	34 19	19 66	20 21
Sm	2 94	4 38	6 44	8 17	8 47	5 44	4 05	3 96	7 26	5 87	3 74	5 05	6 99	6 88	4 69	4 81
Eu	1 06	1 54	1 62	1 91	1 99	1 53	1 30	1 26	1 73	1 18	1 15	1 39	0 55	1 65	1 48	1 45
Gd	3 38	5 07	5 51	7 18	7 39	5 41	4 24	3 93	6 35	5 43	3 70	4 76	6 29	5 94	4 86	5 00
Tb	0 61	0 87	0 79	1 07	1 14	0 86	0 67	0 64	0 96	0 95	0 58	0 76	1 05	0 89	0 77	0 80
Dy	3 80	5 41	4 37	6 14	6 56	5 08	4 01	3 73	5 52	5 62	3 44	4 56	6 29	4 98	4 72	4 88
Ho	0 78	1 12	0 81	1 19	1 30	1 04	0 78	0 75	1 06	1 17	0 68	0 91	1 25	0 98	0 92	0 98
Er	2 35	3 27	2 26	3 45	3 82	2 98	2 27	2 18	3 10	3 56	1 98	2 67	3 75	2 79	2 72	2 78
Tm	0 34	0 48	0 31	0 49	0 56	0 44	0 33	0 32	0 45	0 55	0 29	0 40	0 58	0 40	0 40	0 42
Yb	2 23	3 13	2 00	3 21	3 69	2 82	2 13	2 11	2 98	3 70	1 88	2 60	3 85	2 52	2 59	2 63
Lu	0 35	0 49	0 31	0 50	0 57	0 44	0 33	0 33	0 47	0 60	0 29	0 42	0 60	0 40	0 41	0 40
Hf	2 15	3 29	4 60	5 48	7 11	3 13	2 57	2 64	6 04	6 75	2 41	4 13	4 94	4 99	2 89	2 97
Ta	0 21	0 46	0 99	1 13	1 46	0 42	0 43	0 47	1 13	1 08	0 41	0 58	1 14	0 80	0 39	0 35
Tl	0 29	0 27	0 78	0 98	0 67	0 19	0 02	0 11	0 39	0 77	0 23	0 55	0 72	0 90	0 19	0 07
Pb	3 58	4 77	9 15	41 20	19 78	8 32	12 86	8 10	12 65	4 99	7 83	14 18	3 67	12 69	10 13	7 26
Bi	0 04	<0 02	0 06	0 13	0 20	<0 02	0 11	0 03	0 14	0 11	0 05	0 15	0 04	0 04	<0 02	<0 02
Th	0 93	1 97	8 35	13 31	14 09	3 05	1 88	4 24	12 51	13 61	2 24	6 74	15 50	10 86	2 40	2 45
U	0 27	0 57	2 49	3 47	3 72	0 88	0 66	1 30	3 23	3 19	0 70	1 98	4 46	2 86	0 75	0 79